UNIVERSIDADE TÉCNICA DE LISBOA
INSTITUTO SUPERIOR TÉCNICO

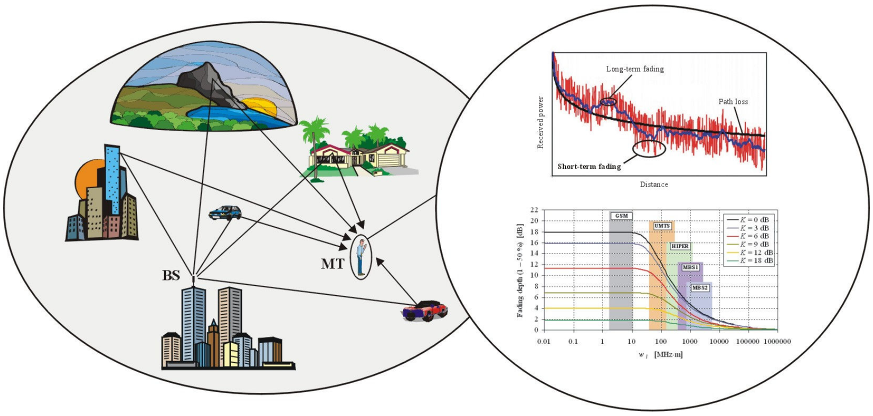

Short-Term Fading Characterisation in Wideband Mobile Communication Systems

Filipe Duarte dos Santos Cardoso
(Master)

Dissertation Submitted for Obtaining the Degree of
Doctor in Electrical and Computer Engineering

Supervisor: Doctor Luís Manuel de Jesus Sousa Correia

Jury

President: Rector of the Technical University of Lisbon

Members: Doctor Michel Daoud Yacoub
Doctor Carlos Eduardo do Rego da Costa Salema
Doctor Carlos António Cardoso Fernandes
Doctor Luís Manuel de Jesus Sousa Correia
Doctor Armando Carlos Domingues da Rocha

June 2004

To the memory of my father and my mother.
Wherever you are, I know that
you are thinking of me.

To my wife, Paula,
and our children, Ana and João,
for their love, encouragement and support.

Acknowledgments

This work was only possible due to the encouragement and support of many people, who drove me along this long, and sometimes sinuous, journey.

Among them, I would like to start by expressing all my deeply gratitude to Prof. Luis Correia, my supervisor, whose technical excellence, way of being and unconditional support was undoubtedly the master stone for achieving this goal. I would like to thank him for giving me the opportunity of sharing all of his knowledge and experience; I will never forget the encouragement and motivation during the most sinuous parts of this journey, always driving me along the best route.

To Instituto das Telecomunicações, I express my sympathy for all the support and the opportunity of sharing of its facilities. I would like to express my gratitude to all of my colleagues from the "*Group for Research on Wireless*" (GROW), and to many friends who have encouraged me during this journey. Foremost among them, I would like to thank to João Gil for his encouragement and the fruitful discussions. I would also thank to Gabriela Marques, Jorge Aguiar, Lúcio Ferreira, João Serrador, Jorge Venes, David Xavier and Silvia Taccori, among many others.

Thanks to all of my colleagues from Escola Superior de Tecnologia de Setúbal, who have always encouraged me; it is not easy to enumerate all of them, nevertheless, they know to whom I am referring to. To Escola Superior de Tecnologia de Setúbal, I would like to thank for giving me the opportunity and support for doing my Ph.D. This work was supported in part via a grant from *"Programa de Desenvolvimento Educativo para Portugal"* (PRODEP), action 4\5.3\PRODEP\2000, which gave me the opportunity of having a leave from teaching responsibilities.

Part of this work was developed within the framework of IST-FLOWS and COST 273 European Projects, whose colleagues have contributed with fruitful discussions and suggestions.

To my father, who unfortunately has left me in the last part of this journey, thanks for the encouragement and almost a whole life devoted to me.

I would like to express all my heartfelt gratitude to my wife for the support in the best and the worst moments, and to my children for all the times that I did not had time to play with them and to share their experiences.

Abstract

This thesis addresses short-term fading depth dependence on system bandwidth and environment characteristics. Two different and independent approaches are proposed, an environment-geometry based and a time-domain one. It is observed that statistical Rayleigh and Rice distributions are appropriate for evaluating the fading margins for GSM in some environments; nevertheless, for UMTS, HIPERLAN/2 and MBS, fading margins are usually well below the ones obtained from considering these narrowband distributions. A simple relationship between both approaches is derived, allowing one to use any of the proposed approaches for evaluating the fading depth, starting either from a geometrical description of the working environment or the power delay profile of the propagation channel. The use of directional antennas either at the mobile terminal or the base station is also studied, therefore, providing a framework for evaluating the fading depth in these conditions. Finally, link budget evaluation and cell range estimation is addressed, considering that the short-term fading margins are evaluated as for the narrowband case, as usually found in literature, and by using the proposed approaches. For the case of GSM, besides some exceptions, a reduction in the number of cells up to 35 %, is obtained by considering the proposed fading margins; for UMTS, a cell number reduction up to 39 % can be achieved; in the case of HIPERLAN/2 and MBS, these values decrease to 26 and 18 %, respectively. Thus, for a given service area, a significant reduction in the required number of cells is achieved when considering the proposed fading margins, allowing a better system planning and a better link quality. Hence, the work presented in this thesis, contributes for filling in the gap for proper approaches for evaluating the fading depth in wideband mobile communication systems, while providing a large set of data for different systems working in different standard reference environments.

Keywords: Mobile communications. Wideband systems. Channel characterisation. Short-term fading. Fading margin. Link budget.

Resumo

Esta tese aborda a dependência do desvanecimento rápido em função da largura de banda do sistema e das características do ambiente de propagação. São propostas duas abordagens independentes, uma baseada nas características geométricas do ambiente de propagação, e outra numa análise no domínio temporal. Verifica-se que as distribuições estatísticas de Rayleigh e Rice são apropriadas para a avaliação da margem de desvanecimento em GSM para alguns ambientes de propagação; contudo, as margens de desvanecimento em UMTS, HIPERLAN/2 e MBS são inferiores às obtidas habitualmente a partir destas distribuições de banda-estreita. É apresentada uma relação simples entre ambas as abordagens, permitindo desta forma a utilização de ambas, quer a partir da descrição geométrica do ambiente de propagação, quer a partir do perfil de potência do canal de propagação. A utilização de antennas direcionais no terminal móvel ou na estação base, é também abordada, fornecendo-se assim uma ferramenta para a avaliação da profundidade de desvanecimento nestas condições. Finalmente, apresentam-se balanços de potência e estimativas de cobertura, assumindo margens de desvanecimento rápido obtidas com base no pressuposto de banda estreita, como habitualmente encontrado na literatura, ou a partir das abordagens propostas. No caso do GSM, com excepção de alguns ambientes de propagação, a utilização das margens de desvanecimento propostas conduz uma redução do número de células que pode atingir os 35 %; no caso do UMTS verifica-se uma redução até 39 %; para HIPERLAN/2 e MBS estes valores decrescem para 26 e 18 %, respectivamente. Assim, quando se consideram as margens de desvanecimento propostas, verifica-se uma redução significativa do número de células necessárias para garantir a cobertura duma determinada área de serviço, permitindo efectuar um melhor planeamento da rede, associado a uma melhoria de desempenho da mesma. Desta forma, o trabalho apresentado nesta tese, representa uma contribuição para o preenchimento da lacuna existente em termos de abordagens adequadas para o cálculo da profundidade de desvanecimento em sistemas de comunicações móveis de banda larga, fornecendo simultaneamente um vasto conjunto de dados para diversos sistemas funcionando em diferentes cenários de referência.

Palavras Chave: Comunicações móveis. Sistemas de banda-larga. Caracterização do canal. Desvanecimento rápido. Margem de desvanecimento. Balanço de potência.

Table of Contents

List of Figures

List of Tables

List of Acronyms and Abbreviations

2D	Two dimensional
3D	Three dimensional
3GPP	Third Generation Partnership Project
ACTS	Advanced Communications Technologies and Services
AMPS	Advanced Mobile Phone System
AoA	Angle-of-Arrival
AoD	Angle-of-Departure
AP	Access Point
ATM	Asynchronous Transfer Mode
B-ISDN	Broadband Integrated Services Digital Network
BS	Base Station
C-450	German analogue mobile communications system at the 450 MHz band
CDF	Cumulative Distribution Function
CDMA	Code Division Multiple Access
CIR	Channel Impulse Response
COST	European cooperation in the field of scientific and technical research
DCIR	Directional CIR
DCM	Directional Channel Model
DL	Downlink
DoA	Direction-of-Arrival
DoD	Direction-of-Departure
DS	Direct Sequence
DSP	Digital Signal Processing

EDGE	Enhanced Data Rates for GSM Evolution
EIRP	Equivalent Isotropic Radiated Power
ERO	European Radiocommunications Office
ETSI	European Telecommunications Standards Institute
FDD	Frequency Division Duplex
FDMA	Frequency Division Multiple Access
FLOWS	Flexible Convergence of Wireless Standards and Services
GAoA	Gaussian Angle-of-Arrival
GBSB	Geometrically-Based Single Bounce
GBSBCM	GBSB Circular Model
GBSBEM	GBSB Elliptical Model
GBSM	Geometrically-Based Stochastic Model
GPRS	General Packet Radio Service
GSM	Global System for Mobile Communications
GWSSUS	Gaussian WSSUS
HIPERLAN	High Performance Radio Local Area Network
HSCSD	High-Speed Circuit Switched Data
IEEE	Institute of Electrical and Electronics Engineers
IIR	Infinite Impulse Response
IMT-2000	International Mobile Telecommunications 2000
IP	Internet Protocol
IS-136	Interim Standard for U.S. digital cellular
IS-95	Interim Standard for U.S. CDMA
ISDN	Integrated Services Digital Network
IST	Information Society Technologies
ITU	International Telecommunications Union
JTACS	Japan Total Access Communication Systems
JTC/PCS	Joint Technical Committee for Personal Communication Systems
LoS	Line-of-Sight
MBS	Mobile Broadband System
MC	Multi-Carrier
MIMO	Multiple-Input-Multiple-Output
MOMENTUM	Models and simulations for network planning and control of UMTS

MRC	Maximal Ratio Combining
MT	Mobile Terminal
NLoS	Non-Line-of-Sight
NMT	Nordic Mobile Telephone
OFDM	Orthogonal Frequency Division Multiplexing
OQAM	Offset QAM
OQPSK	Offset Quadrature Phase Shift Keying
PAP	Power-Azimuth Profile
PDC	Pacific Digital Cellular
PDF	Probability Density Function
PDP	Power-Delay Profile
PSK	Phase Shift Keying
QAM	Quadrature Amplitude Modulation
RACE	Research in Advanced Communications in Europe
RAM	Random Access Memory
rms	root mean square
SAMBA	System for Advanced Mobile Broadband Applications
SCM	Spatial Channel Model
TD	Time Division
TDD	Time Division Duplex
TDMA	Time Division Multiple Access
ToA	Time-of-Arrival
UCA	Uniform Circular Array
UHF	Ultra High Frequency
UL	Uplink
ULA	Uniform Linear Array
ULA_{wB}	Uniform Linear Array with Backplane
UMTS	Universal Mobile Telecommunications System
VCIR	Vector CIR
WCDMA	Wideband Code Division Multiple Access
WLAN	Wireless Local Area Network
WPAN	Wireless Personal Area Network
WSSUS	Wide-Sense Stationary Uncorrelated Scattering

List of Symbols

α_i	Excitation magnitude of the i-th antenna element
$\alpha_{3\text{dB}}$	Antenna half-power beamwidth
$\alpha_{3\text{dB}(BS)}$	BS antenna half-power beamwidth
$\alpha_{3\text{dB}(BS)th}$	Threshold value for the BS antenna half-power beamwidth
$\alpha_{3\text{dB}(MT)}$	MT antenna half-power beamwidth
β	Progressive phase between antenna array elements (linear array)
β_i	Phase excitation of the i-th element of a circular array
$\delta(\cdot)$	Dirac delta function
Δd_{max}	Cell range variation
Δd_r	Relative cell range variation
δf	Incremental bandwidth
ΔFD_p	Fading depth variation
Δf_{uv}	Difference between the u-th and v-th frequency components
Δh_{BS}	Difference between the BS antenna height and the average building height
Δh_{MT}	Difference between the average building height and the MT antenna height
$\Delta h_{BS\text{-}MT}$	Difference between BS and MT antenna height
ΔK	Rice factor variation
Δl_{ij}	Path length difference between the i-th and j-th multipath components
Δl_{max}	Maximum difference in propagation path length
$\Delta l_{max(dir)}$	Value of Δl_{max} observed with directional antennas
$\Delta l_{max(omni)}$	Value of Δl_{max} observed with omnidirectional antennas
ΔN_{cr}^{l}	Relative variation of the number of cells for a linear geometry

ΔN_{cr}^{a}	Relative variation of the number of cells for a regular geometry (area)
$\Delta\tau_{ref}$	Reference delay between consecutive arriving waves
ε	Absolute error
ε_r	Relative error
ϕ_i	Phase of the *i*-th multipath component
$\mathbf{\Gamma}$	Covariance matrix
Γ_{uv}	Covariance between the *u*-th and *v*-th frequency component
γ_O	Oxygen attenuation
γ_R	Rain attenuation
φ	Azimuth angle
$\varphi_{(xy)i}$	Angular position (*x*-*y* plane) of the *i*-th element of an UCA
φ_b	Main beam orientation in azimuth
φ_i	AoA of the *i*-th multipath component
φ_s	Street orientation relative to the direct path
λ	Wavelength
λ_m	Eigenvalue of the covariance matrix
μ_L	Mean value of the log-normal distribution
θ	Elevation angle
θ_b	Main beam orientation in elevation
$\rho(\cdot)$	Correlation function
ρ_{off}	Rolloff factor
σ	Standard deviation
σ_φ	*rms* azimuth angle spread
σ_L	Standard deviation of the log-normal distribution
σ_s	Standard deviation of the PDF of AoAs
σ_τ	*rms* delay spread
$\sigma_{\tau,i}$	*rms* delay spread of the *i*-th multipath component
$\sigma_{\tau_{ref}}$	Reference *rms* delay spread
τ	Delay
$\bar{\tau}$	Mean delay
$\overline{\tau_A}$	Average fade duration

τ_{f_i}	Duration of the *i*-th fade
τ_i	Delay of the *i*-th multipath component
ξ	Total attenuation
ψ_i	Phase of the *i*-th frequency component

A	Reference signal magnitude
$\mathbf{A}$	Complex matrix of channel coefficients
a	Signal magnitude
$a(f)$	Signal magnitude at frequency f
A_c	Cell area
a_d	Magnitude of the LoS component
AF	Array factor
AF_{lin}	Array factor of a linear array
AF_{circ}	Array factor of a circular array
a_i	Magnitude of the *i*-th arriving wave (multipath component)
A_T	Coverage area
b	Building separation
B	System bandwidth
B_c	Coherence bandwidth
B_N	Noise bandwidth
c	Speed of light
d	Distance
d_e	Separation between antenna array elements
d_{max}	Cell range
E_b	Energy per bit
$E_{element}$	Electric far-field of a single antenna element
E_{total}	Electric far-field of an antenna array
f	Frequency
F	Receiver noise figure
f_c	Carrier frequency
FD_p	Fading depth measured between p and 50% of the CDF of the received power
$FD_{p(dir)}$	Value of FD_p observed with directional antennas

$FD_{p(omni)}$	Value of FD_p observed with omnidirectional antennas
f_i	i-th frequency component
f_m	Maximum Doppler shift
g	Cell shape factor
G_{extra}	Additional gain
G_p	Processing gain
G_r	Receiver antenna gain
G_t	Transmitter antenna gain
$\mathbf{H}$	Complex channel matrix
$h(\tau,t)$	Time-variant channel impulse response
$h(\tau,t,\varphi)$	Time-variant directional channel impulse response
$H(f)$	Frequency response of the transmitting equipment
h_{BS}	BS antenna height
h_{MT}	MT antenna height
h_{roof}	Average building height
$I_0(\cdot)$	Modified zero-th order Bessel function of the first kind
K	Rice factor
k	Wave number
k_a	Path loss increase for BS antenna below the average rooftop building height
k_d	Multi-screen diffraction loss as a function of distance
K_{dir}	Rice factor observed with a directional antenna
k_f	Multi-screen diffraction loss as a function of frequency
K_{omni}	Rice factor observed with an omnidirectional antenna
L_0	Free-space path loss
L_{bsh}	Correction factor for the BS height
L_c	Cable losses
l_i	Path length of the i-th multipath component
L_{msd}	Multiple screen diffraction loss
L_{ori}	Empirical correction factor
L_p	Path loss
$\overline{L_p}$	Average path loss
$L_{p_{max}}$	Maximum allowable path loss
$\overline{L_r}$	Average reference path loss

L_{rts}	Rooftop to street diffraction and scatter loss
l_s	Street length
L_u	Losses due to the presence of the user
L_w	Building penetration loss
$L_{w_{ref}}$	Reference building penetration loss
M	Number of multipath components
$M_{ff,90\,\%}$	Short-term fading (fast fading) margin for 90 % coverage probability
M_i	Interference margin
M_{sf}	Long-term fading (slow fading) margin
M_t	Total margin
N	Number of antenna elements
n	Path loss exponent
N_0	Noise power
N_A	Level crossing rate
N_{BS}	Number of BS antennas
N_c	Number of cells
N_{cRR}	Number of cells obtained from considering Rayleigh or Rice distributions
N_{cWB}	Number of cells obtained from considering the wideband approach
N_d	Noise density
N_{exp}	Number of exponential multipath components
N_f	Number of fades
N_{MT}	Number of MT antennas
n_s	Number of samples (interpolation points)
p	Lower limit for fading depth evaluation
P_A	Reference power level
$p_{\mathrm{AoA}(\cdot)}$	PDF of AoAs
$p_d(\tau)$	Time-invariant power delay profile
$p_d(\tau,t)$	Time-variant power delay profile
P_i	Power of the i-th arriving wave
$P_{i_{max}}$	Power of the strongest arriving wave
$p_{LoS}(\cdot)$	PDF of the total received power under LoS
$p_{LoS_i}(\cdot)$	PDF of the power of the i-th multipath component under LoS
$p_{NLoS}(\cdot)$	PDF of the total received power under NLoS

$p_{NLoS_i}(\cdot)$	PDF of the power of the i-th multipath component under NLoS
P_r	Received power
P_{rT}	Total received power
P_{RX}	Power at the receiver input
$P_{RX_{min}}$	Minimum received power at the receiver input
P_t	Transmitted power
P_{TX}	Power at the transmitter output
$P_{\tau,i}$	Value of $p_d(\tau)$ for $\tau = \tau_i$
$Q(\cdot)$	Q function
q_{ds}	Ratio between τ_2 and $\sigma_{\tau,1}$
q_p	Ratio between $P_{\tau,2}$ and $P_{\tau,1}$
q_s	Ratio between $\sigma_{\tau,2}$ and $\sigma_{\tau,1}$
r	Radius of UCA
R_b	Bit rate
R_c	Chip rate
r_s	Radius of the scattering scenario
r_w	Room width
s	Power level
s_i	i-th scatterer
s_{ref}	Reference power level
t	Time
T	Time window
T_c	Coherence time
t_k	Time sample
v_{MT}	Relative speed between the MT and the BS
$w_{b,p}$	Breakpoint value
$w_{bn,p}$	n-th breakpoint value
w_l	Equivalent received bandwidth
$w_{l(\mathrm{dir})}$	Value of w_l observed with directional antennas
$w_{l(\mathrm{omni})}$	Value of w_l observed with omnidirectional antennas
w_s	Street width
w_t	Product between the system bandwidth and the *rms* delay spread of the propagation channel

$\mathbf{x}(t)$	Signal at the MT
$x_i(t)$	Signal at the i-th MT antenna element
X_L	Zero-mean Gaussian distributed random variable
$\mathbf{y}(t)$	Signal at the BS
$y_i(t)$	Signal at the i-th BS antenna element

Chapter 1

Introduction

1.1. Historical Perspective

During the last century, the notion of transmitting information without wires experienced rapid and extraordinary developments, driving the world to a global communications sphere, aiming at providing wireless communication services to anyone and everywhere, i.e., global coverage.

Starting from the very early beginning in the 18th century, with the theoretical postulates of James C. Maxwell and further experimental work by Heinrich R. Hertz and Gugliemo Marconi, among many others, the first wireless mobile telephone system was installed in the beginning of the 19th century, for car dispatching in the Detroit Police Department [Pras98]. From that time on, the increasing demand for system capacity in order for accommodating more and more users and services drives the technology to new solutions, required for achieving all the needs within the scarce spectrum resources. Trunked systems were introduced in the mid 20th century, in order to increase system capacity; these systems make a group of radio channels available to a large number of users, by tuning the mobile radio to any available channel when the call connection is established. Nevertheless, this solution, and the available spectrum, was not also capable to cope with the increasing demand for capacity; hence, some years later cellular systems were finally introduced. These systems allow accommodating a large number of users within a large geographic area, with a limited amount of spectrum, by limiting the coverage of each transmitter to a certain restricted area, the cell; this way, the same channels can be reused by different transmitters located in such a way that there is only a limited amount of interference among different transmitters operating with the same channels [Yaco93]. This was the first generation of mobile cellular systems, having channel bandwidths of the order of a few tenths of kHz, which were intended only for voice services, being entirely based on analogue technology and circuit switched connections; capacity and quality was a major problem. Furthermore, there was no compatibility among different systems developed in different countries, e.g., Advanced Mobile Phone Service (AMPS) in the United States, Nordic Mobile Telephone (NMT) in some European countries, Total Access Communication System (TACS) in United Kingdom, Japanese TACS (JTACS) in Japan, and C-450 in Germany and Portugal, among many others. Besides being designed for voice, some of these systems allow low data rate communications, of the order of several kbps, by using appropriate modems.

With the advances in digital technologies, namely digital signal processing and speech coding techniques, new possibilities for increasing system capacity arose. The second generation of mobile cellular systems, with bandwidths ranging from several tenths of kHz to approximately 1 MHz, were characterised by the digitalisation of the networks. The Global System for Mobile Communications (GSM) developed in Europe is the more elaborated and well-accepted standard worldwide [MoPa92], [GSMW03]. However, the compatibility problem among different systems developed at different countries, e.g., Pacific Digital Cellular (PDC) in Japan, and IS-136 (Interim Standard for U.S. digital cellular) in North America, still persists. Besides the increased system capacity and quality of service introduced by these second generation systems, they also provide, for the first time, the possibility of transmitting data at data rates up to several tenths of kbps without the need for any additional modems. Nevertheless, these systems, being naturally limited in terms of available bandwidth, pose some problems in terms of the maximum achievable data rates.

During the last years, computer communications have grown exponentially. Multimedia communications, which allow combining text, data, graphics, sound, images and video, are now playing an important role in the society, creating new challenges to those working in the development of communication systems. The need for higher bit rates has driven the development of wired network standards in order to accommodate the desired data rates and services. Broadband Integrated Services Digital Network (B-ISDN) enlarges the possibilities of the current ISDN, by offering higher data rates and a huge diversity of services [Pras98]. However, a big problem still needs to be solved: the extension of these possibilities to mobile users.

Several enhancements were made to GSM in order to accomplishing such demand for higher data rates, e.g., High Speed Circuit Switched Data (HSCSD) and General Packet Radio Service (GPRS) [VrLa02]. HSCSD enables data rates up to 64 kbps; nevertheless, it still is circuit-switched based, being inefficient for data communications due to their bursty nature. GPRS was designed to provide packet-switched services over the GSM radio interface with "always on" connectivity characteristics, supporting simultaneous voice calls and data services at data rates up to 171 kbps; however, a significant degradation is verified as the number of users increases, thus, decreasing the net user rate. Nevertheless, many operators in different countries started implementing GPRS solutions in order to provide some of the new services foreseen for the next third generation systems, e.g., image and low quality video transfer. Further upgrades to GSM include Enhanced Data Rates for GSM Evolution (EDGE), which allows improving existing networks, by including advanced features that increase spectrum efficiency, enabling new higher bit rate services (up to 384 kbps) to be deployed. Several enhancements were also proposed for the different standards worldwide, e.g., Multi-Carrier Code Division Multiple Access (MC-CDMA) for cdma2000, and further improvements for cdmaOne, an IS-95 (Interim Standard for U.S. CDMA) based system [Yaco01].

In 1992, some frequency bands around 2 GHz were identified to be used by third generation mobile cellular systems. Known as International Mobile Telecommunications 2000 (IMT-2000) within International Telecommunications Union (ITU), in Europe this is called Universal Mobile Telecommunications System (UMTS) [HoTo00], [UMTS03]. One of the main objectives of third generation systems was to provide a common interface, allowing, at some degree, the convergence to a universally accepted standard, while providing multimedia communications among mobile users with enhanced high quality images and video, and access to a wide diversity of services, enhanced by higher data rates and flexible communication capabilities. UMTS is intended to deliver data rates up to 2 Mbps in a 5 MHz channel bandwidth, depending on the cell coverage and mobility scenario, aiming at providing multimedia services anytime and anywhere, i.e., global coverage.

A hierarchical cellular structure similar to the one of GSM allows supplying various applications in different environments, with different cell ranges and mobility characteristics, Figure 1.1. The lower layer is composed of in- and outdoor pico-cells, with cell ranges below 100 m. The second layer is composed of micro- and macro-cells with cells ranges about 100 m to 1 km, and above 1 km, respectively. It should be noted that these figures for the cell range are only reference values, in order for the reader to understand what is typically meant when referring to macro-, micro-, and pico-cellular environments. The upper layer (mega-cell) consists of satellite systems with global coverage and full mobility for broadband downlink distribution towards the user.

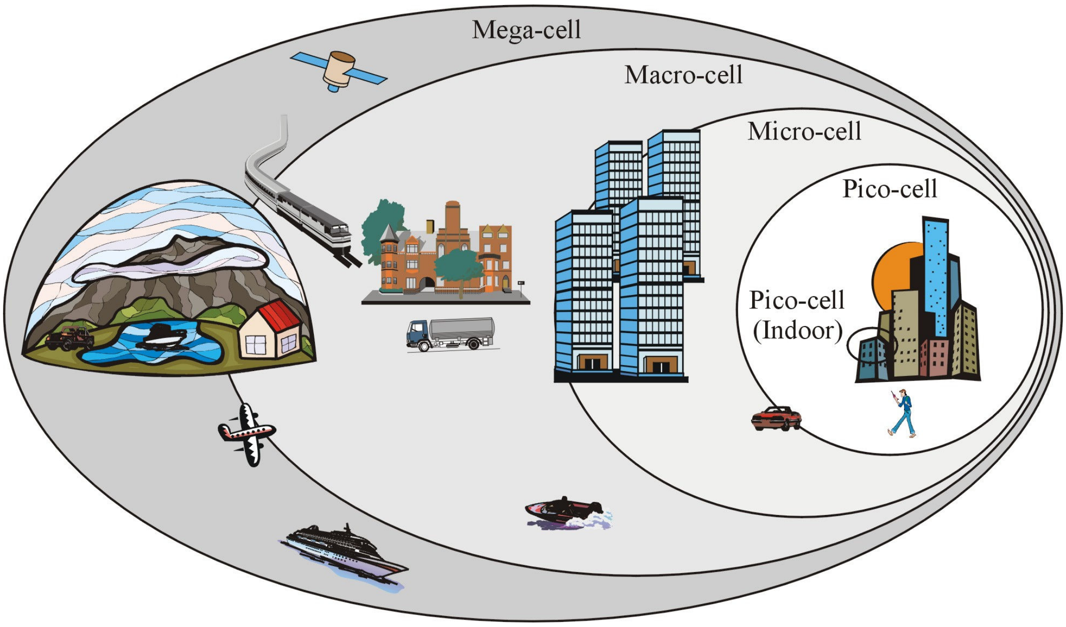

Figure 1.1 – Hierarchical cellular structure providing global coverage.

This hierarchical cellular structure will be connected to the wired broadband network, allowing to transparently accessing the applications and services provided for the wired user. Naturally, the ability to access all these functionalities will be dependent on the environment and mobility scenarios. In the macro-layer, at least 144 kbps at a maximum speed of 500 km/h should be possible. In the micro-layer, 384 kbps at a maximum speed of 120 km/h should be supported. At the pico-layer level, data rates up to 2 Mbps with a maximum speed of 10 km/h should be achieved [TUWi03].

Meanwhile, Wireless Local Area Networks (WLANs) and Wireless Personal Area Networks (WPANs) at the 2 and 5 GHz bands, supporting broadband multimedia communications, are being developed and standardised all over the world [VrLa02]. Current WLAN standards include IEEE 802.11b at the 2 GHz band, and IEEE 802.11a and High Performance Radio Local Area Network version two (HIPERLAN/2) at the 5 GHz one, the latter providing data rates up to 54 Mbps in a 20 MHz channel bandwidth. WLANs differ from mobile cellular systems, since they are mainly intended for providing wireless connectivity between computers and other equipments, as well as to access the core network in public and home environments. Concerning mobility, these systems are not intended for high or even medium mobility scenarios, rather being designed for low mobility pico-cellular environments, i.e., cell ranges on the order of hundreds of metres and, at most, pedestrian mobility. WPANs, such as Bluetooth, enable connectivity among portable user equipments and communication devices within a reduced coverage area (several tenths of metres), providing data rates up to 1 Mbps [Blue01], [Bisd01]. Further improvements in terms of achievable data rate are being standardised within the scope of IEEE 802.11 and IEEE 802.15 working groups [Kara01].

Since recent developments on WLANs technology are focused on extending the possibilities concerning cell range, speed and mobility, these networks are emerging not only as a natural complement of existing and next generation wireless mobile cellular communication systems, such as UMTS, but also in some cases as direct competitors. The task of defining where and how all these emerging technologies will co-exist and interoperate will be one of the hardest that should be rapidly carried out by all the entities involved in this process, namely, regulating bodies, operators, manufacturers and service providers, among others. Some effort is being done in order to assess how these competing technologies can interoperate, allowing the convergence of multiple wireless standards, such that a mobile user can be simultaneously connected to several networks operating according to different standards, allowing the user to transparently access a wider variety of services [KMRV01], [FLOW03].

Besides being suited for high data rate communications, UMTS and WLANs are limited by the scarce amount of spectrum at the 2 and 5 GHz bands. Hence, Mobile Broadband Systems (MBSs) are seen as the next step for achieving even higher data rates, allowing to implement even more demanding services, e.g., high definition video [CoPr97], [VeCo00a].

Frequency bands of [39.5, 43.5] and [62, 66] GHz, with 2 GHz spacing in between 1 GHz bands, are being considered for the implementation of future MBSs, solving the problem of spectrum congestion in lower frequency bands, while providing larger available bandwidths, hence, higher data rates. The concept of future MBSs is strongly different from UMTS and WLANs. Although most of user needs can be reasonably satisfied by using UMTS, the upper data rate limit of 2 Mbps may not be enough when a user wants to access multimedia information, especially if high-definition video is required. MBS is supposed to be a universal system, allowing terminals to communicate while in motion (supporting handover functions) and at higher speeds within any public MBS coverage area, which can be small cells or large continuous ones with different access environments. MBS is seen as a natural evolution from third generation systems, such UMTS, and a wireless extension of

B-ISDN, giving users the access to a large range of broadband services that exists or will exist for the fixed broadband communications network [PSRC94], [Pras98].

Figure 1.2 illustrates the relative positioning between MBS and other existing systems, regarding achievable data rates and mobility [Vele00], [GSMW03]. Although a staircase behaviour is expected to characterise the upper data rates for MBS in different mobility scenarios, there is no current data for these figures, since MBS is not yet completely defined; nevertheless, one still considers that data rates up to 155 Mbps will be achievable. Data rates for HSCSD, GPRS and EDGE correspond to theoretical peak data rates; average data rates are usually lower, depending on the system configuration and network capacity, e.g., 28, 40 and 120 kbps are typically obtained for HSCSD, GPRS and EDGE, respectively [GSMW03]. Besides some superposition, it is clear that each system has its own place, so it is expected that MBS will act not as an alternative to the existing systems, but as their natural complement. One thing is common to all of these emerging technologies, their wideband/broadband nature, required for accommodating the increased demand for higher data rates [CoPr97].

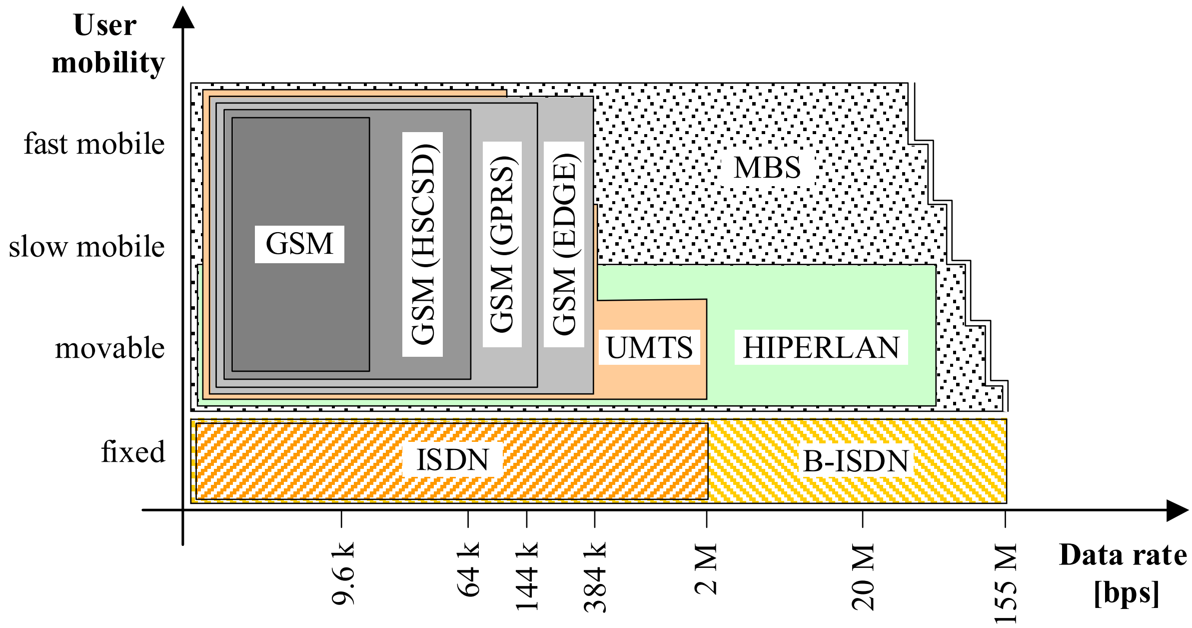

Figure 1.2 – Data rate versus user mobility for different systems.

Focusing on the lower level of the network planning process, i.e., the radio level, most of the assumptions usually made for the case of first and almost all second generation systems are no longer valid, in the sense that the working frequencies are changing (increasing), different propagation phenomena being usually involved. Additionally, system bandwidths are also increasing significantly, thus, radio propagation (namely, the variation properties of the wideband signals) can no longer be seen as for the narrowband case, as usually assumed in most of the situations, which has a huge impact on the overall network planning process.

Furthermore, new processing techniques for exploiting the directional properties of the propagation channel in order to improve system capacity are emerging. New technologies include smart antennas, either adaptive or switched beam approaches, spatial diversity combining, digital beamforming and Multiple-Input-Multiple-Output (MIMO) techniques [LiLo96], [LiRa99], [MuLe02], [DGIM02], [GiCo03]. Since the inclusion of antenna directionality into the radio channel modelling is relatively new, as far as wideband mobile systems are concerned, a large effort has to be done for assessing its impact on the variation properties of wideband signals, therefore, on the overall system performance.

1.2. Motivation

A complete understanding of the wireless communications channel is a key issue for the design, implementation and operation of a wireless system. Since the multipath nature of the propagation channel modifies the transmitted signal, causing fading, it is of relevance to completely characterise the signal at the receiver, enabling the system to be designed such that the receiver will be able to cope with such effects, thus, eliminating transmission errors and distortion as much as possible.

Apart from the additive noise introduced by the transmitting and receiving equipments themselves, the atmospheric effects and the interference, the signal at the receiver is usually characterised by the combination of different effects [Yaco93]: path loss, long-term fading (or slow fading) and short-term fading (fast fading), Figure 1.3. All these effects depend on the relative positioning of the Base Station (BS), the Mobile Terminal (MT) and any objects contributing to the total amount of reflected/diffracted power arriving at the receiver. Path loss corresponds to the variation of power with distance; when averaged over several tenths of wavelengths, the received signal varies around the average path loss value due to the varying nature of the obstructions between the BS and the MT, being usually called long-term fading. Short-term fading, due to the interference among multiple waves arriving from distinct paths (multipath components), imposes an additional signal variation at the scale of roughly half a wavelength. The combination of these effects is responsible for the signal variation at the receiver, significantly affecting system performance.

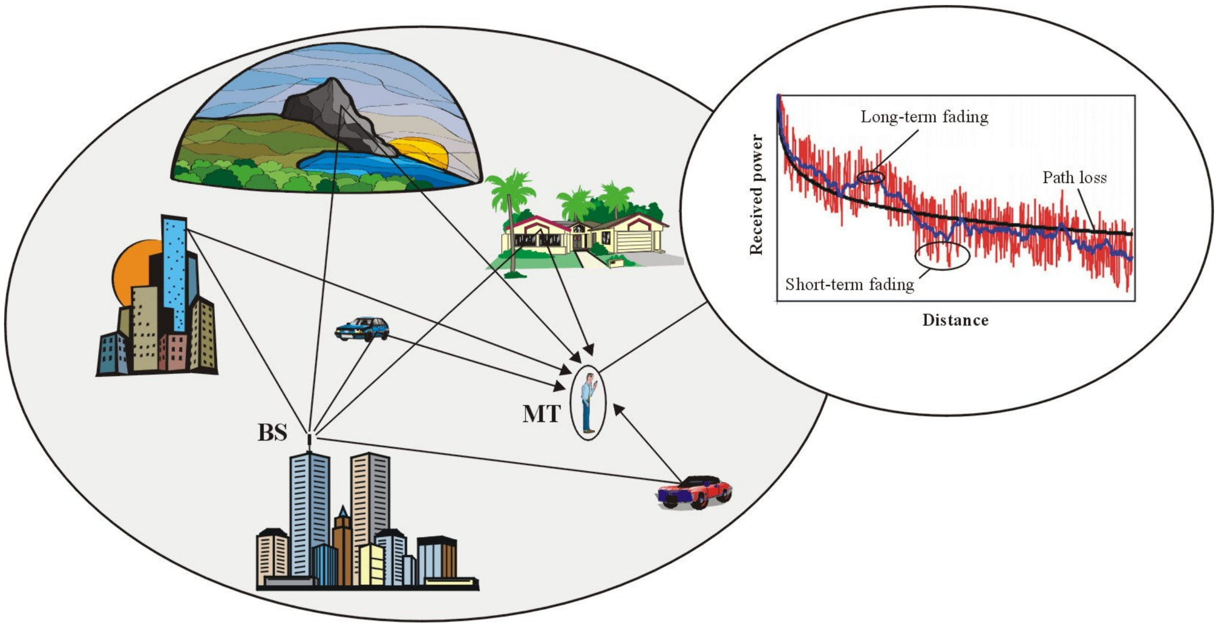

Figure 1.3 – Multipath fading channel, path loss and fading effects.

A complete network planning procedure within a specific radio environment involves several steps, during which an approximate number of BSs, their configuration and other elements on the network should be specified according to several requirements, such as coverage, capacity and quality of service. These steps include link budget calculation and cell range evaluation, capacity estimation, quality of service evaluation, and network optimisation, among others [HoTo00].

Link budget evaluation and cell range estimation is one of the first and most important steps in the overall network planning process; since it is the calculation of power, noise, and signal-to-noise ratios for a given communications link, it enables to evaluate the maximum allowable path loss for achieving a given system performance [Saun99]. The path loss is usually subdivided into different components: the distance dependent path loss value, and two fading margins to be accounted for, in order for the system to be able to cope with long- and short-term fading effects, while achieving the desired performance.

An accurate link budget evaluation is needed in order to achieve the required coverage probability, capacity and quality of service; as previously referred, the link budget allows evaluating the maximum allowable path loss under given criteria, namely, the type and data rate of the service, the type of environment, MT and BS characteristics, the required coverage probability, and financial and economic factors that force the operator to decide whether to use expensive and better quality equipment or a cheaper option. Once the maximum allowable distance dependent path loss is obtained, the maximum cell range in a given environment can be evaluated from well-known propagation models in literature, [Yaco93], [Saun99].

Besides a link budget evaluation being usually a rough approximation to the real network working conditions, in the sense that many assumptions and simplifications during the planning process are usually made in order to simplify calculations, while allowing to reasonably predict the number of BSs, as well as their range and localisation, it is desirable to use a set of system and environment parameters as accurate as possible. In this way, cellular planning results will be closer to the ones observed in real network operating conditions, therefore, reducing the effort needed for future network optimisation procedures.

System characteristics themselves are usually well defined; however, uncertainty is involved in the proper description of the working environment and users behaviour, affecting system parameters that depend on the propagation conditions and MT mobility. As mentioned before, in a multipath fading environment, the received signal fades, leading to the need to provide additional power (fading margin) in order to achieve the desired link quality. When performing link budget calculations, fading margins must be accounted for, since a pure average or deterministic behaviour is not acceptable; accurate short- and long-term fading margins (usually referred as fast and slow, or log-normal, fading margins) should be considered, in order to achieve the desired link capacity and quality of service for the desired coverage probability.

Long-term fading margins are usually evaluated from considering that long-term fading effects can be reasonably modelled as being log-normal distributed, which seems to be a reasonable approximation for most communication systems. Different values for the standard deviation are usually assumed, depending on the system and working environment being considered. Short-term fading margins are not many times accounted for in link budget calculations or, instead, Rayleigh or Rice distributions are used for modelling short-term fading effects, depending on the existence of a Line-of-Sight (LoS) component between the BS and the MT. This approach is valid for narrowband systems, whose bandwidth is much smaller compared to the coherence bandwidth of the propagation channel. However, when one considers wideband systems, whose bandwidth is usually greater than the coherence bandwidth, e.g., UMTS, HIPERLAN/2 and MBS, the signal at the receiver is distorted, but the fading depth is smaller than the one obtained from the Rayleigh or Rice distributions. Overestimating short-term fading margins, by considering those distributions, leads to shorter cells, or to higher transmitting powers, thus, higher interference. These effects are not desirable, and they can be overcome by taking more accurate values for the fading margins. By considering more appropriate fading margins, a significant reduction in the number of cells can be achieved, allowing a better system planning, and enabling network optimisation, while reducing deployment and maintenance costs.

Since the necessary short-term fading margin depends on the system bandwidth and working environment, one will focus on the fading depth evaluation for different systems working in different environments, this way, allowing to properly estimate the short-term fading margins that should be considered for a proper link budget evaluation. It should be remembered that the narrow- or wideband nature of a given system depends not only on its bandwidth but also on the coherence bandwidth of the propagation channel, i.e., on the environment properties. This implies that any given system can behave as narrow- or wideband, depending on the working environment being considered.

The analysis of the signal variability in narrowband systems is already well studied, however, the variation properties of wideband signals are almost exclusively based on numerical simulation and field measurements, and only a few apply to the case of LoS [Corr01]. Since systems like UMTS, HIPERLAN/2 and MBS, usually behave as wideband/broadband ones, operating many times in LoS conditions, for the former, or intended to work mainly under LoS, for the latter, two different and independent approaches for the study of wideband signal transmission in LoS and NLoS (Non-Line-of-Sight) situations are proposed, contributing for filling in the gap of short-term fading characterisation in wideband systems.

The first one is an environment-geometry based approach for the study of the short-term fading depth dependence on system bandwidth and environment specific features. An expression for the evaluation of fading depth, accounting for the maximum difference in propagation path length among different arriving components and having the Rice factor as a parameter, is derived from fitting simulated data from a model in the literature [KoSN96]. This approach aims at eliminating the need for heavy computer simulations, while allowing the determination of the fading depth through the evaluation of a simple equation. Application examples, which give some insight into the fading depth behaviour for different systems, e.g., GSM, UMTS, HIPERLAN/2 and MBS, working in macro-, micro- and pico-cellular environments, are presented and discussed. On the other hand, time-domain techniques, using statistical models, are one of the most popular methods for simulation of in- and outdoor mobile communication systems; standard-setting bodies usually recommend generalised and simple time-domain statistical models for different environments. A time-domain level variation analysis technique of wideband signals in NLoS environments is proposed in [InKa99], being based on the eigenvalue decomposition technique, which allows evaluating the Probability Density and Cumulative Distribution Functions (PDF and CDF) of the received power for various fading channels, whose Power Delay Profiles (PDPs) are expressed as continuous or discrete functions. In this thesis, a time-domain based approach for fading depth characterisation in wideband LoS and NLoS environments is also proposed. New expressions for the PDF and CDF of the received power are derived, extending the approach in [InKa99] to the LoS case. The short-term fading depth for continuous and discrete channel models is evaluated from the CDF of the received power and represented as a function of the Rice factor, and of the product between the system bandwidth and the *rms* delay spread of the propagation channel. Results for the fading depth observed by GSM, UMTS and HIPERLAN/2 working in standard reference environments are presented and discussed; some results for MBS, obtained from considering typical PDPs derived from measurements in different environments, are also presented.

Since there is a close relationship between the environment characteristics and the PDP of the propagation channel, one derives a simple relationship between the maximum difference in propagation path length and the *rms* delay spread of the propagation channel, thus, establishing an equivalence between the two approaches and allowing one to use them for evaluating the fading depth in a given environment, defined either by its physical and geometrical properties, or by the PDP; this perspective establishes a relationship between the two approaches, independently derived from the two models proposed by different authors. By using the proposed relationship, fading depth results from the two different approaches being proposed are compared.

With the emergence of third generation systems, new techniques for exploiting the directional properties of the propagation channel are being developed, using antenna arrays and spatial processing algorithms, in order to improve system capacity, by providing enhanced coverage with less transmitted power and reduced levels of interference. Although some work has been done concerning the implementation of these techniques, it is not yet clear how short-term fading depth for different systems working in different environments will be affected by the use of antenna arrays whose beamwidth is usually narrower compared to the ones usually found in most existing systems. Since a characterisation of this phenomenon is of practical interest for system design and network planning purposes, this issue is also addressed in this thesis.

Results on the fading depth variation, due to considering the use of directional antennas rather than omnidirectional ones, are presented and discussed. This dependence is modelled through the variation of the Rice factor and the maximum possible difference in propagation path length among different arriving components, and analytical expressions are derived for the variation of these parameters as a function of the half-power beamwidth of the antenna array. Results on the fading depth variation due to the use of directional antennas for different systems (GSM, UMTS, HIPERLAN/2 and MBS) working in macro-, micro-, and pico-cellular environments represented by single bounce scatterer channel models [Corr01] are presented and discussed.

The main novelties of this thesis include the two different and independent approaches for short-term fading depth evaluation in wideband systems being proposed, filling in the gap in short-term fading evaluation techniques intended for wideband systems working in LoS and NLoS environments. Moreover, the simple relationship between the two different approaches being proposed, allows one to use different perspectives for evaluating the fading depth in a given environment, defined either by its physical and geometrical properties, or by the PDP. The main emphasis is given to simplicity and applicability, therefore, analytical expressions for evaluating the fading depth are derived, that way, reducing the need for heavy computer simulations. Short-term fading margins are proposed for UMTS, HIPERLAN/2 and MBS working in different environments, which is valuable for system evaluation purposes. Additionally, the impact of using directional antennas at either the MT or the BS is addressed, and its influence on the short-term fading depth is studied. For illustrating the impact of using more appropriate fading margins for link budget evaluation and cell range estimation, a simple link budget exercise for GSM, UMTS, HIPERLAN/2 and MBS working in rural, urban and suburban standard environments is presented. Furthermore, indoor coverage by outdoor BSs, i.e., including building penetration, is also addressed. Globally, the approaches being proposed allow to properly evaluating short-term fading margins, by considering the dependence on system bandwidth and environments characteristics, therefore, eliminating the error usually introduced from considering the narrowband assumption.

The work being presented in this thesis was already reflected in several papers that were published or submitted to various conferences and journals:

- Short-term fading depth dependence on antenna characteristics in wideband mobile communications [CaCo04].
- On the equivalence between time-domain and environment-geometry based approaches for fading evaluation in wideband mobile communication systems [CaCo03d].
- Short-term fading evaluation in wideband mobile communication systems [CaCo03c].

- Fading depth dependence on system bandwidth in mobile communications – an analytical approximation [CaCo03b].
- A comparison between different approaches for fading evaluation in wideband mobile communication systems [CaCo03a].
- Fading depth evaluation in mobile communications – from GSM to future MBS [CaCo02b].
- A time-domain technique for fading depth characterisation in wideband mobile communication systems [CaCo02a].
- An analytical approach to fading depth dependence on bandwidth for mobile communication systems [CaCo01].

Also, some contributions were made within the framework of the IST (Information Society Technologies) European projects FLOWS (Flexible Convergence of Wireless Standards and Services) [FLOW03] and MOMENTUM (Models and Simulations for Network Planning and Control of UMTS) [MOME03]:

- Fading statistics and wideband fading characterisation is addressed, and several results on the short-term fading depth observed by GSM and UMTS in different environments are presented [CCKL02].
- A technique for short-term fading evaluation in wideband mobile communications is proposed, and fading margins for GSM, UMTS and HIPERLAN/2 working in standard reference environments, as proposed by standard-setting bodies, are suggested [CaTC02].

Additionally, most of the relevant work was, and still is, being presented in regular meetings of the European project COST273 (European Cooperation in the Field of Scientific and Technical Research – Action 273) [COST03].

1.3. Thesis Structure

This thesis is organised as follows. Chapter 2 addresses channel characterisation and modelling. General considerations about propagation are drawn, and long- and short-term fading effects are addressed. Fading and time dispersion parameters are also presented, this way, giving an insight into fading and time dispersion properties of the propagation channel. As usual, long-term fading is assumed as being log-normal distributed around the mean path loss value, and Rayleigh and Rice distributions are presented for modelling short-term fading effects; Suzuki distribution is also presented, since it is usually used for modelling the composite effect of both long- and short-term fading. Moreover, classical stochastic narrow- and wideband non-directional channel models are briefly described; additionally, directional channel models and MIMO ones are also presented, giving an insight into some existing state-of art channel models.

In Chapter 3, a brief description of GSM, UMTS, HIPERLAN/2 and MBS is made, and a general theoretical background on link budget evaluation is given; some specific parameters for this purpose are presented. Additionally, out- and indoor path loss models, usually used for cell range evaluation purposes in different environments, are presented, therefore, fulfilling the requirements for properly evaluating the maximum cell range. Building penetration is also addressed, and a measurement-based model that accounts for both outer and inner wall losses is described.

The proposed environment-geometry based analytical approximation for short-term fading depth evaluation in wideband mobile communication systems is detailed in Chapter 4. The wideband propagation model, on which the proposed approach is based, is described, the method for deriving the analytical approximation is presented, and the approximation error is characterised. Several results on the fading depth observed by GSM, UMTS, HIPERLAN/2 and MBS working in macro- micro- and pico-cellular environments are presented and discussed.

The time-domain based approach for wideband short-term fading depth evaluation is developed in Chapter 5. The method for deriving the PDF and CDF of the received power, which apply to both LoS and NLoS cases, is presented, and a study on the influence of the PDP parameters on the observed values of fading depth is made. The results obtained from considering continuous or discrete PDPs are discussed, and general considerations are drawn. Moreover, an analytical approximation for the short-term fading depth dependence on the Rice factor and the product between the system bandwidth and the *rms* delay spread of the propagation channel, similar to the one derived in Chapter 4 is also proposed.

In Chapter 6, results on the fading depth observed by the different systems working in standard reference environments as proposed by standard-setting bodies are presented and discussed. Moreover, a simple relationship between the environment-geometry based approach and the time-domain one is also presented. By using the proposed relationship, results on the fading depth observed in the standard reference environments, obtained from the different approaches being proposed, are compared and discussed.

The use of directional antennas at the MT and/or the BS, and its influence on the observed values of fading depth, is addressed in Chapter 7; this influence is modelled through the variation of the Rice factor and the maximum difference in propagation path length among different arriving components, relative to the case when omnidirectional antennas are used. Expressions for the Rice factor variation as a function of the antenna beamwidth, for different statistical distributions for the Angle-of-Arrival (AoA) of arriving waves, and different types of antennas are presented. Typical scattering channel models are used for modelling macro-, micro- and pico-cellular environments, and the maximum difference in propagation path length dependence on the antenna beamwidth is evaluated. Results on the fading depth observed by GSM, UMTS, HIPERLAN/2 and MBS in different environments, and for different antenna beamwidths, are presented and discussed.

Link budget evaluation and cell range estimation is addressed in Chapter 8. Link budgets are evaluated for GSM, UMTS, HIPERLAN/2 and MBS, considering that the short-term fading margins are obtained either from Rayleigh or Rice distributions or from using the proposed approaches, and the results are compared. An analysis on the BS number reduction, due to considering the use of appropriate fading margins is made, illustrating how it can influence deployment and network optimisation, while allowing to reduce network deployment and maintenance costs.

Conclusions are drawn in Chapter 9, where further improvements to the proposed models and suggestions for future research are also presented.

Chapter 2

Channel Characterisation and Modelling

2.1. General Propagation

Radio propagation in a wireless system usually involves some degree of complexity, due to the physical and morphological aspects of the surrounding environment. In such systems, the direct path between the transmitter and the receiver is sometimes blocked by walls, ceilings, floors, doors, and a multiplicity of objects within an indoor environment; in the case of outdoors, a large diversity of natural and man-made obstacles can be found within the vicinity of the transmitter and/or the receiver. Therefore, the signal at the receiver results from a multiplicity of signals arriving from different paths with distinct magnitudes, phases and arrival times, proportional to the path length, and also depending on the diffraction and reflection properties of the objects within the vicinity of the transmitter and the receiver. Additionally, in the case of outdoor systems working at the microwave and millimetre wavebands, there is a non-negligible attenuation imposed by atmospheric elements, such as oxygen, water vapour, rain and fog; in indoor environments, the cell coverage is usually small, and these effects are not relevant when compared with the blocking effect by walls, ceiling, floor and furniture [Pars92]. Besides, the typical scenarios found in a wireless mobile communications system are usually more specific than other wireless systems, such as fixed ones, this specificity resulting from the randomness imposed by the non-static environment properties and the moving terminal.

Propagation in a wireless communications channel depends on several phenomena: reflection, diffraction, scattering, absorption and shadowing. Reflection occurs when waves propagating in one medium impinge on objects of large dimensions, compared to the wavelength, having different electrical properties. The magnitude of the reflected and transmitted waves are related to the incident wave in the medium of origin through the reflection coefficient, which depends on the material properties, wave polarisation, angle of incidence and working frequency. Diffraction occurs when the path between the transmitter and the receiver is obstructed by a surface with sharp edges, e.g., buildings, allowing waves to propagate behind obstructions. The received signal in a mobile radio environment may be stronger than the prediction from considering only reflection and diffraction: when a wave impinges on a rough surface or on a large number of small objects (compared to the wavelength), the reflected energy is spread (diffused) in several directions due to scattering, providing an additional amount of energy at the receiver. Scattered waves are usually produced when waves impinge in foliage and rough surfaces, e.g., some kinds of walls. Absorption (or penetration) losses result from path obstruction in in- and outdoor environments by a multiplicity of natural and man-made objects, such as walls, furniture, buildings and trees. When considering outdoors, also atmospheric elements can cause extra absorption [ITUR86]; nevertheless, in mobile communications, it can be usually neglected for frequencies below 30 GHz. Shadowing occurs when the LoS component is blocked by an object of large dimensions, compared to the wavelength, due to the moving terminal or objects in the vicinity of the transmitter and/or the receiver, thus, decreasing the received power.

The complete analysis of these mechanisms requires large amounts of data regarding the morphological and physical properties, as well as the non-static properties of the environment. The deterministic analysis of these mechanisms is usually restricted to simpler cases, in more complex situations a statistical analysis is of great usefulness [PaLe95]. In general, the signal at the receiver can be decomposed into a long-term component and a short-term one [Yaco93]. The long-term component is usually modelled by a path loss component plus a slow-varying one, usually referred as slow or long-term fading, which defines the changes in the signal power at the receiver as a consequence of shadowing. Although the path loss is usually evaluated by averaging the power at the receiver in a range from tens to thousands of wavelengths, an extreme variation in the transmission path can usually be found; this phenomenon can cause an extreme variation in the propagation channel characteristics, ranging from LoS to NLoS, which is usually accounted for by taking different values of path loss factors depending on the existence of a LoS component. The fast variations of the received signal over distances of the order of a few wavelengths, or short periods of time, due to the multipath behaviour of the signal, are usually referred to as fast- or short-term fading.

Most of existing wireless mobile systems, being designed for voice and low bit rate data applications, use small bandwidths, hence, they can be considered as having pure narrowband characteristics, i.e., short-term fading results from the path length difference between different waves arriving from distinct scatterers. Nevertheless, all rays arrive essentially at the same time compared to the system resolution, and all frequencies within a given bandwidth are affected in the same way. However, if the relative delay between different arriving waves is significant, i.e., if it is large compared to the symbol duration (or other reference time interval adequate for the system under analysis), the resulting signal will experience significant distortion, which varies across the channel bandwidth; such kind of channel is usually called a wideband fading one. In order to properly assess the influence of these effects, an appropriate channel model should account for the corresponding mechanisms. Furthermore, novel technologies allow exploiting not only the time domain but also the spatial one, enabling to discriminate waves arriving from different directions and at different delays, hence, an accurate channel model should account for both the time and the spatial channel properties.

In this chapter, path loss and fading characterisation is addressed, fading and time dispersion parameters, commonly used for characterising the propagation channel, being presented. Existing narrow- and wideband channel models intended for system simulation purposes are also presented. Moreover, since nowadays much of the research on channel modelling is focused on the use of Directional Channel Models (DCMs) and MIMO ones, they will also be briefly addressed herein; this way a general insight into the current state-of-art on propagation channel modelling is given.

2.2. Path Loss and Fading Characterisation

The average path loss is defined as the ratio between the transmitted and the received average power, including all possible loss effects associated with the interactions between the propagating wave and the objects within the propagation space, its mean value being usually expressed as [Rapp96]

$$\overline{L_p}_{[\mathrm{dB}]} = \overline{L_r}_{[\mathrm{dB}]} + 10 \cdot n \cdot \log(d) \tag{2.1}$$

where $\overline{L_r}$ is the average path loss measured at a given reference distance (1 m is usually considered for indoor environments and outdoor pico- and micro-cellular ones), n is the path loss exponent, and d the distance between the transmitter and the receiver.

For free-space a value of $n = 2$ is obtained, but in wireless and mobile environments, typical values of n for the Ultra-High-Frequency (UHF) band are usually between 1.6 and 6.0, depending on the environment characteristics [Rapp96], [Pras98]. As previously referred, at lower frequencies the attenuation by atmospheric elements can be neglected; however, at the millimetre waveband, namely for the frequency bands allocated to MBS, this effect cannot be ignored, having a significant impact on the value of n [CoRF97].

Besides the dependence of n on the scenario characteristics, the model in (2.1) does not consider the effect of shadowing along a measured path, leading to theoretical values of path loss that can be significantly different from the measured ones. Several deterministic approaches can be used for predicting path loss in every location; nevertheless, the amount of data needed in order to properly describe the environment is usually large, hence, the computational effort needed in order to accomplish such task is prohibitive. Moreover, even assuming that enough resources are available, the network designer is usually interested in the overall area to be covered, rather than specific values at given locations. As a consequence, several path loss models derived from experimental measurements in different environments and from theoretical approaches can be found in literature [Saun99]; some of the most common ones will be briefly described in the next chapter.

Measurements at the UHF band, e.g., reported in [Rapp96], show that the path loss is random and log-normal distributed around the mean distance-dependent value calculated from (2.1), i.e., the path loss including the long-term fading component, can be represented as

$$L_{p\,[\mathrm{dB}]} = \overline{L_p}_{\,[\mathrm{dB}]} + X_{L[\mathrm{dB}]} \tag{2.2}$$

where X_L is a zero-mean Gaussian random variable expressed in dB, with standard deviation σ_L and mean value μ_L, also expressed in dB; in general, its PDF being given by

$$p(a) = \frac{1}{\sqrt{2\pi} \cdot a \cdot \sigma_L} \cdot e^{-\frac{(\ln(a)-\mu_L)^2}{2\sigma_L^2}} \tag{2.3}$$

Since path loss has a normal distribution in dB, so has the received power, P_r. The probability that the received power will exceed a particular reference level, P_A, is obtained as

$$\mathrm{Prob}(P_r > P_A) = Q\left(\frac{P_A - \overline{P}_r}{\sigma_L}\right) \tag{2.4}$$

where

$$Q(z) = \frac{1}{\sqrt{2\pi}} \cdot \int_{z}^{\infty} e^{-\frac{x^2}{2}} \cdot dx \tag{2.5}$$

Typical values of σ_L at the UHF band are around 7 to 9 dB for outdoor environments and 1.5 to 16.3 dB for indoors [Rapp96]; values of σ_L in the range [1.0, 5.7], [0.3, 3.6], [0.8, 4.1] and [0.6, 5.0] dB are reported from indoor measurements at 1.9, 2.4, 4.75 and 11.5 GHz, respectively [Pras98]. Although some work is being done at the microwave and the millimetre wavebands, a complete study and generalisation of the results for these frequency bands are far from being completed; values of σ_L in [1.0, 3.4] dB are obtained from the analysis of experimental results from outdoor measurements at 62 GHz [Vasc98].

The short-term fading variations of the received signal over distances of the order of a few wavelengths, or short periods of time, due to its multipath behaviour, can be represented by the sum of a LoS component (if it exists) plus several reflected and/or diffracted ones, resulting from the presence of several objects in the vicinity of the transmitter and the receiver. Assuming the existence of LoS, the short-term signal level variation around the local mean is usually described by a Rice distribution, its PDF being given by [Proa83]

$$p(a) = \frac{a}{\sigma^2} \cdot e^{-\frac{a^2 + a_d^2}{2\sigma^2}} \cdot I_0\left(\frac{a \cdot a_d}{\sigma^2}\right) \tag{2.6}$$

where I_0 is the modified Bessel function of the first kind, a_d represents the magnitude of the LoS component, and σ^2 corresponds to the mean signal power of the reflected/diffracted components. In this case, there is no closed form for the CDF, but it can be obtained from numerical integration or based on the Q-function, as defined in (2.5). The ratio between the power of the LoS component and the power of the reflected/diffracted ones is usually named Rice or Ricean factor, and is expressed by

$$K = \frac{a_d^2}{2\sigma^2} \tag{2.7}$$

Values of K in decibel ($10 \cdot \log(K)$) around 6 to 10 dB are typically used for modelling the radio channel fluctuations at the UHF band [PaLe95]. It should be noted that the value of K is a useful measure of the communications link performance, its proper estimation being of practical importance for an accurate channel characterisation. Recent advances in space-time coding techniques have shown that the capacity and performance of MIMO systems depends on this factor, leading to the development of adaptive schemes for MIMO systems where the adaptation procedure is based on the value of the Rice factor, rather than on instantaneous channel coefficients. The estimation of the Rice factor and the associated estimation errors is still a topic of interesting research [TeAG03].

Under NLoS ($a_d = 0$, $K = 0$), Rice PDF reduces to the Rayleigh one [Proa83]

$$p(a) = \frac{a}{\sigma^2} \cdot e^{-\frac{a^2}{2\sigma^2}} \tag{2.8}$$

with CDF, for a given reference value A,

$$\text{Prob}(a \le A) = 1 - e^{-\frac{A^2}{2\sigma^2}} \tag{2.9}$$

For large values of K, the contribution of the reflected/diffracted paths is not significant, and (2.6) reduces to the almost free-space situation, where the signal distribution is well modelled by a Gaussian distribution with mean value a_d and variance σ^2, the PDF and CDF being given by [Proa83]

$$p(a) = \frac{1}{\sqrt{2\pi} \cdot \sigma} \cdot e^{-\frac{(a-a_d)^2}{2\sigma^2}} \tag{2.10}$$

$$\text{Prob}(a \le A)) = 1 - Q\left(\frac{A - a_d}{\sigma}\right) \tag{2.11}$$

As previously referred, under NLoS the long-term fading effect is usually modelled by a log-normal distribution, while a Rayleigh one is used for modelling the short-term fading. The overall signal distribution can be modelled by a distribution that is a mixture of log-normal and Rayleigh ones, the PDF of the signal magnitude being represented by [Gued96]

$$p(a) = \sqrt{\frac{\pi}{8}} \cdot \frac{1}{\sigma_L} \cdot \int_{-\infty}^{\infty} \frac{a}{10^{x/10}} \cdot e^{-\frac{\pi \cdot a^2}{4 \cdot 10^{x/10}}} \cdot e^{-\frac{(x-\mu_L)^2}{2\sigma_L^2}} \cdot dx \tag{2.12}$$

This distribution was proposed by Suzuki [Suzu77] and named after him. Besides its clear physical interpretation, this equation is not commonly used in most practical situations due to its increased mathematical complexity. Other distributions are used for modelling the propagation channel, which can be found in literature [PaLe95]; examples are the Weibull and Nakagami ones. When properly parameterised, these distributions degenerate to different ones: the Weibull distribution reduces to Rayleigh and exponential ones if the proper parameterisation is used, while the Nakagami one can degenerate to Rayleigh and one-sided

Gaussian ones; moreover, with a proper adjustment of parameters it can closely fit Rice and log-normal distributions.

Appropriate fading statistics are of great relevance for the development of new techniques for improving systems performance, e.g., error-control codes and diversity schemes among others. Assuming that the short-term fading behaviour of the propagation channel can be well described by a Rayleigh or Rice distribution, statistical parameters for the fading characterisation can be derived; usual parameters are the level crossing rate and the average fade duration. Similar results for the Nakagami distribution can be found in [Gued96].

Considering that the MT moves relatively to the BS with constant velocity, v_{MT}, the frequency observes a maximum drift, referred to as Doppler drift or Doppler shift of $f_m = \pm (v_{MT}/c) \cdot f_c$, c being the speed of light, and f_c the carrier frequency; the signal plus corresponds to the situation when the MT moves towards the BS. In the frequency domain, if a harmonic signal is transmitted in a multipath environment, this effect corresponds to a maximum spectrum spread of $2f_m$ near the carrier frequency [Jake74], this phenomenon being usually mentioned as Doppler spread.

The level crossing rate, N_A, is defined as the expected rate at which the signal envelope crosses a specified signal level, A, in a positive-going direction. It is expressed in number of crossings per unit time or distance (usually wavelength). For a signal with a Rice distribution, N_A, is calculated from [Gued96]

$$N_A = \sqrt{\frac{\pi}{\sigma^2}} \cdot f_m \cdot A \cdot I_0\left(\frac{A \cdot a_d}{\sigma^2}\right) \cdot e^{-\frac{A^2 + a_d^2}{2\sigma^2}} \tag{2.13}$$

while for a Rayleigh distribution ($a_d = 0$) the value of N_A can be calculated from

$$N_A = \sqrt{\frac{\pi}{\sigma^2}} \cdot f_m \cdot A \cdot e^{-\frac{A^2}{2\sigma^2}} \tag{2.14}$$

The average fade duration, $\overline{\tau_A}$, is defined as the average duration of time (or space) for which the signal is below a specified level, A, and is calculated as the ratio between the probability that the signal is below that level and the level crossing rate, N_A,

$$\overline{\tau_A} = \frac{\sum_{i=1}^{N_f} \tau_{f\,i}}{T \cdot N_A} = \frac{\mathrm{Prob}(a \le A)}{N_A} \tag{2.15}$$

with τ_{f_i} representing the fade duration below the level A, N_f the number of fades, and T the interval considered for the analysis. For a signal with a Rice distribution, $\overline{\tau_A}$ is given by

$$\overline{\tau_A} = \frac{\int_0^A \frac{a}{\sigma^2} \cdot e^{-\left(\frac{a^2+a_d^2}{2\sigma^2}\right)^2} \cdot I_0\left(\frac{a \cdot a_d}{\sigma^2}\right) \cdot da}{N_A} \tag{2.16}$$

while for a Rayleigh one it can be calculated from

$$\overline{\tau_A} = \frac{e^{\frac{A^2}{2\sigma^2}} - 1}{\sqrt{\frac{\pi}{\sigma^2}} \cdot f_m \cdot A} \tag{2.17}$$

2.3. Time Dispersion

The propagation channel can be described by a Channel Impulse Response (CIR) that is a continuous function of the time and delay variables, and that depends on the environment and system characteristics, e.g., antennas type and system bandwidth (system resolution), among others. As a simplification, discrete propagation models are derived from continuous ones, allowing to reasonably reproducing the results obtained with the equivalent continuous ones. These propagation models are usually modelled as a linear filter with impulse response [Pars92]

$$h(\tau,t) = \sum_{i=1}^{M} a_i(t) e^{j\phi_i(t)} \cdot \delta[t - \tau_i(t)] \tag{2.18}$$

where $\tau_i(t)$, $a_i(t)$ and $\phi_i(t)$ represent the time-dependent delay, magnitude and phase of each one of the M multipath components; δ is the Kronecker function. In many situations, the time delay is modelled as being time-independent, i.e., $\tau_i(t) = \tau_i$.

This type of models, being usually recommended by standard-setting bodies for simulating the propagation channel, can be easily implemented by using a tapped-delay line structure, characterised by the number of taps, the time delay, magnitude and Doppler spectrum of each tap, Figure 2.1 [Fail89], [Corr01].

Since in a real channel each wave results from the sum of several ones arriving so close to one another that they are not distinguishable by the receiving system, the receiver ability to discriminate waves arriving at different delays depends on its resolution, which is inversely proportional to the system bandwidth. In this way, the number of distinct waves observed at time t_k depends on the system bandwidth. If there is NLoS between the BS and the MT, the magnitudes of the arriving waves are modelled as being Rayleigh distributed; under LoS, the first arriving wave is modelled by a Rice distribution, Figure 2.2 [Corr01].

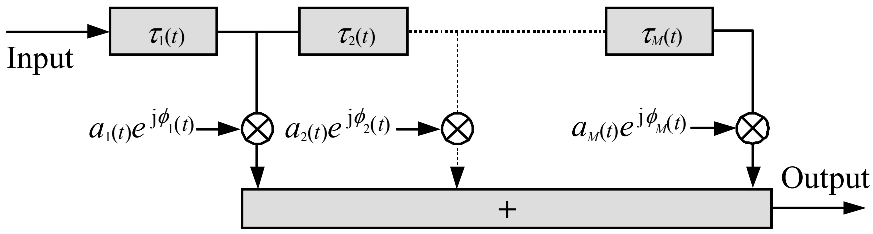

Figure 2.1 – Tapped-delay line structure.

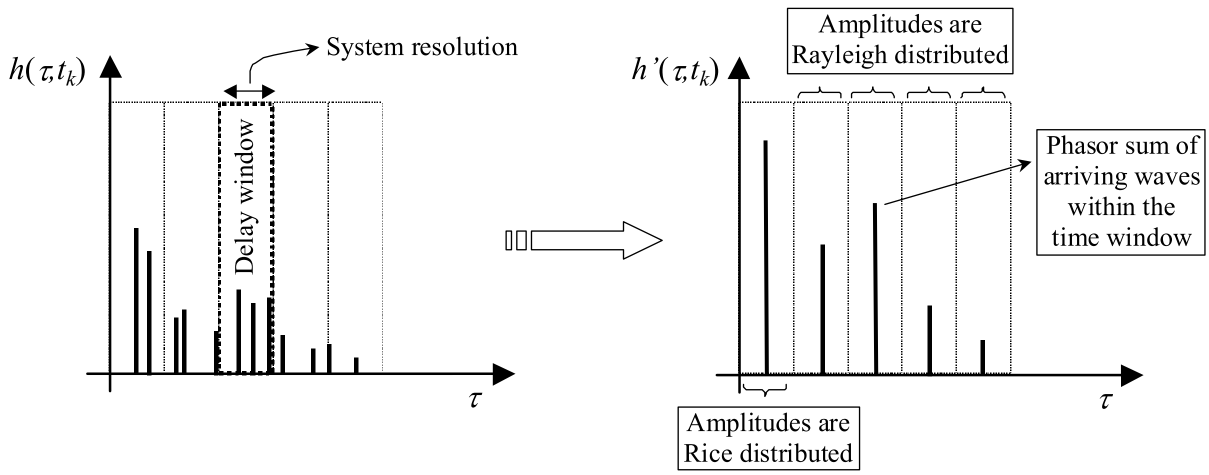

Figure 2.2 – CIR dependence on system resolution, LoS case.

Once the CIR has been identified, the PDP, which gives a measure of the received power distribution, is obtained as

$$p_d(\tau,t) = |h'(\tau,t)|^2 \tag{2.19}$$

Wide-Sense Stationary Uncorrelated Scattering (WSSUS), which is valid for most radio channels [PaLe95], is usually assumed, therefore, waves arriving at different delays, τ_i, are uncorrelated, and the correlation properties of the channel are stationary, i.e., they do not change with the time variable, t, i.e., the PDP, $p_d(\tau, t)$, can be represented as $p_d(\tau) = p_d(\tau, 0)$. The total received power, P_{rT}, being given by

$$P_{rT} = \int_{-\infty}^{+\infty} p_d(\tau) \cdot d\tau \tag{2.20}$$

There are several types of PDPs that have been used for modelling the propagation channel, WSSUS being assumed. These models are not intended to cover all possible operating environments. Instead, they are designed in order to span the overall possible range of environments. The exponential and two-stage exponential ones are commonly used for the evaluation mobile communication systems, such as GSM, UMTS and HIPERLAN/2 [Fail89], [Pras98], [Corr01].

The exponential one is usually found to be appropriate when there is only one relevant group of scattering objects [Pras98]. Its PDP is expressed by an exponential decaying function

$$p_d(\tau) = P_{\tau,1} \cdot e^{-\frac{\tau-\tau_1}{\sigma_{\tau,1}}} \quad , \quad \tau \geq \tau_1 \tag{2.21}$$

where τ_1, $P_{\tau,1}$ and $\sigma_{\tau,1}$ are the initial delay of the exponential distribution, the value of $p_d(\tau)$ for $\tau = \tau_1$ and the *rms* delay spread of the propagation channel, respectively.

The two-stage exponential is usually used when the propagation paths can be decomposed into two distinct groups: the first is a short-delay group, resulting from obstacles at a short distance of the BS and/or the MT, and the second one corresponds to the paths from a distant group of obstacles. The two-stage exponential PDP is expressed as

$$p_d(\tau) = \begin{cases} P_{\tau,1} \cdot e^{-\frac{\tau-\tau_1}{\sigma_{\tau,1}}} & , \quad \tau_1 \leq \tau < \tau_2 \\ P_{\tau,2} \cdot e^{-\frac{\tau-\tau_2}{\sigma_{\tau,2}}} & , \quad \tau \geq \tau_2 \end{cases} \tag{2.22}$$

where τ_1 and $\sigma_{\tau,1}$ are the initial delay and the *rms* delay spread of the first exponential component, and τ_2 and $\sigma_{\tau,2}$, are those of the second one; $P_{\tau,i}$ correspond to the value of $p_d(\tau)$ for $\tau = \tau_i$, Figure 2.3 (τ_1 = 0 s).

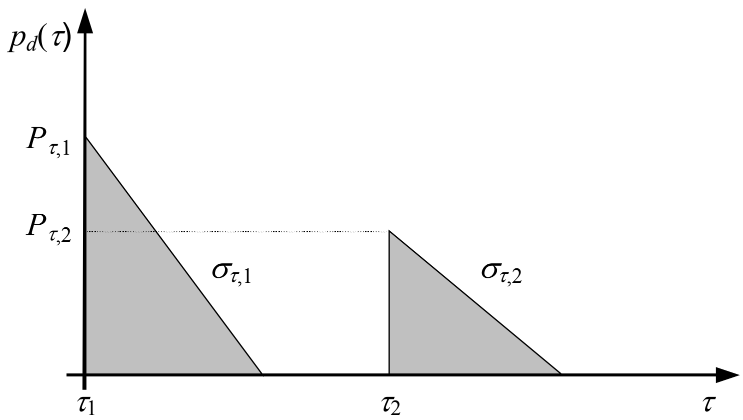

Figure 2.3 – Two-stage exponential PDP (logarithmic scale).

As referred before, channel simulators can be based on a tapped-delay line structure, therefore, discrete propagation models are usually derived from continuous ones, allowing to reasonably approximate the results obtained with the corresponding continuous ones. This type of PDPs is defined by a set of taps with specified arrival delays, τ_i, and average powers, P_i, Figure 2.4. A common procedure consists of specifying relative values for these parameters rather than absolute ones themselves.

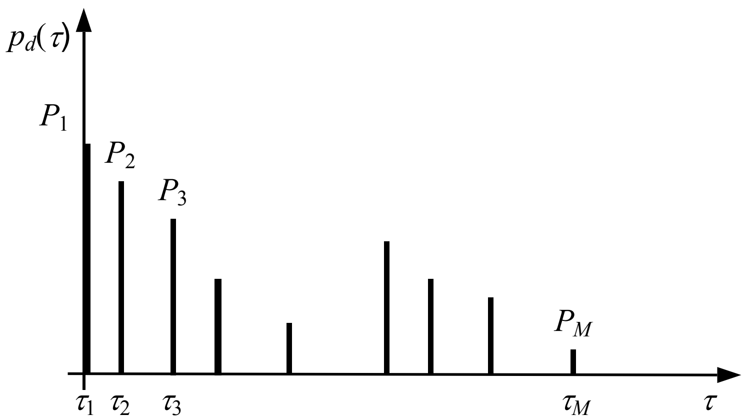

Figure 2.4 – Discrete PDP.

Since the performance of a wireless system depends on the multipath characteristics of the propagation channel, time dispersion parameters that roughly quantify the multipath channel are derived from its PDP, allowing to compare different multipath channels and to develop general guidelines for system design. The mean excess delay is defined as the first central moment of the PDP of the propagation channel

$$\bar{\tau} = \frac{\sum_{i=1}^{M}(P_i \cdot \tau_i)}{\sum_{i=1}^{M} P_i} \tag{2.23}$$

The *rms* delay spread, σ_τ, is defined as the square root of the second central moment of the PDP

$$\sigma_\tau = \left[\frac{\sum_{i=1}^{M} P_i \cdot (\tau_i - \bar{\tau})^2}{\sum_{i=1}^{M} P_i} \right]^{1/2} \tag{2.24}$$

Additional time dispersion parameters can be used for characterising the PDP of the propagation channel, examples being maximum excess delay, excess delay spread, fixed window delay and sliding window delay [Rapp96]. The expressions presented above apply to discrete PDPs, nevertheless, an equivalent formulation can be used for the continuous case [Pars92].

A frequency domain measure of the delay spread is the coherence bandwidth, B_c, which gives a measure of the bandwidth where the channel can be considered flat. Though there is no exact relation between delay spread and coherence bandwidth, it can be defined as the bandwidth over which the signal envelope correlation is above a given value; typical values for the correlation are 0.5 and 0.9, yielding [Rapp96]

$$B_c \approx \frac{1}{50\sigma_\tau} \qquad \text{(for a correlation of 0.9)} \tag{2.25}$$

$$B_c \approx \frac{1}{5\sigma_\tau} \qquad \text{(for a correlation of 0.5)} \tag{2.26}$$

Since there is no exact relationship between B_c and σ_τ, (2.25) and (2.26) are only rough estimates, therefore, spectral analysis techniques and simulation are usually required for assessing the value of B_c.

The delay spread and the coherence bandwidth are parameters describing the time dispersive nature of the propagation channel; nevertheless, they do not account for time varying properties due to relative movement between the MT and the BS, or by movement of objects that influences the channel properties. Another parameter used to describe the channel is the coherence time, T_c, defined as the time over which two received signals have a strong envelope correlation so that the channel can be considered time invariant during that interval. There is no exact relation between the maximum Doppler shift and the coherence time; nevertheless, a measure for the coherence time, assuming a frequency correlation of 0.5 is given by [Rapp96]

$$T_c = \frac{9}{16\pi \cdot f_m} = \frac{0.179}{f_m} \tag{2.27}$$

while another rule of thumb gives

$$T_c = \frac{0.423}{f_m} \tag{2.28}$$

There is a strict relationship between T_c and the type of channel fading: for a signal with symbols narrower than T_c, the channel could be considered static over some symbol duration (time flat-fading); if the symbol is larger than T_c, the channel changes during the symbol transmission and the received symbol is distorted. This kind of distortion is called time selective-fading. In conclusion, the coherence time, defines the minimum symbol rate for which the channel could be considered as a time flat-fading one.

2.4. Channel Models

2.4.1. Initial Considerations

One of the main challenges of propagation channel modelling is to develop accurate and realistic models for predicting the performance of wireless/mobile communication systems. It must be stressed out that the level of detail and the type of output provided by a channel model are highly dependent on the type of system and desired performance parameters. For classical analogue and digital mobile communication systems (e.g., GSM), it can be acceptable to consider only the received signal power (narrowband models) and/or time-varying characteristics of the received signal (wideband models). However, with emerging techniques, such as smart antennas, spatial diversity and MIMO systems, new features that depend on the spatial properties of the operating environment, namely the spatial distribution of MTs and scatterers/reflectors should be exploited; thus, new spatial channel models (usually referred as DCMs) are needed. Basically, those models must account for the physical and geometrical properties of scattering objects located in the vicinity of the antenna of interest (the number and location of these scattering objects being usually related to the heights of the antennas relative to the mean rooftop height of the surrounding environment), while providing time and spatial properties of the received signal.

This type of channel models are classified as single- or double-directional ones, depending on whether they provide spatial information only for the BS or the MT, or both, respectively [StMB01]. Moreover, they can be classified as 2D or 3D, depending on whether only one spatial freedom degree (usually azimuth) or both (azimuth and elevation) are considered. For the latter, Direction-of-Arrival (DoA) and Direction-of-Departure (DoD) are used, for referring to the direction of arrival and departure of each multipath component; for the former, usually referred to as the planar case, AoA and AoD are used, standing for Angle-of-Arrival and Angle-of-Departure, respectively.

Furthermore, channels models are also classified in different categories according to their nature, two main categories being considered: the deterministic and the stochastic ones. Within the deterministic category, a distinction is made between the reproduction of recorded impulses responses and ray-tracing techniques. Despite many measurement campaigns, it is not very usual that the recorded impulses responses are used to simulate radio channels; naturally, this approach suffers from the need of huge memory resources, and it is site-specific. Concerning ray-tracing techniques, it allows to predict the multipath propagation in a given environment, based on a physical and geometrical description of the propagation environment, being also site-specific and computationally demanding.

As opposite to these techniques, there are the stochastic ones. Stochastic models do not rely on a sit-specific description neither on specific measurements (besides being commonly assessed with results from measurements), the observed propagation phenomenon being modelled by means of statistical distributions of the involved parameters. Within this category, three sub-categories are usually considered [Corr01], [ScBM02]: parametric, geometrically-based and correlation models.

In the parametric models, the received signal is evaluated from the superposition of waves arriving at the receiver. The tapped-delay line structure is a common implementation of such kind of models, where each tap represents the signal resulting from a given propagation path [TCJF72], [Rapp96], [Corr01].

Geometrically-Based Stochastic Models (GBSM) are based either on the placement of scatterers in given positions with the scattered signal characteristics, e.g., magnitude and phase, being modelled by statistical distributions, or on a statistical distribution of scatterers, or clusters of scatterers, around one or the two ends of a connection (scattered signal characteristics being also modelled by statistical distributions). These models are usually derived by applying fundamental laws of specular reflection, diffraction and scattering of electromagnetic waves, allowing one to evaluate the PDP and the Power-Azimuth Profile (PAP) of the propagation channel. The shape of the scattering area depends on the type of environment being considered: macro- and pico-cellular environments are simulated by distributing scatterers around the MT or the BS, respectively; micro-cellular ones are usually based on an elliptical scatterer distribution whose foci are the BS and the MT. Nevertheless, different approaches can be found in literature [Corr01]. These two techniques (geometrically-based and parametric) are interrelated, thus, it is possible to derive both the PDP and PAP from the scatterer geometry, or inversely, to find a scatterer distribution that matches the given PDP and PAP.

Stochastic parametric and geometrically-based channel models are the most popular ones for simulating the propagation channel in wireless/mobile environments, however, several correlation models are also proposed in literature, mainly for MIMO approaches. These models are based on the assumption that channel coefficients are Gaussian distributed, and first and second order moments fully characterise the statistical behaviour of the channel [ScBM02].

A different distinction among channel models is done concerning channel model purposes: link- and system-level ones. Link-level models account only for the short-term characteristics of the propagation channel, long-term effects, such as path loss and shadowing, not being modelled. At the system level, long-term variations are included; moreover, multiple MTs and interference is usually accounted for large MT displacements or over large periods of time.

In this section one presents a survey of existing classical and state-of-art stochastic channel models, proposed for system design and evaluation purposes, this way, covering most of the above-mentioned approaches. These models were developed and are used for different purposes. Some of them provide information only about some channel characteristics, while others aim at giving all the properties of the wireless channel. Deterministic channel models will not be addressed, since they are not within the main scope of this thesis.

2.4.2. Classical Non-Directional Channel Models

Until nowadays, pure time-domain techniques based on stochastic models, are the most usual ones for modelling the wideband wireless propagation channel. The tapped-delay line structure (see Figure 2.1) is one of the most common ones, being usually recommended by standard-setting bodies for simulating the propagation channel. This model was first proposed for modelling the propagation channel in urban environments [TCJF72], [Suzu77], and later improved for modelling the propagation channel in indoor environments [GaPa91], [RaST91], [YeMc91], [Hash93]. Similar models were recommended by standard-bodies for simulating GSM [Fail89], [ETSI99] and UMTS [ETSI97], [3GPP02a] propagation channels. In order to use this formulation, a big effort was done concerning appropriate statistics for the delays, magnitudes and phases of multipath components.

Assuming that the scattering objects that cause multipath are randomly distributed within the space surrounding the BS and the MT, a Poisson distribution was first devised as a good solution for modelling delays; however, as observed by [TCJF72], [Suzu77], [GaPa89], [YeMc91] and [Hash93], it does not match the results from measurements. Globally, it is observed that different waves arrive in groups, rather than being totally random, thus, a modified Poisson model was proposed for modelling delays in outdoor urban environments [Suzu77], [Hash79], and further extended to indoor ones [GaPa89].

Different approaches are also suggested for modifying the Poisson process. According to [SaVa87], it is assumed that in an indoor environment waves arrive in clusters; cluster arrivals and path arrivals within each cluster are both modelled as being random Poisson distributed variables. A different approach is proposed in [YeMc91]: basically, it consists of analysing inter-arrival times (time difference between consecutive arriving delays) rather than the delays themselves. From experimental measurements in indoor environments, it was concluded that inter-arrival times are well modelled by a Weibull distribution. Concerning path magnitudes, short-variations are modelled using Rayleigh and Rice distributions, depending on the existence of a LoS component; as usual, long-term variations are modelled by a log-normal distribution.

Channel modelling in the frequency-domain is not so usual, nevertheless, an autoregressive frequency-domain modelling technique is proposed in [HoPa92]. Basically, the auto-regressive modelling technique consists of mapping a large set of points, obtained from measurements, into a limited number of parameters that are the poles of a linear filter. In practice, this modelling technique consists of evaluating the statistics of the poles obtained from a large set of measurements, such that it can be incorporated in the autoregressive modelling, allowing to generate samples of the frequency response of the propagation channel. These samples can be further transposed to the time-domain by using the inverse Fourier transform. Since time-domain techniques are the most popular ones, the propagation channel is usually characterised by its PDP, thus, in order to apply the proposed approach, poles are usually obtained from the frequency correlation function that corresponds to the given PDP. A main drawback of the frequency-domain approach is that, while in time-domain modelling a physical interpretation of the propagation phenomena is quite evident and can be directly related to the results from measurements, in the frequency-domain one a physical interpretation is not straightforward.

Besides being wideband (in the sense that they account for time-domain properties of the propagation channel), the above-mentioned models are usually used for modelling the propagation channel for specific systems working in specific environments, therefore, issues such as the dependence on system bandwidth and on environment characteristics are not directly addressed.

A time-domain level variation analysis technique of wideband signals in Rayleigh fading environments that accounts for both system bandwidth and environment properties is proposed in [InKa99], the approach being based on the eigenvalue decomposition technique. As described in [InKa99], starting from the continuous or discrete PDP of the propagation channel, a covariance matrix is obtained by generating a matrix whose elements are given by the product between the correlation function between different frequency components, evaluated as the Fourier transform of the PDP, the frequency response of the filter used in the transmitting equipment, and an incremental bandwidth that depends on the system bandwidth. Performing the eigenvalue decomposition of the covariance matrix, the obtained eigenvalues correspond to the power of the signals that fade incoherently. The CDF of the received power is then evaluated as a function of the obtained eigenvalues.

2.4.3. Directional Channel Models

As previously referred, DCMs differ from the previous existing wideband channel models basically in the introduction of spatial information. The extension of the classical time-domain CIR to the spatial-domain is done through the inclusion of the dependence on the direction of arrival (or departure) of each multipath component, being referred to as a Directional CIR (DCIR). When the influence of the antenna array is also included the channel response at each antenna element is represented as a Vector CIR (VCIR) that is related to the DCIR through the antenna array factor [LiRa99].

Similarly to the case of time-variant channels that are usually characterised through a set of delay spread statistical parameters, directional channels are also characterised according to the observed angular spread. When the spatial distribution of multipath components is characterised by a PDF, it can be used to estimate the statistical parameters of angle spread. However, when the spatial PDF is not available, one can estimate the *rms* azimuth angle spread of a narrowband channel as [LiRa99]

$$\sigma_\varphi = \sqrt{\langle \varphi^2 \rangle - \langle \varphi \rangle^2} \tag{2.29}$$

where

$$\langle \varphi \rangle = \frac{\int_0^{2\pi} \varphi \cdot P_r(\varphi) \cdot d\varphi}{\int_0^{2\pi} P_r(\varphi) \cdot d\varphi} \qquad \text{and} \qquad \langle \varphi^2 \rangle = \frac{\int_0^{2\pi} \varphi^2 \cdot P_r(\varphi) \cdot d\varphi}{\int_0^{2\pi} P_r(\varphi) \cdot d\varphi} \tag{2.30}$$

with $P_r(\varphi)$ representing the power received from angle φ. It must be noted that (2.29) applies to the 2D case, i.e., only azimuth is considered; nevertheless, it can be easily extrapolated to the 3D case, since it can also be applied if elevation together with azimuth is considered.

Depending on the narrow- or wideband nature of the propagation channel in the time-domain, and on the relation between the angle spread and the 3 dB beamwidth of the receiving antenna, the channel is usually classified as low- or high-rank [LiRa99]; a channel is said to be low-rank if it is narrowband and the angle spread is narrower than the 3 dB beamwidth of the antenna; if any of these conditions is not satisfied, the channel is considered as high-rank.

An extension of the traditional tapped-delay line channel model to the case of a 2D parametric wideband directional channel model is described in [LiRa99]. The proposed channel model was obtained from the classic one by including AoA information

$$h(\tau,t,\varphi)=\sum_{i=1}^{M}a_i(t)e^{\phi_i(t)}\cdot\delta(\tau-\tau_i)\cdot\delta(\varphi-\varphi_i) \tag{2.31}$$

where M is the number of taps (multipath components). Parameters $a_i(t)$, $\phi_i(t)$, τ_i and φ_i correspond to the magnitude, phase, delay and AoA of the i-th multipath component, respectively.

Since the DCIR given by (2.31) is a generic one, no application environment is defined, i.e., there is no standard statistics for $a_i(t)$, $\phi_i(t)$, τ_i and φ_i, those statistics being usually obtained from measurements.

An extension of the work in [Bell63], where the non-directional channel is characterised by means of correlation functions or power spectral densities, is presented in [Katt99], where the channel model is represented as a tapped-delay-line structure resembling the directional properties of the propagation channel.

A narrowband time-variant vector model, for NLoS environments, that provides both short-term Rayleigh fading and theoretical correlation properties, is proposed in [RaPa95]. It is assumed that the MT has a single antenna, while the BS has an array. The propagation environment is characterised by several dominant reflectors, hence, multipath components are taken into account. It is assumed that the magnitude of each multipath component is frequency invariant over the signal bandwidth, and that the relative time delay between different multipath components is small compared to the inverse of the signal bandwidth. Moreover, it is also assumed that the array factor is also invariant over the signal bandwidth, thus, corresponding to the narrowband case.

A wideband non-directional channel model for indoor environments is proposed in [SaVa87]. From the analysis of indoors measurement data, a certain type of clustering phenomenon was observed. Basically, it is seen that multipath components arrive in clusters, and that both clusters and rays within a cluster decay in magnitude with time. An extension of this model accounting for AoA, assuming that time and angle are statistically independent, is presented in [SRJJ97].

The wideband DCM proposed in [InKa00], being based on the eigenvalue decomposition technique, is an extension of the non-directional model in [InKa99]. Globally, it is assumed that multipath components, densely distributed and resolved in the spatial and time domains, are independent and vary according to the Rayleigh distribution. The magnitude and phase variations of the resolvable components are kept constant within the symbol period of a signal. The PAP is a Gaussian random distributed variable of the AoA, and the PDP is given by an exponential function of the time delay. The analysis in the spatial and time domains is done by assuming that multipath waves are independently distributed in those domains, however, according to [InKa00], the proposed method is available even though the spatial and time distributions are not independent. The model was theoretically assessed for a continuous exponential PDP, and a good agreement was verified with the results from simulations.

A 2D wideband DCM for the study of wideband signal transmission under NLoS, which accounts directly for the influence of system bandwidth and environment specific features, is presented in [Kozo94], being further extended to the LoS case in [KoSN96]. The model incorporates physical parameters, such as the number and magnitude of arriving waves, the propagation path length, the signal bandwidth, and the carrier frequency. It is assumed that the path length, magnitude and AoA of the arriving multipath waves, are independent and uniformly distributed within a given range. Furthermore, the bandwidth of each arriving wave is greater than the receiver bandwidth, and the power spectral density is assumed to be flat.

An extended version of the model in [KoSN96] to the case of a 3D wideband DCM is presented in [ZhRV01]. The number of arriving waves is modelled as a Poisson distributed random variable, and their magnitudes follow either Rayleigh or Rice distributions. AoAs are assumed as being uniformly and Gaussian distributed in azimuth and elevation, respectively, delays being characterised by an exponential distribution. The received power is evaluated from the same expression as the one corresponding to the non-directional case [KoSN96].

As referred before, GBSMs are based either on the placement of scatterers in given positions with the signals characteristics, e.g., magnitude and phase, being modelled by statistical distributions, or by a statistical distribution of scatterers or clusters of scatterers around one or the two ends of a connection, where the shape of the scattering area depends on channel model and on the type of environment being considered. For the former, scatterers are usually positioned over a circumference or a sector surrounding the MT or the BS, depending on the type of environment being considered. In the latter, macro- and pico-cellular environments are usually simulated by randomly distributing scatterers around the MT or the BS, respectively; micro-cellular models are usually based on an elliptical scatterers distribution whose foci are the BS and the MT [LiRa99].

As proposed in [Lee73], scatterers are uniformly spaced over a circumference surrounding the MT, each scatterer representing the effect of many scatterers within a region. It is assumed that all waves come from scatterers, i.e., NLoS is considered, the magnitude of each scattered wave being modelled as a zero mean independent complex Gaussian variable. An extension of this model, in order to account for Doppler shift by imposing an angular velocity on the ring of scatterers, is presented in [StCM94]. The joint AoA and ToA channel derives a "U-shaped" PDP [LiRa99], which is not consistent with measurements. A second extension to the model proposed by the same authors [StCM96] considers additional scatterer rings in order to obtain the desired PDPs. A similar model, usually referred as discrete uniform distribution model, is proposed in [Aszt96]. Basically, this model differs from the previous one only on the scatterers placement, these being equally spaced within a narrow beamwidth centred at the LoS to the MT.

The Geometrically-Based Single Bounce (GBSB) statistical channel models [LiRa99] are defined by a spatial scatterer density function, being useful for both simulation and analysis purposes. The simplifying assumptions of these models are to consider that, while each multipath signal travels between the MT and the BS, only a single specular reflection in a scatterer occurs. Therefore, no other effects, such as rough surface scattering, diffraction, and multiple bounce by surfaces and volumes, are accounted for. Scatterers are assumed to be omnidirectional re-radiating elements, with associated complex scattering coefficients. As mentioned above, a PDF is associated to the scatterers positioning, it being restricted to a delimited region, which shape depends on the considered environment.

From a simulation point of view, the use of these models for simulation purposes involves randomly placing scatterers in the scattering region, according to the spatial scatterer density function; the shape and size of the spatial scatterer density function, and the validation of these models through extensive measurement campaigns, still is an area of intensive research. Basically, two different models are well accepted: the GBSB Circular Model (GBSBCM) and the GBSB Elliptical Model (GBSBEM), which are based on a scatterer region of circular and elliptical shapes, respectively, Figure 2.5.

The GBSBCM for macro-cells, also called GBSB macro-cell model, is applicable to high tier, macro-cellular environments, where the BS is higher than potential scatterers, and the

MT is surrounded by a circular scatterer area, centred at the MT. A similar GBSBCM model in which scaterers are distributed on a circular area around the BS is also commonly used for modelling pico-cellular environments; in that case, it is assumed that the MT can be positioned anywhere within the scattering scenario, i.e., the distance between the BS and the MT is always lower than the radius of the scattering scenario.

The GBSBEM (also called GBSB micro-cell model) is used for low tier, micro-cellular systems, where the BS and the MT are both surrounded by local scatterers (the BS is at about the same height as local scatterers), and where it is assumed that scatterers exist predominantly along the BS-MT axis, the scattering area being defined by an ellipse.

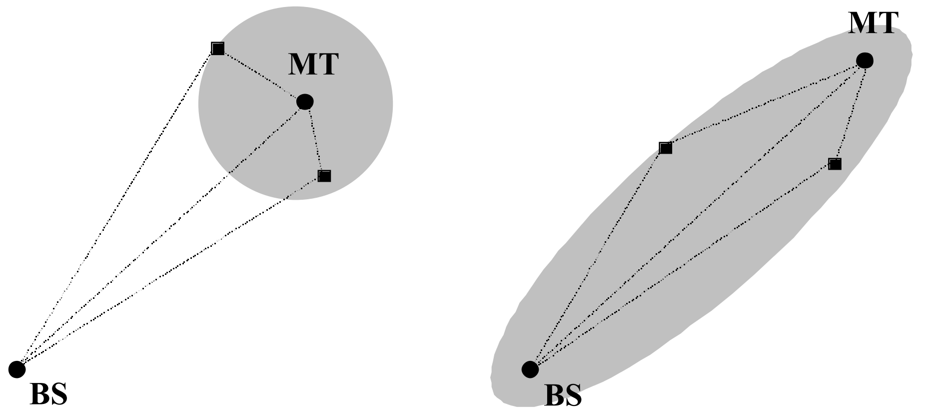

a) GBSBCM for macro-cells b) GBSBEM for micro-cells

Figure 2.5 – Typical GBSB geometries.

A Modified GBSBEM model is described in [Marq01], [MPKZ01], being designed for simulation purposes in urban street environments, while taking into account the temporal evolution of the channel due to motion. The street guiding effect through multiple reflections along the street is accounted for in a simplified way, by assuming an effective street width, thus, emulating multiple specular reflections through longer distanced single reflections, as in geometric optics methods. Given the fact that measurement results have shown signals arriving in clusters [KLTH00], scatterers are fixed in space and grouped into clusters, which are uniformly distributed in space; scatterers within each cluster are Gaussian distributed. Scattering coefficients are random variables whose magnitude and phase are uniformly distributed within [0,1] and [0, 2π[, respectively.

Different scattering spatial distributions can be found in literature. In the Gaussian WSSUS (GWSSUS) model, scatterers are grouped into clusters in space with intra-cluster delay differences that are not resolvable within the transmission bandwidth [ZeEs96];

however, it can still be considered as a wideband channel model. It is also assumed that there is no correlation between clusters. A particular case of the GWSSUS model is the Gaussian Angle-of-Arrival (GAoA) channel model, in which it is assumed that the number of scatterers within each cluster is infinite. Other models have been reported in literature with this same name, e.g., [Otte95], which is a narrowband model with only one cluster, whose AoA statistics are assumed to be Gaussian distributed around a nominal angle.

Based on the classic non-directional Typical Urban and Bad Urban GSM models, two extended directional versions of these models were developed for simulation purposes [ZeEs96]. These extended versions were designed to have time properties similar to the ones of the non-directional versions, having nearly identical PDPs, Doppler spectra and delay spreads.

A model in which scatterers are assumed as being uniformly distributed in a section of a circular crown, within a given angle and radial range centred at the mobile is proposed in [NøAn94]. The magnitude and phase associated to the scatterers are uniformly distributed within the intervals [0, 1] and [0, 2π[, respectively. A partially 3D model is proposed by [NøAn98], while considering the scattering region to be the ellipse defined by the intersection between the ground plane and an ellipsoid with foci at the BS and the MT.

The elliptical sub-regions model [LuLL97] is based on the distribution of scatterers in elliptical sub-regions whose foci are the BS and the MT; each elliptical sub-region corresponds to one possible range of excess delays. There are many similarities between this model and the GBSBEM one; the main difference between both models is in the selection of the number of scatterers and the corresponding distribution within the elliptical sub-regions. Since local scatterers around the MT, and around the path from the MT to the BS, have more significant effects on the signal components arriving to the receiver, it is proposed, that scatterers will be distributed within a 2D ellipse (as in the GBSBEM model). The ellipse is divided into a number of equal width elliptical crowns, large enough to guarantee the required delay distribution. The number of scatterers in each crown is given by a Poisson distribution whose mean must be chosen from measurements. Taking into account that, as observed from measurements, multipath components tend to arrive in clusters, it is assumed that there are several scatterers composed by reflecting points. The complex components magnitudes depend on the number of reflecting points of the scatterer, and the phases are assumed as being uniformly distributed in [0, 2π[. Additionally, the AoAs from each reflecting point are assumed to be Gaussian distributed around the angle between the BS and the considered scatterer. For macro-cellular environments, where the BS antenna is usually mounted at heights higher than the surrounding obstacles, a circular area around it can be set scatterer free, since scattering effects in the vicinity of the BS become weaker.

A unified modelling approach intended for macro-, micro- and pico-celullar environments, under LoS and NLoS is presented in [FuMB98]. In order to account for different types of environments, scattering regions are placed around both the MT and the BS; moreover, distant reflectors are also considered. A Rice factor and log-normal shadowing is assigned to the LoS component. A spatial distribution is assumed for the discrete scatterers around the BS and the MT, in order to compute the impulse response at the BS. For this purpose, two distributions are suggested: a uniform distribution within a circle or a Gaussian one. An extension of this model, by including the polarisation properties of the channel, is presented in [Svan01].

The modelling approach proposed in [PiTs99], [PiMT01] is based on the GBSB and GWSSUS model assumptions. The combination of these two models is done by considering a GBSB model composed of clusters instead of discrete scatterers; these clusters will satisfy the GWSSUS assumptions. The cluster spatial distribution assumptions are such that clusters are fixed in space according to a uniform distribution. During MT motion, the scattering influence region will move along with it, and so new multipath components will appear and others will be discarded, therefore, the number of multipath components will vary as the MT moves; the authors prove that this number is Poisson distributed. Also the statistics for the multipath components lifetime are derived. Since the model is driven by GBSB assumptions, the channel characteristics of delay spread, angle spread and correlation functions remain the same as the ones for the original model.

The Space-Time Channel Model (STCM) [SJBF99] combines advantages from purely stochastic and geometrical channel models with stochastic fading simulation. The model is based on the assumption that multipath propagation is characterised by local scatterers around the MT and a few dominant spatially separated remote reflectors. Slow fading effects and MT movement, which includes appearance and disappearance of remote reflectors, are also taken into account. Independent short-term fading is assumed for each resolvable path, with a specific time delay and AoA. The short-term fading coefficient is Rayleigh distributed being generated from a complex Gaussian random process that is filtered using an Infinite Impulse Response (IIR) filter with the typical Jakes spectrum [Jake74]. The long-term fading coefficient is a log-normal random variable and the time correlation is modelled as a simple decreasing correlation function, implemented with a simple first order IIR filter. Globally, the proposed model accounts for the influence of Doppler, fading and antenna array characteristics. A mobility model is also implemented.

A modelling framework from which channel models can be deduced is presented in [Corr01]. The structure of the COST259 Directional Channel Model (COST259/DCM) consists of the cell type, the radio environment (different types of radio environment are defined, associated to the given cell types) that stands for a whole class of environments of similar properties concerning the propagation conditions related to the surroundings in which the system operates, and the propagation scenarios. The model, being general and versatile, does not specify a certain implementation method, increasing the complexity of specification and implementation. However, two possibilities are recommended: a stochastic approach based on a tapped-delay line model or a geometrically-based one.

An implementation of a COST259/DCM GBSM at the system-level for macro- and micro-cellular environments can be found in [HoMS01]. In the proposed approach, a geometrical distribution of scatterers is done from which multipath delays and AoAs are evaluated by using a simple geometrical approach, assuming that each scatterer is responsible for one multipath component to the BS. Multiple scattering is emulated by placing virtual clusters of scatterers at certain locations in order to obtain the desired delays and AoAs. Basically, one cluster is placed around the MT, and additional far clusters may be distributed in the cell depending on the specific global scenario.

A parametric implementation of the COST259/DCM is presented in [NeBB01], which is done by implementing it as a tapped delay-line structure. As suggested in [Corr01], Laplacian and one-sided exponential-decaying functions are used for characterising both the PAP and the PDP.

2.4.4. MIMO Channel Models

The remarkable theoretical capacity gain obtained from using multiple antennas at the MT and the BS has generated significant interest in the past years [MaYJ03]. Large capacity is obtained from the signal decorrelation between different pairs of antenna elements, which can be exploited to create some parallel sub-channels. This decorrelation depends on the multipath richness of the channel; higher capacity can be achieved in high decorrelation rich multipath channels. Until nowadays, most of the studies were carried out from considering a fully correlated/decorrelated channel, nevertheless, a partially correlated channel is expected in practice. Therefore, new channel models suited for simulation purposes in partially correlated MIMO communication channels are emerging.

According to [YuOt02], MIMO channel models are divided into two main groups: the physically and non-physically based ones. The non-physical ones are derived from the statistical properties of the MIMO channels obtained from measurements, while the physical ones are based on some relevant physical parameters that provide a reasonable channel description, e.g., AoA, AoD and ToA among others; scattering models are commonly used for this type of MIMO channel modelling. Additionally, they can be classified according to their narrow- or wideband nature.

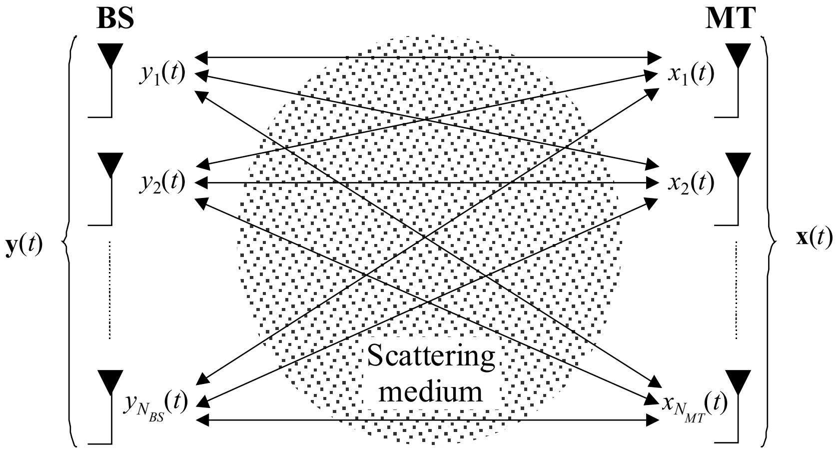

Figure 2.6 – MIMO channel structure.

The MIMO channel structure depicted in Figure 2.6 is composed of N_{BS} and N_{MT} antennas at the BS and MT, respectively. The signals at the BS are represented by $\mathbf{y}(t) = [y_1(t), y_2(t), \ldots, y_{N_{BS}}(t)]^T$, where $y_m(t)$ is the signal at the m-th antenna and $[\cdot]^T$ denotes transposition; similarly, the signals at the MT are represented as $\mathbf{x}(t)=[x_1(t), x_2(t), \ldots, x_{N_{MT}}(t)]^T$, thus, the relation between the transmitted and received signals can be represented as

$$\mathbf{y}(t) = \mathbf{H}(t) * \mathbf{x}(t) \tag{2.32}$$

where $\mathbf{H}(t)$ is a $N_{BS}\times N_{MT}$ complex channel impulse response matrix and $*$ stands for convolution.

Several approaches have been proposed for modelling the channel matrix $\mathbf{H}$; among them one can find wide- and narrowband channel models, mostly derived either from measurements or from well known scattering models. A good survey on recent techniques for MIMO channel modelling can be found in [YuOt02]. For illustration, one briefly describes some models that have been recently proposed in literature.

The model in [PAKM00] was designed for simulation purposes, allowing existing wideband tapped-delay-line models to be extrapolated to the MIMO case. Since it is assumed that antenna arrays are used at both ends, the BS and the MT, the relation between the signals at the MT and the BS can be expressed as a simple tapped-delay-line where the channel coefficients at the M delays are represented by matrices

$$\mathbf{H}(t) = \sum_{m=1}^{M} \mathbf{A}_m \delta(t - \tau_m) \tag{2.33}$$

where $\mathbf{A}_m$ is a $N_{BS} \times N_{MT}$ matrix of complex coefficients that describes the linear transformation between the considered antenna arrays at delay τ_m, and can be chosen according to well-known profiles, such as the ones proposed by standard-setting bodies [ETSI97], [3GPP02a]. For simplification, it is assumed that the coefficients of $\mathbf{A}_m$ are zero-mean complex Gaussian distributed random variables. Furthermore, it is assumed that the average power of the transmission coefficients is identical for a given delay, and uncorrelated among different delays.

A wideband channel model intended for the study of MIMO systems is proposed in [XuCV02]. The channel model is generated based on any given channel statistics for the PDP and PAP, these statistics being easily obtained from measurements, or from standard models such as the ones provided in [Corr01]. Two different levels of simulation are assumed, i.e., link-, and system-levels. For the former, a single MT and a single BS is assumed, and the classical approach that the total electromagnetic field is generated by a superposition of many wave components is used. The discrete-time wideband MIMO channel is described by a four-dimensional channel transfer matrix; by using this approach, channel matrices are generated based on standard statistics for the PDP and PAP. Despite the number of scatterers in the channel or the nature of the propagation mechanisms, these parameters represent the statistical properties of the propagation channel. Moreover, since the coordinates of the MT antenna are tracked in time as a function of MT speed, Doppler effect is implicitly included. The choice of the model parameters depends on the statistical properties of the channel and on the propagation environment; it is suggested to extract the PDPs directly from measurements or from well-known standard models. In the model, the PAP is realised by considering that the AoA and AoD are uniformly distributed random variables, power being Laplacian distributed. Concerning the antennas, the model allows any antenna configuration.

The described link-level model is easily extended to the system-level model case, i.e., when multiple BSs and MTs are considered. The proposed model having as input parameters the PDP, PAP, MT speed and antennas configuration, provide four dimensional matrices for characterising wideband time-varying fading channels. Effects such as long- and short-term fading and Doppler shift are also accounted for in the model.

The increasing need for Spatial Channel Models (SCMs) intended for MIMO simulation purposes has driven Third Generation Partnership Project (3GPP) and 3GPP2 SCM working groups to propose a SCM for MIMO simulations [3GPP03d]. The proposed model is intended for system- and link-level simulations; nevertheless, the link-level one is only intended for the comparison of performance for different implementations of a given algorithm, not for comparing the performance of different algorithms themselves; this should be accomplished by using the system-level model. Three different environments are considered: suburban macro-, urban macro- and urban micro-cellular. Reference configurations with ULA antennas at both the BS and the MT sides are provided; however, the model allows any type of antenna configuration to be selected. For these environments, several parameters are provided, e.g., the number of paths and sub-paths, angle spread statistics at both the BS and the MT, azimuth and delay spread statistics, log-normal shadowing statistics and path loss models among others. The model output is a matrix of channel coefficients for each multipath component. The overall procedure for generating the channel matrixes can be summarised as follows: (i) specify an environment; (ii) obtain the parameters associated with that environment and (iii) generate the channel model. Optional system simulation features includes the use of polarised arrays, the inclusion of far scatterer clusters as usually found in bad-urban environments, the definition of LoS or NLoS conditions and the urban canyon case usually found in both macro- and micro-cellular urban environments; these functionalities are user selectable and configurable. Further functionalities include the definition of correlation between channel parameters and the possibility of modelling inter-cell interference.

2.5. Conclusions

Channel characterisation and modelling is one of the most important issues from the point of view of system design, implementation and evaluation purposes. By properly modelling path loss, long- and short-term fading effects, it is possible to make an accurate system and network designs while allowing to closely fitting the results from measurements. At different scales, propagation models are of great usefulness for the definition of the system to be implemented, being determinant to coverage study issues and system specific features dimensioning, such as frame dimension, synchronism and automatic gain control circuits, and protocols choice. An accurate characterisation of the propagation channel is of extreme importance, reducing the need for measurements campaigns every time a system has to be set up on a new scenario.

In this chapter, path loss and fading effects were addressed; moreover a survey of existing channels models is done. The main emphasis was given to stochastic parametric and geometrically-based directional channel models, since they are commonly used for simulating the propagation channel while accounting for the influence of spatial channel properties, therefore, being suited for future wireless mobile systems being deployed. Some of the presented models do not account for the influence of the type of antennas; however, in general, they can be easily extended in order to account for this effect. Also, most of the models are single-directional ones, nevertheless, in some cases, they can be easily improved in order to become double-DCMs. Thus, one concludes that some of these models can be extended in order to allow simulating double-directional MIMO channels. It must be noted that in order to accomplish this, an additional effort has to be made in order to include also effects related to the correlation properties of the received signal and polarisation of antennas. Specific channel models for simulating MIMO channels were also briefly addressed, aiming at giving a general insight into state-of-art channel models.

Chapter 3

Link Budget and Cell Range Evaluation

3.1. Initial Considerations

Radio network planning is the process of estimating possible required network configurations in order for the operator to be able to achieve the required coverage with the desired capacity and quality of service. Coverage is usually dependent on the propagation conditions within the working environment and on system specific features, such as transmitted power, receiver sensitivity, antenna gains and others, like the use of some kind of diversity technique. Capacity is closely related to the amount of available spectrum, i.e., system bandwidth, number of users and traffic density. These issues need to be considered together in order to achieve the desired quality of service, e.g., the desired blocking probability and signal-to-interference noise ratio. Basically, a complete dimensioning process includes link budget evaluation, cell range estimation, capacity evaluation, and finally estimation of the number of BSs.

Some existing systems, e.g., GSM, are coverage limited in the sense that the maximum cell range only depends on the maximum allowable path loss, which is a function of the distance between the BS and the MT, and the environment properties; nevertheless, cell sectorisation and splitting is usually done in order for the system to accommodate the required density of users within a given area, this way, providing the required capacity. The UMTS network behaviour is quite different, since the maximum allowable path loss depends not only on the distance and environment properties but also on the required data rate, i.e., the higher the data rate the lower the maximum allowable path loss, hence, the lower the cell range.

Usually, coverage is uplink (UL) limited due to the lower MT transmitted power compared to the BS, while capacity is downlink (DL) limited; therefore, coverage discussions concentrate on the uplink [HoTo00].

Since this work is mainly focused on coverage issues, one will not address capacity matters. A brief description of GSM, UMTS, HIPERLAN and MBS is done, with the main emphasis on working frequencies, transmitted power and receiver sensitivities, since these parameters are the most relevant ones for evaluating the link budget. Additionally, general considerations about link budget evaluation are drawn, and some specific parameters for this purpose are presented. Well-known path loss models are also presented, fulfilling the requirements for properly evaluating the maximum cell range in different environments.

3.2. Systems Characteristics

3.2.1. GSM

GSM [MoPa92] was first devised as a cellular system in the 900 MHz band, usually called "primary band". This primary band includes two sub-bands of 25 MHz each, [890, 915] MHz for UL and [935, 960] MHz for DL. In 1990, a second frequency band was specified, being divided into two 75 MHz bandwidth sub-bands, [1 710, 1 785] MHz and [1 805, 1 880] MHz for the UL and DL, respectively, Table 3.1.

Table 3.1 – GSM frequency bands (extracted from [ETSI99]).

Parameter	Value
GSM900 UL frequency band [MHz]	[890, 915]
GSM900 DL frequency band [MHz]	[935, 960]
GSM1800 UL frequency band [MHz]	[1 710, 1 785]
GSM1800 DL frequency band [MHz]	[1 805, 1 880]
Channel bandwidth [kHz]	200

Speech and data are mapped onto 8 timeslots of TDMA frames. The central frequencies of the radio channels are spread evenly every 200 kHz within these bands, starting 200 kHz away from the band borders. There are 124 different radio channels in the 900 MHz band, and 375 in the 1 800 MHz one; nevertheless, the border frequencies are usually avoided and so the number of radio channels is usually limited to 122 and 373, for the 900 and 1 800 MHz bands, respectively. The BS and the MT are classified into different classes according to the output power and the frequency band, Table 3.2 and Table 3.3.

Table 3.2 – GSM BS characteristics (extracted from [ETSI99]).

Parameter	Value	
	GSM900	**GSM1800**
Maximum output power [dBm]		
Power class 1:	[55, 58[	
Power class 2:	[52, 55[	
Power class 3:	[49, 52[	[43, 46[
Power class 4:	[46, 49[	[40, 43[
Power class 5:	[43, 46[	[37, 40[
Power class 6:	[40, 43[	[34, 37[
Power class 7:	[37, 40[	
Power class 8:	[34, 37[	
Micro BS output power per carrier [dBm]		
Power class M1:	]19, 24]	]27, 32]
Power class M2:	]14, 19]	]22, 27]
Power class M3:	]9, 14]	]17, 22]
Reference sensitivity level [dBm]		
Micro BS M1:	-97	-102
Micro BS M2:	-92	-97
Micro BS M3:	-87	-92
Normal BS:	-104	-104

Table 3.3 – GSM MT characteristics (extracted from [ETSI99]).

Parameter	Value	
	GSM900	**GSM1800**
Maximum output power [dBm]		
Power class 1:		30
Power class 2:	39	24
Power class 3:	37	36
Power class 4:	33	
Power class 5:	29	
Reference sensitivity level [dBm]		
Class 1/2/3 MT:	-104	-102
Class 4/5 MT:	-102	-102

Adaptive RF power control with a time step of 480 ms, i.e., a rate of 2 Hz, is mandatory for the MT, but optional for the BS. This feature allows reducing co-channel interference while maintaining the desired link quality; moreover, it also decreases power consumption, which is important for hand-held MTs. Provisions are made for 16 different power control levels with 2 dB spacing between adjacent steps. The lowest power level for all MTs, regardless of their power class, is 13 dBm and the highest power level is equal to the maximum peak power corresponding to the class of the particular MT. For BSs, also 16 steps of 2 dB spaced power levels are provided to achieve adaptive RF power. The output power of the BS can be reduced from its maximum level at least six steps of 2 dB to adjust the radio coverage.

GSM is intended to work in outdoor macro-, micro- and pico-cellular environments, and indoor pico-cellular ones. Typical cell ranges in outdoor macro-cellular environments can be on the order of a few tenths of kilometres in rural areas, while in urban and suburban ones typical cell ranges are usually below a few kilometres. In outdoor micro- and in- and outdoor pico-cellular environments (usually found in urban and suburban zones), these values are usually below 1 km, for the case of micro-cellular environments, and a few hundreds of metres, for pico-cellular ones.

3.2.2. UMTS

UMTS [HoTo00] has two Direct Sequence-Code Division Multiple Access (DS-CDMA) variants: Wideband Code Division Multiple Access - Frequency Division Duplex (WCDMA-FDD) and Time Division - Code Division Multiple Access - Time Division Duplex (TD-CDMA-TDD). These variants use similar bandwidths: WCDMA-FDD uses the frequency band of [2 110, 2 170] MHz for DL, and [1 920, 1 980] MHz for UL, with a duplex separation of 190 MHz; TD-CDMA-TDD uses the frequency bands of [1 900, 1 920] MHz and [2 010, 2 025] MHz, Table 3.4.

Typical values for the maximum BS output power in macro-, micro- and pico-cellular environments and reference sensitivity levels for the FDD mode are presented in Table 3.5. Since the receiver sensitivity depends on the type of service, results are provided for voice, real-time data and non-real-time data, as suggested in [3GPP03c]. The MT is classified in different classes according to its maximum output power. For the FDD mode, output powers of 33, 27, 24 and 21 dBm are specified for classes 1, 2, 3 and 4, respectively [3GPP03c]. Output powers of 30, 24, 21 and 10 dBm are specified for TDD classes 1, 2, 3 and 4, respectively [3GPP03e]. Additional data for FDD and TDD modes can be found in [3GPP03a], [3GPP03b], [3GPP03c], [3GPP03e], [HoTo00].

Table 3.4 – UMTS frequency bands (extracted from [3GPP03a], [3GPP03b]).

Parameter	Value
Chip rate [Mcps] FDD: TDD:	 3.84 1.28, 3.84
Channel bandwidth [MHz] FDD: TDD (1.28 Mcps): TDD (3.84 Mcps):	 5.00 1.60 5.00
TDD frequency bands [MHz]	[1 900, 1 920] [2 010, 2 025]
FDD DL frequency band [MHz]	[2 110, 2 170]
FDD UL frequency band [MHz]	[1 920, 1 980]

Table 3.5 – UMTS BS characteristics, FDD (extracted from [3GPP03a], [HoTo00]).

Parameter	Value
Maximum output power [dBm] Macro-cell: Micro-cell: Pico-cell:	 43 38 24
Reference sensitivity level[1] [dBm] 12.2 kbps voice: 144 kbps real-time data: 384 kbps non-real-time data:	 -122 -115 -111

Fast power control is one of the most important aspects in UMTS, in particular in UL, since an overpowered MT could block a whole cell, giving rise to the so-called near-far problem. The optimum strategy for maximising capacity is to continuously equalise the received power per bit of all MTs [HoTo00]. Open-loop power control provides a coarse initial power setting of the MT at the beginning of a connection, and then fast closed-loop

[1] Reference sensitivity level assumes 4.0 dB BS noise figure, an interference margin of 2 dB, and E_b/N_d equal to 5.0, 1.5 and 1.0 dB for 12.2 kbps speech, 144 kbps real-time data and 384 kbps non-real-time data, respectively.

power control is used. This is performed at 1.5 kHz, so that the system reaction time is faster than any significant change in path loss for low to moderate MT speeds, preventing any power unbalance among all UL signals at the MT.

Closed-loop power control is also used in DL, however, in this case, the main motivation is not the near-far problem but the need for providing a marginal amount of power to the MTs positioned at the cell edge, hence, suffering from increased inter-cell interference. Moreover, closed-loop power control in DL allows enhancing weak signals caused by short-term fading effects at low speeds, and when other correcting methods such as interleaving and error correcting codes cannot work effectively.

As specified for the case of GSM, UMTS is intended to work in outdoor macro- and micro-cellular environments and in- and outdoor pico-cellular ones. Typical cell ranges for voice and low data rate services (12.2 kbps) are of the same order as the ones for GSM; for higher data rate services, e.g., 144 and 384 kbps the cell range is usually below the one for GSM. These values are naturally dependent on the working environment and on the mobility characteristics, e.g., MT speed.

3.2.3. HIPERLAN

HIPERLAN is a set of WLANs communication standards [Pras98], with four different variants: HIPERLAN/1, HIPERLAN/2, HIPERACCESS and HIPERLINK. HIPERLAN/1 was designed for providing high-speed communications between portable devices in the 5 GHz range; it could be used to allow flexible wireless data networks, and as an extension of a wired LAN. HIPERLAN/2 will offer high-speed access (up to 54 Mbit/s) to a variety of networks, including Asynchronous Transfer Mode (ATM) and Internet Protocol (IP) based ones. HIPERACCESS is intended for point-to-multipoint and high-speed access by residential and small business users to a wide variety of networks including UMTS, ATM and IP based ones. The HIPERLINK variant will provide short-range high-speed interconnection of HIPERLAN and HIPERACCESS.

The frequency band allocated to HIPERLAN/1 is [5 150, 5 300] MHz, with a channel spacing of 23.5 MHz. The frequency band for HIPERACCESS is [40.5, 43.5] GHz. Spectrum for HIPERLINK is available at the 17 GHZ band.

Since HIPERLAN development and implementation appears to be strictly confined to HIPERLAN/2, if succeeded, one basically focuses on it, Table 3.6.

Table 3.6 – HIPERLAN/2 characteristics (extracted from [ETSI01]).

Parameter	Value
Frequency band [MHz]	[5 150, 5 350] [5 470, 5 725]
Channel bandwidth [MHz]	20
Bit rate [Mbps]	≤ 54
Mean EIRP [dBm] [5 150, 5 350] MHz: [5 470, 5 725] MHz:	 23 30
Minimum sensitivity [dBm] 6 Mbps: 9 Mbps: 12 Mbps: 18 Mbps: 27 Mbps: 36 Mbps: 54 Mbps:	 -85 -83 -81 -79 -75 -73 -68

Two frequency bands are allocated for HIPERLAN/2: a lower frequency band, [5 150, 5 350] MHz, and an upper one, [5 470, 5 725] MHz. The former is intended for indoor applications, while the latter is foreseen for outdoor ones. In both cases, Orthogonal Frequency Division Multiplexing (OFDM) is used as the transmission scheme, hence, data is divided into several interleaved, parallel bit stream that modulate separate carriers; different types of Phase Shift Keying (PSK) and Quadrature Amplitude Modulation (QAM) techniques are used for modulating each sub-carrier, depending on the operating mode. The channel spacing is 20 MHz, and 52 sub-carriers are used per channel (48 sub-carriers for data and 4 sub-carriers tracking the phase for coherent demodulation).

Currently, WLAN standards at the 5 GHz band include IEEE802.11a, an evolution of the widely used IEEE803.11b. This system, being similar to HIPERLAN/2, namely concerning system bandwidth, provides the same theoretical maximum data rate as the one expected for HIPERLAN/2 [DABN02].

As previously referred, WLANs differ from mobile cellular systems, since they are mainly intended for providing wireless connectivity between computers and other equipments, being designed for operating in low mobility pico-cellular environments, or at most, micro-cellular ones; typical cell ranges being usually on the order of tenths to several hundreds of metres.

3.2.4. MBS

MBS deployment and specification depend on a large set of economic, service and technical factors [Pras98]. The target for MBS is its integration with the future integrated broadband communication structure, providing data rates up to 155 Mbps for the mobile user. Due to the spectrum scarcity at lower frequency bands, and the required data rates, MBS is expected to work at the millimetre waveband, 40 and 60 GHz bands being foreseen as strong candidates. The European Radiocommunications Office (ERO) has recommended the frequency bands of [39.5, 43.5] and [62, 66] GHz, with an interval of 2 GHz in between 1 GHz bands, while recommending the use of the former for link paths exceeding 1 km. Based on this recommendation, the use of [65, 66] and [62, 63] GHz for the UL and DL, respectively, was assumed within the European project RACE-MBS (Research in Advanced Communications in Europe - Mobile Broadband System) [RoSc95]; nevertheless, other frequency bands are being considered, e.g., [24.5, 29.5] GHz. From the physical level point of view, one of the main differences between MBS and existing third generation systems, such as UMTS, is the usage of higher carrier frequencies in order for accommodating larger bandwidths, needed for achieving the required data rates. Due to the propagation effects at high frequencies, MBS is supposed to be deployed only (or mainly) for LoS communications; moreover, the additional attenuation effects from atmospheric elements, such as oxygen and rain, will have a strong influence on system performance. Concerning the cellular structure, MBS is expected to use a cellular structure such as the one for GSM (nevertheless, different cellular structures can be used), while being also an interference limited system. Although, MBS is not yet specified, some work was done within the scope of European projects, e.g., RACE-MBS [MBS03] and ACTS-SAMBA (Advanced Communications Technologies and Services - System for Advanced Mobile Broadband Applications) [SAMB03], among others, aiming at providing some general insight into the system characteristics that should be adopted for the proper MBS deployment and implementation. Offset Quadrature Amplitude Modulation (OQAM), Offset Phase Shift Keying (OQPSK) and OFDM, and FDMA/TDMA, were foreseen as candidates for the modulation and multiplexing schemes, respectively. There are no actual figures for the transmitter and receiver characteristics, however, from the work developed within the scope of RACE-MBS and ACTS-SAMBA, system bandwidths ranging from 20 to 200 MHz are devised; moreover, several figures for the transmitting equipment as well as for the antennas are given [RoSc95]. Transmitting powers of 17 to 22 and 20 to 27 dBm are proposed for the MT and BS, respectively; antennas gains of 3 to 6 dBi for an MT equipped with an omnidirectional antenna and 9 to 15 dBi if an adaptive one is used are foreseen; antennas gains of 17 to 20 dBi are assumed for the BS.

It is not yet possible to have a clear view on the MBS deployment scenarios, nevertheless, some are already identified, namely, business city centres, urban residential areas, primary roads, trains, commercial zones, offices, factory plants and home [VeCo00b]. In this context, the shape and range of cells are very much dependent on the working environment, nevertheless, typical cell ranges are expected to be on the order of a few tenths of metres in indoor environments to several hundreds of metres in outdoor ones.

As a conclusion, one should stress that none of these figures are definitive, since a full MBS specification is far from being complete, and its deployment and implementation is not foreseen for the next couple of years. Significant work is, and has to be, carried out in order to properly assess MBS characteristics; therefore, in the next chapters one will use some of these figures only for illustrative purposes.

3.3. Link Budget Analysis

As referred before, link budget evaluation is essential for system design and evaluation purposes, e.g., cell coverage and interference analysis. Basically, it consists of estimating the power at the receiver for a given transmitted power, while accounting for both gain and loss between the transmitter output and the receiver input [Pars92]

$$P_{r[\mathrm{dBm}]} = P_{t[\mathrm{dBm}]} + G_{r[\mathrm{dBi}]} + G_{t[\mathrm{dBi}]} - L_{p[\mathrm{dB}]} \tag{3.1}$$

where P_t and P_r correspond to the transmitted and received powers at the antenna terminals, respectively, G_t and G_r are the transmitter and receiver antenna gains, and L_p is the path loss between the transmitter and the receiver. When EIRP (Equivalent Isotropic Radiated Power) is given instead of P_t, the received power is obtained as

$$P_{r[\mathrm{dBm}]} = EIRP_{[\mathrm{dBm}]} + G_{r[\mathrm{dBi}]} - L_{p[\mathrm{dB}]} \tag{3.2}$$

The value of EIRP depends on which link is considered; for the UL one obtains

$$EIRP^{UL}{}_{[\mathrm{dBm}]} = P_{TX[\mathrm{dBm}]} - L_{u[\mathrm{dB}]} + G_{t[\mathrm{dBi}]} \tag{3.3}$$

with L_u representing the loss due to the presence of the user's head near the antenna (this being usually around zero for data terminals), and P_{TX} the power at the transmitter output. For the DL the EIRP can be evaluated as

$$EIRP^{DL}{}_{[\mathrm{dBm}]} = P_{TX[\mathrm{dBm}]} - L_{c[\mathrm{dB}]} + G_{t[\mathrm{dBi}]} \tag{3.4}$$

with L_c representing the coupling and cable losses between the transmitter output and the antenna.

Similarly, for the case of the received power at the receiver input, P_{RX}, one obtains for the UL and DL, respectively

$$P^{UL}_{RX\,[\mathrm{dBm}]} = P_{r[\mathrm{dBm}]} - L_{c[\mathrm{dB}]} \tag{3.5}$$

$$P^{DL}_{RX\,[\mathrm{dBm}]} = P_{r[\mathrm{dBm}]} - L_{u[\mathrm{dB}]} \tag{3.6}$$

Therefore, the path loss is evaluated as

$$L_{p[\mathrm{dB}]} = P_{TX[\mathrm{dBm}]} + G_{t[\mathrm{dBi}]} + G_{r[\mathrm{dBi}]} - L_{c[\mathrm{dB}]} - L_{u[\mathrm{dB}]} - P_{RX[\mathrm{dBm}]} \tag{3.7}$$

Depending on the system being considered, the receiver sensitivity, i.e., the minimum possible received power at the receiver input, $P_{RX_{min}}$, depends on the type of service and/or the data rate. The receiver sensitivity is usually expressed as

$$P_{RX_{min}[\mathrm{dBm}]} = N_{0[\mathrm{dBm}]} + \frac{S}{N_0}_{[\mathrm{dB}]}$$

where N_0 is the noise power, defined as

$$N_{0[\mathrm{dBm}]} = -174 + 10\log(B_{N[\mathrm{Hz}]}) + F_{[\mathrm{dB}]} \tag{3.8}$$

B_N is the noise bandwidth (considered as the chip rate in the case of UMTS), F is the receiver noise figure, and S/N_0 is the desired signal to noise ratio, which in the case of CDMA based systems, can be defined as the ratio between the energy per bit, E_b, and the noise spectral density, N_d. Also, in CDMA based systems, such as UMTS, the receiver sensitivity depends also on the processing gain, G_p, and the interference margin, M_i, which is a function of the considered system load

$$P_{RX_{min}[\mathrm{dBm}]} = N_{0[\mathrm{dBm}]} + \frac{E_b}{N_d}_{[\mathrm{dB}]} + M_{i[\mathrm{dB}]} - G_{p[\mathrm{dB}]} \tag{3.9}$$

with

$$G_{p[\mathrm{dB}]} = 10\log\left(\frac{R_c}{R_b}\right) \tag{3.10}$$

where R_c and R_b correspond to the chip and bit rates, respectively.

Since in a multipath fading environment the signal experiences different kinds of propagation phenomena, additional margins should be considered for evaluating the maximum possible path loss; the total margin to be considered, M_t, is given by

$$M_{t[\mathrm{dB}]} = M_{sf[\mathrm{dB}]} + M_{ff[\mathrm{dB}]} + L_{int[\mathrm{dB}]} - G_{extra[\mathrm{dB}]} \tag{3.11}$$

where: M_{sf} and M_{ff} are the fading margins accounting for long- and short-term fading, respectively (also referred as slow and fast fading); L_{int} is an extra margin that should be accounted for when considering into building penetration; G_{extra} results from the contribution of additional gains, e.g., soft handover (in the case of UMTS), diversity schemes, power control and any additional feature. The maximum allowable path loss is then evaluated as

$$L_{p_{max}[\mathrm{dB}]} = \underbrace{L_{p[\mathrm{dB}]}}_{P_{RX}=P_{RX_{min}}} - M_{t[\mathrm{dB}]} \tag{3.12}$$

One must remember that for an appropriate link budget evaluation one needs accurate short- and long-term fading margins, among many other parameters. The long-term fading is modelled as being log-normal distributed, which is usually in good agreement with the results from measurements; however, short-term fading margins are not usually accurately defined, since no dependence on the considered system bandwidth and working environment characteristics is accounted for, instead Rayleigh and Rice distributions being commonly used. It should be remembered that these distributions are only valid for the narrowband case. By considering more accurate fading margins, an accurate link budget evaluation can be achieved. This will be addressed in the next chapters. Several useful parameters for link budget evaluation in GSM, UMTS, HIPERLAN/2 and MBS are presented in Table 3.7 to Table 3.9. Additional data can be found in [MoPa92], [HoTo00], [ETSI01], [RoSc95].

Table 3.7 – Parameters for link budget evaluation, GSM.

Parameter	Value	
MT output power [dBm]	GSM 900	GSM 1800
	33	30
Antenna gain for MT [dBi]	0	
Body loss [dB]	Voice	Data
	3	0
Cable loss at the BS [dB]	2	
Antenna gain for BS [dBi]	13	
BS sensitivity [dBm]	-104	

Table 3.8 – Parameters for link budget evaluation, UMTS.

Parameter	Value		
MT output power [dBm]	24		
Antenna gain for MT [dBi]	0		
Body loss [dB]	Voice	Data	
	3	0	
Cable loss at the BS [dB]	2		
Antenna gain for BS [dBi]	13		
Thermal noise density [dBm/Hz]	-174		
BS sensitivity [dBm]	Voice 12.2 kbps	Data 144 kbps	Data 384 kbps
	-122	-115	-111
BS receiver noise figure [dB]	4		
Interference margin [dB]	2		
Required E_b/N_d [dB]	Voice 12.2 kbps	Data 144 kbps	Data 384 kbps
	5.0	1.5	1.0

Table 3.9 – Parameters for link budget evaluation, HIPERLAN/2.

Parameter	Value	
Mean EIRP [dBm]	Indoor	Outdoor
	23	30
Antenna gain for MT [dBi]	0	
Cable loss at the BS [dB]	2	
Antenna gain for BS [dBi]	5	
Sensitivity level [dBm]	54 Mbps	6 Mbps
	-68	-85

Table 3.10 – Parameters for link budget evaluation, MBS.

Parameter	Value
MT output power [dBm]	22
Antenna gain for MT [dBi]	6
Cable loss at the BS [dB]	2
Antenna gain for BS [dBi]	17
Sensitivity level [dBm]	-75

3.4. Cell Range Evaluation

3.4.1. Outdoor Path Loss Models

Since one has evaluated the maximum allowable path loss in order to achieve the desired system performance for a given coverage probability, one can estimate the cell range from using well-known path loss models. Outdoor environments are considered in what follows.

Several path loss models for evaluating the path loss in outdoor environments can be found in literature [Pars92], [Yaco93], [Saun99]; one will focus on the most widely used since many years, namely Okumura-Hata, Walfisch-Bertoni, Ikegami and their extensions made within the framework of COST 231 European project [DaCo99].

Assuming free-space propagation, the average path loss, $\overline{L_p}$, is evaluated as [Pars92]

$$\overline{L_p}_{[\mathrm{dB}]} = L_{0[\mathrm{dB}]} = 32.44 + 20 \cdot \log\left(f_{[\mathrm{MHz}]}\right) + 20 \cdot \log\left(d_{[\mathrm{km}]}\right) \tag{3.13}$$

where f is the working frequency and d represents the distance between the transmitter and the receiver.

The free-space propagation model applies only under very restricted conditions; in practice there are almost always obstructions to the propagation path or surfaces from which radio waves can be reflected. The two-ray ground reflection model is a useful propagation model that is based on geometric optics and considers both the direct path and a ground reflected one, being approximated for large distances $\left(d > (10 \cdot h_{BS} \cdot h_{MT})/\lambda\right)$ by [Pars92]

$$\overline{L_p}_{[\mathrm{dB}]} = 120 + 40 \cdot \log\left(d_{[\mathrm{km}]}\right) - 20 \cdot \log\left(h_{BS[\mathrm{m}]}\right) - 20 \cdot \log\left(h_{MT[\mathrm{m}]}\right) \tag{3.14}$$

where h_{BS} and h_{MT} correspond to the BS and MT antenna heights, respectively. As one can observe, the received power falls with a rate of 40 dB/decade, while the decay rate for the free-space model is 20 dB/decade.

Although being simple, these two models are not of great practical interest, since radio propagation in a wireless mobile communications system usually takes place over irregular terrain, varying from a simple flat earth profile to a highly mountainous one, with both the MT and BS antennas positioned at different heights, according to the type of cellular structure and environment being considered. Moreover, the presence of natural and man-made obstacles should also be accounted for; hence, more elaborated models, especially those based, or at least accessed, from a systematic interpretation of measurement data in different environments, should be used instead.

The Okumura-Hata model [Hata80] is an empirical formulation of the graphical path loss data provided by Okumura [OkOF68], and is valid from 150 to 1 500 MHz. Hata presented the urban area propagation loss as a standard formula and supplied correction factors for application to other situations. The results from the Okumura-Hata model are closely related to the original Okumura model, as long as distance exceeds 1 km, therefore, this model is intended for macro-cellular environments; nevertheless, it usually provides good results only for distances above 5 km.

The median path loss in an urban area (equivalent to the average one, under the assumption that the long-term fading is modelled by a log-normal distribution) is given by

$$\begin{aligned}\overline{L_p}_{\,[\mathrm{dB}]} = {} & 69.55+26.16\cdot\log\left(f_{[\mathrm{MHz}]}\right)-13.82\cdot\log\left(h_{BS[\mathrm{m}]}\right)+ \\ & \left[44.9-6.55\cdot\log\left(h_{BS[\mathrm{m}]}\right)\right]\cdot\log\left(d_{[\mathrm{km}]}\right)-a\left(h_{MT[\mathrm{m}]}\right)-\sum(\mathit{Correction\ factors})\end{aligned} \tag{3.15}$$

where for a smaller to medium sized city

$$a\left(h_{MT[\mathrm{m}]}\right)=\left(1.1\cdot\log f_{[\mathrm{MHz}]}-0.7\right)\cdot h_{MT[\mathrm{m}]}-\left(1.56\cdot\log f_{[\mathrm{MHz}]}-0.8\right) \tag{3.16}$$

where h_{BS} and h_{MT} correspond to the BS and MT heights, respectively. The function $a(h_{MT})$ is a correction factor for effective MT antenna height, which depends on the size of the coverage area. Several correction factors are provided, extending the model applicability to rural and suburban environments [PaLe95].

Within the framework of the COST 231 European Project, an extended version of the Okumura-Hata model was developed. COST 231 proposes extending the model to the frequency band [1 500, 2 000] MHz by analysing Okumura's propagation curves in the upper frequency band [DaCo99]. This model, usually referred as COST 231-Hata model, is restricted to large and small macro-cells, i.e., BS antenna heights above rooftop levels adjacent to the BS [DaCo99]

$$\begin{aligned}\overline{L_p}_{\,[\mathrm{dB}]} = {} & 46.3+33.9\cdot\log\left(f_{[\mathrm{MHz}]}\right)-13.82\cdot\log\left(h_{BS[\mathrm{m}]}\right)+ \\ & \left[44.9-6.55\cdot\log\left(h_{BS[\mathrm{m}]}\right)\right]\cdot\log\left(d_{[\mathrm{km}]}\right)-a\cdot\left(h_{MT[\mathrm{m}]}\right)+C_m-\sum(\mathit{Correction\ factors})\end{aligned} \tag{3.17}$$

with

$$C_m=\begin{cases}0\ \mathrm{dB} & ,\quad \text{medium sized city and suburban centres}\\ 3\ \mathrm{dB} & ,\quad \text{metropolitan centres}\end{cases} \tag{3.18}$$

The model applicability is restricted to a given range of parameters, differing from the ones for the original Okumura-Hata model only on the value of the allowable frequency range, Table 3.11.

Table 3.11 – Validity domain of COST 231-Hata model

Parameter	Value
Frequency (f) [MHz]	[1 500, 2 000]
BS height (h_{BS}) [m]	[30, 200]
MT height (h_{MT}) [m]	[1, 10]
Distance (d) [km]	[1, 20]

The COST 231-Walfisch-Ikegami model (COST 231-WI) [DaCo99] allows improving the estimation of the path loss in urban and suburban environments where the building heights are quasi-uniform, by considering additional data, namely: average height of surrounding buildings, h_{roof}, street width, w_s, building separation, b, and street orientation with respect to the direct path, φ_s. Moreover, this model is also valid when the BS antenna is positioned below the rooftop level. Although this model may be subject to corrections and improvements, e.g., [HaWC99], it was assessed by measurement campaigns, and extensively used. A detailed description of the environment geometry being considered in the model can be found in [DaCo99]. Distinction is made between LoS and NLoS conditions: for the LoS case, within a street canyon, the average path loss is evaluated from

$$\overline{L_p}_{[\mathrm{dB}]} = 42.6 + 26 \cdot \left(d_{[\mathrm{km}]}\right) + 20 \cdot \log\left(f_{[\mathrm{MHz}]}\right) \quad , \qquad d \geq 20\mathrm{m} \tag{3.19}$$

while under NLoS, it is obtained as

$$\overline{L_p}_{[\mathrm{dB}]} = \begin{cases} L_{0[\mathrm{dB}]} + L_{rts[\mathrm{dB}]} + L_{msd[\mathrm{dB}]} & , \quad L_{rts[\mathrm{dB}]} + L_{msd[\mathrm{dB}]} > 0 \\ \\ L_{0[\mathrm{dB}]} & , \quad L_{rts[\mathrm{dB}]} + L_{msd[\mathrm{dB}]} \leq 0 \end{cases} \tag{3.20}$$

where L_0 is the free space loss, L_{msd} is the multiple screen diffraction loss, and L_{rts} describes the coupling of the wave propagating along the multiple-screen path into the street where the MT is located (rooftop-to-street diffraction loss). The latter is given by

$$L_{rts[\mathrm{dB}]} = -16.9 - 10 \cdot \log\left(w_{s[\mathrm{m}]}\right) + 10 \cdot \log\left(f_{[\mathrm{MHz}]}\right) + 20 \cdot \log\left(\Delta h_{MT[\mathrm{m}]}\right) + L_{ori[\mathrm{dB}]} \tag{3.21}$$

where L_{ori} is an empirical correction factor, obtained from a few experimental measurements

$$L_{ori[\mathrm{dB}]} = \begin{cases} -10 + 0.354 \cdot \varphi_{s[^\circ]} & , \quad 0^\circ \le \varphi_s < 35^\circ \\ 2.5 - 0.075 \cdot \left(\varphi_{s[^\circ]} - 35\right) & , \quad 35^\circ \le \varphi_s < 55^\circ \\ 4.0 - 0.114 \cdot \left(\varphi_{s[^\circ]} - 55\right) & , \quad 55^\circ \le \varphi_s < 90^\circ \end{cases} \tag{3.22}$$

and

$$\Delta h_{MT} = h_{roof} - h_{MT} \tag{3.23}$$

The multiple screen diffraction loss, L_{msd}, is defined as

$$L_{msd[\mathrm{dB}]} = L_{bsh[\mathrm{dB}]} + k_a + k_d \cdot \log\left(d_{[\mathrm{km}]}\right) + k_f \cdot \log\left(f_{[\mathrm{MHz}]}\right) - 9 \cdot \log\left(b_{[\mathrm{m}]}\right) \tag{3.24}$$

where

$$L_{bsh[\mathrm{dB}]} = \begin{cases} -18 \cdot \log\left(1 + \Delta h_{BS[\mathrm{m}]}\right) & , \quad h_{BS} > h_{roof} \\ 0 & , \quad h_{BS} \le h_{roof} \end{cases} \tag{3.25}$$

$$k_a = \begin{cases} 54 & , \quad h_{BS} > h_{roof} \\ 54 - 0.8 \cdot \Delta h_{BS[\mathrm{m}]} & , \quad d \ge 0.5\,\mathrm{km} \text{ and } h_{BS} \le h_{roof} \\ 54 - 0.8 \cdot \Delta h_{BS[\mathrm{m}]} \dfrac{d_{[\mathrm{km}]}}{0.5} & , \quad d < 0.5\,\mathrm{km} \text{ and } h_{BS} \le h_{roof} \end{cases} \tag{3.26}$$

$$k_d = \begin{cases} 18 & , \quad h_{BS} > h_{roof} \\ 18 - 15 \cdot \dfrac{\Delta h_{BS}}{h_{roof}} & , \quad h_{BS} \le h_{roof} \end{cases} \tag{3.27}$$

$$k_f = -4 + \begin{cases} 0.7 \cdot \left(\dfrac{f_{[\mathrm{MHz}]}}{925} - 1\right) & , \quad \text{medium sized city and suburban centres} \\ 1.5 \cdot \left(\dfrac{f_{[\mathrm{MHz}]}}{925} - 1\right) & , \quad \text{metropolitan centres} \end{cases} \tag{3.28}$$

with

$$\Delta h_{BS} = h_{BS} - h_{roof} \tag{3.29}$$

The parameter k_a represents the increase of the path loss for BS antennas below the rooftops of the adjacent buildings; k_d and k_f controls the dependence of the multi-screen diffraction loss versus distance and radio frequency, respectively.

When building and street data is unknown, default values are recommended [DaCo99]

- $h_{roof[\mathrm{m}]} = 3 \times \text{number-of-floors} + \text{roof-height}_{[\mathrm{m}]}$

  with

  $$\text{roof-height}_{[\mathrm{m}]} = \begin{cases} 3 & , \quad \text{pitched} \\ 0 & , \quad \text{flat} \end{cases} ;$$

- $20 \le b \le 50$ m, $w_s = \frac{b}{2}$, $\varphi_s = 90^{\mathrm{o}}$.

The validity domain of COST 231-WI model is in Table 3.12. The estimation of path loss agrees rather well with the measurements for BS antenna heights above rooftop level. The mean error is in the range of ±3 dB and the standard deviation is about 4 to 8 dB [DaCo99]. However, the prediction error becomes large for $h_{BS} \approx h_{roof}$ compared to situations where $h_{BS} >> h_{roof}$; moreover, the performance of the model is poor for $h_{BS} << h_{roof}$. Additionally, parameters b, w_s and φ_s are not considered in a physically meaningful way for small micro-cells; in this way, the prediction error for this type of environments can be quite large. The reliability of the model also decreases, if terrain is not flat or the land cover is inhomogeneous.

Table 3.12 – Validity domain of COST 231-WI model

Parameter	Value
Frequency (f) [MHz]	[800, 2 000]
BS height (h_{BS}) [m]	[4, 50]
MT height (h_{MT}) [m]	[1, 3]
Distance (d) [km]	[0.02, 5]

Both Okumura-Hata or COST 231-Hata (depending on the frequency band being considered) and COST 231-WI models can be applied for evaluating the path loss in GSM and UMTS, since they are valid for carrier frequencies up to 2 GHz. Nevertheless, they are not suited for HIPERLAN/2 and MBS, for which different propagation models are usually used. Since COST 231-WI allows improving the path loss estimation in urban environments from considering the influence of additional propagation effects, while being intended for cell ranges from 20 m to 5 km, it will be used for evaluating the path loss in urban and suburban environments where typical cell ranges for GSM and UMTS are usually below 5 km. In rural environments cell ranges from several to a few tenths of kilometres are usually used, therefore, Okumura-Hata or COST 231-Hata is used depending on the working frequency.

In the case of HIPERLAN/2, path loss models derived from the free-space one, and further assessed from measurements, are usually used. Propagation in urban LoS street-canyon environments can be reasonable modelled from considering the free-space path loss law with a power decay exponent usually found to be around or slightly below the one for free-space [Corr01]

$$\overline{L_p} = 47.4 + 20 \cdot \log(d) \tag{3.30}$$

The propagation phenomena at the millimetre waveband is quite different from the one observed at lower frequency bands, therefore, specific propagation models for this band should be used for MBS. One model for short-range radio links at 60 GHz for mobile inter-vehicle communication accounting for rain and oxygen attenuation is proposed in [Scha91]. A similar model intended for MBS purposes is presented in [CoFr94]; this model, obtained from the free-space propagation equation, accounts for oxygen and rain attenuation, enabling the estimation of the average path loss as

$$\overline{L_p}_{[\mathrm{dB}]} = 32.4 + 30 \cdot n + 10 \cdot n \cdot \log\left(d_{[\mathrm{km}]}\right) + 20 \cdot \log\left(f_{[\mathrm{GHz}]}\right) + \gamma_{R[\mathrm{dB/km}]} \cdot d_{[\mathrm{km}]} + \gamma_{O[\mathrm{dB/km}]} \cdot d_{[\mathrm{km}]} \tag{3.31}$$

where γ_O and γ_R are the oxygen and rain attenuation coefficients, respectively. A drawback of this model is that in many calculations of system design and assessment, the evaluation of the received power is not straightforward, since the model does not present a unique term depending on the distance. A simpler model, similar to the previous one, in which there is a global dependence of power with distance, is proposed in [CoRF97]

$$\overline{L_p}_{[\mathrm{dB}]} = C + 10 \cdot \xi \cdot \log\left(d_{[\mathrm{km}]}\right) + 20 \cdot \log\left(f_{[\mathrm{GHz}]}\right) \tag{3.32}$$

where C is a constant depending on the distance interval and on the frequency. The parameter ξ, depending on frequency, accounts for the total attenuation, including the one due to oxygen and rain. The dependence of C and ξ on distance and frequency can be found in [Bedi98]. This type of models requires an environment classification according to different values of n. A survey from outdoor measurements at the 60 GHz band, can be found in [CoRF97]. These values are almost the same as the one obtained for free-space, i.e., $n = 2$, which is not surprising since for this frequency band the breakpoint distance is of the order of several kilometres for typical antenna heights.

3.4.2. Indoor Path Loss and Building Penetration Models

In indoor radio channels, propagation is strongly influenced by the layout of buildings, construction materials and building type, e.g., type of partitions (soft or hard partitions) and multi-floor buildings. Moreover, when outdoor to indoor building penetration is involved, an additional complexity exists, since the received signal inside the building varies with height. It is usually considered that the received power increases with height, due to the urban clutter effect.

Being one of the simplest models for path loss evaluation in indoor environments, the one slope model is based on the assumption that there is a linear dependence between the path loss and the distance between the transmitter and the receiver (see (2.1)). This model, being simple, is useful and easy to use for cell planning purposes, since only the distance between the transmitter and the receiver appears as a parameter. However, its use is of low practical interest if an accurate power estimation is needed, since all propagation mechanisms are implicitly included together in the value of the average reference path loss, $\overline{L_r}$, and the power decay rate, n. Nevertheless, if $\overline{L_r}$ and n are assessed from measurements, this model gives reasonable results when used for cell range evaluation purposes. Hence, it will be used for evaluating path loss in HIPERLAN/2 indoor environments; as proposed in [DaCo99], n = 3.4 is considered, which extrapolating for the HIPERLAN/2 working frequency gives

$$\overline{L_p} = 46.8 + 34 \cdot \log(d) \tag{3.33}$$

This expression apply to multi-floor buildings, therefore, penetration among neighbouring floors is implicitly included. Similar models, that include some additional effects, e.g., two-slope, multiple breakpoint and linear attenuation models, can be found in literature [PaLe95], [DaCo99]. More elaborated models account for the influence of different types of walls and floor while allowing to evaluate the path loss as a function of the number and type of penetrated walls and floor. A well-known example is the COST 231 Multi-Wall Model [DaCo99] for which the path loss is given by the sum of the free space loss plus additional losses introduced by different types of walls and floor. Nevertheless, it should be noted that model parameters do not represent physical wall and floor losses, instead they are only model parameters that should be optimised with measurement data, since implicitly they include the composite effect of any objects within the rooms, e.g., furniture, as well as the effect of signal paths guided through corridors.

Concerning outdoor to indoor building penetration, several models can also be found in literature [DaCo99]. The COST 231 model for building penetration allows characterising outdoor to indoor penetration of signals impinging on a certain building. The model was developed for the frequency band of [900, 1 800] MHz and distances up to 500 m. Besides being of easy applicability, the above-mentioned model should also be carefully assessed with results from measurements in order to provide good results.

There is an extensive list of building penetration measurements, allowing to evaluate with some degree of accuracy the penetration losses for different buildings and working frequencies [Rapp96], [DaCo99], [Corr01]. Results from several measurements in isolated and integrated high- and low-rise buildings in the city of Lisbon can be found in [XaVC03]. These measurements allow estimating the additional building attenuation due to wall losses relative to an outdoors reference level at 1.5 m height. Several positions within the buildings are measured for the GSM 1800 band, accounting for both exterior and interior wall losses. For each class of buildings, it is observed that the PDF of the received power looks like a double-Gaussian function (in dB), i.e., different standard deviations were obtained for the left and right half parts of the PDF. When accounting for all kinds of buildings, the PDF approaches a Gaussian one, this being a consequence of the central limit theorem. For the measured buildings, a mean attenuation and a standard deviation of 10.19 and 13.85 dB were obtained, respectively. The CDF of the building attenuation, i.e., the probability that the building penetration loss, L_w, is below a given level, $L_{w_{ref}}$, is given by, Figure 3.1,

$$\mathrm{Prob}\left(L_w \le L_{w_{ref}}\right) = 1 - Q\left(\frac{L_{w_{ref}} - 10.19}{13.85}\right) \tag{3.34}$$

One can then easily evaluate the building attenuation that should be considered in order to ensure a desired indoor coverage probability, e.g., building attenuations of 13.7 and 27.9 dB are obtained for the GSM1800 band for indoor coverage probabilities of 60 and 90 %, respectively. It should be remembered that these values account for both outer and inner wall losses, thus, becoming significantly large than the ones usually found when only the attenuation from the outer wall is considered.

As previously referred, these results where obtained for the GSM1800 frequency band, nevertheless, they can be extrapolated for different frequency bands (e.g., UMTS and HIPERLAN/2) by considering the dependence on $20\cdot\log(f)$. However, one should be aware that such an assumption can lead to some approximation error [XaVC03]; anyhow, these errors are not usually significant, compared to the uncertainty associated to the proper description of a given class of buildings itself. For the case of MBS, such an extrapolation can lead to significant errors, since the propagation phenomena at the millimetre waveband is quite different from the one at lower frequencies [CoFr95].

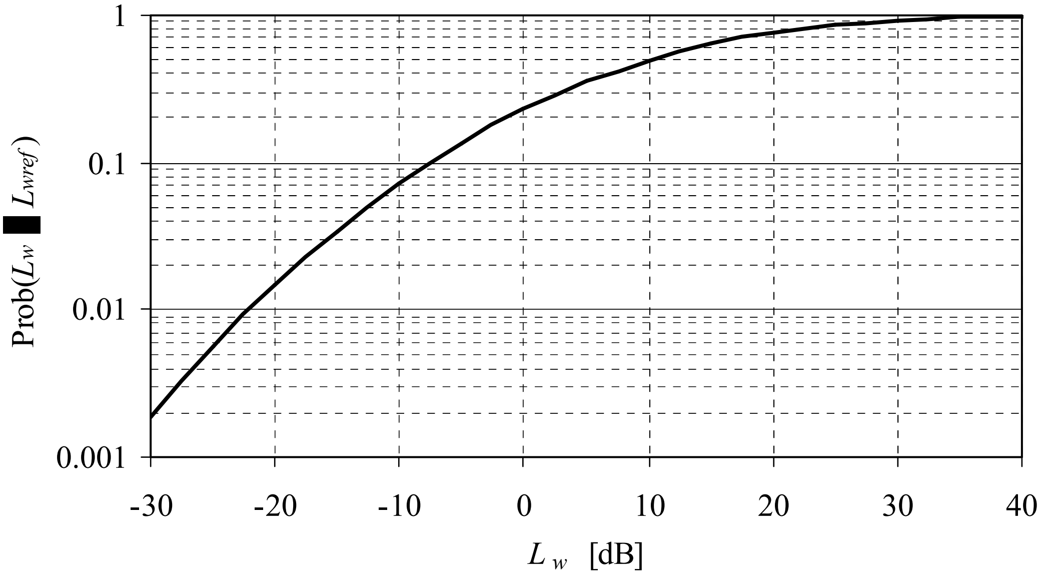

Figure 3.1 – CDF of building attenuation (GSM1800).

COST 231 indoor and building penetration models, being designed for GSM, are not specific for any working frequency; when correctly parameterised, they can be used for evaluating the path loss for UMTS, HIPERLAN/2 and MBS. Nevertheless, its proper parameterisation depends on the results from measurements; the main drawback is that there is not usually many available data for doing a proper assessment in different environments, for the working frequencies being considered; therefore, simple and usually less accurate models, e.g., one-slope model, usually assessed from a few measurements, are commonly used.

3.5. Conclusions

In this chapter, a brief description of GSM, UMTS, HIPERLAN and MBS is made, being mainly focused on working frequency bands and power characteristics. Link budget evaluation is addressed and several useful parameters for this purpose are presented.

Outdoor, indoor and building penetration path loss models, usually used for estimating path loss in different environments are described, and its applicability to the different systems being considered is discussed. Since the propagation phenomena at the millimetre waveband is quite different from the one observed at lower frequencies, a specific path loss model for outdoor MBS environments, which accounts for both rain and oxygen attenuation, is also presented. A general theoretical background on link budget evaluation and path loss estimation is given, allowing to evaluate the cell range in different environments. It should be stressed that a complete system planning procedure involves additional steps such as capacity estimation and quality of service requirements, nevertheless, general considerations on these topics are not drawn, since one is mainly focused on coverage issues.

Chapter 4

Environment-Geometry Based Approach for Fading Depth Evaluation

4.1. Initial Considerations

As previously referred, the received signal level characteristics in relatively narrowband mobile communication systems, such as GSM, are already well known [Pras98]. Nowadays, much of the recent research on mobile communication systems is focused on wideband transmission, providing high data rates, aiming at satisfying the increasing demand for new and better quality services, such as multimedia ones. Nearly existing systems, such as UMTS and HIPERLAN/2, and future ones, MBS, work or are intended to work in the frequency range from 2 to 60 GHz, with bandwidths ranging from a few to several tenths of MHz. Therefore, the study of the signal level at the receiver in wideband transmission systems is a key issue for the development of such systems, as well as for their design, assessment and implementation.

A theoretical model for the study of wideband signals is proposed in [Kozo94]. The proposed model clarifies the fundamental characteristics of signal behaviour, through the theoretical and experimental investigation of the signal level variation at the receiver. The model incorporates physical parameters, such as the number and magnitude of arriving waves, the propagation path lengths, the signal bandwidth, and the carrier frequency. An expression for the received signal level under NLoS is derived and examined for various propagation parameters. A generalisation of this model to the LoS case, and the introduction of a new propagation parameter, the equivalent received bandwidth, defined as the product between the system bandwidth and the maximum difference in propagation path length among different arriving components, can be found in [KoSN96]. Results on the validation of the equivalent received bandwidth to characterise the received signal level variation are presented in [NYMI01].

In this chapter, a simple and computationally inexpensive analytical approach, to study the signal level characteristics in narrow- and wideband systems, is proposed, describing fading depth dependence on the equivalent received bandwidth, and having the Rice factor as a parameter. An expression is obtained through fitting the simulation data from the model in [KoSN96]. This approach aims at eliminating the need for heavy computer simulations, while allowing the determination of the fading depth through the evaluation of a simple equation. Applications examples for different systems, e.g., GSM, UMTS, HIPERLAN/2 and MBS, working in macro-, micro- and pico-cellular environments are shown, giving some insight into the fading depth behaviour for different systems working in different environments.

4.2. Channel Model

The model presented in [KoSN96], being suited for macro-, micro- and pico-cellular environments, has been assessed from outdoor measurements, and used for deriving several results on the observed fading depth and correlation properties of the received signal in wideband mobile communication systems [YaKo99], [NYMI01], [ZhRV01], [NaKo02]. It will be used as the basis for deriving the proposed approach.

The model, depicted in Figure 4.1, assumes that multipath waves arrive at the MT under the following conditions:

(i) each of the M arriving waves (M-1 reflected and/or diffracted, plus the LoS one) has a path length l_i, which is independent and uniformly distributed within a given range. The angles of arrival, φ_i (i >1), are independent and uniformly distributed in a horizontal plane over an angle of 2π;

(ii) each arriving wave has magnitude a_i (i >1), which is also independent and uniformly distributed within a given range;

(iii) the magnitude of the LoS wave is a_1, its path length l_1 is the minimum path length among the arriving waves, and $\varphi_1 = 0^{\circ}$;

(iv) the bandwidth of each arriving wave is greater than the receiver bandwidth, B, and the power spectral density is assumed flat and centred on f_c.

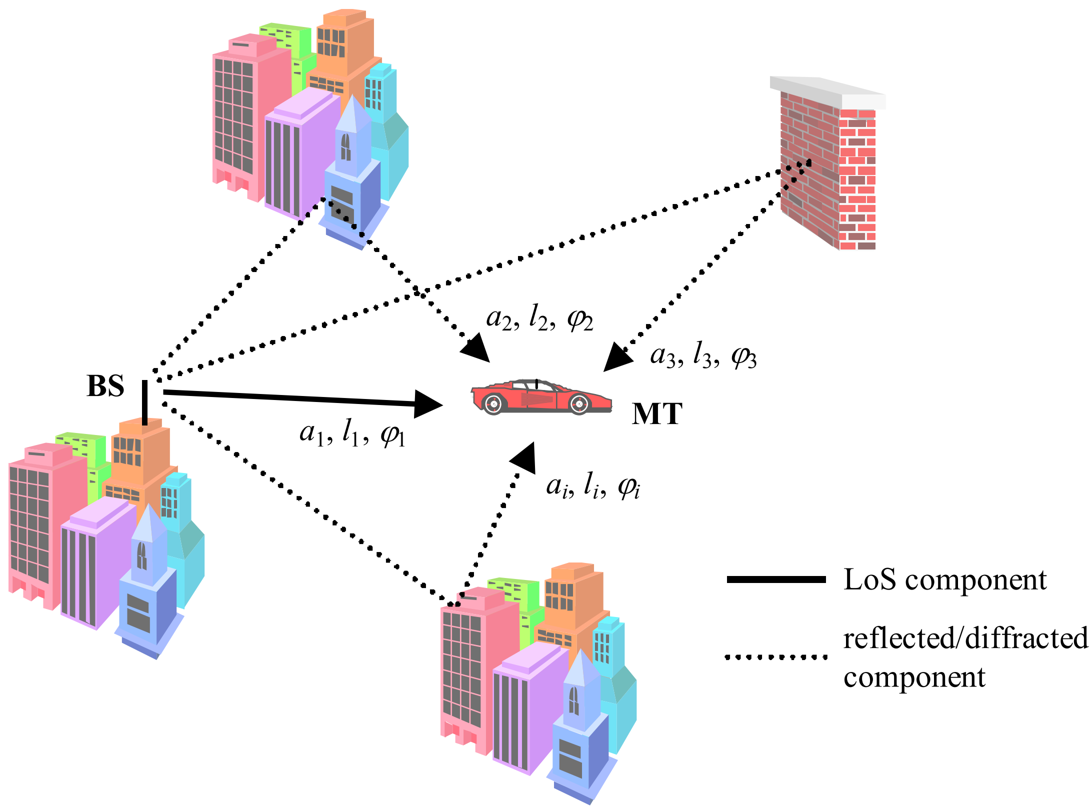

Figure 4.1 – Propagation model.

For the model shown in Figure 4.1, it is assumed that the received signal magnitude at frequency f, $a(f)$, is expressed by [Kozo94]

$$a(f) = \sum_{i=1}^{M} a_i \cdot \cos(2\pi f t + \psi_i) \tag{4.1}$$

where

$$\psi_i = \frac{2\pi \cdot l_i}{\lambda} \tag{4.2}$$

and λ is the wavelength. Therefore, expanding (4.1) one obtains

$$\begin{aligned} |a(f)| &= \left(\sum_{i=1}^{M} \sum_{j=1}^{M} a_i \cdot a_j \cdot [\cos(\psi_i) \cdot \cos(\psi_j) + \sin(\psi_i) \cdot \sin(\psi_j)] \right)^{\frac{1}{2}} \\ &= \left(\sum_{i=1}^{M} \sum_{j=1}^{M} a_i \cdot a_j \cdot \cos\left(\frac{2\pi}{c} \cdot f \cdot \Delta l_{ij} \right) \right)^{\frac{1}{2}} \end{aligned} \tag{4.3}$$

where the parameter Δl_{ij}, associated to the difference between path lengths, varies in time depending on the MT speed, v_{MT}, and on the angles of arrival, φ_i,

$$\Delta l_{ij} = l_i - l_j - v_{MT} \cdot t \cdot \left[\cos(\varphi_i) - \cos(\varphi_j)\right] \tag{4.4}$$

The received power is then obtained by integrating the square of $|a(f)|$ over the whole receiver bandwidth

$$P_r = \int_{f_c - B/2}^{f_c + B/2} |a(f)|^2 \cdot df = B \cdot \left(\sum_{i=1}^{M} a_i^2 + \sum_{i=1}^{M} \sum_{\substack{j=1 \\ i \neq j}}^{M} a_i \cdot a_j \cdot \left[\cos\left(\frac{2\pi}{c} \cdot f_c \cdot \Delta l_{ij}\right) \cdot \frac{\sin\left(\frac{\pi}{c} \cdot B \cdot \Delta l_{ij}\right)}{\frac{\pi}{c} \cdot B \cdot \Delta l_{ij}} \right] \right) \tag{4.5}$$

The first term of (4.5) represents the mean value of the wideband received power, and the second one its instantaneous variation around the mean value. As usual, the Rice factor is defined as the power ratio between the LoS component and the reflected/diffracted ones

$$K = \frac{a_1^2}{\sum_{i=2}^{M} a_i^2} \tag{4.6}$$

In order to clarify the characteristics of the received signal, as a function of system bandwidth and environment specific features, a new propagation parameter, the equivalent received bandwidth, w_l, is proposed, which is defined as the product between the system bandwidth, B, and the maximum possible difference in the propagation path length, Δl_{max},

$$w_{l[\mathrm{Hz \cdot m}]} = B_{[\mathrm{Hz}]} \cdot \Delta l_{max[\mathrm{m}]} \tag{4.7}$$

with

$$\Delta l_{max} = \max\left|\Delta l_{ij}\right| \quad , \quad i \neq j \tag{4.8}$$

The relation between this new parameter and the fading depth was evaluated, and it was found that they are closely related; globally, it can be stated that the fading depth decreases as w_l increases. This is not surprising, since as one can observe from (4.5) the received power variation around the mean value is highly dependent on the value of

$$\cos\left(\frac{2\pi}{c} \cdot f_c \cdot \Delta l_{ij}\right) \cdot \frac{\sin\left(\frac{\pi}{c} \cdot B \cdot \Delta l_{ij}\right)}{\frac{\pi}{c} \cdot B \cdot \Delta l_{ij}} \tag{4.9}$$

therefore, decreasing as $B \cdot \Delta l_{ij}$ increases. It should be noted that $f_c >> B$, hence, the second term of (4.9) varies much slower than the first one, limiting the variation range of (4.9), hence, the received power variation around the mean value.

4.3. Simulation Results

The model has been implemented in C programming language, aiming at reducing the computational burden needed for performing simulations. Random parameters, e.g., a_i, l_i and φ_i, were generated using C standard built-in functions. As far as flexibility is concerned, consecutive simulations were carried out, by specifying a list of input parameters for each simulation.

In order to assess the fading depth dependence on w_l, as a function of the Rice factor, K, computer simulations were carried out. The carrier frequency was set to 60 GHz, a candidate for future MBS; however, according to [Kozo94] and [KoSN96], the fading depth is practically independent of the carrier frequency, so these results can be applied, with some degree of accuracy, to systems operating at different carrier frequencies. As suggested in [Kozo94], the number of arriving waves should be chosen large enough in order for the results to become almost independent of it; a value of $M = 11$ (10 reflected/diffracted waves, plus the LoS one) was chosen in order to reduce the computational effort required for performing simulations, while being sufficiently large as required. Parameter w_l ranges from 0.01 to 1 000 000 MHz·m, and different values of K are considered (0, 3, 5, 7, 10, and 20 dB).

Under these conditions, and for each combination of K and w_l, 10 000 points are evaluated from (4.5). The fading depth is computed as the difference in signal power corresponding to p and 50 % of the CDF of the relative (referenced to its mean value) received power, Figure 4.2.

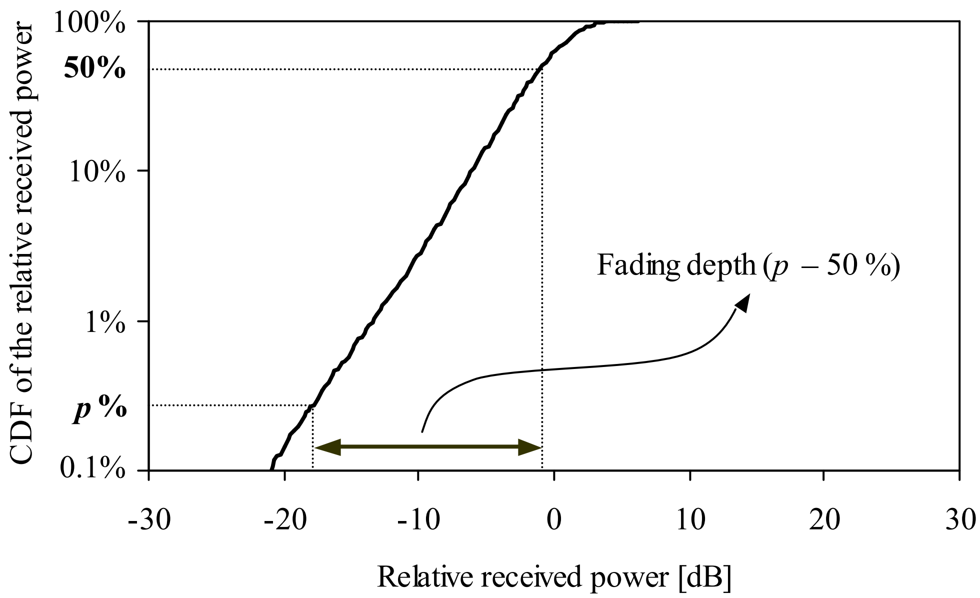

Figure 4.2 – Fading depth evaluation.

The fading depth presents some randomness due to the random behaviour of some parameters. In order to reduce this inherent randomness, six simulations were carried out for each combination of K and w_l; this value was chosen in order to achieve reasonable results, while keeping the simulation time within acceptable limits. The average value of the fading depth is computed as the mean value obtained from each set of simulations. The average fading depth, for p = 0.1, 1 and 10 %, is represented in Figure 4.3 to Figure 4.5; detailed data can be found in Appendix I.

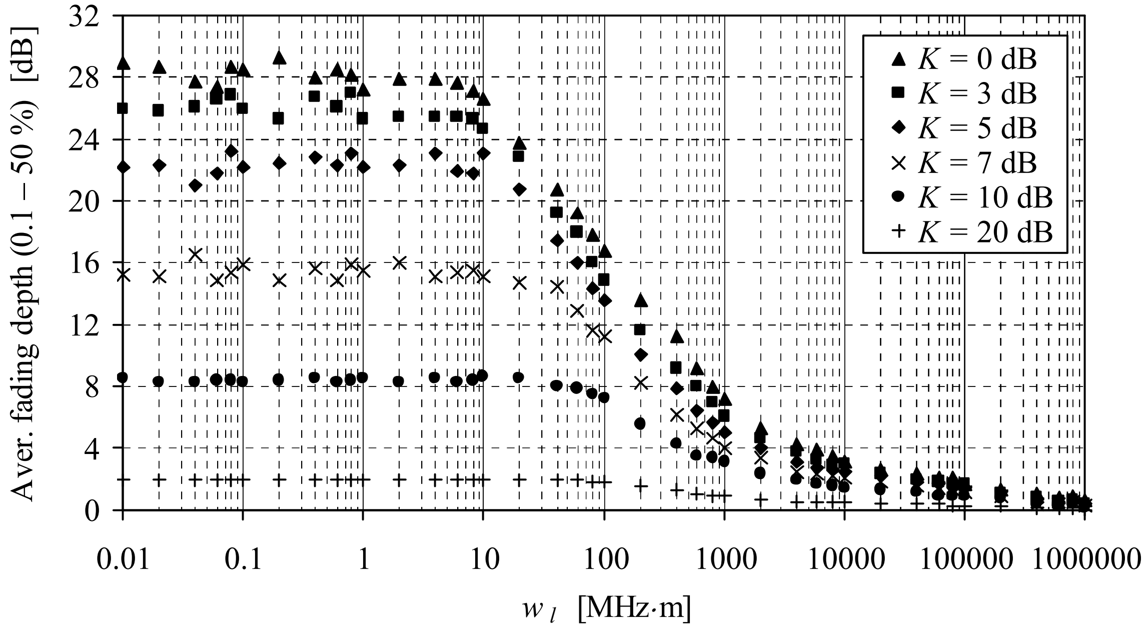

Figure 4.3 – Average fading depth, p = 0.1 %.

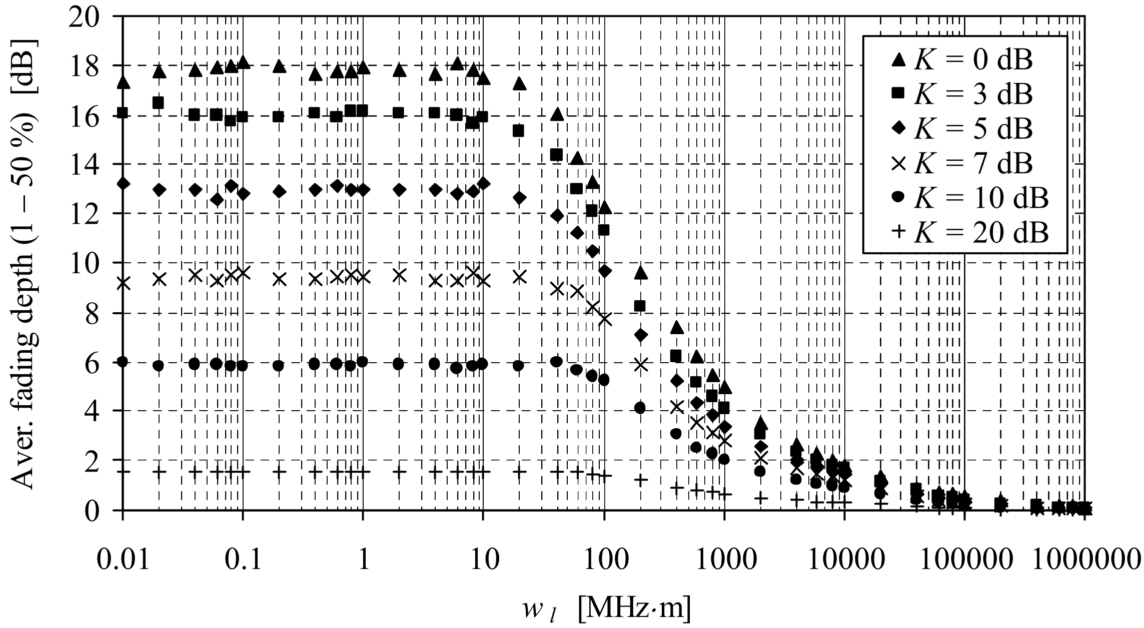

Figure 4.4 – Average fading depth, p = 1 %.

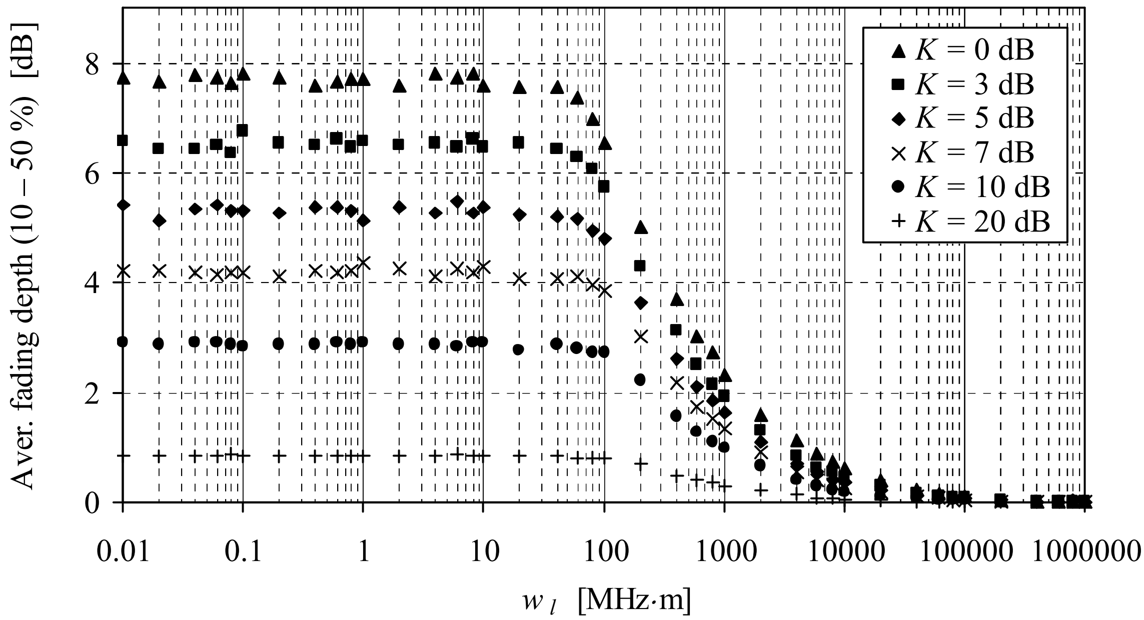

Figure 4.5 – Average fading depth, p = 10 %.

For each value of p and K, 41 values of fading depth (for different values of w_l) were evaluated, the different values of w_l being chosen in order to reasonably cover the range of variation of the parameter, i.e., $0.01 < w_l < 1\,000\,000$ MHz·m. For the given simulation parameters, the evaluation of the data in each figure correspond to a simulation time of approximately 3h16 on a 933 MHz Pentium® III processor with 128 MB of RAM.

From the results, it can be observed that the fading depth is almost constant until a specific value of w_l is reached, after which it decreases; this breakpoint value depends on p, increasing as it increases. Hence, two different behaviours are observed; the first one, in which the fading depth remains constant and almost independent of w_l, corresponds to the narrowband situation, and the second one, for which the fading depth decreases as w_l increases, therefore, corresponding to the wideband case. It should be stressed that the narrow- or wideband nature of the propagation channel, depends not only on B, but also on the coherence bandwidth of the propagation channel, therefore, being related to Δl_{max}.

For the same value of w_l, the fading depth becomes shallower as K increases; this is not surprising, since an increase in K corresponds to an increased contribution of the LoS wave, hence, reducing the influence of the reflected/diffracted ones. Concerning the dependence on p, one can see that, as expected, the fading depth decreases as p increases. One must note that p defines the length of the fading depth evaluation interval, a larger value of p representing a narrower fading depth evaluation interval.

The rate at which the fading depth decreases for values of w_l above the breakpoint depends on both p and K, decreasing as these parameters increase. Regarding K, when the contribution of the LoS component becomes more significant (higher values of K), the decreasing rate goes smaller, i.e., the power at the receiver becomes less sensitive to w_l, i.e., there is a weaker dependence on system bandwidth and environment characteristics. Concerning the dependence on p, as it increases the maximum levels of the fading depth decrease and the breakpoint value increases; however, the increase in the breakpoint is not significant, compared to the decrease of the maximum level of fading depth, which causes the reduction in the fading depth decreasing rate.

Since one is making a statistical analysis, it is of relevance to characterise the standard deviation of fading depth for different values of p, Appendix I. As expected, for each value of p, the standard deviation decreases as w_l increases, since the absolute value of fading depth decreases. The standard deviation is usually lower than 1.5, 0.7 and 0.35 dB, for $p = 0.1$, 1 and 10%, respectively; for $p = 0.1$ % a worst value of 2.4 dB is observed.

4.4. Analytical Approximation

From the analysis of the simulated data, one can extract that the fading depth, measured between p and 50 % of the CDF of the received signal power, can be approximated by[2]

$$FD_p(K, w_l)_{[\mathrm{dB}]} = \begin{cases} S_p(K) & , \quad w_l \leq w_{b,p} \\ \dfrac{S_p(K) - A_{1,p}(K)}{1 + A_{2,p}(K) \cdot \left[\log\left(\dfrac{w_l}{w_{b,p}} \right) \right]^{A_{3,p}(K)}} + A_{1,p}(K) & , \quad w_l > w_{b,p} \end{cases} \tag{4.10}$$

where $FD_p(K, w_l)$ is the fading depth (in decibel) measured between p and 50 % of the CDF of the received power, and $w_{b,p}$ is the breakpoint, defined as the value of w_l for which the fading depth starts to decrease, hence, experiencing lower values than the ones observed for the narrowband case. The mathematical functions, $S_p(K)$, $A_{1,p}(K)$, $A_{2,p}(K)$ and $A_{3,p}(K)$ must be chosen to be simple enough, in order not to unnecessarily increase the mathematical complexity of the proposed approach, while allowing a good fitting between (4.10) and the simulated data obtained from (4.5). Using a simplifying notation, from now on, whenever there is no confusion about the value of p and the dependence on K, functions $S_p(K)$, $A_{1,p}(K)$, $A_{2,p}(K)$ and $A_{3,p}(K)$ are referred as S, A_1, A_2 and A_3, respectively. The breakpoint value, $w_{b,p}$, is

[2] The proposed matemathical equation was derived empirically.

assumed as 4, 10 and 40 MHz·m for $p =$ 0.1, 1, 10 % respectively. For each value of p, the fitting process consists of the evaluation of S, A_1, A_2 and A_3 that fit the simulated data as a function of K. Results for p = 0.1, 1, 10 % are presented in Table 4.1.

Table 4.1 – Fitted parameters and associated error.

	p [%]	K [dB] 0	3	5	7	10	20
S [dB]	0.1	28.22	26.01	22.38	15.44	8.38	1.95
	1.0	17.81	15.98	12.98	9.41	5.86	1.51
	10.0	7.68	6.51	5.30	4.18	2.87	0.84
A_1 [dB]	0.1	-1.44	-0.67	-0.04	0.00	0.00	0.00
	1.0	-0.84	-0.53	-0.27	-0.08	-0.05	-0.04
	10.0	-0.52	-0.32	-0.24	-0.17	-0.10	-0.03
A_2	0.1	0.315	0.317	0.258	0.135	0.072	0.045
	1.0	0.414	0.423	0.348	0.236	0.163	0.113
	10.0	0.973	1.009	0.950	0.848	0.757	0.637
A_3	0.1	2.259	2.473	2.867	3.310	3.523	3.530
	1.0	2.427	2.575	2.850	3.218	3.403	3.392
	10.0	2.019	2.251	2.349	2.533	2.702	2.842
$\sqrt{\overline{\varepsilon^2}}$ [dB]	0.1	0.50	0.40	0.43	0.40	0.23	0.06
	1.0	0.15	0.15	0.16	0.05	0.11	0.03
	10.0	0.08	0.07	0.07	0.06	0.04	0.01
$\overline{\varepsilon_r}$ [%]	0.1	-0.8	0.8	2.5	4.3	4.2	2.9
	1.0	-0.6	-0.7	-0.4	0.2	0.5	0.4
	10.0	-6.4	-6.4	-5.3	-5.2	-7.0	-7.7

The *rms* error and mean relative error are evaluated from [Leon93]

$$\sqrt{\overline{\varepsilon^2}} = \sqrt{\frac{1}{n_s}\sum_{i=1}^{n_s}\varepsilon_i^2} \tag{4.11}$$

$$\overline{\varepsilon_r} = \frac{1}{n_s}\sum_{i=1}^{n_s}\left(\frac{\varepsilon_i}{y_i}\right) \tag{4.12}$$

with ε_i defined as

$$\varepsilon_i = y_i - \hat{y}_i \tag{4.13}$$

where y_i corresponds to the value obtained from simulation, and $\hat{y}_i$ to the one estimated from (4.10). The parameter n_s stands for the number of samples (interpolation points).

The fitting process is based on the least-squares technique, being implemented in two steps: first, the range of variation of y_i is identified, and then, $\hat{y}_i$ is estimated as the one that minimises the mean square error.

Since the fading depth for values of w_l greater than 100 000 tend to zero, the mean relative error tends to infinity and the *rms* error is negligible, hence, the results in Table 4.1 are obtained for w_l ranging from 0.01 to 100 000 MHz·m.

As one can see from Table 4.1, the relative error and the *rms* error are acceptable, ranging from -7.7 to 4.3 % and 0.01 to 0.5 dB, respectively. The error standard deviation is not presented, since its values are similar to the ones of the *rms* error. One can then conclude that the error from this approximation is negligible.

From the analysis of Table 4.1, one can note that, for each value of p, the fitting of S, A_1, A_2 and A_3, as a function of K, can be obtained from

$$S_{[\mathrm{dB}]} = \frac{(b_1 - b_2)}{1 + b_3 \cdot \left(\frac{K_{[\mathrm{dB}]}}{10} - b_4 \right)^{b_5}} + b_2 \tag{4.14}$$

$$A_{1[\mathrm{dB}]} = c_{11} \cdot \arctan\left(c_{12} \cdot K_{[\mathrm{dB}]} - c_{13}\right) - c_{14} \tag{4.15}$$

$$A_2 = c_{21} \cdot \left[\frac{\pi}{2} - \arctan\left(c_{22} \cdot K_{[\mathrm{dB}]} - c_{23}\right)\right] + c_{24} \tag{4.16}$$

$$A_3 = c_{31} \cdot \arctan\left(c_{32} \cdot K_{[\mathrm{dB}]} - c_{33}\right) + c_{34} \tag{4.17}$$

where parameters b_j $\{j = 1, \ldots, 5\}$ and c_{ik} $\{i = 1, \ldots, 3; k = 1, \ldots, 4\}$ depend on the value of p. The parameters b_j and c_{ik}, derived from the fitting of data in Table 4.1, with p = 1 %, are presented in Table 4.2 and Table 4.3.

Table 4.2 – Fitting of *S* and associated error, *p* = 1 %.

S						
b_1	b_2	b_3	b_4	b_5	$\sqrt{\overline{\varepsilon^2}}$ [dB]	$\overline{\varepsilon_r}$ [%]
18.089	0.569	0.939	-0.298	3.593	0.13	-0.6

Table 4.3 – Fitting of A_i and associated error, $p = 1$ %.

	A_1	A_2	A_3
c_{i1}	0.328	0.118	0.351
c_{i2}	0.553	0.486	0.720
c_{i3}	1.810	3.020	3.750
c_{i4}	0.489	0.099	2.907
$\sqrt{\overline{\varepsilon^2}}$	0.024	0.012	0.026
$\overline{\varepsilon_r}$ [%]	1.3	-0.2	0.0

As one can observe, the relative error and the *rms* error are acceptable, ranging from -0.6 % for S to 1.3 % for A_1, and 0.012 for A_2 to 0.13 dB for S, respectively. The error standard deviation is not presented for reasons similar to the previous case. Figure 4.6 illustrates the fitting results: the dots correspond to the results from Table 4.1, and the lines are obtained from the analytical approach with the parameterisation in Table 4.2 and Table 4.3.

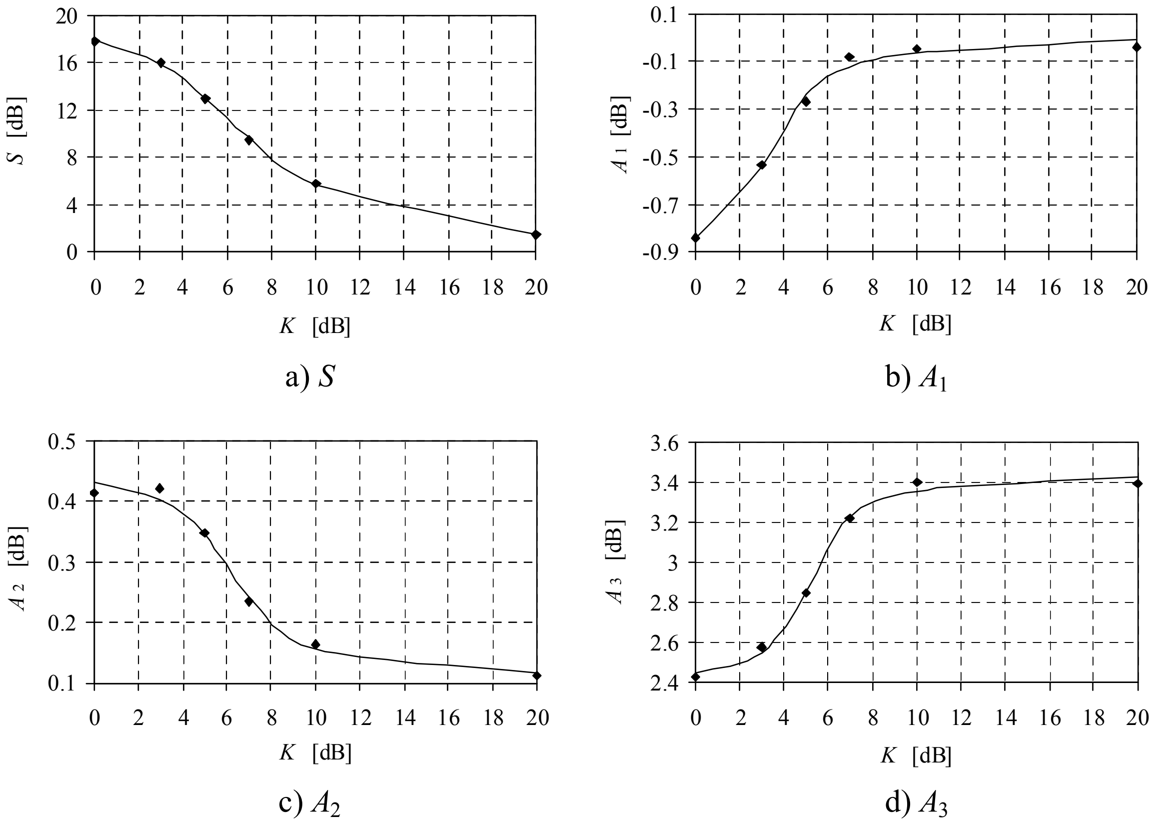

Figure 4.6 – Fitting of parameters S, A_1, A_2 and A_3, $p = 1$ %.

As described, the complete fitting process, for each value of p, consists of the following:

(i) find S, A_1, A_2 and A_3, that fits (4.10) to the simulated data, for the given values of K;

(ii) find the parameters b_j and c_{ik} that fits (4.14), (4.15), (4.16) and (4.17) to the values of S, A_1, A_2 and A_3 obtained in (i).

The approximate values of S, A_1, A_2 and A_3, evaluated from (4.14), (4.15), (4.16) and (4.17), are presented in Table 4.4. It must be noted that the *rms* error and the relative error are evaluated for w_l ranging from 0.01 to 100 000 MHz·m, for reasons similar to the previous case. With the parameterisation of S, A_1, A_2 and A_3, in Table 4.4, the fading depth for each value of K, can be evaluated from (4.10). The result from this evaluation corresponds to the solid lines in Figure 4.7, dots representing the simulated data.

Table 4.4 – Calculated parameters and associated error, p = 1 %.

	K [dB]					
	0	3	5	7	10	20
S [dB]	17.89	15.84	12.94	9.64	5.73	1.46
A_1 [dB]	-0.84	-0.54	-0.24	-0.12	-0.06	-0.01
A_2	0.432	0.403	0.347	0.241	0.158	0.116
A_3	2.447	2.553	2.855	3.227	3.359	3.425
$\sqrt{\overline{\varepsilon^2}}$ [dB]	0.19	0.20	0.16	0.22	0.16	0.05
$\overline{\varepsilon_r}$ [%]	2.2	-3.2	-0.9	0.6	0.9	1.2

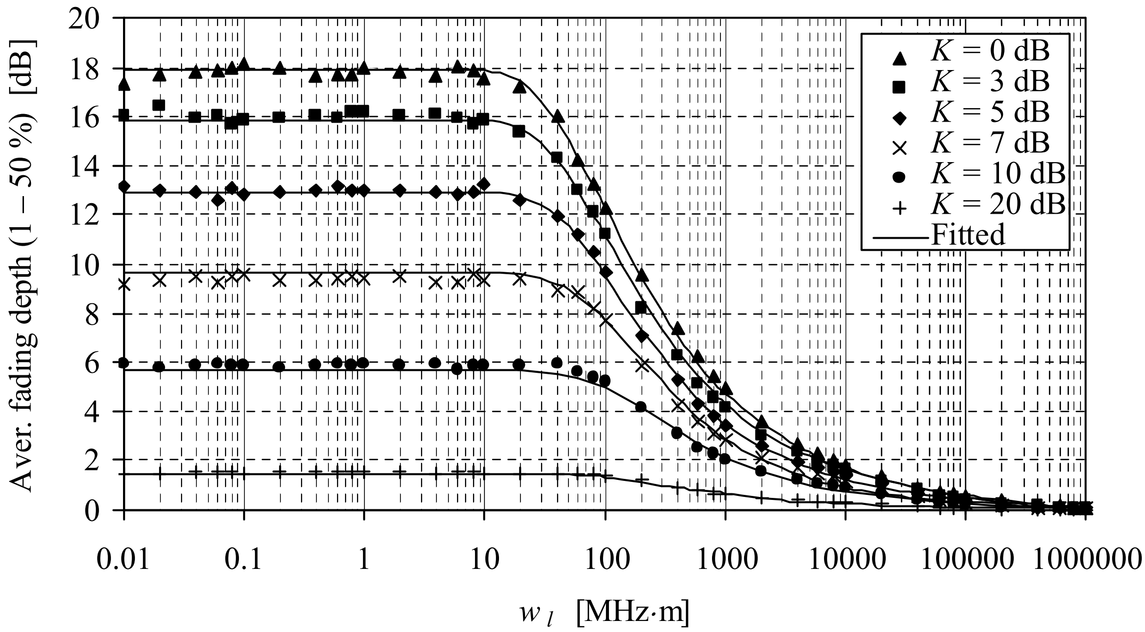

Figure 4.7 – Fading depth fitting results, p = 1 %.

The approximation relative error is depicted in Figure 4.8. It must be noted that as the fading depth approaches zero the relative error tends to infinity. However, these values are not significant, since they only represent a variation around a fading depth value that is virtually zero. In general, it can be stated that the approximation error is comprised between 0.0 and 5.0 %, for the range of interest. Similar results, obtained with p = 0.1 % and p = 10 %, can be found in Appendix I.

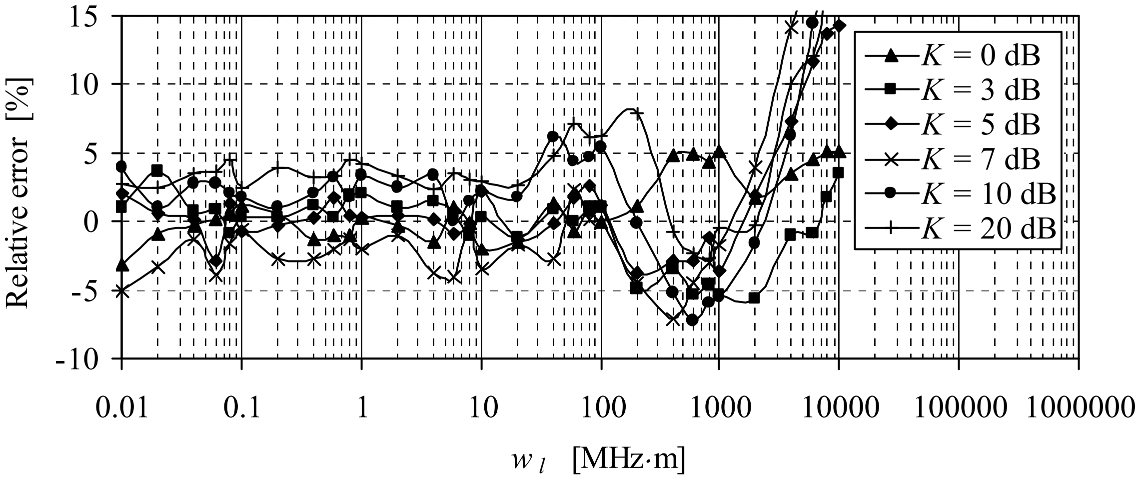

Figure 4.8 – Approximation relative error, p = 1 %.

As one can see from (4.10), the function S represents the maximum possible value of fading depth for any given value of K, i.e., the one observed for the narrowband case. The dependency of S on K, as a function of p, evaluated from (4.14) is represented in Figure 4.9; the dots correspond to the value of S for the given values of p, and the lines to the fading depth evaluated from considering the Rice distribution for the same values of p.

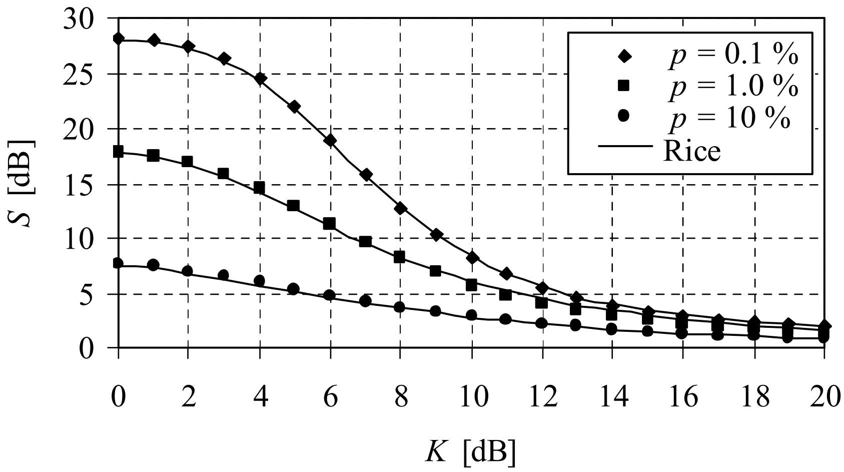

Figure 4.9 – Dependence of S on K, having p as a parameter.

It can be observed that S depends on K in a similar way as FD_p (K, w_l) depends on w_l; as it was expected, the value of S decreases with increasing values of p. It must be remembered that p defines the fading depth evaluation interval, with the higher value of p corresponding to the narrower fading depth evaluation interval. Moreover, both S and the fading depth obtained from the Rice distribution are practically superimposed, therefore, the proposed approach, is appropriate for evaluating the fading depth in narrow- (for which it gives similar results as the ones obtained from the Rice distribution) and wideband systems.

4.5. Application Examples

4.5.1. Micro-Cellular Environments

Once correctly parameterised, the evaluation of the fading depth is straightforward. By representing the fading depth dependence on w_l, as a function of K, for different systems working in typical environments (characterised by their morphological and physical properties), one can easily obtain a range of possible values for the fading depth, depending on the system bandwidth and environment specific features that influence the values of w_l and K. Such a result is of great usefulness for the design, assessment and implementation of mobile communication systems.

In order to illustrate the application, one considers a typical micro-cellular environment, an urban street about 1 km long. The BS is positioned above rooftops, at 25 m high, and the MT can move along the axis of the street at 1.5 m high, Figure 4.10.

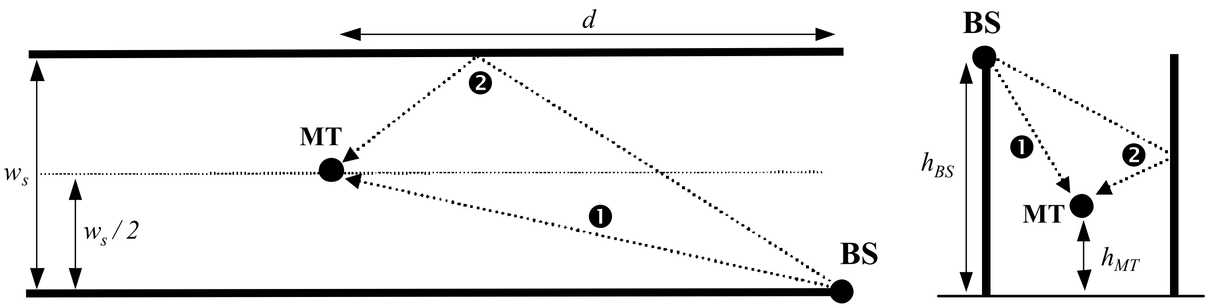

Figure 4.10 – Urban street environment.

As a first approach, only first order reflections from building walls and ground are considered (two-path model); this model has been found to be appropriate for LoS micro-cellular urban environments [Rapp96]. For simplification, BS and MT antennas are assumed as isotropic, and no polarisation influence is considered.

In order to assess the fading depth dependence on the street width, it is assumed that it can range from 15 to 60 m. Within this environment, the maximum difference in propagation path length, Δl_{max}, at the distance d, results from a wall reflection, and can be evaluated from the path length difference between the LoS component, marked as ❶ in Figure 4.10, and the reflected one, marked as ❷

$$\Delta l_{max}(d) = \sqrt{\left(\frac{3w_s}{2}\right)^2 + d^2 + \Delta h_{BS-MT}^2} - \sqrt{\left(\frac{w_s}{2}\right)^2 + d^2 + \Delta h_{BS-MT}^2} \quad (4.18)$$

with

$$\Delta h_{BS-MT} = h_{BS} - h_{MT} \quad (4.19)$$

where h_{BS} and h_{MT} correspond to the BS and MT heights respectively, and w_s is the street width.

Note that, depending on the street width and on the BS and MT antennas positioning and characteristics, the maximum difference in propagation path length difference can result from a floor reflection rather than a wall one, meaning that a new equation for Δl_{max} has to be derived.

Within this environment, different systems are considered: GSM, UMTS, HIPERLAN/2, and MBS1 (B = 50 MHz) and MBS2 (B = 100 MHz) standing for possible fourth generation systems. Although HIPERLAN/2 and MBS are intended to work mainly in pico-cellular environments, they are considered here, since one can assume that for lower values of d the conclusions derived for the micro-cellular environment can be applied, with some restrictions, to the case of a pico-cellular one. The results corresponding to larger distances can also be of usefulness, if one considers the study of future implementations of HIPERLAN/2 and MBS within micro-cellular environments.

In order to gain some insight into the fading depth dependence on the street width, as a function of d, three distinct situations are considered, d = 0, 500, 1 000 m. The first is the one yielding the best results regarding fading depth, since smaller fading depths are usually verified near the BS; the last one corresponds to the worst case, which occurs when the MT is in the vicinity of the cell range, assumed as 1 km long. Results for different values of d and w_s are presented in Table 4.5; for illustration, results for d = 500 m are presented in Figure 4.11 (results for d = 0 and 1 000 m can be found in Appendix I), the coloured zones associated to each system correspond to the possible values of w_l for a street width ranging from 15 to 60 m; the leftmost part of each zone corresponding to narrower streets.

Table 4.5 – Equivalent received bandwidth for different values of d and w_s.

System	w_l [MHz·m]					
	d = 0 m		d = 500 m		d = 1 000 m	
	w_s		w_s		w_s	
	15 m	60 m	15 m	60 m	15 m	60 m
GSM	1.57	10.98	0.09	1.43	0.04	0.72
UMTS	39.33	274.55	2.25	35.65	1.12	17.95
HIPERLAN/2	157.34	1 098.18	8.99	142.57	4.50	71.82
MBS1	393.34	2 745.45	22.50	356.50	11.25	179.55
MBS2	786.68	5 490.91	45.00	713.00	22.49	359.09

As one can observe, as d increases, a significant reduction of w_l is verified, therefore, significantly increasing the possible values of fading depth observed for the different systems being considered. This is not surprising, since higher fading depths are usually observed at larger distances between the BS and the MT. Concerning the dependence on w_s, small values of w_l are observed in narrower streets, thus, higher fading depths are expected.

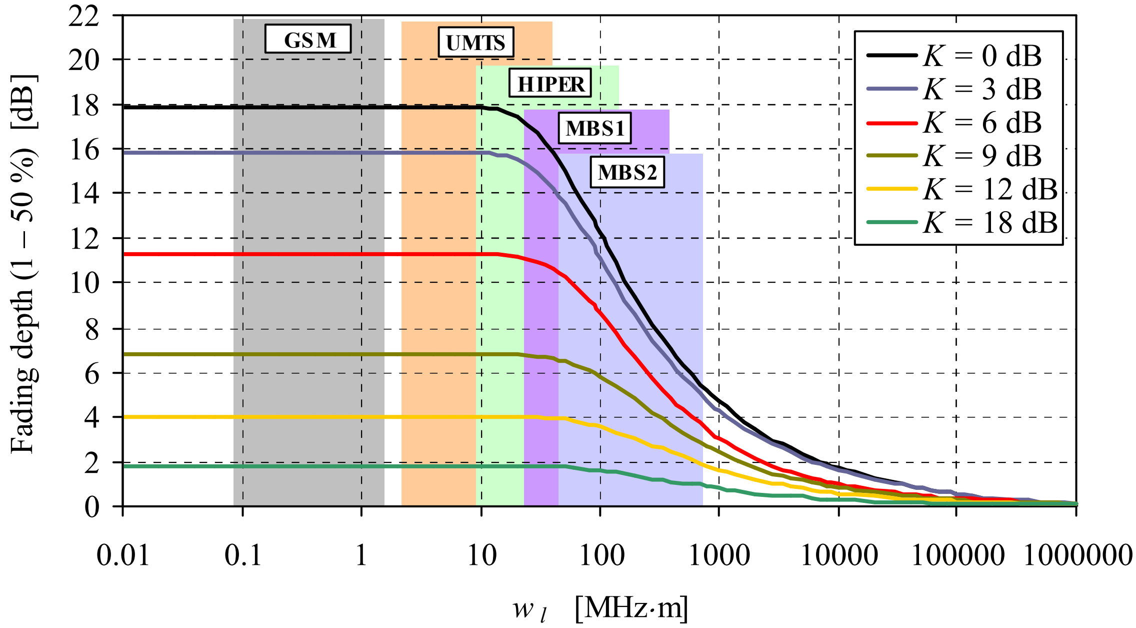

Figure 4.11 – Fading depth at d = 500 m.

For a given value of K, e.g., K = 6 dB, one can extract values for the fading depth, depending on the street width, the system bandwidth, and the distance between the BS and the MT, as presented in Table 4.6 and illustrated in Figure 4.12 and Figure 4.13.

Table 4.6 – Fading depth for K = 6 dB.

System	$FD_{1\%}$ [dB]					
	d = 0 m		d = 500 m		d = 1 000 m	
	w_s		w_s		w_s	
	15 m	60 m	15 m	60 m	15 m	60 m
GSM	11.3	11.3	11.3	11.3	11.3	11.3
UMTS	10.6	5.8	11.3	10.7	11.3	11.2
HIPERLAN/2	7.4	2.9	11.3	7.7	11.3	9.5
MBS1	4.9	1.9	11.1	5.1	11.3	7.0
MBS2	3.5	1.3	10.4	3.7	11.1	5.1

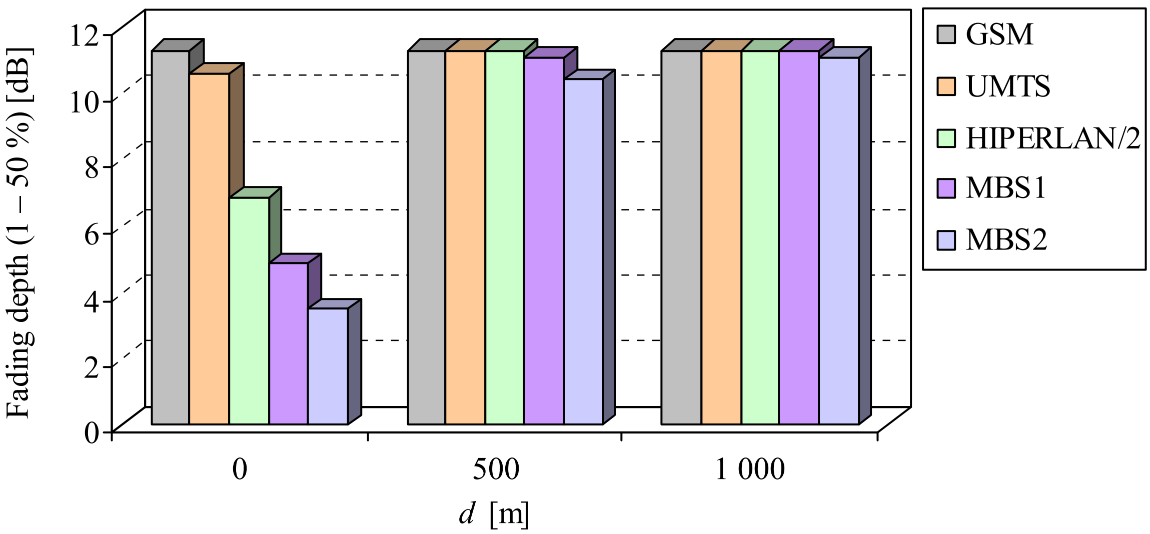

Figure 4.12 – Fading depth in the micro-cellular environment, K = 6 dB, w_s = 15 m.

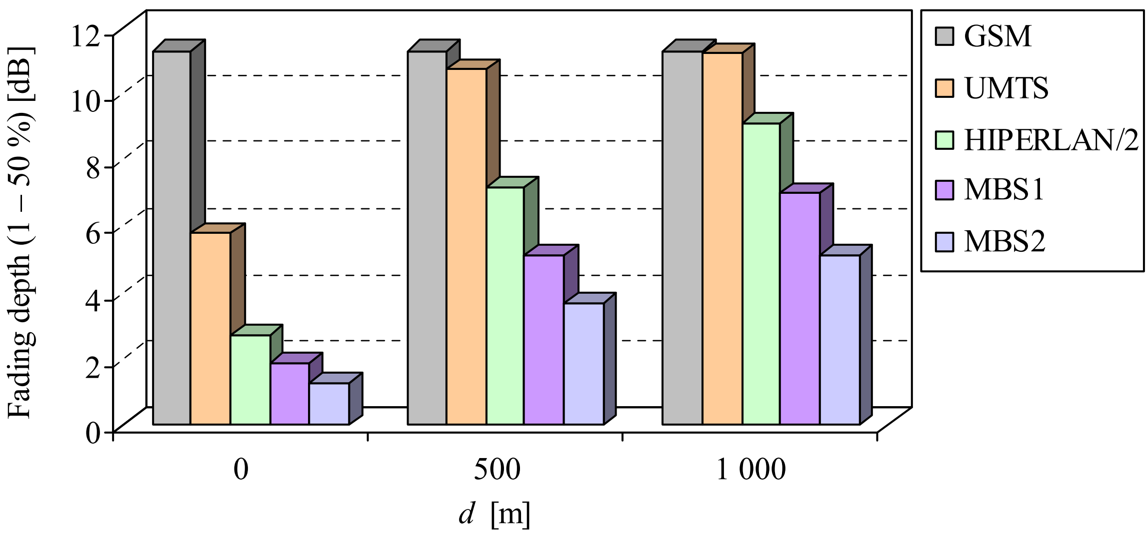

Figure 4.13 – Fading depth in the micro-cellular environment, K = 6 dB, w_s = 60 m.

When the MT is several hundreds of metres away from the BS, e.g., $d = 500$ m and $d = 1\,000$ m, and for a street width of 15 m, a fading depth about 11 dB is observed for each of the considered system bandwidths. For wider streets, e.g., $w_s = 60$ m, the dependence on system bandwidth becomes more significant; one can observe that, when d is comprised between 500 and 1 000 m, the fading depth experienced by HIPERLAN/2, MBS1, and MBS2 is below the one for GSM by 1.8 to 3.6, 4.3 to 6.2, and 6.2 to 7.6 dB, respectively. If one considers UMTS, there is no significant dependence on street width, and the observed fading depth is approximately the same as for GSM. Considering the MT in the close vicinity of the BS, e.g., $d = 0$ m, the dependence of fading depth on system bandwidth and street width increases. When the street width ranges from 15 to 60 m, the fading depth experienced by UMTS, HIPERLAN/2, MBS1, and MBS2 is below the one for GSM by 0.7 to 5.5, 3.9 to 8.4, 6.4 to 9.4, and 7.8 to 10.0 dB respectively.

As expected, GSM behaves always as a narrowband system, hence, experiencing the larger fading depths. UMTS, HIPERLAN/2 and MBS usually behave as wideband ones, nevertheless, in narrower streets, and for large values of d, they can be considered as being narrowband, since the observed fading depths are almost the same as the one for GSM.

4.5.2. Pico-Cellular Environments

To illustrate a possible application to the case of pico-cellular environments, one can consider a square room with the BS positioned in its middle. A geometrical based approach, such as the one used for the micro-cells, can be applied in order to evaluate the value of Δl_{max}, depending on the environment characteristics and the MT position in the room. However, for illustrative purposes, it seems reasonable to assume a value of Δl_{max} equal to the room width, and independent of the MT position in the room. This results from considering that the scattering objects are placed around the BS within a radius of about one half of the room width, r_w, as proposed in [Corr01], which corresponds to consider that the given pico-cellular environment is modelled by a GBSBCM as described in Chapter 2. The value of w_l as a function of Δl_{max}, for the pico-cellular environment is presented in Table 4.7. The fading depth for $K = 6$ dB is presented in Table 4.8 and illustrated in Figure 4.14. One can observe that, within the considered pico-cellular environment, the fading depth experienced by UMTS and GSM is similar, and that the dependence on room width is not significant. HIPERLAN/2, MBS1, and MBS2 experience fading depths of 2.6 to 4.6, 5.2 to 6.9, and 6.9 to 8.2 dB below the ones for GSM, as a function of the room width.

Table 4.7 – Equivalent received bandwidth for the pico-cellular environment.

System	w_l [MHz·m] r_w 5 m	w_l [MHz·m] r_w 10 m
GSM	1	2
UMTS	25	50
HIPERLAN/2	100	200
MBS1	250	500
MBS2	500	1 000

Table 4.8 – Fading depth for *K* = 6 dB.

System	$FD_{1\%}$ [dB] r_w 5 m	$FD_{1\%}$ [dB] r_w 10 m
GSM	11.3	11.3
UMTS	11.1	10.2
HIPERLAN/2	8.7	6.7
MBS1	6.1	4.4
MBS2	4.4	3.1

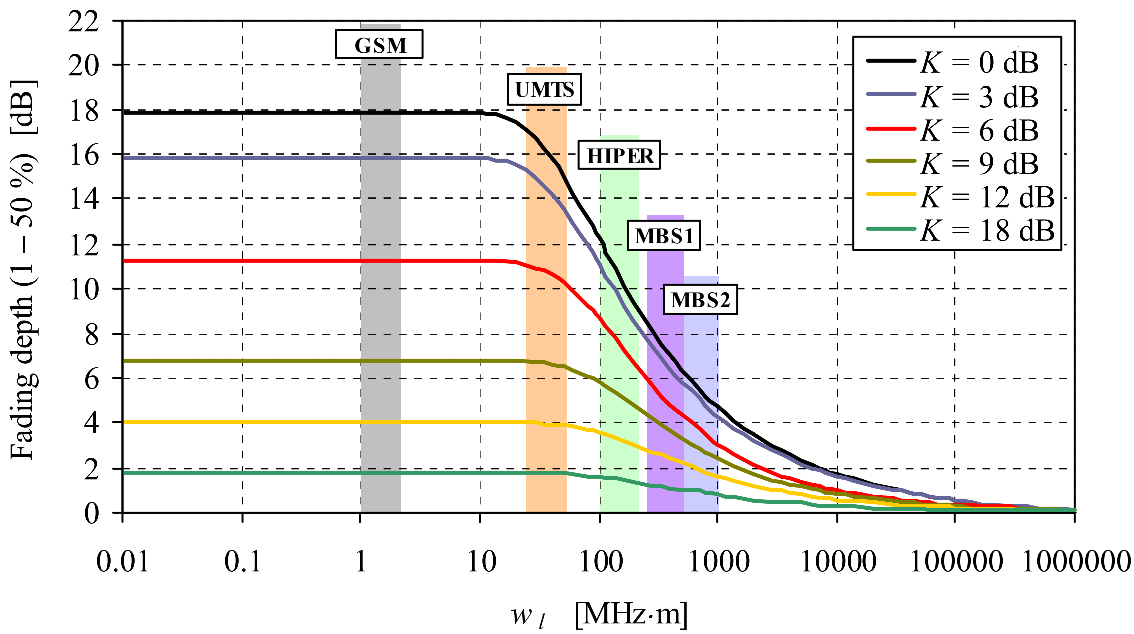

Figure 4.14 – Fading depth in the pico-cellular environment.

As previously, GSM can be taken as a reference for the narrowband case; for the given values of r_w, UMTS, HIPERLAN/2 and MBS behave as wideband systems, therefore, experiencing lower fading depths. Nevertheless, the difference in fading depth between UMTS and GSM, is not significant, hence, it behaves almost as a narrowband system.

4.5.3. Macro-Cellular Environments

Within macro-cellular environments, the existence of LoS is not usually assumed. From the work presented in [KoSN96], one can conclude that, under NLoS, the fading depth is about 1 to 2 dB above the one obtained with K = 0 dB. So, it seems that the proposed approach can be applied to the case of a macro-cellular environment, with the results for K = 0 dB resembling the case of NLoS. Basically, for the narrowband case, it corresponds to consider that the Rayleigh distribution is reasonably approximated by the Rice one for that value of K. In fact, the difference in fading depth for p = 1 %, resulting from considering the Rayleigh distribution or the Rice one with K = 0 dB is 0.8 dB, which is not significant. It should be noted that it is possible to derive an analytical approximation for the NLoS case, similarly as done for the LoS one; however, the error introduced by considering that the NLoS case can be approximated by considering K = 0 dB is negligible, compared with the uncertainty associated to the proper description of the environment itself. One considers that this is a reasonable approximation, thus, simplifying the applicability of the proposed approach.

A simple approach to the evaluation of Δl_{max} can be done by assuming that the relevant scattering objects are positioned within a radius of about 100 to 800 m around the MT [Corr01] (as previously, it is assumed that the propagation environment is modelled by a GBSCM). With this assumption, the maximum difference in propagation path length can be calculated as twice the radius of the scattering scenario, r_s. The value of w_l as a function of Δl_{max} is shown in Table 4.9.

Table 4.9 – Equivalent received bandwidth for the macro-cellular environment.

	w_l [MHz·m]	
System	r_s	
	100 m	800 m
GSM	40	320
UMTS	1 000	8 000

The shadowed zones in Figure 4.15 correspond to the possible values of w_l for a scattering radius ranging from 100 to 800 m. The leftmost part of each coloured zone corresponds to the smaller scattering radius.

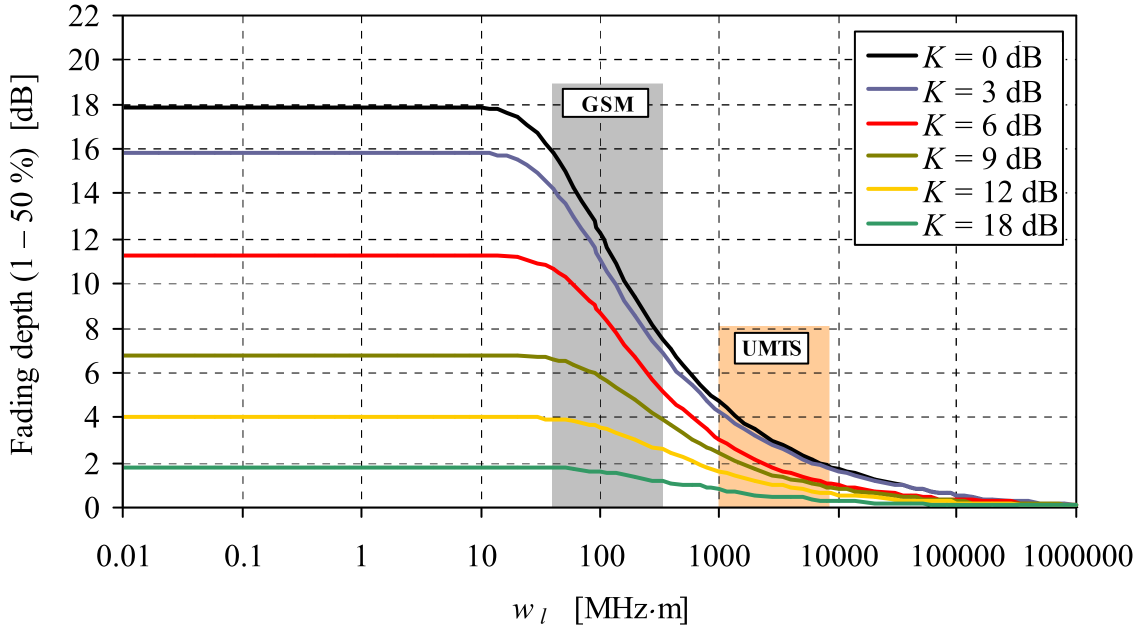

Figure 4.15 – Fading depth in the macro-cellular environment.

Assuming that usually there is NLoS between the transmitter and the receiver, the results in Table 4.10 illustrate the difference between the fading depth observed by GSM and UMTS within this environment.

Table 4.10 – Average fading depth under NLoS (≈ $K = 0$ dB).

	$FD_{1\%}$ [dB]	
System	r_s 100 m	r_s 800 m
GSM	15.8	7.8
UMTS	4.7	1.9

While for GSM typical values of fading depth are between 7.8 and 15.8 dB, for UMTS a value of 1.9 to 4.7 dB is achieved; hence, the difference between UMTS and GSM is around 5.9 to 11.1 dB, depending on the radius of the scattering scenario. Besides the dependence on K, under LoS this difference is smaller than the one for NLoS, nevertheless, it being still of the order of several dB. One main difference, compared to previous cases, is that, for the given values of r_s, even GSM behaves as a wideband system, thus, experiencing lower fading depths, compared to the ones observed in pico- and micro-cellular environments. HIPERLAN/2, MBS1, and MBS2 are not mentioned here, since these systems are not intended for macro-cellular environments.

4.6. Conclusions

In this chapter, a method for deriving the fading depth as a function of the equivalent received bandwidth and the Rice factor, from a simple analytical approximation, is presented. The proposed mathematical equation, is derived through fitting of simulated data from a model in the literature [KoSN96], thus, overcoming the need for heavy computer simulations or huge databases management every time a fading depth value has to be calculated, within a given environment and for a specific system bandwidth. A similar approach can be used to fit data from experimental measurements; one should remember that the model in which the proposed approach is based was already assessed from measurements in different environments and for different system bandwidths. By using the proposed approximation, which approximation error is negligible compared to the results from simulation, one can evaluate the fading depth, for any system bandwidth, starting from a simple geometrical description of the working environment, or from the PDP of the propagation channel, from which the value of Δl_{max} can be derived, as it will be presented in Chapter 6. Moreover, the results for the narrowband case are in good agreement with the ones obtained from classical narrowband distributions, e.g., the Rice one; therefore, the proposed approach being effective for evaluating the fading depth in wideband systems (as required), is also accurate for modelling short-term fading effects for the narrowband case.

Some application examples are presented. An urban street is used as a typical micro-cellular environment, and the fading depth dependence on the street width and on the distance between the BS and the MT is evaluated for a set of typical system bandwidths. Pico- and macro-cellular environments were also considered.

In the micro-cellular environment, when the MT is several hundreds of metres away from the BS, the difference in fading depth between UMTS and GSM, is practically independent of the street width and is not significant; however, if one considers HIPERLAN/2, MBS1, or MBS2, this difference, increases and becomes dependent on the street width, with the lower values of fading depth being observed for wider streets. At smaller distances between the MT and the BS, there is an increased dependency on street width. The difference between UMTS and GSM, for a value of $K = 6$ dB, is about 0.7 to 5.5 dB, for a street width ranging from 15 to 60 m. Also HIPERLAN/2, MBS1 and MBS2, experience lower fading depths than the ones observed at larger distances.

Within the pico-cellular environment, the fading depth experienced by UMTS and GSM is similar, and the dependence on room width is not significant. However, HIPERLAN/2, MBS1 and MBS2 experience fading depths that are several dB below the ones for GSM, and significant dependence on room width is observed, with the larger values of fading depth being observed for smaller rooms.

In the macro-cellular environment, the fading depth experienced by UMTS is well below the one for GSM. Globally, it can be stated that the fading depth in UMTS is about 6 to 11 dB lower than the one observed for GSM, for a scattering scenario radius ranging from 800 to 100 m respectively.

Globally, GSM can be considered as a reference system for the narrowband case, exception being done for the case of the considered macro-cellular environments. UMTS, HIPERLAN/2 and MBS, usually behave as wideband systems, hence, experiencing lower fading depths; nevertheless, in micro- and pico-cellular environments, UMTS behaves almost as a narrowband system. This way, when evaluating the fading depth, the influence of system bandwidth and environment characteristics should always be taken into account, otherwise, the obtained fading margins, can be clearly overestimated, leading to lower cell range and higher interference, and as a consequence, higher deployment costs and lower network quality.

As a final conclusion, one can state that, as expected, the fading depth decreases when the bandwidth increases, the amount of fading depth reduction depending on the environment characteristics.

Chapter 5

Time-Domain Based Approach for Fading Depth Evaluation

5.1. Initial Considerations

Since a complete description of the physical and geometrical environment properties is difficult to obtain, the propagation channel is commonly described by a PDP. Moreover, most of the channel models, as proposed by standard-setting bodies, are usually based on a typical PDP characterisation; hence, time-domain techniques are commonly used for simulating the propagation channel [Corr01]. A time-domain analysis technique for the evaluation of fading of wideband signals in NLoS environments is presented in [InKa99]. This approach, which is based on the eigenvalue decomposition technique [KlLa80], [Leon93], allows one to evaluate the short-term fading depth from the CDF of the received power, as a function of the system bandwidth and the *rms* delay spread of the propagation channel. However, this model is not applicable to LoS cases, which is a drawback if one wants to use it for the design of systems working in this type of scenarios.

Therefore, a time-domain technique for wideband fading depth evaluation is proposed, which is an extension of [InKa99] to the LoS case, being suited for fading depth evaluation in wideband mobile communication systems under either NLoS or LoS conditions; new expressions are derived for the PDF and the CDF of the received power, which apply to both LoS and NLoS cases. The short-term fading depth is evaluated from the CDF of the received power, and represented as a function of the Rice factor, and a new variable defined as the product between the system bandwidth and the *rms* delay spread of the propagation channel. The influence of PDP parameters on the fading depth for theoretical continuous and discrete PDPs is presented and discussed. Moreover, an analytical approximation for the fading depth dependence on the Rice factor and the product between the system bandwidth and the *rms* delay spread of the propagation channel, similar to the one derived in Chapter 4 is also proposed.

5.2. Proposed Time-Domain Technique

As presented in [InKa99], the proposed technique for the analysis of the signal variability is based on the eigenvalue decomposition technique [KlLa80]. By using this approach, the CDF of the received power can be derived from the PDP of the propagation channel, expressed as either continuous or discrete functions of the delay variable. Since WSSUS is assumed, there is no dependence on the time variable as referred before.

Assuming that the PDP of the propagation channel is expressed as $p_d(\tau)$, the frequency correlation function between the f_u and f_v frequency components is obtained through the Fourier transform of $p_d(\tau)$, as

$$\rho(\Delta f_{uv}) = \int_0^\infty p_d(\tau) \cdot e^{-j \cdot 2\pi \cdot \Delta f_{uv} \cdot \tau} \cdot d\tau \tag{5.1}$$

with

$$\Delta f_{uv} = f_u - f_v \tag{5.2}$$

Dividing the bandwidth of the received signal, B, by an incremental bandwidth $\delta f = \frac{B}{M'}$, where M' is a large number, the u-th frequency component, f_u, is given by [InKa99]

$$f_u = \delta f \cdot \left(u - \frac{M'+1}{2}\right) \quad , \quad u = 1,2,\ldots,M' \tag{5.3}$$

and the covariance between the u-th and v-th frequency components is expressed as

$$\Gamma_{uv} = \rho(\Delta f_{uv}) \cdot H^*(f_u) \cdot H(f_v) \cdot \delta f \tag{5.4}$$

where $H(f)$ is the frequency response of the pulse-shaping filter used in the transmitting equipment. Since raised-cosine filters have been used extensively for system design purposes, one considers [PaLe95]

$$H(f)=\begin{cases}\dfrac{1}{B} & ,\quad 0\le|f|<(1-\rho_{off})\cdot\dfrac{B}{2}\\ \dfrac{1}{2B}\cdot\left[1-\sin\left(\dfrac{\pi}{\rho_{off}\cdot B}\cdot\left(|f|-\dfrac{B}{2}\right)\right)\right] & ,\quad (1-\rho_{off})\cdot\dfrac{B}{2}\le|f|\le(1+\rho_{off})\cdot\dfrac{B}{2}\end{cases} \tag{5.5}$$

where ρ_{off} is the rolloff factor. In simulations, ρ_{off}= 0.5 is assumed, which is a typical value in digital radio systems design.

The covariance matrix is then obtained by generating a matrix, $\mathbf{\Gamma}$, whose element in the u-th row and v-th column is given by Γ_{uv}. Performing the eigenvalue decomposition of $\mathbf{\Gamma}$, the obtained eigenvalues, λ_m (m = 1, 2, …, $M \le M'$), correspond to the decomposition of the M signals that fade incoherently. The respective decomposed signals and their powers correspond to the eigenvectors and eigenvalues respectively.

Assuming that each of the signals magnitude is Rayleigh distributed (see Chapter 2), which is true if NLoS is assumed, and that Maximal Ratio Combining (MRC) is carried out for M-branch independently varying signals, which is equivalent to consider that signals arrive from M independent paths [InKa99], the PDF of the signal power at the receiver can be obtained through the convolution of the PDF of the signal power at each branch. Since all path magnitudes are assumed to be Rayleigh distributed, the PDF of the received power for the i-th branch can be obtained from a simple transformation [Leon93]

$$s=\frac{a^2}{2} \tag{5.6}$$

corresponding to the exponential distribution

$$p_{\mathrm{NLoS}_i}(s)=\frac{1}{\sigma_i^2}\cdot e^{-\frac{s}{\sigma_i^2}} \tag{5.7}$$

The PDF of the received power at the receiver can then be obtained through the convolution of the PDF of the received power at each branch, the resulting PDF being [Pras96]

$$p_{\mathrm{NLoS}}(s)=p_{\mathrm{NLoS}_1}(s)*p_{\mathrm{NLoS}_2}(s)*\cdots*p_{\mathrm{NLoS}_M}(s) \tag{5.8}$$

where the symbol * denotes convolution, thus

$$p_{\mathrm{NLoS}}(s)=\frac{1}{\sigma_1^2}\cdot e^{-\frac{s}{\sigma_1^2}}*\frac{1}{\sigma_2^2}\cdot e^{-\frac{s}{\sigma_2^2}}*\cdots*\frac{1}{\sigma_M^2}\cdot e^{-\frac{s}{\sigma_M^2}}=\sum_{m=1}^{M}\frac{\lambda_m^{M-2}\cdot e^{-\frac{s}{\lambda_m}}}{\prod\limits_{\substack{k=1\\k\neq m}}^{M}(\lambda_m-\lambda_k)} \tag{5.9}$$

The CDF of the received power, i.e., the probability that the received power is below a given level s_{ref}, is then

$$\mathrm{Prob}_{\mathrm{NLoS}}(s \le s_{ref}) = 1 - \sum_{m=1}^{M} \frac{(\lambda_m)^{M-1} \cdot e^{-\frac{s_{ref}}{\lambda_m}}}{\prod_{\substack{k=1 \\ k \ne m}}^{M} (\lambda_m - \lambda_k)} \tag{5.10}$$

Equations (5.9) and (5.10) are derived for NLoS, hence, if there is a LoS component these equations are no longer appropriate to describe the received power, since the magnitude of the first arriving wave follows a Rice distribution (see Chapter 2) rather than a Rayleigh one. By applying (5.6), the PDF of the power of the LoS component is given by

$$p_{\mathrm{LoS}_1}(s) = \frac{2K}{a_d^2} \cdot e^{-\frac{K(2s+1)}{a_d^2}} \cdot I_0\left(\frac{2K \cdot \sqrt{2s}}{a_d}\right) \tag{5.11}$$

where K is defined as usual and a_d is the magnitude of the LoS component. The PDF of the received power is then obtained from the convolution of the PDF of the LoS component with M-1 scattered ones

$$p_{\mathrm{LoS}}(s) = p_{\mathrm{LoS}_1}(s) * p_{\mathrm{NLoS}_2}(s) * \cdots * p_{\mathrm{NLoS}_M}(s) \tag{5.12}$$

thus

$$p_{\mathrm{LoS}}(s) = \int_{-\infty}^{+\infty} \frac{2K}{a_d^2} \cdot e^{-\frac{K(2x+1)}{a_d^2}} \cdot I_0\left(\frac{2K \cdot \sqrt{2x}}{a_d}\right) \cdot \sum_{m=2}^{M} \frac{(\lambda_m)^{M-3} \cdot e^{-\frac{s-x}{\lambda_m}}}{\prod_{\substack{k=2 \\ k \ne m}}^{M} (\lambda_m - \lambda_k)} \cdot dx \tag{5.13}$$

where

$$a_d = \sqrt{\lambda_1 \cdot \frac{2K}{1+K}} \tag{5.14}$$

with λ_1 representing the eigenvalue associated to the first arriving wave, i.e., the LoS component.

There is no closed-form expression for (5.13), in a similar way as for (5.9), hence, the evaluation of the CDF of the received power has to be performed by means of numerical methods

$$\mathrm{Prob}_{\mathrm{LoS}}(s \le s_{ref}) = 1 - \int_{s_{ref}}^{+\infty} \int_{-\infty}^{+\infty} \frac{2K}{a_d^2} \cdot e^{-\frac{K(2x+1)}{a_d^2}} \cdot I_0\left(\frac{2K\cdot\sqrt{2x}}{a_d}\right) \cdot \sum_{m=2}^{M} \frac{(\lambda_m)^{M-3} \cdot e^{-\frac{s-x}{\lambda_m}}}{\prod_{\substack{k=2 \\ k\neq m}}^{M} (\lambda_m - \lambda_k)} \cdot dx \cdot ds \tag{5.15}$$

Since when K tends to zero the Rice distribution degenerates to the Rayleigh one, (5.13) and (5.15) tend to (5.9) and (5.10), respectively.

The process for the evaluation of the CDF of the received power can then be summarised into the following steps:

(i) derive the frequency correlation function, $\rho(\Delta f_{uv})$;

(ii) obtain the covariance matrix, $\mathbf{\Gamma}$;

(iii) find the eigenvalues of $\mathbf{\Gamma}$;

(iv) obtain the CDF of the received power by substituting the obtained eigenvalues in (5.10) or (5.15), depending on if NLoS or LoS is considered.

The evaluation of $\rho(\Delta f_{uv})$ depends on whether a discrete or a continuous PDP is considered; for the former, (5.1) reduces to

$$\rho(\Delta f_{uv}) = \sum_{i=1}^{M} P_i \cdot e^{-j\cdot 2\pi\cdot\Delta f_{uv}\cdot\tau_i} \tag{5.16}$$

where P_i and τ_i represent the power and delay of the i-th multipath component, and M is the number of multipath components. For the latter, $p_d(\tau)$ is described by a reduced set of parameters (e.g., (2.21) and (2.22)), hence, (5.1) is also evaluated analytically, reducing the required computation time

$$\rho(\Delta f_{uv}) = \sum_{i=1}^{N_{exp}} P_{\tau,i} \cdot e^{\frac{\tau_i}{\sigma_{\tau,i}}} \cdot \left(\frac{e^{\frac{\tau_i}{\sigma_{\tau,i}}\cdot(1+j\cdot 2\pi\cdot\Delta f_{uv}\cdot\sigma_{\tau,i})} - e^{\frac{\tau_i'}{\sigma_{\tau,i}}\cdot(1+j\cdot 2\pi\cdot\Delta f_{uv}\cdot\sigma_{\tau,i})}}{1 + j\cdot 2\pi\cdot\Delta f_{uv}\cdot\sigma_{\tau,i}} \right) \tag{5.17}$$

where N_{exp} is the number of exponential components (N_{exp} = 1 and 2 corresponding to the exponential and two-stage exponential cases, respectively); $P_{\tau,i}$, τ_i and $\sigma_{\tau,i}$ are defined as presented in Chapter 2, and τ'_i corresponds to the delay above which the contribution of the i-th exponential component is considered as being negligible, i.e., set to zero.

Note that the value of the incremental bandwidth, $\delta(f)$, hence, Δf_{uv}, must be carefully determined, since the smaller the value of $\delta(f)$ the larger the number of eigenvalues, and consequently the larger the size of $\mathbf{\Gamma}$. On the other hand, if the value of $\delta(f)$ is not small enough, the eigenvalues corresponding to higher signal bandwidths will oscillate. From experiments, one concludes that the value of $\delta(f)$ must be at least 100 to 500 times lower than the signal bandwidth, depending on the type of the PDP.

Since the use of the proposed model for simulation purposes requires the implementation of integration, eigenvalue extraction, and matrix manipulation procedures, it was implemented in MATLAB®, built-in functions being used for performing these operations. The default numerical precision of $2\cdot10^{-16}$ provided by MATLAB®, was used for the calculations, and numerical integration (Simpson's method) was performed with an absolute accuracy of $1\cdot10^{-6}$. These values were chosen in order to achieve a reasonable compromise among simulation time and accuracy.

As expected, there is a significant dependence of the required computational effort for evaluating $\mathbf{\Gamma}$, for a given value of B, depending on the value of M' being considered. The hardware platform was the same as the one in Chapter 4. Average simulation times of 1 and 23 s are obtained for M' = 100 and 300, respectively. Since one has evaluated the eigenvalues (the simulation time being negligible, compared to the one required for evaluating $\mathbf{\Gamma}$), the CDF of the received power, and the corresponding fading depth is evaluated. Average simulation times of roughly 0.06 and 56 s (these values being almost independent of M'), are obtained for the NLoS and LoS case, respectively. It should be remembered that, while for the NLoS case, the CDF is obtained from a closed-form expression, for the LoS one, it has to be evaluated from numerical integration, hence, significantly increasing simulation time. Naturally, there is a dependence of the required simulation time on the type of PDP being considered, nevertheless, for the cases under study, it is not significant, compared to the total simulation time required for evaluating the fading depth for a given value of B.

5.3. Analysis of Theoretical Cases

5.3.1. Initial Considerations

Besides the PDP dependence on the antennas type and environment characteristics, there is a set of typical channel models that has been proposed by standard-setting bodies for simulating the propagation channel. These models are usually (or obtained from) exponential or two-stage exponential continuous ones. Several examples are presented for some propagation channels, represented by their continuous or discrete PDPs. The evaluation of the CDF of the received power is obtained from the PDP of the propagation channel through the evaluation of (5.15), and the fading depth is evaluated as the difference in power corresponding to 1 and 50 % of the CDF, and represented as a function of the product between the system bandwidth and the *rms* delay spread of the propagation channel

$$w_{t[\mathrm{Hz \cdot s}]} = B_{[\mathrm{Hz}]} \cdot \sigma_{\tau[\mathrm{s}]} \tag{5.18}$$

Results for different fading depth evaluation intervals, namely [0.1, 50] % and [10, 50] %, are also presented.

The fading depth dependence on the PDP parameters is studied for the case of continuous and discrete PDPs. For the former, several results are derived in order to study the influence of the *rms* delay spread and initial delay of each exponential component on the observed fading depth, moreover, the dependence on the relative power of arriving components is also addressed. For the latter, several situations are considered in order to assess the influence of the number and relative time delay of arriving waves; moreover, the use of regular or non-regular PDPs is briefly addressed. An analytical approximation for the fading depth dependence on w_t, for the case of exponential PDPs is also proposed. For simulation purposes, the parameter M' in (5.3) is fixed as 100 for continuous models and 300 for discrete ones. These values are chosen in order to reduce computational needs, while giving accurate results.

5.3.2. Continuous Propagation Models

In order to study the dependence of the fading depth on the PDP of the propagation channel, two channel models are considered, exponential and two-stage exponential, as presented in Chapter 2. As previously referred, exponential PDPs are completely defined by the set of parameters τ_1, $P_{\tau,1}$ and $\sigma_{\tau,1}$, which correspond to the initial delay of the exponential distribution, the value of $p_d(\tau)$ for $\tau = \tau_1$ and the *rms* delay spread of the propagation channel, respectively. One must remember that these parameters depend on the environment characteristics and on the transmitted power. A graphical representation of $p_d(\tau)/P_{\tau,1}$ is presented in Figure 5.1; for illustrative purposes $\sigma_{\tau,1}$ is fixed to 100 ns. The eigenvalue characteristics of the covariance matrix, $\mathbf{\Gamma}$, normalised by the total received power, P_{rT}, as defined in Chapter 2, are shown in Figure 5.2. As one can observe, the number of eigenvalues increases with increasing w_t; this is not surprising, since, for a given PDP, this corresponds to increasing system bandwidth, thus, an increasing receiver ability to discriminate arriving waves.

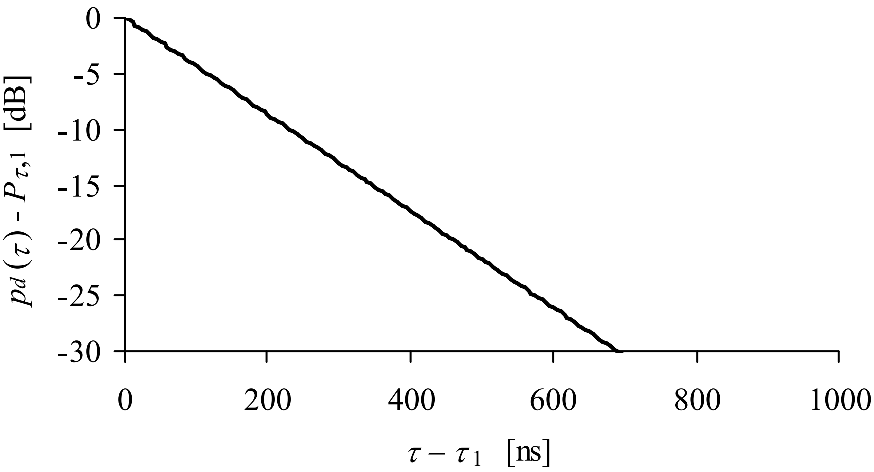

Figure 5.1 – PDP, exponential model.

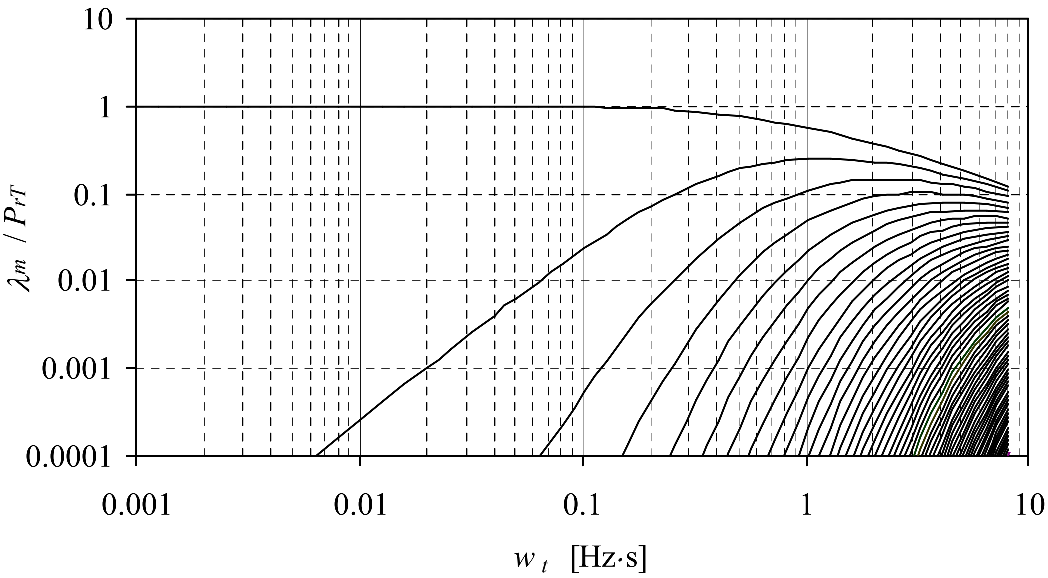

Figure 5.2 – Eigenvalue characteristics, exponential model.

The fading depth dependence on w_t and K is represented in Figure 5.3, each point corresponding to a value of fading depth, evaluated as previously described. These points were chosen as being regularly spaced (in logarithmic scale), within the range of variation of w_t. A large number of points being considered for the NLoS case, since simulation time is not so restrictive, compared to the one for LoS. As one can observe, under NLoS the fading depth remains practically constant for w_t below 0.02 Hz·s, and then decreases with increasing w_t. This breakpoint value corresponds roughly to the coherence bandwidth of the propagation channel, when defined for a frequency correlation of 90 %

$$B_c = \frac{1}{50 \cdot \sigma_\tau} = \frac{0.02}{\sigma_\tau} \tag{5.19}$$

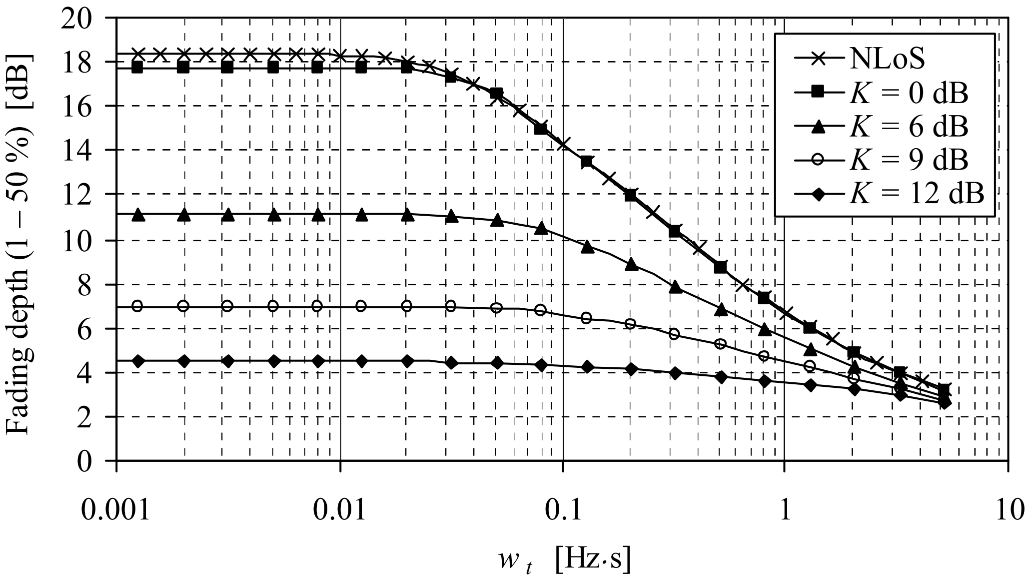

Figure 5.3 – Fading depth, exponential model.

Under LoS, the fading depth decrease rate above the breakpoint decreases with increasing values of K. Hence, one can distinguish different behaviours; the first one, which corresponds to a system bandwidth below the coherence bandwidth of the propagation channel (the narrowband case), and the second, which corresponds to the wideband case, i.e., the system bandwidth is above the coherence bandwidth of the propagation channel. In the former, the fading depth depends only on the value of K rather than on the system bandwidth, while for the latter, besides the dependence on K, the fading depth decreases with increasing system bandwidths, similarly as observed in Chapter 4. Also, as the system bandwidth increases, the fading depth becomes less sensitive to the value of K, since for different values of K the curves become closer. Since the fading depth is represented as a function of w_t, the obtained results are valid for any exponential PDP, independently on the value of σ_τ; moreover, they are independent of $P_{\tau,1}$ and τ_1.

The two-stage exponential model is completely defined by the set of parameters τ_1, $\sigma_{\tau,1}$, $P_{\tau,1}$ and τ_2, $\sigma_{\tau,2}$, $P_{\tau,2}$, corresponding to the initial delay, *rms* delay spread and the maximum value of value of $p_d(\tau)$ for the first and second exponential components, respectively (see Chapter 2). A graphical representation of $p_d(\tau)/P_{\tau,1}$ with $P_{\tau,1} = P_{\tau,2}$, and $\tau_2 = 2\cdot\sigma_{\tau,1}$ is presented in Figure 5.4; for illustrative reasons $\sigma_{\tau,1} = \sigma_{\tau,2} = 100$ ns. The normalised eigenvalue characteristics of the covariance matrix are shown in Figure 5.5; as one observes, these characteristics are identical to the ones for the exponential model, however, they slightly oscillate for $w_t > 1$ Hz·s, due to the existence of two arriving components at different delays.

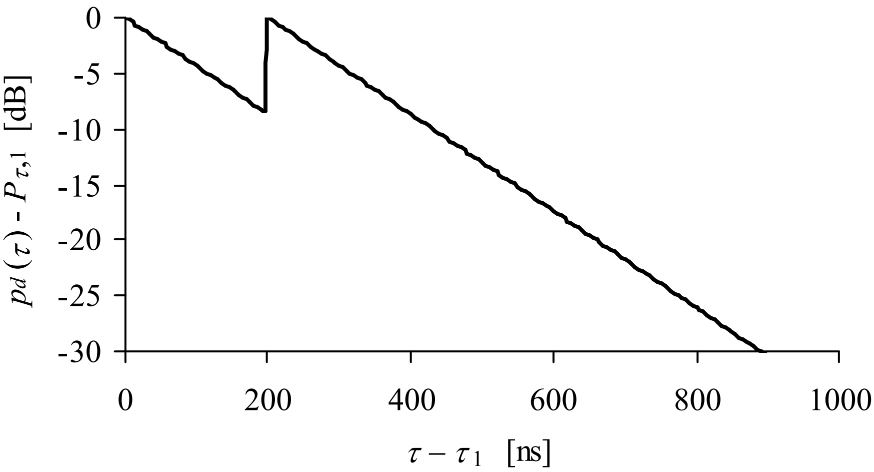

Figure 5.4 – PDP, two-stage exponential model.

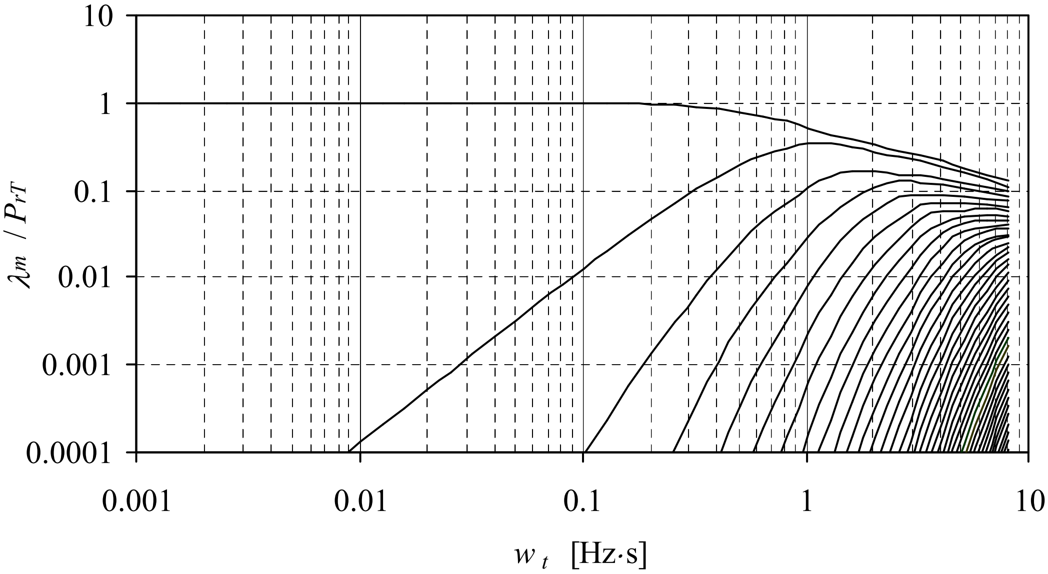

Figure 5.5 – Eigenvalue characteristics, two-stage exponential model.

The fading depth dependence on w_t and K, Figure 5.6, is identical to the one for the exponential model (a small difference is observed for $w_t > 0.02$ Hz·s, i.e., the fading depth is slightly above the one for the exponential case). This should not be seen as a surprise, since the channel models used above are quite similar, i.e., the initial delay for the second exponential component is quite close to the one corresponding to the first exponential one. This way, a study on the fading depth dependence on PDP parameters must by carried out in order to extract detailed conclusions. It is expected that the observed fading depth depends on the relative initial delay and the *rms* delay spread of the second arriving component, compared to *rms* delay spread of the first arriving one. Moreover, a dependence on the ratio $P_{\tau,2}/P_{\tau,1}$ is also expected, thus, some results are presented for different PDP parameters.

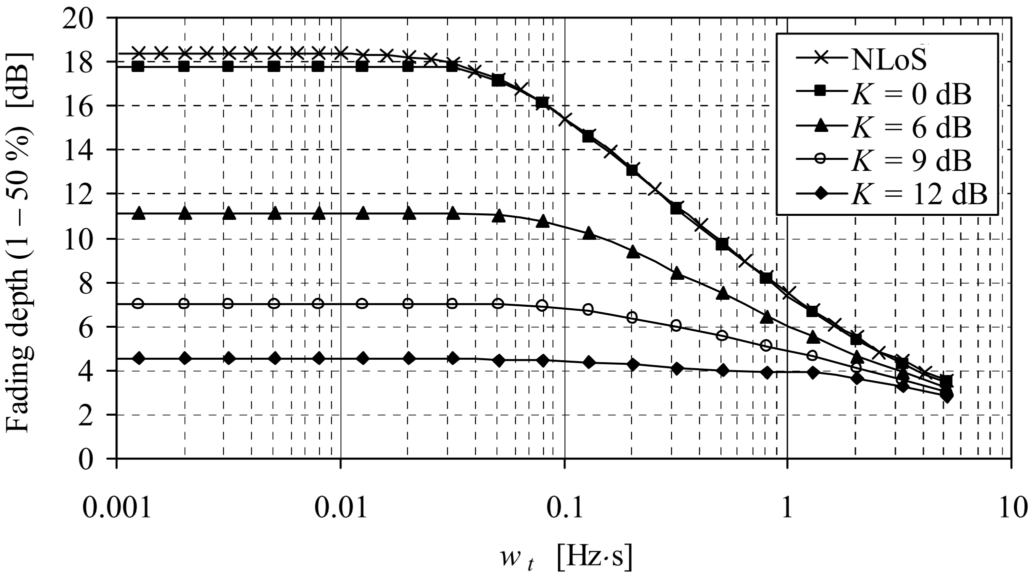

Figure 5.6 – Fading depth, two-stage exponential model.

As a simplification of the comparison among different systems, one only considers the NLoS case, however, the results can be easily extrapolated to any value of *K*, since, as previously presented, besides the dependence on the value of *K*, the fading depth curves variation law is similar both for NLoS and LoS cases.

In order to study the dependence on the ratio between the *rms* delay spread of the second arriving component and the one for the first, one considers $\sigma_{\tau,2} = q_s \cdot \sigma_{\tau,1}$, with $q_s = 0.25, 0.5, 1, 2, 4$; also, $P_{\tau,1} = P_{\tau,2}$ is assumed. Two different situations are considered: $\tau_2 = 2 \cdot \sigma_{\tau,1}$ (a situation similar to the previous one), Figure 5.7, and $\tau_2 = 80 \cdot \sigma_{\tau,1}$, Figure 5.8, which corresponds to a situation when the second arriving component is significantly delayed from the first one. The difference in fading depth, relative to the case of a single exponential PDP, is shown in Appendix II.

As can be observed from Figure 5.7, when both arriving components are close to each other, the influence of q_s is not significant; the difference in fading depth is usually below 2 dB, for the considered values of q_s. From Figure 5.8 one observes that, when the second arriving component is significantly delayed from the first one, e.g., $\tau_2 = 80 \cdot \sigma_{\tau,1}$, the fading depth observed for $w_t > 0.2$ Hz·s is higher than the one obtained for the exponential case; the difference relative to the case of a single exponential is usually below 6.5 dB, which is due to the existence of a second arriving component at a distant delay, causing each arriving component to be discriminated separately. However, the influence of q_s still is not significant, as verified in the previous case.

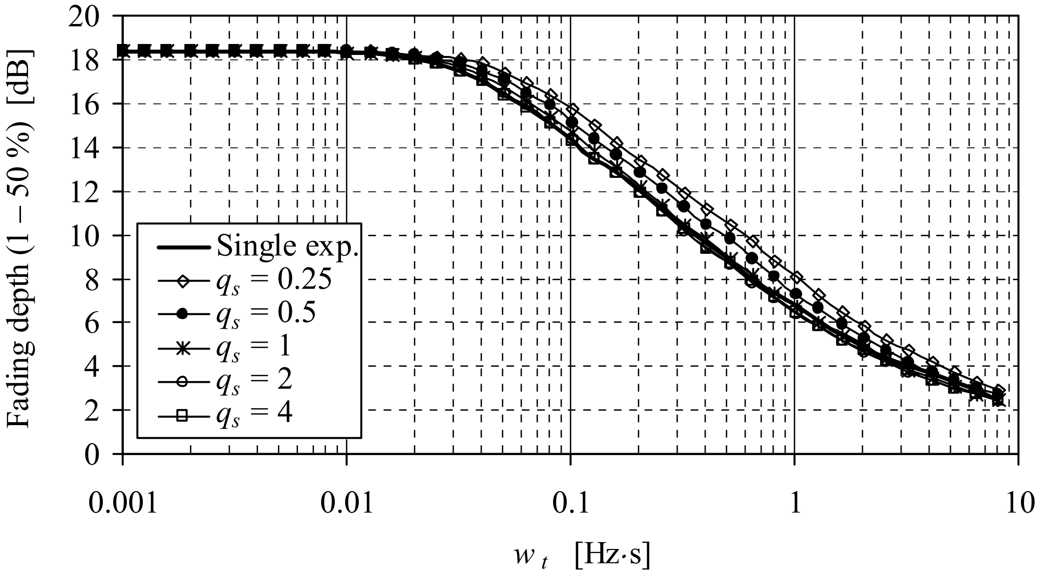

Figure 5.7 – Fading depth for different values of q_s, $\tau_2 = 2 \cdot \sigma_{\tau,1}$.

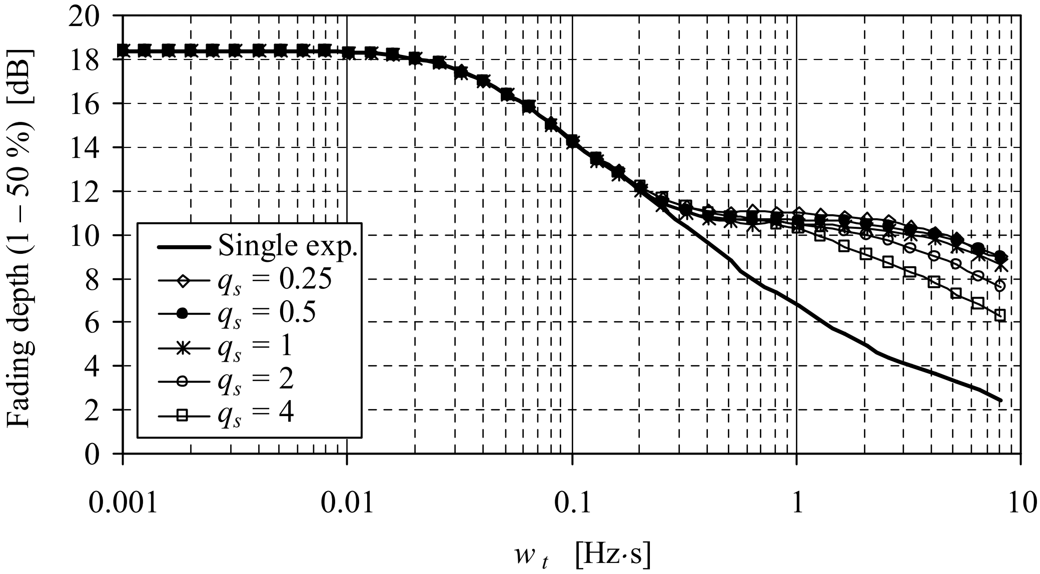

Figure 5.8 – Fading depth for different values of q_s, $\tau_2 = 80 \cdot \sigma_{\tau,1}$.

In order to study the dependence on the ratio between the initial delay of the second arriving component and the *rms* delay of the first arriving one, one considers, $\tau_2 = q_{ds} \cdot \sigma_{\tau,1}$, with q_{ds} = 2, 4, 8, 10, 20, 40, 80; also $P_{\tau,1} = P_{\tau,2}$ is assumed. Two different situations are considered, $\sigma_{\tau,2} = 0.5 \cdot \sigma_{\tau,1}$, Figure 5.9, and $\sigma_{\tau,2} = 2 \cdot \sigma_{\tau,1}$, Figure 5.10. The difference in fading depth, relative to the case of an exponential PDP is shown in Appendix II.

From Figure 5.9, one concludes that, for $q_{ds} < 4$, the observed fading depth is close to the one for the exponential case. However for small values of q_{ds}, e.g., $q_{ds} = 2$, and $w_t > 0.2$ Hz·s, the observed fading depth is usually above the one for the exponential case. This is due to considering $\sigma_{\tau,2} = 0.5\cdot\sigma_{\tau,1}$, hence, $p_d(\tau)$ decreases rapidly for $\tau > \tau_2$, when compared to the case of a single exponential function with *rms* delay spread $\sigma_{\tau,1}$. As expected, for large values of q_{ds} and, $w_t > 0.2$ Hz·s, an increase in q_{ds}, i.e., on the initial delay of the second arriving component, causes an increase in fading depth. The difference in fading depth for different values of q_{ds} is usually below 6.5 dB.

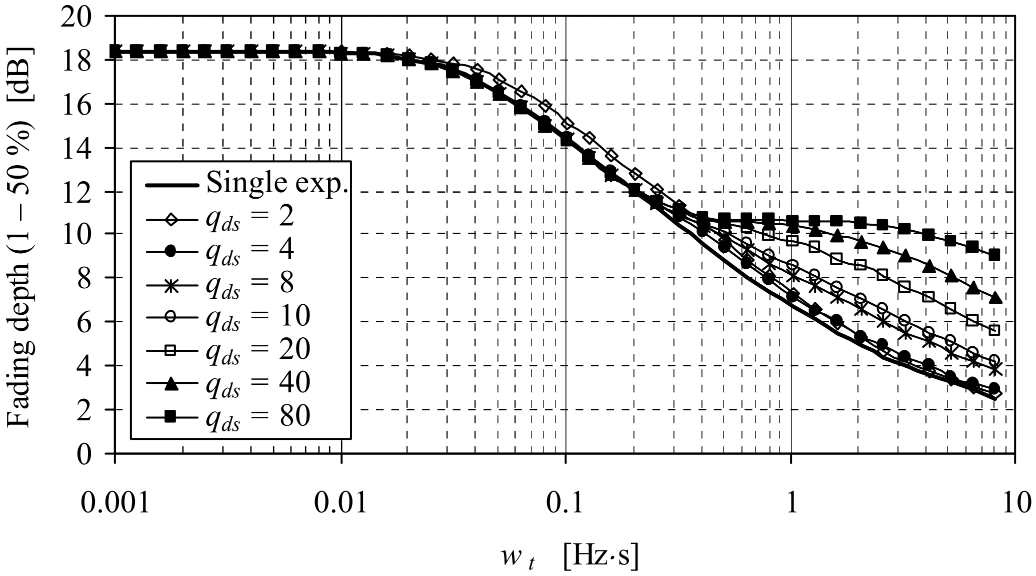

Figure 5.9 – Fading depth for different values of q_{ds}, $\sigma_{\tau,2} = 0.5\cdot\sigma_{\tau,1}$.

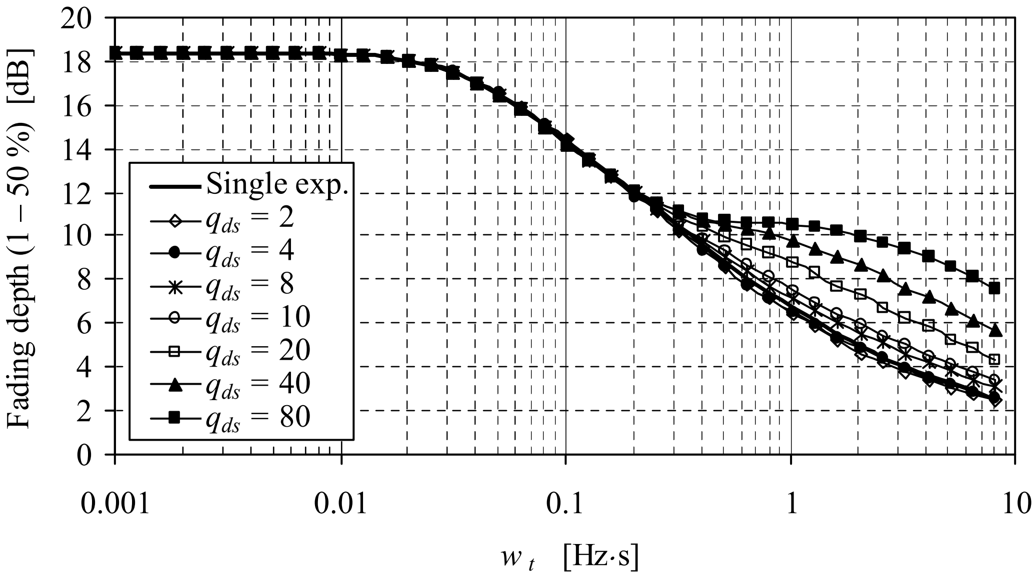

Figure 5.10 – Fading depth for different values of q_{ds}, $\sigma_{\tau,2} = 2\cdot\sigma_{\tau,1}$.

A similar behaviour is observed for $\sigma_{\tau,2} = 2\cdot\sigma_{\tau,1}$, Figure 5.10; exception is made for $q_{ds} = 2$, since one considers $q_s = 2$ ($\sigma_{\tau,2} = 2\cdot\sigma_{\tau,1}$) while for the previous case $q_s = 0.5$ (see

Figure 5.7). The difference in fading depth for different values of q_{ds} slightly decreases, being usually below 5.5 dB.

In both, $\sigma_{\tau,2} = 0.5 \cdot \sigma_{\tau,1}$ and $\sigma_{\tau,2} = 2 \cdot \sigma_{\tau,1}$, the difference in fading depth for $w_t > 0.2$ Hz·s, relative to the one for the case of a single exponential increases with increasing delay of the second arriving component. Moreover, it also increases as the *rms* delay spread of the second arriving component decreases, nevertheless, this difference is not significant for $q_{ds} < 10$, i.e., $\tau_2 < 10 \cdot \sigma_{\tau,1}$, since it is usually below 1 to 2 dB relative to the case of a single exponential. For large values of q_{ds}, the difference is usually below 6.5 dB for the cases under study.

For studying the dependence on the relative power of arriving components, one considers, $P_{\tau,2} = q_p \cdot P_{\tau,1}$, with $q_{p[\mathrm{dB}]} = -6, -12, -18, -24$ dB; also $\sigma_{\tau,2} = \sigma_{\tau,1}$ is assumed. The results for $\tau_2 = 2 \cdot \sigma_{\tau,1}$ are in Figure 5.11. The difference in fading depth, relative to the case of an exponential PDP, is shown in Appendix II.

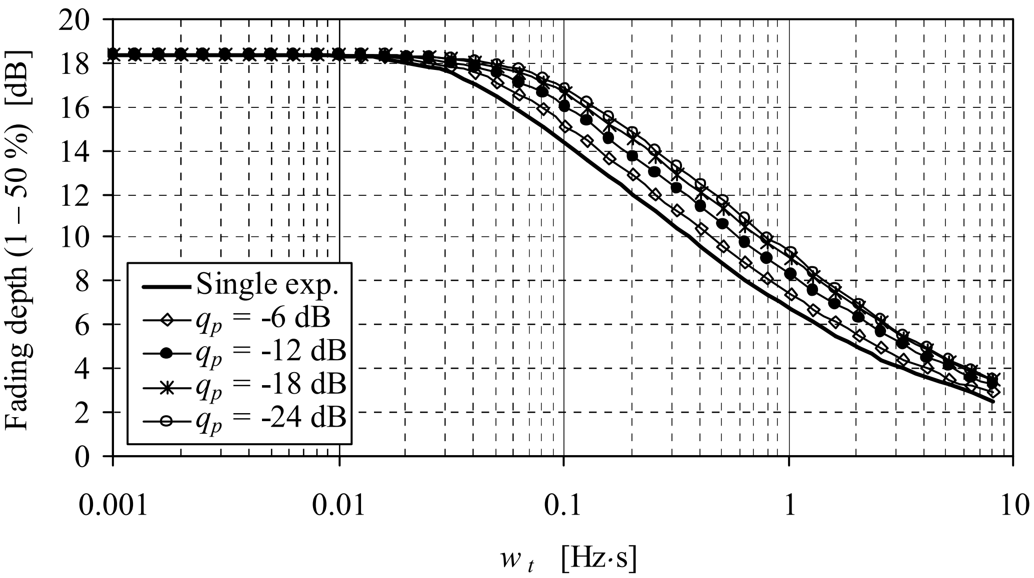

Figure 5.11 – Fading depth for different values of q_p, $\tau_2 = 2 \cdot \sigma_{\tau,1}$.

From Figure 5.11, one concludes that, compared to the case of an exponential PDP, the observed fading depth increases with decreasing values of q_p, i.e., the fading depth increases with decreasing relative power of the second arriving component. However, this variation is not significant, since for the cases under study, it is usually below 3 dB. This is not surprising, since for $\tau_2 = 2 \cdot \sigma_{\tau,1}$ the given PDP is close the one for the exponential case. However, one must refer that the observed fading depth is above the one for the exponential case, since $P_{\tau,2}$ is always below $P_{\tau,1}$, hence, increasing the observed fading depth.

For $\tau_2 = 80 \cdot \sigma_{\tau,1}$, Figure 5.12, the influence of q_p is more significant; moreover, one observes that the relative power of the second arriving component has a strong influence on the value of w_t above which the fading depth curves start to diverge from the one for the exponential model, this value decreasing with decreasing values of q_p.

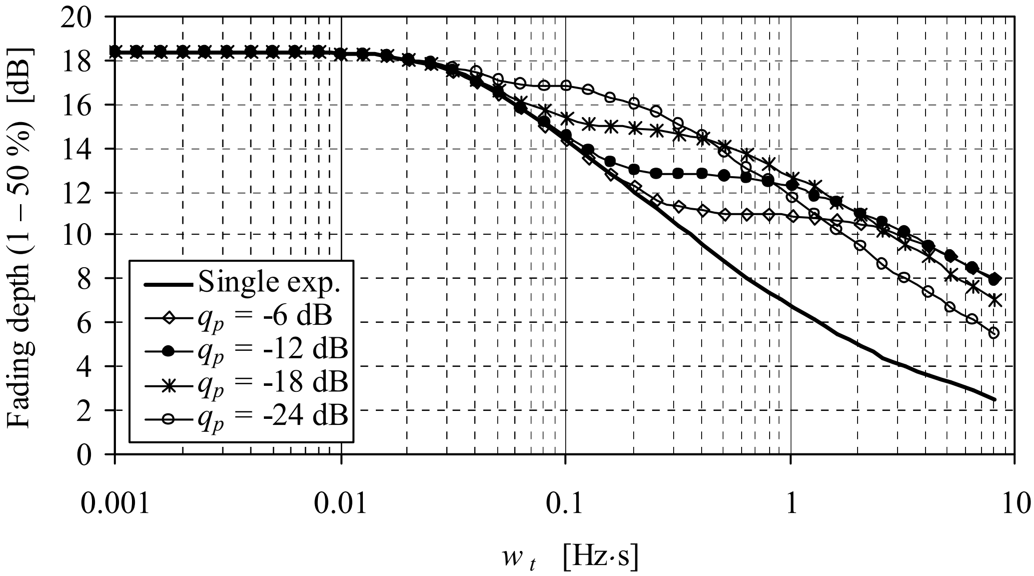

Figure 5.12 – Fading depth for different values of q_p, $\tau_2 = 80 \cdot \sigma_{\tau,1}$.

As a conclusion, one can state that the relative power and the initial delay of the second arriving component influences the results for the fading depth. Globally, one observes that the relative power of arriving components is mainly responsible by defining the value of w_t from which the fading depth curves start to differ from the one for the exponential model. The initial delay of the second component clearly influences the difference in fading depth observed between the exponential and two-stage exponential models.

Since continuous propagation models for different environment are usually proposed for system evaluation [Fail89], one uses some of the proposed models, aiming at giving some insight into the eigenvalue characteristics and observed fading depth for typical PDPs. These models are commonly used for the evaluation of GSM; however, it is not restrictive for the presented analysis, since, besides some differences, namely on the value of the *rms* delay spread of the propagation channel, similar models are used for the evaluation of systems such as UMTS [ETSI97] and HIPERLAN/2 [Corr01]. Hence, one assumes that these models are representative of typical environments usually found in mobile communication systems.

Since WSSUS is considered, the channel properties depend on the difference in delay and relative power of arriving components, rather than on the absolute values, i.e., $\tau_1 = 0$ ns and $P_{\tau,1} = 1$ is assumed for the proposed channel models.

The proposed channel models, commonly used for modelling the GSM propagation channel in Rural Area and Typical Urban environments, are single exponential functions, as shown in Appendix III [Fail89]

$$p_d(\tau)=\begin{cases} e^{-\frac{\tau[\mu s]}{0.12}} & , \quad 0<\tau<0.7\,\mu s \\ 0 & , \quad \text{elsewere} \end{cases} \qquad \text{for Rural Area environments} \tag{5.20}$$

$$p_d(\tau)=\begin{cases} e^{-\frac{\tau[\mu s]}{1.0}} & , \quad 0<\tau<7\,\mu s \\ 0 & , \quad \text{elsewere} \end{cases} \qquad \text{for Typical Urban environments} \tag{5.21}$$

The normalised eigenvalue characteristics of the covariance matrix, $\mathbf{\Gamma}$, are also shown in Appendix III. As expected, in both cases the eigenvalue characteristics are equal to the ones for the case of an exponential PDP, which is not surprising, since when represented as a function of w_t, the obtained results are valid for any exponential PDP, independently of the value of σ_τ, as previously referred.

The channel models proposed for GSM Bad Urban and Hilly Terrain environments, shown in Appendix III, are defined by two-stage exponential functions [Fail89]

$$p_d(\tau)=\begin{cases} e^{-\frac{\tau[\mu s]}{1.0}} & , \quad 0<\tau<5\,\mu s \\ 0.5\cdot e^{-\frac{5.0-\tau[\mu s]}{1.0}} & , \quad 5<\tau<10\,\mu s \\ 0 & , \quad \text{elsewere} \end{cases} \qquad \text{for Bad Urban environments} \tag{5.22}$$

$$p_d(\tau)=\begin{cases} e^{-\frac{\tau[\mu s]}{0.29}} & , \quad 0<\tau<2\,\mu s \\ 0.1\cdot e^{-\frac{15.0-\tau[\mu s]}{1.0}} & , \quad 15<\tau<20\,\mu s \\ 0 & , \quad \text{elsewere} \end{cases} \qquad \text{for Hilly Terrain environments} \tag{5.23}$$

The normalised eigenvalue characteristics of the covariance matrix, $\mathbf{\Gamma}$, are shown in Appendix III as well. For the case of Bad Urban environments, besides the similarities between the eigenvalue characteristics and the ones for the two-stage exponential model in Figure 5.5, one can observe some differences for $w_t > 0.2$ Hz·s, since the eigenvalue characteristics depend on the shape of the PDP, namely on the power, *rms* delay spread and initial delay of each exponential component, as previously described. For the case of Hilly Terrain ones, the eigenvalue characteristics for $w_t > 0.2$ Hz·s are different from the previous two-stage exponential cases. This would be expected, since the PDP for the Hilly Terrain environment is composed of two distinct groups of arriving components at distant delays, compared to the *rms* delay spread of each group of arriving components.

In order to assess the fading depth dependence on the PDP of the propagation channel, one presents the fading depth curves for the different channel models, Figure 5.13.

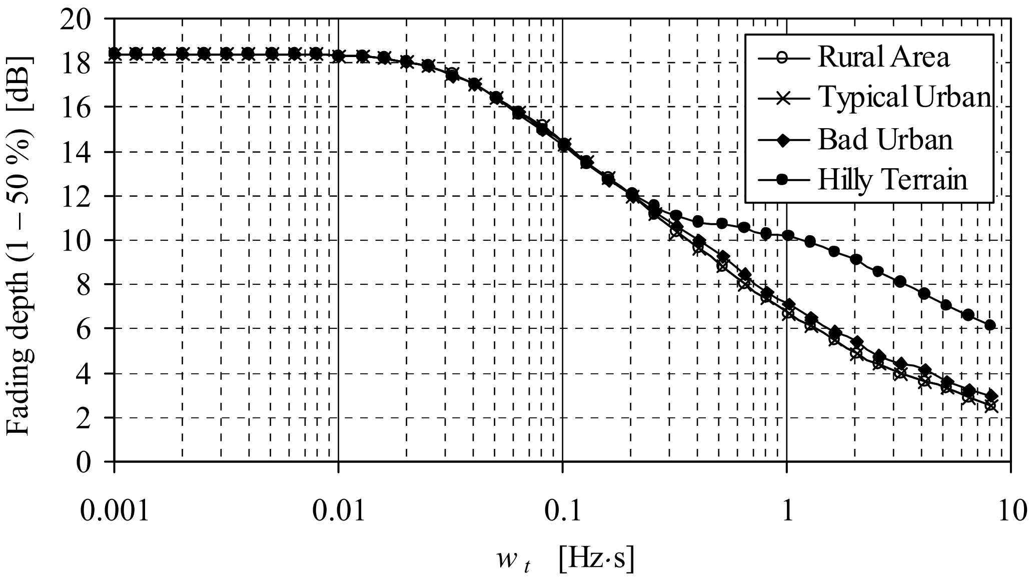

Figure 5.13 – Fading depth for different GSM continuous channel models.

In order to simplify the comparison among different systems, one only considers the NLoS case, however, these results can be easily extrapolated to any value of *K*, since, as previously referred, besides the fading depth dependence on the value of *K*, the curves variation law is similar. As one can observe from Figure 5.13, the curves for the Rural Area and Typical Urban environments (exponential PDPs) are superimposed, which means that the observed fading depth depends only on w_t, as previously referred. For the case of Bad Urban and Hilly Terrain environments (two-stage exponential PDPs), the fading depth curves are superimposed with the previous ones for $w_t \leq 0.2$ Hz·s. For higher values of w_t, there is a dependence on the shape of the PDP, namely the relative initial delay, power and *rms* delay spread of each exponential component. As previously referred, this dependence is more significant with increasing initial delay between different arriving components.

5.3.3. Discrete Propagation Models

In order to assess the fading depth dependence on the type of PDP, several situations are presented, in order to gain some insight on the influence of PDP parameters for the discrete case, namely, the number of arriving waves, the time delay between different arriving waves, and the influence of using regularly or non-regularly spaced PDPs. The discrete PDPs being considered for simulations are derived from an exponential continuous one. For simulation and illustration purposes, the *rms* delay spread of the continuous PDP is fixed to $\sigma_{\tau_{ref}} = 50$ ns; however, a different value can be considered. For the same reason, unless otherwise noted, the reference time delay between arriving waves is fixed to $\Delta\tau_{ref} = \sigma_{\tau_{ref}}$.

Several simulations are carried out in order to understand the influence of the number of arriving waves, M, different values being considered $M = 2$, 4, 8 and 16. Arriving waves are assumed as being regularly spaced. The value of σ_τ for different values of M is in Table 5.1.

Table 5.1 – Value of σ_τ for different values of M.

M	σ_τ [ns]	$\sigma_\tau / \sigma_{\tau_{ref}}$
2	22.17	0.41
4	39.26	0.78
8	47.41	0.95
16	47.98	0.96

The results for the fading depth observed for different values of M are depicted in Figure 5.14. As one can observe, the curves for different values of M behave like the ones for the continuous case until a given value of w_t is reached; for large values of w_t, the curves remain practically constant, hence, independent of w_t. This was expected, since in the case of discrete PDPs, one considers a discrete number of arriving waves, hence, the fading depth remains constant for a system bandwidth that is large enough in order to discriminate all arriving waves; moreover, for $M > 4$ the fading depth curves are practically superimposed and independent of the value of the number of arriving waves. One also observes that, as expected, the system bandwidth from which the fading depth remains constant, hence, independent on w_t, is roughly equal to the inverse of the time delay between arriving waves, i.e., $1/\sigma_{\tau_{ref}}$.

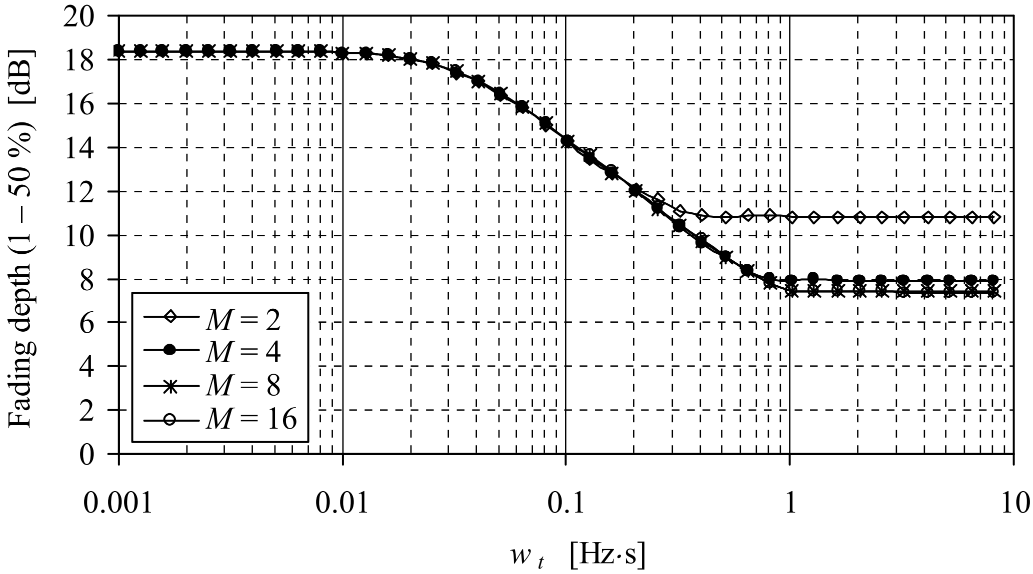

Figure 5.14 – Fading depth for different values of M.

It is expected that the time delay between arriving waves also affects the results, hence, with $M = 8$, different simulations were carried out for different values of time delay between arriving waves, different values being considered, $\Delta\tau/\Delta\tau_{ref} = 0.1$, 1.0 and 2.0, Figure 5.15.

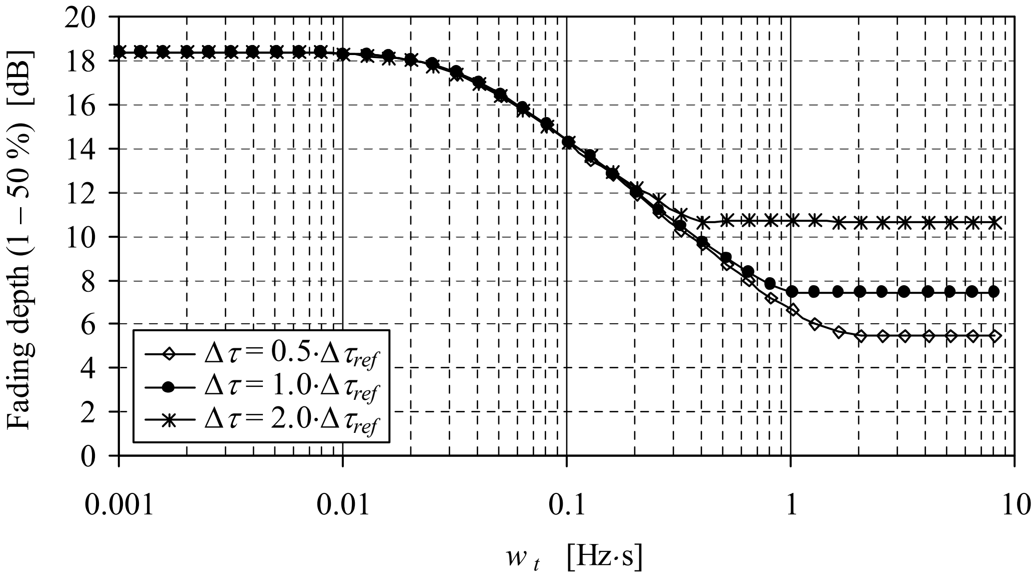

Figure 5.15 – Fading depth for different values of $\Delta\tau/\Delta\tau_{ref}$.

As previously, one concludes that the value of w_t from which the curves remain constant depends on the time delay between arriving waves. Globally, one can state that these values increase with decreasing time delay between arriving waves, which is expected, since as the time delay decreases consecutive arriving waves become closer, hence, a higher system bandwidth is needed to discriminate them. For illustrating such dependence, one assumes that the system bandwidth that is large enough in order to discriminate all arriving waves, *B'*, can be roughly obtained from

$$B' = \frac{1}{\Delta\tau} \tag{5.24}$$

hence,

$$B' \cdot \sigma_\tau = \frac{\sigma_\tau}{\Delta\tau} \tag{5.25}$$

Considering the case $\Delta\tau/\Delta\tau_{ref} = 0.5$, one obtains, Table 5.2,

$$B' \cdot \sigma_\tau = \frac{0.82\sigma_{\tau_{ref}}}{0.5\Delta\tau_{ref}} = 1.64 \tag{5.26}$$

Table 5.2 – Value of σ_τ for different values of $\Delta\tau/\Delta\tau_{ref}$.

$\Delta\tau/\Delta\tau_{ref}$	σ_τ [ns]	$\sigma_\tau/\sigma_{\tau_{ref}}$
0.5	41.09	0.82
1.0	47.41	0.95
2.0	42.55	0.85

As one can observe, this value corresponds to the one in Figure 5.15, for $\Delta\tau/\Delta\tau_{ref} = 0.5$, from which the fading depth curves becomes constant, i.e., independent on w_t. One must remember that, for simulation purposes, one considers $\Delta\tau_{ref} = \sigma_{\tau_{ref}}$; however, similar results are achieved when considering different values of $\Delta\tau_{ref}$ and $\sigma_{\tau_{ref}}$.

When deriving a discrete PDP from a continuous one, several rules are usually recommended [Fail89]. One of these rules consists of using non-regular spacing between arriving waves, in order to avoid regularities in the correlation properties of the received signal. In order to understand how this affects the results for the fading depth, several experiments were carried out. A non-regular PDP with $M = 8$ is considered, the minimum and maximum spacing between arriving waves being $0.5\Delta\tau_{ref}$ and $\Delta\tau_{ref}$, respectively.

As one can observe from Figure 5.16, the use of non-regular spacing influences the obtained results. Moreover, the fading depth curve for the case of non-regular spacing is within the limits imposed by the ones corresponding to the cases for $\Delta\tau = 0.5 \cdot \Delta\tau_{ref}$ and

$\Delta\tau = \Delta\tau_{ref}$. These results aim only at illustrating the influence of using non-regularly spaced PDPs; nevertheless, although not being within the main scope of this work, an accurate study is needed in order to properly assess such influence.

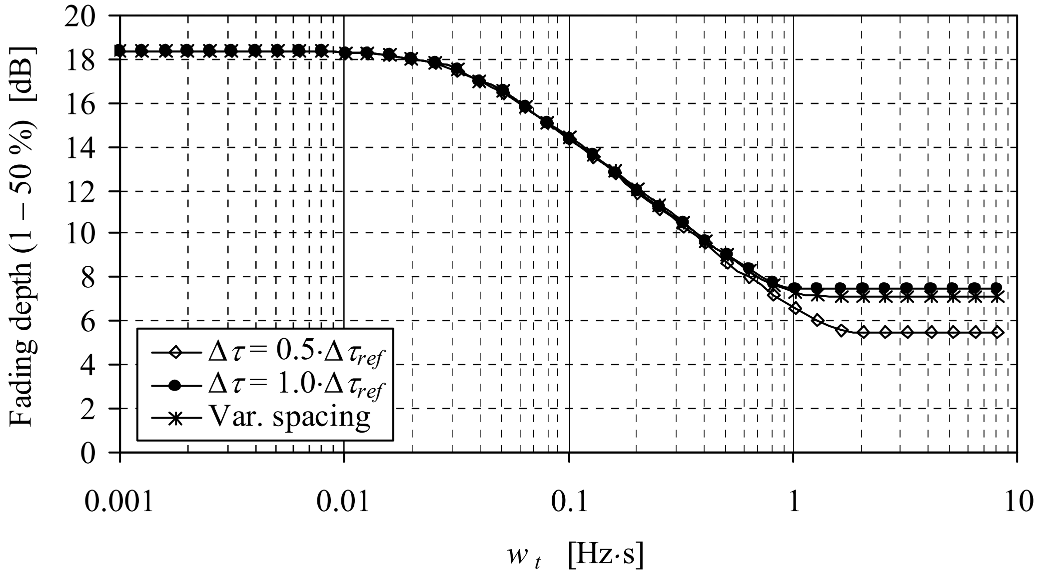

Figure 5.16 – Influence of using regular/non-regular spacing.

As previously, one uses some typical environments in order to properly assess the fading depth dependence on the considered discrete channel model. Since for the continuous case the fading depth in Bad Urban GSM environments is close to the one for Rural Area and Typical Urban ones, Bad Urban environments are not considered here, since regarding fading depth the obtained results do not give additional information from the point of view of comparison among different systems. Discrete channel models are derived from the equivalent continuous ones as described in [Fail89]. The results for the fading depth observed in different environments are presented in Figure 5.17. As for the case of continuous PDPs, the fading depth curves are practically superimposed for $w_t \leq 0.2$ Hz·s, and become dependent on the shape of the PDP for large values of w_t. One main difference between the observed fading depth curves and the ones for the continuous models is that the fading depth remains constant for large values of w_t. One would expect this, since for the case of discrete PDPs one considers a discrete number of arriving waves, thus, the fading depth remains constant for a system bandwidth above the one that is large enough in order to discriminate all arriving waves, as previously referred.

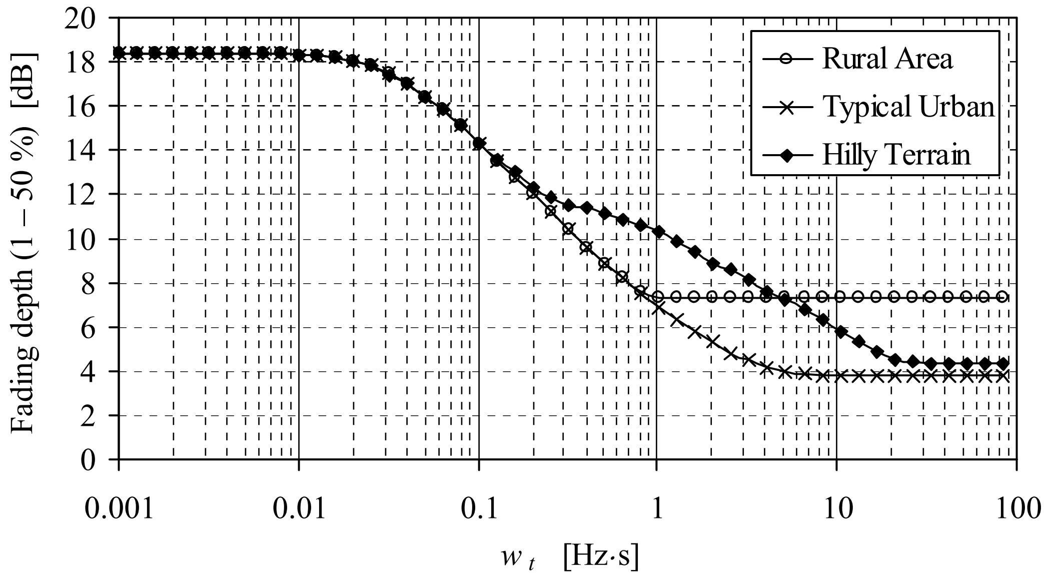

Figure 5.17 – Fading depth, discrete channel models, NLoS.

From Figure 5.18 and Figure 5.19, one can observe the differences between the results obtained with continuous and discrete PDPs. One must remember that the latter are simple realisations of the former. It should be noted that for Rural Area and Typical Urban, the curves for the continuous case are superimposed, since both PDPs are single-exponential ones, Figure 5.18.

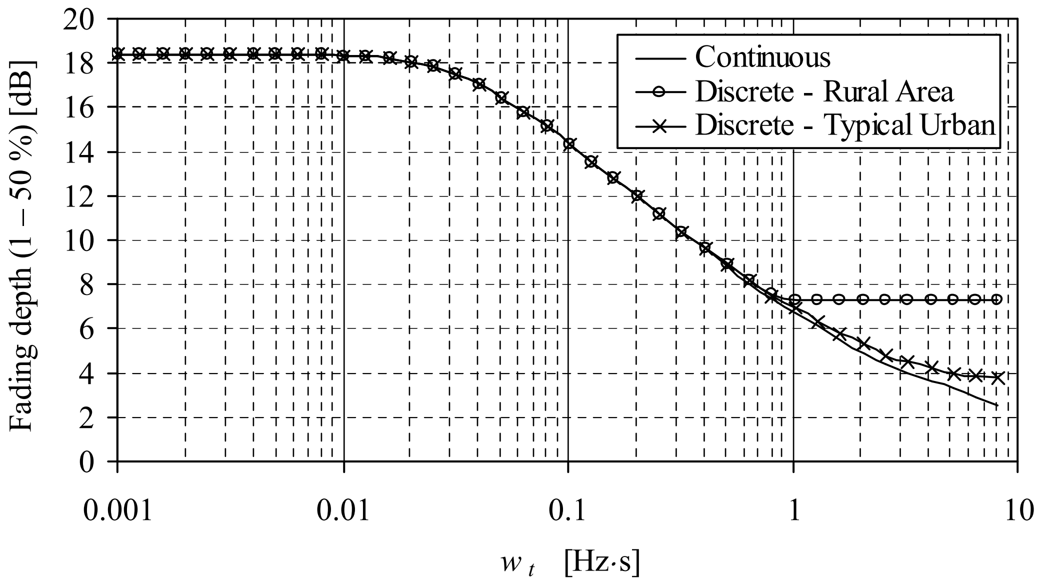

Figure 5.18 – Comparison between continuous and discrete channel models, Rural Area and Typical Urban.

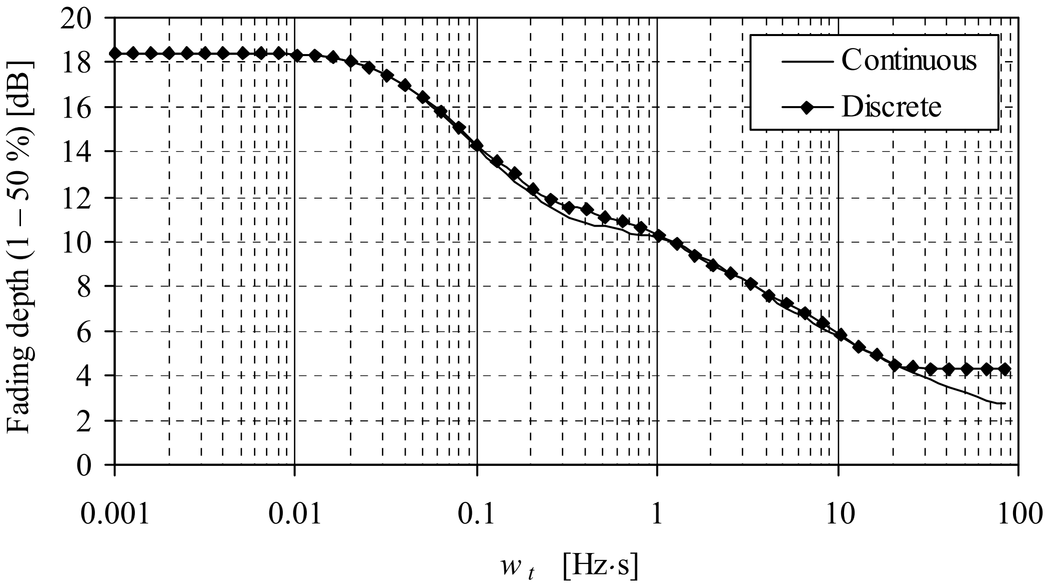

Figure 5.19 – Comparison between continuous and discrete channel models, Hilly Terrain.

As previously stated, the fading depth remains constant for a system bandwidth greater than the one needed in order to discriminate all arriving waves. One must refer that this behaviour is due to considering a simplified discrete channel model, rather than inherent characteristics of the propagation channel, hence, for a given system bandwidth one must carefully determine if for a given model the considered system bandwidth is above or below that point. In the first case, one can consider that the obtained fading depth is an accurate estimation, besides the uncertainty introduced by considering the model; in the second one, the obtained fading depth results from the error introduced by considering a discrete model rather than an inherent characteristic of the propagation channel.

5.3.4. Fading Depth Evaluation Interval

In previous sections, one evaluates the fading depth as the difference in power corresponding to 1 and 50 % of the CDF of the received power, however, it is of relevance to realise if similar results were obtained when one considers a different fading depth evaluation interval, e.g., [0.1, 50] % and [10, 50] %. The results in Figure 5.20 correspond to the ones for the continuous exponential model, under NLoS, when different fading depth evaluation intervals are considered. As previously, one assumes that, with proper adjustment, the conclusions drawn from the analysis of Figure 5.20 can be extrapolated to the LoS case.

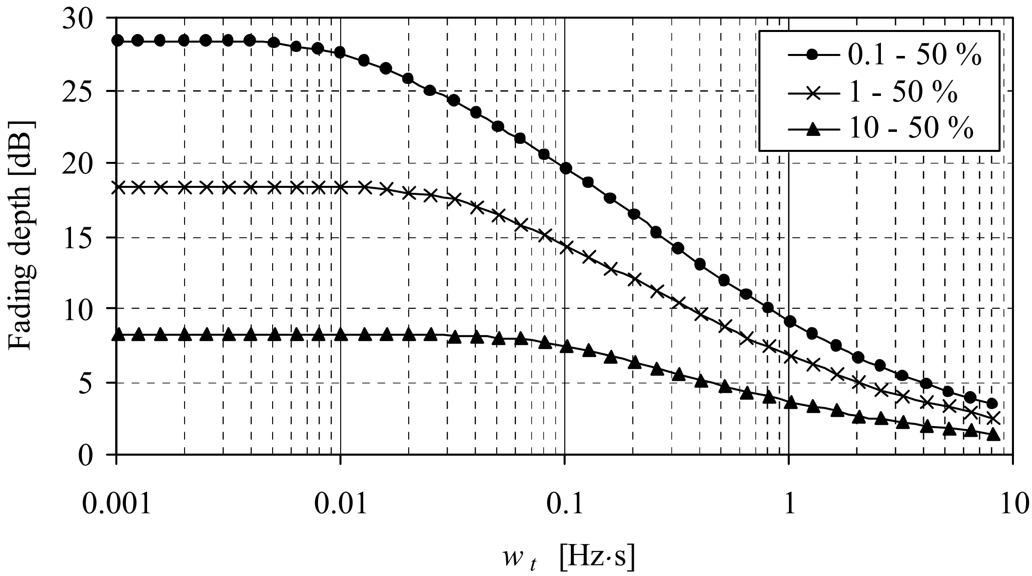

Figure 5.20 – Fading depth measured over different intervals, exponential model, NLoS.

As one observes, the fading depth varies in a similar way when one considers different values for the fading depth evaluation interval. As expected, for each value of w_t, the larger fading depth evaluation interval the larger observed fading depth.

The main difference among the curves in Figure 5.20 is that the point from which the fading depth starts to decrease (breakpoint) depends on the fading depth evaluation interval. As previously referred, when the fading depth is measured between 1 and 50 % of the CDF of the received power the breakpoint value is around 0.02 Hz·s, which corresponds to the correlation bandwidth of the propagation channel. If one considers an interval of [0.1, 50] % or [10, 50] % the breakpoint value is around 0.004 and 0.04 Hz·s respectively, which roughly correspond to 0.2 and 2.0 times the coherence bandwidth of the propagation channel. Different breakpoint values are expected if one considers a different fading depth evaluation interval.

5.3.5. Analytical Approximation

As verified in previous sections, when the PDP is represented by a single continuous exponential function, the fading depth depends only on w_t and K. Moreover, the curves for the two-stage exponential models are almost superimposed with the ones for the exponential case when $w_t \leq w_{b2,p}$, where $w_{b2,p}$ depends on the relative initial delay, *rms* delay spread and power of the exponential components. For large values of w_t, the fading depth becomes dependent on the shape of the PDP, hence, this influence has to be accounted for.

By comparing the results derived in this chapter with the ones in Chapter 4, one realises that the fading depth depends on w_t in a similar way as it depends on the product between the system bandwidth and the maximum difference in propagation path length, w_l, which is not surprising, since the value of the *rms* delay spread of the propagation channel is closely related with the difference in propagation path length of arriving waves. Thus, the fading depth can be reasonable approximated by (see Chapter 4):

$$FD_p^t(K,w_t)_{[\mathrm{dB}]} = \begin{cases} S_p^t(K) & , \; w_t \le w_{b1,p} \\ \dfrac{S_p^t(K) - A_{1,p}^t(K)}{1 + A_{2,p}^t(K) \cdot \left[\log\left(\dfrac{w_t}{w_{b1,p}} \right) \right]^{A_{3,p}^t(K)}} + A_{1,p}^t(K) + f(K,w_t) & , \; w_t > w_{b1,p} \end{cases} \tag{5.27}$$

where $S_p^t(K)$, $A_{1,p}^t(K)$, $A_{2,p}^t(K)$ and $A_{3,p}^t(K)$, are functions that also depend on the interval used for the fading depth evaluation, as well as the breakpoint, $w_{b1,p}$. The function $f(K,w_t)$ is equal to zero for the case of exponential PDPs, while for two-stage PDPs, $f(K, w_t)$ is equal to zero only for $w_t \le w_{b2,p}$, where $w_{b2,p}$ depends on the relative power, *rms* delay spread and initial delay of each exponential component.

In the case of an exponential PDP, the fitting process consists on the evaluation of $S_p^t(K)$, $A_{1,p}^t(K)$, $A_{2,p}^t(K)$ and $A_{3,p}^t(K)$ that fit the simulated data for each value of K. For a two-stage PDP, $f(K,w_t)$ needs also to be evaluated. Results from fitting data for an exponential PDP are presented in Table 5.3.

Table 5.3 – Fitted parameters and associated error, exponential model, p = 1 %.

***K* [dB]**	$S_p^t(K)$ [dB]	$A_{1,p}^t(K)$ [dB]	$A_{2,p}^t(K)$	$A_{3,p}^t(K)$	$\sqrt{\overline{\varepsilon^2}}$ [dB]	$\overline{\varepsilon_r}$ [%]
-∞ (NLoS)	18.40	-2.98	0.23	2.37	0.06	-0.05
12	4.49	-0.03	0.04	2.90	0.03	0.08

Two different situations are considered, NLoS, and K = 12 dB; the breakpoint value is assumed as being $w_{b1,p}$ = 0.02 Hz·s, and p = 1.0 % is considered. The *rms* error and mean relative error are evaluated as in Chapter 4. From Table 5.3, one observes that both errors are negligible, hence, a very accurate fitting is expected. The results from the evaluation of (5.27) with the parameterisation in Table 5.3 are presented in Figure 5.21.

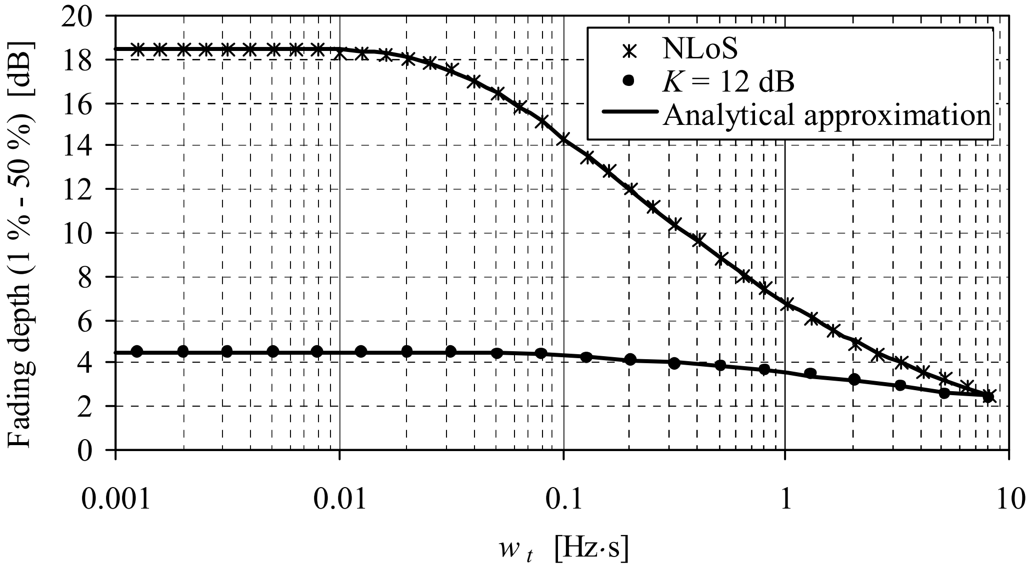

Figure 5.21 – Fitting results, exponential model.

As one can observe, both the results from the evaluation of (5.27) and the dots, which correspond to the simulated data, are practically superimposed, hence, it seems that the proposed analytical approximation can be of interest for modelling the fading depth behaviour for different channel models. Similarly to the work presented in Chapter 4, one also concludes that the same approach can be used to fit results for different values of the Rice factor since the variation law of the fading depth is quite similar to the one for the NLoS case. Nevertheless, it should be remembered that, for the case of discrete PDPs the fading depth curves remain constant for values of w_t above a value that depends on the minimum required bandwidth needed for discriminating all arriving waves; hence, this should be taken into account when using such analytical approximation. For simplicity, the analytical expressions for $S_p^t(K)$, $A_{1,p}^t(K)$, $A_{2,p}^t(K)$ and $A_{3,p}^t(K)$ were not derived, nevertheless, a similar approach as the one described in Chapter 4 can be used.

Alternatively, the fading depth curves for the case of discrete two-stage exponential PDPs can be approximated in a piecewise manner from considering that it can be decomposed into several parts, each part being approximated by a different analytical expression, (5.28), where, $S_{1,p}^t(K)$, $A_{11,p}^t(K)$, $A_{12,p}^t(K)$, $A_{13,p}^t(K)$, $S_{2,p}^t(K)$ $A_{21,p}^t(K)$, $A_{22,p}^t(K)$, $A_{23,p}^t(K)$ and $S_{3,p}^t(K)$ are functions that depend on the fading depth evaluation interval, as previously. The breakpoints, $w_{b1,p}$, $w_{b2,p}$, $w_{b3,p}$ and $w_{b4,p}$ depend on the fading depth evaluation interval, and on the type of channel model being considered. Moreover, for the case of continuous two-stage exponential PDPs, there is no breakpoint above which the fading depth remains constant and independent on w_t, therefore, $w_{b4,p}$ should be set to infinity and $S^t_{3,p}(K)=0$ for all values of K.

$$FD^t_p(K,w_t)_{[\mathrm{dB}]}=\begin{cases} S^t_{1,p}(K) & , w_t \le w_{b1,p} \\ \dfrac{S^t_{1,p}(K)-A^t_{11,p}(K)}{1+A^t_{12,p}(K)\times\left[\log\left(\dfrac{w_t}{w_{b1,p}}\right)\right]^{A^t_{13,p}(K)}}+A^t_{11,p}(K) & , w_{b1,p} < w_t \le w_{b2,p} \\ S^t_{2,p}(K) & , w_{b2,p} < w_t \le w_{b3,p} \\ \dfrac{S^t_{2,p}(K)-A^t_{21,p}(K)}{1+A^t_{22,p}(K)\times\left[\log\left(\dfrac{w_t}{w_{b2,p}}\right)\right]^{A^t_{23,p}(K)}}+A^t_{21,p}(K) & , w_{b3,p} < w_t \le w_{b4,p} \\ S^t_{3,p}(K) & , w_t > w_{b4,p} \end{cases} \quad (5.28)$$

As an illustration, one presents the results for the fading depth observed for a two-stage exponential discrete PDP (which corresponds to the proposed channel model for UMTS Hilly Terrain environments [3GPP02a]), Figure 5.22. The fitted parameters are presented in Table 5.4. The breakpoints for this model were fixed to 0.01, 0.2, 0.3 and 100.0, respectively; as previously, p = 1 % is considered.

As one can observe, the approximation error is negligible, hence, the proposed analytical approximation is effective for fitting the fading depth results from two-stage exponential continuous or discrete channel models.

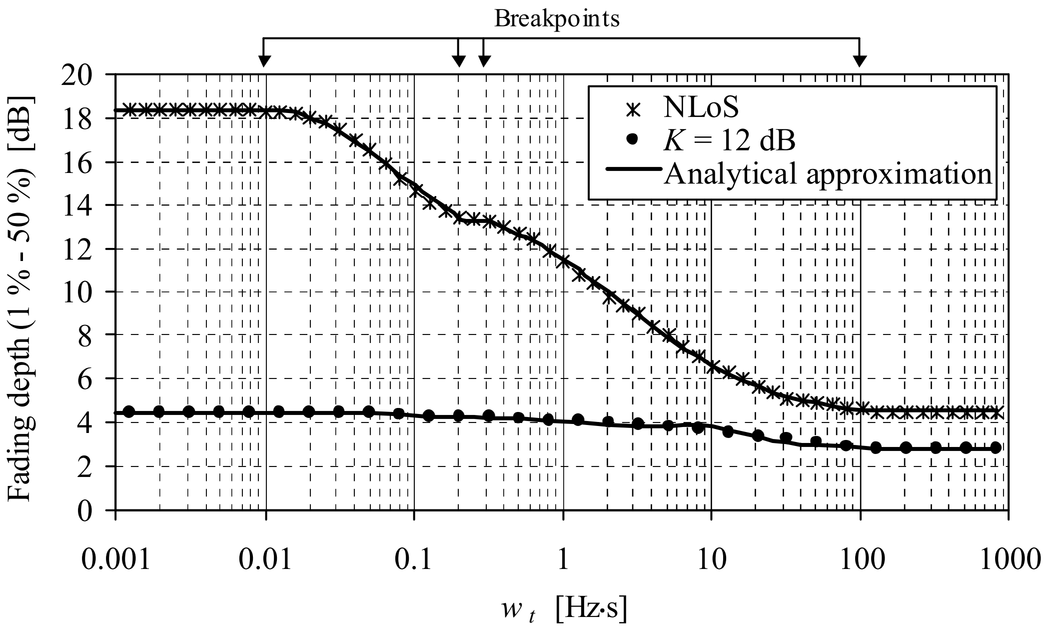

Figure 5.22 – Fitting results, two-stage exponential model.

Table 5.4 – Fitted parameters and associated error, two-stage exponential model, $p = 1$ %.

	NLoS	K = 12 dB
$S_{1,p}^{t}(K)$ [dB]	18.40	4.49
$A_{11,p}^{t}(K)$ [dB]	4.90	4.00
$A_{12,p}^{t}(K)$	0.36	0.37
$A_{13,p}^{t}(K)$	2.10	3.20
$S_{2,p}^{t}(K)$ [dB]	13.25	4.25
$A_{21,p}^{t}(K)$ [dB]	3.90	1.60
$A_{22,p}^{t}(K)$	0.004	0.002
$A_{23,p}^{t}(K)$	5.80	4.50
$S_{3,p}^{t}(K)$ [dB]	4.54	2.81
$\sqrt{\overline{\varepsilon^2}}$ [dB]	0.11	0.07
$\overline{\varepsilon_r}$ [%]	-0.27	0.23

As referred in Chapter 4, one of the main novelties of this type of analytical approximation is that, since an analytical fitting for a given channel model is obtained, the fading depth for any value of K and w_t can be easily evaluated from a simple expression, rather than for a more elaborated and computationally demanding model, allowing to easily evaluate the fading depth with a negligible error. It should be noted that this approach does not substitute the model in Section 5.2; the model is always the starting point for generating simulated data that can be used directly for evaluating the fading depth for given values of K and w_t or for evaluating the parameters for the analytical approximation, which allows to evaluate the fading depth for any value of K and w_t without the need for additional model simulations.

5.4. Conclusions

A time-domain based approach for fading depth characterisation in Rayleigh and Rice fading environments is proposed. The approach, based on the eigenvalue decomposition technique, allows deriving the CDF of the received power for various fading channels whose PDPs are expressed as continuous or discrete functions of the delay. The fading depth is evaluated as a function of the Rice factor, and the product between the system bandwidth and the *rms* delay spread of the propagation channel, w_t.

There are some similarities regarding the fading depth observed in different environments. For values of w_t below 0.02 Hz·s, the observed fading depths are similar and independent of the PDP of the propagation channel. This corresponds to a situation where the system bandwidth is below the coherence bandwidth of the propagation channel, thus, signals are in a frequency flat fading environment; for large values of w_t, fading depths depend on the type of the PDP. In order to assess this dependence, several simulations were carried out for continuous and discrete exponential and two-stage exponential PDPs, and the fading depth dependence on the type of PDP being considered is studied. Moreover, the results obtained from considering equivalent continuous and discrete PDPs are compared. It is concluded that the results obtained with discrete propagation models are similar to the ones for the continuous models; however, this is valid only below a value of w_t that depends on the minimum system resolution needed in order to resolve all paths, i.e., the inverse of the minimum difference in delay between two consecutive arriving waves.

An analytical approximation for the fading depth dependence on w_t is also proposed, allowing to accurately fitting the results from simulation, enabling to evaluate the fading depth from a simple expression. This approach reduces the computational effort needed, compared to the one required when the proposed time-domain based approach is used every time a fading depth value has to be evaluated for any value of K and w_t.

Chapter 6

Observed Fading Depth – A Comparative Analysis

6.1. Initial Considerations

In this chapter, results for the fading depth observed by GSM, UMTS and HIPERLAN/2 in standard reference environments as proposed by standard-setting bodies are presented and discussed. The observed fading depth is also evaluated whenever the considered system bandwidth is below the one for which the models are designed for, as well as the one observed by GSM with the models for UMTS and HIPERLAN/2; a similar approach is used for UMTS. Results from MBS, derived from experimental PDPs obtained from measurements in different environment, are also presented. This way, the whole set of results presented in Chapter 4 is enhanced by providing an exhaustive set of data for the most well-known channel models, allowing the proper design and assessment of such systems.

Moreover, since there is a link between the environment properties and the PDP of the propagation channel (hence, the *rms* delay spread), a simple (but accurate enough in most cases) relationship between the maximum difference in propagation path length among different arriving components and the *rms* delay spread of the propagation channel is also proposed, which also constitutes a novelty. The main objective of the proposed relationship is to bridge the gap between the models presented in [KoSN96] and [InKa99] in which the approaches proposed in Chapters 4 and 5 are based, allowing one to use any of the proposed approaches for evaluating the fading depth in a given environment, defined either by its physical and geometrical properties, or by the PDP of the propagation channel. By using the proposed relationship, fading depth results obtained from the proposed time-domain approach are compared with the ones from the environment geometry-based analytical one. Furthermore, since the presented models for wideband fading characterisation account for the influence of system bandwidth, more accurate fading margins are provided, leading to a better power budget evaluation, and enabling a better and less costly planning of future networks, as well as the optimisation of existing ones.

6.2. GSM Fading Depth Models

There is a large set of channel models for GSM that has been proposed by the Joint Technical Committee for Personal Communication Systems (JTC/PCS) [PaLe95] and the European Telecommunications Standards Institute (ETSI) [ETSI99], with the latter being the most commonly used for system evaluation purposes. The channel models recommended by ETSI for GSM are defined by 12 tap settings; a reduced configuration with only 6 taps is also provided for simple simulators, but the full configuration should be used whenever possible. For each model, two equivalent alternative tap settings are given (Appendix IV). The channels models, and the corresponding average *rms* delay spread, are presented in Table 6.1.

Table 6.1 – Average *rms* delay spread for GSM environments.

Environment	Cell type	Average *rms* delay spread [ns]	
		Type 1	Type 2
Rural Area	Macro-cell	98	126
Typical Urban	Macro-cell	1 026	1 000
Bad Urban	Macro-cell	2 553	2 488
Hilly Terrain	Macro-cell	5 100	4 984

The referenced channels models were already used in the previous chapter as a basis for the study of the fading depth dependence on the type of the PDP. Since for each environment two equivalent alternative channel models are given, one only considers Type 1 channel models in here.

In order to evaluate the fading depth observed in different environments, one has to evaluate the value of w_t for each environment, Table 6.2. It should be remembered that for a system bandwidth below the coherence bandwidth of the propagation channel, i.e.,

$w_t \leq 0.02$ Hz·s, a system is said to be narrowband and experiences the highest fading depth; however, small variations on the propagation conditions, which affects the value of the *rms* delay spread of the propagation channel, are not significant regarding the observed fading depth. When $w_t > 0.02$ Hz·s, the wideband case, small changes on the propagation conditions are more significant regarding the observed fading depth.

Table 6.2 – Value of w_t for GSM Type 1 environments.

Environment	w_t [Hz·s]
Rural Area	0.02
Typical Urban	0.21
Bad Urban	0.51
Hilly Terrain	1.02

As can be observed from Table 6.2, in Rural Area environments one has $w_t = 0.02$ Hz·s, hence, it is expected that the observed fading depth does not depend significantly on small variations of the propagation environments. For Typical Urban, Bad Urban and Hilly-Terrain environments, the observed fading depth is more sensitive to environment changes, since the value of w_t is well above 0.02 Hz·s. Globally, one can state that a decrease in w_t due to a decrease of σ_τ causes an increase in fading depth.

Since one has the value of w_t for each environment, the observed fading depth in different environments can be evaluated from (5.15), as illustrated in Figure 6.1.

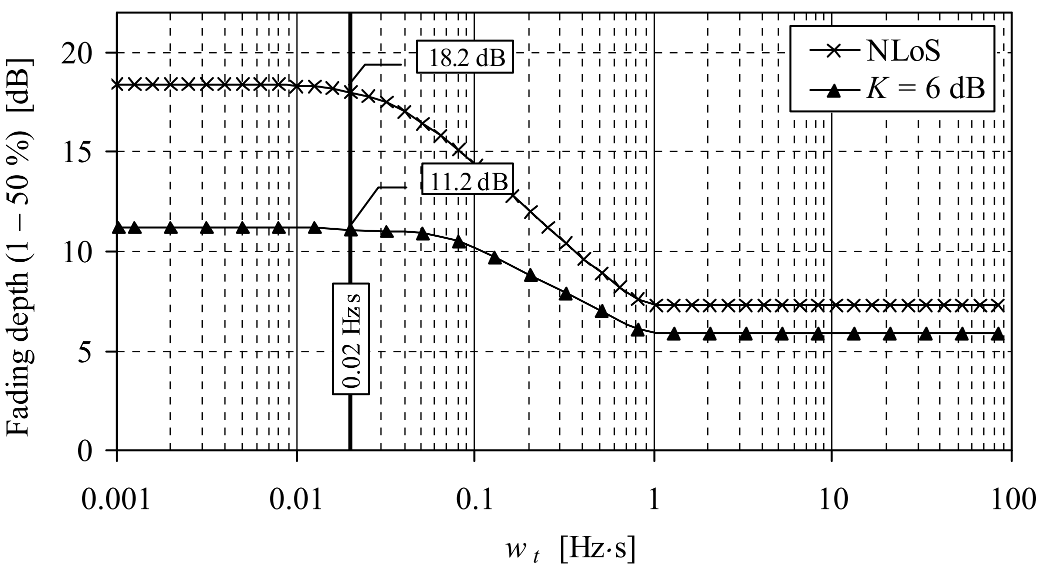

Figure 6.1 – Observed fading depth.

The Rural Area model applies to macro-cellular environments, and LoS is assumed in principle. The corresponding PDP is depicted in Figure 6.2, where $P_{i_{max}}$ corresponds to the power of the strongest arriving wave, and parameters P_i and τ_i standing for the power and delay of the i-th arriving wave. The eigenvalue characteristics are represented in Figure 6.3.

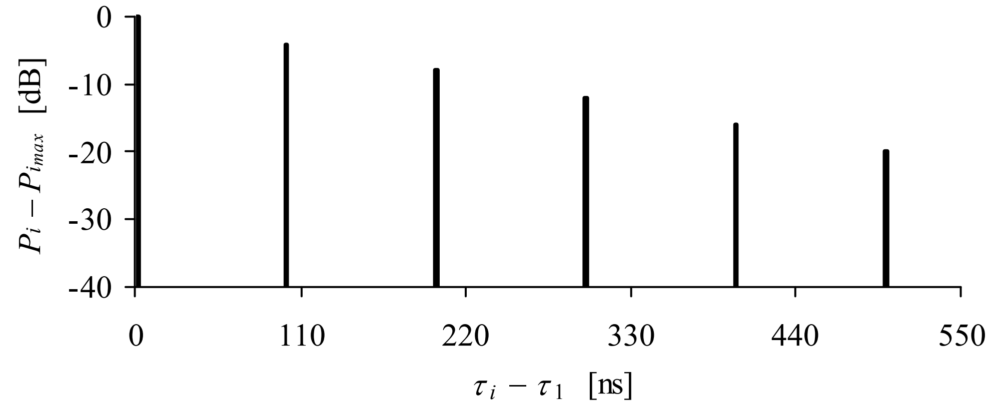

Figure 6.2 – PDP, GSM Rural Area.

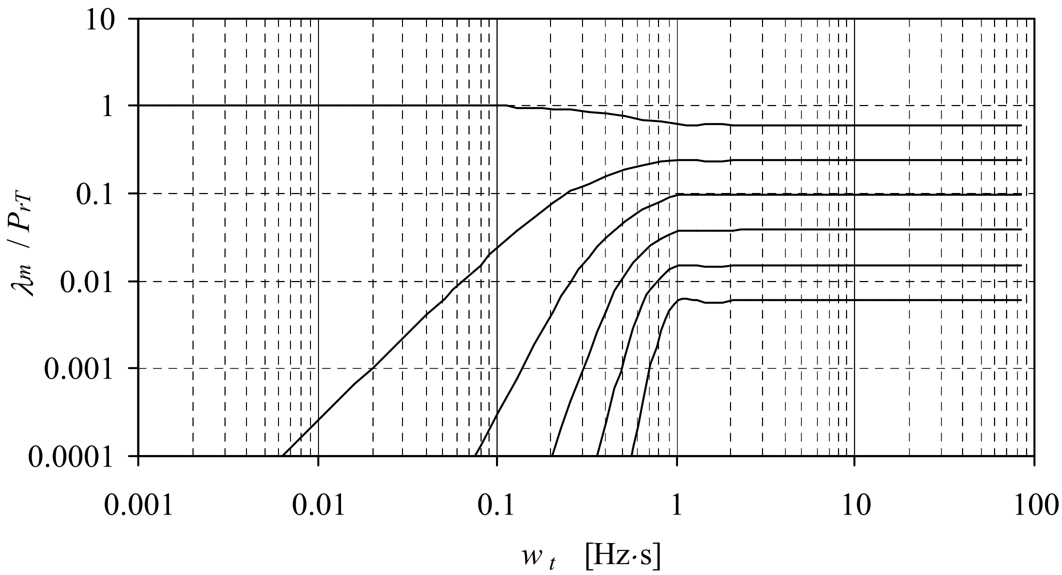

Figure 6.3 – Eigenvalue characteristics, GSM Rural Area.

As one can observe, the eigenvalue characteristics are similar to the ones of the continuous case for $w_t \leq 1.0$ Hz·s (see Chapter 5), and then converge to the relative power of each arriving wave, meaning that all paths are resolved. One must remember that the value of w_t for which the eigenvalue characteristics converge can be evaluated as the inverse of the minimum time delay between consecutive arriving waves, that is, the minimum system resolution needed to resolve all paths.

The fading depth curves for the Rural Area model are depicted in Figure 6.4. As expected, for each K and $w_t < 1.0$ Hz·s, the observed fading depth is similar to the one of the continuous exponential model. A fading depth of 18.2 and 11.2 dB is observed for NLoS and $K = 6$ dB, respectively.

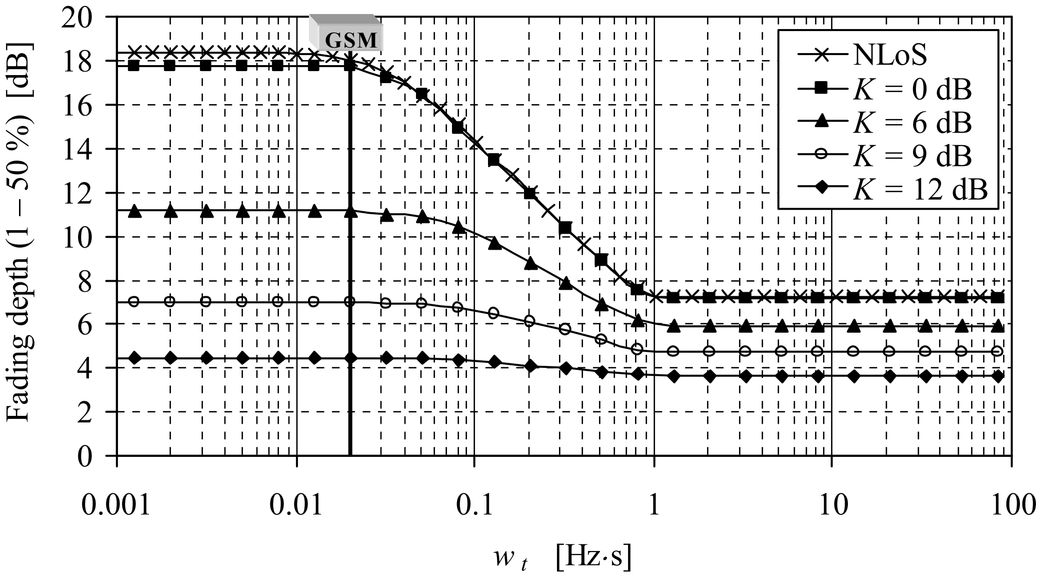

Figure 6.4 – Fading depth, GSM Rural Area.

The Typical Urban model applies to macro-cellular environments, and a NLoS situation is considered. The corresponding PDP is depicted in Figure 6.5.

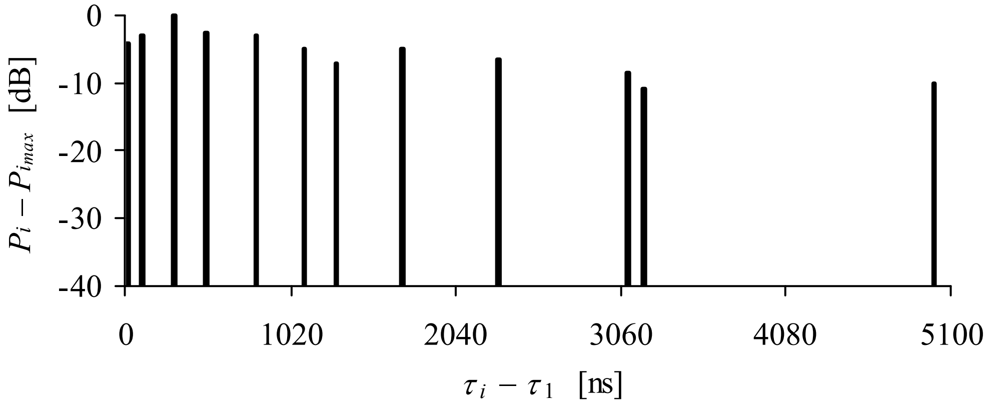

Figure 6.5 – PDP, GSM Typical Urban.

From Figure 6.6, it can be observed that the eigenvalues oscillate near $w_t = 10.0$ Hz·s and finally converge for $w_t > 20.0$ Hz·s. This value is significantly large, compared to the one of the previous case, due to presence of waves arriving at close delays, since a higher system resolution is needed to resolve all paths.

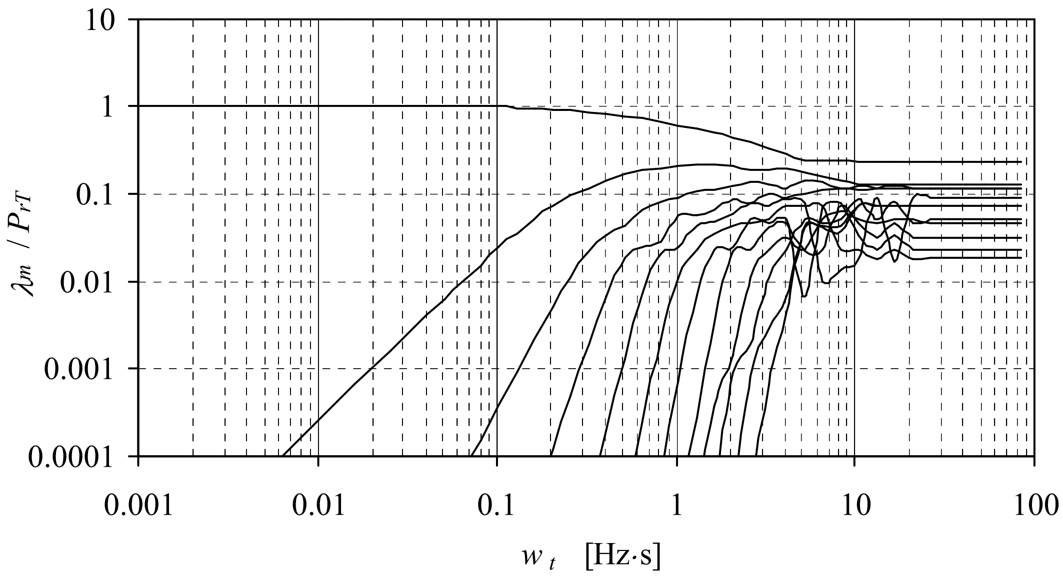

Figure 6.6 – Eigenvalue characteristics, GSM Typical Urban.

The fading depth curve is depicted in Figure 6.7. A fading depth of 12 dB is observed for NLoS; LoS conditions are not considered, since this model is not intended for LoS. As one can observe, the fading depth is similar to the one for the Rural Area model, however, the value of w_t above which the fading depth remains constant and independent of w_t is larger than the one for the Rural Area case, as expected from the behaviour of the eigenvalues.

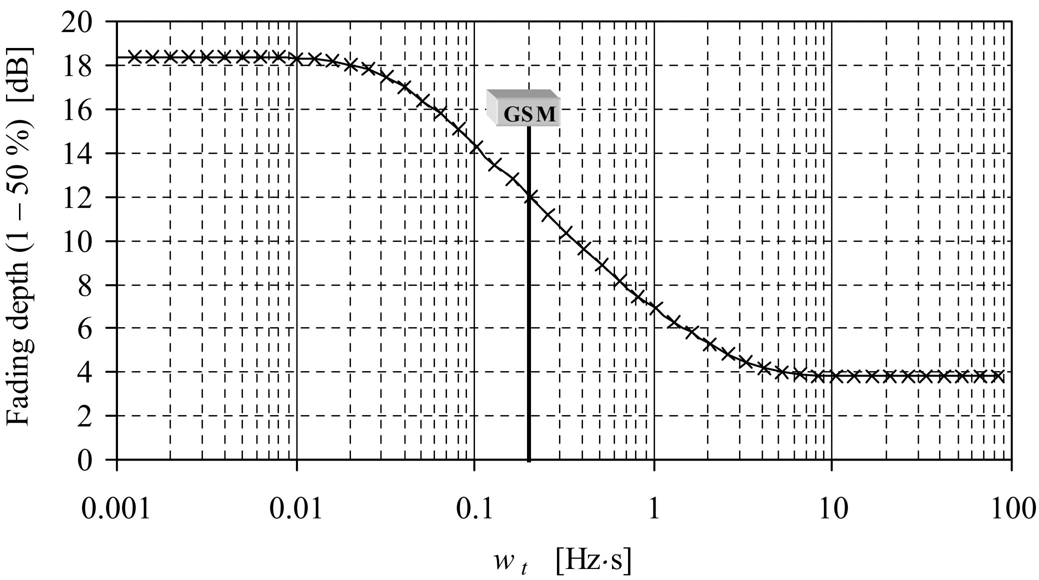

Figure 6.7 – Fading depth, GSM Typical Urban.

For simplicity, from now on, the graphical representation of the PDPs and the eigenvalue characteristics will be omitted; they can be found in Appendix V.

The Bad Urban model, applies to macro-cellular environments characterised by two distinct groups of arriving waves, a typical situation in hilly urban areas; as previously, one only considers the NLoS case. It can be observed that the eigenvalue characteristics oscillate near $w_t = 10.0$ Hz·s, and finally converge for $w_t > 20.0$ Hz·s, being quite similar to the ones for the Typical Urban model; as a consequence, the fading depth curves are also close to the ones for the Typical Urban model. Nevertheless, a lower fading depth is obtained, since the *rms* delay spread of the propagation channel is well above the one for the Typical Urban model; a fading depth of 9.2 dB is observed under NLoS.

The Hilly Terrain model applies to macro-cellular environments, also characterised by two distinct groups of arriving waves, in the NLoS case, Figure 6.8. Eigenvalues oscillate near $w_t = 40.0$ Hz·s, and finally converge for $w_t > 200.0$ Hz·s. As expected, the fading depth curve is typical of a two-stage exponential model with two distinct groups of arriving waves at distant delays, a fading depth of 10.3 dB being registered.

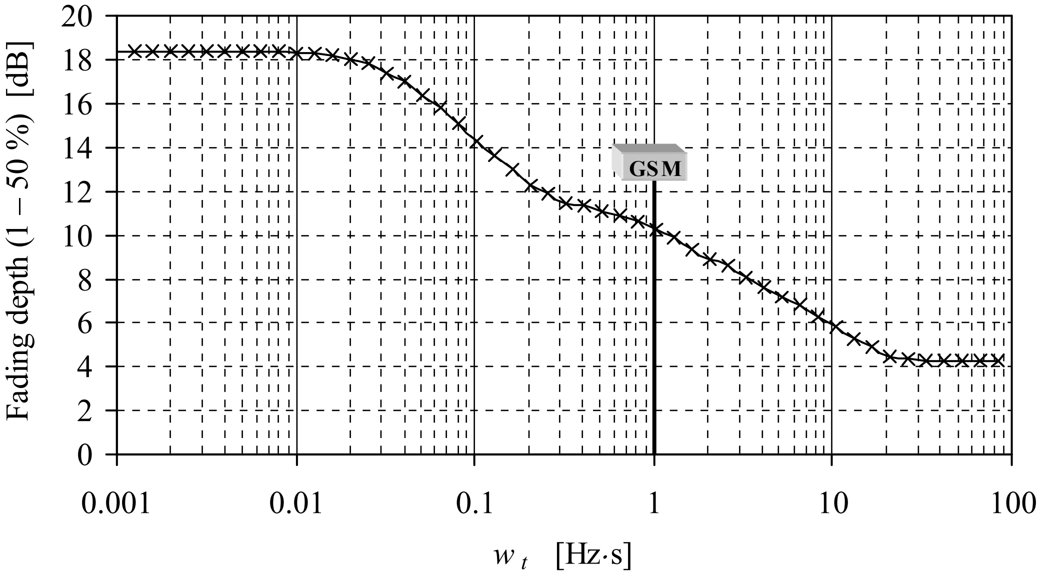

Figure 6.8 – Fading depth, GSM Hilly Terrain.

A summary on the fading depth observed in different environments is presented in Table 6.3. For each system, the fading depth observed in each environment is evaluated, for both NLoS and LoS cases, when appropriate; for LoS, a Rice factor of $K = 6$ dB is assumed. As one can see from Table 6.3, the fading depth observed by GSM under NLoS ranges from 18.2 dB in Rural Areas to 9.2 dB verified in Bad Urban environments. However, if one considers the existence of LoS in Rural Area environments and $K = 6$ dB, the observed fading depth decreases to 11.2 dB. As presented, the fading depth observed by GSM, under NLoS, in different environments is always significantly below the one obtained from considering the Rayleigh distribution, for which a fading depth of 18.4 dB is obtained for the given value of *p*; this corresponds to the narrowband case, i.e., $w_t < 0.02$ Hz·s, exception made for the case of the Rural Area model for which this difference is not significant. Under LoS, the fading depth observed in Rural Area environments is the same as the one obtained from the Rice distribution for the given value of *K*, i.e., 11.2 dB.

Table 6.3 – Fading depth observed in GSM Type 1 environments, *p* = 1%.

Environment	Fading depth [dB]	
	GSM	
	NLoS	K = 6 dB
Rural Area	18.2	11.2
Typical Urban	12.0	–
Bad Urban	9.2	–
Hilly Terrain	10.3	–

Therefore, one concludes that Rayleigh and Rice distributions still are appropriate for evaluating the fading depth in GSM Rural Area environments. For the remaining NLoS environments, the Rayleigh distribution is no longer appropriate, hence, lower fading margins than the ones obtained from this distribution should be considered for link budget evaluation purposes.

6.3. UMTS Fading Depth Models

Several channel models were proposed for UMTS by ETSI [ETSI97] and Third Generation Partnership Project (3GPP) [3GPP02a]. Since most of the time, *rms* delay spreads are relatively small, but there are "worst cases" when multipath characteristics lead to much larger delay spreads, ETSI proposes two channel models for each environment; within a given test environment, Channel A corresponds to the low delay spread and Channel B to the median delay spread that occurs frequently, Table 6.4. 3GPP only defines one channel model for each environment, Table 6.5.

As previously, the tapped-delay line parameters, the corresponding PDPs and the eigenvalues characteristics, for each model, can be found in Appendix V.

Table 6.4 – Average *rms* delay spread for UMTS environments.

Environment	Cell type	Average *rms* delay spread [ns]	
		Channel A	Channel B
Indoor Office	Pico-cell	35	100
Outdoor to Indoor and Pedestrian	Micro-cell	45	750
Vehicular - High Antenna	Macro-cell	370	4 000

Table 6.5 – Average *rms* delay spread for UMTS environments.

Environment	Cell type	Average *rms* delay spread [ns]
Rural Area	Macro-cell	100
Typical Urban	Macro-cell	500
Hilly Terrain	Macro-cell	3 000

Using the proposed channel models for UMTS, one can compare the observed fading depth for different systems, namely GSM and UMTS. The results for w_t for each system and environment are presented in Table 6.6. For simplicity, from now on, one refers to "Outdoor to Indoor and Pedestrian" model as the "Pedestrian" model.

Table 6.6 – Value of w_t for UMTS environments.

Environment	w_t [Hz·s]	
	GSM	UMTS
Indoor-A	0.01	0.18
Pedestrian-A	0.01	0.23
Vehicular-A	0.07	1.85
Indoor-B	0.02	0.50
Pedestrian-B	0.15	3.75
Vehicular-B	0.80	20.00
Rural Area	0.02	0.50
Typical Urban	0.10	2.50
Hilly Terrain	0.60	15.00

From Table 6.6, one concludes that UMTS behaves as a wideband system in all kind of environments, since w_t is well above 0.02 Hz·s, hence, the observed fading becomes significantly dependent on environment changes that affect the value of σ_τ. Regarding GSM, one concludes that this effect is not significant in Indoor, Pedestrian-A and Rural Area environments. For the remaining classes of environments, GSM behaves like a wideband system, experiencing lower fading depths, but being more sensitive to environment changes that affect propagation.

Vehicular channel models are intended for macro-cellular environments. For the case of Vehicular-A, one can assume the existence of a LoS component. As expected, the eigenvalue characteristics are similar to the ones for the continuous case for $w_t \leq 1.0$ Hz·s, and then converge to the relative power of each arriving wave.

As one can observe from Figure 6.9, for each value of K, and $w_t \leq 1.0$ Hz·s, the fading depth curves behave in a similar way as for continuous exponential models. For large values of w_t, the curves become independent of w_t, and converge to a fading depth value that is a function of K, since all paths are resolved, as previously referred.

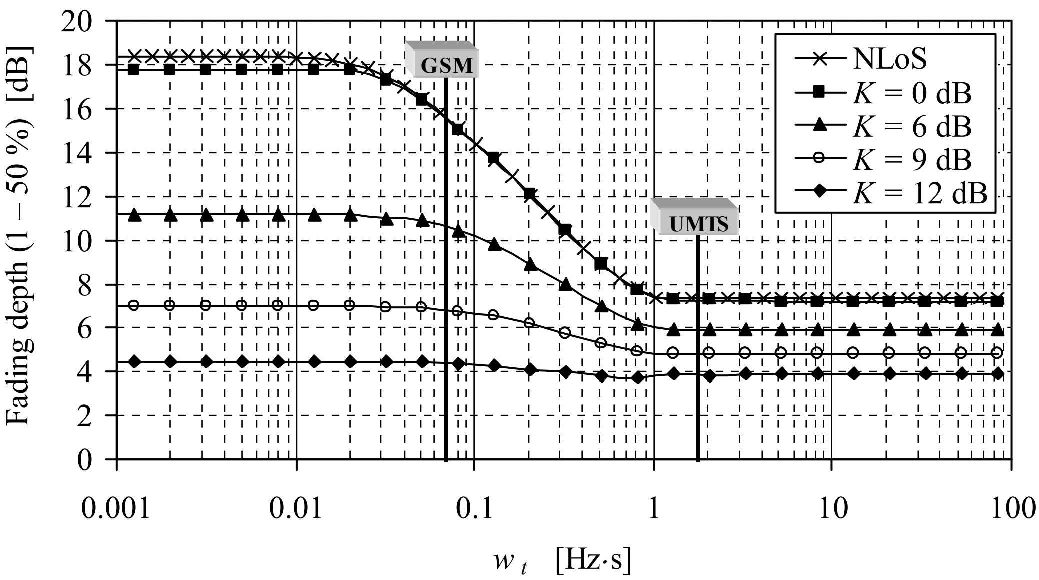

Figure 6.9 – Fading depth, UMTS Vehicular-A.

It must be noted that the value of w_t for UMTS in this type of environments is above the one for which the fading depth remains constant, i.e., independent on the system bandwidth. Therefore, this model is not well appropriate for UMTS fading depth evaluation purposes, since there is always an approximation error, introduced from considering a discrete channel model whose characteristics are not adequate for UMTS. If NLoS is assumed, a fading depth of 3 and more than 11 dB below the one for the narrowband case, is observed for GSM and UMTS, respectively. Under LoS and $K = 6$ dB, these values decreases to 0.6 and more than 5.3 dB, respectively.

In the case of the Vehicular-B, the eigenvalue characteristics converge slower than for the case of Vehicular-A, due to the effect of the first two strong propagation paths located at close delays, since, a large system bandwidth is needed to discriminate them. From Figure 6.10, one concludes that, as expected, the fading depth for the Vehicular-B model varies in a similar way as for the case of a two-stage exponential model. This is not surprising, since the PDP is composed of two distinct groups of arriving waves: two arriving waves at close delay, and the remaining ones together in a group significantly delayed from the first one. As expected, the value of w_t above which the fading depth remains constant is larger than the one for the Vehicular-A model. For the same reasons as previously, this model is not well appropriate for UMTS fading depth evaluation purposes. Under NLoS, a fading depth of 8.1 and more than 10.7 dB below the one for the narrowband cases, is observed for GSM and UMTS, respectively; this model is not intended for LoS.

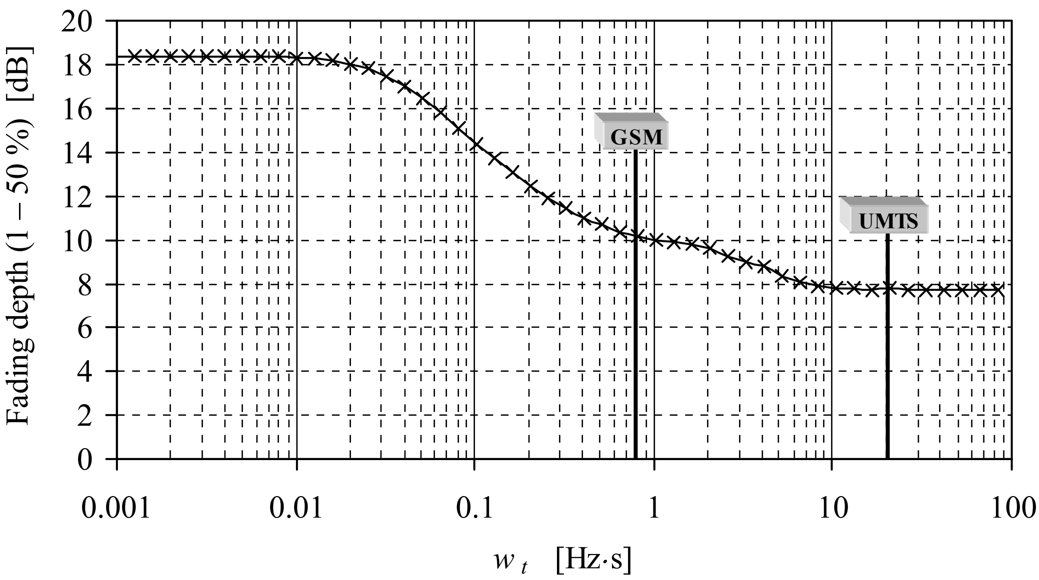

Figure 6.10 – Fading depth, UMTS Vehicular-B.

Indoor models are adequate to describe environments characterised by small cells (pico-cellular) and low transmit powers, with both antennas and users located indoors. Besides the difference on the relative powers of arriving waves that compose the PDP, the eigenvalue characteristics for the Indoor-A model behave almost like the ones for the Vehicular-A model. Nevertheless, the value of w_t for the different systems being considered is well below the one observed in Vehicular-A environments, therefore, for each value of K, the observed fading depths are above the ones for Vehicular-A, Figure 6.11. As expected, GSM behaves as a narrowband system. If NLoS is assumed, a fading depth of 5.9 dB below the one for GSM is observed for UMTS; for K = 6 dB, this value decreases to 2.1 dB.

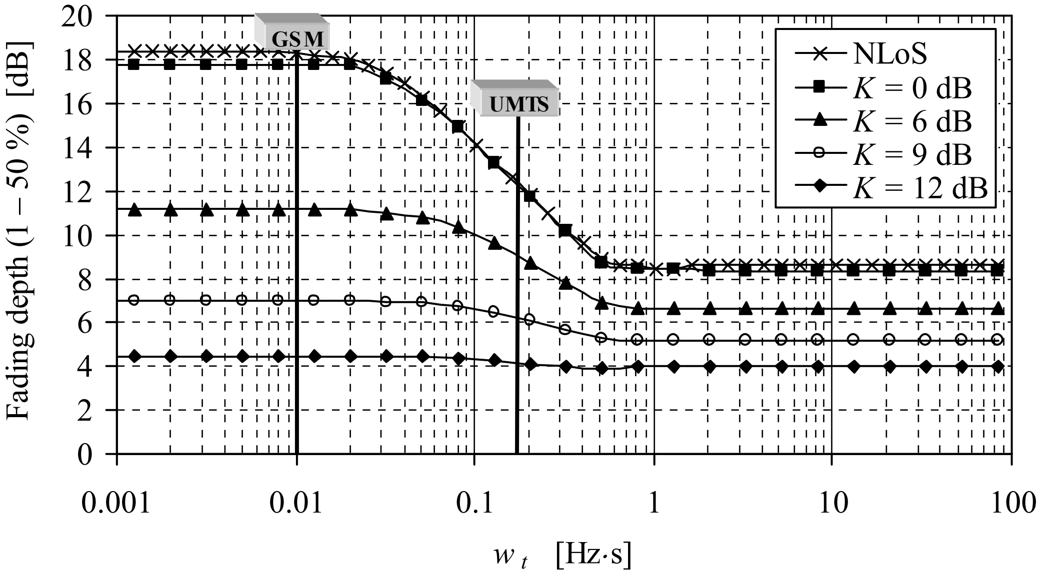

Figure 6.11 – Fading depth, UMTS Indoor-A.

It is observed that the eigenvalue characteristics for the Indoor-B model are similar to the ones for Indoor-A. As expected from the value of w_t, the observed values of fading depth are below the ones for Indoor-A, nevertheless, GSM behaves almost as a narrowband system. For UMTS, a fading depth of 9.4 and 4.2 dB below the ones for the narrowband case, are observed for NLoS and $K = 6$ dB, respectively.

Pedestrian models apply to both, micro- and pico-cellular environments, and low transmit powers. Antennas are located outdoors at low heights, and users can be either on the streets or inside buildings. Eigenvalues for the Pedestrian-A model vary around $w_t = 0.25$ Hz·s, and then converge. As previously, GSM behaves as a narrowband system. UMTS experiences fading depths of 6.1 and 2.1 dB below the ones for GSM, for NLoS and $K = 6$ dB, respectively. The eigenvalue characteristics for Pedestrian-B model are similar to the ones for Vehicular-B. Besides the similarities with the Vehicular-B model, the fading depth, observed for large values of w_t, is below the one for the Vehicular-B model, due to the differences in relative power and delay of arriving waves. As verified for the case of Vehicular models, the value of w_t for UMTS is above the one for which the fading depth remains constant, thus, this model is not well appropriate for UMTS fading depth evaluation purposes. If NLoS is assumed, a fading depth of 4.9 and more than 12.1 dB below the one for the narrowband case, is observed for GSM and UMTS; for $K = 6$ dB, these values decrease to 1.4 and more than 6 dB, respectively.

The Rural Area model applies to macro-cellular environments. Since the number of arriving paths is higher than the ones for the previous models, the eigenvalues behaviour is closer to the one of the continuous models. If NLoS is assumed, a fading depth of 9.7 dB below the one for the narrowband case, is observed for UMTS; for $K = 6$ dB, this value decreases 4.3 dB, respectively. GSM behaves almost as a narrowband system.

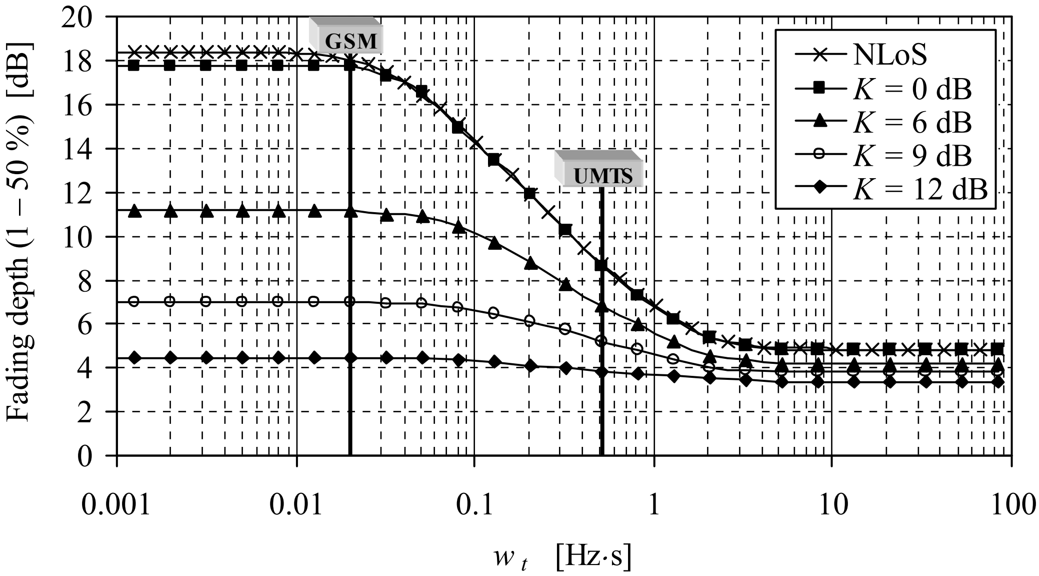

Figure 6.12 – Fading depth, UMTS Rural Area.

The Typical Urban model applies to macro-cellular environments. The behaviour of the eigenvalue characteristics for the Typical urban model is similar to the one for the Rural Area model for $w_t < 1.0$ Hz·s; however, for large values of w_t, it varies very much, due to the existence of arriving waves at close delays. The fading depth dependence on w_t is similar to the one for the Rural Area model. Nevertheless, this model is not well appropriate for UMTS fading depth evaluation purposes, for the same reasons as previously explained. If NLoS is assumed, a fading depth of 4.1 and more than 13.3 dB below the one for the narrowband case, is observed for GSM and UMTS, respectively; for $K = 6$ dB, these values decreases to 1 and more than 6.9 dB, respectively.

The Hilly Terrain model applies to macro-cellular environments. This model is characterised by two distinct groups of arriving waves, which is the most common situation for this type of environments. The eigenvalues behaviour is typical for a PDP with two distinct exponential groups of arriving waves. For large values of w_t, the eigenvalues vary even more than in the previous cases. The fading depth dependence on w_t is presented in Figure 6.13. As expected, the observed fading depth is similar to the one obtained for the case of a two-stage exponential model; as one can observe, the fading depth remains almost constant and independent of w_t, for $0.2 \leq w_t \leq 0.3$ Hz·s, and then starts to decrease as

w_t increases, since the PDP is composed of two groups of arriving components at distant delays. If NLoS is assumed, a fading depth of 5.8 and 12.3 dB below the one for the narrowband case, is observed for GSM and UMTS, respectively; for $K = 6$ dB, these values decrease to 1.8 and 6.1 dB, respectively.

A summary on the observed fading depths in different environments is presented in Table 6.7. As previously, for each system, the fading depth is evaluated both for NLoS and LoS cases, when appropriate; for LoS conditions, a Rice factor of $K = 6$ dB is assumed.

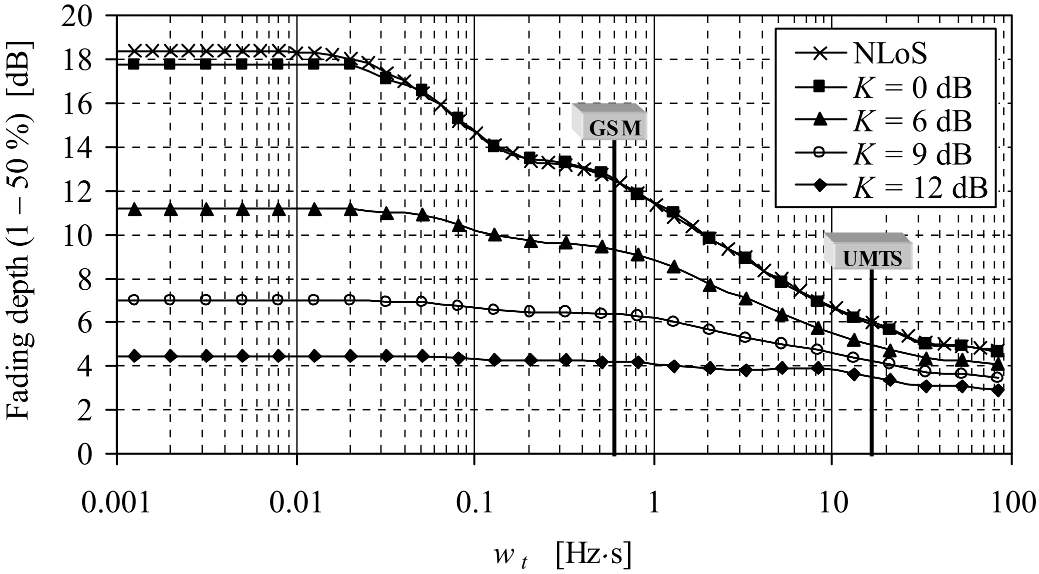

Figure 6.13 – Fading depth, UMTS Hilly Terrain.

Table 6.7 – Fading depth observed in UMTS environments, *p* = 1%.

Environment	Fading depth [dB]			
	GSM		UMTS	
	NLoS	$K = 6$ dB	NLoS	$K = 6$ dB
Indoor-A	18.4	11.2	12.5	9.1
Pedestrian-A	18.4	11.2	12.3	9.1
Vehicular-A	15.4	10.6	< 7.4	< 5.9
Indoor-B	18.1	11.2	9.0	7.0
Pedestrian-B	13.5	9.8	< 6.3	< 5.2
Vehicular-B	10.3	–	< 7.7	–
Rural Area	18.2	11.2	8.7	6.9
Typical Urban	14.3	10.2	< 5.1	< 4.3
Hilly Terrain	12.6	9.4	6.1	5.1

Under NLoS, GSM experiences fading depths between 10.3 and 18.4 dB; one must note that these values are close to the ones obtained with the channel models proposed for GSM. Fading depths between 9.4 and 11.2 dB are observed for $K = 6$ dB, thus, being close to the ones obtained from the Rice distribution, for the given value of K. The difference in fading depth between LoS and NLoS is usually lower than 7.2 dB.

The fading depths observed by UMTS, under NLoS, are between less than 5.1 and 12.5 dB; under LoS, these values decrease to less than 4.3 and 9.1 dB; the difference between LoS and NLoS being usually below 3.4 dB. One must remember that the real fading depths observed for Vehicular, Pedestrian-B and Typical Urban models, are below the ones presented in Table 6.7, due to the error introduced by using a discrete model (see Chapter 5).

From the difference in fading depth observed between the LoS and NLoS situations, one then concludes that, regarding fading depth, UMTS is less sensitive to the existence of LoS. Moreover, the fading depth experienced by UMTS is below the one for the narrowband case, for NLoS and LoS respectively; therefore, the fading margins for UMTS can be significantly reduced, compared to the ones obtained from the narrowband distributions. Rayleigh and Rice distributions are not appropriate for evaluating the fading depth for UMTS in different environments, hence, the fading margins derived from using the proposed approach should be used, otherwise, they will be clearly overestimated. For GSM, in NLoS environments, there is a closer proximity to the values for the narrowband case, nevertheless, the proposed approach should also be used, since the difference in fading depth still is significant for some environments, e.g., it can be as large as 8.1 dB for Vehicular-B environments; under LoS, the Rice distribution still is a reasonable approximation (a maximum difference of 1.8 dB is observed in Hilly Terrain environments).

6.4. HIPERLAN Fading Depth Models

Five channels models A, B, C, D and E were established for HIPERLAN/2 simulation purposes in different environments [MeSc98]: Model A corresponds to a typical office environment; Model B corresponds to a typical large open space environment with NLoS conditions, or an office environment with large delay spread; Models C and E correspond to typical large open space indoor and outdoor environments with large delay spread; Model D corresponds to LoS conditions in a large open space indoor, or an outdoor environment. The average *rms* delay spread for each environment is presented in Table 6.8. As previously, the tapped-delay line parameters for each model are presented in Appendix IV, the graphical representation of the PDPs and the eigenvalues characteristics can be found in Appendix V. The value of w_t for each system is presented in Table 6.9.

Table 6.8 – Average *rms* delay spread for HIPERLAN/2 environments.

Environment	Cell type	Average *rms* delay spread [ns]
Model A	Pico-indoor	50
Model B	Pico-indoor	100
Model C	Pico-indoor	150
Model D	Pico-indoor	140
Model E	Pico-indoor	250

Table 6.9 – Value of w_t for HIPERLAN/2 environments.

Environment	w_t [Hz·s]		
	GSM	UMTS	HIPERLAN/2
Model A	0.01	0.25	1.00
Model B	0.02	0.50	2.00
Model C	0.03	0.75	3.00
Model D	0.03	0.70	2.80
Model E	0.05	1.25	5.00

As one observes, while UMTS and HIPERLAN/2 are sensitive to environment changes that affect the *rms* delay spread of the propagation channel, GSM is less sensitive to those changes, since the value of w_t is usually around 0.02 Hz·s.

From the eigenvalue characteristics for Model A, Appendix V, one observes that, for $w_t < 5.0$ Hz·s, they are similar to the ones for continuous exponential models, and the two-stage exponential ones when the initial delay of the second exponential component is not significantly large, compared to the *rms* delay spread of the first exponential component. This should not come as a surprise, since the number of arriving waves is significantly large, approaching the case of a continuous channel model. The fading depth for different values of K is presented in Figure 6.14. As expected from the eigenvalue characteristics, the fading depth curves are similar to the ones for the continuous exponential case for $w_t < 5$ Hz·s. For higher values of w_t, the fading depth remains constant since all paths are resolved. As expected from Table 6.9, GSM behaves as a narrowband system. If NLoS is assumed, a fading depth of 7.2 and 11.7 dB below the one for GSM, is observed for UMTS and HIPERLAN/2, respectively; for $K = 6$ dB, these values decrease to 2.7 and 5.7 dB, respectively.

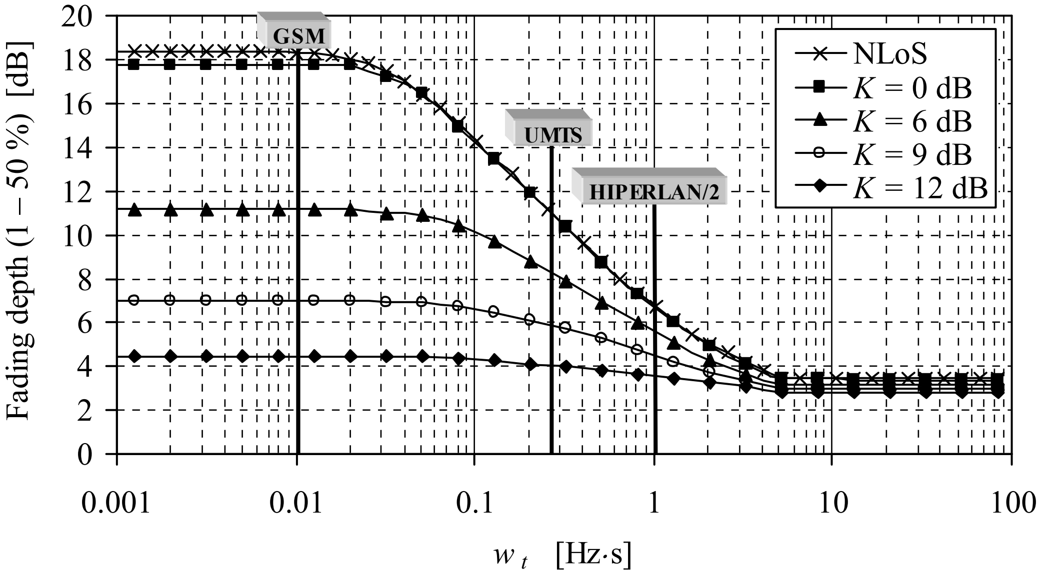

Figure 6.14 – Fading depth, HIPERLAN/2 Model A.

As previously, the eigenvalue characteristics for Model B are similar to the ones for continuous exponential and two-stage exponential models. The fading depth for different values of K is presented in Figure 6.15.

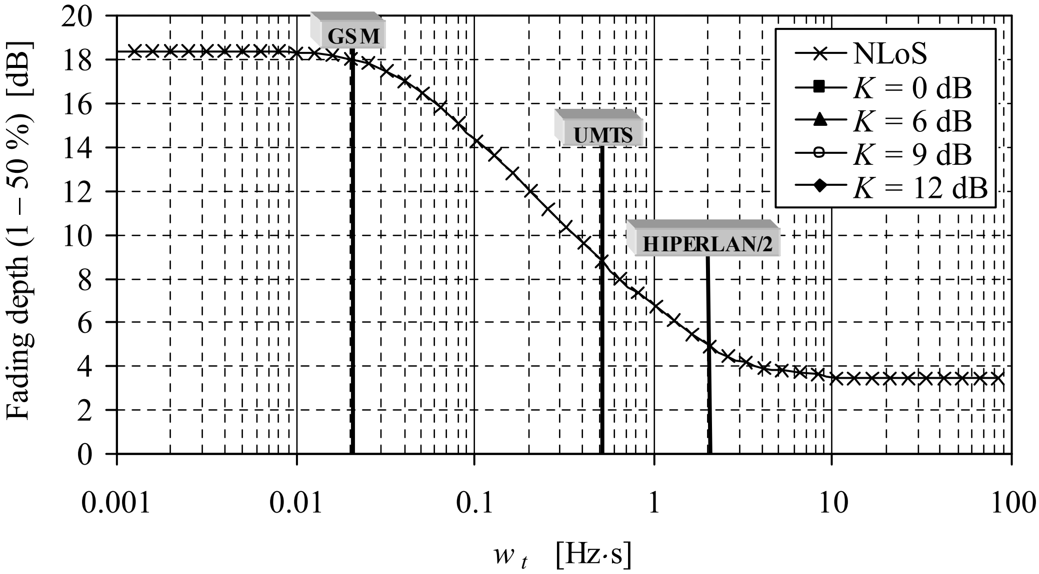

Figure 6.15 – Fading depth, HIPERLAN/2 Model B.

As expected, GSM behaves almost as a narrowband system. Under NLoS, fading depths of 9.5 and 13.5 dB below the one for the narrowband case, are observed for UMTS and HIPERLAN/2, respectively. LoS is not considered, since this model is not intended for LoS.

Also, the eigenvalue characteristics for Model C are similar to the ones for continuous exponential and two-stage exponential models, however, they oscillate around $w_t = 10$ Hz·s. As previously, GSM behaves almost as a narrowband system, UMTS and HIPERLAN/2 experiencing lower fading depths. Similar results for Model D and E can be found in Appendix V.

A summary on the fading depth observed in different environments is presented in Table 6.10. As previously, for each system, the fading depth observed within different environments is evaluated, both for NLoS and LoS cases.

Table 6.10 – Fading depth observed in HIPERLAN/2 environments, *p* = 1%.

Environment	Fading depth [dB]					
	GSM		UMTS		HIPERLAN/2	
	NLoS	$K = 6$ dB	NLoS	$K = 6$ dB	NLoS	$K = 6$ dB
Model A	18.4	11.2	11.2	8.5	6.7	5.5
Model B	18.1	–	8.9	–	4.9	–
Model C	17.6	–	7.6	–	4.2	–
Model D	17.6	11.1	7.8	6.2	4.1	3.6
Model E	16.5	–	6.2	–	3.9	–

As one can observe, under LoS, which corresponds to the situation for which HIPERLAN/2 is mainly intended to work, it experiences a fading depth between 3.6 and 5.5 dB; under NLoS, the fading depth ranges from 3.9 to 6.7 dB. Hence, in the considered environments, the difference in fading depth between LoS and NLoS is usually below 1.2 dB. The fading depths observed by GSM and UMTS are usually lower than the ones obtained with the UMTS Indoor channel models. Concerning the fading margin for HIPERLAN/2, one concludes that it can be lower than the one for UMTS, since the experienced fading depth is usually between 2.3 to 4.5 dB and 2.6 to 3.0 dB below the one for UMTS, for the NLoS and LoS cases, respectively.

One concludes that the fading margins for HIPERLAN/2 are well below the ones obtained from Rayleigh and Rice distributions, hence, these distributions are no longer appropriate for evaluating the fading depth for HIPERLAN/2.

6.5. MBS Fading Depth Models

While for GSM, UMTS and HIPERLAN/2 there is a lot of proposed channel models, from which one can derive some interesting results, for MBS no definitive channel models have been proposed yet; moreover, the system itself is not yet defined, namely regarding bandwidths. Hence, one has to use some results from measurements, such as the ones in [MLAR94] for 59 GHz, and to assume possible system bandwidths, in order to obtain some preliminary results for the fading depth verified within different environments, and for different system bandwidths.

From experimental measurements in [MLAR94], it seems that the PDP of the MBS propagation channel in different environments can be modelled by exponential and two-stage exponential PDPs. In order to derive some preliminary results for the fading depth observed for MBS, one assumes an exponential PDP as representative of typical environments. Two different system bandwidths are considered, 50 and 100 MHz for MBS1 and MBS2 respectively, as before.

Typical values of *rms* delay spread were extracted from measurements in different environments [MLAR94]: City Street, City Square, Small Room and Corridor. For each type of environment, different experiments were carried out in different places, in order to cover a complete range of environments within a given class. The range of variation of the *rms* delay spread for each class of environments and the corresponding value of w_t is presented in Table 6.11.

Table 6.11 – *rms* delay spread and w_t for MBS environments.

Environment	*rms* delay spread [ns]	w_t [Hz·s]	
		MBS1	MBS2
City Street	6 – 48	0.30 – 2.40	0.60 – 4.80
City Square	55 – 92	2.75 – 4.60	5.50 – 9.20
Small Room	8 – 27	0.40 – 1.35	0.80 – 2.70
Corridor	8 – 21	0.40 – 1.05	0.80 – 2.10

From Table 6.11, one observes that w_t is always well above 0.02 Hz·s, meaning that MBS is clearly a wideband system, independently of which environment it works on, being sensitive to environment changes that affect propagation parameters, namely the *rms* delay spread of the propagation channel.

By using the curves for the fading depth that correspond to the case of an exponential PDP, one evaluates the fading depth in different environments, Table 6.12.

Table 6.12 – Fading depth observed in MBS environments, p = 1%.

Environment	Fading depth [dB]			
	MBS1		MBS2	
	NLoS	K = 6 dB	NLoS	K = 6 dB
City Street	4.6 – 10.6	4.0 – 8.0	3.3 – 8.3	3.1 – 6.6
City Square	3.4 – 4.3	3.2 – 3.8	2.5 – 3.1	2.5 – 3.0
Small Room	6.1 – 9.7	5.1 – 7.4	4.5 – 7.3	3.9 – 6.0
Corridor	6.7 – 9.7	5.5 – 7.4	4.9 – 7.3	4.3 – 6.0

From Table 6.12 one realises that, under LoS, the fading depth observed by MBS1 ranges from 3.2 to 8.0 dB in outdoors, and 5.1 to 7.4 dB in indoors; if one considers MBS2 the fading depth is usually between 0.7 to 1.4 dB below the ones for MBS1. Under NLoS, there is an increase in fading depth, relative to the LoS case, of about 0.2 to 2.6 dB and 0.1 to 1.7 dB for MBS1 and MBS2, respectively.

Globally, one concludes that the fading depth for MBS is well below the one for GSM and UMTS and close to the one for HIPERLAN/2. However, since these results are based only on a few measurements within specific environments, future work is needed in order to properly identify adequate channel models for MBS. Nevertheless, the proposed approach should be used, since the obtained values of fading depth are well below the ones observed for the narrowband case.

6.6. Relationship between Propagation Path Length and Delay Spread

6.6.1. Proposed Relationship

A time-domain technique for evaluating the short-term fading depth dependence on the system bandwidth and the *rms* delay spread of the propagation channel is proposed in Chapter 5. An approach for the study of the short-term fading depth dependence on system bandwidth and environment specific features is proposed in Chapter 4; the approach, being based on geometrical environment properties, allows evaluating the fading depth as a function of the system bandwidth and the maximum difference in propagation path length.

Since there is a close relation between environment characteristics and the power delay profile of the propagation channel, in this section one derives the relationship between the maximum difference in propagation path length and the *rms* delay spread of the propagation channel, thus, allowing a direct comparison between the results from the two different approaches.

The PDP of the propagation channel depends on a huge set of system and environment specific parameters, as a consequence, an extensive analysis of the dependence between Δl_{max} and σ_τ, i.e., w_l and w_t, can be cumbersome, and not easily applicable to practical cases. Since the main purpose of this approach is to provide a simple and effective way of defining a simple relationship between w_l and w_t, which allows evaluating the fading depth in different environments by using different approaches, one considers a two-path fading channel. Nevertheless, this approach can be extended to more complicated models, but then the simple relationship between the two models would be lost, without a significant increase in accuracy, hence, not being too much of value; a possible approach is presented in [NYMI01]. The PDP of a two-path fading channel is composed of two arriving waves with different delays, Figure 6.16.

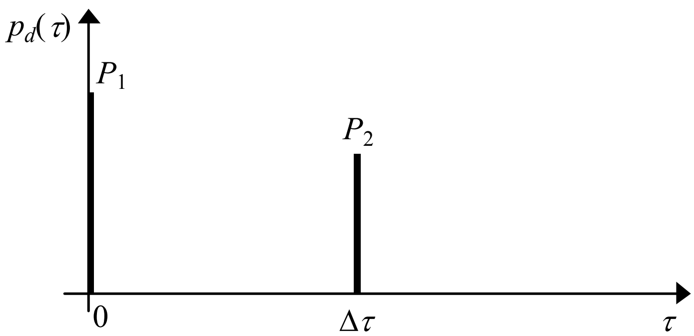

Figure 6.16 – Two-ray model.

Assuming a normalised received power, $P_1 + P_2 = 1$, one can evaluate the *rms* delay spread of the PDP in Figure 6.16 from (2.24)

$$\sigma_\tau = \Delta\tau \cdot \sqrt{P_2 - P_2^2} \tag{6.1}$$

hence

$$\sigma_\tau = \Delta\tau \cdot \frac{\sqrt{K}}{K+1} \tag{6.2}$$

where $K = P_1/P_2$. If expressed as a function of the maximum difference in propagation path length between different arriving components, Δl_{max}, which in this case corresponds to the difference in propagation path length between the LoS component and the reflected one, one obtains for the relative delay

$$\Delta\tau = \frac{\Delta l_{max}}{c} \tag{6.3}$$

thus,

$$\sigma_\tau = \frac{\Delta l_{max}}{c} \cdot \frac{\sqrt{K}}{K+1} \tag{6.4}$$

or inversely

$$\Delta l_{max} = c \cdot \sigma_\tau \cdot \frac{K+1}{\sqrt{K}} \tag{6.5}$$

The relation between Δl_{max} and σ_τ, as a function of the Rice factor is depicted in Figure 6.17. As expected from (6.5), for $K \geq 0$ dB, the ratio $\Delta l_{max}/c\cdot\sigma_\tau$ increases with increasing values of K; as K tends to infinity so does $\Delta l_{max}/c\cdot\sigma_\tau$, since it corresponds to a situation when the PDP is represented by only one single arriving wave, i.e., $\sigma_\tau = 0$ s.

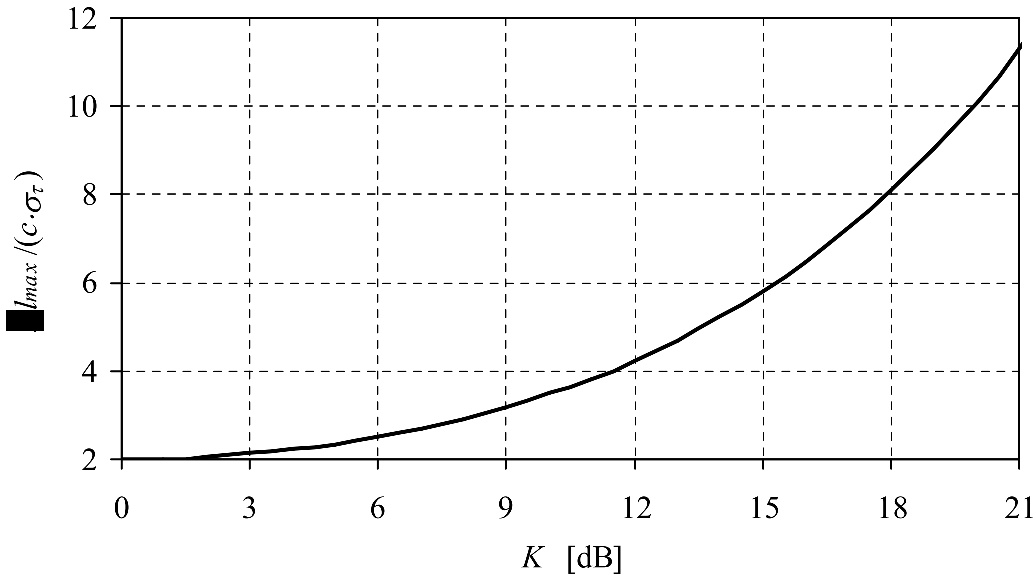

Figure 6.17 – $\Delta l_{max}/c\cdot\sigma_\tau$ as a function of K.

The value of Δl_{max} as a function of σ_τ, for different values of K, is shown in Figure 6.18. The slope decreases as K decreases, i.e., for the same value of Δl_{max}, the lower the K the higher the *rms* delay spread, since there is an increased contribution of the reflected wave.

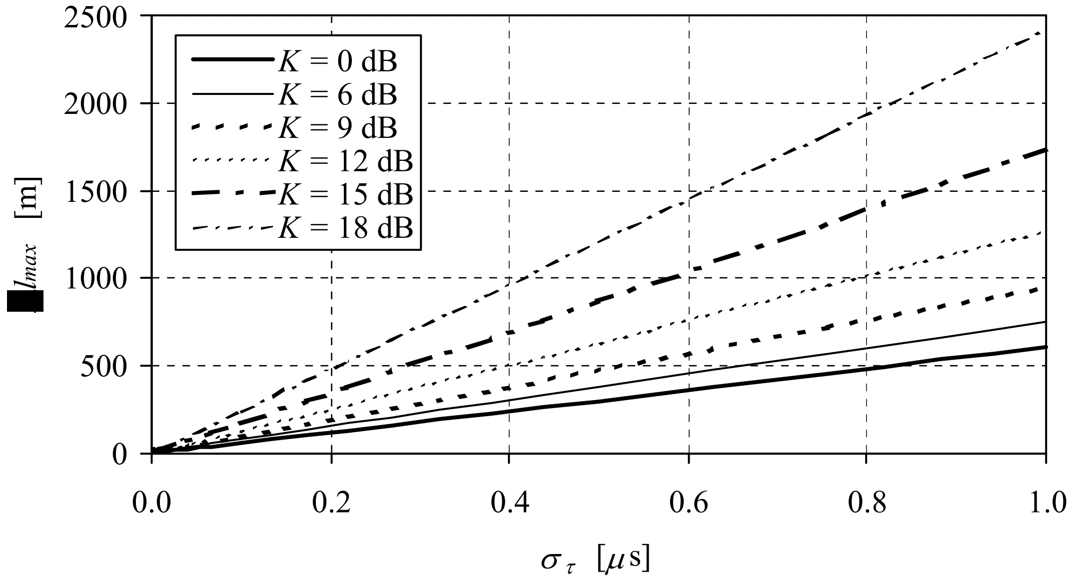

Figure 6.18 – Relation between Δl_{max} and σ_τ.

Since one has defined a simple relation between Δl_{max} and σ_τ, one can easily evaluate w_l from w_t, and vice-versa, allowing to use any of the above presented approaches for evaluating the fading depth in different environments, defined either by geometrical considerations or by its PDP

$$\frac{w_l}{w_t} = \frac{\Delta l_{max}}{\sigma_\tau} = c \cdot \frac{K+1}{\sqrt{K}} \tag{6.6}$$

6.6.2. Comparison of Results

In this section one compares the results from the time-domain based approach for the fading depth dependence on bandwidth with the ones from the environment-geometry based approach. This comparison is made as follows: for each environment, represented by its PDP, one evaluates w_t; the value of w_l, is then evaluated from (6.6); substituting the obtained value in the analytical approximation in Chapter 4, one obtains the observed fading depth. Two distinct situations are considered, LoS and NLoS: for the former, a value of K = 6 dB is considered, while for the latter one assumes that the NLoS situation can be reasonable approximated by considering K = 0 dB, as previously referred.

In the following, APPROACH T refers to the value of fading depth obtained from the time-domain based approach, and APPROACH G to the one obtained from the analytical approximation for the environment-geometry based one.

One starts here with GSM, as previously, with only Type 1 channel models. The value of w_t and w_l, for the different environments being considered, is presented in Table 6.13.

Table 6.13 – Values of w_t and w_l for GSM Type 1 environments.

Environment	w_t [Hz·s]	w_l [MHz·m]	
		NLoS	K = 6 dB
Rural Area	0.02	11.76	14.68
Typical Urban	0.21	123.12	153.68
Bad Urban	0.51	306.36	382.41
Hilly Terrain	1.02	612.00	763.91

The fading depth obtained from the different approaches is in Table 6.14. For the given environments, the difference in fading depth between APPROACH T and APPROACH G is below 1.3 and 0.1 dB for the NLoS and LoS cases, respectively; the lower values of fading depth are obtained from APPROACH G. However, a worst case of 4.4 dB is verified for the Hilly Terrain environment; this is not surprising, since APPROACH G is suited for PDPs composed of a single group of arriving waves, and the PDP that corresponds to the Hilly Terrain environment is composed of two distinct groups at distant delays. Hence, the fading depth evaluated from APPROACH G is well below the one that corresponds to the given PDP.

Table 6.14 – Fading depth observed in GSM Type 1 environments, p = 1 %.

Environment	Fading depth [dB]			
	NLoS		K = 6 dB	
	T	**G**	**T**	**G**
Rural Area	18.2	17.9	11.2	11.3
Typical Urban	12.0	11.4	–	–
Bad Urban	9.2	7.9	–	–
Hilly Terrain	10.3	5.9	–	–

The values of w_t and w_l, for UMTS environments, are presented in Table 6.15. As one can observe from Table 6.16, for the given environments, the difference in fading depth between APPROACH T and APPROACH G is below 1.3 and 2.0 dB for the NLoS and LoS cases, respectively. Worst cases are verified for Vehicular-B and Hilly Terrain environments; as previously explained, this is not surprising, since the PDP for Vehicular-B and Hilly Terrain environments are composed of two distinct groups of arriving waves at distant delays. As verified for GSM, one also observes that the lower values of fading depth are obtained with APPROACH G.

Table 6.15 – Values of w_t and w_l for UMTS environments.

Environment	w_t [Hz·s]	w_l [MHz·m]	
		NLoS	K = 6 dB
Indoor-A	0.18	105.00	131.06
Pedestrian-A	0.23	135.00	168.51
Vehicular-A	1.85	1 110.00	1 385.53
Indoor-B	0.50	300.00	374.47
Pedestrian-B	3.75	2 250.00	2 808.51
Vehicular-B	20.00	12 000.00	14 978.70
Rural Area	0.50	300.00	374.47
Typical Urban	2.50	1 500.00	1 872.34
Hilly Terrain	15.00	9 000.00	11 234.02

Table 6.16 – Fading depth observed in UMTS environments, p = 1 %.

Environment	Fading depth [dB]			
	NLoS		K = 6 dB	
	T	**G**	**T**	**G**
Indoor-A	12.5	12.0	9.1	7.9
Pedestrian-A	12.3	11.0	9.1	7.2
Vehicular-A	< 7.4	4.5	< 5.9	2.6
Indoor-B	9.0	8.0	7.0	5.0
Pedestrian-B	< 6.3	3.3	< 5.2	1.8
Vehicular-B	< 9.6	1.6	–	–
Rural Area	8.7	8.0	6.9	5.0
Typical Urban	< 5.1	4.0	< 4.3	2.2
Hilly Terrain	6.1	1.8	5.1	0.9

The values of w_t and w_l for HIPERLAN/2 environments are presented in Table 6.17. As one can observe from Table 6.18, the difference in fading depth between APPROACH T and

APPROACH G is below 1.0 and 1.9 dB for the NLoS and LoS cases respectively. As previously, the lower values of fading depth are obtained from APPROACH G.

Table 6.17 – Values of w_t and w_l for HIPERLAN/2 environments.

Environment	w_t [Hz·s]	w_l [MHz·m]	
		NLoS	K = 6 dB
Model A	1.00	600.00	748.93
Model B	2.00	1 200.00	1 497.87
Model C	3.00	1 800.00	2 246.80
Model D	2.80	1 680.00	2 097.02
Model E	5.00	3 000.00	3 744.67

Table 6.18 – Fading depth observed in HIPERLAN/2 environments, p = 1 %.

Environment	Fading depth [dB]			
	NLoS		K = 6 dB	
	T	**G**	**T**	**G**
Model A	6.7	5.9	5.5	3.6
Model B	4.9	4.4	–	–
Model C	4.2	3.7	–	–
Model D	4.1	3.8	3.6	2.1
Model E	3.9	2.9	–	–

The variation range of w_t and w_l, for MBS1 environments, is presented in Table 6.19. As one can observe from Table 6.20, for the given environments, the difference in fading depth between APPROACH T and APPROACH G is below 0.9 and 1.6 dB for the NLoS and LoS cases respectively. Besides the difference in the absolute values of fading depth, similar results are obtained for MBS2; for the given environments, the difference in fading depth between APPROACH T and APPROACH G is below 0.9 and 2.0 dB for the NLoS and LoS cases, respectively. In both cases, MBS1 and MBS2, the lower values of fading depth corresponding to APPROACH G.

Globally, the difference in fading depth between both approaches is usually below 2.0 dB, exception is made for the case of environments characterised by a PDP composed of two distinct groups of arriving waves at large delays, as previously explained.

Table 6.19 – Values of w_t and w_l for MBS1 environments.

Environment	w_t [Hz·s]	w_l [MHz·m]	
		NLoS	K = 6 dB
City Street	0.30 – 2.40	180.00 – 1 440.00	224.68 – 1 797.44
City Square	2.75 – 4.60	1 650.00 – 2 760.00	2 059.57 – 3 445.10
Small Room	0.40 – 1.35	240.00 – 810.00	299.57 – 1 011.06
Corridor	0.40 – 1.05	240.00 – 630.00	299.57 – 786.38

Table 6.20 – Fading depth observed in MBS1 environments, p = 1 %.

Environment	Fading depth [dB]			
	NLoS		K = 6 dB	
	T	**G**	**T**	**G**
City Street	4.6 – 10.6	4.0 – 9.8	4.0 – 8.0	2.3 – 6.4
City Square	3.4 – 4.3	3.0 – 3.8	3.2 – 3.8	1.7 – 2.1
Small Room	6.1 – 9.7	5.2 – 8.8	5.1 – 7.4	3.1 – 5.6
Corridor	6.7 – 9.7	5.8 – 8.8	5.5 – 7.4	3.5 – 5.6

6.7. Conclusions

Results on the fading depth observed by different systems working in different environments are presented and discussed. The fading depth experienced by GSM is between 9.2 and 18.4 dB, while for UMTS fading depths range from less than 4.3 to 12.5 dB, and HIPERLAN/2 experiences fading depths between 3.6 and 6.7 dB. In the considered environments, and for the given system bandwidths, the fading depth observed by MBS is usually between 2.5 and 9.7 dB (a worst case of 10.6 dB is observed in City Streets under NLoS). Hence, one can state that, since the observed fading depth depends on the system bandwidth and environment specific features, different fading margins should be considered according to different system bandwidths and working environments when performing link budget calculations. The fading margins for UMTS, HIPERLAN/2 and MBS can be significantly reduced, when compared to the ones for GSM (i.e., the ones usually obtained by using Rayleigh or Rice distributions), while achieving the desired link quality; this enables a more efficient and less costly radio network planning.

By using a simple relationship between the maximum difference in propagation path length among different arriving components and the *rms* delay spread of the propagation channel, fading depth results obtained from the proposed time-domain approach for wideband fading characterisation are compared with the ones for the environment geometry-based analytical one. It must be remembered that the approaches being considered are completely independent and based on different models.

Since a good agreement is verified (the difference between both approaches is usually below 2 dB), one concludes that the proposed relationship, being simple, is effective for evaluating the fading depth in different environments and for different system bandwidths. This allows one to use different approaches for fading depth evaluation, taking as a starting point either physical and geometrical environment properties, or the PDP of the propagation channel. Besides being based on a two-path fading channel, the proposed relationship is used for channels with arbitrary PDPs. However, it must be remembered that one of the objectives of this relationship is simplicity, while allowing one to use different approaches for evaluating the fading depth starting from different environment descriptions. Moreover, by using the proposed relationship, a good agreement between both approaches is verified, therefore, from a practical point of view, a more complex and general approach does not seem to be of great usefulness in the sense that the difference in fading depth between both approaches, obtained with the proposed relationship, is not significant, since a proper environment description itself is always associated to a given uncertainty.

Chapter 7

Fading Characterisation Using Directional Channel Models

7.1. Initial Considerations

In most of existing wireless and mobile communication systems, the spatial domain is not usually exploited. Therefore, no techniques for improving systems capacity by using spatial properties of the propagation channel, e.g., spatial distribution of arriving waves, are accounted for. In this way, classical non-directional channel models that provide only information about signal level distribution and time domain characteristics are used. Additionaly, the influence of the antennas radiation pattern is not often accounted for.

With the emergence of third generation systems, the improvements in Digital Signal Processing (DSP) hardware, and the increasing demand for a larger capacity in mobile communication systems, the spatial domain appears to be one of the last frontiers for exploiting the possibility of increasing systems capacity. This can be achieved by using different types of antennas, at either the BS, or the MT, or both. Also, new signal processing techniques for exploiting the directional properties of the propagation channel are being explored, therefore, directional channel models including both temporal and spatial characteristics of the propagation channel are becoming of practical interest. New antenna techniques include smart antennas, either adaptive or switched beam, spatial diversity combining, and MIMO. These technologies, usually implying the use of antenna arrays, allow improving system capacity by providing enhanced coverage, with less transmitted power and reduced levels of interference.

A lot of work has been done concerning the implementation of algorithms for achieving the desired link quality and system capacity using these techniques. However, it is not clear how the values of short-term fading depth observed by the different systems, working in different environments, depend on the antenna arrays being considered, namely the half-power beamwidth. Since a characterisation of this phenomenon is of practical interest for system design and radio network planning purposes, this issue is addressed herein.

As proposed in Chapter 4, the short-term fading depth in a given environment is evaluated from an equation that is a function of the Rice factor and the product between the system bandwidth and the maximum possible difference in the propagation path length among different arriving components, reflecting the influence of physical and geometrical environment properties. However, the above-mentioned approach does not account for the influence of spatial propagation channel characteristics, since omnidirectional antennas are assumed at both ends of the link. In order to account for these characteristics, one proposes to extend the presented approach by including the influence of the antennas radiation pattern, therefore, allowing to evaluate the fading depth observed when directional antennas are used, which is of practical interest for the analysis of some existing systems (e.g., directional antennas are usually used for cell sectorisation), and future ones (which will probably use some kind of beamforming, combining diversity or MIMO scheme).

The approach proposed in this Chapter is based on the assumption that, for a given set of channel parameters, the observed fading depth in a LoS environment (depending on the value of the Rice factor) is directly related with the antenna characteristics, namely the half-power beamwidth. Moreover, the changes in the maximum difference in propagation path length, due to using directional antennas, are also accounted for. Since this influence is modelled through the variation of the Rice factor and the maximum possible difference in propagation path length among different arriving components, relative to the case of using omnidirectional antennas, expressions for the variation of these parameters as a function of the half-power beamwidth of the antenna array are analytically derived.

Results on the fading depth variation due to considering the influence of using directional antennas are presented and discussed. Moreover, by using the relationship between the maximum difference in propagation path length and the *rms* delay spread of the propagation channel, as described in Chapter 6, results on the fading depth observed by GSM, UMTS, HIPERLAN/2 and MBS in different environments, and for different system bandwidths, are presented.

7.2. Theoretical Considerations on the Rice Factor Variation

Since the Rice factor depends on the ratio between the power of the LoS component and the reflected/diffracted one, the use of directional antennas at the MT, the BS or both, will modify its value, since all arriving waves coming from different directions will be affected by the antenna gain in that direction, therefore, affecting the observed value of the Rice factor, hence, the observed fading depth. This way, one proposes evaluating the value of the Rice factor as a function of the half-power antenna beamwidth.

Since the half-power beamwidth of a single-element antenna is usually high, a larger directivity can be achieved by increasing the electrical size of the antenna. One of the ways of doing this, without increasing the size of each element itself, can be done by the use of antenna arrays, formed as an assembly of radiating elements with a given electrical and geometrical configuration. The total field of the array is determined by the sum of the fields of each radiating element, the overall antenna radiation pattern depending on [Bala82]:

- the geometrical array configuration;
- the separation between elements;
- the excitation magnitude and phase of each element;
- the radiation pattern of the individual elements.

By correctly setting these characteristics, it is possible to direct the main beam of the antenna array in a desired direction, while achieving a desired overall radiation pattern. This increased directivity means increased gain, therefore, the use of directional antennas also influences the transmitted signal power needed in order to achieve a desired signal power at the receiver, i.e., for the same signal level at the receiver the required amount of transmitted power decreases as the antenna directivity increases.

The use of antenna arrays becomes one of the key factors for exploiting the spatial domain, either by allowing different waves arriving from different directions to be discriminated through the use of different receiving algorithms, or by eliminating undesired signal interference through the use of directional beams, obtained from beamforming schemes [LiLo96], [GiCo03].

An exhaustive description of antenna arrays is not within the main scope of this thesis, however, in order to provide the reader with some basic knowledge, some usual terminology is briefly presented [LiLo96]. The array factor represents the far-field pattern of an array of isotropic elements as a function of both azimuth and elevation angles; the overall far-field of an array, E_{total}, is obtained as the product among the field of a single antenna element, $E_{element}$, and the array factor of that array, AF

$$E_{total} = E_{element} \times AF \tag{7.1}$$

This is valid for arrays with any number of identical elements that do not necessarily have identical magnitudes, phases and/or spacing among them. Moreover, the array factor does not depend on the characteristics of each radiating element. The half-power beamwidth (or 3 dB beamwidth), is defined as the angle between the two directions in a plane containing the maximum of a beam, for which the radiation intensity corresponds to one half of the maximum of the beam, giving a measure on the ability of an antenna to discriminate signals arriving from distinct paths.

One of the most practical and simple array configurations is the one in which antenna elements are placed along a line, which is referred as a linear array, Figure 7.1. For a linear array of elements positioned symmetrically along the x-axis, with a constant phase shift, the array factor, AF_{lin}, can be expressed as [Bala82]

$$AF_{lin}(\theta,\varphi) = \sum_{i=1}^{N} \alpha_i \cdot e^{j[(i-1)(k \cdot d_e \cdot \sin(\theta)\cdot\cos(\varphi)+\beta)]} \tag{7.2}$$

where k is the wave number, α_i is the excitation magnitude of the i-th antenna element and β is the phase difference between consecutive antenna elements; d_e corresponds to the separation between antenna elements and N is the number of antenna elements. A similar definition can be easily derived for the case in which the phase excitation between antenna elements is not constant [Bala82].

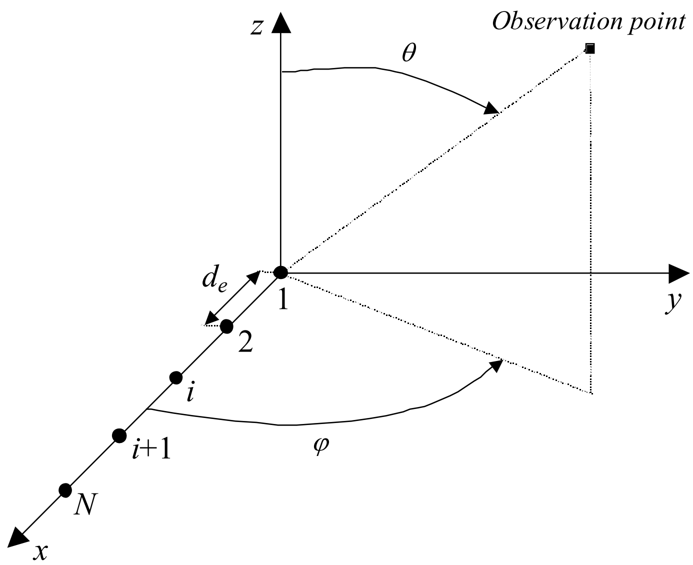

Figure 7.1 – Geometry of a linear array.

When all the elements have equal excitation magnitudes and the phase lead current of each element relative to the preceding one is constant, the array is referred as a Uniform Linear Array (ULA) with progressive phase. The main beam can be oriented in any direction by controlling the progressive phase, β. Two distinct situations are usually considered $\beta = 0$ and $\beta = \pm k \cdot d_e$, corresponding to the ordinary broadside and end-fire arrays, respectively: in the former, the main beam is oriented towards $\varphi = \pm 90^{\circ}$, i.e., perpendicular to the array axis; in the latter, it is oriented in the direction of the axis ($\beta = -k \cdot d_e$ for $\varphi = 0^{\circ}$ and $\beta = +k \cdot d_e$ for $\varphi = 180^{\circ}$). Globally, if the main beam is required to be oriented at an angle φ_b, the value of β should be adjusted such that

$$\beta = -k \cdot d_e \cdot \cos(\varphi_b) \tag{7.3}$$

The same objective can be achieved by individually setting the phase excitation of each antenna element, rather than using a progressive phase.

In a circular array, N elements are equally spaced along a circular ring of radius r, as illustrated in Figure 7.2. In this case, the array factor, AF_{circ}, can be derived as [Bala82]

$$AF_{circ}(\theta,\varphi) = \sum_{i=1}^{N} \alpha_i \cdot e^{j\left(k \cdot r \cdot \sin(\theta) \cdot \cos\left(\varphi - \varphi_{(xy)i}\right) + \beta_i\right)} \tag{7.4}$$

where α_i and β_i are the magnitude and phase (relative to the array centre) excitation of the i-th antenna element and $\varphi_{(xy)i}$ represents its angular position on the x-y plane

$$\varphi_{(xy)i} = 2\pi \cdot \left(\frac{i}{N}\right) \tag{7.5}$$

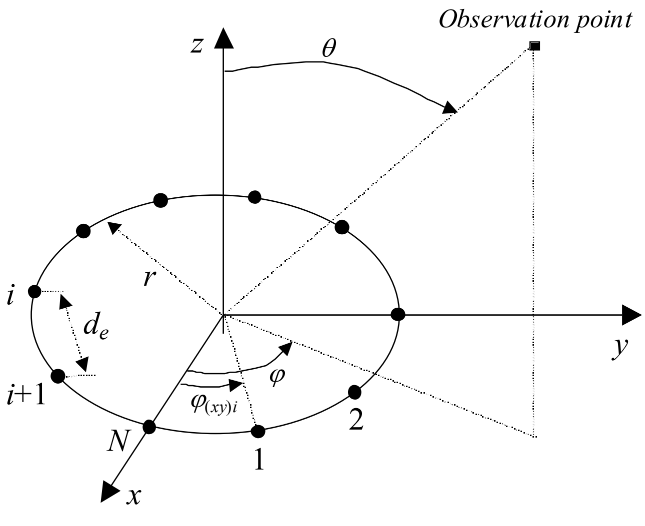

Figure 7.2 – Geometry of a circular array.

To direct the main beam in the (θ_b,φ_b) direction, the phase excitation of the i-th element has to be chosen as

$$\beta_i = -k \cdot r \cdot \sin(\theta_b) \cdot \cos\left(\varphi_b - \varphi_{(xy)i}\right) \tag{7.6}$$

In order for the antenna elements to be positioned such that the distance between consecutive antenna elements is d_e the radius of the antenna can be evaluated from

$$r = \frac{d_e}{2 \cdot \sin\left(\frac{\pi}{N}\right)} \tag{7.7}$$

When all elements have equal excitation magnitude, the array is referred as a Uniform Circular Array (UCA). Basically, for the same number of antenna elements and equal intra-element spacing, UCA radiation patterns differ from ULA ones due to the presence of high sidelobe levels in their radiation patterns. For a circular array with equally spaced elements and uniform weighting, the lowest peak sidelobe level is around 8 dB, when referred to the maximum of the main lobe.

In the model proposed in Chapter 4, omnidirectional antennas are assumed at both the BS and the MT; if directional antennas are used, at either the BS, or the MT, or both, waves arriving from different azimuth angles are differently affected by the antenna radiation pattern, causing the value of the Rice factor to differ from the one obtained with omnidirectional antennas. It can be evaluated as

$$K_{dir[\mathrm{dB}]} = K_{omni[\mathrm{dB}]} + \Delta K(\alpha_{3\mathrm{dB}})_{[\mathrm{dB}]} \tag{7.8}$$

where K_{omni} and K_{dir} are the values of the Rice factor obtained with omnidirectional and directional antennas, respectively, $\alpha_{3\mathrm{dB}}$ is the antenna half-power beamwidth, and $\Delta K(\alpha_{3\mathrm{dB}})$ is the Rice factor variation due to considering the influence of using directional antennas.

For illustrative purposes, let us consider that the AoAs, at the location where the directional antenna is placed (the BS or the MT), are uniformly distributed in the spatial domain, as considered in the model, which is usually assumed from the BS or the MT points of view in micro- and pico-cellular environments [Corr01]; in macro-cellular environments, signals arriving at the MT are also commonly modelled as being uniformly distributed in the angular domain. Therefore, the PDF of the AoAs is given by, Figure 7.3,

$$p_{\mathrm{AoA}}(\varphi) = \begin{cases} \frac{1}{2\pi} & , \ |\varphi| \le \pi \\ 0 & , \ |\varphi| > \pi \end{cases} \tag{7.9}$$

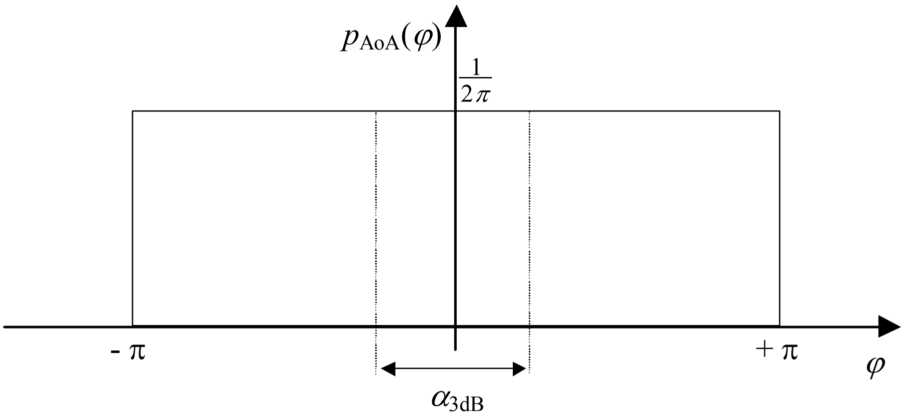

Figure 7.3 – Uniform distribution.

Assuming that all rays arriving within the antenna beamwidth contribute to the observed signal level distribution, the number of arriving waves within the antenna beamwidth, corresponding to a given range of angles, decreases proportionally to the antenna beamwidth, hence, so does the received reflected/refracted power. One must remember that the power of each arriving wave is also considered as having a uniform distribution within a given range, thus, when expressed in dB, the Rice factor increases logarithmically as the antenna beamwidth decreases, and $\Delta K(\alpha_{3\mathrm{dB}})$ can be obtained from

$$\Delta K(\alpha_{3\mathrm{dB}})_{[\mathrm{dB}]} = 10 \cdot \log\left(\frac{1}{\mathrm{Prob}\left(|\varphi| \le \frac{\alpha_{3\mathrm{dB}}}{2} \right)} \right) = 10 \cdot \log\left(\frac{2\pi}{\alpha_{3\mathrm{dB}}} \right) = -10 \cdot \log\left(\alpha_{3\mathrm{dB}[^\circ]} \right) + 25.56 \quad (7.10)$$

A truncated Gaussian distribution is also usually found appropriate for modelling the AoAs at the BS and/or the MT in some environments [PeMF00], [3GPP03d], thus, if a truncated zero mean Gaussian distribution with standard deviation σ_s is assumed, Figure 7.4, the PDF of the AoAs is given by

$$p_{\mathrm{AoA}}(\varphi) = \begin{cases} \frac{1}{\sqrt{2\pi} \cdot \sigma_s} e^{-\frac{\varphi^2}{2\sigma_s^2}} & , \ |\varphi| \le \pi \\ 0 & , \ |\varphi| > \pi \end{cases} \quad (7.11)$$

As a simplification, one assumes that the truncated Gaussian distribution is obtained from the equivalent Gaussian one by discarding all the contributions that are not within [-π, +π[. In practice, all arriving waves are within [-π, +π[, nevertheless, considering a normalised truncated Gaussian distribution such that $\mathrm{Prob}(|\varphi| \le \pi) = 1$ would increase the mathematical complexity of the approach, while not influencing significantly the presented results. It should be noted that one wants to evaluate the ratio between the values of the Rice factor obtained with a directional antenna relative to the case of an omnidirectional one, which is related to the ratio among PDF areas rather than absolute values of probabilities themselves.

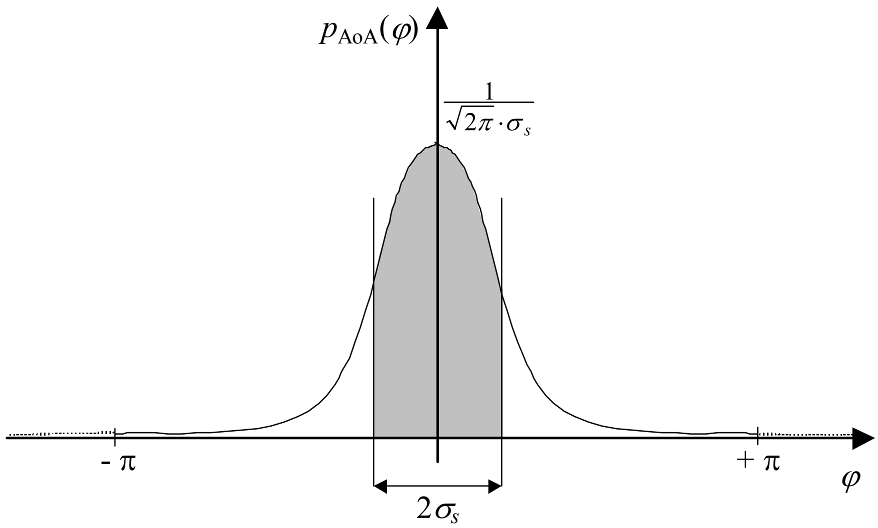

Figure 7.4 – Truncated Gaussian distribution.

Assuming that, as previously, the power of each arriving wave is uniformly distributed, the value of ΔK is obtained as

$$\Delta K(\alpha_{3\mathrm{dB}})_{[\mathrm{dB}]} = 10\cdot\log\left(\frac{\mathrm{Prob}(|\varphi|\le\pi)}{\mathrm{Prob}\left(|\varphi|\le\frac{\alpha_{3\mathrm{dB}}}{2}\right)}\right)$$

$$= 10\cdot\log\left[1-2Q\left(\frac{\pi}{\sigma_s}\right)\right] - 10\cdot\log\left[1-2Q\left(\frac{\alpha_{3\mathrm{dB}}}{2\sigma_s}\right)\right] \tag{7.12}$$

For small values of σ_s the first term is close to zero, i.e., $\mathrm{Prob}(|\varphi|\le\pi)\approx 1$, hence, (7.12) can be approximated by

$$\Delta K(\alpha_{3\mathrm{dB}})_{[\mathrm{dB}]} = -10\cdot\log\left[1-2Q\left(\frac{\alpha_{3\mathrm{dB}}}{2\sigma_s}\right)\right] \tag{7.13}$$

An error below 0.1 dB is observed for values of σ_s below 80°, increasing to 0.5 dB for σ_s = 112°.

The expressions above were derived assuming a hypothetical ideal directional antenna[3]. If an antenna array is considered, one has to account for the influence of the antenna array parameters that defines the overall radiation pattern of the array, since waves arriving at different angles are affected differently by the radiation pattern of the antenna array. A mathematical description of ΔK as a function of the antenna array type and parameters cannot be easily extrapolated for any array configuration, therefore, in the next sections several simulation results are presented aiming at illustrating how the antenna radiation pattern influences the value of ΔK.

7.3. Simulation Results

7.3.1. Initial Analysis

In order to verify the influence of the antenna array radiation pattern on the value of ΔK several simulations were carried out. This was implemented in two steps: first, the minimum number of arriving waves to be considered in the model is studied, since one has to ensure that the considered number of arriving waves is large enough in order not to significantly influence the results; second, the Rice factor variation, ΔK, is evaluated for different antennas, an ideal directional antenna, ULA and UCA, being considered. The process for evaluating the value of ΔK consists of the following, Figure 7.5,

(i) generate M-1 pairs (a_i, φ_i) corresponding to M-1 scattered waves; as proposed in Chapter 4, magnitudes a_i are uniformly distributed, AoAs φ_i being obtained from uniform or truncated Gaussian distributions;

(ii) generate the LoS component ($a_1 = 1$, $\varphi_1 = 0^o$);

(iii) evaluate K_{omni};

(iv) multiply magnitudes a_i by the antenna gain in direction φ_i;

(v) evaluate K_{dir} and ΔK;

(vi) repeat the process for each simulation.

The simulator was implemented in C programming language, and designed in order to reduce the computational effort needed for performing simulations, while providing the required flexibility, for the definition of input simulation parameters.

[3] Hypothetical antenna with constant directional gain within the antenna half-power beamwidth and zero outside.

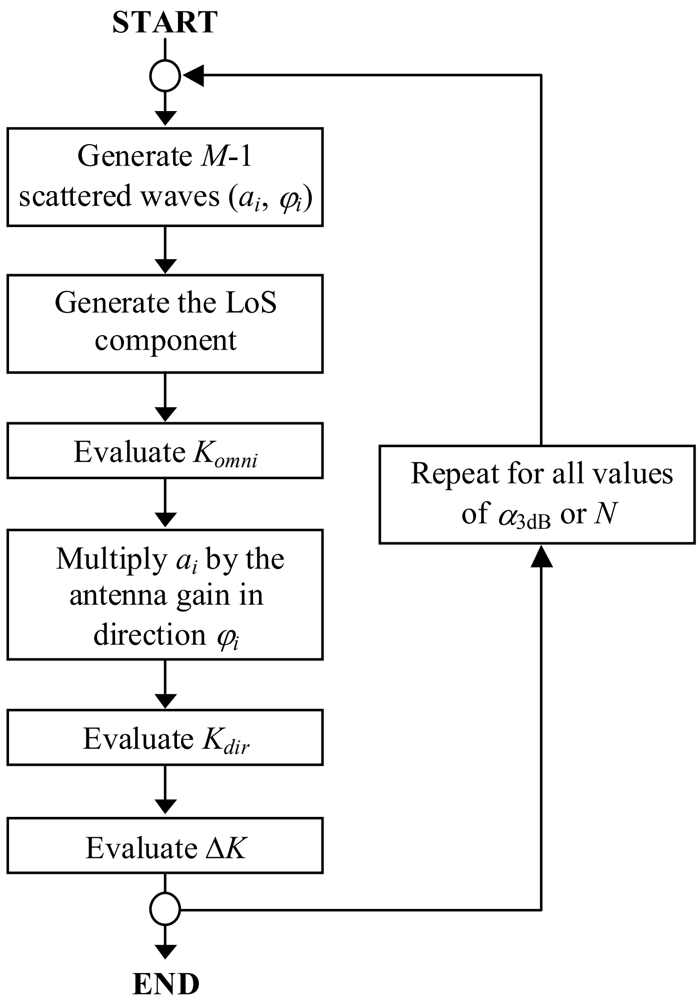

Figure 7.5 – Simulation procedure.

In order to assess the minimum number of arriving waves, M, needed to be considered so that the results become almost independent of it, 500 simulations were carried out for different antenna beamwidths, α_{3dB} = 5, 10, 20, 30, 60 and 90°; an ideal directional antenna is considered. The results in Figure 7.6 correspond to the mean value obtained from each set of simulations. Under these conditions, the total simulation time was 45 s (using the same hardware platform, as previously referred), hence, on average 0.08 s is required for evaluating each value of ΔK (in this case, the dependence on M is not significant). Standard deviations of 0.07 and 0.11 dB were obtained for α_{3dB} = 5, and 90°, respectively, hence, being negligible (here, and in the cases that follows).

As one can observe, as the number of arriving waves being considered increases, smaller beamwidths can be analysed. This is not surprising, since the probability of having a sufficiently large number of arriving waves within the antenna beamwidth (such that the results become almost independent of the value of M) increases with M. Globally, one concludes that a value of $M = 200$ can be used for α_{3dB} above roughly 20°. For small values of M, the value of ΔK tends to infinity, since in some simulation runs no reflected/refracted waves are found within the antenna beamwidth.

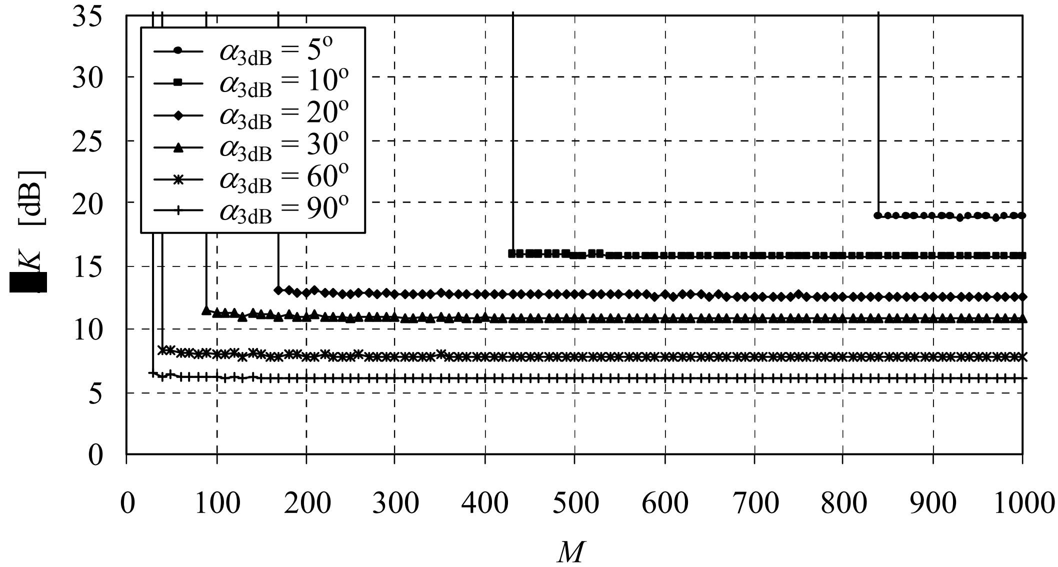

Figure 7.6 – Influence of the number of arriving waves, ideal directional antenna.

It must be noted that such a higher value of M is due to considering that all rays not lying within the antenna array beamwidth do not contribute to the signal level distribution. It is expected that this value will significantly reduce when considering real antenna arrays, since all rays are considered as being relevant; naturally, the magnitude of these rays is affected by the antenna gain in each direction. The results in Figure 7.7 (as previously, 500 simulations were carried out for each value of N) are obtained for a broadside ULA of isotropic elements equally spaced of $d_e = 0.5\lambda$, aligned such that the maximum of the radiation pattern corresponds to the direction connecting the BS to the MT; a different number of antenna elements is considered N = 2, 4, 8, 16, 32 and 64. Expected values for UMTS and HIPERLAN/2 are usually below $N = 8$; nevertheless, higher values of N will be probably used for MBS, working at the millimetre waveband, e.g., for the given value of d_e, and a working frequency of 60 GHz, 64 elements can be placed within a segment of 32 cm or a 16×16 cm^2 square area, which is not exaggerated, e.g., compared to the typical dimensions of a laptop. In these conditions the total simulation time for evaluating the data in Figure 7.7 was 41 minutes, being well above the one for the previous case; moreover, a significant dependence of M is found. This is due to consider the influence of the radiation pattern of the array; for the ideal case, the magnitude of each arriving wave is simply multiplied by one or zero, depending on if the AoA is, or not, within the antenna half-power beamwidth; in this case, for each arriving wave, the antenna gain in direction AoA has to be evaluated.

From Figure 7.7, it can be concluded that for $M \geq 200$ the results become almost independent of M. Similar results are obtained when considering an ULA with a backplane ($\mathrm{ULA_{wB}}$) such that signals arriving from behind are not considered, or even an UCA.

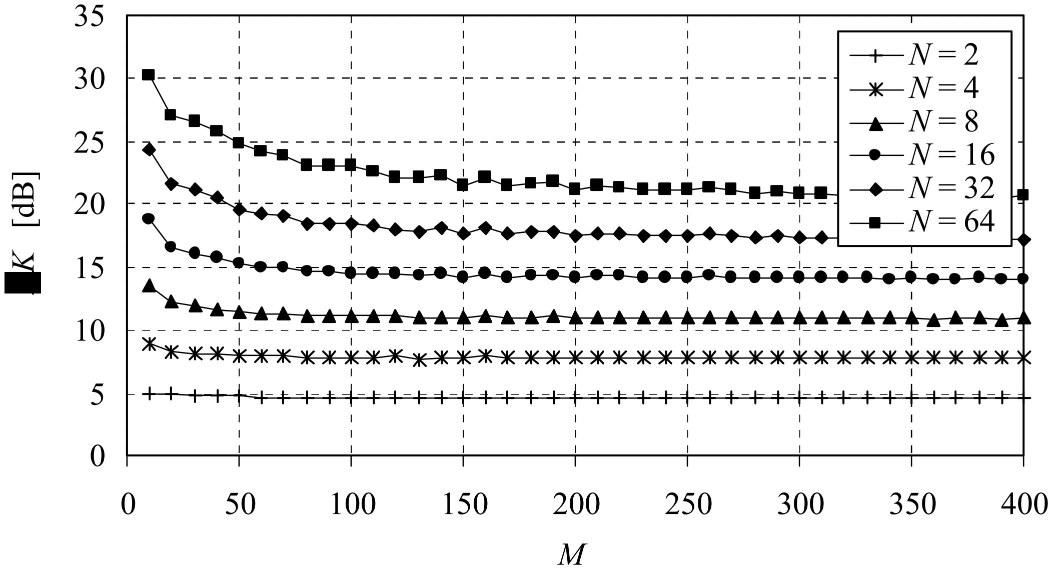

Figure 7.7 – Influence of the number of arriving waves, ULA, $d_e = 0.5\lambda$.

In order to assess the variation of ΔK as a function of $\alpha_{3\mathrm{dB}}$, 500 simulations were carried out for each value of $\alpha_{3\mathrm{dB}}$ (or N in the case of ULA and UCA). The results in Figure 7.8 correspond to the mean values obtained from each set of simulations, an ideal directional antenna is assumed, and different values of M are considered, $M = 200$, 400 and 1 000. As expected from (7.10), the value of ΔK varies linearly with $\log(\alpha_{3\mathrm{dB}})$.

The results in Figure 7.9 correspond to the case of ULA, $\mathrm{ULA_{wB}}$ and UCA antennas; the separation between antenna elements for different values of N is $d_e = 0.5\lambda$, $M = 200$ being considered. As one can observe, the results corresponding to $\mathrm{ULA_{wB}}$ are almost superimposed to the ones obtained with the ideal antenna. If a backplane is not considered, the results are 3 dB below the previous ones, since a "main lobe" exists in the opposite direction to the LoS, contributing significantly for the total amount of received reflected/refracted power, roughly doubling its value. In the case of the UCA, the obtained results are close to the ones for the ULA, however, a slightly lower decreasing rate is observed. Besides having higher sidelobe level than ULAs, UCAs have only one main beam, this way, for large beamwidths UCAs behave slightly better than ULAs; for small beamwidths, the contribution of the secondary main beam of ULAs is not relevant, compared to the higher sidelobe level of UCAs, hence, ULAs behave better, i.e., a higher value of ΔK is achieved.

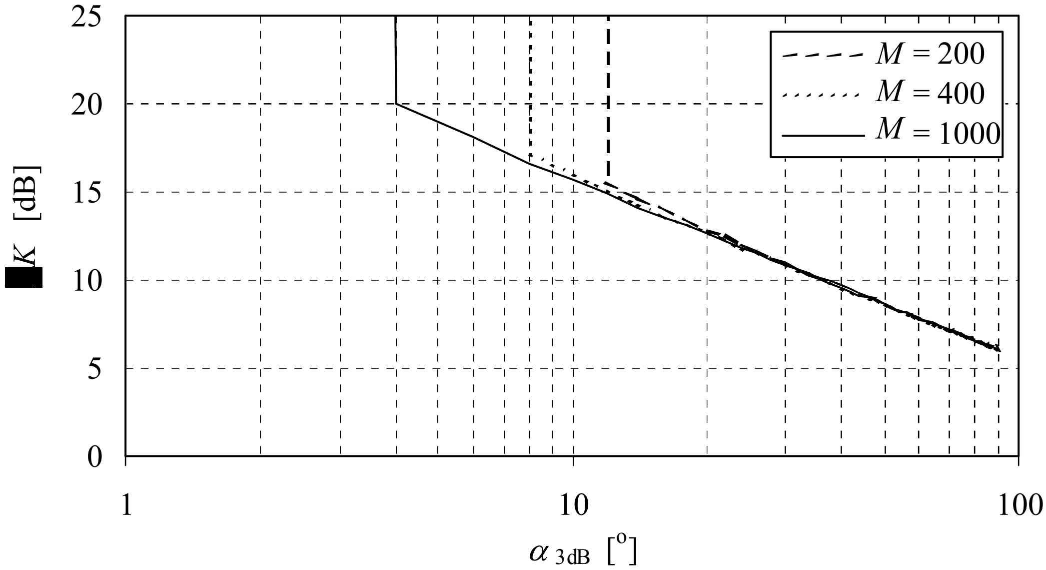

Figure 7.8 – Relation between ΔK and α_{3dB}, ideal directional antenna.

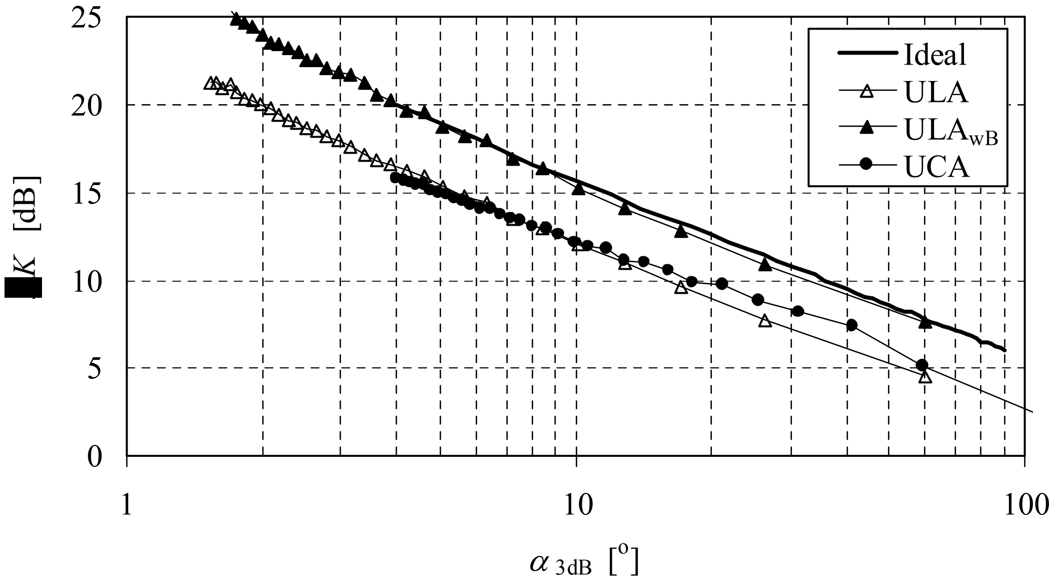

Figure 7.9 – Relation between ΔK and α_{3dB}, $d_e = 0.5\lambda$.

With the given assumptions, for the same number of antenna elements, ULAs and UCAs exhibit different beamwidths, Appendix VI; therefore, it is of relevance to compare the results, i.e., the value of ΔK, for the same number of antenna elements, Figure 7.10 (the dots correspond to the results from simulation and the lines were obtained from linear interpolation).

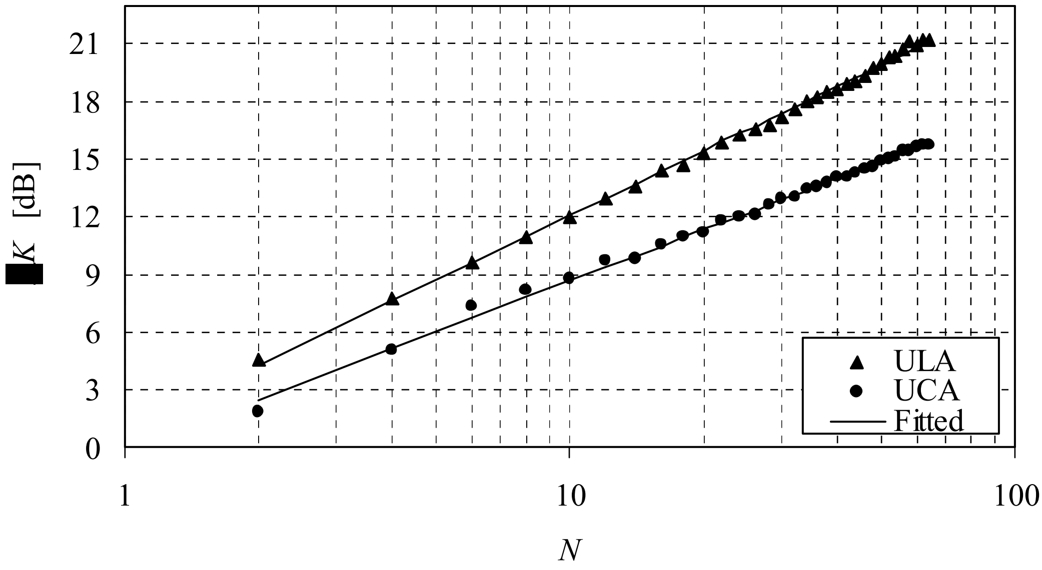

Figure 7.10 – Relation between N and ΔK, $d_e = 0.5\lambda$.

As expected from the relation between $\alpha_{3\text{dB}}$ and N, ΔK varies linearly with log(N), being approximated by

$$\Delta K_{[\text{dB}]} = 11.20 \cdot \log(N) + 0.88 \qquad \text{(ULA)} \tag{7.14}$$

$$\Delta K_{[\text{dB}]} = 8.87 \cdot \log(N) - 0.18 \qquad \text{(UCA)} \tag{7.15}$$

As one can observe from Figure 7.10, for the same number of antenna elements (it must be remembered that the separation between antenna elements for different values of N is assumed to be constant and equal to $d_e = 0.5\lambda$) ULA behaves better, since it provides a larger value of ΔK. For a large number of antenna array elements ($N > 60$) ULA provides an improvement in K_{omni} around 21 dB, while roughly 16 dB are provided by UCA, i.e., a difference of the order of 5 dB. This is not surprising, since, for the same number of antenna elements, ULAs present narrower beamwidths than UCAs, lowering the total amount of received reflected/diffracted power, and leading to a higher value of ΔK. It should be noted that the maximum possible number of antenna elements depends on if the directional antenna is to be used at the BS or the MT: in the former, there are no significant space limitations, and so the number of antenna elements can be as large as needed; for the latter, typical values of N are foreseen to be around 4 to 8, therefore, values of ΔK ranging from 5 to 11 dB are expected.

In order to properly evaluate the value of $K = K_{dir}$ to be used in the model proposed in Chapter 4 for evaluating the fading depth, while accounting for the influence of the antennas, a rule of variation of ΔK as a function of α_{3dB} should be derived. A theoretical approach for the case of using an ideal directional antenna was already presented. A similar study can be done for ULAs and UCAs, taking into account the antenna array radiation pattern for a given antenna configuration, however, it can be of considerable complexity. As a simplification, in this section, one proposes a simpler approach based on fitting of simulation data. A uniform distribution is used for modelling AoAs; the dependence on the type of statistical distribution being considered will be addressed as well. In order that the results are almost independent on the number of arriving waves, $M = 200$, was considered. The simulation results, depicted in Appendix VI, were obtained as the mean value of a set of 500 simulations. The curve that corresponds to the ideal antenna case can be approximated by

$$\Delta K_{[\mathrm{dB}]} = -10.17 \cdot \log\left(\alpha_{3\mathrm{dB}[^\circ]}\right) + 25.89 \tag{7.16}$$

A mean absolute error and standard deviation of 0.03 and 0.04 dB are obtained, respectively, which are negligible. As expected, there is a good agreement with the theoretical results given by (7.10). For the case of ULA and $\mathrm{ULA_{wB}}$ one obtains

$$\Delta K_{[\mathrm{dB}]} = -10.85 \cdot \log\left(\alpha_{3\mathrm{dB}[^\circ]}\right) + 23.13 \qquad \text{(ULA)} \tag{7.17}$$

$$\Delta K_{[\mathrm{dB}]} = -11.81 \cdot \log\left(\alpha_{3\mathrm{dB}[^\circ]}\right) + 27.48 \qquad (\mathrm{ULA_{wB}}) \tag{7.18}$$

A mean absolute error and standard deviation of 0.16 and 0.14 dB respectively, are obtained for ULA, if a $\mathrm{ULA_{wB}}$ is considered these values increase to 0.25 and 0.22 dB, respectively; again, those values are negligible. For UCA, one obtains

$$\Delta K_{[\mathrm{dB}]} = -9.05 \cdot \log\left(\alpha_{3\mathrm{dB}[^\circ]}\right) + 21.34 \tag{7.19}$$

A mean absolute error and standard deviation of 0.13 and 0.17 dB are obtained, respectively.

7.3.2. Dependence on the Statistical AoA Distribution

As previously referred, the relation between ΔK and α_{3dB} depends on the statistical distribution of the AoAs, at either the MT or the BS, as well as on the type of working environment. These two assumptions usually define the type of statistical distribution to be considered. For illustrating the influence of the statistical distribution of AoAs being considered, one presents some results for the case of an ideal directional antenna and a zero-mean truncated Gaussian distribution of AoAs, Figure 7.11. The results correspond to the mean value obtained from a set of 500 simulations; the number of arriving waves was set to M = 200. As can be observed, for small values of α_{3dB}, i.e., α_{3dB} roughly below $2\sigma_s$, ΔK varies almost linearly with $\log(\alpha_{3dB})$, similarly as observed for the case of a uniform distribution of AoAs, nevertheless, a lower value of ΔK is observed since all angles of the arriving waves are mainly concentrated around the main beam orientation due to considering a Gaussian distribution of AoAs. For $\alpha_{3dB} > 2\sigma_s$ the value of ΔK rapidly approaches zero, since almost all reflected/refracted power lie within the antenna beamwidth. As the value of σ_s increases, the observed fading depth variation approaches the one for the case of a uniform distribution of AoAs, which is not surprising, since as the value of σ_s increases the Gaussian distribution approaches the uniform one.

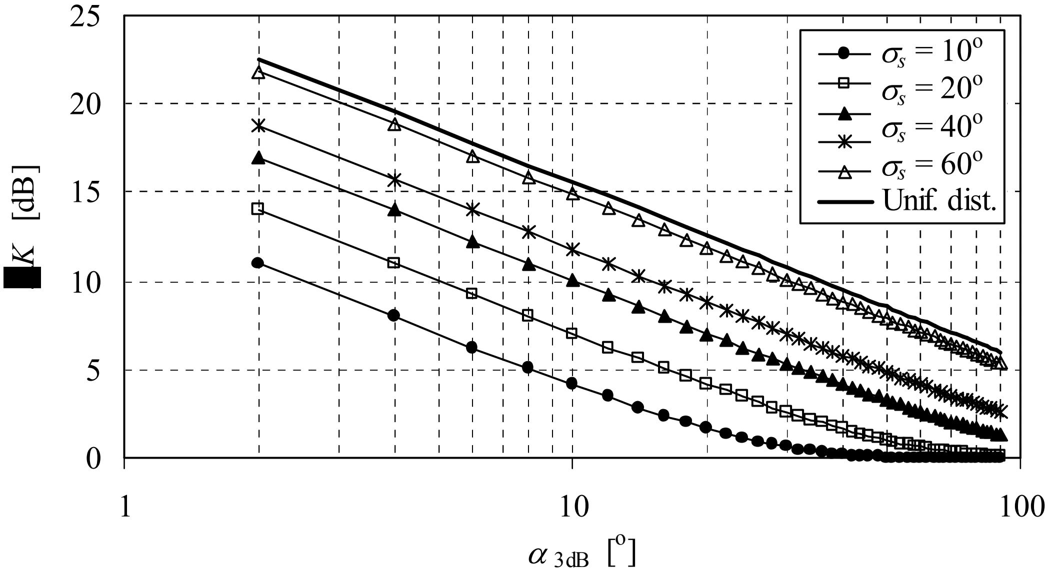

Figure 7.11 – Relation between ΔK and α_{3dB}, ideal directional antenna, Gaussian AoA.

The results in Figure 7.12 correspond to the case of ULA and UCA antennas, a value of σ_s = 10° being considered in the simulations, since as σ_s increases the results approach the one for a uniform distribution of AoAs. ULA_{wB} is not presented since the results are almost superimposed with the ones for ULA, which would be expected, since all arriving waves lie within a small angular range around the LoS direction (this range, depending on the value of σ_s, is usually small enough such that there are no arriving waves from the opposite direction to the LoS component, therefore, nulling the influence of the secondary main lobe of ULA). One must remember that these results are obtained for σ_s = 10°; it is expected that for higher values of σ_s, ULA_{wB} perform better, since all waves with relevant magnitude arriving from the back (which number increases as σ_s increases) will not contribute to the total amount of reflected power, thus, increasing the value of ΔK.

As shown in Figure 7.12, for larger beamwidths, $\alpha_{3dB} > 15^{\circ}$ ($1.5\sigma_s$), ULA behaves better than the ideal directional antenna. This is due to the fact that in the case of an ideal antenna the gain is constant within the whole beamwidth; in the case of ULA, the gain decreases with the angular distance to the main beam orientation, thus, decreasing the influence of the total amount of reflected power. For narrower beamwidths, the influence of sidelobes in the case of ULA becomes more significant and ULA behaves worst. In the case of UCA, it is observed that for $\alpha_{3dB} > 15^{\circ}$ ($1.5\sigma_s$) UCA behaves as a ULA. For narrower beamwidths, UCA behaves worst, for similar reasons as previously explained. Globally, one concludes that the ideal directional antenna still is a reasonable approximation to the ULA and UCA cases, the difference in the value of ΔK being usually below 2 dB.

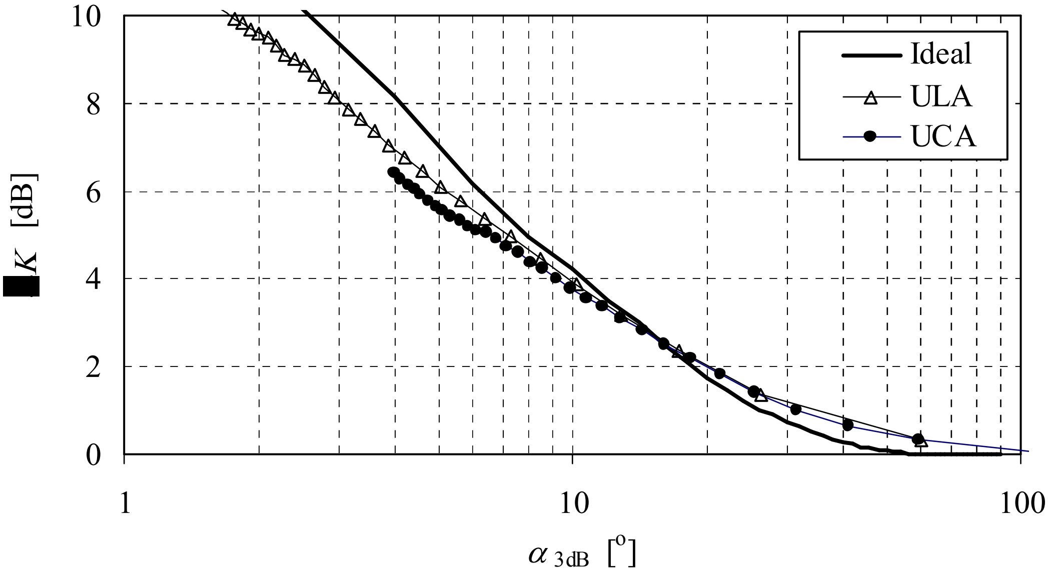

Figure 7.12 – Relation between ΔK and α_{3dB}, Gaussian AoA.

Until now, it is being assumed that the antenna main beam is oriented such that the direction of the maximum gain is aligned with the direction that connects the BS and the MT, such that the LoS component is always within the half-power beamwidth of the antenna, being multiplied by the antenna gain in that direction. Assuming a different main beam orientation (it can happen naturally as a result of well-known beamforming algorithms, or resulting from the MT positioning within a cell), the LoS component will be affected differently as a function of the angle deviation relative to the LoS direction and the radiation pattern of the antenna array. In order to give some insight into this phenomenon, one presents some results for illustrating such behaviour. The results in Figure 7.13 where obtained for an ULA and for different main beam orientations, φ_b = 0, 2, 5 and 10°, a uniform distribution of AoAs being considered. As can be observed, the value of ΔK rapidly decreases for $\alpha_{3\text{dB}} < 2\varphi_b$; as expected, for large values of $\alpha_{3\text{dB}}$ the curves approach the one for $\varphi_b = 0°$. For $\alpha_{3\text{dB}} < \varphi_b$ the curves start to vary complexly (not represented) due to the influence of the nulls and minor lobes of the antenna array radiation pattern, since the LoS component is no longer within the antenna half-power beamwidth. As expected, apart from an increase of approximately 3 dB on the value of ΔK, in the case of ULA_{wB}, similar conclusions are derived for ULA_{wB} and UCA, Appendix VI.

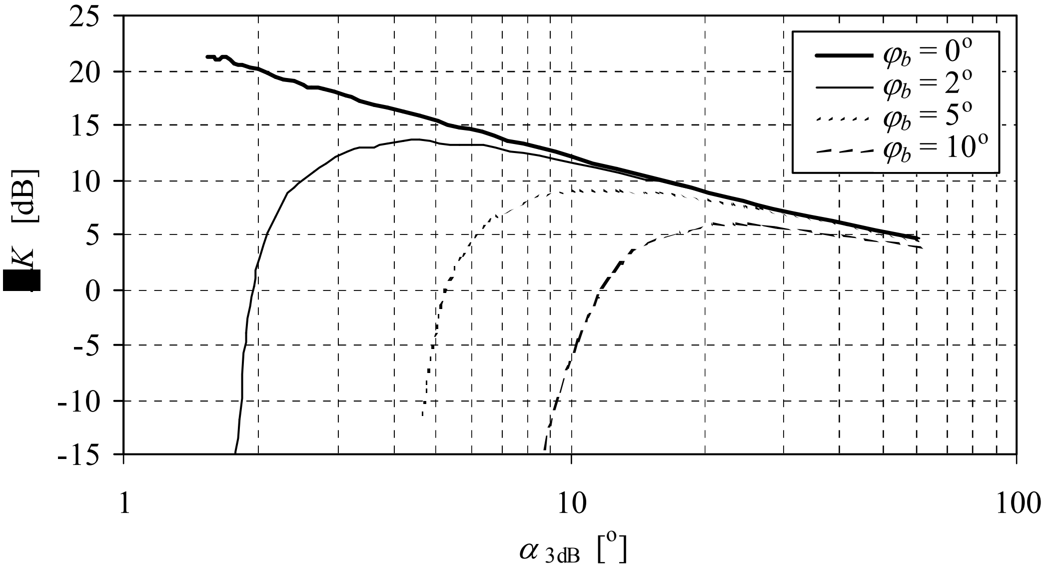

Figure 7.13 – Relation between ΔK and $\alpha_{3\text{dB}}$, dependence on the main beam orientation, ULA, uniform AoA.

The results in Figure 7.14 were obtained for a Gaussian distribution of AoAs; a value of $\sigma_s = 10°$ is used, for the same reasons as previously explained. Similar results for ULA_{wB} and UCA antennas are presented in Appendix VI. As expected, besides the difference in the absolute values of ΔK, the curves behaviour is almost similar to the one corresponding to a uniform distribution of AoAs: globally, the value of ΔK rapidly decreases for $\alpha_{3\text{dB}} < 2\varphi_b$; for large values of $\alpha_{3\text{dB}}$ the curves approach the one for $\varphi_b = 0°$; for values of roughly $\alpha_{3\text{dB}} < \varphi_b$ the curves start to vary complexly (not represented) for the same reasons as previously explained. Moreover, a similar behaviour is observed for the different type of antennas being considered; nevertheless, for the same value of $\alpha_{3\text{dB}}$ the value of ΔK is below the one for the ideal directional antenna case, this difference decreasing as σ_s increases (see Figure 7.11).

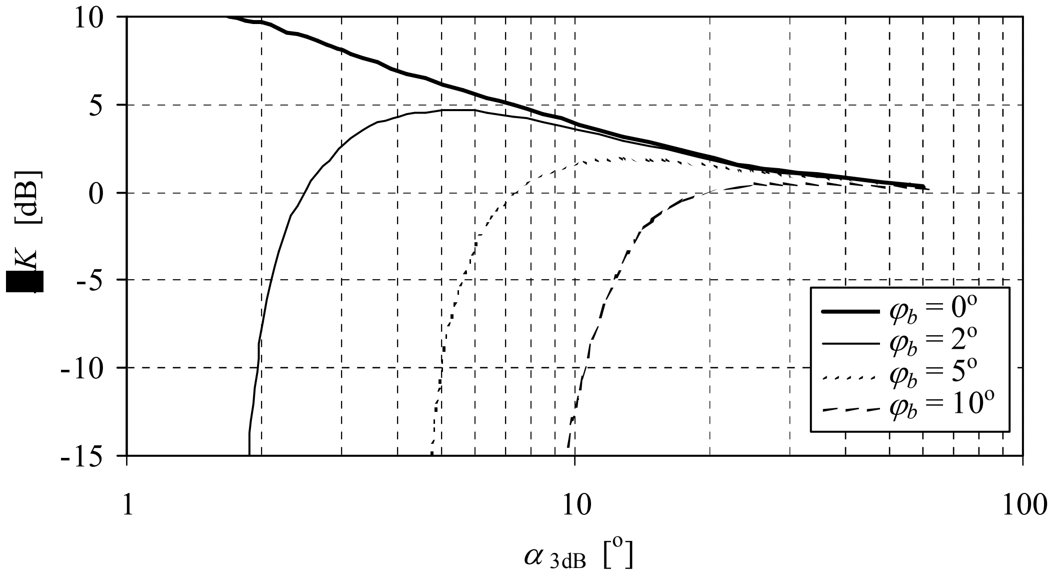

Figure 7.14 – Relation between ΔK and $\alpha_{3\mathrm{dB}}$, dependence on the main beam orientation, ULA, Gaussian AoA.

7.3.3. Fading Depth Reduction

As previously referred, a fading depth reduction will occur due to the Rice factor variation, ΔK, resulting from using directional antennas. Since the observed fading depth also depends on the equivalent received bandwidth, w_l, i.e., on the system bandwidth and environment properties, different fading depth variations will be observed as a function of Δw_l and ΔK, these parameters being related to $\alpha_{3\mathrm{dB}}$ (from now on, one refers to $w_{l(omni)}$ and $w_{l(dir)}$ as the value of w_l observed with omnidirectional and directional antennas, respectively). As an illustration of such behaviour, results on the fading depth variation, ΔFD_p, for different values of K_{omni} are presented; an ideal directional antenna and a uniform distribution of AoAs are considered. The variation in fading depth is evaluated as the difference between the fading depth observed with an omnidirectional antenna and the one corresponding to a directional one

$$\Delta FD_{p[\mathrm{dB}]} = FD_p(K_{omni}, w_{l(omni)})_{[\mathrm{dB}]} - FD_p(K_{dir}, w_{l(dir)})_{[\mathrm{dB}]} \tag{7.20}$$

where FD_p is evaluated as described in Chapter 4. A positive value of ΔFD_p corresponds to a reduction in fading depth, relative to the case of using an omnidirectional antenna.

As a first approach, only the fading depth dependence on ΔK is considered, i.e., $w_{l(omni)} = w_{l(dir)} = w_l$. Such assumption is valid for some environments, e.g., micro-cells, as it will be detailed in further sections, where the composite effect of both the variation of K and

w_l as a function of α_{3dB} will be addressed. In the following, p = 1 % is assumed, i.e., the fading depth is measured between 1 and 50 % of the CDF of the received power. The results in Figure 7.15 correspond to the case of an ideal directional antenna (a 3D representation of such data can be found in Appendix VI).

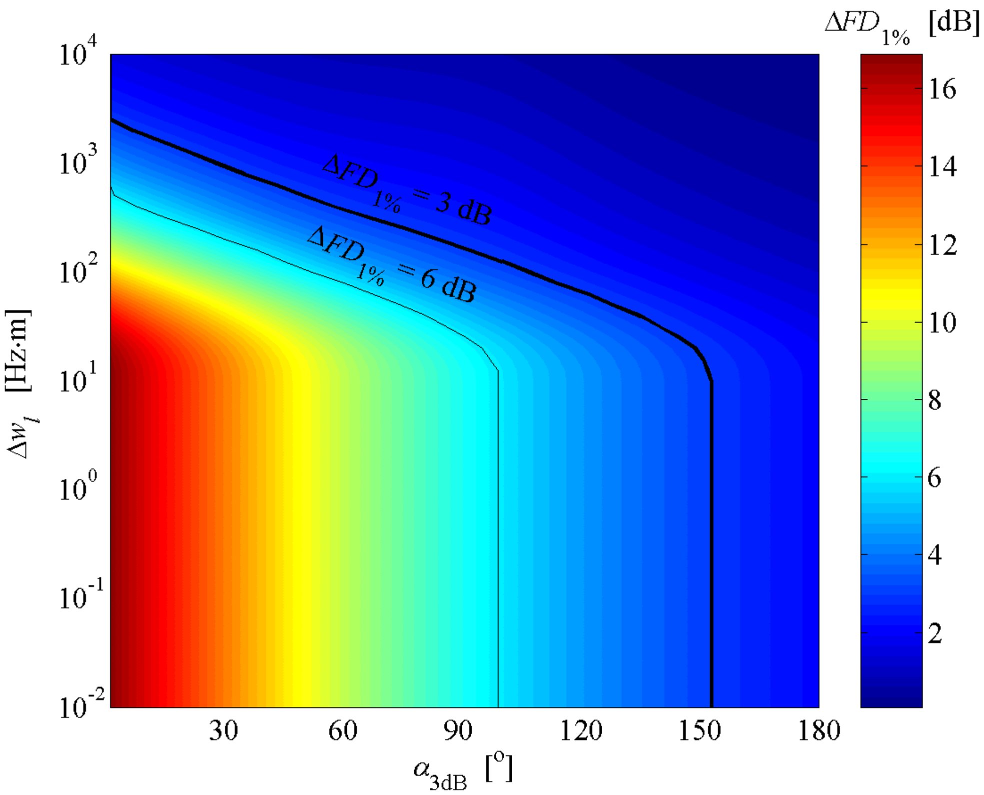

Figure 7.15 – Fading depth reduction as a function of Δw_l and α_{3dB}, K_{omni} = 0 dB.

As expected, the fading depth decreases more significantly (higher values of $\Delta FD_{1\%}$) with decreasing values of α_{3dB} and Δw_l. As shown in Figure 7.15, for K_{omni} = 0 dB, there is a significant reduction (above 6 dB) in fading depth for roughly $\alpha_{3dB} < 100^{\circ}$ and $\Delta w_l < 10$ Hz·m. For large values of Δw_l this reduction is not significant, since the absolute values of observed fading depth are usually low, even considering the use of omnidirectional antennas (see Chapter 4).

The results for K_{omni} = 6 dB are depicted in Figure 7.16. A reduction above 6 dB is observed for roughly $\alpha_{3dB} < 130^{\circ}$ and $\Delta w_l < 10$ Hz·m, while a reduction above 3 dB is observed for $\alpha_{3dB} < 180^{\circ}$ and $\Delta w_l < 100$ Hz·m. For K_{omni} = 12 dB, Appendix VI, a significant reduction of fading depth is still achieved but only for narrow antenna beamwidths; a fading depth reduction slightly above 3 dB is observed for $\alpha_{3dB} < 20^{\circ}$ and $\Delta w_l < 10$ Hz·m, no significant reduction being observed for large values of α_{3dB}.

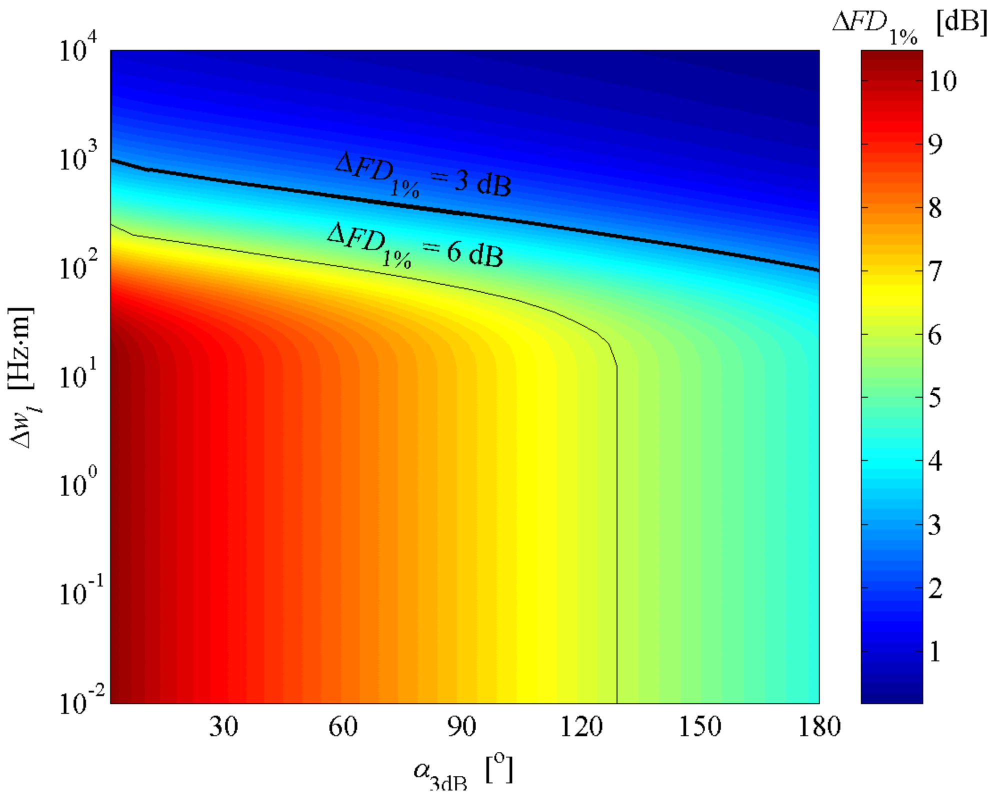

Figure 7.16 – Fading depth reduction as a function of Δw_l and α_{3dB}, $K_{omni} = 6$ dB.

In the case of ULA and UCA antennas, one briefly presents some results on the observed fading depth as a function of the number of antenna elements, corresponding to a given half-power antenna beamwidth. The results for an ULA and $K_{omni} = 0$ dB are in Figure 7.17, where a maximum fading depth reduction of 3 dB is observed for $N = 2$, which corresponds to an antenna beamwidth of 60°. Moreover, for $N < 16$ ($\alpha_{3dB} > 6.3°$), there is a significant dependence of $\Delta FD_{1\%}$ on the number of antenna elements; for large values of N no significant dependence is observed. For $K_{omni} = 6$ dB, Figure 7.18, the maximum reduction in fading depth is around 10 dB, for $N \geq 16$; no significant increase in fading depth reduction is observed for a larger number of antenna elements. It must be noted that besides the decrease in the maximum fading depth reduction with the increasing value of K_{omni}, the value of $\Delta FD_{1\%}$ for $N = 2$ and $K_{omni} = 6$ dB is above the one verified for $K_{omni} = 0$ dB, which can be explained by the rule of variation of the maximum possible value for the fading depth as a function of K_{omni} (see Figure 4.9). If a higher value of K_{omni} is considered, e.g., $K_{omni} = 12$ dB, no significant increase in fading depth reduction is observed for $N > 16$, as previously verified for different values of K_{omni}, Appendix VI. For $N \geq 8$ the maximum fading depth reduction is around 3 dB; it must be remembered that, for $K_{omni} = 12$ dB, the maximum value of fading depth observed with omnidirectional antennas is usually below 4 dB.

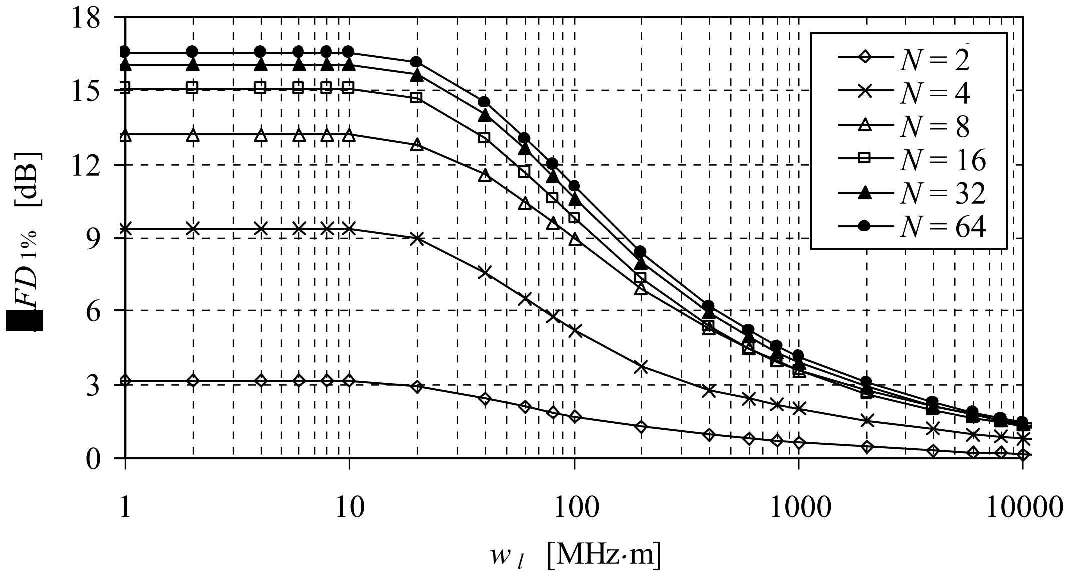

Figure 7.17 – Fading depth reduction for K_{omni} = 0 dB, ULA.

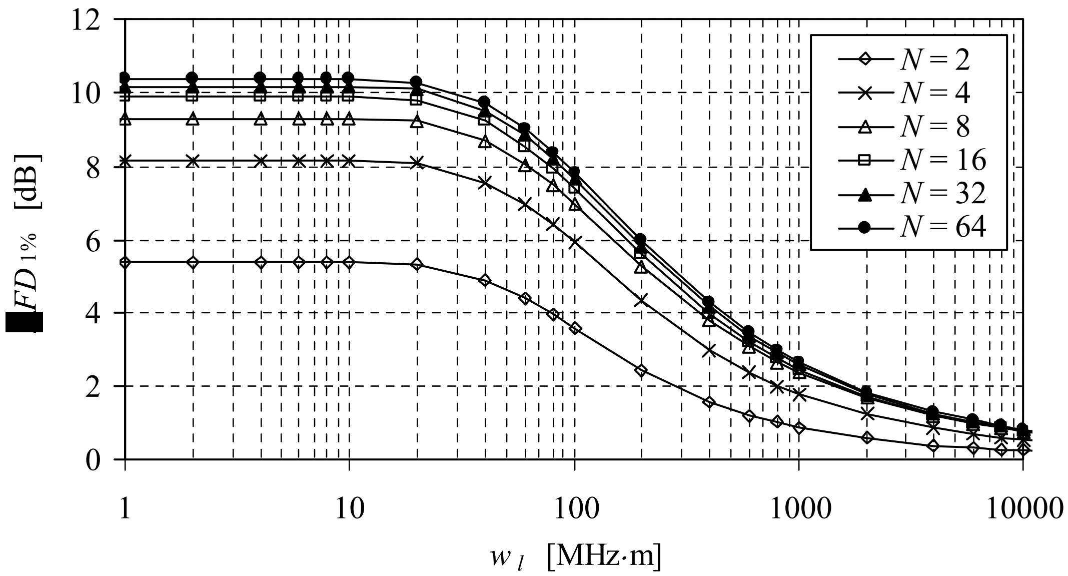

Figure 7.18 – Fading depth reduction for K_{omni} = 6 dB, ULA.

The results for UCA with K_{omni} = 0 dB are illustrated in Figure 7.19. A maximum fading depth reduction above 3 dB is observed for $N > 2$ ($\alpha_{3\text{dB}} < 120^{\text{o}}$). For values of N above 32 ($\alpha_{3\text{dB}} \leq 8.1^{\text{o}}$), no significant improvement in fading depth is observed, the fading depth reduction being of the order of 15 dB. Results for K_{omni} = 6 and 12 dB are in Appendix VI. For K_{omni} = 6 dB, a maximum fading depth reduction above 3 dB is observed for $N \geq 2$; for values of N above 16 ($\alpha_{3\text{dB}} \leq 16^{\text{o}}$), it increases to roughly 9 to 10 dB; no significant increase in fading depth reduction is observed for larger values of N. For K_{omni} = 12 dB, the maximum decrease in fading depth is around 3 dB, obtained for $N > 16$.

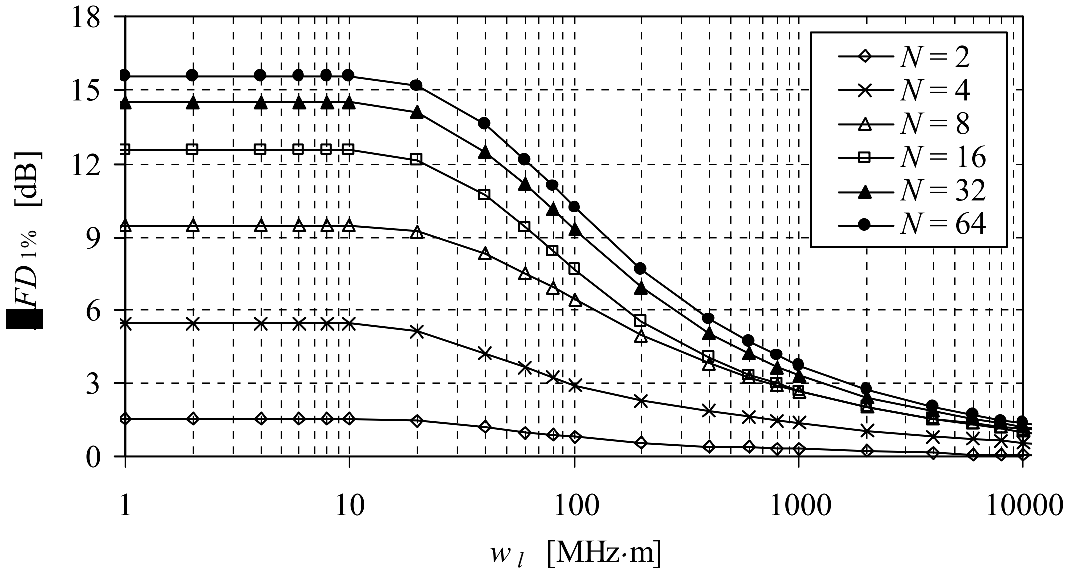

Figure 7.19 – Fading depth reduction for K_{omni} = 0 dB, UCA.

Globally, one observes that a considerable reduction in fading depth can be obtained with ULA and UCA antennas. This reduction can be as high as 9 to 10 dB for a value of K_{omni} = 6 dB; for large values of K_{omni}, the absolute reduction of fading depth is not so large, however, it must be remembered that as the value of K_{omni} increases the absolute value of fading depth decreases significantly, and so does the reduction in fading depth. No significant improvement in fading depth reduction is observed for values of N larger than 16 and 32 for ULA and UCA, respectively. As expected, for the same number of antenna elements and inter-element spacing, ULA antennas performs better, yielding larger fading depth reduction than UCA ones. This is not surprising, since, as previously explained, for the same number of antenna elements (equal spacing among elements is assumed), ULAs experience narrower beamwidths; moreover, besides having a secondary main lobe, they have a small sidelobe level than UCA.

7.4. Propagation Path Length Dependence on Antenna Beamwidth

As previously referred, the maximum difference in propagation path length among different arriving components depends on the geometrical environment characteristics. Assuming that the propagation channel can be modelled by a GBSB, such as the ones described in Chapter 2, the scattering area to be considered depends on the antenna beamwidth; it can be assumed that only scatterers within the area illuminated by the antenna, i.e., within the antenna half-power beamwidth, contribute significantly for the received scattered power. Depending on the type of environment being considered, macro-, micro- or pico-cellular, the value of Δl_{max} depends on the environment characteristics, therefore, on the propagation model being considered, and on the antenna half-power beamwidth. In order to derive some preliminary results on the dependence of Δl_{max} on the antenna beamwidth, for different environments, when a directional antenna is assumed at the BS or the MT (for illustration, results are also presented for directional antennas at both, the BS and the MT), an ideal directional antenna is considered. From now on, one refers to $\Delta l_{max(dir)}$ and $\Delta l_{max(omni)}$ as the maximum difference in propagation path length obtained with directional and omnidirectional antennas, respectively.

A simple geometrical approach for evaluating $\Delta l_{max(omni)}$ and $\Delta l_{max(dir)}$ from the scattering area of interest, for a given antenna configuration, is used. Nevertheless, one must be aware that the approximation error of the proposed approach will increase with decreasing number and density of clusters and scatterers within clusters, which will be further explained in the next sections. The main novelty of the proposed approach is to provide a simple framework for evaluating the maximum difference in propagation path length obtained with directional antennas, thus, allowing to evaluate the fading depth (or fading depth variation) in different environments and for different systems, when directional antennas are used. As referred in Chapter 3, in a micro-cellular environment, the scattering scenario is usually modelled by a GBSBEM, where the scattering area is defined as an ellipse whose foci are the BS and the MT, Figure 7.20.

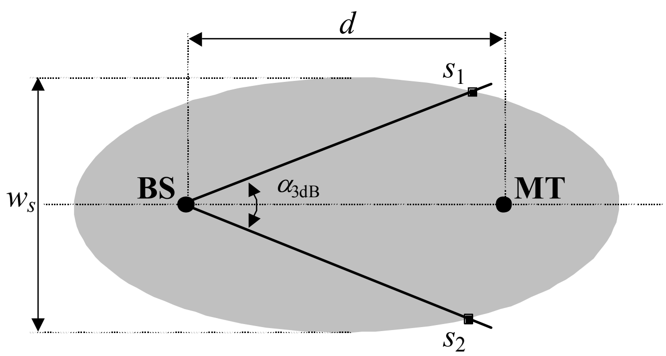

Figure 7.20 – Micro-cellular environment.

This type of model is commonly used for modelling the propagation channel in street-type micro-cellular scenarios [Corr01]. With the given assumptions, the maximum difference in propagation path length is independent of the value of α_{3dB} (according to the ellipse properties), and corresponds to the path length difference between the LoS component and the one reflected from a scatterer, s_1 and/or s_2, positioned at the geometrical limit of the scattering scenario

$$\Delta l_{max(dir)} = \Delta l_{max(omni)} = \sqrt{w_s^2 + d^2} - d \tag{7.21}$$

where w_s usually corresponds to a street width (as previously referred, this type of model is commonly used for modelling micro-cellular street-type scenarios), and d represents the distance between the BS and the MT.

It must be referred that, depending on the number and density of clusters and scatterers within clusters, there is some uncertainty associated to the evaluation of $\Delta l_{max(dir)}$, since there is no certainty if a scatterer is always positioned in the limits of the scattering environment. However, such an assumption seems to be appropriate, since unless the number and density of clusters and scatterers within clusters become really low, which is not usually the case, it seems reasonable to assume that a scatterer is positioned at least at a close distance from the scattering region limits; therefore, the error introduced from considering the above assumption is negligible.

Assuming a GBSBCM, the macro-cellular environment is modelled by a set of scatterers/clusters of scatterers positioned within a circle (scattering scenario) of radius r_s centred at the MT [LiRa99]. It is assumed that the distance between the BS and the MT is larger than the radius of the scattering scenario, Figure 7.21.

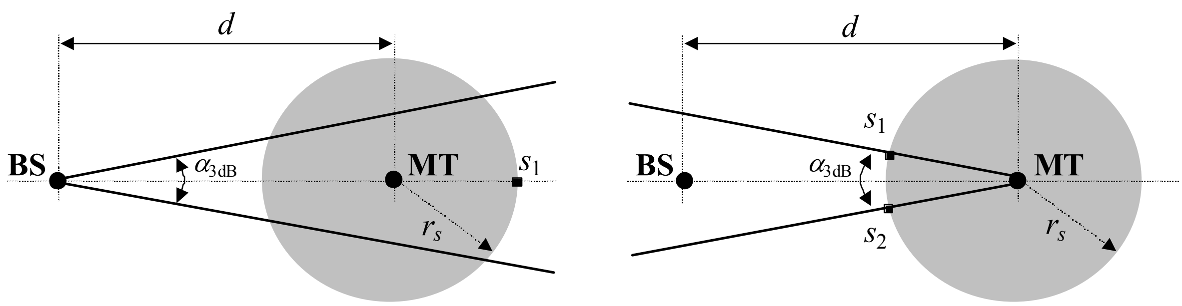

a) Directional antenna at the BS b) Directional antenna at the MT

Figure 7.21 – Macro-cellular environment.

The maximum possible difference in propagation path length depends on if a directional antenna is used at either the BS or the MT. In the former, the value of $\Delta l_{max(dir)}$ is independent on α_{3dB}, since it is obtained as the difference in path length between the LoS component and the reflected one from scatterer s_1

$$\Delta l_{max(dir)} = \Delta l_{max(omni)} = 2 \cdot r_s \tag{7.22}$$

For the latter, the maximum path length of reflected waves results from a reflection in s_1 or s_2

$$\Delta l_{max(dir)} = (r_s - d) + \sqrt{r_s^{\,2} + d^2 - 2 \cdot d \cdot r_s \cdot \cos\left(\frac{\alpha_{3\text{dB}}}{2}\right)} \tag{7.23}$$

As previously, it is assumed that a scatterer is usually positioned at s_1, s_2 or both, or at least, the cluster density in the scattering environment is sufficiently large such that a scatterer exists in the near vicinity of these points. If this is not the case, the value of $\Delta l_{max(dir)}$ will be smaller and, as a consequence, a lower fading depth reduction will be observed.

In pico-cellular environments, Figure 7.22, the scattering scenario is usually delimited by a circle of radius r_s centred at the BS, smaller than the distance between the BS and the MT. Besides the fact that the scattering scenario is assumed as being centred at the BS and $d \le r_s$, a similar expression for $\Delta l_{max(dir)}$ can be derived, since this geometry is similar to the one for the case of the macro-cellular one, Table 7.1.

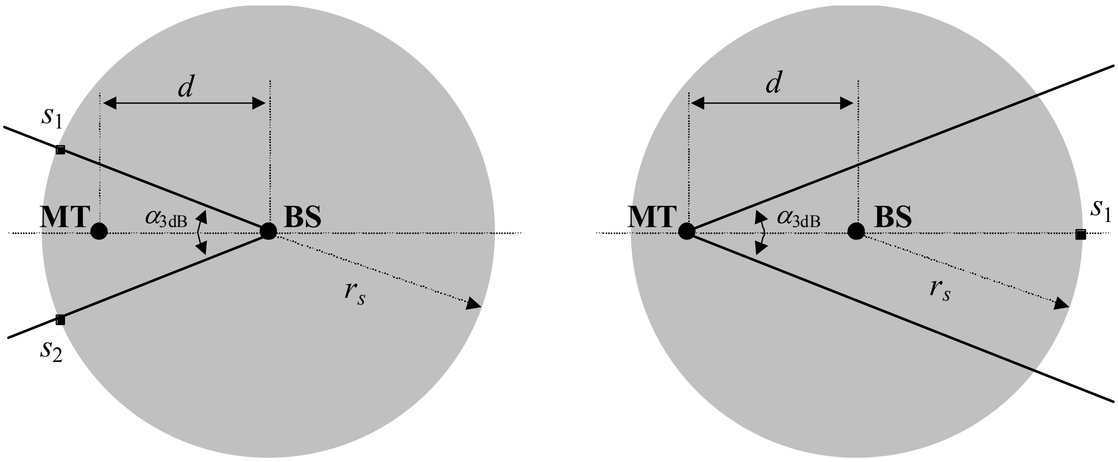

a) Directional antenna at the BS b) Directional antenna at the MT

Figure 7.22 – Pico-cellular environment.

Globally, in macro-cellular environments, the value of $\Delta l_{max(dir)}$ depends on the antenna beamwidth when a directional antenna is used at the MT, but no dependence is found when a directional antenna is used at the BS. A similar behaviour is observed in pico-cellular environments, however, the dependence of $\Delta l_{max(dir)}$ on $\alpha_{3\text{dB}}$ is found for the case of a directional antenna at the BS. As referred before, besides the dependence on the typical values of r_s and d to be considered for macro- and pico-cellular environments, the same expressions for $\Delta l_{max(dir)}$ can be used in both cases, Table 7.1. In micro-cellular environments no dependence of $\Delta l_{max(dir)}$ on $\alpha_{3\mathrm{dB}}$ is found, due to considering an elliptical scattering scenario.

Table 7.1 – Maximum difference in propagation path length with directional antennas.

$\Delta l_{max(dir)}$ [m]	Environment					
	Macro		Micro		Pico	
	BS	MT	BS	MT	BS	MT
$\Delta l_{max(dir)} = \Delta l_{max(omni)} = \sqrt{w_s^2 + d^2} - d$			✓	✓		
$\Delta l_{max(dir)} = (r_s - d) + \sqrt{r_s^2 + d^2 - 2 \cdot d \cdot r_s \cdot \cos\left(\frac{\alpha_{3\mathrm{dB}}}{2}\right)}$		✓			✓	
$\Delta l_{max(dir)} = \Delta l_{max(omni)} = 2 \cdot r_s$	✓					✓

The use of directional antennas at both the BS and the MT may not be easy to accomplish, since small angular main beam deviations, either at the BS or the MT, have large impact on the overall link performance. This configuration can be somehow associated to the establishment of a fixed link between the BS and the MT. The main drawback is that the MT position varies in time; however, following a similar simple geometrical approach, one can define some expressions for evaluating the maximum difference in propagation path length under these conditions, Figure 7.23.

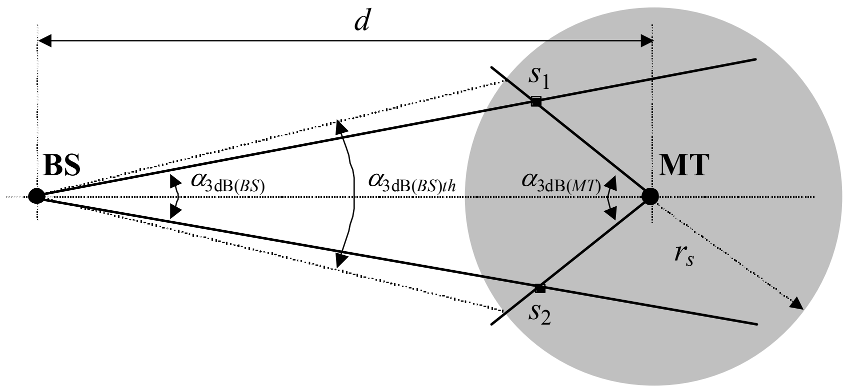

Figure 7.23 – Directional antennas at the BS and the MT.

As depicted in Figure 7.23, for $\alpha_{3\mathrm{dB}(BS)} > \alpha_{3\mathrm{dB}(BS)th}$ the value of $\Delta l_{max(dir)}$ is evaluated as for the case when considering only a directional antenna at the MT, since it defines the maximum possible difference in propagation path length resulting from a scatterer reflection in the scattering area boundary. For smaller values of $\alpha_{3\mathrm{dB}(BS)}$ the value of $\Delta l_{max(dir)}$ results from a reflection within the scattering area, and it can be evaluated as

$$\Delta l_{max(dir)} = \frac{d - x_l}{\cos\left(\dfrac{\alpha_{3\mathrm{dB}(BS)}}{2}\right)} + \frac{x_l}{\cos\left(\dfrac{\alpha_{3\mathrm{dB}(MT)}}{2}\right)} - d \tag{7.24}$$

with

$$x_l = \frac{d \cdot \tan\left(\dfrac{\alpha_{3\mathrm{dB}(BS)}}{2}\right)}{\tan\left(\dfrac{\alpha_{3\mathrm{dB}(BS)}}{2}\right) + \tan\left(\dfrac{\alpha_{3\mathrm{dB}(MT)}}{2}\right)} \tag{7.25}$$

For a given MT antenna beamwidth, the value of $\alpha_{3\mathrm{dB}(BS)}$ below which $\Delta l_{max(dir)}$ is evaluated as (7.24) is given by

$$\alpha_{3\mathrm{dB}(BS)th} = 2 \cdot \mathrm{atan}\left(\frac{\sin\left(\dfrac{\alpha_{3\mathrm{dB}(MT)}}{2}\right)}{\dfrac{d}{r_s} - \cos\left(\dfrac{\alpha_{3\mathrm{dB}(MT)}}{2}\right)} \right) \tag{7.26}$$

As previously referred, for $\alpha_{3\mathrm{dB}(BS)} > \alpha_{3\mathrm{dB}(BS)_{th}}$ the value of $\Delta l_{max(dir)}$ should be evaluated as for the case when only a directional antenna at the MT is considered.

Since the observed values of fading depth depend not only on the value of K_{dir} but also on $\Delta w_{l(dir)}$, thus, $\Delta l_{max(dir)}$, it is of interest to evaluate the dependence of $\Delta l_{max(dir)}$ on the considered antenna beamwidth (for simplicity, the use of directional antennas at the BS and the MT is not adressed). As previously presented, the value of $\Delta l_{max(dir)}$ in micro-cellular environments is independent of $\alpha_{3\mathrm{dB}}$, hence, one focus on macro- and pico-cellular ones.

The results in Figure 7.24 illustrate the relation between $\Delta l_{max(dir)}$ and $\Delta l_{max(omni)}$ in a macro-cellular environment as a function of $\alpha_{3\mathrm{dB}}$, d/r_s = 1, 2, 5, 10 and 80 being considered. A directional antenna is assumed only at the MT; as previously explained, if a directional antenna is used only at the BS no dependence of $\Delta l_{max(dir)}$ on $\alpha_{3\mathrm{dB}}$ is observed, thus, $\Delta l_{max(dir)} = \Delta l_{max(omni)}$. It is observed that, as expected, $\Delta l_{max(dir)}$ tends to zero as $\alpha_{3\mathrm{dB}}$ decreases. For large values of $\alpha_{3\mathrm{dB}}$, it approaches the one obtained with an omnidirectional antenna. Moreover, there is not a significant dependence on d/r_s, this dependence having its maximum for $\alpha_{3\mathrm{dB}} = 120^{\circ}$, and no significant dependence being observed for $d/r_s > 5$.

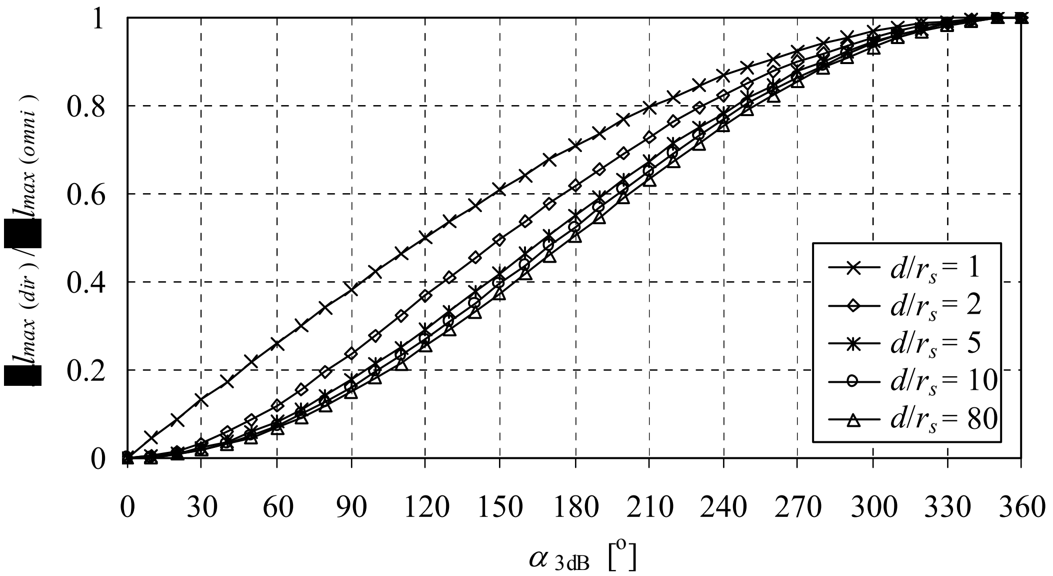

Figure 7.24 – Dependence of $\Delta l_{max(dir)}$ on $\alpha_{3\mathrm{dB}}$, macro-cellular, directional antenna at the MT.

In pico-cellular environments, it is assumed that the MT is positioned within the scattering scenario, hence, d/r_s = 0.01, 0.1, 0.2, 0.4, 0.6, 0.8 and 1.0 is considered, Figure 7.25. A directional antenna is assumed only at the BS; if a directional antenna is used only at the MT, no dependence of $\Delta l_{max(dir)}$ on $\alpha_{3\mathrm{dB}}$ is observed, as previously, $\Delta l_{max(dir)} = \Delta l_{max(omni)}$. As one can observe, a significant dependence on d/r_s is verified: for small values of d/r_s, e.g., $d/r_s < 0.1$, the value of $\Delta l_{max(dir)}$ is practically independent of $\alpha_{3\mathrm{dB}}$; as d/r_s increases, i.e., for large values of d (higher distance between the BS and the MT) or small values of r_s (smaller scattering scenarios) the dependence of $\Delta l_{max(dir)}$ on $\alpha_{3\mathrm{dB}}$ becomes increasingly significant.

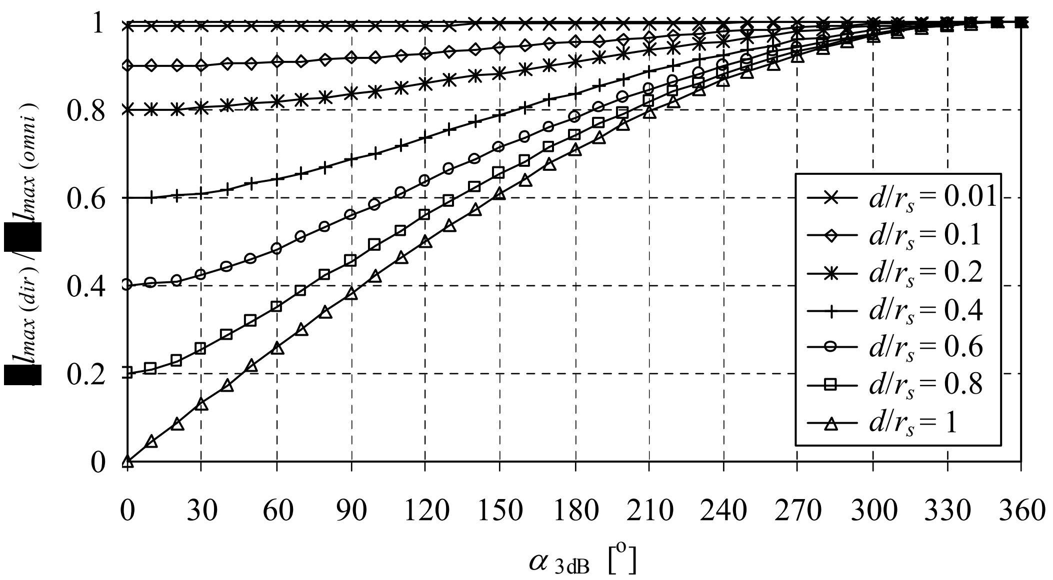

Figure 7.25 – Dependence of $\Delta l_{max(dir)}$ on $\alpha_{3\mathrm{dB}}$, pico-cellular, directional antenna at the BS.

Globally, a significant dependence of $\Delta l_{max(dir)}$ on $\alpha_{3\text{dB}}$ is found in macro- and pico-cellular environments. Nevertheless, in pico-cellular ones, no significant dependence is observed for $d/r_s < 0.1$; this corresponds to consider that the MT is close to the BS, compared to the radius of the scattering scenario. Concerning the dependence of $\Delta l_{max(dir)}$ on d/r_s, in macro-cellular environments, no significant dependence is observed for $d/r_s > 5$, which is usual in this kind of environments, since the MT is usually far away from the BS, compared to the radius of the scattering scenario; in pico-cellular ones, an increased dependence on d/r_s is found.

7.5. Observed Fading Depth

7.5.1. Micro-Cellular Environments

Since one has already characterised K_{dir} and $\Delta l_{max(dir)}$ as a function of $\alpha_{3\text{dB}}$, the fading depth observed by different systems can be easily evaluated. For simplicity, one considers the use of an ideal directional antenna.

As previously referred, in micro-cellular environments the value of $\Delta l_{max(dir)} = \Delta l_{max(omni)}$, i.e., $w_{l(dir)} = w_{l(omni)}$, is constant and independent of $\alpha_{3\text{dB}}$, thus, the value of $\Delta FD_{1\%}$ depends only of K_{dir}, as assumed in Section 7.3. A micro-cellular environment as the one in Figure 7.20 is considered for the simulations; different separations between the BS and the MT are assumed, d = 50, 100 and 500 m, for different street widths, w_s = 15 and 60 m.

In the case of GSM, the results are valid for any of the considered street widths and BS-MT separation distances, thus, no dependence on distance and street width is found. This results from the fact that in the considered micro-cellular environments, GSM behaves always as a narrowband system, therefore, not being affected by the change in propagation conditions that affects the value of $\Delta l_{max(dir)} = \Delta l_{max(omni)}$. For the case of a uniform distribution of AoAs, and $K_{omni} > 3$ dB, Figure 7.26, $\Delta FD_{1\%}$ varies almost linearly with $\alpha_{3\text{dB}}$, decreasing as it increases; for lower values, e.g., K_{omni} = 0 and 3 dB, this rule of variation is no longer valid (the rule of variation is more like a n-th power law of $\alpha_{3\text{dB}}$), which results from the fading depth variation behaviour as a function of $K = K_{dir}$, for the different values of $\alpha_{3\text{dB}}$ (see Chapter 4).

Results for a Gaussian distribution of AoAs are presented in Figure 7.27, $\sigma_s = 10^{\circ}$ being considered. It is observed that the value of $\Delta FD_{1\%}$ is below 3 dB for $\alpha_{3\text{dB}} > 20^{\circ}$, i.e.,

$\alpha_{3dB} > 2\sigma_s$, which is not surprising, since almost all refracted/reflected waves are within the antenna half-power beamwidth. For higher values of σ_s, a similar behaviour is observed, nevertheless, for the same value of α_{3dB} a higher value of $\Delta FD_{1\%}$ is obtained, Appendix VII.

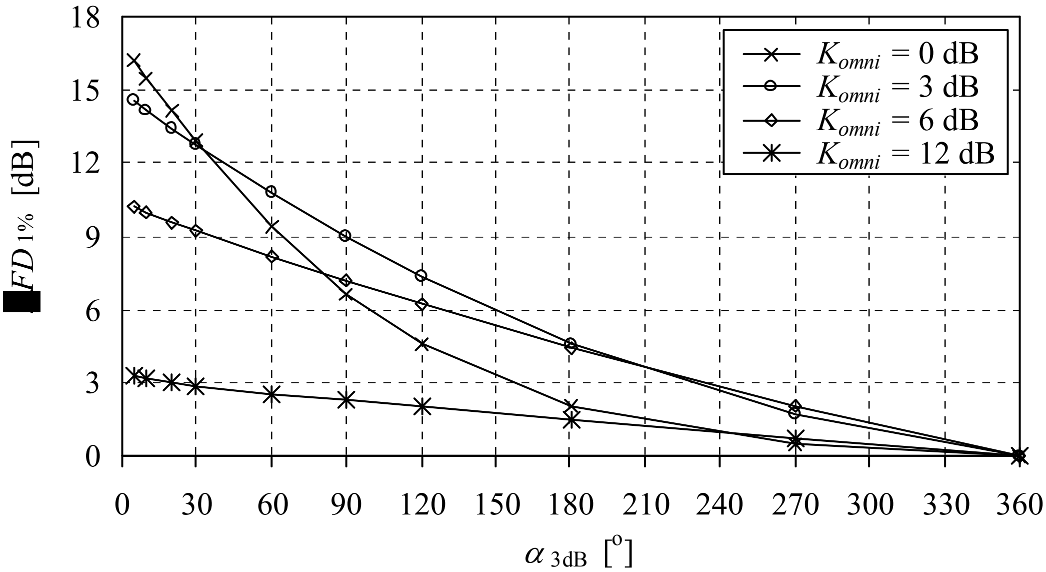

Figure 7.26 – Fading depth variation, micro-cellular, GSM.

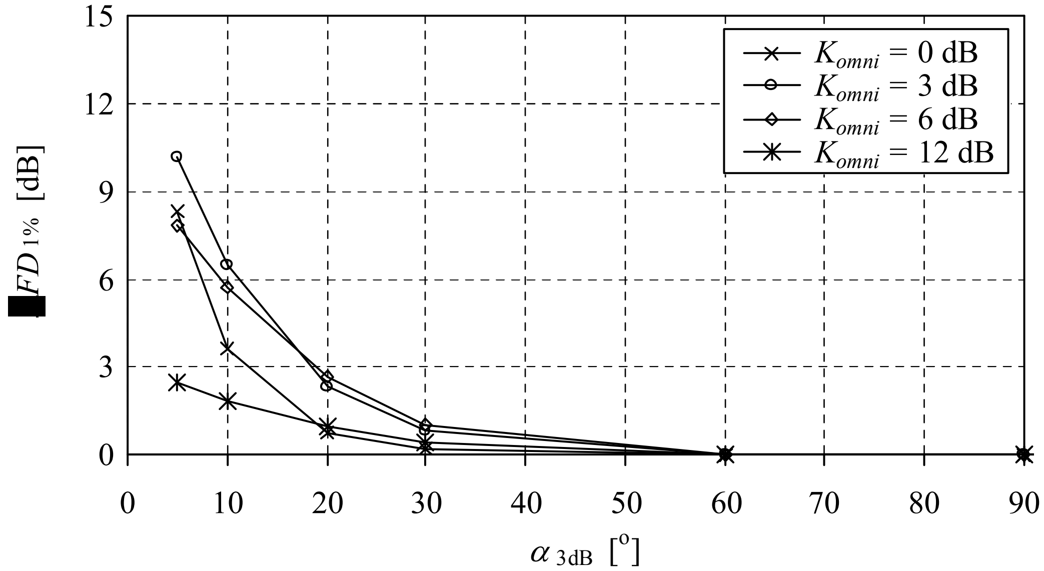

Figure 7.27 – Fading depth variation, micro-cellular, $\sigma_s = 10^{\circ}$, GSM.

In the case of UMTS, for a uniform distribution of AoAs, a significant dependence on the BS-MT separation is observed, Figure 7.28 and Figure 7.29. In fact, UMTS has a bandwidth larger than GSM, therefore, the value of $\Delta l_{max(dir)} = \Delta l_{max(omni)}$ observed at different BS-MT distances has a larger impact on $\Delta FD_{1\%}$.

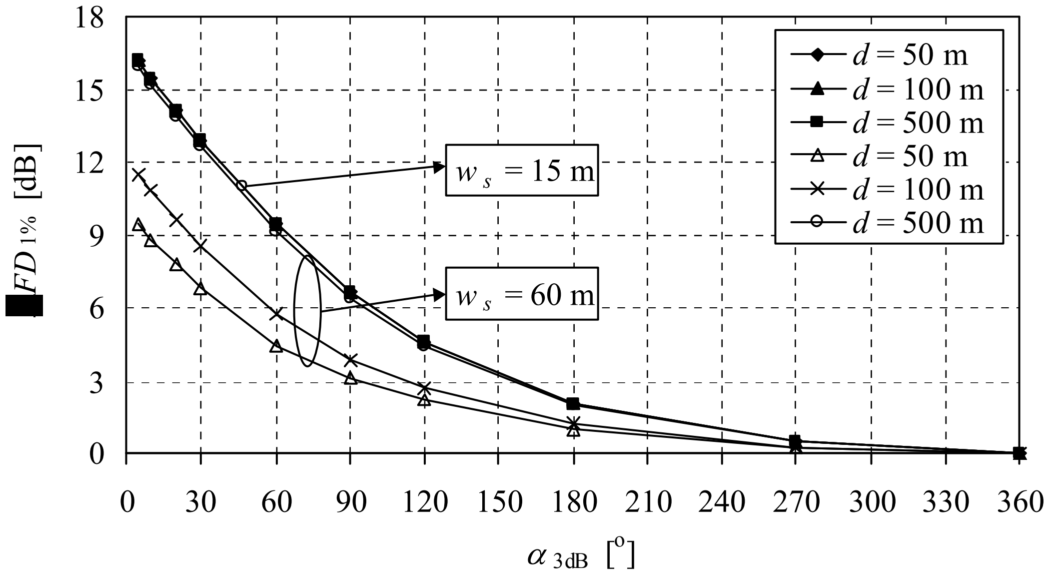

Figure 7.28 – Fading depth variation, micro-cellular, K_{omni} = 0 dB, UMTS.

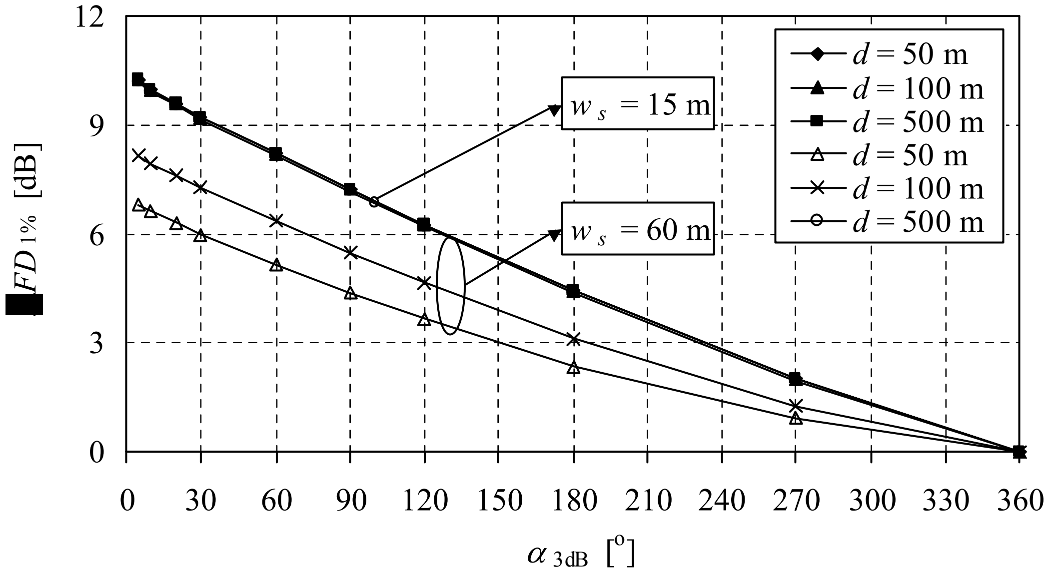

Figure 7.29 – Fading depth variation, micro-cellular, K_{omni} = 6 dB, UMTS.

This dependence is more significant in wider streets and for small values of the Rice factor (results for K = 12 dB can be found in Appendix VII). A complete understanding of such behaviour can be accomplished by evaluating the values of $\Delta l_{max(dir)}$ and K_{dir} corresponding to the different BS-MT separation distances; as expected, lower values of $\Delta FD_{1\%}$ are observed for large values of K_{omni}. As far as the street width is concerned, narrower streets, e.g., w_s = 15 m, exhibits large values of $\Delta FD_{1\%}$ and no significant dependence on d is observed; in wider streets, e.g., w_s = 60 m, a significant dependence on d is observed, the larger values of $\Delta FD_{1\%}$ being obtained for larger values of d, i.e., large BS-MT distance.

Besides the fact that for UMTS a higher dependence on the street width is observed, the effect of considering a Gaussian distribution of AoAs rather than a uniform one is quite similar to the GSM case. Results can be found in Appendix VII.

Similar results for HIPERLAN/2 are presented in Appendix VII. It is observed that there is an increased dependency on the BS-MT separation distance even for narrower streets, this being more significant for small values of K_{omni}. Therefore, one concludes that the dependence on the street width increases with increasing system bandwidths and decreasing values of K_{omni}. As far as the reduction in fading depth is concerned, the narrower the street and the larger the value of d, the higher the value of $\Delta FD_{1\%}$.

Results for the case of a Gaussian distribution of AoAs are also presented in Appendix VII. Besides the increased dependency on d/r_s, a similar behaviour to the one for UMTS is observed.

7.5.2. Macro-Cellular Environments

Macro-cellular environments are considered now. For illustration, one considers r_s = 100 and 800 m, and d/r_s = 1, 2, 5, 10 and 80. A directional antenna is assumed for the MT, since the results obtained by considering a directional antenna at the BS are similar to the ones obtained only from considering the dependence of K_{dir} on $\alpha_{3\text{dB}}$ (see Section 7.3.3). In the following, one presents some results on the fading depth variation observed by GSM and UMTS, HIPERLAN/2 and MBS not being considered, since these systems are not intended to work in this type of environments. As previously, uniform and Gaussian distributions of the AoAs are used.

The results in Figure 7.30 illustrate the fading depth variation for GSM in a macro-cellular environment for the case of a uniform distribution of AOAs. A scattering radius of 100 m and K_{omni} = 0 dB is assumed. For the considered parameters, no significant dependence on d/r_s is observed, i.e., different values $\Delta l_{max(dir)}$ observed for different antenna beamwidths do not significantly affect the observed reduction in fading depth. This reduction is mainly due to the change in the value of K_{dir} resulting from considering the influence of the directional antenna at the MT. This results from the fact that, in this environment, GSM behaves almost like a narrowband system, being significantly independent of environment changes that affect propagation path length of arriving waves. One also observes that for K_{omni} = 0 dB no significant (lower than 3 dB) reduction in fading depth is observed for

$\alpha_{3dB} > 120^o$. For small beamwidths, e.g., $\alpha_{3dB} < 60^o$, a fading depth reduction ranging from 7 to 15 dB is observed. For large values of K_{omni}, e.g., K_{omni} = 6 and 12 dB, Appendix VII, $\Delta FD_{1\%}$ depends almost linearly on α_{3dB}; as expected the larger K_{omni} the lower the value of $\Delta FD_{1\%}$.

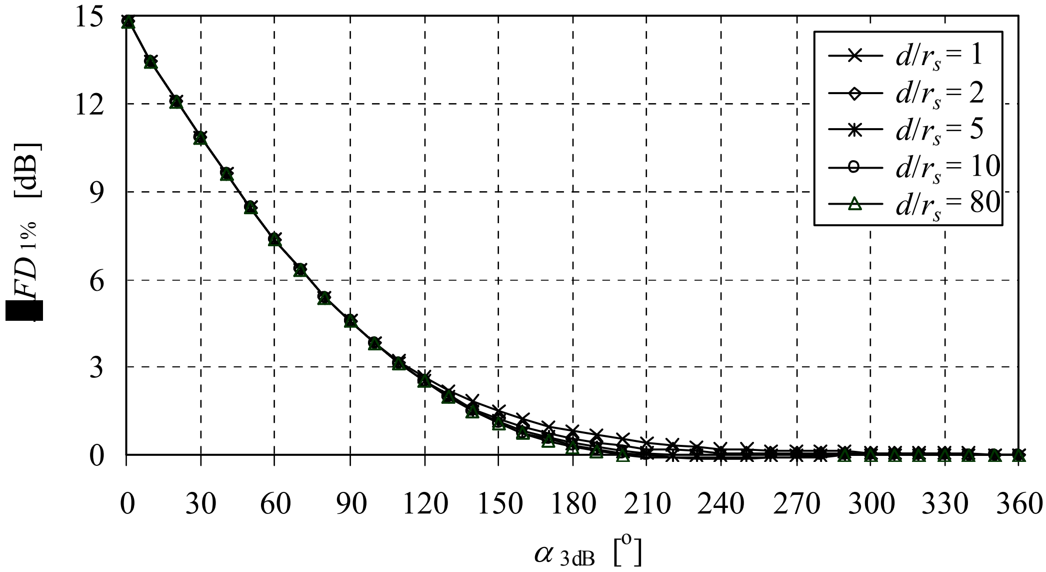

Figure 7.30 – Fading depth variation, macro-cellular, r_s = 100 m, K_{omni} = 0 dB, GSM.

For large scattering radius, e.g., r_s = 800 m, and K_{omni} = 0 dB, a significant dependence on d/r_s is observed, Figure 7.31. Moreover, a fading depth degradation (negative values of $\Delta FD_{1\%}$) is observed for roughly $\alpha_{3dB} > 60^o$, since the observed value of K_{dir} is above the one observed with an omnidirectional antenna; however, the value of $\Delta l_{max(dir)}$ is below $\Delta l_{max(omni)}$ (see Figure 7.24), these two effects resulting on a fading depth degradation. This degradation is more significant for large values of d/r_s, i.e., large BS-MT separation distances, which is not surprising, since for the same value of α_{3dB}, small values of $\Delta l_{max(dir)}/\Delta l_{max(omni)}$ are observed for large values of d/r_s, being predominant compared to the increase in K_{dir}. One must remember that the fading depth decreases with increasing values of K_{dir} and $\Delta l_{max(dir)}$; for values of $\alpha_{3dB} < 30^o$ a fading depth reduction above 3 dB is observed independently of d/r_s; for large values of K_{omni}, e.g., K_{omni} = 6 dB, Appendix VII, no degradation is observed. Also a fading depth reduction above 3 dB is observed for $\alpha_{3dB} < 40^o$; no significant fading depth reduction is observed for larger values of K_{omni}, since the values of fading depth observed with an omnidirectional antenna are usually very low for the given values of d/r_s.

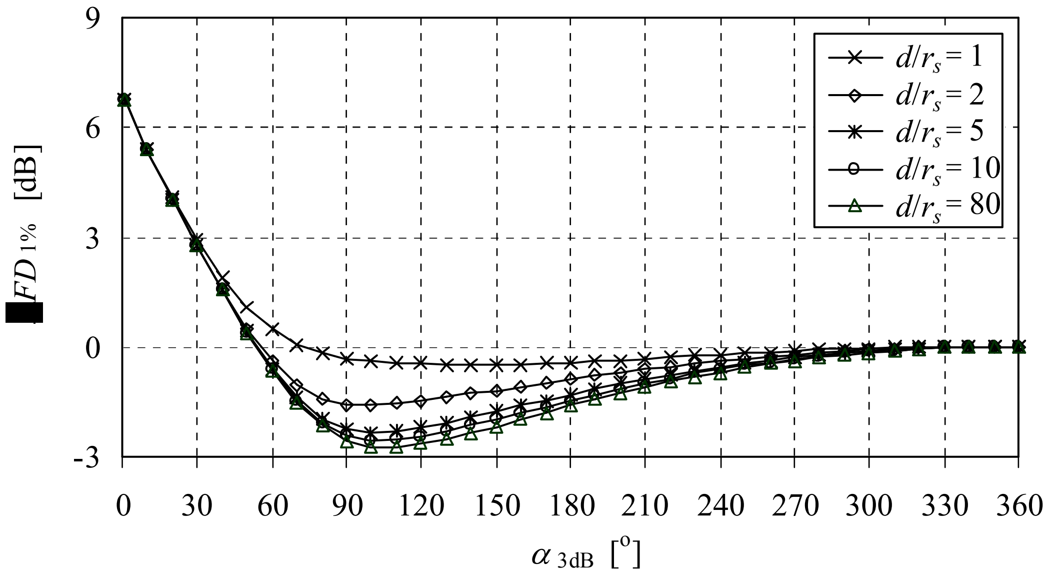

Figure 7.31 – Fading depth variation, macro-cellular, r_s = 800 m, K_{omni} = 0 dB, GSM.

When assuming a Gaussian distribution of AoAs, a different behaviour is expected, as previously, results are derived for different values of σ_s and d/r_s. As one can observe from Figure 7.32, for r_s = 100 m, σ_s =10° and K_{omni} = 0 dB a degradation in fading depth is observed for α_{3dB} > 15° (1.5σ_s). Moreover, the results are practically independent of d/r_s. As the value of K_{omni} increases also the value of α_{3dB} above which there is fading depth degradation increases, the degradation being smaller with increasing values of K_{omni}.

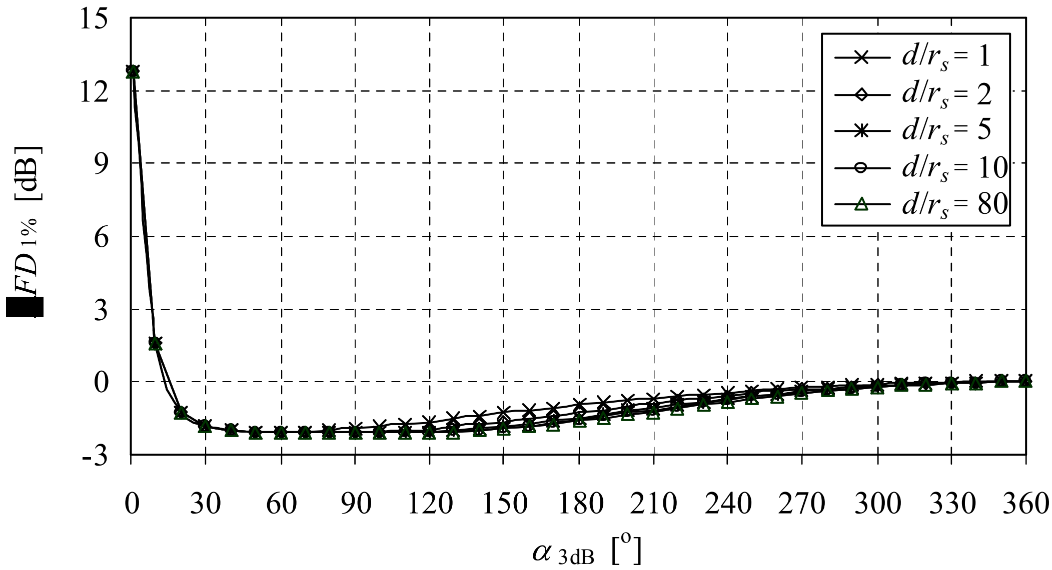

Figure 7.32 – Fading depth variation, macro-cellular, r_s = 100 m, K_{omni} = 0 dB, σ_s = 10°, GSM.

For $K_{omni} = 6$ dB, Appendix VII, it is observed that an improvement in fading depth is observed for $\alpha_{3\mathrm{dB}} < 30^{\mathrm{o}}$ ($3\sigma_s$); for large values of $\alpha_{3\mathrm{dB}}$ still is a degradation, however, it is not significant. For large values of K_{omni}, the results are similar, globally, the maximum value of $\Delta FD_{1\%}$ decreases with increasing values of K_{omni}, Appendix VII.

As the value of σ_s increases, e.g., $\sigma_s = 40^{\mathrm{o}}$, the value of $\alpha_{3\mathrm{dB}}$ above which there is fading depth degradation, also increases, Figure 7.33. Results for $K_{omni} = 6$ dB can be found in Appendix VII; it is observed that degradation occurs for roughly $\alpha_{3\mathrm{dB}} > 1.5\sigma_s$ and $\alpha_{3\mathrm{dB}} > 3.0\sigma_s$ for $K_{omni} = 0$ and 6 dB, respectively.

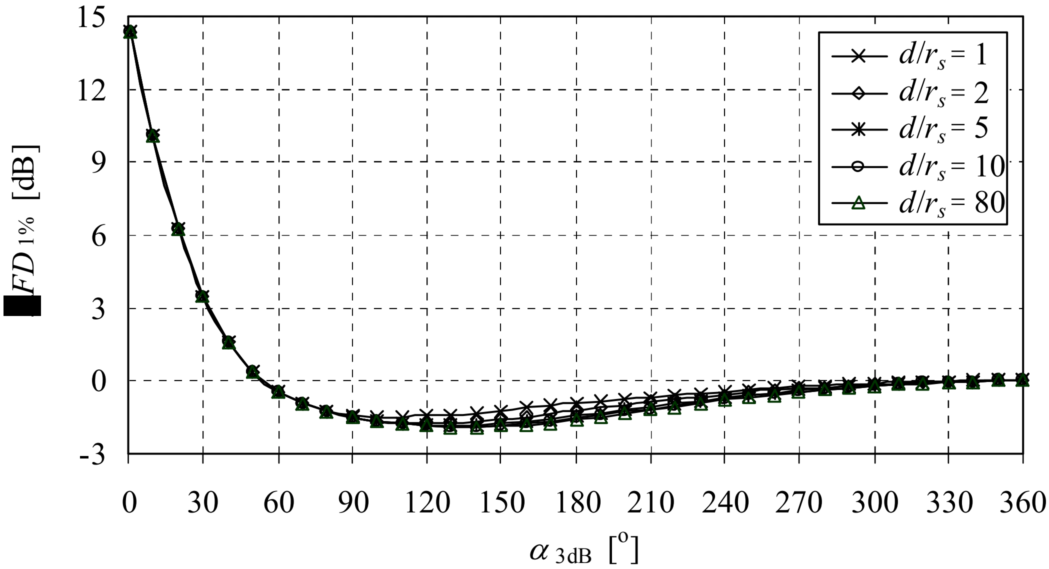

Figure 7.33 – Fading depth variation, macro-cellular, $r_s = 100$ m, $K_{omni} = 0$ dB, $\sigma_s = 40^{\mathrm{o}}$, GSM.

For large values of r_s, e.g., $r_s = 800$ m, a higher degradation is observed, Figure 7.34. It is observed that there is almost always an increase in the observed value of fading depth, as previously, this being more significant for large BS-MT separation distances (large values of d/r_s). As the value of K_{omni} increases, there a slightly increase on the value of $\alpha_{3\mathrm{dB}}$ above which there is fading depth degradation and a decrease in the maximum fading depth degradation, Appendix VII.

Again, as the value of σ_s increases the value of $\alpha_{3\mathrm{dB}}$ above which there is fading depth degradation increases and the maximum fading depth degradation decreases, Figure 7.35. Globally, it is observed that fading depth degradation is observed for roughly $\alpha_{3\mathrm{dB}} > 0.5\sigma_s$ and $\alpha_{3\mathrm{dB}} > 1.0\sigma_s$ for $K_{omni} = 0$ and 6 dB, respectively.

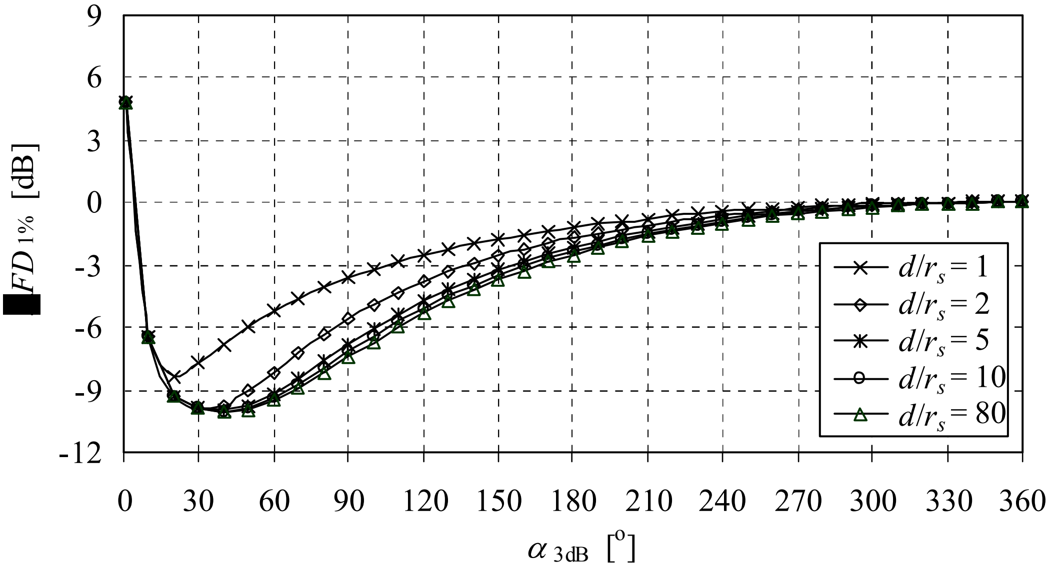

Figure 7.34 – Fading depth variation, macro-cellular, r_s = 800 m, K_{omni} = 0 dB, σ_s = 10^o, GSM.

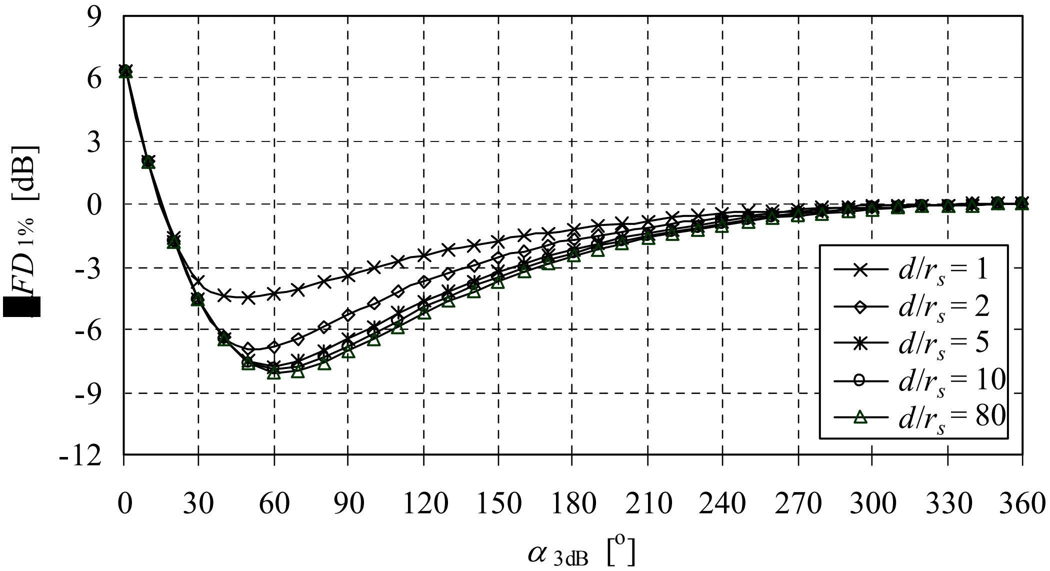

Figure 7.35 – Fading depth variation, macro-cellular, r_s = 800 m, K_{omni} = 0 dB, σ_s = 40^o, GSM.

The results in Figure 7.36 illustrate the fading depth behaviour for UMTS, a uniform distribution of AoAs being assumed. As one can observe, there is a degradation of fading depth for roughly α_{3dB} > 30^o and K_{omni} = 0 dB. This degradation is more significant for large BS-MT separations; for d/r_s > 5, the results are almost independent of d/r_s. As previously, as K_{omni} increases, the value of α_{3dB} above that there is fading depth degradation also increases and the maximum fading depth degradation decreases. For K_{omni} = 6 dB, no significant degradation is observed, however, even for smaller beamwidths, no significant improvement is obtained; the value of $\Delta FD_{1\%}$ is always below 3 dB, Appendix VII.

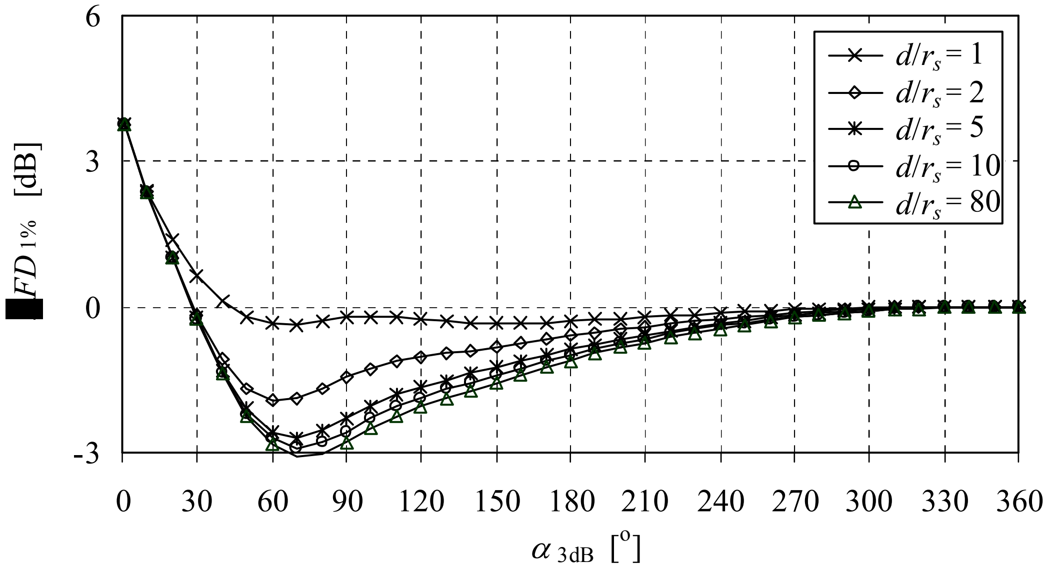

Figure 7.36 – Fading depth variation, macro-cellular, r_s = 100 m, K_{omni} = 0 dB, UMTS.

For large values of r_s, no significant improvement is observed for K_{omni} = 0 dB, instead, degradation is observed, Figure 7.37. For large values of K_{omni} no significant dependence on α_{3dB} is verified, Appendix VII.

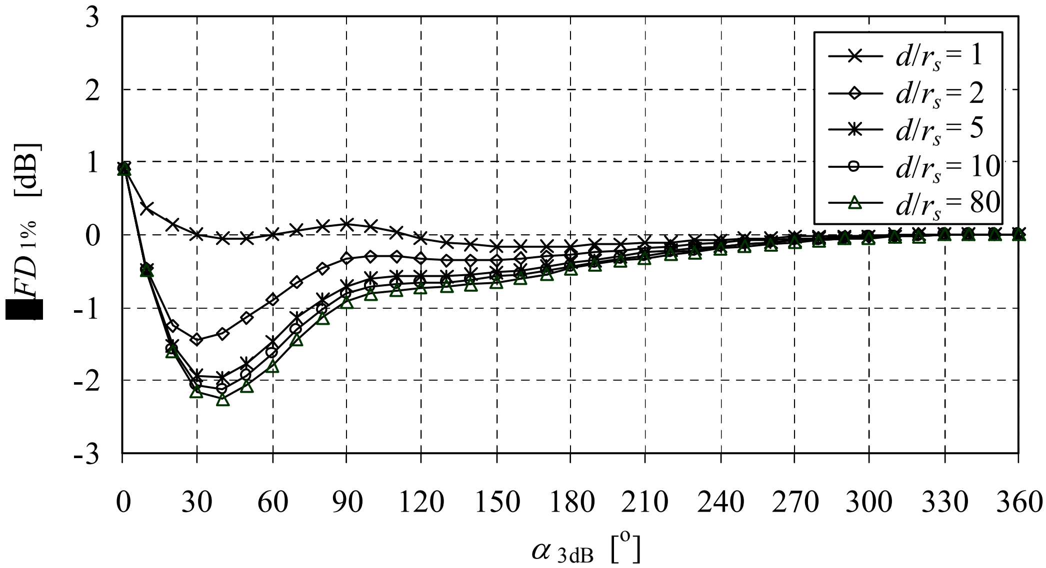

Figure 7.37 – Fading depth variation, macro-cellular, r_s = 800 m, K_{omni} = 0 dB, UMTS.

Assuming a Gaussian distribution of the AoAs the results are even worst, i.e., a large degradation is found; it can be as large as -12 dB depending on the considered values of d/r_s

and σ_s, the larger degradation being observed for large values of d/r_s and small values of σ_s, Appendix VII.

Globally, fading depth reduction is observed for narrow antenna beamwidths. As the system bandwidth and the radius of the scattering scenario increases, lower fading depth reduction is observed and fading depth degradation can occur. Moreover, there is a significant dependence on d/r_s, which increases with increasing system bandwidth.

7.5.3. Pico-Cellular Environments

For illustrating the results obtained in pico-cellular environments, one considers r_s = 2.5 and 5 m, and d/r_s = 0.01, 0.1, 0.2, 0.4, 0.6, 0.8 and 1.0. A directional antenna is assumed for the BS, since the results when considering a directional antenna at the MT are similar to the ones obtained only from considering the dependence of K_{dir} on $\alpha_{3\mathrm{dB}}$ (see Section 7.3.3). In the following, one presents some results on the fading depth variation observed by GSM, UMTS and HIPERLAN/2.

Since GSM is not usually intended to work mainly in pico-cellular environments, the results are not presented herein; however, one briefly illustrates the obtained results in Appendix VII. As for the case of micro-cellular environments, these results are valid for any of the considered values of r_s and d/r_s; therefore, for the given parameters no dependence is observed as a function of the distance between the BS and the MT, i.e., the changes in the value of $\Delta l_{max(dir)}$ do not affect the observed reduction in fading depth. This reduction is only due to the change in the value of K_{dir} due to considering the influence of using a directional antenna at the MT. As previously, this results from the fact that, in this type of environment, GSM behaves as a narrowband system, being significantly independent of environment changes that affect the propagation path length of arriving waves.

If a Gaussian distribution of AoAs is assumed, there is always a fading depth reduction independently on the value of d/r_s. Nevertheless, this reduction approaches zero for roughly $\alpha_{3\mathrm{dB}} > 4.0\sigma_s$. As far as the dependence on K_{omni} is concerned, a similar behaviour as for the case when considering a uniform distribution of AoAs is observed, however, the value of $\Delta FD_{1\%}$ rapidly decreases with increasing values of $\alpha_{3\mathrm{dB}}$, this decreasing rate increasing as σ_s decreases, Appendix VII.

The results for UMTS for K_{omni} = 0, 6 and 12 dB are presented in Appendix VII. It is observed that there is always an improvement in fading depth. As expected this improvement increases with decreasing values of $\alpha_{3\mathrm{dB}}$; moreover, there is no significant dependence on d/r_s, however, a slightly increased dependency is observed for large values of r_s and lower values of K_{omni}. The results in Figure 7.38 illustrate the dependency on d/r_s observed in larger rooms (r_s = 20 m is assumed); a uniform distribution of AoAs is considered.

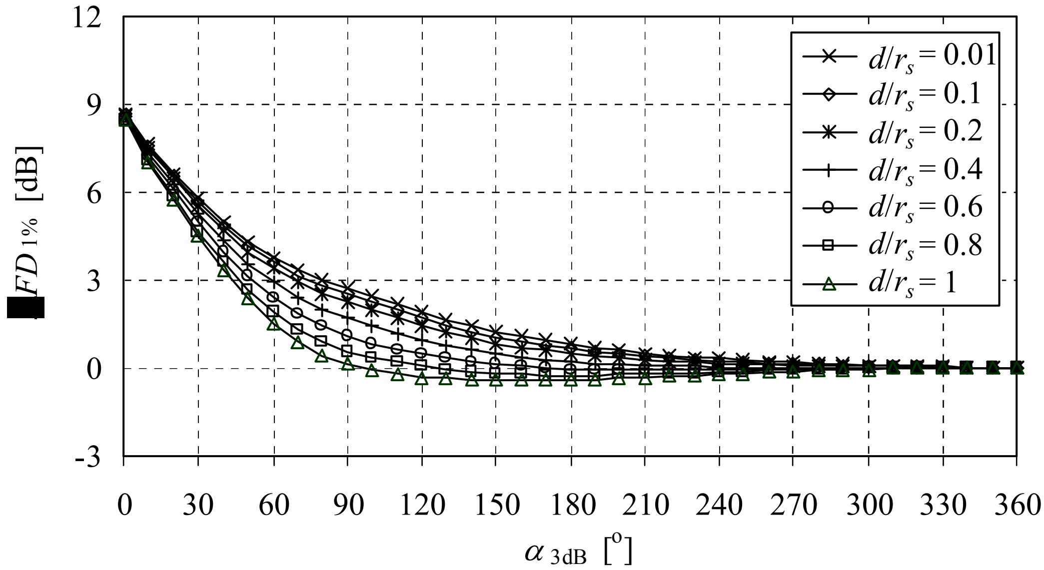

Figure 7.38 – Fading depth variation, pico-cellular, r_s = 20 m, K_{omni} = 0 dB, UMTS.

In large rooms, the fading depth reduction is more significant for small values of d/r_s, thus, small BS-MT distances. As previously, if large values of K_{omni} are considered, a lower dependence on d/r_s is observed, however, the value of $\Delta FD_{1\%}$ also reduces significantly.

Results for HIPERLAN/2 with K_{omni} = 0, 6 and 12 dB are presented in Appendix VII as well. Globally, an increased dependency on d/r_s compared to the case for UMTS is observed, the value of $\Delta FD_{1\%}$ being usually below the corresponding one for UMTS. Similarly, the best results concerning fading depth reduction are observed for small values of r_s; nevertheless, the difference is not significant. Additionally, the fading depth reduction for large values of K_{omni}, e.g., K_{omni} = 12 dB, is below 3 dB for the values of r_s being considered. Similarly to the case of UMTS, the fading depth reduction observed in larger rooms is presented in Figure 7.39, r_s = 20 m and K_{omni} = 0 dB being considered. As verified for UMTS, a smaller fading depth reduction is observed in larger rooms independently of d/r_s. For large values of K_{omni}, no significant reduction in fading depth is observed.

In general, an improvement in fading depth is usually observed, which, as previously, decreases with increasing system bandwidth and for large antenna beamwidths. Compared to the case of macro-cellular environments, a lower dependence on d/r_s is found, no dependence being observed for the case of GSM.

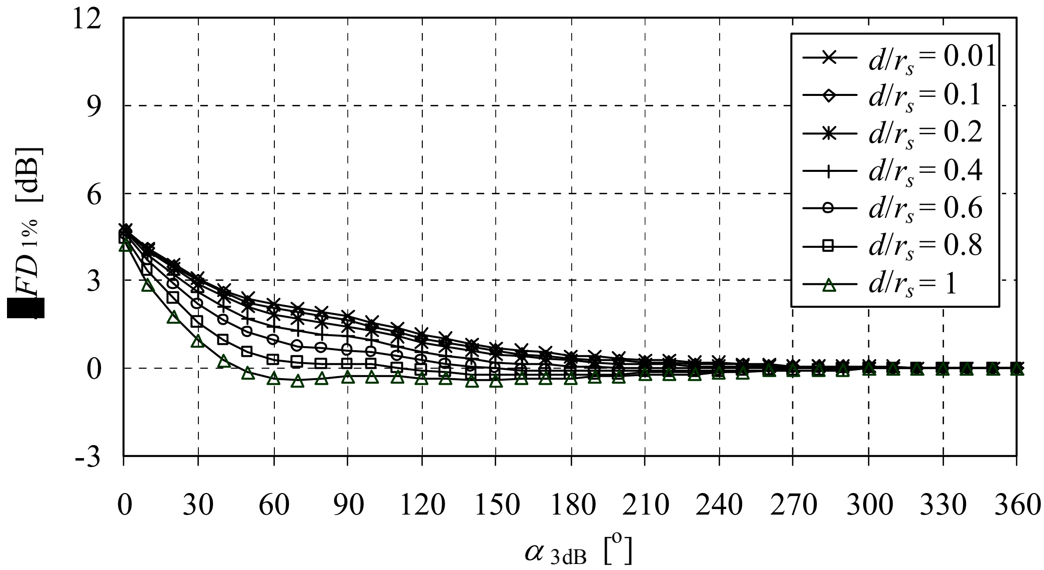

Figure 7.39 – Fading depth variation, pico-cellular, r_s = 20 m, K_{omni} = 0 dB, HIPERLAN/2.

7.5.4. Non-Line-of-Sight Environments

As previously, it is assumed that the NLoS case can be reasonably approximated from considering the fading depth curves for K_{omni} = 0 dB. Nevertheless, there is a main difference, compared to the LoS case: in LoS environments the fading depth depends only on K_{dir}, or on the composite effect of both K_{dir} and $\Delta l_{max(dir)}$; in NLoS ones, the changes in fading depth results only from the variation of $\Delta l_{max(dir)}$, since a LoS component does not exist, hence, it does not make sense to refer to the Rice factor.

For illustration, one presents the results for GSM and UMTS in macro-cellular environments and HIPERLAN/2 in pico-cellular ones; a uniform distribution of AoAs being considered. The value of $\Delta l_{max(dir)}$ is evaluated as for the LoS case, which can be reasonable, if one assumes that the object that is blocking the LoS component is small when compared to the BS-MT separation distance. If this is not the case lower values of $\Delta l_{max(dir)}$ are obtained, and, as a consequence, higher fading depth degradation can be obtained.

For the case of GSM and r_s = 100 m, Figure 7.40, it can be observed that fading depth degradation occurs for any value of d/r_s; moreover, different behaviours are observed for different values of α_{3dB}. It should be remembered that in the wideband case the observed fading depth depends on $\Delta l_{max(dir)}$, basically increasing as $\Delta l_{max(dir)}$ decreases. In the narrowband one, the fading depth is almost independent of $\Delta l_{max(dir)}$, hence, on α_{3dB}.

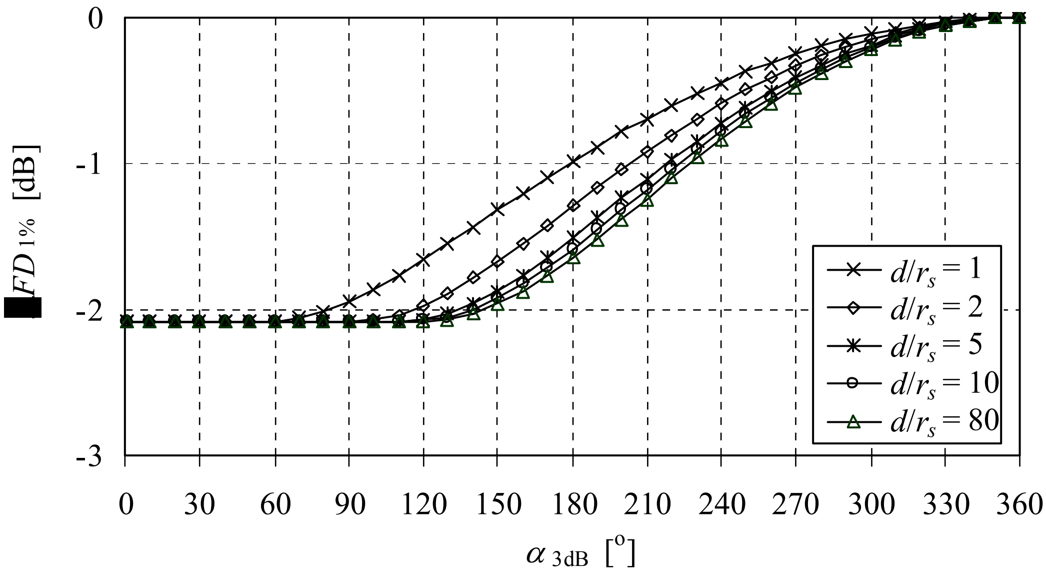

Figure 7.40 – Fading depth variation, macro-cellular, r_s = 100 m, GSM, NLoS.

From Figure 7.40, it is observed that for $\alpha_{3dB} < 90^o$ the value of $\Delta FD_{1\%}$ is constant and practically independent of α_{3dB}, therefore, it can be concluded that the propagation channel behaves as a narrowband one. It must be noted that, when the influence of BS and MT antennas is considered, the narrow- or wideband nature of the propagation channel depends on the considered antenna beamwidth; in this case, the propagation channel behaves as a narrowband channel for $\alpha_{3dB} < 90^o$, while for larger values of α_{3dB} it can be considered as being wideband. Globally, for $\alpha_{3dB} > 120^o$ the fading depth degradation is usually below 2 dB independently of the value of d/r_s. When a large scattering radius are considered, e.g., r_s = 800 m, Appendix VII, the propagation channel behaves as narrowband for $\alpha_{3dB} < 30^o$ and $d/r_s \geq 2$, experiencing a maximum fading depth degradation of roughly -10 dB, i.e., there is an increased fading depth degradation when compared to the case of smaller scattering radius.

In the case of UMTS, Figure 7.41, the results for r_s = 100 m are close to the ones obtained for GSM with r_s = 800 m, resulting from the fact that UMTS has a system bandwidth larger than GSM. For r_s = 800 m, Appendix VII, a lower degradation is usually observed compared to GSM. Higher degradation is observed only for narrow antenna beamwidths, e.g., α_{3dB} roughly below 20^o.

Globally, smaller degradation occurs for smaller values of d/r_s, increasing as the antenna beamwidth decreases. It is also observed that, for narrow antenna beamwidths, UMTS usually experiences higher fading depth degradation than GSM; nevertheless, it should be remembered that the fading depth observed for UMTS when omnidirectional antennas are used is usually well below the one for GSM. Concerning the influence on the distance between the BS and the MT, no significant dependence on d/r_s is observed for $d/r_s > 5$; globally, larger fading depth degradation is observed at larger distances.

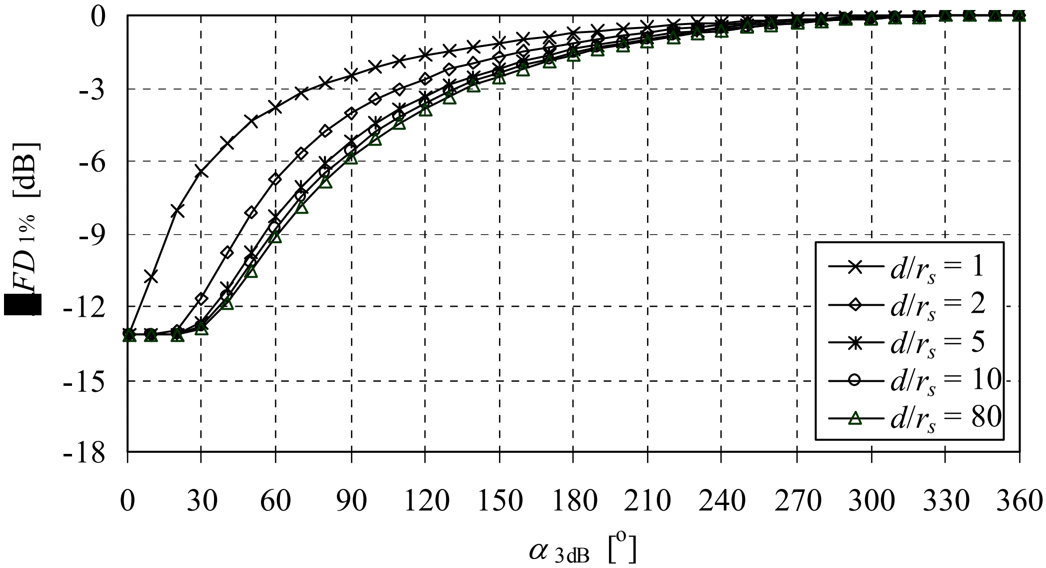

Figure 7.41 – Fading depth variation, macro-cellular, r_s = 100 m, UMTS, NLoS.

The fading depth variation for HIPERLAN/2 in pico-cellular environments is represented in Figure 7.42, r_s = 2.5 m being considered.

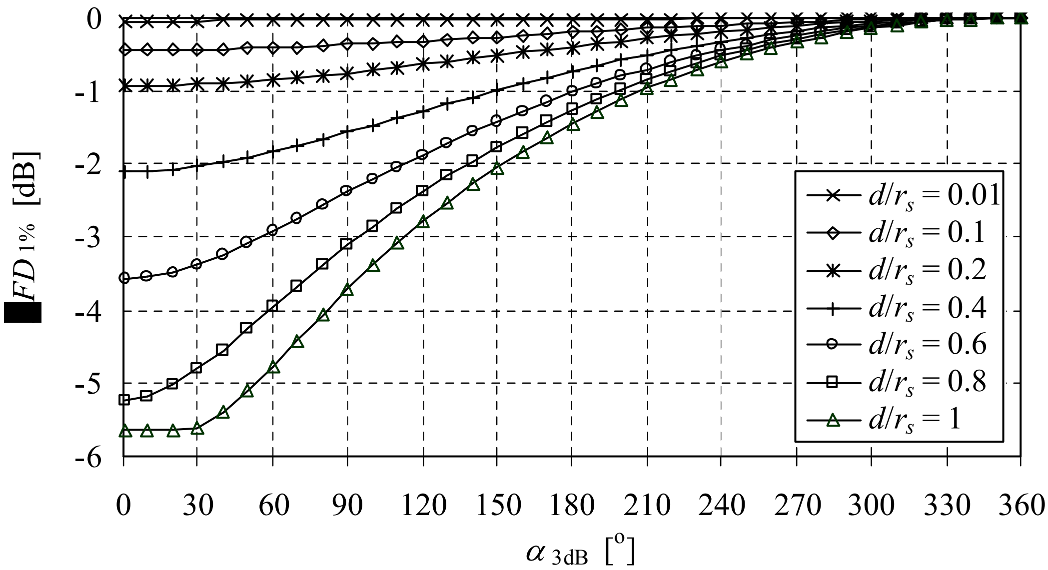

Figure 7.42 – Fading depth variation, pico-cellular, r_s = 2.5 m, HIPERLAN/2, NLoS.

As illustrated in Figure 7.42, there is a significant dependence on d/r_s, a higher degradation being observed for large values of d/r_s; moreover, this degradation increases with increasing values of r_s, Appendix VII. Also, the fading depth degradation decreases with increasing values of $\alpha_{3\text{dB}}$; a degradation below 3 dB is observed for $\alpha_{3\text{dB}} > 120^{\circ}$ for the given values of d/r_s.

Overall, the main difference, compared to previous cases, is that there is always fading depth degradation, which increases for narrower antenna beamwidths, and for increasing system bandwidths. It should be remembered that in NLoS environments, the fading depth observed with directional antennas, depends only on $\Delta l_{max(dir)}$, therefore, increasing as $\Delta l_{max(dir)}$ decreases (smaller values of $\Delta l_{max(dir)}$ being obtained for narrower antenna beamwidths).

7.5.5. Comparative Analysis

In this section, one presents some results on the observed fading depth by different systems, e.g., GSM, UMTS, HIPERLAN/2 and MBS, in different environments. Different situations are considered LoS and NLoS; for the former a value of K_{omni} = 6 dB is assumed. An ideal directional antenna is assumed, different antenna beamwidths being considered, $\alpha_{3\text{dB}}$ = 10, 30, 60 and 120°. For each environment, the fading depth observed with an omnidirectional antenna is also presented, this way, allowing to evaluate the benefit (from the point of view of fading depth reduction) of using directional antennas in different environments.

This evaluation is made as follows:

- for each environment, characterised by its PDP, the value of σ_τ is evaluated;
- by using the equivalence between Δl_{max} and σ_τ, as presented in Chapter 6, one evaluates the value of $\Delta l_{max(omni)}$ for the given value of K_{omni} (as previously K_{omni} = 0 dB is considered for NLoS);
- for each value of $\alpha_{3\text{dB}}$ the value of $\Delta l_{max(dir)}$ is evaluated as described in previous sections;
- the value of K_{dir} is evaluated as a function of $\alpha_{3\text{dB}}$, the AoA being modelled by a uniform distribution;
- the observed fading depth with omnidirectional and directional antennas is obtained by substituting the values of K and Δl_{max} in (4.10) by K_{omni} and $\Delta l_{max(omni)}$, and K_{dir} and $\Delta l_{max(dir)}$, respectively.

Since the lower fading depth reduction, or higher fading depth degradation occurs, almost always for larger BS-MT distances, one considers d/r_s = 80 and d/r_s = 1 for macro- and pico-cellular cases, respectively, therefore, illustrating the worst case fading depth behaviour observed by different systems. In the following, $FD_{1\%(omni)}$ and $FD_{1\%(dir)}$ refers to the value of $FD_{1\%}$, obtained with omnidirectional and directional antennas, respectively.

Using the channel models for GSM the fading depth observed in LoS Rural Area environments is evaluated, Table 7.2; different scenarios are not considered, since they are not suited for LoS. It is observed that a significant reduction in fading depth is obtained for α_{3dB} = 10, 30 and 60°, this reduction increasing as the antenna beamwidth decreases.

Table 7.2 – Fading depth in GSM environments, LoS.

<table>
<tr><th rowspan="3">Environment</th><th rowspan="3">Cell type</th><th rowspan="3">$FD_{1\%(omni)}$ [dB]</th><th colspan="4">$FD_{1\%(dir)}$ [dB]
α_{3dB} [°]</th></tr>
<tr><th>10</th><th>30</th><th>60</th><th>120</th></tr>
<tr><td>Rural Area</td><td>Macro-cell</td><td>11.3</td><td>1.3</td><td>2.0</td><td>3.1</td><td>5.0</td></tr>
</table>

As expected from previous sections, when there is no LoS component a different behaviour is observed, Table 7.3. Fading depth degradation is usually observed for any of the considered antenna beamwidths. As far as the antenna beamwidth is concerned, lower degradation is verified for large values of α_{3dB}.

Table 7.3 – Fading depth in GSM environments, NLoS.

<table>
<tr><th rowspan="2">Environment</th><th rowspan="2">Cell type</th><th rowspan="2">$FD_{1\%(omni)}$ [dB]</th><th colspan="4">$FD_{1\%(dir)}$ [dB]
α_{3dB} [°]</th></tr>
<tr><th>10</th><th>30</th><th>60</th><th>120</th></tr>
<tr><td>Rural Area</td><td>Macro-cell</td><td>17.9</td><td colspan="4">17.9</td></tr>
<tr><td>Typical Urban</td><td>Macro-cell</td><td>11.4</td><td colspan="3">17.9</td><td>16.6</td></tr>
<tr><td>Bad Urban</td><td>Macro-cell</td><td>7.9</td><td colspan="2" rowspan="2">17.9</td><td>17.4</td><td>13.3</td></tr>
<tr><td>Hilly Terrain</td><td>Macro-cell</td><td>5.9</td><td>15.7</td><td>10.4</td></tr>
</table>

Using the channel models for UMTS the fading depth observed under LoS is presented in Table 7.4; Vehicular-B is not considered since it is not intended for LoS conditions. Globally, a fading depth reduction is observed when using directional antennas, however, degradation is observed in Vehicular-A, Typical Urban and Hilly Terrain environments. Nevertheless, this degradation is not significant, since the fading depth observed with a directional antenna is usually less than 0.5 dB above the one observed with an omnidirectional one.

Under NLoS, Table 7.5, fading depth degradation is usually observed, exceptions being Pedestrian environments; this results from the fact that these environments are modelled as micro-cellular ones, i.e., no variation of $\Delta l_{max(dir)}$ is considered.

Table 7.4 – Fading depth in UMTS environments, LoS.

Environment	Cell type	$FD_{1\%(omni)}$ [dB]	$FD_{1\%(dir)}$ [dB] α_{3dB} [°] 10	30	60	120
Indoor-A	Pico-cell	7.9	1.3	2.0	3.0	4.7
Pedestrian-A	Micro-cell	7.2	1.0	1.6	2.4	3.8
Vehicular-A	Macro-cell	2.6	1.3	2.0	2.7	3.0
Indoor-B	Pico-cell	5.0	1.3	2.0	2.7	3.7
Pedestrian-B	Micro-cell	1.8	0.4	0.6	0.8	1.2
Rural Area	Macro-cell	5.0	1.3	2.0	3.1	4.4
Typical Urban	Macro-cell	2.2	1.3	2.0	2.6	2.7
Hilly Terrain	Macro-cell	0.9	1.3	1.6	1.4	1.2

Table 7.5 – Fading depth in UMTS environments, NLoS.

Environment	Cell type	$FD_{1\%(omni)}$ [dB]	$FD_{1\%(dir)}$ [dB] α_{3dB} [°] 10	30	60	120
Indoor-A	Pico-cell	12.0	17.9	17.8	16.9	14.8
Pedestrian-A	Micro-cell	11.0	11.0			
Vehicular-A	Macro-cell	4.5	17.9	17.5	13.4	8.2
Indoor-B	Pico-cell	8.0	17.8	15.9	13.3	10.6
Pedestrian-B	Micro-cell	3.3	3.3			
Vehicular-B	Macro-cell	1.6	17.2	9.3	5.2	2.9
Rural Area	Macro-cell	8.0	17.9	17.9	17.4	13.4
Typical Urban	Macro-cell	4.0	17.9	17.0	12.2	7.2
Hilly Terrain	Macro-cell	1.8	17.6	10.4	5.9	3.3

When considering HIPERLAN/2 environments, the fading depth obtained in different LoS environments is below 3.6 dB, observed with omnidirectional antennas, Table 7.6.

Nevertheless, a reduction in fading depth still is achieved when using directional antennas. A reduction of 2.3 and 0.9 dB is observed for Model A and B, respectively, for an antenna beamwidth of 10^{o}.

Table 7.6 – Fading depth in HIPERLAN/2 environments, LoS.

Environment	Cell type	$FD_{1\%(omni)}$ [dB]	$FD_{1\%(dir)}$ [dB] α_{3dB} [^{o}]			
			10	30	60	120
Model A	Pico-cell	3.6	1.3	1.8	2.3	2.9
Model D	Pico-cell	2.1	1.2	1.4	1.6	1.9

If one considers the NLoS situation, a different behaviour is observed, i.e., as the antenna beamwidth decreases larger fading depths are obtained. The difference relative to the case when using directional antennas can be as large as 11.1 dB, observed for Model A environments and an antenna beamwidth of 10^{o}.

Table 7.7 – Fading depth in HIPERLAN/2 environments, NLoS.

Environment	Cell type	$FD_{1\%(omni)}$ [dB]	$FD_{1\%(dir)}$ [dB] α_{3dB} [^{o}]			
			10	30	60	120
Model A	Pico-cell	5.9	17.0	13.3	10.4	7.8
Model B	Pico-cell	4.4	14.9	10.4	7.9	5.9
Model C	Pico-cell	3.7	13.2	8.9	6.6	5.0
Model D	Pico-cell	3.8	13.5	9.1	6.8	5.1
Model E	Pico-cell	2.9	11.1	7.1	5.3	4.0

As previously referred, besides some experimental PDPs obtained from experimental measurements in different environments, proposed channel models for MBS are not available yet, hence, typical values of *rms* delay spread, as presented in Chapter 5, and an exponential PDP are assumed. Different environments are modelled by assuming the scattering models previously described. City Streets and Corridors are modelled as micro-cellular environments. Nevertheless, one must be aware that the propagation phenomena in Corridors is usually different from that observed in City Streets, thus, it is expected that the theoretical results presented herein can be somehow not so close to reality as for that case of City Streets, for which the micro-cellular scattering model is designed for. In the case of Small Rooms and City Squares they are modelled as pico-cellular environments; again, it should be stressed that in the case of City Squares the scattering model is more likely the one for macro-cellular environments, since the BS is usually placed on a wall or a corner the scattering area being the one around the MT. Nevertheless, since one assumes the worst fading situation in all kind of environments, i.e., a large BS–MT separation distance ($d/r_S = 1$ is assumed for the case of pico-cellular environments), the results obtained by considering the pico-cellular environment are the same as for the case of the macro-cellular with $d/r_S = 1$. One should remember that the same expression for evaluating $\Delta l_{max(dir)}$ applies to macro- and pico-cellular environments, the difference being the possible range of variation of d/r_S.

The results in Table 7.8 were obtained in LoS conditions for a system bandwidth of 50 MHz; as previously a value of $K = 6$ dB is considered.

Table 7.8 – Fading depth in MBS environments, LoS.

Environment	**Cell type**	$FD_{1\%(omni)}$ **[dB]**	$FD_{1\%(dir)}$ **[dB]** α_{3dB} **[°]** 10	30	60	120
City Street	Micro-cell	2.3 – 6.4	0.4 – 1.0	0.7 – 1.5	0.8 – 2.2	1.5 – 3.5
City Square	Pico-cell	1.7 – 2.1	1.1 – 1.2	1.2 – 1.4	1.3 – 1.7	1.5 – 1.9
Small Room	Pico-cell	3.1 – 5.6	1.2 – 1.3	1.7 – 2.0	2.1 – 2.8	2.6 – 4.0
Corridor	Micro-cell[4]	3.5 – 5.6	0.6 – 0.9	1.0 – 2.4	1.4 – 2.1	2.2 – 3.2

It is observed that a decrease in fading depth is obtained with the use of directional antennas. Globally, a significant reduction is obtained in City Streets, Small Rooms and Corridors; a best situation of 5.4 dB fading depth reduction is observed for an antenna beamwidth of 10° in City Street environments. In Small Rooms and Corridors this reduction is usually below 4.3 and 4.7 dB, respectively; these values decrease to 4.2, 3.6 and 3.2 dB for an antenna beamwidth of 60°. No significant decrease in fading depth is verified in City Squares.

[4] The scattering model being considered is based on the assumption that, from a geometrical point of view, a Corridor is almost similar to a City Street. Nevertheless, one must be aware that different propagation phenomena are usually involved.

As expected, under NLoS, Table 7.9, fading depth degradation is usually observed; however, no degradation is verified in City Streets and Corridors since a micro-cellular environment is assumed, hence, the value of $\Delta l_{max(dir)}$ does not depend on the antenna beamwidth, as previously explained.

Table 7.9 – Fading depth in MBS environments, NLoS.

Environment	Cell type	$FD_{1\%(omni)}$ [dB]	$FD_{1\%(dir)}$ [dB] α_{3dB} [º] 10	30	60	120
City Street	Micro-cell	4.0 – 9.8	4.0 – 9.8			
City Square	Pico-cell	3.0 – 3.8	11.5 – 13.6	7.4 – 9.2	5.5 – 6.9	4.1 – 5.2
Small Room	Pico-cell	5.2 – 8.8	16.2 – 17.9	12.0 – 16.5	9.3 – 14.2	7.0 – 11.5
Corridor	Micro-cell	5.8 – 8.8	5.8 – 8.8			

From Table 7.9, one concludes that a larger degradation is observed for narrower antenna beamwidths, e.g., a degradation of 9.8 dB is observed in City Squares for an antenna beamwidth of 10º. This degradation is not significant for large antenna beamwidths, e.g., $\alpha_{3dB} > 120$º.

7.6. Conclusions

An approach for short-term fading depth evaluation using wideband directional channel models is presented. The use of directional antennas is modelled through the variation of the Rice factor and the maximum difference in propagation path length, relative to the case of using omnidirectional antennas. Expressions for the Rice factor and the maximum difference in propagation path length variation as a function of the half-power antenna beamwidth are derived. Different statistical distributions are used for modelling AoAs.

When considering only the variation in fading depth resulting from the Rice factor variation, a uniform distribution of AoAs, and $K_{omni} = 6$ dB, a maximum fading depth reduction of roughly 10 dB is observed when using ULA or UCA antennas. As expected, this fading depth reduction decreases with increasing values of K_{omni} and for increasing system bandwidths. For a number of antenna elements higher than 16 and 32 for ULA and UCA, respectively, no significant improvement in the maximum fading depth reduction is observed.

When a truncated Gaussian distribution is used for modelling AoAs a lower variation of the Rice factor is obtained; consequently, a lower fading depth reduction is observed, however, still being a function of the angular standard deviation of the AoA, i.e., the higher the value of the standard deviation the higher the maximum Rice factor variation.

Typical scattering models are used for modelling the propagation channel. In the micro-cellular environment no dependence of the maximum difference in propagation path length dependence on the half-power beamwidth is found; the fading depth observed for any antenna beamwidth depends only on the Rice factor variation. In the considered micro-cellular environments there is fading depth variation dependence on the street width and on the value of K_{omni}; this dependence increases for increasing system bandwidths and decreasing values of K_{omni}. As far as the reduction in fading depth is concerned, the narrower the street and the larger the BS-MT separation, the higher the fading depth reduction. When considering a Gaussian distribution of AoAs, it is observed that the fading depth reduction is usually below 3 dB for $\alpha_{3\text{dB}} > 2\sigma_s$. Globally, for the same value of $\alpha_{3\text{dB}}$, the higher the value of σ_s the higher the maximum fading depth reduction.

In macro-cellular environments, the results depend on the value of r_s and on the system bandwidth, among others. Basically, the maximum fading depth reduction is obtained for small scattering radius and low system bandwidths; moreover, with increasing system bandwidth and for increasing values of r_s, an increased fading depth degradation is observed; the results when considering a Gaussian distribution of AoAs being even worst.

In pico-cellular environments there is almost always an improvement in fading depth, nevertheless, degradation, besides not being significant, still is observed for large system bandwidths and large values of r_s. In the case of GSM there is no significant dependence on d/r_s; some dependence is observed for systems with larger bandwidths, e.g., UMTS and HIPERLAN/2.

Under NLoS the changes in fading depth results only from the variation of $\Delta l_{max(dir)}$ since a LoS component does not exist, hence, it does not make sense to refer to the Rice factor. Globally, fading depth degradation occurs for any value of d/r_s. This degradation increases with increasing system bandwidth and r_s; moreover, a significant dependence on d/r_s is found, this dependence increasing with increasing system bandwidth.

Using the channel models for GSM, UMTS and HIPERLAN/2, as proposed by standard-setting bodies, the fading depth observed in different environments and for different system bandwidths is evaluated. As expected, under NLoS, degradation is usually verified;

under LoS, there is almost always an improvement in fading depth for the antenna beamwidths being considered; nevertheless, for some channel models, besides not being significant, degradation occurs.

In the case of MBS, City Streets and Corridors are modelled as for the case of micro-cellular environments, and Small Rooms and City Squares are modelled as pico-cellular ones. Globally, under LoS, a significant fading depth reduction is obtained in City Streets, Small Rooms and Corridors; no significant improvement is verified in City Squares. As expected, under NLoS, fading depth degradation is usually observed, nevertheless, no degradation is verified in City Streets and Corridors.

Overall, one concludes that the use of directional antennas can be of usefulness for systems that are mainly intended to work under LoS. Nevertheless, one must be aware that a significant degradation can occur in NLoS situations, and even in LoS ones, depending on the system and environment parameters. It should be stressed that the results presented herein are not intended to provide a complete description on the influence of using directional antennas, but rather giving an insight into this phenomenon. In order to go deeper into the subject, further study should be focused on: (i) the use of different antenna types and parameters; (ii) a complete characterisation of the dependence of the Rice factor variation and the maximum difference in propagation path length as a function of the angular standard deviation of the AoAs, and its relation with propagation model parameters, e.g., the radius of the scattering environments, among many others; (iii) further assessment of the presented results with additional results from simulations and measurements in different environments. Nevertheless, the obtained results are of usefulness for properly identifying the main issues concerning the influence of using directional antennas on the observed values of fading depth. Moreover, it seems that assuming a given approximation error, this characterisation can be done by considering an ideal directional antenna, since the obtained results for ULA and UCA are usually close to the ones of the ideal one, or at least, being related to them, e.g., the Rice factor variation for the case of ULA and UCA is usually 3 dB (in the case of a uniform distribution of AoAs) below the one for the ideal antenna.

As a final conclusion, it should be also stressed that, besides the fading depth degradation observed under certain conditions, this does not necessarily mean that the use of directional antennas is not adequate. One must remember that the use of such techniques is broader in scope, aiming at eliminating interference from different sources, e.g., other MTs, while achieving increased system capacity. In this way, the work presented in this Chapter should be seen as a contribution for properly characterising the short-term fading depth when directional antennas are used, rather than for individually assessing if directional antennas should be used for improving system performance in a given system and working environment.

Chapter 8

Cell Range Evaluation

8.1. Initial Considerations

As referred in previous Chapters, the radio network planning process consists of estimating possible network configurations and equipment required by the operator to be able to achieve the required coverage with the desired capacity and quality of service. Systems such as GSM are usually coverage limited, since the maximum cell range only depends on the maximum allowable path loss between the MT and the BS (for simplicity, besides the different terminologies for naming the BSs, e.g., Node B and Access Point (AP) are commonly used for UMTS and HIPERLAN/2, respectively; one globally refers to BS); the UMTS network behaviour is quite different, since the maximum allowable path loss depends not only on the distance and environment properties but also on the data rate. Coverage is usually uplink limited due to the lower MT transmitted power compared to the BS. Globally, for data rates below several hundreds of kbps, cell coverage in UMTS is basically limited by the uplink, while capacity is downlink limited. Since this work is mainly concerned with coverage issues, one will focus on the uplink.

In order to properly assess the influence from considering more appropriate fading margins, rather than the ones obtained from Rayleigh or Rice distributions, link budgets are evaluated for GSM, UMTS, HIPERLAN/2 and MBS, working in different environments (a broader classification being used): Rural, Suburban and Urban are considered for GSM and UMTS; Urban ones are considered for HIPERLAN/2 and MBS. Building penetration, i.e., indoor coverage by outdoor BSs is also addressed.

Coverage results obtained from considering that short-term fading margins are obtained either from Rayleigh or Rice distributions, or from the approach proposed in Chapter 5 are presented and discussed. Similar results can be derived when considering that short-term fading margins obtained from the environment-geometry based approach in Chapter 4; it should be remembered that a relationship between the approaches proposed in Chapters 4 and 5 is presented in Chapter 6. One uses the time-domain based one, since it allows evaluating the short-term fading margins directly from the PDPs of the propagation channel, as proposed by standard-setting bodies. As usual a log-normal distribution is used for modelling long-term fading effects.

The difference in cell range obtained from considering that the short-term fading margins are evaluated from Rayleigh or Rice distributions is computed. Finally, results on the cell number reduction due to considering the use of more appropriate fading margins, obtained from the proposed approach, are presented and discussed. This way, the applicability of Rayleigh and Rice distributions is discussed, not only from the point of view of the absolute fading depth reduction, obtained from considering more appropriate fading margins, but also on the basis of the effective cell number reduction that can be achieved.

The use of directional antennas is not accounted for, since the obtained results greatly depend on the considered type of antenna, their characteristics, usage (at the BS, the MT, or both) and working environment, hence, a huge set of results needs to be produced in order for covering all the typical configurations that are expected to be found in future mobile communication systems. Nevertheless, the results in Chapter 7 provide a framework for evaluating the fading margins when directional antennas are used, therefore, allowing to estimate the maximum cell range for a given system and working environment.

8.2. Short-term Fading Margins

The use of appropriate short-term fading margins enables a more accurate cell range prediction, this way, allowing a better radio network planning. Most of the existing examples in literature are derived from assuming that there is no need for an additional short-term fading margin, or that a similar fading margin can be applied to different systems working in different environments. Globally, short-term fading margins are usually derived from Rayleigh or Rice distributions, i.e., system bandwidth and environment characteristics are not usually accounted for. However, as presented in previous chapters, the short-term fading margin depends on the environment being considered and on the system bandwidth; therefore, the results obtained from not considering this influence can lead to cell range estimation errors, leading to smaller cells. Additionally, a higher number of BSs is estimated for a given coverage area, therefore, increasing initial network deployment costs.

For illustration purposes, a possible application to the case of cell range prediction in GSM, UMTS, HIPERLAN/2 and MBS is presented. Several classes of environments are considered: Rural, Suburban, Urban and Indoor; building penetration is also accounted for. For cell planning purposes, coverage probabilities around 90 % are usually considered; hence, a coverage probability of 90 % is assumed, corresponding to a fading margin that leads to the fading depth measured between 10 and 50 % of the CDF of the received power; nevertheless, different probabilities can be taken. For this coverage probability, short-term fading margins of 8.2 and 4.6 dB are obtained from considering that the short-term fading variations of the signal magnitude follow Rayleigh or Rice (K = 6 dB is assumed) distributions, respectively.

For the given coverage probability, the short-term fading margins (usually referred as fast fading margin), $M_{ff,90\%}$, for the GSM channel models [ETSI99], evaluated as described in Chapter 5, are illustrated in Figure 8.1.

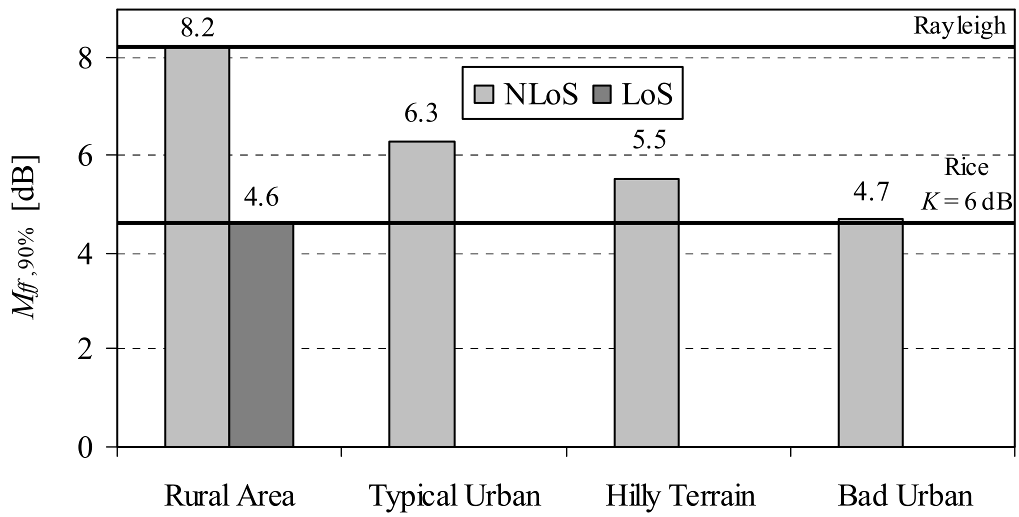

Figure 8.1 – Short-term fading margin for 90 % cell coverage in GSM environments.

It is observed that under NLoS the short-term fading margin, $M_{ff,90\%}$, ranges from 4.7 to 8.2 dB, the higher value corresponding to Rural Area environments. Under LoS, the fading margin in Rural Area environments decreases to 4.6 dB; one should remember that Bad Urban, Typical Urban and Hilly Terrain channel models are not suited for LoS. As expected, under NLoS, the short-term fading margins are well below the ones obtained from considering the Rayleigh distributions; exception is made for the case of Rural Area.

Using the channel models for UMTS [ETSI97], [3GPP02a], the short-term fading margins were evaluated, Figure 8.2. Under NLoS, the fading margins for UMTS range from 2.7 dB observed in Typical Urban environments to 6.4 dB in Indoor-A and Pedestrian-A ones; under LoS, fading margins ranging from 2.2 to 4.0 dB are obtained, being significantly below the ones for the NLoS case. Compared to GSM, lower fading margins are observed both for LoS and NLoS, being usually well below the ones obtained from considering Rayleigh or Rice distributions.

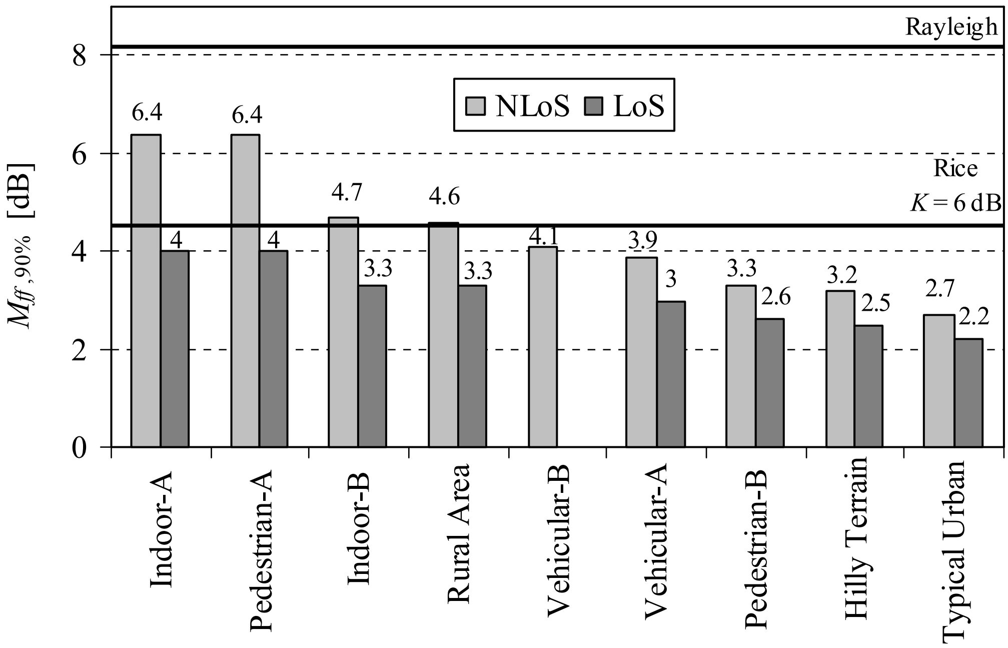

Figure 8.2 – Short-term fading margin for 90 % cell coverage in UMTS environments.

In the case of HIPERLAN/2, for the channel models taken in previous chapters, lower fading margins are obtained, Figure 8.3, they are of the order of 2.0 to 3.5 dB and 1.9 to 2.7 dB for NLoS and LoS, respectively, being significantly below the ones obtained from the usual narrowband distributions.

For MBS, and a 90 % cell coverage probability, short-term fading margins of 2.9 and 2.4 dB are obtained for a system bandwidth of 50 and 100 MHz, respectively, verified for urban street LoS conditions with K = 6 dB (an average *rms* delay spread of 16 ns is assumed [MLAR94]). One should remember that a short-term fading margin of 4.6 dB is obtained from considering the Rice distribution and the same value of K. It must be noted that fading margins for MBS are close to the ones for HIPERLAN/2, since the considered system bandwidths are above the one for HIPERLAN/2, nevertheless, lower values of *rms* delay spread are observed.

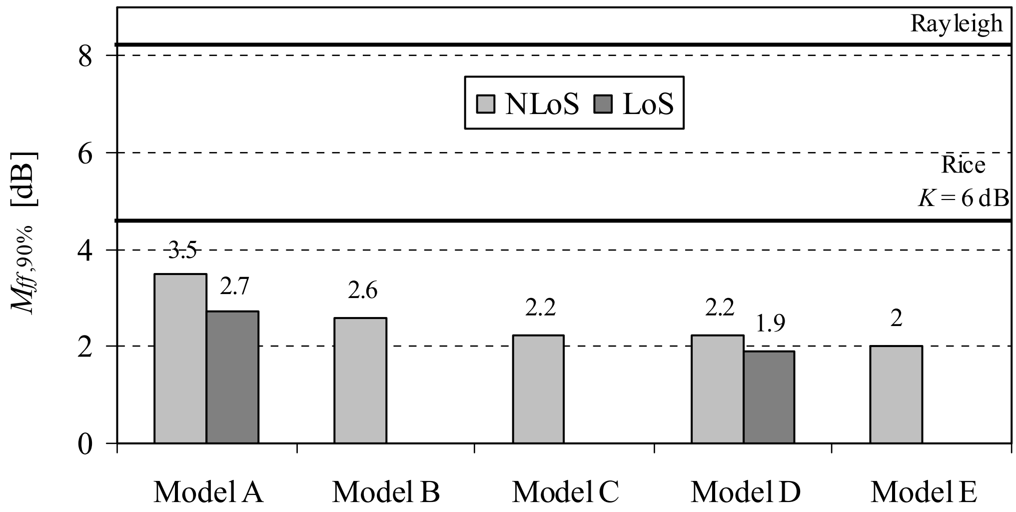

Figure 8.3 – Short-term fading margin for 90 % cell coverage in HIPERLAN/2 environments.

It should be referred that the short-term fading margin depends not only on the environment properties and the system bandwidth but also on the MT speed, power control (especially in the case of UMTS), and transmit/diversity schemes among others. Hence, the proposed margins can be reduced, i.e., lower fading margins should be used when considering the influence of the referred features. Typically, low MT speeds are the limiting factor concerning cell range (higher short-term fading margins), since as the MT speed increases the space/time needed for the MT to get out of a deep fade decreases.

Power control in UMTS is one of the key factors for achieving the desired link quality. Usually a headroom of several dB is reserved for the MT to be able to compensate the short-term fading, allowing to minimise short-term fading effects. Nevertheless, when the MT is already transmitting at the maximum allowable power, no power control is possible, thus, from the point of view of cell range, a short-term fading margin should be accounted for. Concerning the receiver scheme, e.g., Rake and BS antenna structure, additional gains can be obtained in terms of the observed values of fading depth. Although Rake reception and antenna diversity usually compensates for some short-term fading, by combining signals arriving at different delays and paths, this effect greatly depends on the environment characteristics; it is more significant in rich scattering environments, i.e., when there is a larger number of distinct paths between the transmitter and the receiver; when there is no such rich scattering environment, or a strong LoS component exists, this effect becomes less significant.

In the following, one evaluates the link budget and cell range for different systems working in different environments. A worst-case scenario is assumed from considering that the MT is transmitting at maximum power, i.e., no power control effect is possible; moreover, additional gains from using Rake reception schemes and antenna diversity are not accounted for. Additionally, it is assumed that the MT moves at low speeds, this way, experiencing higher fading depths in longer time intervals.

As previously referred, in UMTS the maximum cell range depends on the data rate, hence, different services are considered: voice, real-time data and non-real-time data, with data rates of 12.2, 144 and 384 kbps, respectively [3GPP03c]. In the case of GSM, voice and data services are considered, differing only in the additional body attenuation due to the presence of the user's head near the terminal for the case of voice services. It should be noted that nowadays most of existing terminals allow the user to use voice services without using the terminal near his head, in this case it can be assumed as a data terminal, i.e., no additional body attenuation needs to be considered.

8.3. Rural Environments

Since HIPERLAN/2 and MBS are not intended for Rural environments they are not considered herein. It is assumed that the BS is positioned at 50 m height and that the MT moves at 1.5 m height [Corr01]. As presented in Figure 8.1, the short-term fading margin for GSM in Rural environments is 8.2 and 4.6 dB for the NLoS and LoS cases, respectively. For UMTS fading margins of 4.6 and 3.3 dB are considered for NLoS and LoS, respectively, Figure 8.2. A long-term fading standard deviation of 8 dB is assumed for both systems [Rapp96], [HoTo00], corresponding to a long-term fading margin of 10.25 dB, for 90 % coverage probability. Additional parameters for link budget evaluation were already presented in Chapter 3. For GSM900, the cell range is evaluated from the Okumura-Hata model; for GSM1800 and UMTS, COST 231-Hata is used. Working frequencies of 902.5, 1 747.5 and 1 950 MHz are considered for GSM900, GSM1800 and UMTS, respectively, corresponding to the UL central frequency of each system.

The results for NLoS Rural environments are presented in Table 8.1; L_{pmax} represents the maximum allowable path loss, d_{max} the maximum cell range, obtained as the distance for which $\overline{L_p} = L_{pmax}$ (see Chapter 3), and Δd_{max} the difference in cell range obtained from considering that short-term fading margins are obtained either from Rayleigh or Rice distributions or by using the proposed approach; Δd_r is defined as the ratio between the value of Δd_{max} and d_{max} (obtained from considering that the fading margin is evaluated from

Rayleigh or Rice distributions), hence, representing the relative cell radius increase, obtained from using the proposed fading margins.

Table 8.1 – Cell range in Rural environments, NLoS.

		Rayleigh		Proposed model		Δd_{max} [km]	Δd_r [%]
		$L_{p_{max}}$ [dB]	d_{max} [km]	$L_{p_{max}}$ [dB]	d_{max} [km]		
GSM 900	Voice	130.5	11.36	130.5	11.36	0.00	0.0
	Data	133.5	13.94	133.5	13.94	0.00	0.0
GSM 1800	Voice	127.5	6.10	127.5	6.10	0.00	0.0
	Data	130.5	7.49	130.5	7.49	0.00	0.0
UMTS	12.2 kbps	139.7	13.04	143.3	16.67	3.63	27.8
	144 kbps	135.5	9.78	139.1	12.50	2.72	27.8
	384 kbps	131.7	7.57	135.3	9.67	2.10	27.7

From Table 8.1, one concludes that for GSM900 the cell range in Rural environments ranges from 11.4 to 13.9 km, the higher value corresponding to data transmission. It should be remembered that when considering voice an additional attenuation of 3 dB is considered, due to the influence of the user's head near the antenna. However, assuming that the user can communicate with the mobile terminal away from his head, the cell range will increase by 2.6 km. For GSM1800, a lower a cell range is obtained, 6.1 and 7.5 km for voice and data services, respectively. As expected, in UMTS the cell range is significantly dependent on the type of service being considered. A cell range of 9.7 km is obtained for non-real-time data at 384 kbps; this value increases to 16.7 km for the case of 12.2 kbps voice transmission.

As previously referred, when considering the influence of the system bandwidth and environment characteristics, the fading margins for GSM in Rural Area environments are the same as the ones derived from the Rayleigh distribution, which is not surprising since GSM behaves as a narrowband system in Rural environments. In the case of UMTS, there is a significant decrease in fading margin due to the higher system bandwidth when compared to GSM, i.e., UMTS behaves as a wideband system. For the given coverage probability, the cell range in UMTS increases by 2.1 to 3.6 km (when compared to the Rayleigh case) depending on the type of service being considered, corresponding to an average relative variation of 27.8 %. As expected, under LoS an increased cell range is obtained, Table 8.2. Although, being below the one for the NLoS case, an average cell range increase of 9.3 % is observed for UMTS.

Table 8.2 – Cell range in Rural environments, LoS, K = 6 dB.

		Rice, K = 6 dB		Proposed model		Δd_{max} [km]	Δd_r [%]
		$L_{p_{max}}$ [dB]	d_{max} [km]	$L_{p_{max}}$ [dB]	d_{max} [km]		
GSM 900	Voice	134.1	14.52	134.1	14.52	0.00	0.0
	Data	137.1	17.82	137.1	17.82	0.00	0.0
GSM 1800	Voice	131.1	7.80	131.1	7.80	0.00	0.0
	Data	134.1	9.57	134.1	9.57	0.00	0.0
UMTS	12.2 kbps	143.3	16.67	144.6	18.21	1.54	9.2
	144 kbps	139.1	12.50	140.4	13.66	1.16	9.3
	384 kbps	135.3	9.67	136.6	10.57	0.90	9.3

Globally, it is observed that for GSM in Rural environments there is no need to consider the influence of system bandwidth and environment properties for evaluating the short-term fading margins, instead Rayleigh and Rice distributions can be used.

A different behaviour is observed for UMTS, i.e., the observed fading margins are significantly below the ones for GSM, hence, for the same coverage probability, an increased cell range is obtained. The use of Rayleigh and Rice distributions leads to shorter cells, thus, higher inter-cell interference and lower network quality. Moreover, for a given service area, the number of BSs estimated from using Rayleigh and Rice distributions is higher, increasing network installation, operation, administration and maintenance costs.

8.4. Suburban Environments

As previously, HIPERLAN/2 and MBS are not considered. As proposed in [Corr01] a BS antenna height of 50 m is considered; the MT is positioned at 1.5 m height; buildings with 5 floors and separated by 20 m are assumed. COST 231-WI model is used for path loss estimation, the default parameters for the model being assumed (see Chapter 3); a long-term fading standard deviation of 8 dB is considered. Under NLoS, the short-term fading margins were chosen as 4.7 and 4.1 dB for GSM and UMTS, respectively. In the case of GSM, this value corresponds to the Bad-Urban environment; for UMTS, they were obtained as the mean value of the fading margins for the channel models that can applied to Suburban environments, considering Pedestrian, Vehicular and Typical Urban ones.

From Table 8.3 it is observed that, as expected, the cell range for the different systems significantly decreases when compared to the Rural case. While for GSM900 the cell range is around 3.5 to 4.2 km, for GSM1800 and UMTS it ranges from 1.4 to 2.7 km. As previously, the cell range for UMTS is usually above the one for GSM1800, but below the one observed for GSM900, as opposite to what happens in Rural environments.

Table 8.3 – Cell range in Suburban environments, NLoS.

		Rayleigh		Proposed model		Δd_{max} **[km]**	Δd_r **[%]**
		$L_{p_{max}}$ [dB]	d_{max} [km]	$L_{p_{max}}$ [dB]	d_{max} [km]		
GSM 900	Voice	130.5	2.82	134.0	3.48	0.66	23.4
	Data	133.5	3.38	137.0	4.18	0.80	23.7
GSM 1800	Voice	127.5	1.14	131.0	1.41	0.27	23.7
	Data	130.5	1.37	134.0	1.69	0.32	23.4
UMTS	12.2 kbps	139.7	2.06	143.8	2.65	0.59	28.6
	144 kbps	135.5	1.60	139.6	2.05	0.45	28.1
	384 kbps	131.7	1.27	135.8	1.63	0.36	28.3

Concerning the influence of considering more appropriate fading margins that leads to an increased cell range of around 270 to 800 m. Moreover, this influence is also observed for GSM, since in this kind of environment it no longer behaves as a narrowband system, thus, the Rayleigh distribution is no longer appropriate for evaluating the short-term fading margin. An average cell range increase of 23.6 and 28.3 % is observed for GSM and UMTS, respectively. Similar values are obtained for GSM 900 and 1800, since the difference in cell range depends mainly on the system bandwidth, hence, on the fading margin being considered, rather than on the working frequency.

COST 231-WI provides an expression for path loss evaluation in Urban street-canyon LoS environments. Assuming that, with some approximation error, the same expression can be applied to street-canyon Suburban environments, one evaluates the cell range in LoS conditions, Table 8.4. Short-term fading margins of 4.4 and 3.0 dB are considered for GSM and UMTS, respectively. As previously, the fading margin for UMTS is evaluated as the mean value of the fading margins obtained from the channel models suited for this type of environments; Vehicular-B is excluded, since it is not intended for LoS. Concerning GSM, there are no channel models (as proposed by ETSI) suited for LoS Suburban environments, therefore, one evaluates the fading margin by using the channel models for UMTS for the given GSM system bandwidth, Table 8.5.

Table 8.4 – Cell range in Suburban environments, LoS, K = 6 dB.

		Rice, K = 6 dB		Proposed model		Δd_{max} [km]	Δd_r [%]
		$L_{p_{max}}$ [dB]	d_{max} [km]	$L_{p_{max}}$ [dB]	d_{max} [km]		
GSM 900	Voice	134.1	17.69	134.3	18.00	0.31	1.8
	Data	137.1	23.07	137.3	23.48	0.41	1.8
GSM 1800	Voice	131.1	8.16	131.3	8.30	0.14	1.7
	Data	134.1	10.64	134.3	10.83	0.19	1.8
UMTS	12.2 kbps	143.3	21.96	144.9	25.30	3.34	15.2
	144 kbps	139.1	15.11	140.7	17.41	2.30	15.2
	384 kbps	135.3	10.83	136.9	12.48	1.65	15.2

Table 8.5 – LoS short-term fading margin for 90 % cell coverage in GSM (obtained from the UMTS channel models).

Environment	$M_{ff,90\%}$ [dB] (LoS, K = 6 dB)
Pedestrian-A	4.6
Vehicular-A	4.5
Pedestrian-B	4.2
Typical Urban	4.3

As expected, very large cell ranges are obtained, since propagation in street canyons is usually governed by some kind of wave guiding effect. Nevertheless, one must be aware that the existence of LoS is not usually possible for such large distances, the cell range being inherently limited by the environment topographical properties. Values of 18.0 to 23.5 km, 8.3 to 10.8 km and 12.5 to 25.3 km are obtained for GSM900, GSM1800 and UMTS, respectively. As previously, the lower values are obtained for GSM1800.

A significant dependence from considering lower fading margins is observed for UMTS (a cell range increase of 15.2 % is obtained), nevertheless, for GSM no significant dependence is found, meaning that the Rice distribution still is a reasonable approximation for evaluating the fading margins for GSM in LoS Suburban environments.

When aiming at providing indoor coverage from outdoor BSs, an additional effort has to be done in order to achieve the desired link quality for a given indoor coverage probability. A common approach in existing planning tools is to evaluate the path loss in the outdoor vicinity of buildings, and then adding an additional factor accounting for the additional losses introduced by the walls. Nevertheless, the wall losses depend on several parameters such as the BS height and the existence or not of LoS, among many others. A detailed characterisation of this phenomenon can be found in [DaCo99].

The outdoor path loss is calculated as previously, the wall loss for a given indoor coverage probability being evaluated from the Double-Slope Gaussian Measurement-based Model presented in Chapter 3, by considering the dependence on $20\cdot\log(f)$. The short-term fading margins are the same as previous. It should be remembered that in UMTS, Vehicular channel models are the ones suited for outdoor to indoor penetration, since for these classes of environments the MT is assumed to be within the street or inside a building. Nevertheless, by considering the same average fading margins as previous, those values are in close agreement with the ones obtained from considering only Vehicular models. A maximum difference of 0.1 dB is observed for UMTS under NLoS. The results in Table 8.6 are obtained for GSM and UMTS in Suburban NLoS environments (here LoS or NLoS applies to the path between the BS and the building where the MT is located). It is observed that the cell range for GSM900 is around 1 km while for GSM1800 and UMTS it decreases to 0.26 to 0.47 km. As verified for the case when building penetration is not accounted for, a significant cell radius increase being obtained.

Table 8.6 – Suburban, outdoor-to-indoor building penetration, NLoS.

		Rayleigh		**Proposed model**		**Δd_{max} [km]**	**Δd_r [%]**
		$L_{p_{max}}$ [dB]	d_{max} [km]	$L_{p_{max}}$ [dB]	d_{max} [km]		
GSM 900	Voice	108.6	0.75	112.1	0.92	0.17	22.7
	Data	111.6	0.90	115.1	1.11	0.21	23.3
GSM 1800	Voice	99.6	0.21	103.1	0.26	0.05	23.8
	Data	102.6	0.25	106.1	0.31	0.06	24.0
UMTS	12.2 kbps	111.0	0.36	115.1	0.47	0.11	30.6
	144 kbps	106.8	0.28	110.9	0.36	0.08	28.6
	384 kbps	103.1	0.22	107.2	0.29	0.07	31.8

Assuming street-canyon LoS conditions, a significant improvement in coverage is verified, Table 8.7. A cell range increase of 0.6 to 0.9 km, 0.4 to 0.6 km and 0.8 to 1.7 km is verified for GSM900, GSM1800 and UMTS, respectively, compared to the NLoS case.

Moreover, the best coverage is obtained with UMTS as opposite to the NLoS case for which GSM900 presents the larger cell range; this results from the higher decrease of the short-term fading margin verified for UMTS. One should remember that the fading margin for GSM900 decreases from 4.7 dB for the NLoS case to 4.4 dB in the LoS one, while for UMTS it decreases from 4.1 to 3.0 dB, respectively.

Table 8.7 – Suburban, outdoor-to-indoor building penetration, LoS.

		Rice, K = 6 dB		Proposed model		Δd_{max} [km]	Δd_r [%]
		$L_{p_{max}}$ [dB]	d_{max} [km]	$L_{p_{max}}$ [dB]	d_{max} [km]		
GSM 900	Voice	106.2	1.49	106.4	1.52	0.03	2.0
	Data	109.2	1.94	109.4	1.98	0.04	2.1
GSM 1800	Voice	103.2	0.69	103.4	0.70	0.01	1.4
	Data	106.2	0.90	106.4	0.91	0.01	1.1
UMTS	12.2 kbps	115.3	1.85	116.9	2.13	0.28	15.1
	144 kbps	111.1	1.27	112.7	1.47	0.20	15.7
	384 kbps	107.4	0.91	109.0	1.05	0.14	15.4

As previously, a significant dependence from considering lower fading margins is observed for UMTS, nevertheless, for GSM no significant dependence is found, therefore, the Rice distribution still is a reasonable approximation for evaluating the fading margins for GSM in LoS Suburban environments when building penetration is accounted for.

8.5. Urban Environments

Besides being intended for outdoor urban pico-cellular environments, HIPERLAN/2 and MBS working frequency bands are quiet different from the ones for GSM and UMTS, therefore, they will be addressed separately in further sections.

In Urban environments, a BS antenna height of 30 m is considered, the MT being positioned at 1.5 m height [Corr01]; buildings with 5 floors and separated by 20 m are assumed. As previously, COST 231-WI model is used for path loss evaluation, and a long-term fading standard deviation of 8 dB is considered; the short-term fading margins for NLoS are 6.3 and 4.1 dB for GSM and UMTS, respectively. The fading margin for GSM is the one corresponding to the Typical Urban model, while the one for UMTS was derived based on the same assumptions as previous, i.e., as the mean value obtained from the several models that can be assumed in Urban environments. Since there are no specific models for Urban environments, one assumes that the same models apply to both Suburban and Urban cases. From Table 8.8, it is observed that the cell range is below the one for the Suburban case. Globally, a decrease around 1.5, and 0.6 km is observed for GSM900 and, GSM1800 and UMTS, respectively.

Table 8.8 – Cell range in Urban environments, NLoS.

		Rayleigh		Proposed model		Δd_{max} [km]	Δd_r [%]
		$L_{p_{max}}$ [dB]	d_{max} [km]	$L_{p_{max}}$ [dB]	d_{max} [km]		
GSM 900	Voice	130.5	1.92	132.4	2.15	0.23	12.0
	Data	133.5	2.30	135.4	2.58	0.28	12.2
GSM 1800	Voice	127.5	0.78	129.4	0.87	0.09	11.5
	Data	130.5	0.93	132.4	1.05	0.12	12.9
UMTS	12.2 kbps	139.7	1.41	143.8	1.80	0.39	27.7
	144 kbps	135.5	1.09	139.6	1.40	0.31	28.4
	384 kbps	131.7	0.87	135.8	1.11	0.24	27.6

The effect of considering lower fading margins is relevant in both GSM and UMTS; as verified for the case of Suburban environments, the Rayleigh distribution is no longer appropriate for evaluating the fading margins for these systems.

As previously, COST 231-WI is used for estimating the path loss evaluation in street-canyon LoS situations. Since there are no specific channels models suited for either LoS Urban or Suburban environments, one considers the same assumptions as for the Suburban case, i.e., the same short-term fading margins. Therefore, one obtains the same cell ranges as for Suburban environments, since the path loss estimated from the COST 231-WI model for LoS street canyons only depends on the distance and working frequency, being independent on the environment properties, namely the BS antenna height.

Results for NLoS Urban environments, including building penetration, are presented in Table 8.9, the general assumptions being the same as for the Suburban case. It is observed that the cell range for GSM900 is around 0.6 to 0.7 km while for GSM1800 and UMTS it ranges from 0.16 to 0.32 km. As for the Suburban case, a reduced cell range is observed; also, the Rayleigh distribution is not appropriate for evaluating the fading margins in these environments, since an average cell radius increase of 12.4 and 31.0 % is obtained from considering the proposed fading margins.

Table 8.9 – Urban, outdoor-to-indoor building penetration, NLoS.

		Rayleigh		Proposed model		Δd_{max} [km]	Δd_r [%]
		$L_{p_{max}}$ [dB]	d_{max} [km]	$L_{p_{max}}$ [dB]	d_{max} [km]		
GSM 900	Voice	108.6	0.51	110.5	0.57	0.06	11.8
	Data	111.6	0.61	113.5	0.68	0.07	11.5
GSM 1800	Voice	99.6	0.14	101.5	0.16	0.02	14.3
	Data	102.6	0.17	104.5	0.19	0.02	11.8
UMTS	12.2 kbps	111.0	0.25	115.1	0.32	0.07	28.0
	144 kbps	106.8	0.19	110.9	0.25	0.06	31.6
	384 kbps	103.1	0.15	107.2	0.20	0.05	33.3

The results for LoS are the same as for the Suburban case, for the same reasons as previously explained. It should be remembered that the path loss evaluated from COST 231-WI for LoS environments depends only on the working frequency and the distance between the BS and the MT.

8.6. HIPERLAN Outdoor and Indoor Environments

Since HIPERLAN/2 was mainly designed for outdoor LoS and indoor LoS and NLoS environments, for illustration, one evaluates the cell range in Outdoor LoS urban street-canyon environments and Indoor NLoS ones.

Carrier frequencies of 5.6 (upper band central frequency) and 5.525 GHz (lower band central frequency) are considered for Outdoor and Indoor environments, respectively. The average path loss is evaluated as described in Chapter 3, and a long-term fading standard deviation of 5 dB is considered for both Outdoor and Indoor environments [Rapp96], corresponding to a long-term fading margin of 6.4 dB for 90 % coverage probability. The short-term fading margin is 2.0 and 3.0 dB for Outdoor and Indoor environments, respectively. These values are chosen as being representative of the typical possible values of fading margin for the proposed channel models. It should be remembered that typical values of fading margin ranges from 1.9 to 3.5 dB, the lower ones verified in Outdoor LoS environments. The results in Table 8.10 illustrate the cell range of HIPERLAN/2 for different data rates, 6 and 54 Mbps, which correspond to different receiver sensitivities. As one can observe, the cell radius ranges from 0.18 to 1.3 km and 12.9 to 40.8 m, for Outdoor and Indoor environments, respectively; the lower value corresponds to the higher data rate.

Table 8.10 – Cell range, HIPERLAN/2.

		Rayleigh/Rice		Proposed model		Δd_{max}	Δd_r
		$L_{p_{max}}$ [dB]	d_{max} [m]	$L_{p_{max}}$ [dB]	d_{max} [m]	[m]	[%]
HIPERLAN/2 (Outdoor)	6 Mbps	107.0	954.1	109.6	1 287.1	333.0	34.9
	54 Mbps	90.0	134.8	92.6	181.8	47.0	34.9
HIPERLAN/2 (Indoor)	6 Mbps	96.4	28.7	101.6	40.8	12.1	42.2
	54 Mbps	79.4	9.1	84.6	12.9	3.8	41.6

Compared to the case when the short-term fading margins are obtained from Rayleigh or Rice distributions, the cell range increases by 47.0 to 333.0 m and 3.8 to 12.1 m in Outdoor and Indoor environments, respectively, corresponding to an average cell range variation of 34.9 and 41.9 %, respectively. It should be noted that this increase, when extrapolated to the number of penetrated floors (for the case of indoors), represents an increased cell coverage among neighbouring floors. When Rayleigh or Rice distributions are considered lower cell ranges are obtained, and as a consequence, a large number of BSs is estimated, increasing the interference among adjacent floors.

For illustration, one presents results for the case of Outdoor environments, when building penetration is accounted for; general assumptions being the same as previously described for the case of Urban and Suburban environments. Results for a coverage probability of 90 % are in Table 8.11; one should remember that Rice applies to the path between the BS and the building where the MT is located. As one can observe, indoor coverage by outdoor BSs is not easy to achieve since the estimated cell range is 2.3 to 16.6 m.

Table 8.11 – Cell range, HIPERLAN/2, building penetration, 90 % coverage probability.

		Rice, K = 6 dB		Proposed model		Δd_{max}	Δd_r
		$L_{p_{max}}$ [dB]	d_{max} [m]	$L_{p_{max}}$ [dB]	d_{max} [m]	[m]	[%]
HIPERLAN/2 (Outdoor)	6 Mbps	69.2	12.3	71.8	16.6	4.3	35.0
	54 Mbps	52.2	1.7	54.8	2.3	0.6	35.3

Nevertheless, relaxing the coverage probability from 90 to 60 %, Table 8.12, a cell range of 185.7 and 26.2 m is obtained for the 6 and 54 Mbps cases, respectively; hence, one can assume that a reasonable coverage can be achieved if the BS is in the near vicinity of the building. Moreover, one should remember that the values for building penetration being considered account for the influence of both outer and inner walls, thus, it can be significantly reduced when only the additional loss from the outer wall is considered, extending the coverage range in these conditions. Nevertheless, one should be aware that this strongly depends on the possible MT positioning within the building, for the required coverage probability.

Table 8.12 – Cell range HIPERLAN/2, building penetration, 60 % coverage probability.

		Rice, K = 6 dB		Proposed model		Δd_{max} [m]	Δd_r [%]
		$L_{p_{max}}$ [dB]	d_{max} [m]	$L_{p_{max}}$ [dB]	d_{max} [m]		
HIPERLAN/2 (Outdoor)	6 Mbps	92.4	178.4	92.8	185.7	7.3	4.1
	54 Mbps	75.4	25.2	75.8	26.2	1.0	4.0

Globally, the Rice distribution is not appropriate for evaluating the fading margins in these situations (a cell range reduction of 35.2 % is obtained for 90 % coverage probability), nevertheless, for lower coverage probabilities, e.g., 60 %, the error introduced from considering this distribution is not significant (a cell range reduction of 4.1 % is observed).

8.7. MBS Environments

Since MBS is mainly intended for outdoor and indoor LoS pico-cellular environments, for illustration, one presents some results for the case of an urban street environment. Two different situations are assumed, absence of rain, and a rainfall rate of 50 mm/h that corresponds to a rainfall rate that is seldom exceeded in non-tropical climates.

Carrier frequencies of 43 and 65.5 GHz are considered, corresponding to the centre frequencies foreseen for the UL of each band, a system bandwidth of 50 MHz being taken. A long-term fading standard deviation of 3 dB is assumed from experimental measurements and simulation [Vasc98], corresponding to a long-term fading margin of 3.8 dB for 90 % coverage probability. As previously referred, the short-term fading margin is obtained from considering 16 ns as an average value for the *rms* delay spread in urban street environments [MLAR94]. It should be stressed that these values were obtained for the 60 GHz band; due to the lack of available data for the 40 GHz one, the same values are assumed. For the given parameters, a maximum path loss of 118 dB is obtained (additional data for link budget evaluation was already presented in Chapter 3).

The cell range is evaluated from using the propagation model for the millimetre waveband presented in Chapter 3, parameters C and ξ, extracted from [Bedi98], are presented in Table 8.13.

Table 8.13 – Path loss model parameters.

	40 GHz band		60 GHz band	
	$\gamma_R = 0$ mm/h	$\gamma_R = 50$ mm/h	$\gamma_R = 0$ mm/h	$\gamma_R = 50$ mm/h
C [dB]	92	95	93	99
ξ	2.0	2.3	2.0	2.4

The obtained cell ranges are presented in Table 8.14; as expected, the influence of rain is more significant for the 60 GHz band. As one can observe, an improvement of 30.3 to 38.0 m and 14.9 to 22.2 m in cell range is obtained from considering the proposed fading margins. If a larger system bandwidth is considered, e.g., 100 MHz, slightly larger cell ranges are obtained; an increase of 10 and 12.7 m is verified for the 40 GHz band, the larger value obtained without the influence of rain; these values reduce to 4.9 and 7.4 for the 60 GHz band.

Table 8.14 – Cell range in urban street environments, MBS.

		d_{max} [m]		Δd_{max} [m]	Δd_r [%]
		Rice, K = 6 dB	**Proposed model**		
40 GHz band	$\gamma_R = 0$ mm/h	175.5	213.5	38.0	21.7
	$\gamma_R = 50$ mm/h	163.1	193.4	30.3	18.6
60 GHz band	$\gamma_R = 0$ mm/h	102.7	124.9	22.2	21.6
	$\gamma_R = 50$ mm/h	84.4	99.3	14.9	17.7

From the results, again one concludes that Rice distribution is not appropriate for evaluating the fading margins for MBS, since an average cell radius increase of 19.9 % is obtained for both bands, hence, the proposed fading margins should be used. Building penetration is not addressed, since MBS is mainly intended for LoS pico-cellular environments.

8.8. Coverage Analysis

The increased cell range, estimated from considering that the proposed fading margins for different systems working in different environments, can be extrapolated to an effective cell number reduction, compared to the case when considering Rayleigh or Rice distributions, while allowing to achieve the desired coverage probability, for the desired link quality. Assuming a uniform regular cellular structure, the area of each cell is given by

$$A_c = g \cdot d_{max}^2 \tag{8.1}$$

where g is a real number (shape factor) that depends on the cell geometry, e.g., $g = 3\sqrt{3}/2$ for hexagonal cells. The number of cells needed for covering a given area, A_T, is approximated by

$$N_c = \frac{A_T}{A_c} \tag{8.2}$$

When the cell range, i.e., the cell radius, increases by Δd_r, as previously defined, the value of the relative reduction in the number of cells, ΔN_{cr}^{a}, needed to achieve the same coverage, for the given coverage probability, can be obtained from

$$\Delta N_{cr}^{a} = \frac{N_{cRR} - N_{cWB}}{N_{cRR}} = \left(1 - \frac{1}{(1+\Delta d_r)^2}\right) \tag{8.3}$$

with N_{cRR} and N_{cWB} representing the number of cells obtained from considering Rayleigh or Rice distributions and the ones as proposed in this chapter, respectively.

In the case of HIPERLAN/2 and MBS, working in outdoor environments, a uniform regular structure such as the one for GSM is not usually used, instead linear geometries being assumed, e.g., the BSs are aligned along a street. In this case, the relative cell number reduction, ΔN_{cr}^{l}, can be evaluated as

$$\Delta N_{cr}^{l} = \frac{\Delta d_r}{1+\Delta d_r} \tag{8.4}$$

In the following, building penetration is not considered. The results in Figure 8.4 and Figure 8.5, illustrate the cell radius increase, and cell number reduction, between considering that short-term fading margins are obtained from the Rayleigh distribution or from the proposed approach, i.e., accounting for the system bandwidth and environment properties.

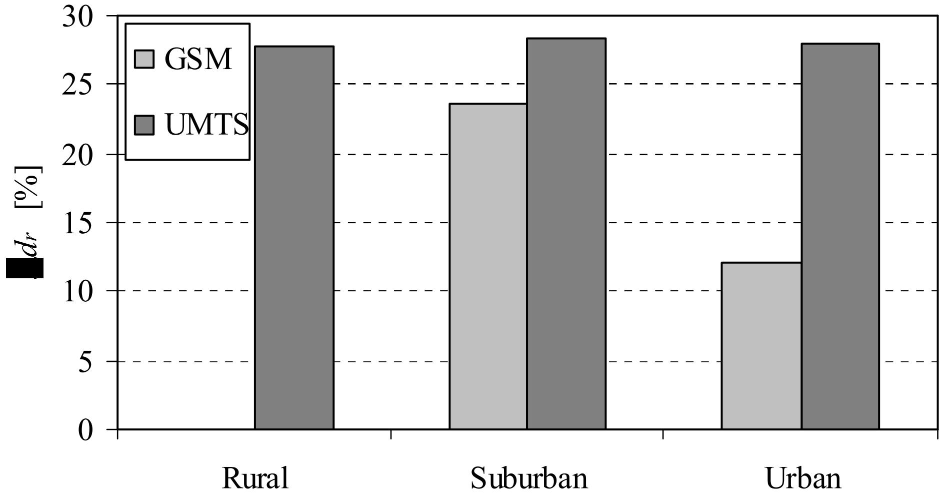

Figure 8.4 – Coverage range variation, NLoS.

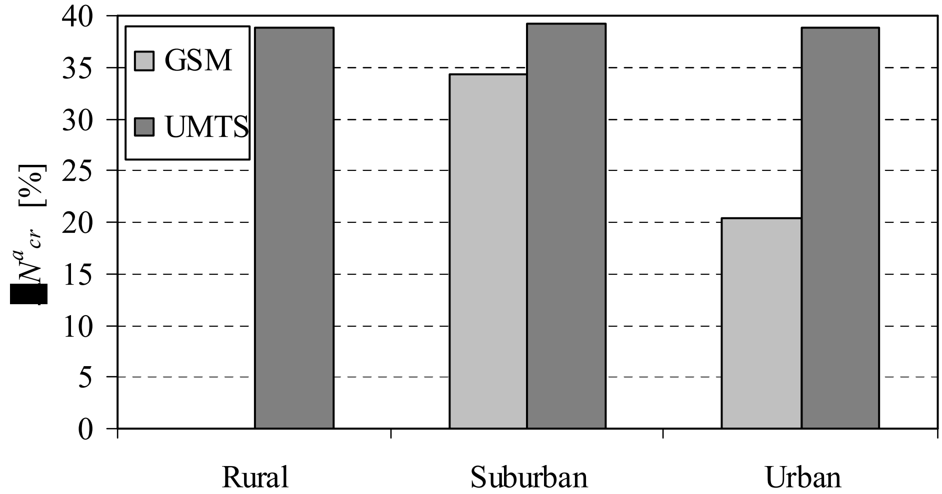

Figure 8.5 – BS number reduction, NLoS.

The values of Δd_r correspond to the mean value for the different services being considered for each system, i.e., voice and data for GSM900 and GSM1800 and voice, non-real-time data and real-time data for UMTS. It should be remembered that for the case of GSM, the results from considering only GSM900, GSM1800, or both, are similar, which is not surprising, since the cell range difference depends mainly on the system bandwidth rather than on the working frequency; therefore, from now on, one refers to GSM900 and GSM1800 purely as GSM.

Globally, one observes that the cell range is always above the one obtained from considering the Rayleigh distribution; exception made for the case of GSM in Rural environments. For the given coverage probability, the number of cells needed in order to obtain the desired link quality within a given coverage area can be reduced by 20.6 and

34.5 % for GSM in Urban and Suburban environments, respectively; for UMTS a reduction between 38.8 and 39.2 % can be achieved.

As previous explained, the results for Suburban and Urban LoS environments are similar, therefore, one refers to both as Suburban/Urban. From Figure 8.6, a lower cell radius increase is observed, hence, a lower cell range reduction is verified, Figure 8.7. For GSM no significant cell number reduction is found; for UMTS a reduction of 16.3 and 24.6 % is observed in Rural and Suburban/Urban environments, respectively. From the results, one concludes that the Rice distribution still is a reasonable approximation for evaluating the short-term fading margins for GSM working in LoS environments; nevertheless, this is no longer valid for UMTS.

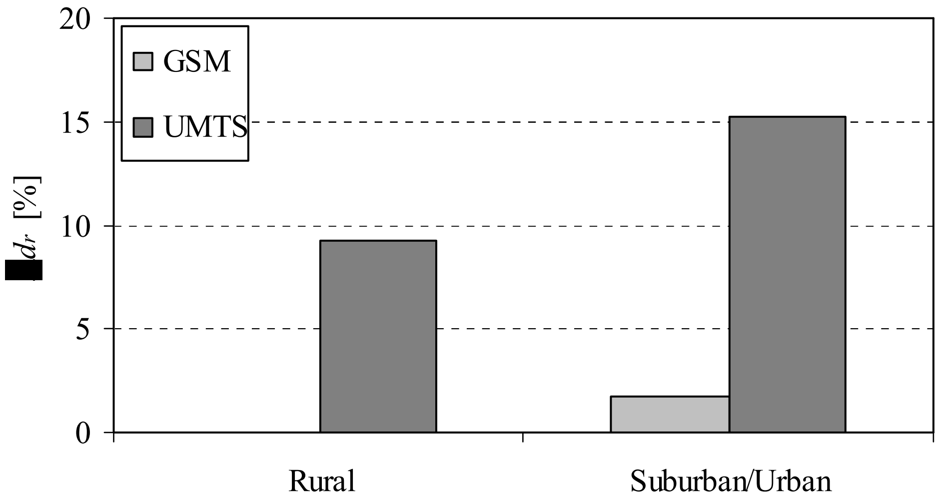

Figure 8.6 – Coverage range variation, LoS, K = 6 dB.

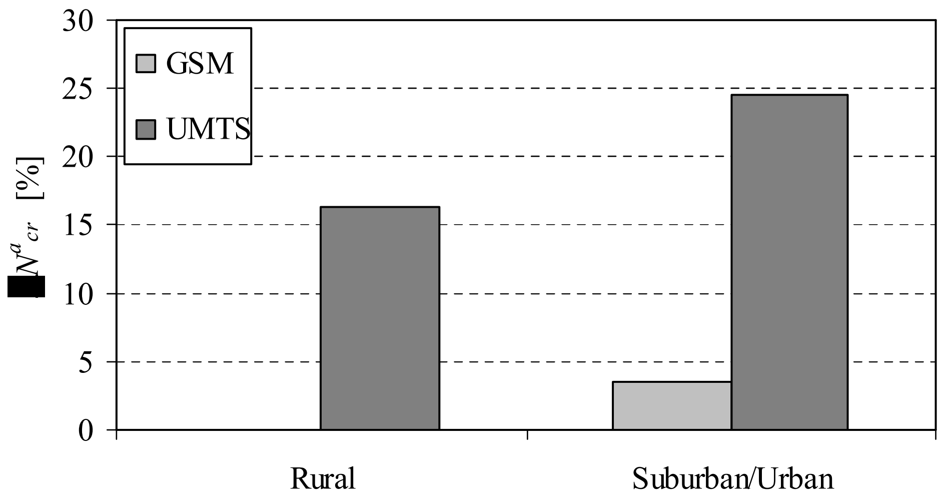

Figure 8.7 – BS number reduction, LoS, K = 6 dB.

For HIPERLAN/2 an even worst situation is verified, i.e., the Rice distribution usually gives short-term fading margins well above the ones obtained from considering the influence of system bandwidth and environment characteristics, yielding a large cell number reduction compared to the Rice case. For a coverage probability of 90 %, a value of Δd_r = 34.9 % is obtained for Outdoor urban street-canyon environments, corresponding to a cell number reduction of 25.7 %, obtained from considering a linear geometry. Indoor environments are not addressed here, since a regular structure such as the ones usually found in Outdoor environments is not found; in this type of environments, the BS positioning is conditioned by the building structure, namely the type and size of partitions, as well as the type of materials being used.

In the case of MBS, a linear geometry with the BSs aligned along a street is also assumed. The results on the cell number reduction are illustrated in Figure 8.8.

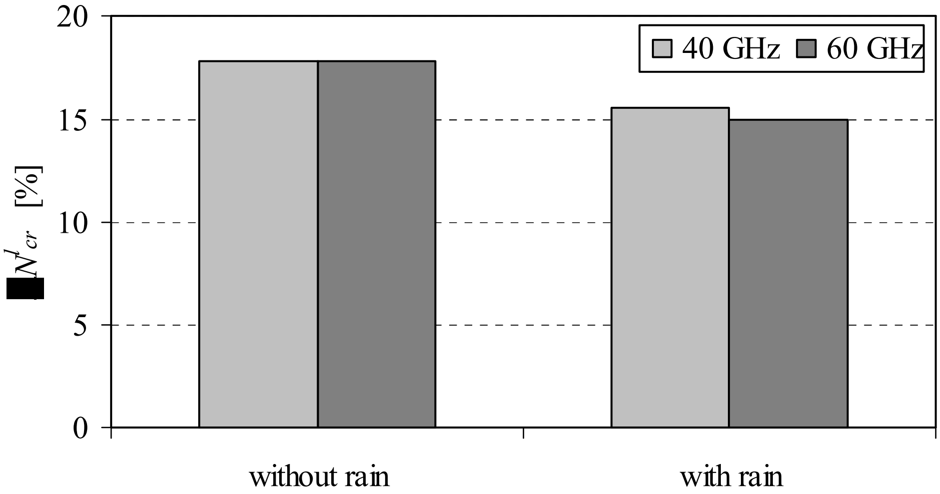

Figure 8.8 – BS number reduction, MBS, LoS, K = 6 dB.

As one can observe, a cell number reduction of 15 to 17.8 % can be achieved by using the proposed fading margins, the higher values being obtained without the influence of rain. Moreover, besides the difference in the maximum cell range for the 40 and 60 GHz bands (see Table 8.14), there is no significant difference in cell number reduction for both bands, which is not surprising, since this value is mainly dependent on the system bandwidth rather than on the working frequency, as already explained for the case of GSM.

Globally, from the point of view of cell number reduction, one can say that the Rayleigh distribution is a good approximation for evaluating the fading margins for GSM in Rural NLoS environments; for the case of Suburban and Urban ones, Rayleigh is no longer appropriate, and the proposed fading margins should be applied. For UMTS, HIPERLAN/2 and MBS, the proposed fading margins should be applied independently of which environment is considered.

Under LoS, the Rice distribution still is a reasonable approximation for evaluating the fading margins for GSM in all of the environments being considered. For UMTS, HIPERLAN/2 and MBS, this is no longer valid, and the proposed margins should be applied.

8.9. Conclusions

Link budget analysis and cell range estimation is addressed from considering that the short-term fading margins are evaluated from Rayleigh or Rice distributions, as usually found in literature, or by considering the proposed approach for fading depth evaluation, thus, accounting for the influence of system bandwidth and environment properties.

For the case of GSM, besides the exceptions for Rural environments, and LoS Suburban and Urban ones, for which Rayleigh or Rice distributions still are appropriate for evaluating the fading margin, a cell number reduction above 20 % is obtained when considering the proposed fading margins. Concerning UMTS, under NLoS, a cell number reduction from 38.8 to 39.2 % can be achieved; under LoS, this value decreases to 16.3 to 24.6 %. In the case of HIPERLAN/2 a reduction of 25.9 % is observed in Outdoor environments. For MBS a cell number reduction around 15.0 to 17.8 % is obtained, being almost independent of the frequency band being considered.

In this way, one concludes that from the point of view of short-term fading depth evaluation, Rayleigh and Rice distributions are not usually appropriate. When considering these distributions, a smaller cell range is obtained and, as a consequence, higher intra-cell interference, and lower link quality. By considering more appropriate fading margins, a significant reduction in the number of cells can be achieved, while allowing a better radio network planning and a better link quality.

As a final conclusion, one can say that the proposed approach, allowing to estimate more accurate short-term fading margins, can be used for radio network optimisation purposes of existing systems, namely GSM, and a better planning of future ones, being or expected to be deployed, e.g., UMTS, HIPERLAN/2 and MBS.

Nevertheless, it should be remembered that in many situations, namely in GSM, short-term fading margins are not usually accounted for, thus, leading to an even higher cell range (when compared to the one obtained from considering Rayleigh or Rice distributions) or, instead, a global fading margin which includes both long- and short-term fading effects is somehow considered. Thus, the cell number reduction figures for the given coverage probability, presented herein, can be significantly higher than the ones that can be achieved in a real existing system optimisation procedure.

Chapter 9

Conclusions and Future Research

9.1. Conclusions

Channel characterisation and modelling is one of the most important steps for the design implementation and optimisation of mobile communication systems. Accurate channel models are needed in order to adequately reproduce the real working conditions of a given system. Work has been done concerning narrowband systems, since most of existing systems are narrowband ones, nevertheless, with the emergence of wideband systems an appropriate characterisation of the wideband propagation channel becomes of great interest. Moreover, with the emergence of new techniques for exploiting the directional properties of the propagation channel, both temporal and spatial characteristics of the propagation channel should be carefully studied, allowing to properly assess appropriate channel models, intended for system design, planning, implementation and optimisation purposes.

Among several steps involved in a radio network planning procedure, link budget evaluation and cell range estimation is one of the first and most important ones in the overall planning process, since an accurate link budget evaluation is needed to achieve the required coverage probability, capacity and quality of service. Although a link budget evaluation is usually a rough approximation of the real network working conditions, it is desirable to use a set of system and environment parameters, as close as possible to the reality, hence, reducing the effort needed for future optimisation procedures. Since in a multipath environment the received signal fades, it is necessary to provide additional power (fading margin) in order to achieve the desired link quality, therefore, when performing link budget calculations, fading margins should always be accounted for. Accurate short- and long-term fading margins should be considered in order to achieve the desired link capacity and quality of service for the desired coverage probability. Long-term fading margins are usually evaluated considering that these effects can be reasonable modelled as being log-normal distributed, which is in good agreement with results from measurements. Short-term fading margins are usually obtained from Rayleigh or Rice distributions; the main drawback is that this approach is valid only for narrowband systems, thus, when one considers wideband systems, the fading depth (hence, the fading margin that should be accounted for) is usually smaller than the one obtained from these distributions. Overestimating fading margins, by considering those distributions, leads to shorter cells, higher transmitting powers, and higher interference; these effects are not desirable, and they can be overcome by taking more accurate values for the fading margins. This was the main motivation for the work being presented in this thesis.

Two different and independent approaches for the study of wideband signal transmission in LoS and NLoS situations are proposed, contributing to filling in the gap of short-term fading characterisation in wideband systems, while allowing to evaluate the fading margins to be considered for a given system working in a given environment, as a function of the system bandwidth, and either geometrical environment properties or the PDP of the propagation channel. With the aim of providing an insight into the influence of using directional antennas, which allows exploiting the directional properties of the propagation channel, a framework for evaluating the fading depth for different systems when directional antennas are used is also presented.

It should be noted that the aim of this work is not to provide a complete fading characterisation, but rather a framework for evaluating the short-term fading margins in wideband mobile communication systems.

Chapter 2 addresses channel characterisation and modelling, path loss and fading effects are characterised, and general considerations about propagation are drawn. Furthermore, a survey of existing channels models is done; the main emphasis is given to stochastic parametric and geometrically-based directional channel models, since they are commonly used for simulating the propagation channel, while accounting for the influence of spatial channel properties. State-of-art channel models for simulating MIMO channels are also presented.

In Chapter 3, GSM, UMTS, HIPERLAN and MBS are briefly characterised; the focus is on working frequencies, transmitted power and receiver sensitivities, since these parameters are the most relevant for evaluating the link budget. Furthermore, general considerations about link budget evaluation are drawn, and some specific parameters for this purpose are presented. Well-known path loss models are also presented, fulfilling the requirements for properly evaluating the maximum cell range in different environments.

In Chapter 4, an environment-geometry based approach for deriving the short-term fading depth as a function of the Rice factor, and the product between the system bandwidth and the maximum difference in propagation path length, from a simple analytical approximation, is presented. The proposed mathematical equation is derived through fitting of simulated data from a model in the literature. Some application examples are presented, pico-, micro- and macro-cellular environments being considered. As expected, in the case of the micro-cellular street-type environment, the difference in fading depth between different systems depends on the distance between the BS and the MT, and on the street width. The difference between UMTS and GSM, for a value of K = 6 dB, is about 0.7 to 5.5 dB, for a street width ranging from 15 to 60 m; HIPERLAN/2, MBS1 and MBS2, experience lower fading depths. Within the pico-cellular environment, the fading depth experienced by UMTS and GSM is similar, and the dependence on room width is not significant. HIPERLAN/2, MBS1 and MBS2 experience fading depths that are several dB below the ones for GSM, and significant dependence on room width is observed, with the larger values of fading depth being observed for smaller rooms. In the macro-cellular environment, the fading depth experienced by UMTS is well below the one for GSM. Globally, it can be stated that the fading depth in UMTS is about 6 to 11 dB lower than the one observed for GSM, for a scattering scenario radius ranging from 800 to 100 m respectively.

In general, GSM behaves as a narrowband system, exception being done for the case of the considered macro-cellular environments. UMTS, HIPERLAN/2 and MBS, usually behaves as wideband systems, therefore, experiencing lower fading depths; nevertheless, depending on the environment geometry, UMTS can behave almost as a narrowband system in micro- and pico-cellular environments. Therefore, when evaluating the fading depth, the influence of system bandwidth and environment characteristics should always be taken into account, otherwise, the obtained fading margins, can be overestimated, therefore, increasing network deployment costs and lowering the network quality.

A time-domain based approach for wideband fading depth evaluation is proposed in Chapter 5. New expressions are derived for the PDF and the CDF of the received power, which apply to both LoS and NLoS cases. The short-term fading depth is evaluated from the CDF of the received power, and represented as a function of the Rice factor, and the product between the system bandwidth and the *rms* delay spread of the propagation channel. The influence of PDP parameters on the fading depth results for theoretical continuous and discrete PDPs is presented and discussed. Moreover, an analytical approximation for the fading depth dependence on the Rice factor and the product between the system bandwidth and the *rms* delay spread of the propagation channel, similar to the one derived in Chapter 4, is also proposed, therefore, allowing to reduce the computational effort needed for evaluating the fading depth in different environments.

In Chapter 6, results on the fading depth observed by GSM, UMTS and HIPERLAN/2 working in different environments, represented by their PDPs (as proposed by ETSI and 3GPP), are presented and discussed; for MBS, an exponential PDP is considered, typical values of *rms* delay spread being obtained from measurements in different environments. There are some similarities regarding the fading depth observed in different environments: for values of Δw_t below 0.02 Hz·s, the observed fading depths are similar and independent of the PDP of the propagation channel, corresponding to a situation where the system bandwidth is below the coherence bandwidth of the propagation channel, i.e., signals are in a frequency flat fading environment; for large values of Δw_t, the fading depth depends on the type of the PDP, namely the number, magnitude and delay of the arriving waves. The fading depth obtained for the channel models for GSM is between 9.2 and 18.4 dB, while for the ones for UMTS fading depths range from less than 4.3 to 12.5 dB, and HIPERLAN/2 experiences fading depths between 3.6 and 6.7 dB. For MBS, in the considered environments, whose characteristics were extracted from measurements, and for the given system bandwidths, the observed fading depth is usually between 2.5 and 9.7 dB (a worst case of 10.6 dB is observed in City Streets under NLoS). Globally, GSM behaves as narrow- or wideband system, depending on the environment being considered; UMTS, HIPERLAN/2 and MBS, behave always as wideband ones. One can state that, since the observed fading depth depends on the system bandwidth and environment specific features, different fading margins should be considered according to different system bandwidths and working environments. Moreover, the fading margins for UMTS, HIPERLAN/2 and MBS can be significantly reduced, when compared to the ones for GSM, while achieving the desired link quality, and enabling a more efficient and less costly radio network planning.

By using a simple relationship between the maximum difference in propagation path length among different arriving components and the *rms* delay spread of the propagation channel, fading depth results obtained from the proposed time-domain approach for wideband fading characterisation are compared with the ones for the environment geometry-based analytical one, establishing a bridge between the two different and independent approaches themselves and the models in which they are based. Since a good agreement is verified (the difference between both approaches is usually below 2 dB), one concludes that the proposed relationship, being simple, is effective for evaluating the fading depth in different environments and for different system bandwidths, allowing to use different approaches for fading depth evaluation, starting either from physical and geometrical environment properties, or the PDP of the propagation channel.

An approach for short-term fading depth evaluation using wideband directional channels is presented in Chapter 7. For each system, working in a given environment, the observed fading depth depends on the type of antennas being used. This influence is modelled through the variation of the Rice factor and the maximum difference in propagation path length, relative to the case of using omnidirectional antennas. Results on the fading depth observed with directional antennas are presented and discussed. Expressions for the Rice factor and the maximum difference in propagation path length variation as a function of the half-power antenna beamwidth are derived. Uniform and Gaussian distributions are used for modelling AoAs.

Since one assumes the use of typical GBSB channel models, in LoS micro-cellular environments no dependence of the maximum difference in propagation path length dependence on the half-power beamwidth is found, thus, the fading depth observed for any antenna beamwidth depends only on the Rice factor variation. It should be remembered that in this type of environments, similar results were obtained when considering a directional antenna at either the BS or the MT. For the considered micro-cellular environments, a fading depth variation dependence on the street width and system bandwidth is observed, this dependence increasing with increasing system bandwidths and for wider streets. When considering a Gaussian distribution of AoAs, it is observed that the fading depth reduction is usually below 3 dB for $\alpha_{3dB} > 2\sigma_s$. Globally, for the same value of α_{3dB}, the higher the value of σ_s the higher the fading depth reduction.

In LoS macro- and pico-cellular environments, the observed fading depth depends not only on the Rice factor variation but also on the maximum difference in propagation path length, which depends on the antenna beamwidth as well. An increase or a reduction in fading depth can be observed (compared to the case when using omnidirectional antennas), depending on the system and environment characteristics; it should be remembered that for the case of the micro-cellular environment, there is always a decrease in fading depth.

Under NLoS, the changes in fading depth result only from the variation of the maximum difference in propagation path length; since a LoS component does not exist, it does not make sense to refer to the Rice factor. There is always fading depth degradation, i.e., an increase in fading depth, the maximum possible degradation increasing for increasing system bandwidths.

Using the channel models for GSM, the fading depth observed in LoS Rural Area environment is evaluated, being observed that a significant reduction in fading depth is obtained; under NLoS a different behaviour is observed, fading depth degradation occurring for any of the considered antenna beamwidths. In the case of UMTS environments, a fading depth reduction is observed when using directional antennas, however, degradation is observed in Vehicular-A, Typical Urban and Hilly Terrain environments; under NLoS, fading depth degradation is usually observed, exceptions being Pedestrian environments. In HIPERLAN/2 environments, the fading depth observed in different LoS environments is usually below 3.6 dB, nevertheless, a reduction in fading depth still is achieved. If one considers the NLoS situation, a different behaviour is observed, i.e., as the antenna beamwidth decreases larger fading depths are obtained; this degradation can be as large as 11.1 dB for Model A and an antenna beamwidth of 10^{o}. In the case of MBS, a significant reduction is obtained in City Streets, Small Rooms and Corridors; the best situation of 5.4 dB reduction in fading depth is observed for an antenna beamwidth of 10^{o} in City Street environments, while in Small Rooms and Corridors this reduction is below 4.3 and 4.7 dB, respectively; no significant improvement is verified in City Squares. Under NLoS, fading depth degradation is usually observed, however, no degradation is verified in City Streets and Corridors.

In Chapter 8, link budget analysis and cell range estimation is addressed, considering that the short-term fading margins are evaluated from Rayleigh or Rice distributions, or by considering the proposed approaches. Besides an exception for the case of GSM in Rural environments, and LoS Suburban and Urban ones, for which Rice or Rayleigh distributions still are appropriate, a reduction in the number of cells above 20 %, is obtained by considering the proposed fading margins. For UMTS, under NLoS, a cell number reduction of roughly 39 % is observed; under LoS, this value decreases to 16 to 25 %. In the case of HIPERLAN/2 a reduction of roughly 26 % is observed in Outdoor urban street-canyon environments. In the case of MBS these values decrease to roughly 15 to 18 %, being almost independent of the frequency band being considered.

The approaches proposed in this thesis, allowing to estimate more accurate short-term fading margins, can be useful for radio network planning and optimisation purposes of existing and future systems, e.g., GSM, UMTS, HIPERLAN/2 and MBS. Nevertheless, it should be remembered that in many situations, namely in GSM, short-term fading margins are not usually accounted for, leading to an even higher cell range (when compared to the one obtained from considering Rayleigh or Rice distributions) or, instead, a global fading margin which includes both long- and short-term fading effects is somehow considered. Thus, the cell number reduction figures presented herein, can be significantly higher than the ones that can be achieved in a real existing system optimisation procedure.

As a final conclusion one can state that, as expected, Rayleigh and Rice distributions are appropriate for evaluating the fading margins for narrowband systems, e.g., GSM in some environments; nevertheless, even GSM can behave as a wideband system, depending on the environment characteristics being considered, hence, lower fading margins should be applied. For UMTS, HIPERLAN/2 and MBS, the situation is even worst, i.e., fading margins are usually well below the ones for the narrowband case, therefore, the influence of system bandwidth and environment characteristics should always be taken into account, thus, the proposed approaches should be applied.

9.2. Suggestions for Future Research

The suggestions for future research can be divided into two distinct groups, the one concerning the extension of the work presented in this thesis, and the one that should be carried out simultaneously in order to achieve a complete understanding of the fading behaviour in wideband mobile communication systems.

For the former, further work should be carried out in order to investigate what is the impact of the presented results in different systems, based on different technologies, e.g., OFDM and CDMA, concerning capacity and link quality. Furthermore, the influence of using antenna diversity techniques at either the BS the MT, or both, should be studied. Also, it should be investigated how the presented results can influence the implementation of MIMO, since in most of existing examples in the literature, the influence of the system bandwidth and environment properties is not usually properly accounted for, i.e., Rayleigh and Rice distributions still are preferred for modelling short-term fading effects. Since, the capacity of a MIMO channel can be derived as the sum of the capacities of the individual sub-channels, each sub-channel should be properly characterised. Also, the achieved increased capacity, depending on the correlation among distinct channels, is related to the environment characteristics as well as the system bandwidth, therefore, the relation between the correlation properties of the fading channel and the observed fading depth should also be investigated, therefore, allowing to properly evaluate capacity and link quality in different environments. Moreover, since the theoretical increased capacity achieved by MIMO is usually based on the application of equalisation, singular value decomposition and space-time coding techniques, among others, being very sensitive to channels estimation errors, it should be investigated how the performance of these techniques depends on the short-term fading effects of the propagation channel.

Since the results presented in this thesis are not intended to provide a complete description on the influence of using directional antennas, at the BS, the MT, or both, but rather giving an insight into this phenomenon, further study should be focused on: (i) the use of different antenna types and parameters, e.g., derived from beamforming techniques; (ii) a complete characterisation of the dependence of the Rice factor variation and the maximum difference in propagation path length as a function of the angular standard deviation of the AoAs, different distributions for the AoA being considered; (iii) further assessment of the obtained results. It should be remembered that the approach being proposed is based on the assumption that the working environments can be reasonably described by using typical scattering channel models that account for spatial properties of the propagation channel; nevertheless, further assessment from measurements should be carried out.

For the latter, work should be carried out in order to investigate the dependence of different fading parameters, e.g., level crossing rate and average fade duration, on the system bandwidth and environment properties, allowing to completely characterise the fading behaviour of the wideband propagation channel. Moreover, the effect of both long- and short-terms fading should be investigated, allowing to properly evaluating the total fading margin that should be considered for link budget evaluation purposes. It should be remembered that one assumes that long-term fading effects are reasonable modelled from a log-normal distribution, which standard deviation depends basically on the working frequency and environment characteristics, i.e., no dependence on system bandwidth is considered.

References

[3GPP02a] 3GPP, *Deployment Aspects*, TSG RAN Technical Report TR 25.943 v4.2.0, Sophia Antipolis, France, June 2002 (http://www.3gpp.org).

[3GPP03a] 3GPP, *BS Radio Transmission and Reception (FDD) (Release 6)*, TSG RAN Technical Specification TS 25.104 v6.1.0, Sophia Antipolis, France, Mar. 2003 (http://www.3gpp.org).

[3GPP03b] 3GPP, *BS Radio Transmission and Reception (TDD) (Release 5)*, TSG RAN Technical Specification TS 25.105 v5.4.0, Sophia Antipolis, France, Mar. 2003 (http://www.3gpp.org).

[3GPP03c] 3GPP, *UE Radio Transmission and Reception (FDD) (Release 6)*, TSG RAN Technical Specification TS 25.101 v6.0.0, Sophia Antipolis, France, Mar. 2003 (http://www.3gpp.org).

[3GPP03d] 3GPP, *Spatial Channel Model for Multiple-Input-Multiple-Output Simulations (Release 6)*, TSG RAN Technical Report TR 25.943 v1.0.0, Sophia Antipolis, France, Mar. 2003 (http://www.3gpp.org).

[3GPP03e] 3GPP, *UE Radio Transmission and Reception (TDD) (Release 5)*, TSG RAN Technical Specification TS 25.102 v5.5.0, Sophia Antipolis, France, June 2003 (http://www.3gpp.org).

[Aszt96] Asztély,D., *On Antenna Arrays in Mobile Communication Systems: Fast Fading and GSM Base Station Receiver Algorithms*, Master Thesis, Royal Institute of Technology, Stockholm, Sweden, Mar. 1996.

[Bala82] Balanis,C.A., *Antenna Theory – Analysis and Design,* John Wiley, Chichester, UK, 1982.

[Bedi98] Bedini,C., *Cellular Planning in Urban Regular Structure for Millimetre Wave Mobile Systems*, Graduation Report, Instituto Superior Técnico, Lisbon, Portugal, Sep. 1998.

[Bell63] Bello,P.A., "Characterization of Ramdomly Time-Variant Linear Channels", *IEEE Transactions on Communication Systems*, Vol. 11, No. 12, Dec. 1963, pp. 360-393.

[Bisd01] Bisdikian,C., "An Overview of the Bluetooth Wireless Technology", *IEEE Communications Magazine*, Vol. 39, No. 12, Dec. 2001, pp. 86-94.

[Blue01] http://www.bluetooth.com/developer/specifications/core.asp, Aug. 2003.

[CaCo01] Cardoso,F.D. and Correia,L.M., "An Analytical Approach to Fading Depth Dependence on Bandwidth for Mobile Communication Systems", in *Proc. of WPMC'01 – The 4th International Symposium on Wireless Personal Multimedia Communications*", Aalborg, Denmark, Sep. 2001.

[CaCo02a] Cardoso,F.D. and Correia,L.M., "A Time-domain Technique for Fading Depth Characterisation in Wideband Mobile Communication Systems", in *Proc. of XXVIIth URSI General Assembly*, Maastricht, The Netherlands, Aug. 2002.

[CaCo02b] Cardoso,F.D. and Correia,L.M., "Fading Depth Evaluation in Mobile Communications – from GSM to Future Mobile Broadband Systems", in *Proc. of PIMRC 2002 – 13th IEEE International Symposium on Personal, Indoor, and Mobile Radio Communications*, Lisbon, Portugal, Sep. 2002.

[CaCo03a] Cardoso,F.D. and Correia,L.M., "A Comparison between Different Approaches for Fading Evaluation in Wideband Mobile Communications", in *Proc. of VTC'03 Spring - 57th IEEE Semiannual Vehicular Technology Conference*, Jeju, Korea, Apr. 2003.

[CaCo03b] Cardoso,F.D. and Correia,L.M., "Fading Depth Dependence on System Bandwidth in Mobile Communications – An Analytical Approximation", *IEEE Transactions on Vehicular Technology*, Vol. 52, No. 3, May 2003, pp. 587-594.

[CaCo03c] Cardoso,F.D. and Correia,L.M., "Short-term Fading Evaluation in Wideband Mobile Communication Systems", submitted to *IEEE Transactions on Wireless Communications*, May 2003.

[CaCo03d] Cardoso,F.D. and Correia,L.M., "On the Equivalence between Time-domain and Environment-geometry Based Approaches for Fading Evaluation in Wideband Mobile Communications", in *Proc. of ConfTele 2003 – 4th Conference on Telecommunications*, Aveiro, Portugal, June 2003.

[CaCo04] Cardoso,F.D. and Correia,L.M., "Short-term Fading Depth Dependence on Antenna Characteristics in Wideband mobile Communications", accepted for publication in *Proc. of PIMRC 2004 – 15th IEEE International Symposium on Personal, Indoor, and Mobile Radio Communications*, Barcelona, Spain, Sep. 2004.

[CaTC02] Cardoso,F.D., Taccori,S. and Correia,L.M., *Initial Propagation models*, IST-FLOWS Project, Deliverable D4, IST Office, Brussels, Belgium, May 2002.

[CCKL02] Cardoso,F.D., Correia,L.M., Kürner,T., Lourenço,P., Gabriela,M. and Matic,D., *Evaluation of Propagation Models*, IST-MOMENTUM Project, Deliverable D4.1, IST Office, Brussels, Belgium, Feb. 2002.

[CoFr94] Correia,L.M. and Francês,P.O., "A Propagation Model for the Average Received Power in an Outdoor Environment in the Millimetrewave band", in *Proc. of VTC'94 – 44th IEEE Vehicular Technology Conference*, Stockholm, Sweden, June 1994.

[CoFr95] Correia,L.M. and Francês,P.O., "Transmission and Isolation of Signals in Buildings at 60 GHz", in *Proc. of PIMRC'95 – 6th IEEE International Symposium on Personal, Indoor and Mobile Radio Communications,* Toronto, Canada, Sep. 1995.

[CoPr97] Correia,L.M. and Prasad,R., "An Overview of Wireless Broadband Communications", *IEEE Communications Magazine*, Vol. 35, No. 1, Jan. 1997, pp. 28-33.

[CoRF97] Correia,L.M., Reis,J.J. and Francês,P.O., "Analysis of the Average Power to Distance Decay Rate at the 60 GHz Band", in *Proc. of VTC'97 – 47th IEEE Vehicular Technology Conference*, Phoenix, AZ, USA, May 1997.

[Corr01] Correia,L.M. (ed.), *Wireless Flexible Personalised Communications (COST 259 Final Report)*, John Wiley, Chichester, UK, 2001.

[COST03] http://www.lx.it.pt/cost273, Aug. 2003

[DABN02] Doufexi,A., Armour,S., Butler,M., Nix,A., Bull,D., McGeehan,J. and Karlsson,P., "A Comparison of the HIPERLAN/2 and IEEE802.11a Wireless LAN Standards", *IEEE Communications Magazine*, Vol. 40, No. 5, May 2002, pp. 104-111.

[DaCo99] Damoso,E. and Correia,L.M. (eds.), *Digital Mobile Radio Towards Future Generation Systems – COST 231 Final Report*, COST Office, European Commission, Brussels, Belgium, 1999.

[DGIM02] Derryberry,R.T., Gray,S.D., Ionescu,D.M., Mandyam,G. and Raghothamam,B., "Transmit Diversity in 3G CDMA Systems", *IEEE Communications Magazine*, Vol. 40, No. 4, Apr. 2002, pp. 68-75.

[ETSI01] ETSI, *Broadband Radio Access Networks (BRAN); HIPERLAN Type 2; Physical (PHY) Layer*, Technical Specification TS 101 475 v1.3.1, Sophia Antipolis, France, Dec. 2001 (http://www.etsi.org).

[ETSI97] ETSI, *Universal Mobile Telecommunications System (UMTS); Selection Procedures for the Choice of Radio Transmission Technologies of UMTS*, Technical Report TR 101 112 v3.1.0, Sophia Antipolis, France, Nov. 1997 (http://www.etsi.org).

[ETSI99] ETSI, *Digital Cellular Telecommunications System (Phase 2); Radio Transmission and Reception*, European Telecommunication Standard ETS 300 577 v4.23.1, Sophia Antipolis, France, Dec. 1999 (http://www.etsi.org).

[Fail89] Failli,M. (ed.), *Digital Land Mobile Radio Communications (COST 207 Final Report)*, COST Secretariat, European Comission, Brussels, Belgium, 1989.

[FLOW03] http://www.flows-ist.org, Aug. 2003

[FuMB98] Fuhl,J., Molisch,A. and Bonek,E., "Unified Channel Model for Mobile Radio Systems with Smart Antennas", *IEE Proceedings – Radar, Sonar Navigation*, Vol. 145, No. 1, Feb. 1998, pp. 32-41.

[GaPa89] Ganesh,R. and Pahlavan,K., "On Arrival of Paths in Fading Multipath Indoor Radio Channels", *Electronic Letters*, Vol. 25, No. 12, June 1989, pp. 763-765.

[GaPa91] Ganesh,R. and Pahlavan,K., "Statistical Modelling and Computer Simulation of Indoor Radio Channel", *IEE Proceedings*, Vol. 138, Part I, No. 3, June 1991, pp. 153-161.

[GiCo03] Gil,J.M. and Correia,L.M., "Impact of Wideband Directional Propagation Channel Characteristics on Adaptive Beamforming", *IEICE Transactions on Communications*, Vol. E83-B, No. 12, Dec. 2002, pp. 1640-1647.

[GSMW03] http://www.gsmworld.com, Aug. 2003.

[Gued96] Guedes,L.G., *Contributions to the statistics of the mobile radio signal* (in Portuguese), Ph.D. Thesis, Campinas State University, Campinas, SP, Brazil, Dec. 1996.

[Hash79] Hashemi,H., "Simulation of the Urban Radio Propagation Channel", *IEEE Transactions on Vehicular Technology*, Vol. 28, No. 3, Aug. 1979, pp. 213-225.

[Hash93] Hashemi,H., "The Indoor Radio Propagation Channel", *Proceedings of IEEE*, Vol. 81, No. 7, July 1993, pp. 943-968.

[Hata80] Hata,M., "Empirical Formula for Propagation Loss in Land Mobile Radio Services", *IEEE Transactions on Vehicular Technology*, Vol. 29, No. 3, Aug. 1980, pp. 317-325.

[HaWC99] Har,D., Watson,A.M. and Chadney,A.G., "Comment on Diffraction Loss of Rooftop-to-Street in COST 231-Walfisch-Ikegami Model", *IEEE Transactions on Vehicular Technology*, Vol. 48, No. 5, Sep. 1999, pp. 1451-1452.

[HoMS01] Hofstetter,H., Molisch,A.F. and Steinbauer,M., "Implementation of a COST 259 Geometry Based Stochastic Model for Macro and Micro Cells", in *Proc. of EPMCC 2001 – 4th European Personal Mobile Communications Conference*, Vienna, Austria, Feb. 2001.

[HoPa92] Howard,S.J. and Pahlavan,K., "Autoregressive Modeling of Wide-Band Indoor Radio Propagation", *IEEE Transactions on Communications*, Vol. 40, No. 9, Sep. 1992, pp. 1540-1552.

[HoTo00] Holma,H. and Toskala,A., *WCDMA for UMTS – Radio Access For Third Generation Mobile Communications*, John Wiley, Chichester, UK, 2000.

[InKa00] Inoue,T. and Karasawa,Y., "Theoretical Analysis on the Perfomance of Multipath Waves Distributed in Spatial and Time Domains", *IEICE Transactions on Communications*, Vol. E83-B, No. 7, July 2000, pp. 1426-1424.

[InKa99] Inoue,T. and Karasawa,Y., "Theoretical Analysis on the Level Variation Properties of Wideband Signals in the Rayleigh Fading Environment", in *Proc. of PIMRC'99 – 10th IEEE International Symposium on Personal, Indoor and Mobile Radio Communications*, Osaka, Japan, Sep. 1999.

[ITUR86] ITU-R, *Attenuation by Hydrometeors, in Particular Precipitation, and Other Atmospheric Particles*, Recommendations and Reports of the ITU-R, Report 721-2, Vol. V (Propagation in Non-Ionized Media), Geneva, Switzerland, 1986.

[Jake74] Jakes,W.C., *Microwave Mobile Communications*, John Wiley, Chichester, UK, 1995.

[Kara01] Karaouguz,J., "High-Rate Wireless Personal Area Networks", *IEEE Communications Magazine*, Vol. 39, No. 12, Dec. 2001, pp. 96-102.

[Katt99] Kattenbach,R., "Statistical Modeling of Short-Term Fading Effects for Directional Radio Channels", *COST259*, TD(99)112, Leidschendam, The Netherlands, Sep. 1999.

[KlLa80] Klema,V.C. and Laub,A.J., "The Singular Value Decomposition: its Computation and Some Applications", *IEEE Transactions on Automatic Control*, Vol. 25, No. 2, Apr. 1980, pp. 164-176.

[KLTH00] Kalliola,K., Laurila,J., Toeltsch,M., Hugl,K., Vainikainen,P. and Bonek,E., "3-D Directional Wideband Dual-Polarized Measurement of Urban Mobile Radio Channel With Synthetic Aperture Technique", in *Proc. of AP2000 – Millennium Conference on Antennas & Propagation*, Davos, Switzerland, Apr. 2000.

[KMRV01] Kalliokulju,J., Meche,P., Rinne,M.J., Vallström,J. and Varshney,P., "Radio Access Selection for Multistandard Terminals", *IEEE Communications Magazine*, Vol. 39, No. 10, Oct. 2001, pp. 116-123.

[KoSN96] Kozono,S., Seino,S. and Nakabayashi,H., "Received Signal-Level Characteristics of Wide-Band Transmission in Mobile Communications", in *Proc. of PIMRC'96 – 7th IEEE International Symposium on Personal, Indoor and Mobile Radio Communications,* Taipei, Taiwan, Oct. 1996.

[Kozo94] Kozono,S., "Received Signal-Level Characteristics in a Wide-Band Mobile Radio Channel", *IEEE Transactions on Vehicular Technology*, Vol. 43, No. 3, Aug. 1994, pp. 480-486.

[Lee73] Lee,W.C.Y., "Effects on Correlation Between two Mobile Base-Station Antennas", *IEEE Transactions on Communications*, Vol. 21, No. 11, Nov. 1973, pp. 1214-1224.

[Leon93] Leon-Garcia,A., *Probability and Random Processes for Electrical Engineering*, Addison-Wesley, Massachusetts, USA, 1993.

[LiLo96] Litva,J. and Lo,T.K., *Digital Beamforming in Wirelless Communications*, Artech House, London, UK, 1996.

[LiRa99] Liberti,J. and Rappaport,T., *Smart Antennas for Wireless Communication: IS-95 and Third Generation CDMA Applications*, Prentice Hall, Upper Saddle River, NJ, USA, 1999.

[LuLL97] Lu,M., Lo.,T. and Litva,J., "A Physical Spatio-Temporal Model of Multipath Propagation Channels", in *Proc. of VTC'97 – 47th IEEE Vehicular Technology Conference*, Phoenix, AZ, USA, May 1997.

[Marq01] Marques,M.G., *A Wideband Directional Model for Micro-Cells in UMTS*, Master Thesis, Instituto superior Técnico, Lisbon, Portugal, May 2001.

[MaYJ03] Matsumoto,T., Ylitalo,J. and Juntti, M., " Overview and Recent Challenges of MIMO Systems, *IEEE Vehicular Technology Society News*, Vol. 50, No. 2, May 2003, pp. 4-9.

[MBS03] http://www.comnets.rwth-aachen.de/project/mbs/, Aug. 2003.

[MeSc98] Medbo,J. and Schramm,P., *Channel Models for HIPERLAN/2 in Different Indoor Scenarios*, ETSI, EP BRAN 3ERI085B, Sophia Antipolis, France, Mar. 1998.

[MLAR94] Mohamed,S.A., Lovnes,G., Antonsen,E., Raekken,R.H., Nigeon,B. and Reis,J.J., *Report on Propagation Measurements*, RACE-MBS Project, Deliverable R2067/BTL/2.2.2/DS/P/031.a1, RACE Office, Brussels, Belgium, Nov. 1994.

[MOME03] http://momentum.zib.de, Aug. 2003.

[MoPa92] Mouly,M. and Pautet,M., *The GSM System for Mobile Communications*, M. Mouly et Marie-B. Pautet, Palaiseau, France, 1992.

[MPKZ01] Marques,G., Pamp,J., Kunisch.J. and Zollinger,E., *Wideband Directional Channel Model, Array Antennas and Measurement Campaign*, IST-ASILUM Project, Deliverable D2.3bis, IST Office, Brussels, Belgium, Nov. 2001.

[MuLe02] Murch,R.D. and Letaief,K.B., "Antenna Systems for Broadband Wireless Access", *IEEE Communications Magazine*, Vol. 40, No. 4, Apr. 2002, pp. 76-83.

[NaKo02] Nakabayashi,H. and Kozono,S., "Theorethical Analysis of Frequency-Correlation Coefficient for Received Signal Level in Mobile Communications", *IEEE Transactions on Vehicular Technology*, Vol. 51, No. 4, July 2002, pp. 729-737.

[NeBB01] Neubauer,T., Baumgartner,T. and Bonek,E., "*Applying COST 259 Channel Models to UMTS Uplink System Level Simulations with Smart Antennas*", ITG Diskkussionssitzung, Ilmenau, Germany, Mar. 2001 (http://www-emt.tu-ilmenau.de/itg91/paper/18_Baumgartner_TU_Wien.pdf).

[NøAn94] Nørklit,O. and Andersen,J.B., "Mobile Radio Environments and Adaptive Arrays", in Proc. *of PIMRC'94 – 5th IEEE International Symposium on Personal, Indoor and Mobile Radio Communications*, The Hague, The Netherlands, Sep. 1994.

[NøAn98] Nørklit,O. and Andersen,J.B., "Diffuse Channel Model and Experimental Results for Array Antennas in Mobile Environments", *IEEE Transactions on Antennas and Propagation*, Vol. 46, No. 6, June 1998, pp. 834-840.

[NYMI01] Nakabayashi,H., Yian,J., Masui,H., Ishii,M., Sakawa,K., Shimizu,H., Kobayashi,T. and Kozono,S., "Validation of Equivalent Received Bandwidth to Characterize Received Signal Level Distribution through Experiment and Simulation," *IEICE Transactions on Communications*, Vol. E84-B, No. 9, Sep. 2001, pp. 2250-2559.

[OkOF68] Okumura,T., Ohmori,E. and Fukuda,K., "Field Strength and its Variability in VHF and UHF Land Mobile Service", *Review Electrical Communication Laboratory*, Vol. 16, No. 9/10, Sep./Oct. 1968, pp. 825-873.

[Otte95] Ottersten,B., "Spatial Division Multiple Access (SDMA) in Wireless Communications", in *Proc. of Nordic Radio Symposium*, Saltsjöbaden, Sweden, Apr. 1995.

[PAKM00] Pedersen,K.I., Andersen,J.B., Kermoal,J.P. and Mogensen,P., "A Stochastic Multiple-Input-Multiple-Output Radio Channel Model for Evaluation of Space-Time Coding Algorithms", in *Proc. of VTC'00 Fall – 52nd IEEE Vehicular Technology Conference*, Boston, MA, USA, Sep. 2000.

[PaLe95] Pahlavan,K. and Levesque,A.H., *Wireless Information Networks*, John Wiley, Chichester, UK, 1995.

[Pars92] Parsons,D., *The Mobile Radio Propagation Channel*, Pentech Press, London, UK, 1992.

[PeMF00] Pedersen,K.I., Mogensen,P.E. and Fleury B.H., "A Stochastic Model of the Temporal and Azimuthal Dispersion seen at the Base Station in Outdoor Propagation Environments", *IEEE Transactions on Vehicular Technology*, Vol. 49, No. 2, Mar. 2000, pp. 437-447.

[PiMT01] Piechocki,R., Mcgeehan,J.P. and Tsoulos,G., "A New Stochastic Spatio-Temporal Propagation Model (SSTPM) for Mobile communications with Antenna Arrays", *IEEE Transactions on Communications*, Vol. 49, No. 5, May 2001, pp. 855-862.

[PiTs99] Piechocki,R. and Tsoulos,G., "Combined GWSSUS and GBSB Channel Model With Temporal Variations", in *Proc. of COST259/260 Joint Workshop on Spatial Channel Models and Adaptive Antennas*, Vienna, Austria, Apr. 1999.

[Pras96] Prasad,R., *CDMA for Wireless Personal Communications*, Artech House, London, UK, 1996.

[Pras98] Prasad,R., *Universal Wireless Personal Communications*, Artech House, London, UK, 1998.

[Proa83] Proakis,J.G., *Digital Communications*, McGraw-Hill, New York, NY, USA, 1983.

[PSRC94] Plassman,D., Scheibenbogen,M., Rommann,J. and Cimmino,A., *Internetworking and MBS Services*, RACE-MBS Project, Deliverable R2067/UA/WP2.1.1/DS/P/28.b1, RACE Office, Brussels, Belgium, Mar. 94.

[RaPa95] Raleigh,G. and Paulraj,A., "Time Varying Vector Channel Estimation for Adaptive Spatial Equalisation", in *Proc. of Globecom'95 – IEEE Global Telecommunications Conference*, Singapore, Nov. 1995.

[Rapp96] Rappaport,T.S., *Wireless Communications – Principles & Practice*, Prentice Hall, Upper Saddle River, NJ, USA, 1996.

[RaST91] Rappaport,T.S., Seidel,S.Y. and Takamizawa,K., "Statistical Channel Impulse Response Models for Factory and Open Plan Building Radio Communication System Design", *IEEE Transactions on Communications*, Vol. 39, No. 5, May 1991, pp. 794-807.

[RoSc95] Rokitansky,C. and Scheibenbogen,M., *Updated Version of SDD*, RACE-MBS Project, Deliverable R2067/UA/WP2.1.5/DS/P/68.b1, RACE Office, Brussels, Belgium, Dec. 95.

[SAMB03] http://cordis.lu/infowin/acts/rus/projects/ac204.htm, Aug. 2003.

[Saun99] Saunders,S.R., *Antennas and Propagation for Wireless Communication Systems*, John Wiley, Chichester, UK, 1999.

[SaVa87] Saleh,A.A.M. and Valenzuela,R.A., "A Statistical Model for Indoor Multipath Propagation", *IEEE Journal on Selected Areas in Communications*, Vol. 5, No. 2, Feb. 1987, pp. 128-137.

[ScBM02] Schumacher,L., Berger,L. and Moreno,J., "Recent Advances in Propagation Characterisation and Multiple Antenna Processing in the 3GPP Framework", in *Proc. of XXVIIth URSI General Assembly*, Maastricht, The Netherlands, Aug. 2002.

[Scha91] Schafer,W., "Channel Modelling of Short-Range Radio Links at 60GHz for Mobile Intervehicle Communication", in *Proc. of VTC'91 – 41st IEEE Vehicular Technology Conference*, St. Louis, MI, USA, May 1991.

[SJBF99] Stege,M., Jelitto,J., Bronzel,M. and Fettweis G., "A Space-Time channel Model with Stochastic Fading Simulation", *ITG – Fachtagung Intelligente Antennen*, Sttutgart, Germany, Apr. 1999.

[SRJJ97] Spencer,Q., Rice,M., Jeffs,B. and Jensen,M., "A Statistical Model for Angle of Arrival in Indoor Multipath Propagation", in *Proc. of VTC'97 – 47th IEEE Vehicular Technology Conference*, Phoenix, AZ, USA, May 1997.

[StCM94] Stapleton,S.P., Carbo,X. and McKeen,T., "Spatial Channel Simulator for Phased Arrays", in *Proc. of VTC'94 – 44th IEEE Vehicular Technology Conference*, Stockholm, Sweden, June 1994.

[StCM96] Stapleton,S.P., Carbo,X. and McKeen,T., "Tracking and Diversity for a Mobile Communications Base Station Array Antenna", in *Proc. of VTC'96 – 46th IEEE Vehicular Technology Conference*, Atlanta, GA, USA, Apr. 1996.

[StMB01] Steinbauer,M., Molisch,A.F. and Bonek,E., "The Double Directional Radio Channel", *IEEE Antennas and Propagation Magazine*, Vol. 43, No. 4, Aug. 2001, pp. 51-63.

[Suzu77] Suzuki,H., "A Statistical Model for Urban Radio Propagation", *IEEE Transactions on Communications*, Vol. 25, No. 7, July 1977, pp. 673-680.

[Svan01] Svantesson,T., "A Physical MIMO Channel Model for Multi-Element Multi-Polarized Antenna Systems", in *Proc. of VTC'01 Fall – 54th IEEE Vehicular Technology Conference*, Atlantic City, NJ, USA, Oct. 2001.

[TCJF72] Turin,G.L., Clapp,F.D., Johnston,T.L., Fine,S.B. and Lavry,D., "A Statistical Model of Urban Multipath Propagation", *IEEE Transactions on Vehicular Technology*, Vol. 21, No. 1, Feb. 1972, pp. 1-9.

[TeAG03] Tepedelenlioğlu,C., Abdi,A. and Giannakis,G.B., "The Ricean *K* Factor: Estimation and Performance Analysis", *IEEE Transactions on Wireless Communications*, Vol. 22, No. 4, July 2003, pp. 799-810.

[TUWi03] http://www.nt.tuwien.ac.at/mobile/projects/UMTS/en/, July 2003.

[UMTS03] http://www.umts-forum.org, Aug. 2003.

[Vasc98] Vasconcelos,P.V., *Propagation Channel Characterisation for 60 GHz Mobile Communnication Systems* (in Portuguese), Master Thesis, Instituto Superior Técnico, Lisbon, Portugal, Jan. 1998.

[VeCo00a] Velez,F.J. and Correia,L.M., "Classification and Characterisation of Mobile Broadband Services", in *Proc. of VTC'2000 Fall – 52nd IEEE Vehicular Technology Conference*, Boston, MA, USA, Sep. 2000.

[VeCo00b] Velez,F.J. and Correia,L.M., "Deployment Scenarios for Mobile Broadband Communications", in *Proc. of PIMRC'2000 – 11th IEEE International Symposium on Personal, Indoor and Mobile Radio Communications*, London, UK, Sep. 2000.

[Vele00] Velez,F.J., *Aspects of Cellular Planning in Mobile Broadband Systems*, Ph.D. Thesis, Instituto Superior Técnico, Lisbon, Portugal, Dec. 2000.

[VrLa02] Vriendt,J. and Lainé,P., "Mobile Network Evolution: A Revolution on the Move", *IEEE Communications Magazine*, Vol. 40, No. 4, Apr. 2002, pp. 104-111.

[XaVC03] Xavier,D.M., Venes,J.M. and Correia,L.M., "Characterization of Signal Penetration into Buildings for GSM", in *Proc. of ConfTele 2003 – 4th Conference on Telecommunications*, Aveiro, Portugal, June 2003.

[XuCV02] Xu,H., Chizhik,D. and Valenzuela,R., "A Wave-Based Wideband MIMO Channel Modeling Technique", in *Proc. of PIMRC' 2002 – 13th IEEE International Symposium on Personal, Indoor, and Mobile Radio Communications*, Lisbon, Portugal, Sep. 2002.

[Yaco01] Yacoub,M.D., *Wireless Technology, Protocols Standards and Technology*, CRC Press, Boca Raton, FL, USA, 2001.

[Yaco93] Yacoub,M.D., *Foundations of Mobile Radio Engineering*, CRC Press, Boca Raton, FL, USA, 1993.

[YaKo99] Yan,J. and Kozono,S., "A Study of Received Signal-Level Distribution in Wideband Transmissions in Mobile Communications", *IEEE Transactions on Vehicular Technology*, Vol. 48, No. 5, Sep. 1999, pp. 1718-1725.

[YeMc91] Yegani,P. and McGillem,C.D., "A Statistical Model for the Factory Radio Channel", *IEEE Transactions on Communications*, Vol. 39, No. 10, Oct. 1991, pp. 1445-1454.

[YuOt02] Yu,K. and Ottersten,B., "Models for MIMO propagation channels: a review", *Wireless Communications and Mobile Computing*, Vol. 2, No. 7, Nov. 2002, pp. 653-666.

[ZeEs96] Zetterberg,P. and Espensen,P.L., "A Downlink Beam Steering Technique for GSM/DCS1800/PCS1900", in *Proc. of PIMRC'96 – 7th IEEE International Symposium on Personal, Indoor and Mobile Radio Communications*, Taipei, Taiwan, Oct. 1996.

[ZhRV01] Zhao,X., Rekanos,I. and Vainikanen,P., "A General Computer Simulation Method for 3-D Received Signal Level in Wideband Mobile Communications", in *Proc. of WPMC'01 – The 4th International Symposium on Wireless Personal Multimedia Communications*", Aalborg, Denmark, Sep. 2001.

Appendix I

Average Fading Depth Evaluation and Fitting Results

Simulation data from which the environment-geometry based approach in Chapter 4 was derived is presented. Fitting results for $p = 0.1$ and 10 % are shown, model parameters are given and the approximation error is quantified. Fading depth results for different systems working in micro-cellular environments are also presented.

I.1. Mean Fading Depth Results

Table I.1 – Mean value and standard deviation of fading depth, p = 0.1 %.

	K [dB]											
	0		3		5		7		10		20	
Δw_{eq} [MHz·m]	$\overline{FD}$ [dB]	σ_{FD} [dB]	$\overline{FD}$ [dB]	σ_{FD} [dB]	$\overline{FD}$ [dB]	σ_{FD} [dB]	$\overline{FD}$ [dB]	σ_{FD} [dB]	$\overline{FD}$ [dB]	σ_{FD} [dB]	$\overline{FD}$ [dB]	σ_{FD} [dB]
0.01	28.92	1.37	25.90	1.51	22.14	1.49	15.23	1.16	8.52	0.35	1.98	0.04
0.02	28.62	0.85	25.85	1.48	22.30	1.37	15.11	1.06	8.31	0.22	1.93	0.04
0.04	27.78	1.32	26.04	0.84	20.99	0.88	16.46	1.03	8.30	0.26	1.96	0.03
0.06	27.41	0.72	26.55	1.13	21.82	0.85	14.90	0.92	8.41	0.34	1.95	0.03
0.08	28.61	0.98	26.81	0.73	23.17	0.71	15.40	0.94	8.38	0.19	1.96	0.04
0.10	28.48	1.22	25.94	1.25	22.22	1.28	15.85	0.87	8.32	0.33	1.99	0.05
0.20	29.35	1.54	25.30	1.45	22.47	1.11	14.89	0.60	8.36	0.14	1.96	0.04
0.40	28.00	1.38	26.65	1.08	22.82	1.09	15.62	1.14	8.45	0.29	1.95	0.06
0.60	28.55	2.41	26.05	0.91	22.31	2.11	14.86	0.44	8.30	0.32	1.94	0.03
0.80	28.18	1.11	26.96	1.04	23.14	2.12	15.84	1.34	8.37	0.31	1.96	0.03
1.00	27.19	0.62	25.34	0.92	22.13	0.93	15.46	0.96	8.49	0.41	1.94	0.04
2.00	27.93	0.75	25.38	0.68	22.34	1.27	16.01	0.71	8.28	0.39	1.91	0.04
4.00	27.84	1.12	25.38	0.65	23.11	1.14	15.15	0.49	8.48	0.21	1.94	0.03
6.00	27.61	1.08	25.48	1.00	21.90	0.77	15.38	1.05	8.24	0.12	1.95	0.04
8.00	27.05	1.05	25.28	0.85	21.78	0.73	15.50	0.74	8.36	0.37	1.95	0.06
10.00	26.52	0.81	24.68	0.84	23.05	0.90	15.14	0.64	8.63	0.27	1.95	0.05
20.00	23.68	0.56	22.84	0.38	20.74	0.51	14.76	0.74	8.56	0.14	1.96	0.04
40.00	20.82	0.33	19.28	0.21	17.41	0.34	14.44	0.60	8.06	0.07	1.91	0.06
60.00	19.23	0.40	17.90	0.14	15.98	0.40	12.97	0.38	7.90	0.18	1.91	0.04
80.00	17.78	0.59	16.05	0.51	14.37	0.41	11.66	0.30	7.50	0.24	1.87	0.02
100.00	16.78	0.97	14.79	0.38	13.58	0.44	11.26	0.50	7.23	0.30	1.79	0.03
200.00	13.52	0.36	11.62	0.30	10.08	0.49	8.27	0.35	5.52	0.28	1.61	0.04
400.00	11.23	0.34	9.17	0.49	7.81	0.34	6.14	0.12	4.27	0.10	1.24	0.04
600.00	9.16	0.27	8.03	0.20	6.46	0.14	5.34	0.25	3.50	0.12	1.09	0.03
800.00	8.01	0.46	7.00	0.22	5.73	0.26	4.65	0.20	3.32	0.09	0.95	0.05
1 000.00	7.23	0.32	6.05	0.17	5.09	0.14	4.02	0.08	3.05	0.25	0.91	0.04
2 000.00	5.29	0.27	4.66	0.14	4.02	0.17	3.30	0.17	2.37	0.08	0.69	0.02
4 000.00	4.28	0.29	3.70	0.20	3.15	0.18	2.51	0.10	1.90	0.05	0.58	0.02
6 000.00	3.86	0.21	3.24	0.24	2.74	0.09	2.36	0.22	1.64	0.06	0.51	0.03
8 000.00	3.44	0.12	2.85	0.14	2.64	0.11	2.15	0.08	1.59	0.10	0.50	0.03
10 000.00	3.11	0.12	2.91	0.15	2.39	0.12	2.05	0.13	1.48	0.04	0.47	0.01
20 000.00	2.62	0.17	2.36	0.14	2.14	0.13	1.76	0.08	1.31	0.08	0.40	0.02
40 000.00	2.28	0.18	1.92	0.07	1.85	0.15	1.54	0.05	1.10	0.05	0.37	0.01
60 000.00	2.03	0.21	1.85	0.07	1.62	0.12	1.46	0.09	0.96	0.06	0.32	0.02
80 000.00	2.02	0.23	1.74	0.10	1.44	0.11	1.25	0.17	0.92	0.11	0.32	0.02
100 000.00	1.65	0.12	1.66	0.10	1.42	0.17	1.16	0.06	0.92	0.16	0.29	0.02
200 000.00	1.35	0.22	1.02	0.14	1.10	0.18	0.91	0.07	0.72	0.08	0.21	0.05
400 000.00	0.97	0.11	0.72	0.13	0.58	0.14	0.44	0.04	0.34	0.12	0.15	0.06
600 000.00	0.75	0.15	0.57	0.10	0.53	0.27	0.42	0.16	0.29	0.09	0.09	0.03
800 000.00	0.85	0.06	0.70	0.14	0.53	0.14	0.53	0.23	0.33	0.12	0.12	0.05
1 000 000.00	0.63	0.10	0.44	0.03	0.34	0.05	0.23	0.04	0.16	0.05	0.05	0.02

Table I.2 – Mean value and standard deviation of fading depth, p = 1 %.

	K [dB]											
	0		3		5		7		10		20	
Δw_{eq} [MHz·m]	$\overline{FD}$ [dB]	σ_{FD} [dB]	$\overline{FD}$ [dB]	σ_{FD} [dB]	$\overline{FD}$ [dB]	σ_{FD} [dB]	$\overline{FD}$ [dB]	σ_{FD} [dB]	$\overline{FD}$ [dB]	σ_{FD} [dB]	$\overline{FD}$ [dB]	σ_{FD} [dB]
0.01	17.35	0.36	16.01	0.63	13.21	0.54	9.18	0.14	5.97	0.10	1.50	0.03
0.02	17.75	0.33	16.45	0.49	13.01	0.28	9.33	0.29	5.79	0.09	1.50	0.03
0.04	17.84	0.46	15.95	0.44	12.96	0.44	9.51	0.16	5.89	0.11	1.51	0.02
0.06	17.92	0.41	15.99	0.60	12.57	0.26	9.29	0.25	5.90	0.12	1.52	0.03
0.08	18.00	0.26	15.72	0.32	13.11	0.26	9.50	0.34	5.85	0.16	1.53	0.02
0.10	18.11	0.29	15.88	0.39	12.85	0.26	9.59	0.19	5.83	0.12	1.50	0.03
0.20	17.99	0.24	15.90	0.29	12.90	0.39	9.39	0.34	5.79	0.15	1.52	0.03
0.40	17.66	0.32	16.03	0.31	12.97	0.39	9.39	0.14	5.85	0.18	1.51	0.03
0.60	17.73	0.41	15.90	0.45	13.16	0.36	9.45	0.24	5.92	0.15	1.51	0.02
0.80	17.72	0.39	16.15	0.33	13.00	0.41	9.53	0.10	5.83	0.19	1.53	0.03
1.00	17.94	0.29	16.16	0.32	12.98	0.34	9.45	0.23	5.93	0.10	1.53	0.03
2.00	17.83	0.57	16.01	0.23	13.00	0.35	9.54	0.14	5.87	0.08	1.51	0.03
4.00	17.64	0.21	16.08	0.60	12.95	0.08	9.30	0.25	5.93	0.15	1.50	0.02
6.00	18.09	0.41	15.95	0.44	12.84	0.46	9.27	0.23	5.73	0.14	1.51	0.02
8.00	17.86	0.33	15.68	0.34	12.92	0.22	9.60	0.23	5.81	0.10	1.51	0.01
10.00	17.54	0.16	15.88	0.30	13.24	0.20	9.31	0.20	5.86	0.13	1.50	0.04
20.00	17.22	0.35	15.36	0.35	12.63	0.38	9.43	0.13	5.82	0.05	1.50	0.02
40.00	16.02	0.45	14.34	0.30	11.94	0.29	8.96	0.17	5.94	0.12	1.50	0.04
60.00	14.24	0.14	12.97	0.17	11.22	0.18	8.90	0.18	5.61	0.12	1.50	0.02
80.00	13.29	0.18	12.08	0.08	10.50	0.16	8.21	0.25	5.40	0.10	1.44	0.03
100.00	12.25	0.11	11.25	0.16	9.66	0.09	7.73	0.18	5.23	0.06	1.39	0.02
200.00	9.56	0.23	8.22	0.13	7.08	0.22	5.86	0.07	4.12	0.10	1.23	0.03
400.00	7.43	0.21	6.25	0.13	5.26	0.10	4.22	0.06	3.06	0.07	0.91	0.01
600.00	6.24	0.11	5.15	0.14	4.35	0.13	3.56	0.07	2.53	0.03	0.77	0.02
800.00	5.47	0.15	4.57	0.11	3.86	0.07	3.12	0.06	2.25	0.05	0.69	0.02
1 000.00	5.00	0.16	4.12	0.09	3.39	0.09	2.82	0.10	2.04	0.07	0.64	0.02
2 000.00	3.56	0.09	3.03	0.07	2.58	0.04	2.11	0.07	1.53	0.03	0.48	0.01
4 000.00	2.67	0.07	2.35	0.06	1.99	0.05	1.67	0.02	1.19	0.03	0.39	0.01
6 000.00	2.25	0.10	1.98	0.03	1.74	0.08	1.44	0.03	1.08	0.04	0.33	0.01
8 000.00	1.99	0.08	1.80	0.06	1.57	0.05	1.35	0.04	0.98	0.03	0.31	0.01
10 000.00	1.80	0.09	1.66	0.04	1.43	0.08	1.18	0.06	0.90	0.02	0.29	0.01
20 000.00	1.38	0.11	1.15	0.06	1.07	0.05	0.88	0.06	0.68	0.03	0.23	0.01
40 000.00	0.92	0.06	0.79	0.04	0.63	0.04	0.56	0.04	0.44	0.03	0.14	0.02
60 000.00	0.75	0.06	0.56	0.04	0.46	0.02	0.38	0.03	0.30	0.04	0.10	0.01
80 000.00	0.65	0.03	0.47	0.02	0.39	0.04	0.30	0.02	0.22	0.02	0.07	0.01
100 000.00	0.60	0.03	0.44	0.03	0.33	0.02	0.27	0.01	0.19	0.03	0.06	0.00
200 000.00	0.40	0.03	0.26	0.02	0.20	0.01	0.15	0.02	0.10	0.02	0.02	0.00
400 000.00	0.20	0.03	0.15	0.03	0.11	0.01	0.09	0.01	0.06	0.01	0.02	0.00
600 000.00	0.16	0.02	0.12	0.01	0.09	0.01	0.07	0.02	0.04	0.01	0.01	0.00
800 000.00	0.12	0.01	0.11	0.02	0.09	0.02	0.06	0.01	0.05	0.01	0.01	0.00
1 000 000.00	0.09	0.02	0.07	0.02	0.05	0.01	0.04	0.01	0.02	0.01	0.01	0.00

Table I.3 – Mean value and standard deviation of fading depth, p = 10 %.

	K [dB]											
	0		3		5		7		10		20	
Δw_{eq} [MHz·m]	$\overline{FD}$ [dB]	σ_{FD} [dB]	$\overline{FD}$ [dB]	σ_{FD} [dB]	$\overline{FD}$ [dB]	σ_{FD} [dB]	$\overline{FD}$ [dB]	σ_{FD} [dB]	$\overline{FD}$ [dB]	σ_{FD} [dB]	$\overline{FD}$ [dB]	σ_{FD} [dB]
0.01	7.73	0.35	6.56	0.14	5.42	0.30	4.21	0.14	2.92	0.06	0.83	0.01
0.02	7.65	0.30	6.42	0.17	5.13	0.19	4.19	0.12	2.86	0.09	0.84	0.02
0.04	7.75	0.09	6.43	0.25	5.32	0.17	4.17	0.09	2.90	0.04	0.83	0.02
0.06	7.74	0.16	6.51	0.28	5.40	0.20	4.15	0.12	2.90	0.09	0.82	0.02
0.08	7.61	0.21	6.36	0.23	5.31	0.14	4.16	0.18	2.86	0.03	0.85	0.02
0.10	7.81	0.20	6.74	0.21	5.28	0.16	4.16	0.11	2.84	0.08	0.82	0.01
0.20	7.72	0.22	6.53	0.31	5.27	0.18	4.11	0.05	2.85	0.08	0.84	0.01
0.40	7.58	0.18	6.49	0.18	5.37	0.16	4.20	0.09	2.88	0.06	0.83	0.01
0.60	7.67	0.18	6.62	0.24	5.37	0.13	4.17	0.17	2.90	0.08	0.85	0.01
0.80	7.70	0.25	6.47	0.16	5.29	0.11	4.22	0.15	2.85	0.09	0.84	0.03
1.00	7.69	0.27	6.56	0.18	5.13	0.12	4.34	0.12	2.90	0.07	0.82	0.03
2.00	7.60	0.14	6.49	0.16	5.37	0.20	4.23	0.10	2.87	0.08	0.82	0.01
4.00	7.80	0.16	6.53	0.22	5.25	0.16	4.09	0.09	2.86	0.08	0.84	0.01
6.00	7.74	0.19	6.48	0.13	5.47	0.18	4.24	0.06	2.85	0.07	0.85	0.02
8.00	7.80	0.16	6.61	0.22	5.28	0.14	4.17	0.09	2.90	0.07	0.84	0.02
10.00	7.59	0.11	6.46	0.14	5.39	0.18	4.29	0.12	2.90	0.08	0.83	0.03
20.00	7.56	0.16	6.52	0.15	5.23	0.09	4.07	0.11	2.76	0.05	0.84	0.01
40.00	7.56	0.16	6.41	0.07	5.19	0.07	4.08	0.07	2.88	0.05	0.83	0.02
60.00	7.36	0.22	6.29	0.11	5.17	0.19	4.10	0.11	2.79	0.07	0.81	0.01
80.00	6.97	0.13	6.07	0.09	4.95	0.11	3.97	0.15	2.72	0.05	0.81	0.02
100.00	6.54	0.13	5.75	0.10	4.78	0.08	3.86	0.04	2.71	0.06	0.79	0.01
200.00	5.01	0.10	4.29	0.07	3.62	0.09	3.03	0.03	2.21	0.08	0.69	0.02
400.00	3.69	0.10	3.13	0.03	2.61	0.06	2.16	0.02	1.55	0.03	0.48	0.02
600.00	3.02	0.12	2.49	0.04	2.10	0.07	1.76	0.05	1.26	0.03	0.40	0.01
800.00	2.71	0.08	2.15	0.12	1.85	0.07	1.53	0.02	1.08	0.04	0.35	0.00
1 000.00	2.33	0.07	1.92	0.05	1.62	0.07	1.33	0.04	0.99	0.03	0.31	0.01
2 000.00	1.61	0.08	1.30	0.07	1.08	0.03	0.92	0.03	0.66	0.03	0.22	0.01
4 000.00	1.12	0.03	0.83	0.06	0.68	0.03	0.56	0.03	0.40	0.04	0.13	0.00
6 000.00	0.87	0.05	0.63	0.03	0.53	0.05	0.40	0.02	0.28	0.01	0.09	0.01
8 000.00	0.71	0.03	0.53	0.03	0.40	0.03	0.31	0.02	0.22	0.02	0.07	0.01
10 000.00	0.61	0.04	0.44	0.02	0.36	0.03	0.26	0.02	0.18	0.01	0.05	0.01
20 000.00	0.38	0.02	0.28	0.03	0.23	0.02	0.17	0.02	0.11	0.01	0.03	0.01
40 000.00	0.20	0.02	0.15	0.01	0.12	0.02	0.10	0.02	0.06	0.00	0.02	0.00
60 000.00	0.16	0.03	0.11	0.02	0.09	0.01	0.07	0.01	0.04	0.01	0.01	0.00
80 000.00	0.12	0.02	0.08	0.02	0.07	0.02	0.05	0.02	0.04	0.01	0.01	0.00
100 000.00	0.09	0.01	0.06	0.02	0.06	0.02	0.04	0.01	0.02	0.01	0.01	0.00
200 000.00	0.05	0.01	0.03	0.02	0.03	0.01	0.02	0.02	0.01	0.01	0.00	0.00
400 000.00	0.01	0.02	0.01	0.01	0.00	0.00	0.00	0.01	0.01	0.01	0.00	0.00
600 000.00	0.02	0.02	0.01	0.01	0.02	0.01	0.01	0.01	0.00	0.01	0.00	0.00
800 000.00	0.02	0.02	0.00	0.00	0.02	0.02	0.00	0.00	0.01	0.01	0.00	0.00
1 000 000.00	0.01	0.01	0.00	0.00	0.00	0.01	0.00	0.01	0.00	0.01	0.00	0.00

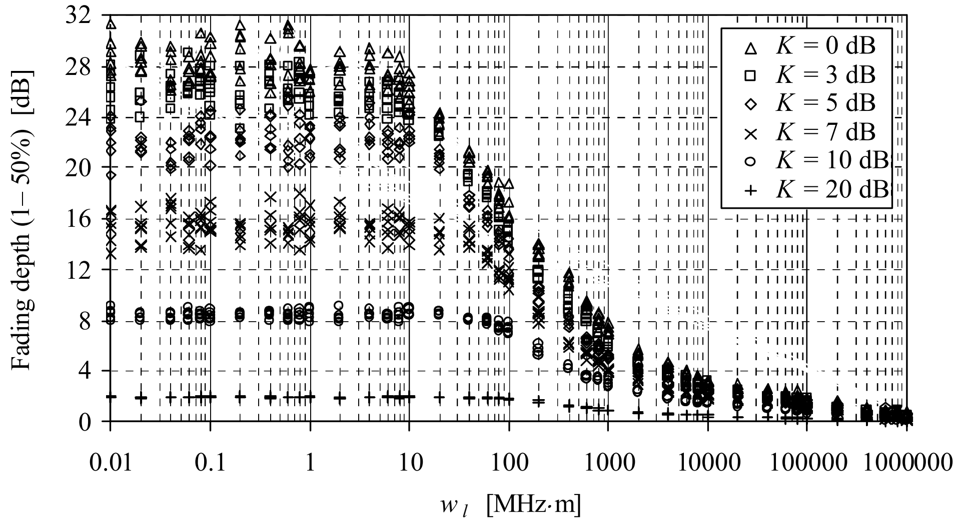

Figure I.1 – Simulation results, p = 0.1 %.

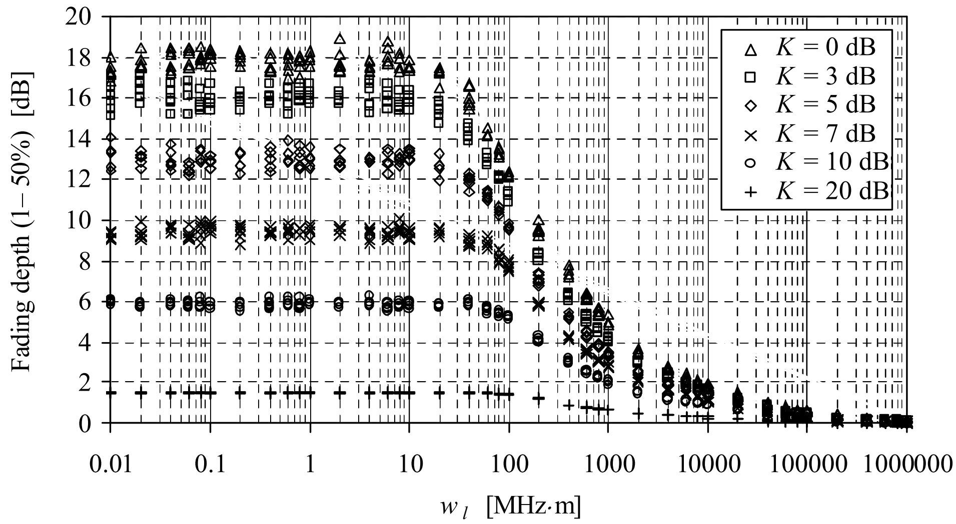

Figure I.2 – Simulation results, p = 1 %.

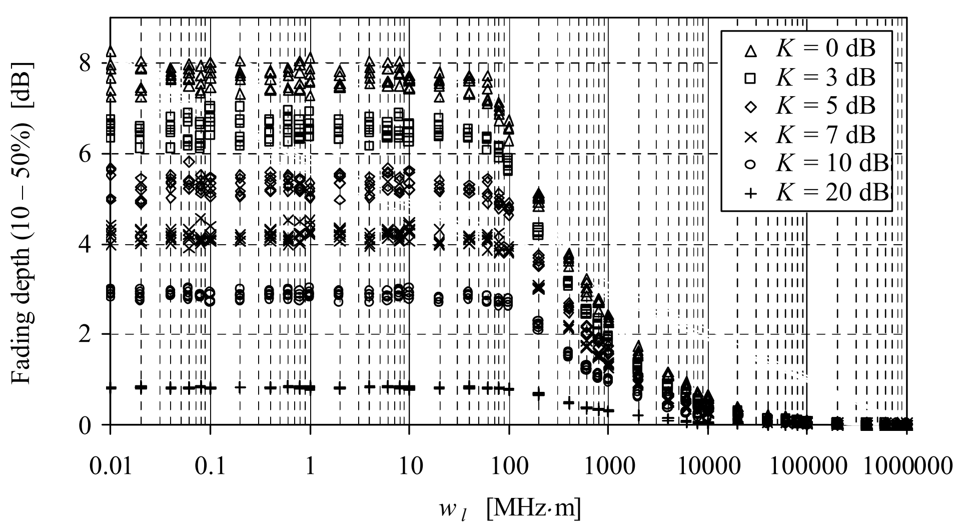

Figure I.3 – Simulation results, p = 10 %.

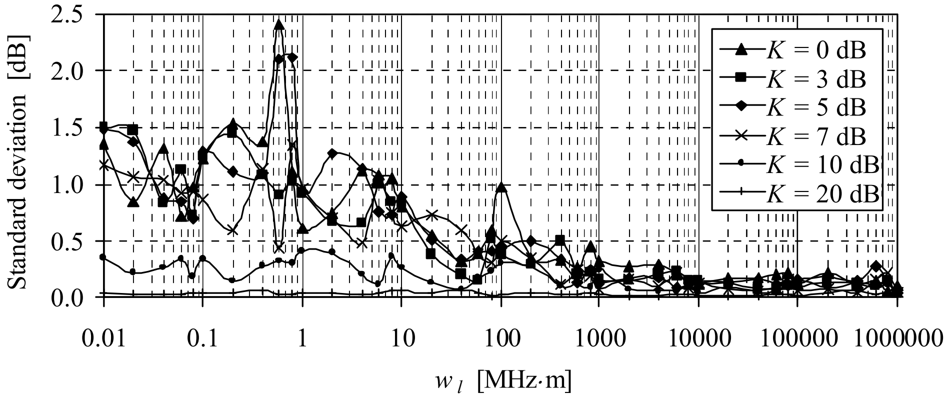

Figure I.4 – Standard deviation, p = 0.1 %.

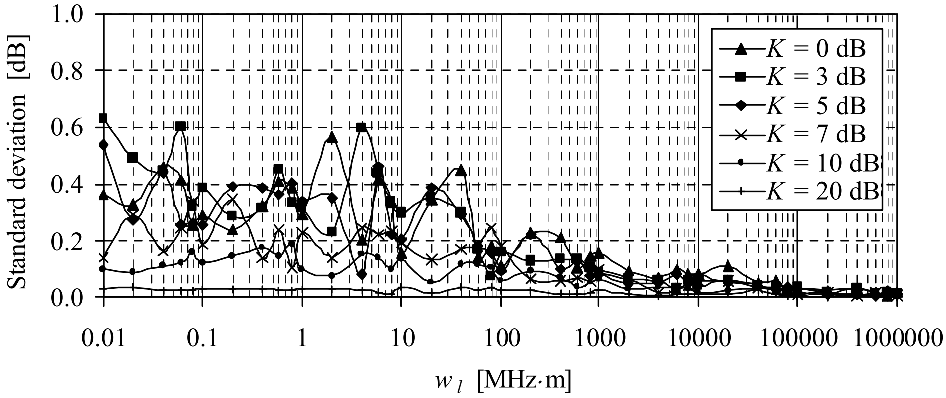

Figure I.5 – Standard deviation, p = 1 %.

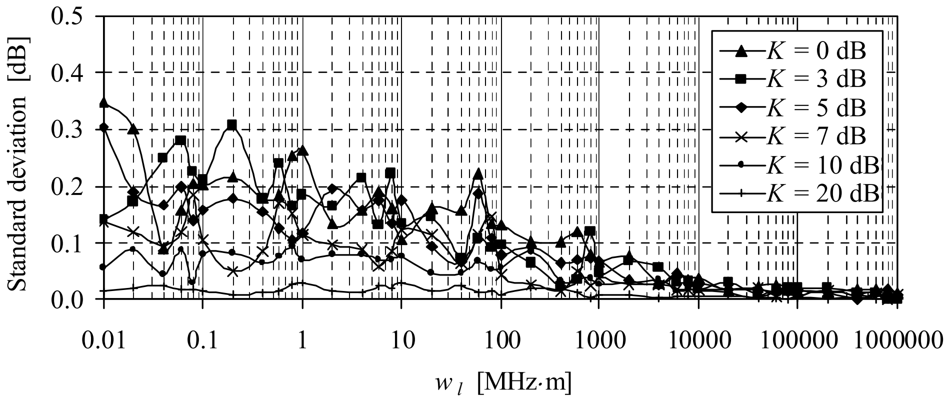

Figure I.6 – Standard deviation, p = 10 %.

I.2. Fitting Results for p = 0.1 %

Table I.4 – Fitting of S and associated error, p = 0.1 %.

S						
b_1	b_2	b_3	b_4	b_5	$\sqrt{\overline{\varepsilon^2}}$ [dB]	$\overline{\varepsilon_r}$ [%]
28.152	1.256	1.323	-0.201	4.191	0.26	0.2

Table I.5 – Fitting of A_i and associated error, p = 0.1 %.

	A_1	A_2	A_3
c_{11}	0.505	0.105	0.464
c_{12}	1.793	0.566	0.688
c_{13}	5.219	3.420	3.450
c_{14}	0.741	0.029	2.881
$\sqrt{\overline{\varepsilon^2}}$	0.023	0.009	0.029
$\overline{\varepsilon_r}$ [%]	–	0.4	0.0

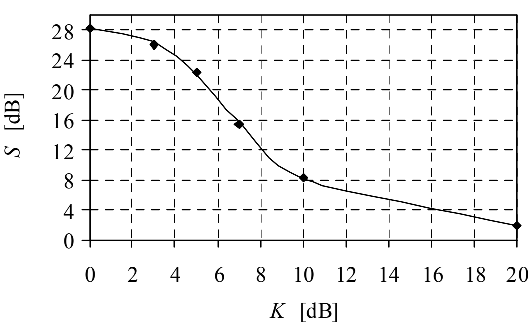

a) S

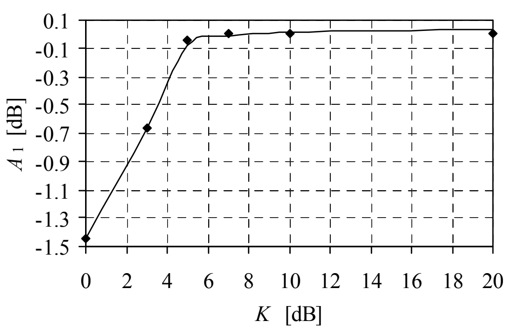

b) A_1

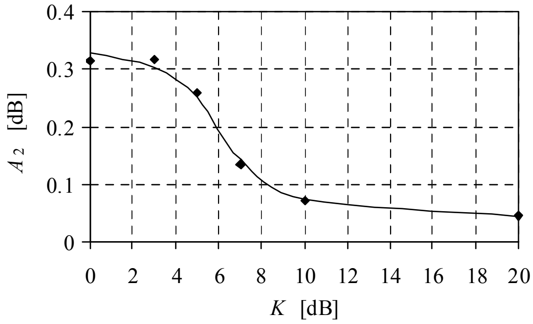

c) A_2

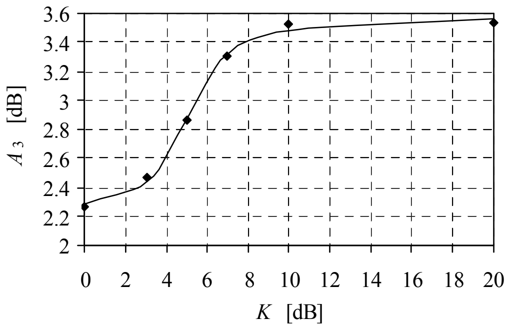

d) A_3

Figure I.7 – Fitting of parameters S, A_1, A_2 and A_3, p = 0.1 %.

Table I.6 – Calculated parameters and associated, p = 0.1 %.

	K [dB]					
	0	3	5	7	10	20
S [dB]	28.11	26.32	21.97	15.76	8.24	1.98
A_1 [dB]	-1.44	-0.66	-0.08	-0.02	0.01	0.04
A_2	0.329	0.304	0.250	0.142	0.073	0.042
A_3	2.283	2.442	2.876	3.317	3.478	3.565
$\sqrt{\overline{\varepsilon^2}}$ [dB]	0.56	0.56	0.53	0.45	0.27	0.06
$\overline{\varepsilon_r}$ [%]	3.1	-4.0	4.0	4.4	4.6	-1.4

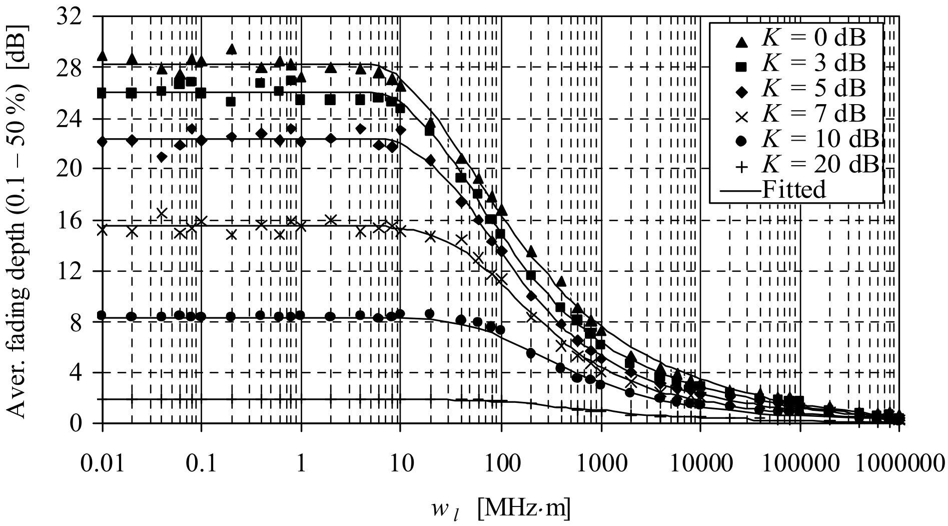

Figure I.8 – Fading depth fitting results, p = 0.1 %.

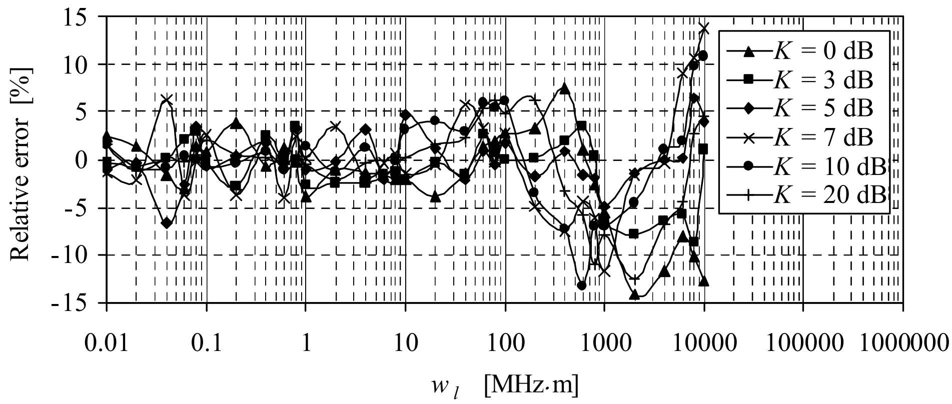

Figure I.9 – Approximation relative error, p = 0.1 %.

I.3. Fitting Results for p = 10 %

Table I.7 – Fitting of S and associated error, p = 10 %.

S						
b_1	b_2	b_3	b_4	b_5	$\sqrt{\overline{\varepsilon^2}}$ [dB]	$\overline{\varepsilon_r}$ [%]
8.080	0.070	0.690	-0.410	2.943	0.03	0.2

Table I.8 – Fitting of A_i and associated error, p = 10 %.

	A_1	A_2	A_3
c_{11}	0.289	0.141	0.452
c_{12}	0.225	0.338	0.180
c_{13}	0.349	2.650	0.689
c_{14}	0.421	0.610	2.295
$\sqrt{\overline{\varepsilon^2}}$	0.010	0.023	0.022
$\overline{\varepsilon_r}$ [%]	-1.6	0.0	-0.1

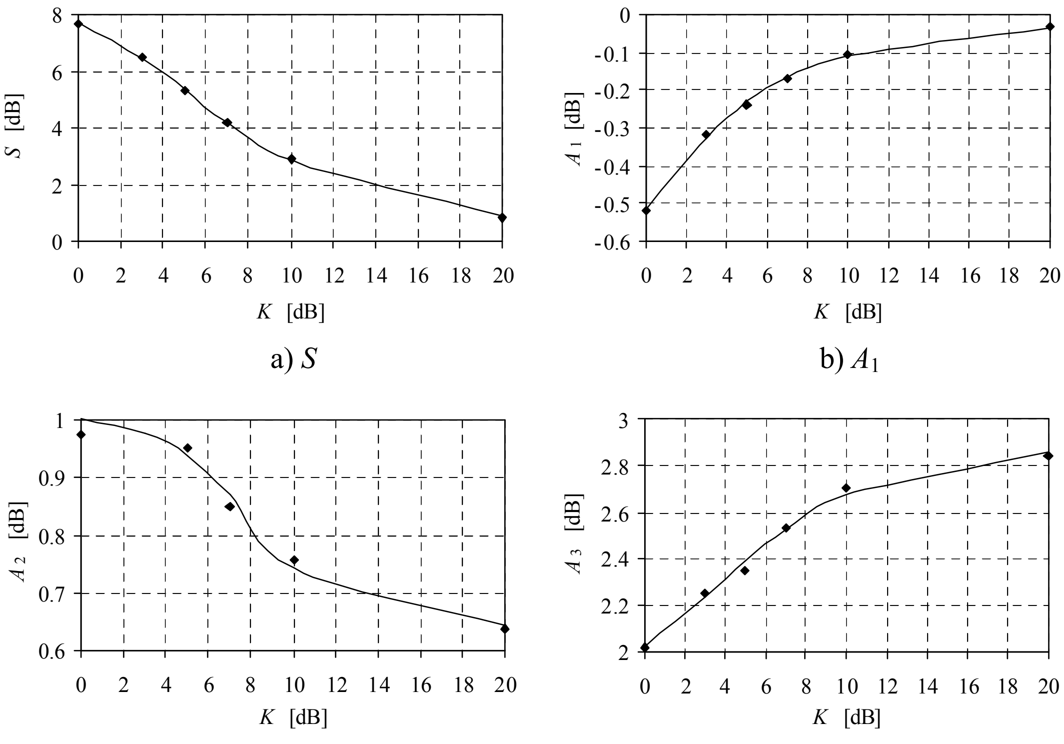

a) S b) A_1

c) A_2 d) A_3

Figure I.10 – Fitting of parameters S, A_1, A_2 and A_3, p = 10 %.

Table I.9 – Calculated parameters and associated error, p = 10 %.

	K [dB]					
	0	3	5	7	10	20
S [dB]	7.70	6.47	5.33	4.20	2.84	0.86
A_1 [dB]	-0.52	-0.32	-0.23	-0.17	-0.11	-0.06
A_2	1.002	0.976	0.940	0.870	0.743	0.643
A_3	2.022	2.228	2.389	2.530	2.674	2.855
$\sqrt{\overline{\varepsilon^2}}$ [dB]	0.08	0.08	0.08	0.06	0.04	0.02
$\overline{\varepsilon_r}$ [%]	-4.3	-8.7	-5.6	-5.2	-7.7	-4.2

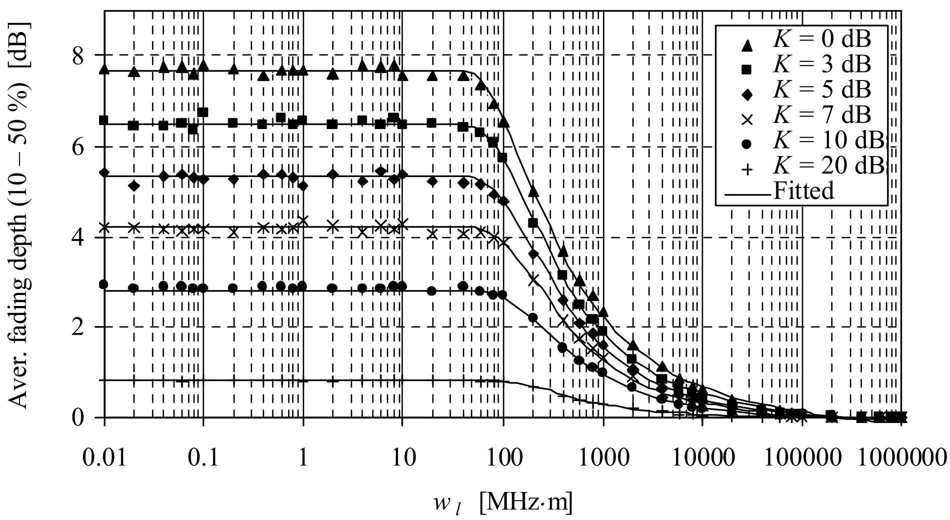

Figure I.11 – Fading depth fitting results, p = 10 %.

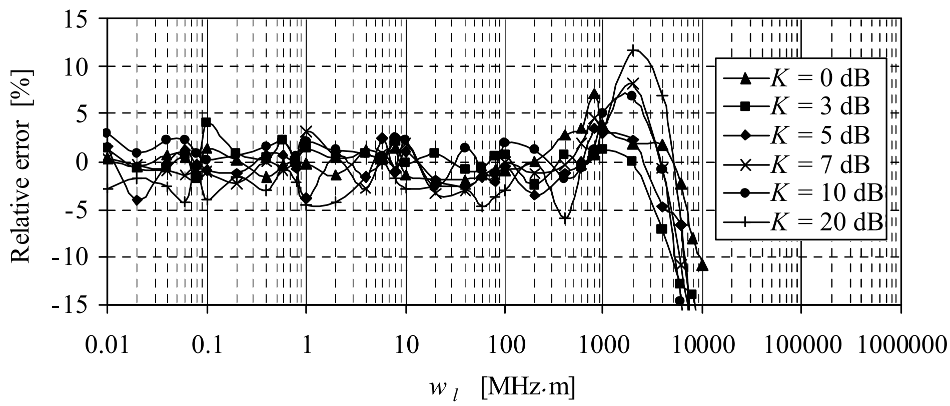

Figure I.12 – Approximation relative error, p = 10 %.

I.4. Fading depth in the micro-cellular environment, $p = 1$ %

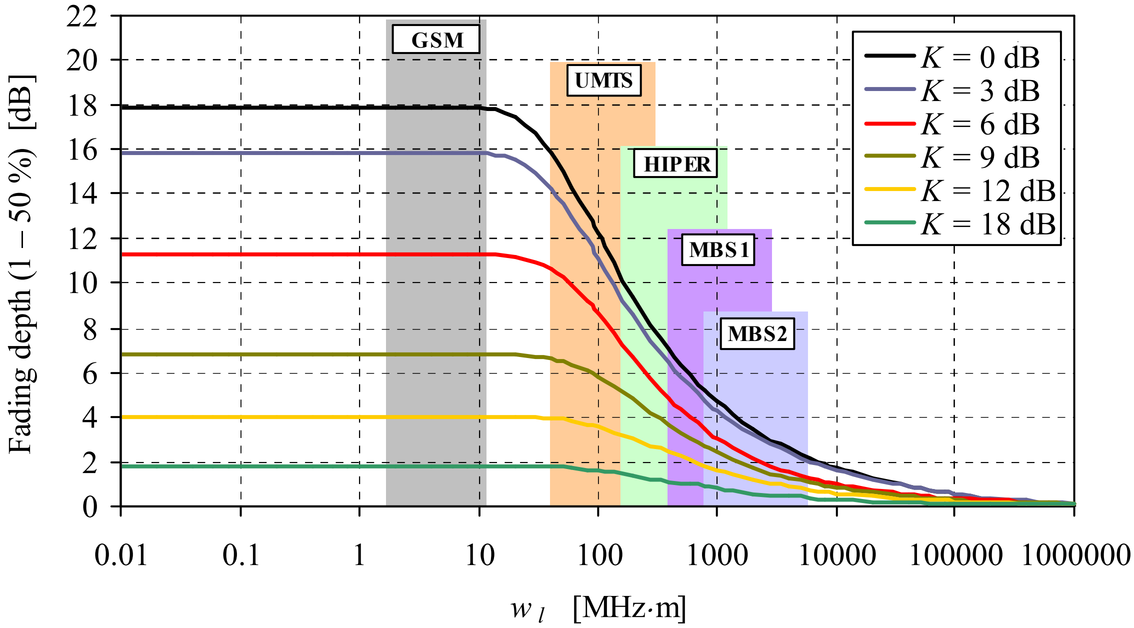

Figure I.13 – Fading depth at $d = 0$ m.

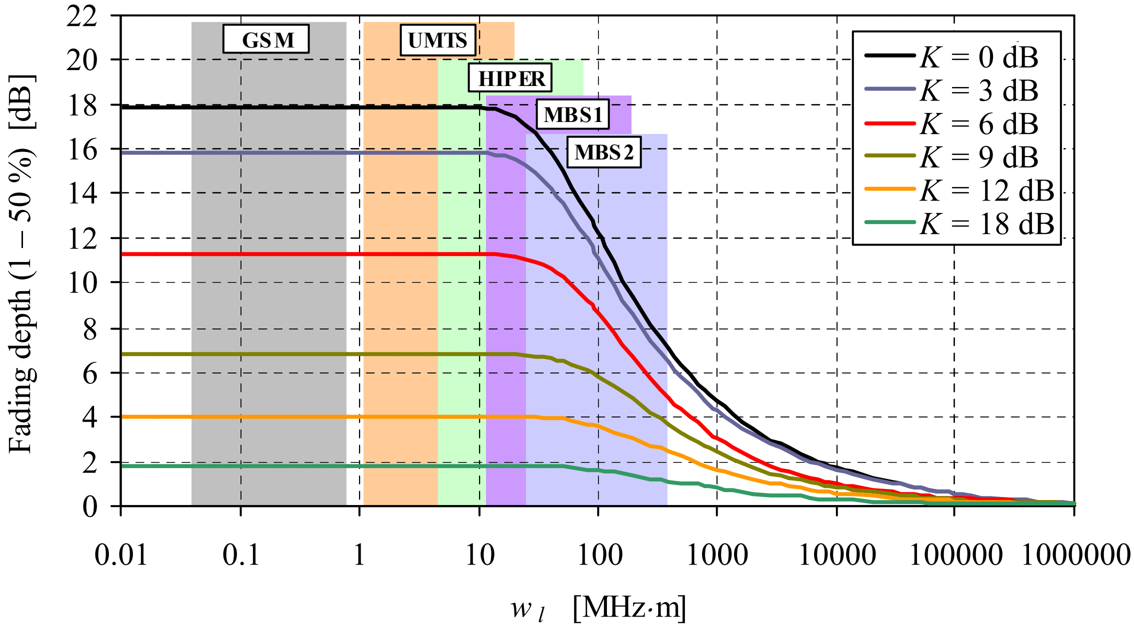

Figure I.14 – Fading depth at $d = 1\,000$ m.

Appendix II

Influence of PDP Parameters

As described in Chapter V, the difference in fading depth between exponential and two-stage exponential PDPs is illustrated for different PDP parameters.

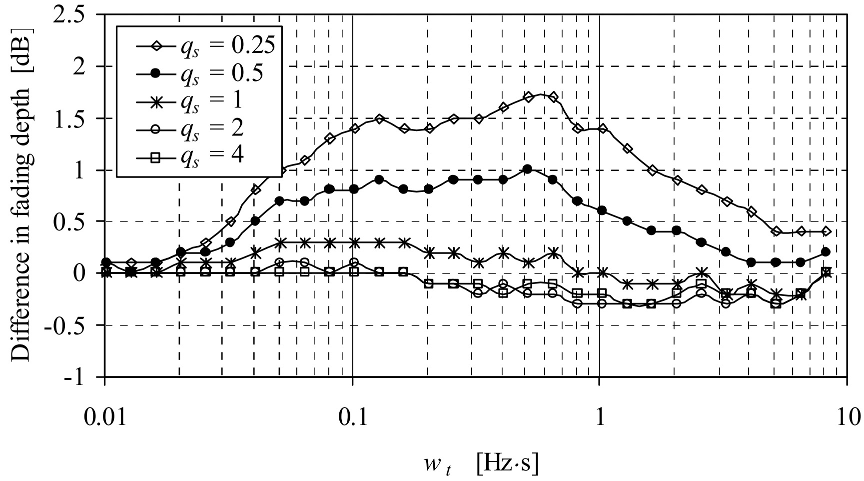

Figure II.1 – Difference between exponential and two-stage exponential PDPs, $\tau_2 = 2\cdot\sigma_{\tau,1}$.

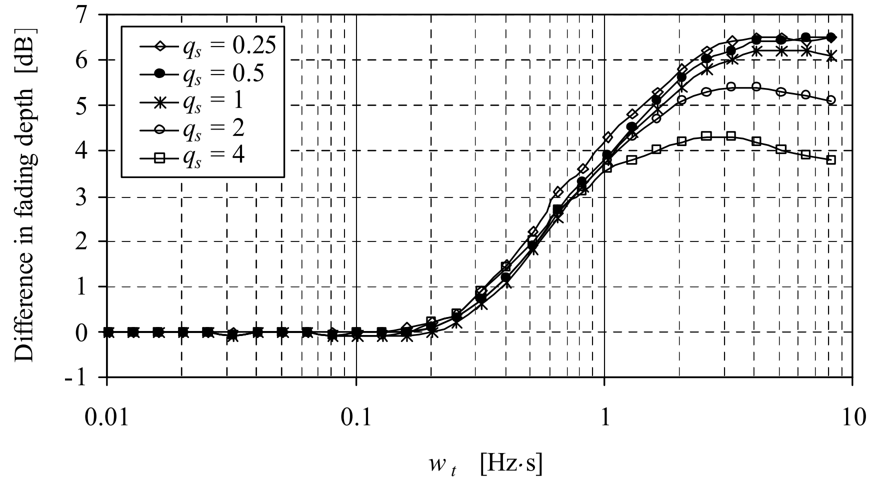

Figure II.2 – Difference between exponential and two-stage exponential PDPs, $\tau_2 = 80\cdot\sigma_{\tau,1}$.

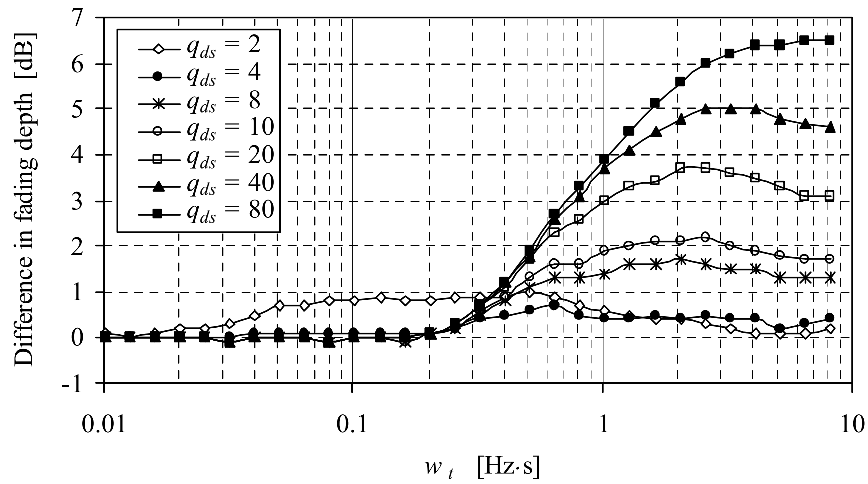

Figure II.3 – Difference between exponential and two-stage exponential PDPs, $\sigma_{\tau,2} = 0.5\cdot\sigma_{\tau,1}$.

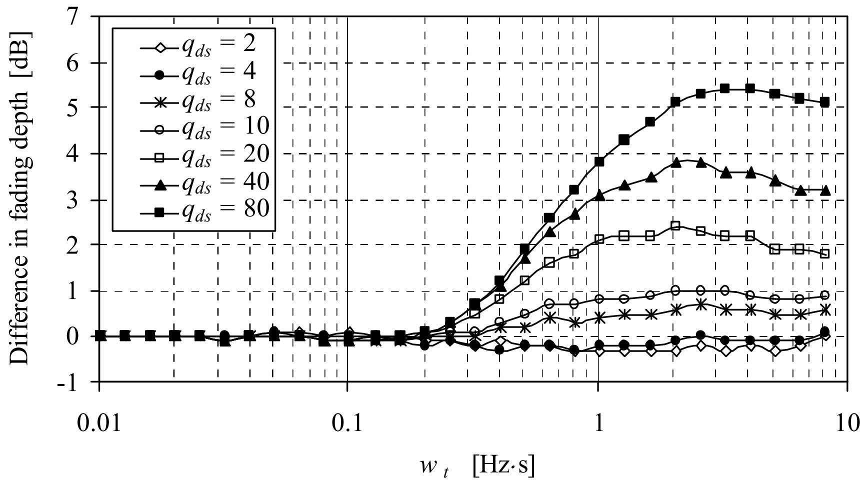

Figure II.4 – Difference between exponential and two-stage exponential PDPs, $\sigma_{\tau,2} = 2 \cdot \sigma_{\tau,1}$.

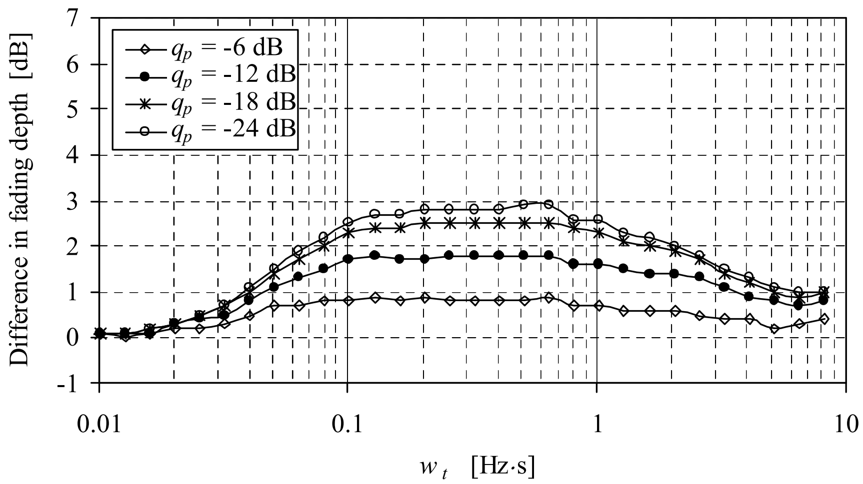

Figure II.5 – Difference between exponential and two-stage exponential PDPs, $\tau_2 = 2 \cdot \sigma_{\tau,1}$.

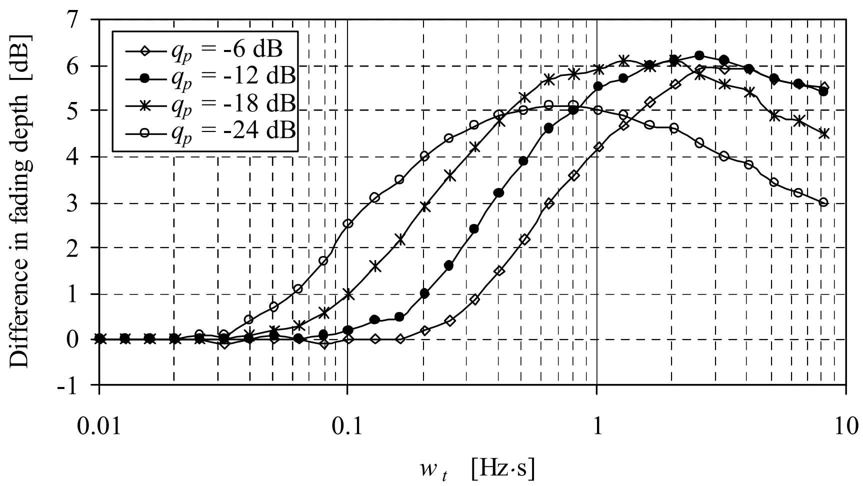

Figure II.6 – Difference between exponential and two-stage exponential PDPs, $\tau_2 = 80 \cdot \sigma_{\tau,1}$.

Appendix III

GSM Continuous Channel Models

In this Appendix, continuous PDPs for GSM in different standard reference environments and the corresponding eigenvalue characteristics are presented.

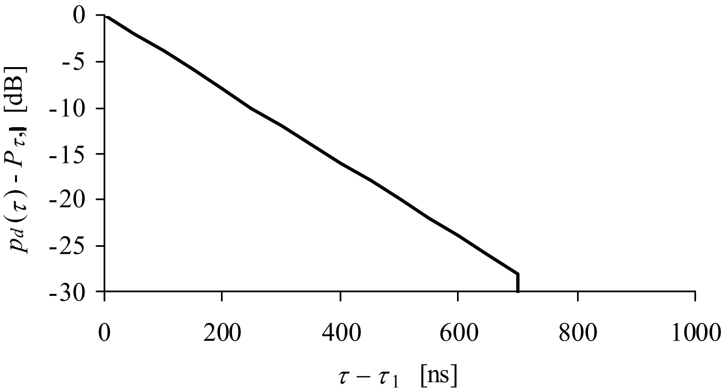

Figure III.1 – PDP, GSM Rural Area.

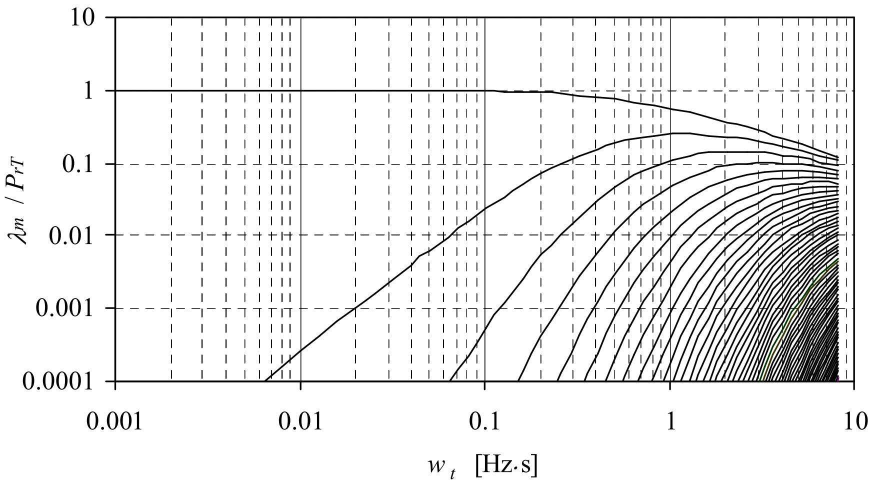

Figure III.2 – Eigenvalue characteristics, GSM Rural Area.

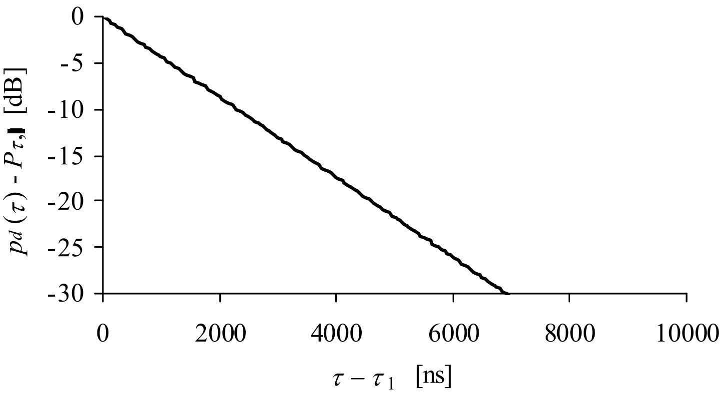

Figure III.3 – PDP, GSM Typical Urban.

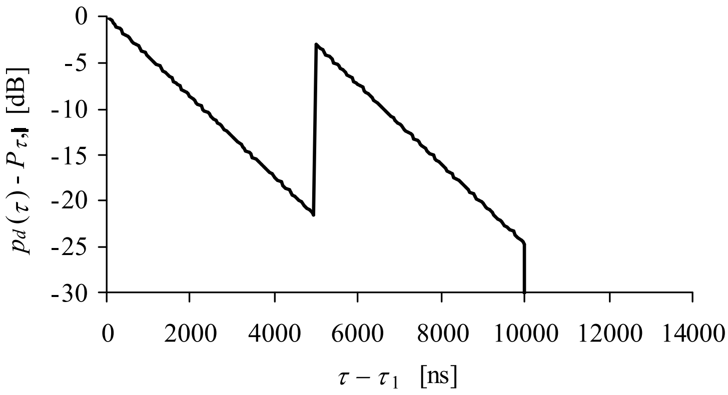

Figure III.4 – PDP, GSM Bad Urban.

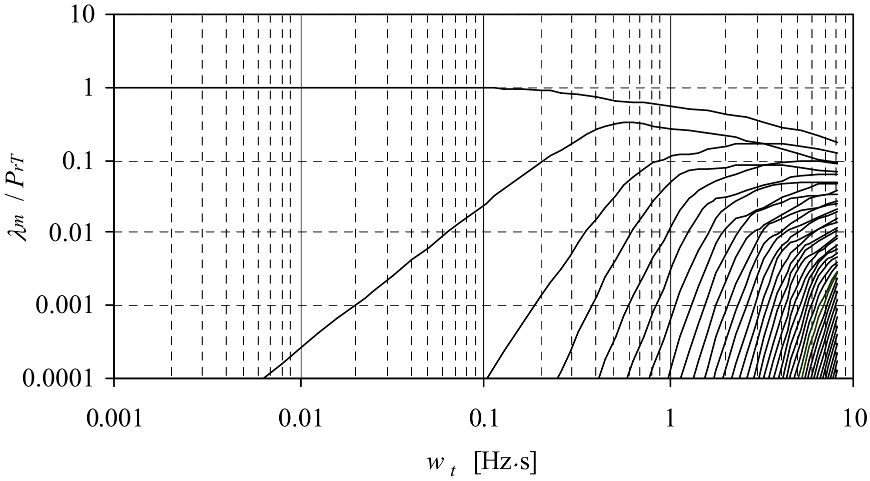

Figure III.5 – Eigenvalue characteristics, GSM Bad Urban.

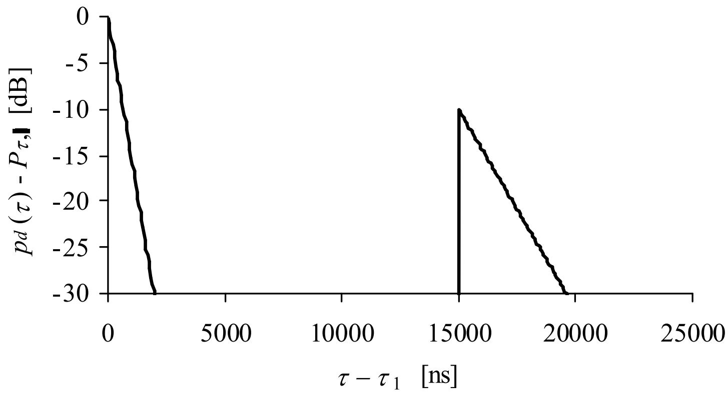

Figure III.6 – PDP, GSM Hilly Terrain.

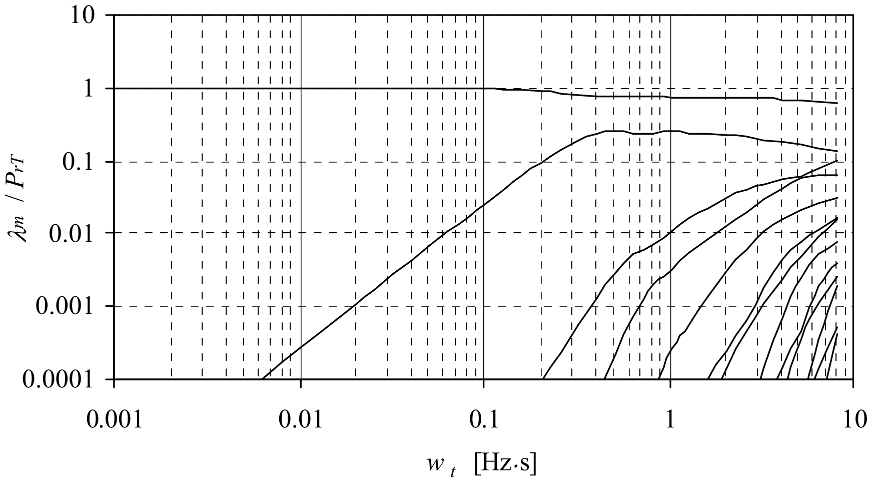

Figure III.7 – Eigenvalue characteristics, GSM Hilly Terrain.

Appendix IV

Tap-Setting for Discrete Channel Models

In this Appendix, tapped-delay line parameters for GSM [ETSI99], UMTS [ETSI97], [3GPP02a], and HIPERLAN/2 [MeSc98] channel models, as recommended by standard-setting bodies, are presented.

IV.1. GSM Channel Models

Table IV.1 – Tapped-delay line parameters, GSM Rural Area.

	Rural Area - Type 1		Rural Area - Type 2	
Tap	τ_i - τ_1 [ns]	P_i - $P_{i_{max}}$ [dB]	τ_i - τ_1 [ns]	P_i - $P_{i_{max}}$ [dB]
1	0	0.0	0	0.0
2	100	-4.0	200	-2.0
3	200	-8.0	400	-10.0
4	300	-12.0	600	-20.0
5	400	-16.0	–	–
6	500	-20.0	–	–

Table IV.2 – Tapped-delay line parameters, GSM Typical Urban.

	Typical Urban - Type 1		Typical Urban - Type 2	
Tap	τ_i - τ_1 [ns]	P_i - $P_{i_{max}}$ [dB]	τ_i - τ_1 [ns]	P_i - $P_{i_{max}}$ [dB]
1	0	-4.0	0	-4.0
2	100	-3.0	200	-3.0
3	300	0.0	400	0.0
4	500	-2.6	600	-2.0
5	800	-3.0	800	-3.0
6	1 100	-5.0	1 200	-5.0
7	1 300	-7.0	1 400	-7.0
8	1 700	-5.0	1 800	-5.0
9	2 300	-6.5	2 400	-6.0
10	3 100	-8.6	3 000	-9.0
11	3 200	-11.0	3 200	-11.0
12	5 000	-10.0	5 000	-10.0

Table IV.3 – Tapped-delay line parameters, GSM Bad Urban.

	Bad Urban - Type 1		Bad Urban - Type 2	
Tap	τ_i - τ_1 [ns]	P_i - $P_{i_{max}}$ [dB]	τ_i - τ_1 [ns]	P_i - $P_{i_{max}}$ [dB]
1	0	-7.7	0	-7.0
2	100	-3.4	200	-3.0
3	300	-1.3	400	-1.0
4	700	0.0	800	0.0
5	1600	-2.3	1 600	-2.0
6	2 200	-5.6	2 200	-6.0
7	3 100	-7.4	3 200	-7.0
8	5 000	-1.4	5 000	-1.0
9	6 000	-1.6	6 000	-2.0
10	7 200	-6.7	7 200	-7.0
11	8 100	-9.8	8 200	-10.0
12	10 000	-15.1	10 000	-15.0

Table IV.4 – Tapped-delay line parameters, GSM Hilly Terrain.

	Hilly Terrain - Type 1		Hilly Terrain - Type 2	
Tap	τ_i - τ_1 [ns]	P_i - $P_{i_{max}}$ [dB]	τ_i - τ_1 [ns]	P_i - $P_{i_{max}}$ [dB]
1	0	-10.0	0	-10.0
2	100	-8.0	200	-8.0
3	300	-6.0	400	-6.0
4	500	-4.0	600	-4.0
5	700	0.0	800	0.0
6	1 000	0.0	2 000	0.0
7	1 300	-4.0	2 400	-4.0
8	15 000	-8.0	15 000	-8.0
9	15 200	-9.0	15 200	-9.0
10	15 700	-10.0	15 800	-10.0
11	17 200	-12.0	17 200	-12.0
12	20 000	-14.0	20 000	-14.0

IV.2. UMTS Channel Models

Table IV.5 – Tapped-delay line parameters, UMTS Vehicular.

	Vehicular-A		Vehicular-B	
Tap	τ_i - τ_1[ns]	P_i - $P_{i_{max}}$ [dB]	τ_i - τ_1 [ns]	P_i - $P_{i_{max}}$ [dB]
1	0	0.0	0	-2.5
2	310	-1.0	300	0.0
3	710	-9.0	8 900	-12.8
4	1090	-10.0	12 900	-10.0
5	1730	-15.0	17 100	-25.2
6	2510	-20.0	20 000	-16.0

Table IV.6 – Tapped-delay line parameters, UMTS Indoor.

	Indoor-A		Indoor-B	
Tap	τ_i - τ_1 [ns]	P_i - $P_{i_{max}}$ [dB]	τ_i - τ_1 [ns]	P_i - $P_{i_{max}}$ [dB]
1	0	0.0	0	0.0
2	50	-3.0	100	-3.6
3	110	-10.0	200	-7.2
4	170	-18.0	300	-10.8
5	290	-26.0	500	-18.0
6	310	-32.0	700	-25.2

Table IV.7 – Tapped-delay line parameters, UMTS Indoor to Outdoor and Pedestrian.

	Indoor to Outdoor and Pedestrian-A		Indoor to Outdoor and Pedestrian-B	
Tap	τ_i - τ_1 [ns]	P_i - $P_{i_{max}}$ [dB]	τ_i - τ_1 [ns]	P_i - $P_{i_{max}}$ [dB]
1	0	0.0	0	0.0
2	110	-9.7	200	-0.9
3	190	-19.2	800	-4.9
4	410	-22.8	1 200	-8.0
5	–	–	2 300	-7.8
6	–	–	3 700	-23.9

Table IV.8 – Tapped-delay line parameters, UMTS Rural Area.

	Rural Area	
Tap	τ_i - τ_1 [ns]	P_i - $P_{i_{max}}$ [dB]
1	0	0.0
2	42	-1.2
3	101	-3.2
4	129	-4.1
5	149	-4.8
6	245	-7.9
7	312	-10.1
8	410	-13.3
9	469	-15.2
10	528	-17.2

Table IV.9 – Tapped-delay line parameters, UMTS Typical Urban and Hilly Terrain.

	Typical Urban		Hilly Terrain	
Tap	τ_i - τ_1 [ns]	P_i - $P_{i_{max}}$ [dB]	τ_i - τ_1 [ns]	P_i - $P_{i_{max}}$ [dB]
1	0	0.0	0	0.0
2	217	-1.9	356	-5.3
3	512	-4.4	441	-6.6
4	514	-4.5	528	-7.9
5	517	-4.5	546	-8.2
6	674	-5.8	609	-9.1
7	882	-7.7	625	-9.4
8	1 230	-10.6	842	-12.6
9	1 287	-11.2	916	-13.7
10	1 311	-11.4	941	-14.1
11	1 349	-11.7	15 000	-14
12	1 533	-13.3	16 172	-19.1
13	1 535	-13.3	16 492	-20.5
14	1 622	-14.1	16 876	-22.2
15	1 818	-15.8	16 882	-22.2
16	1 836	-15.9	16 978	-22.6
17	1 884	-16.4	17 615	-25.4
18	1 943	-16.9	17 827	-26.3
19	2 048	-17.8	17 849	-26.4
20	2 140	-18.6	18 016	-27.1

IV.3. HIPERLAN/2 Channel Models

Table IV.10 – Tapped-delay line parameters, HIPERLAN/2 Model A, B and C.

	Model A		Model B		Model C	
Tap	$\tau_i - \tau_1$ [ns]	$P_i - P_{i_{max}}$ [dB]	$\tau_i - \tau_1$ [ns]	$P_i - P_{i_{max}}$ [dB]	$\tau_i - \tau_1$ [ns]	$P_i - P_{i_{max}}$ [dB]
1	0	0.0	0	-2.6	0	-3.3
2	10	-0.9	10	-3.0	10	-3.6
3	20	-1.7	20	-3.5	20	-3.9
4	30	-2.6	30	-3.9	30	-4.2
5	40	-3.5	50	0.0	50	0.0
6	50	-4.3	80	-1.3	80	-0.9
7	60	-5.2	110	-2.6	110	-1.7
8	70	-6.1	140	-3.9	140	-2.6
9	80	-6.9	180	-3.4	180	-1.5
10	90	-7.8	230	-5.6	230	-3.0
11	110	-4.7	280	-7.7	280	-4.4
12	140	-7.3	330	- 9.9	330	-5.9
13	170	-9.9	380	-12.1	400	-5.3
14	200	-12.5	430	-14.3	490	-7.9
15	240	-13.7	490	-15.4	600	-9.4
16	290	-18.0	560	-18.4	730	-13.2
17	340	-22.4	640	-20.7	880	-16.3
18	390	-26.7	730	-24.6	1 050	-21.2

Table IV.11 – Tapped-delay line parameters, HIPERLAN/2 Model D and E.

	Model D		Model E	
Tap	τ_i - τ_1 [ns]	P_i - $P_{i_{max}}$ [dB]	τ_i - τ_1 [ns]	P_i - $P_{i_{max}}$ [dB]
1	0	0.0	0	-4.9
2	10	-10.0	10	-5.1
3	20	-10.3	20	-5.2
4	30	-10.6	40	-0.8
5	50	-6.4	70	-1.3
6	80	-7.2	100	-1.9
7	110	-8.1	140	-0.3
8	140	-9.0	190	-1.2
9	180	-7.9	240	-2.1
10	230	-9.4	320	0.0
11	280	-10.8	430	-1.9
12	330	-12.3	560	-2.8
13	400	-11.7	710	-5.4
14	490	-14.3	880	-7.3
15	600	-15.8	1 070	-10.6
16	730	-19.6	1 280	-13.4
17	880	-22.7	1 510	-17.4
18	1050	-27.6	1 760	-20.9

Appendix V

Discrete Channel Models

In this Appendix, discrete PDPs for GSM, UMTS and HIPERLAN/2 in different environments, as recommended by standard-setting bodies, and the corresponding eigenvalue characteristics, are presented.

V.1. GSM Channel Models

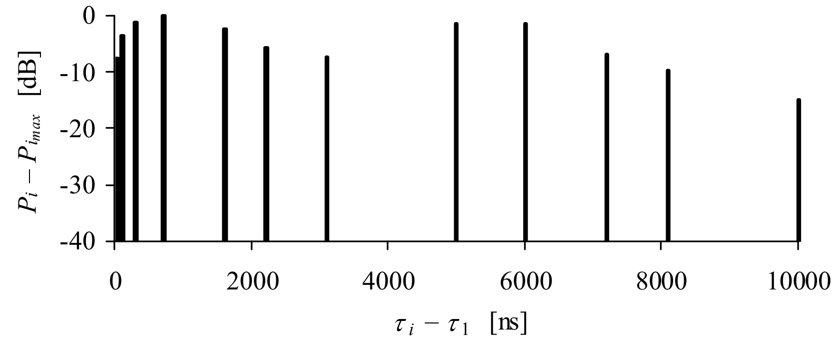

Figure V.1 – PDP, GSM Bad Urban.

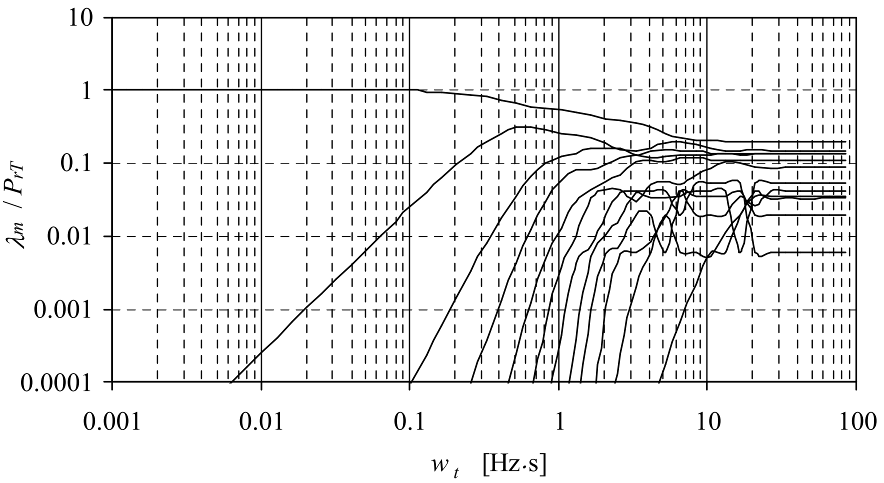

Figure V.2 – Eigenvalue characteristics, GSM Bad Urban.

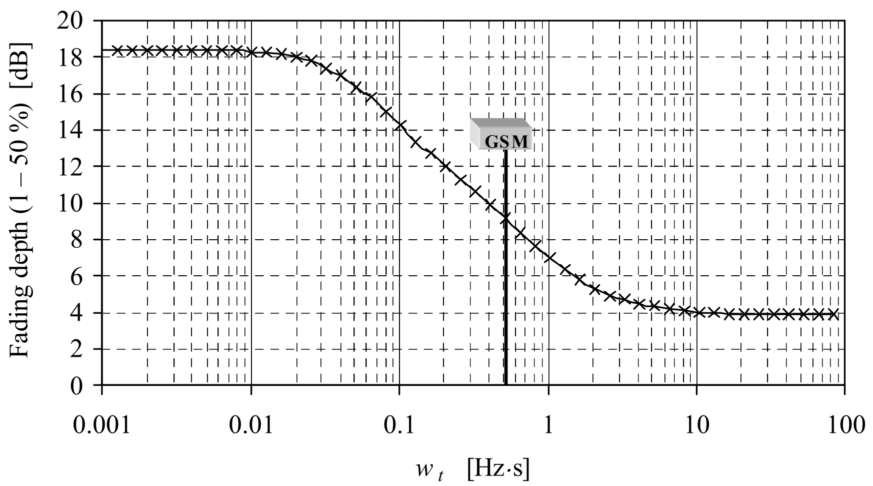

Figure V.3 – Fading depth, GSM Bad Urban.

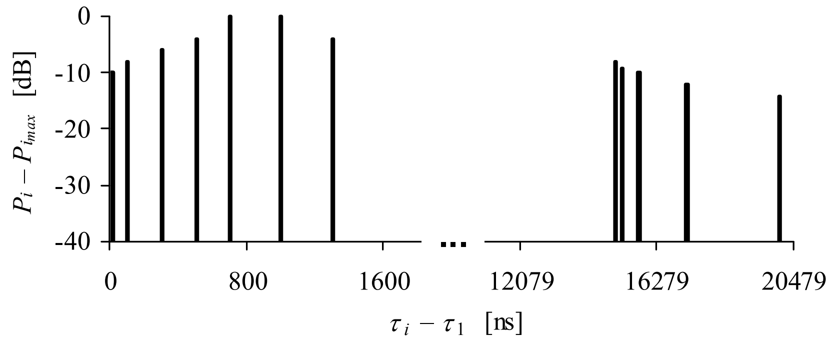

Figure V.4 – PDP, GSM Hilly Terrain.

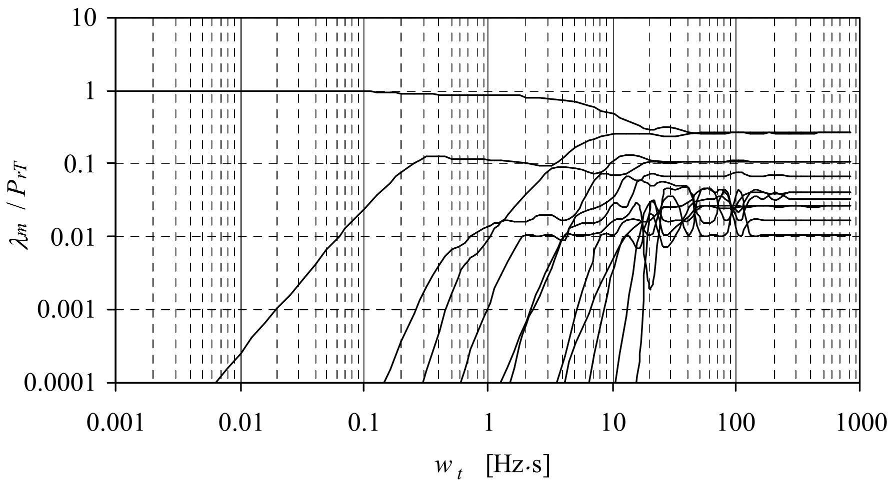

Figure V.5 – Eigenvalue characteristics, GSM Hilly Terrain.

V.2. UMTS Channel Models

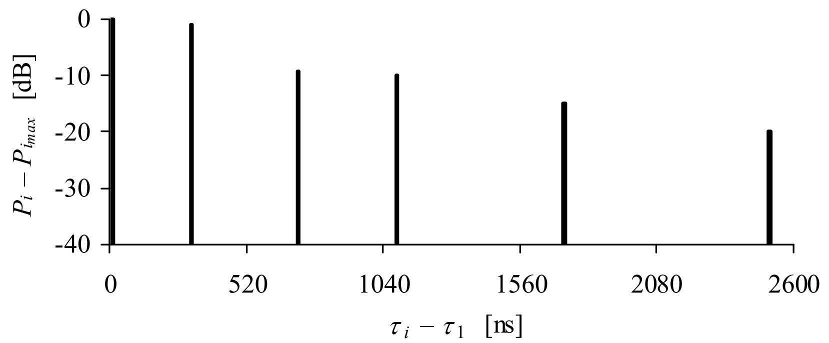

Figure V.6 – PDP, UMTS Vehicular-A.

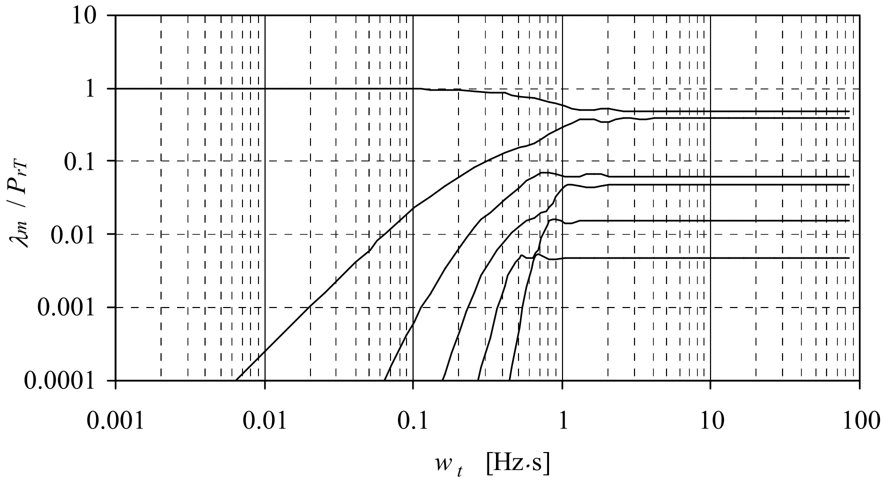

Figure V.7 – Eigenvalue characteristics, UMTS Vehicular-A.

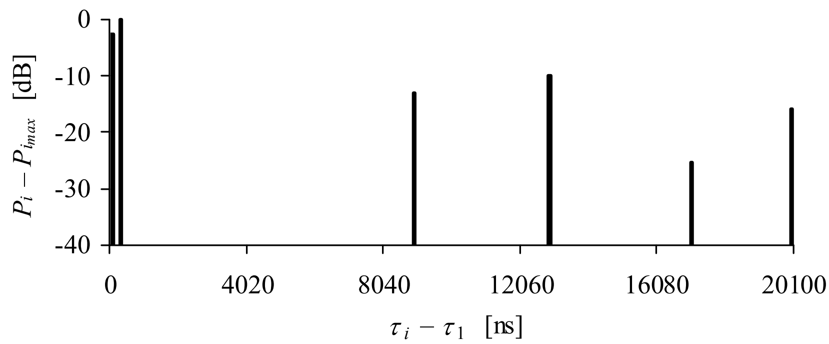

Figure V.8 – PDP, UMTS Vehicular-B.

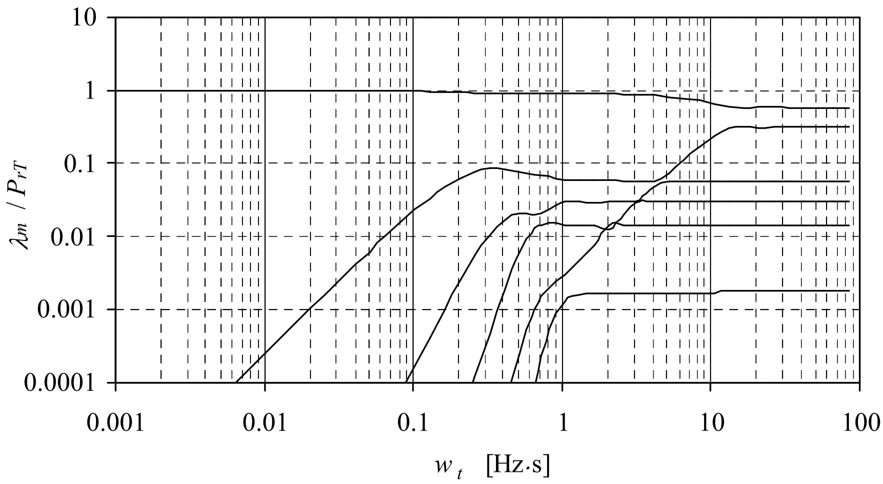

Figure V.9 – Eigenvalue characteristics, UMTS Vehicular-B.

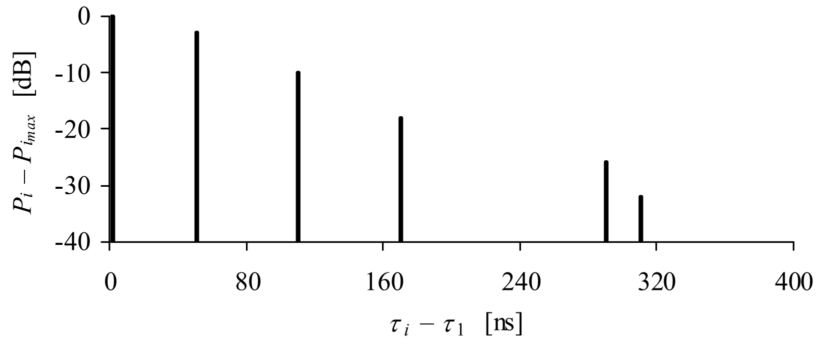

Figure V.10 – PDP, UMTS Indoor-A.

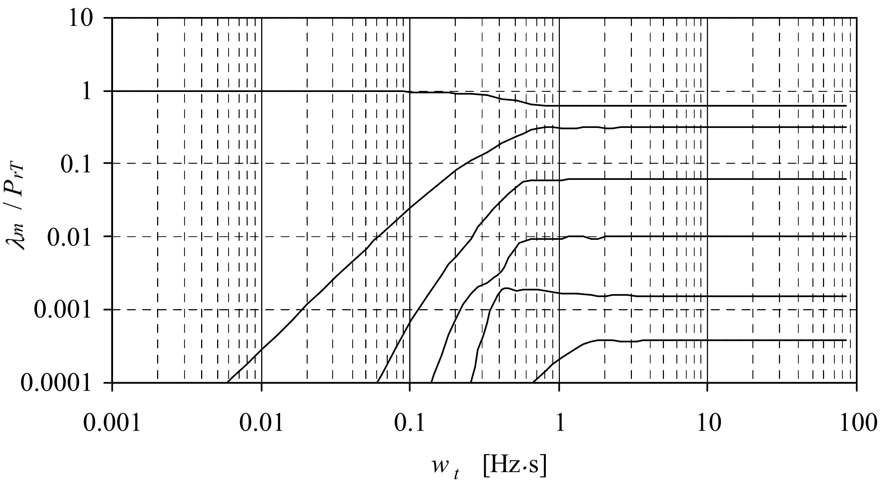

Figure V.11 – Eigenvalue characteristics, UMTS Indoor-A.

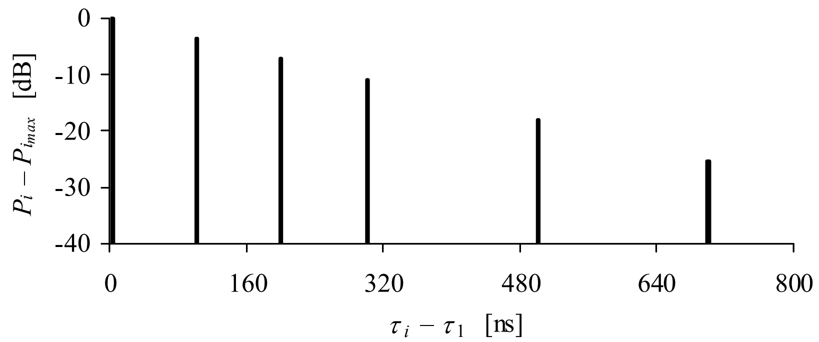

Figure V.12 – PDP, UMTS Indoor-B.

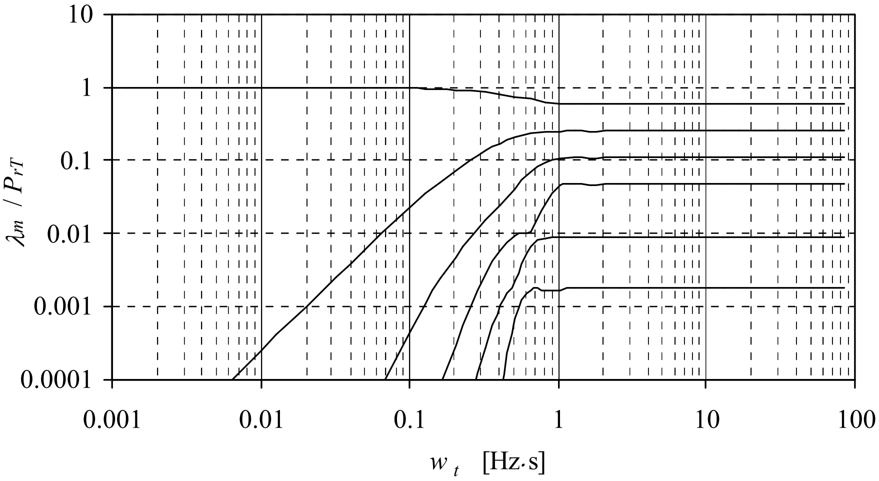

Figure V.13 – Eigenvalue characteristics, UMTS Indoor-B.

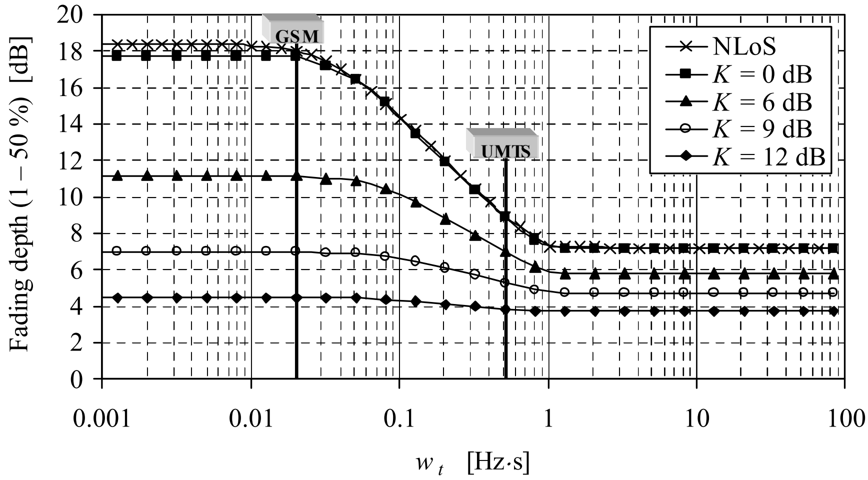

Figure V.14 – Fading depth, UMTS Indoor-B.

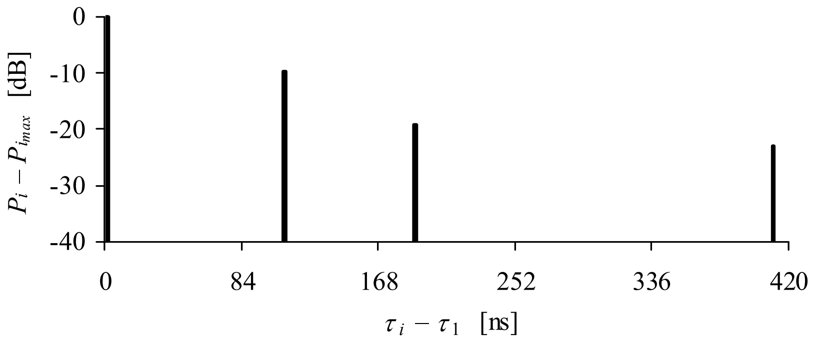

Figure V.15 – PDP, UMTS Pedestrian-A.

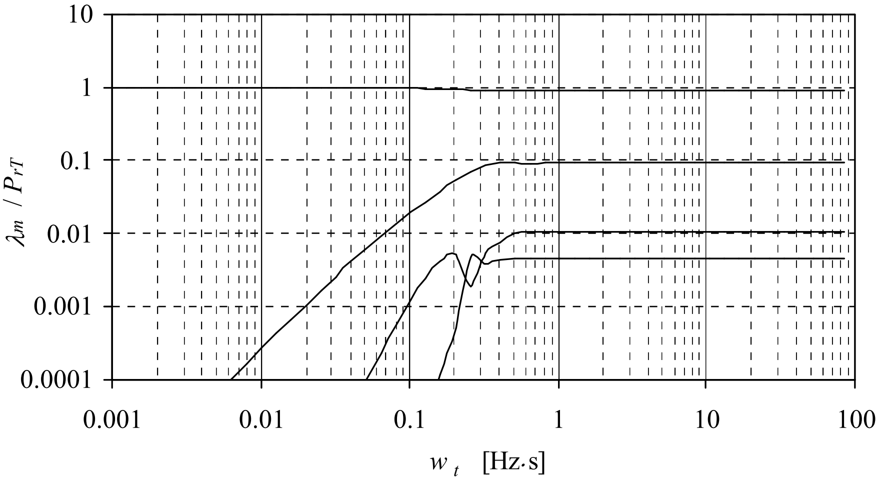

Figure V.16 – Eigenvalue characteristics, UMTS Pedestrian-A.

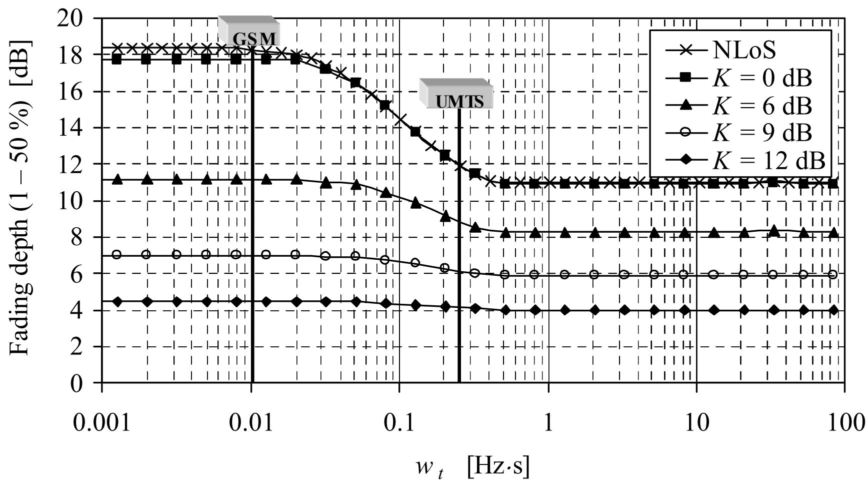

Figure V.17 – Fading depth, UMTS Pedestrian-A.

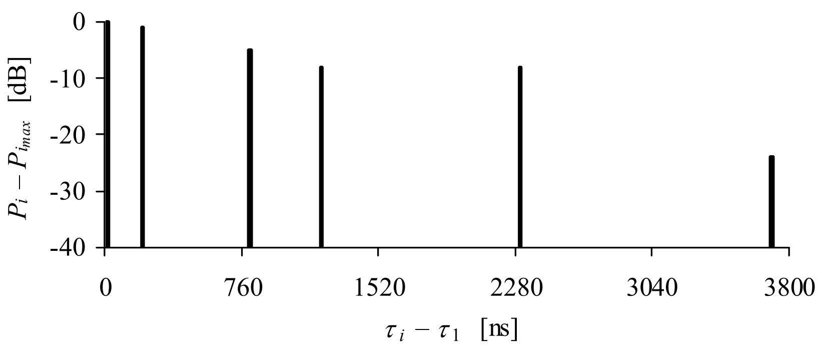

Figure V.18 – PDP, UMTS Pedestrian-B.

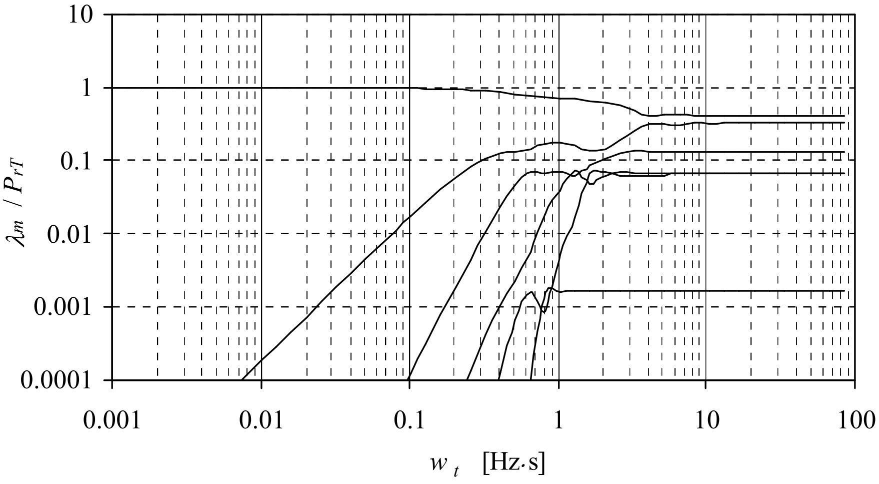

Figure V.19 – Eigenvalue characteristics, UMTS Pedestrian-B.

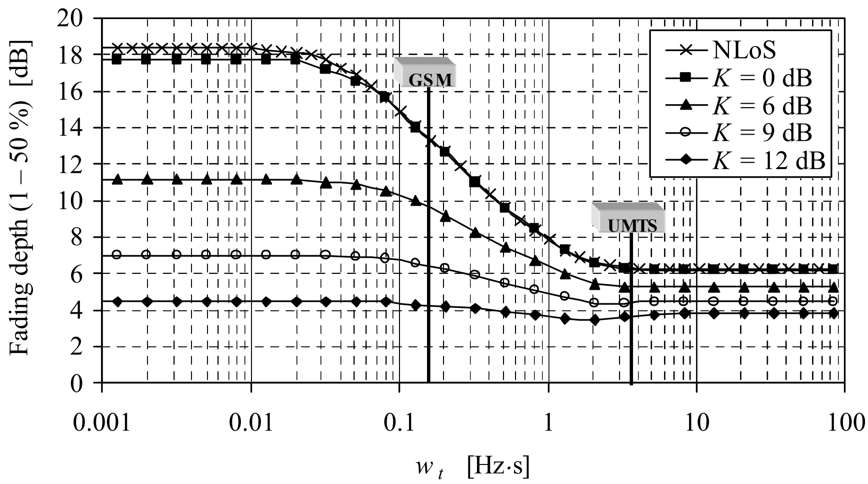

Figure V.20 – Fading depth, UMTS Pedestrian-B.

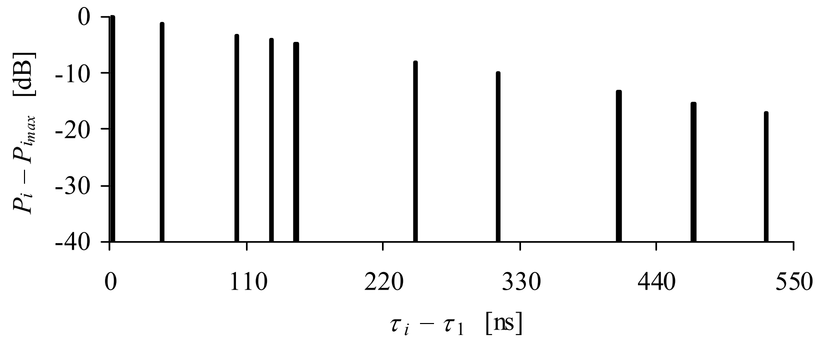

Figure V.21 – PDP, UMTS Rural Area.

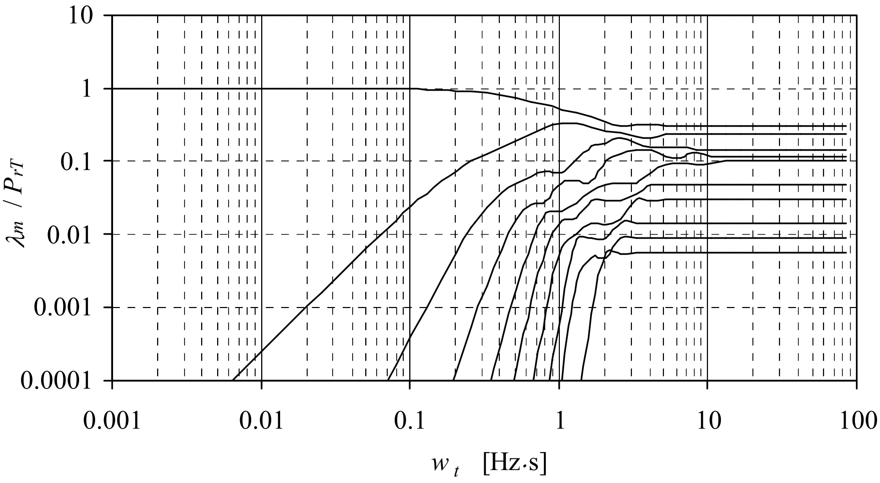

Figure V.22 – Eigenvalue characteristics, UMTS Rural Area.

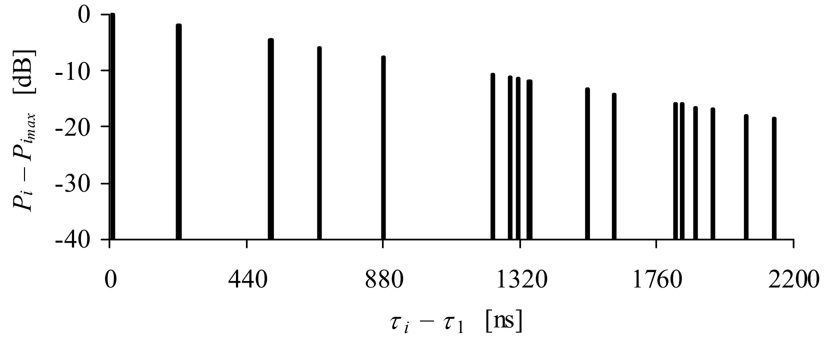

Figure V.23 – PDP, UMTS Typical Urban.

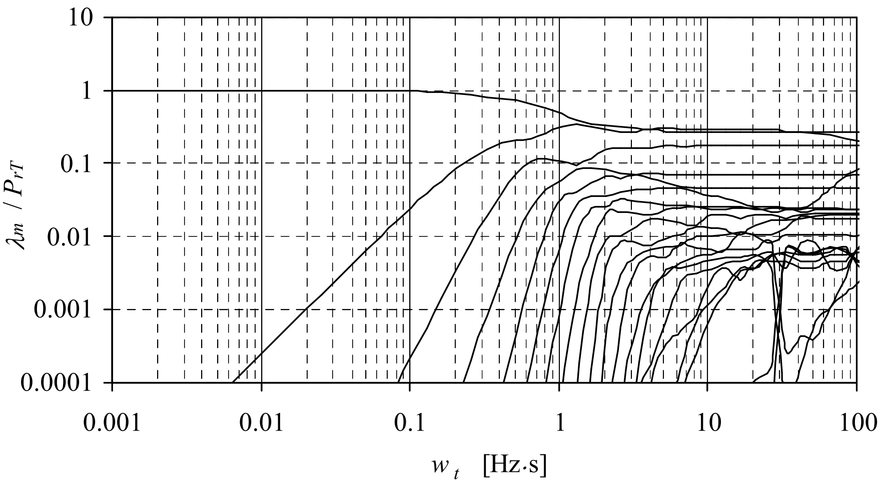

Figure V.24 – Eigenvalue characteristics, UMTS Typical Urban.

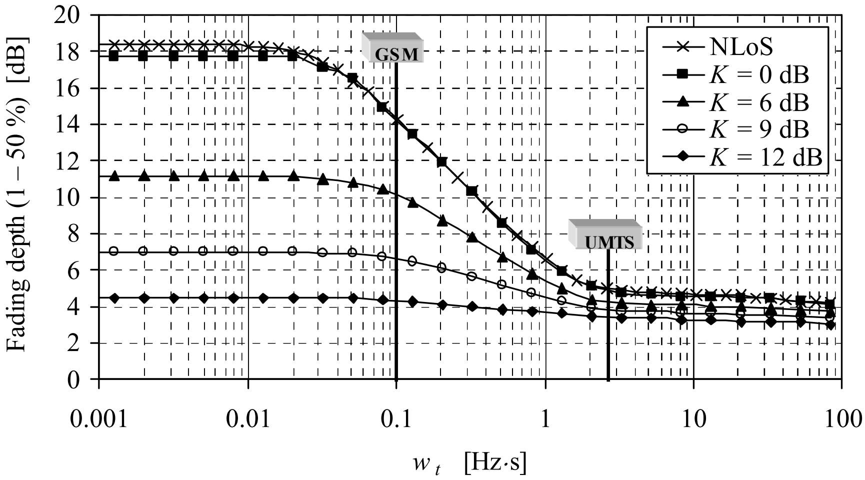

Figure V.25 – Fading depth, UMTS Typical Urban.

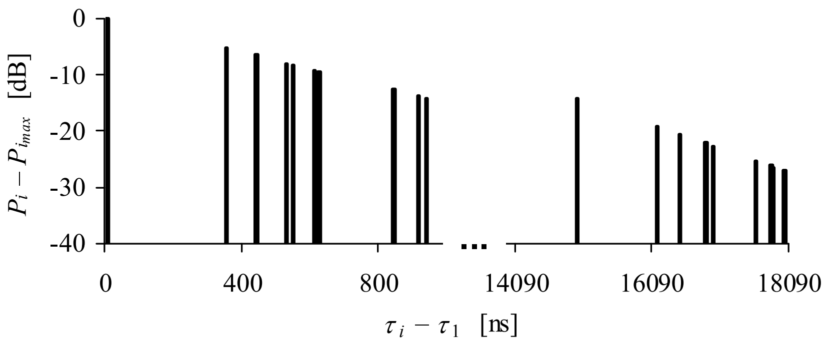

Figure V.26 – PDP, UMTS Hilly Terrain.

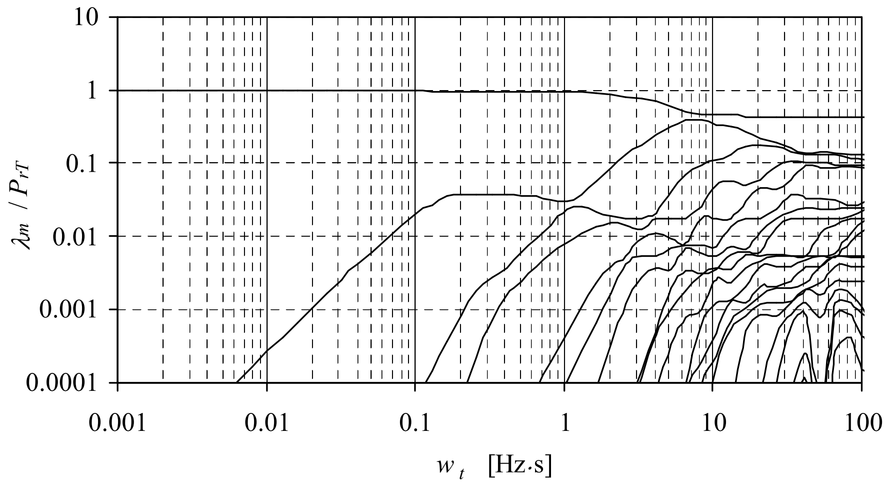

Figure V.27 – Eigenvalue characteristics, UMTS Hilly Terrain.

V.3. HIPERLAN/2 Channel Models

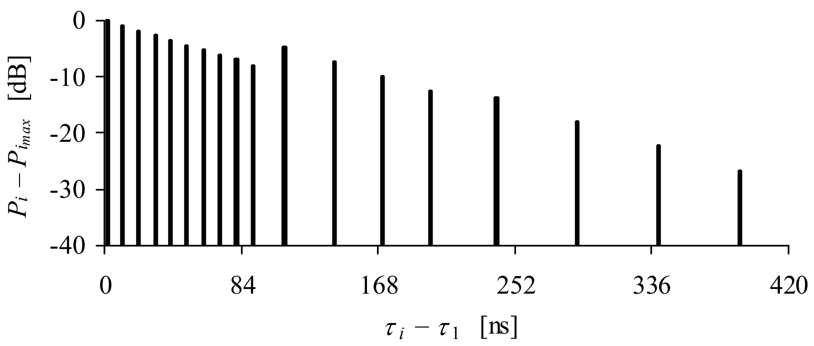

Figure V.28 – PDP, HIPERLAN/2 Model A.

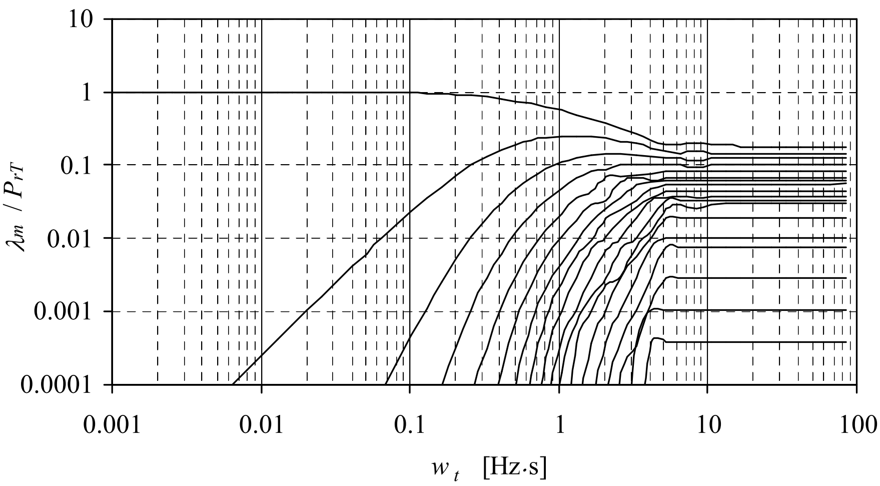

Figure V.29 – Eigenvalue characteristics, HIPERLAN/2 Model A.

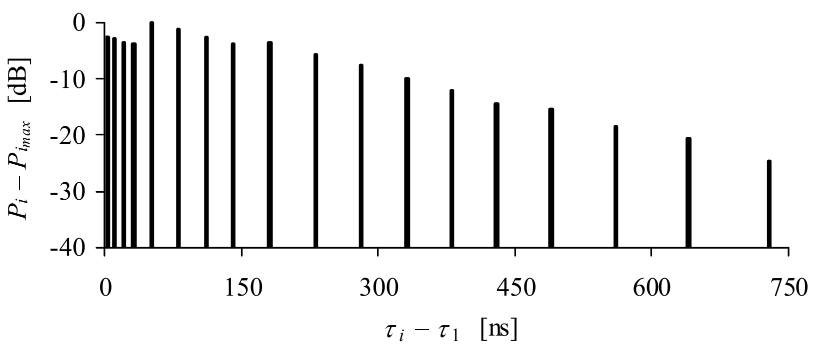

Figure V.30 – PDP, HIPERLAN/2 Model B.

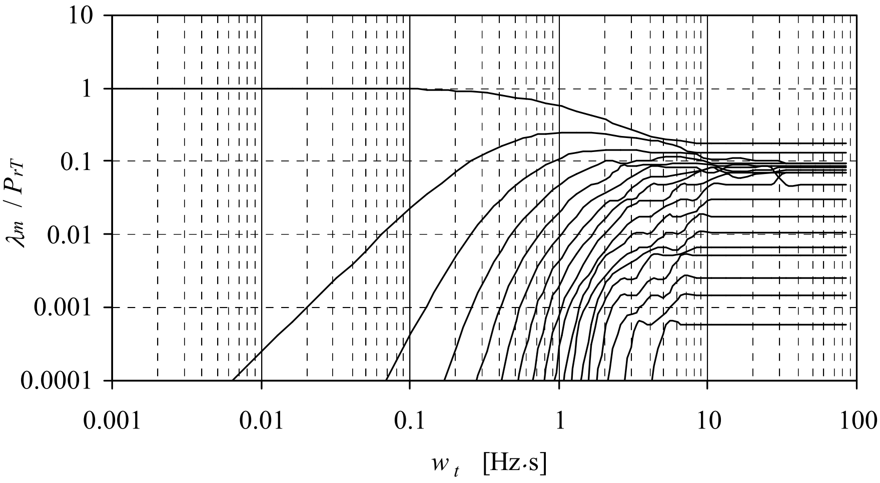

Figure V.31 – Eigenvalue characteristics, HIPERLAN/2 Model B.

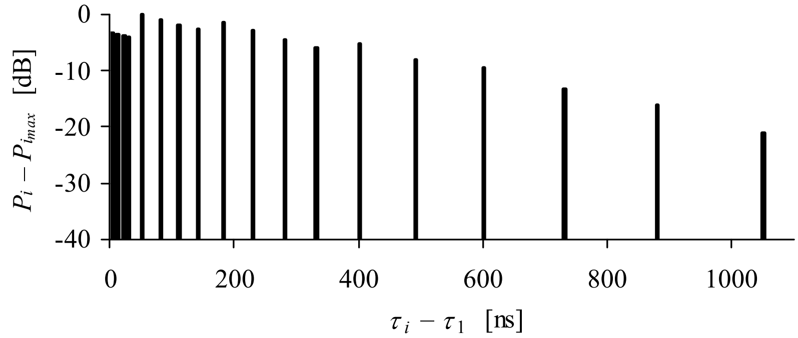

Figure V.32 – PDP, HIPERLAN/2 Model C.

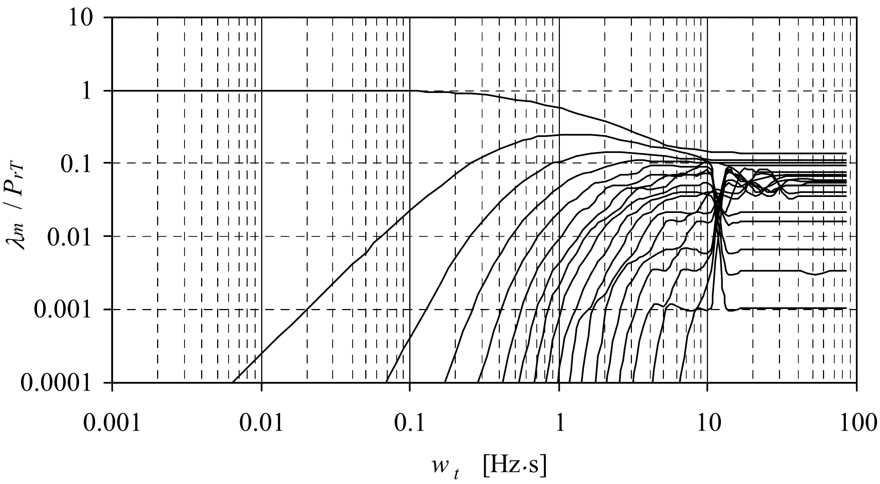

Figure V.33 – Eigenvalue characteristics, HIPERLAN/2 Model C.

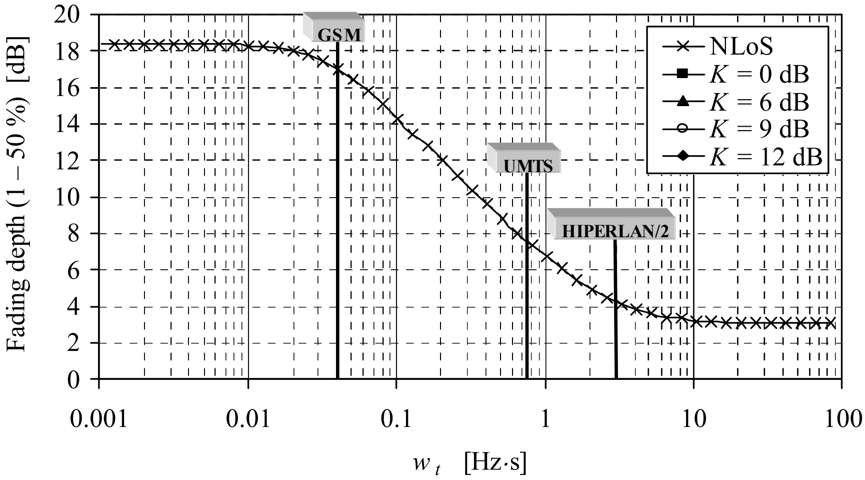

Figure V.34 – Fading depth, HIPERLAN/2 Model C.

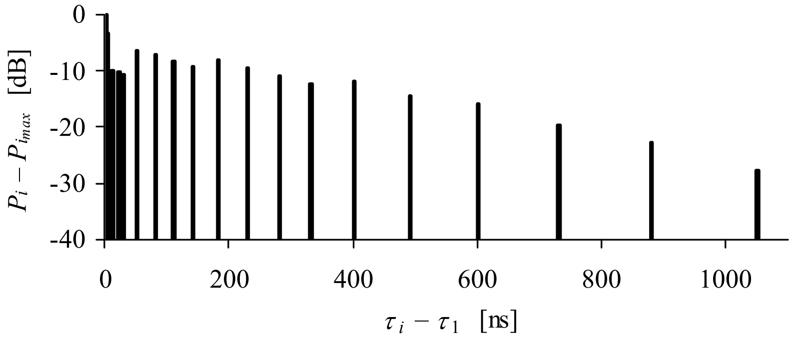

Figure V.35 – PDP, HIPERLAN/2 Model D.

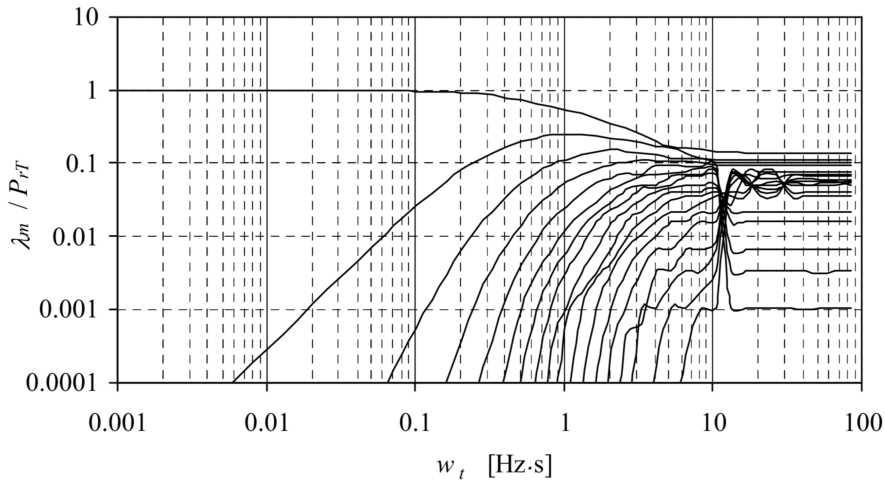

Figure V.36 – Eigenvalue characteristics, HIPERLAN/2 Model D.

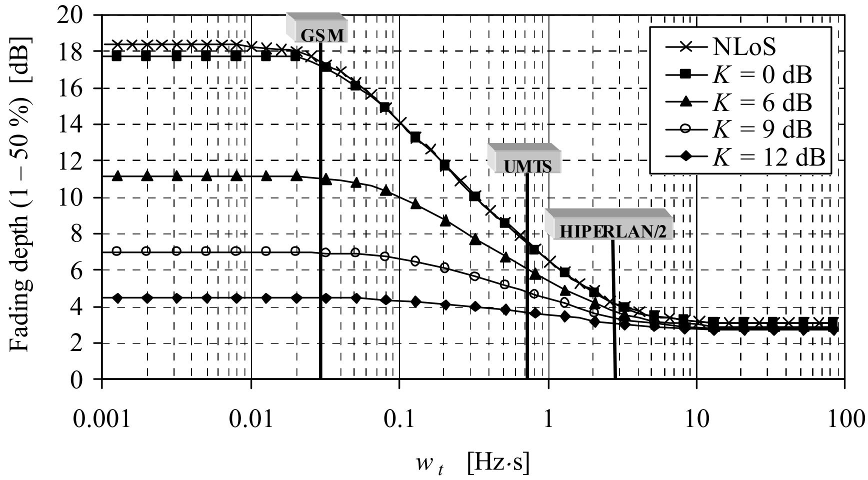

Figure V.37 – Fading depth, HIPERLAN/2 Model D.

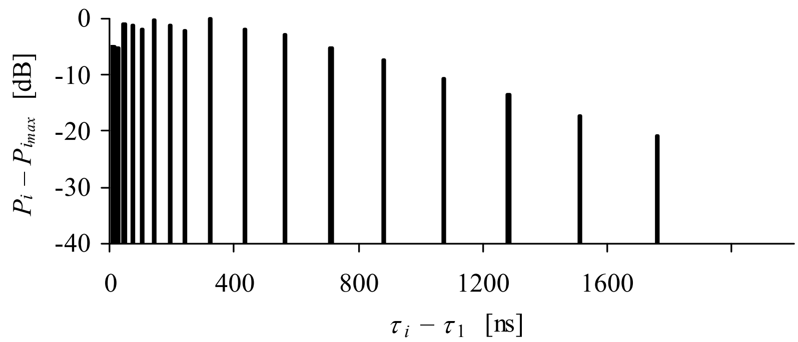

Figure V.38 – PDP, HIPERLAN/2 Model E.

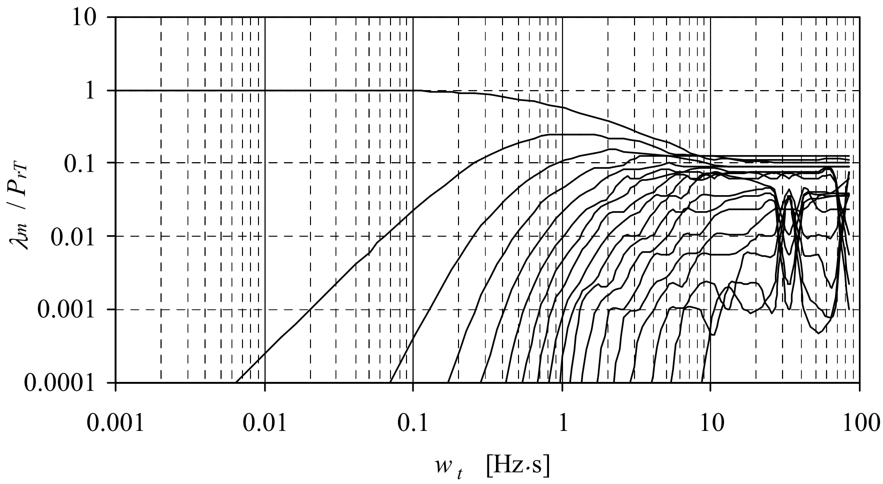

Figure V.39 – Eigenvalue characteristics, HIPERLAN/2 Model E.

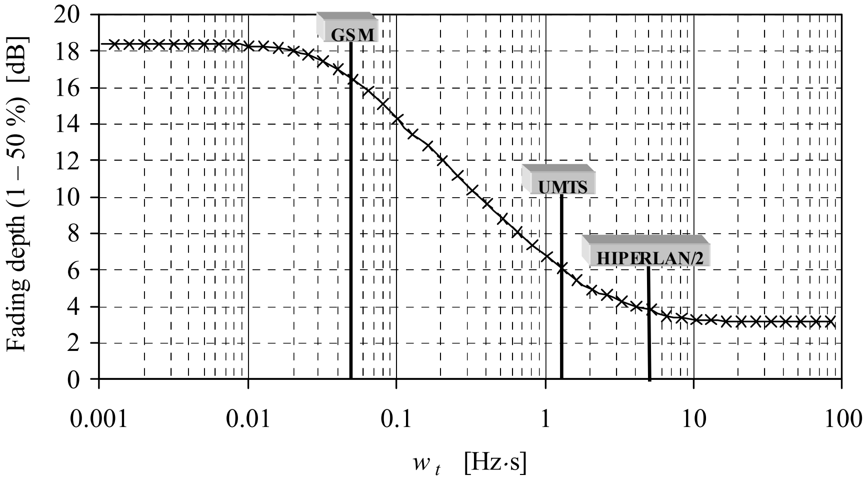

Figure V.40 – Fading depth, HIPERLAN/2 Model E.

Appendix VI

Rice Factor and Fading Depth Variation

In this Appendix, results on the Rice factor and fading depth variation, as a function of the antenna half-power beamwidth and the equivalent received bandwidth, are presented; ideal directional, ULA and UCA antennas, and different distributions for the AoAs, are considered.

VI.1. Rice Factor Variation

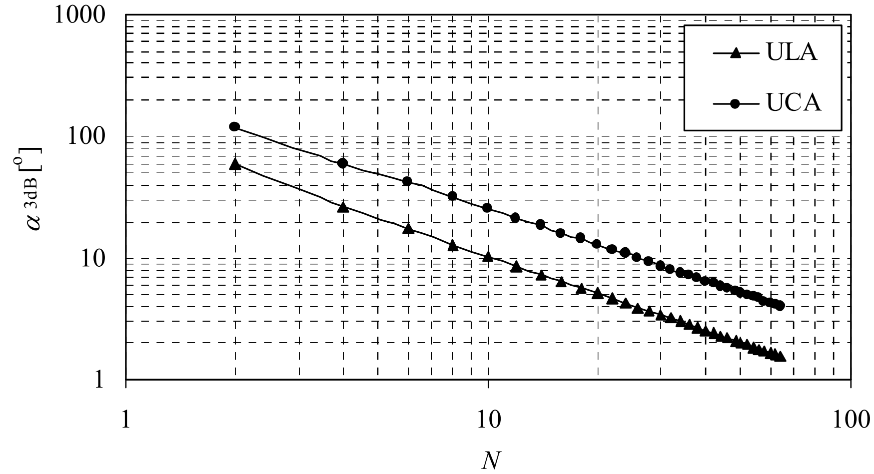

Figure VI.1 – Beamwidth as a function of N, $d_e = 0.5\lambda$.

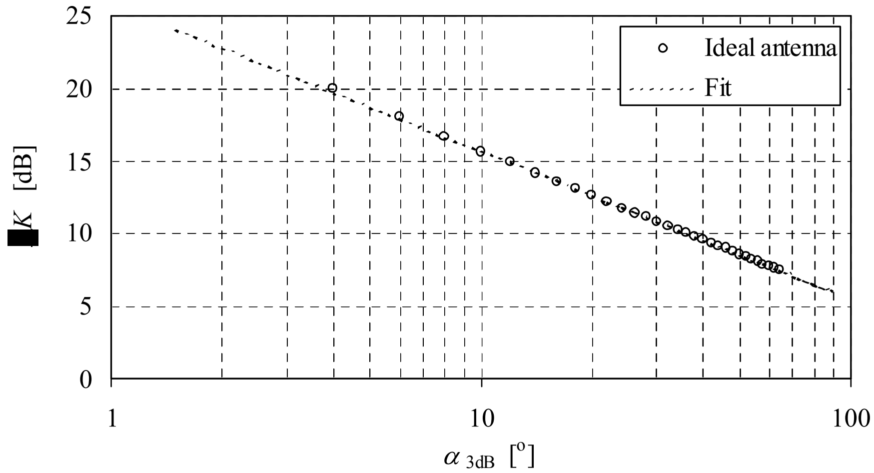

Figure VI.2 – Relation between ΔK and α_{3dB}, Fitting results, ideal directional antenna.

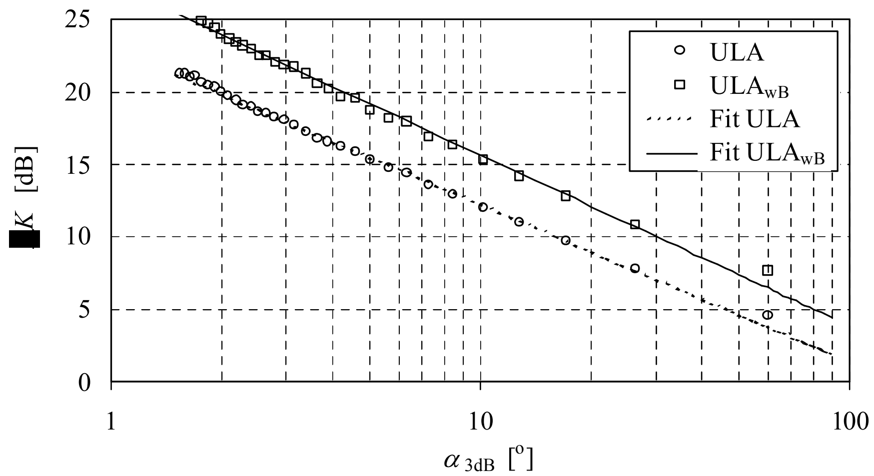

Figure VI.3 – Relation between ΔK and α_{3dB}, Fitting results, ULA.

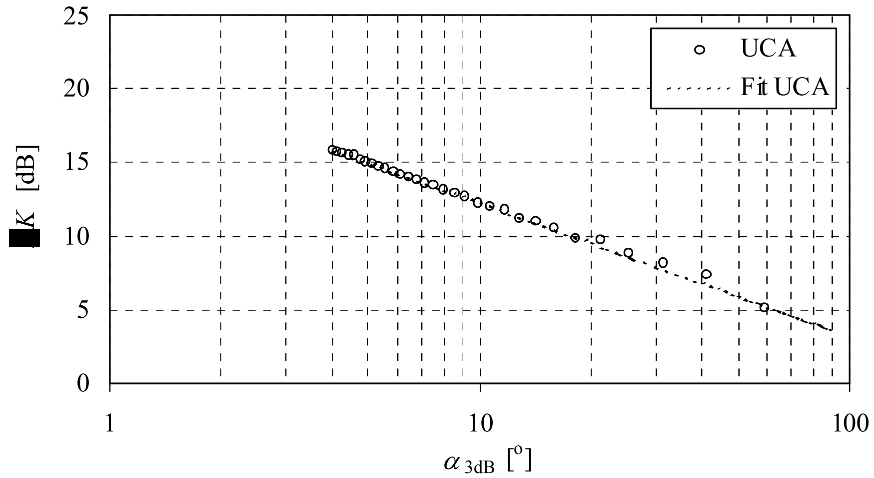

Figure VI.4 – Relation between ΔK and α_{3dB}, Fitting results, UCA.

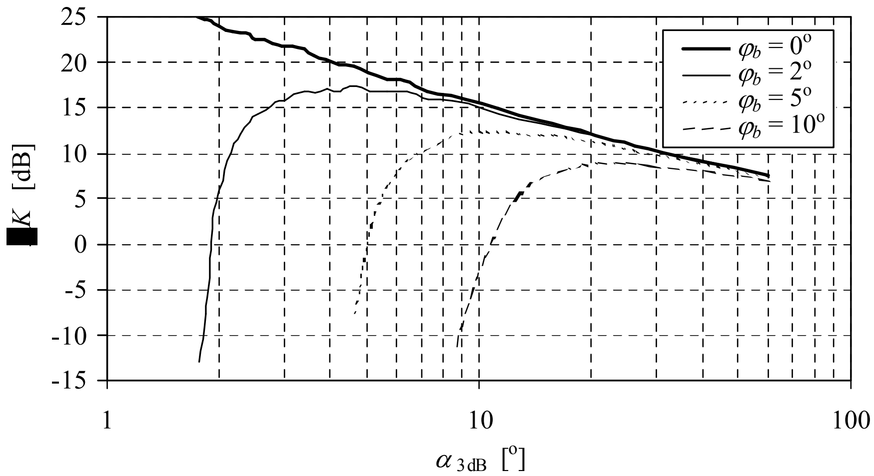

Figure VI.5 – Relation between ΔK and α_{3dB}, dependence on the main beam orientation, ULA_{wB}, uniform AoA.

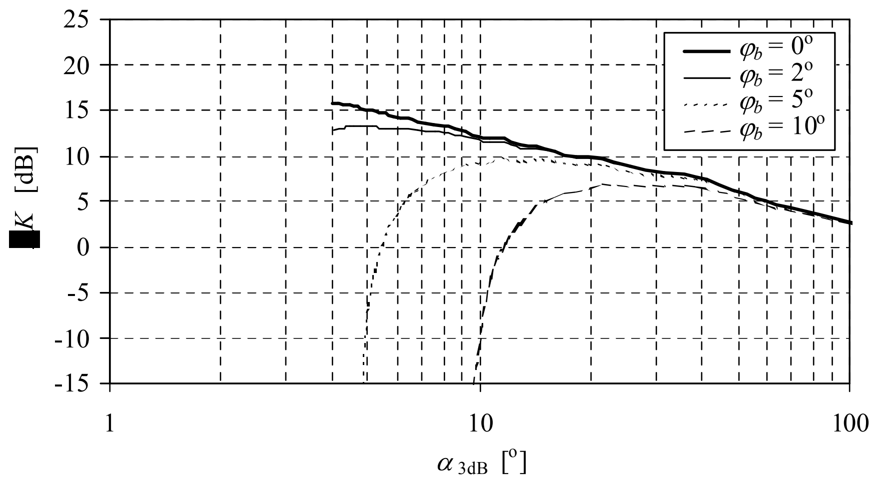

Figure VI.6 – Relation between ΔK and α_{3dB}, dependence on the main beam orientation, UCA, uniform AoA.

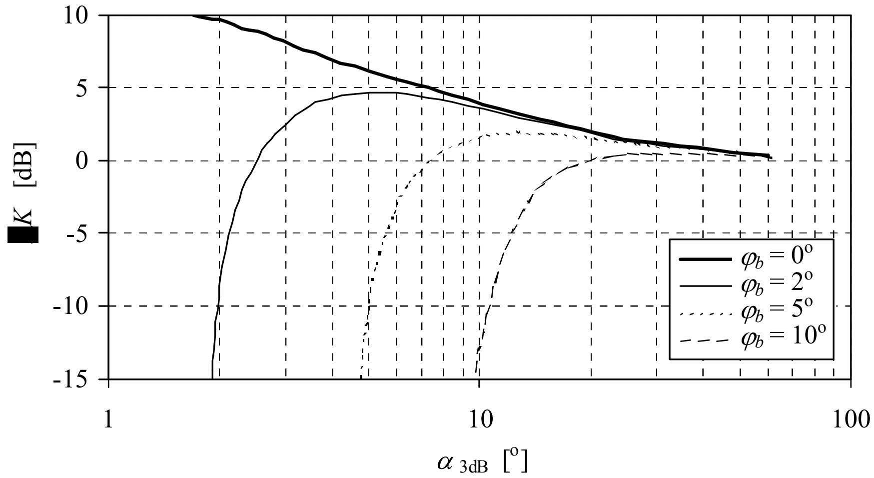

Figure VI.7 – Relation between ΔK and α_{3dB}, dependence on the main beam orientation, ULA_{wB}, Gaussian AoA.

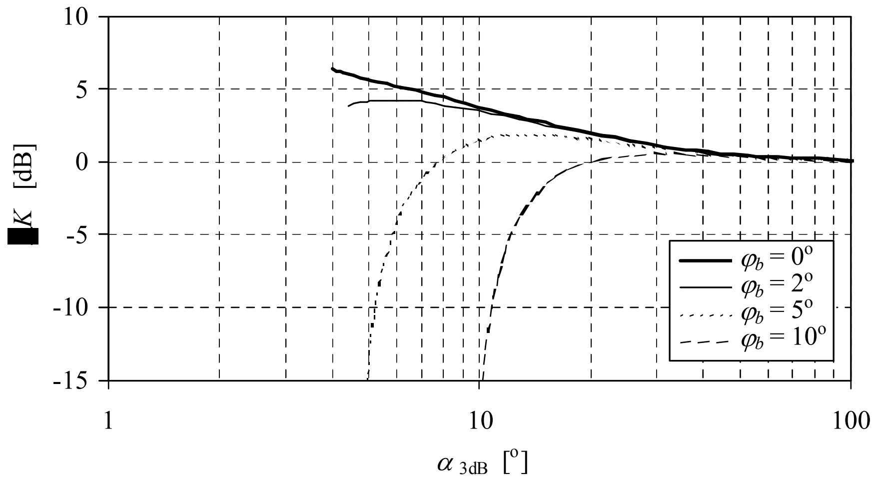

Figure VI.8 – Relation between ΔK and α_{3dB}, dependence on the main beam orientation, UCA, Gaussian AoA.

VI.2. Fading Depth Reduction

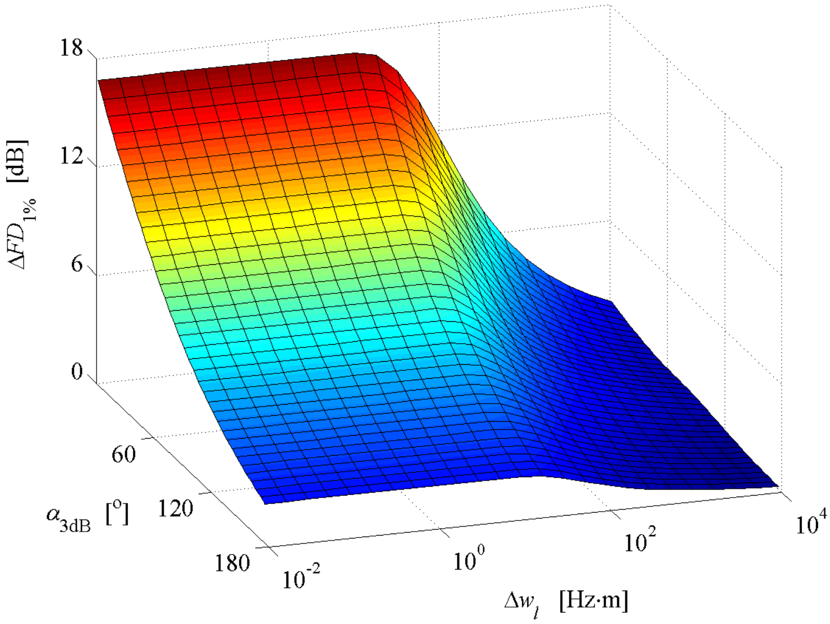

Figure VI.9 – Fading depth reduction as a function of Δw_l and $\alpha_{3\mathrm{dB}}$, $K_{\mathrm{omni}} = 0$ dB.

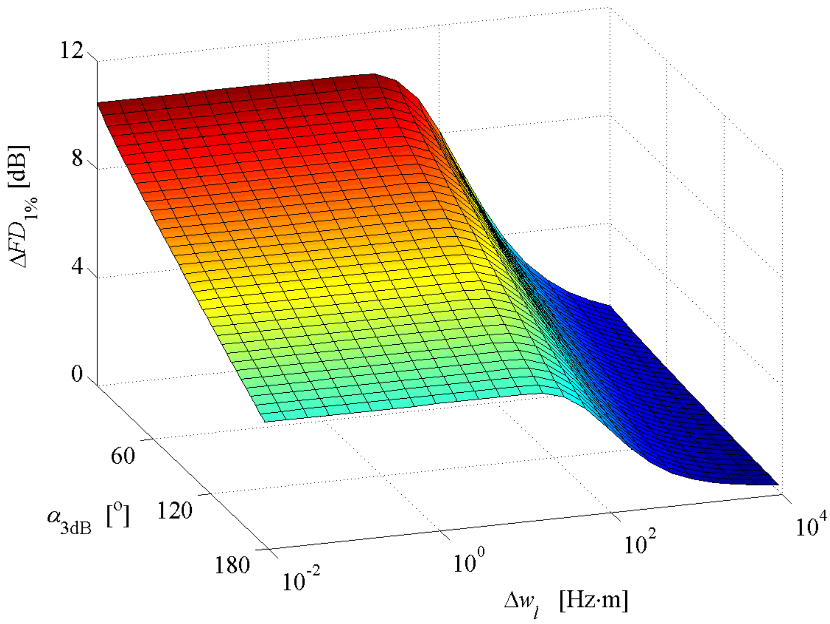

Figure VI.10 – Fading depth reduction as a function of Δw_l and $\alpha_{3\mathrm{dB}}$, $K_{\mathrm{omni}} = 6$ dB.

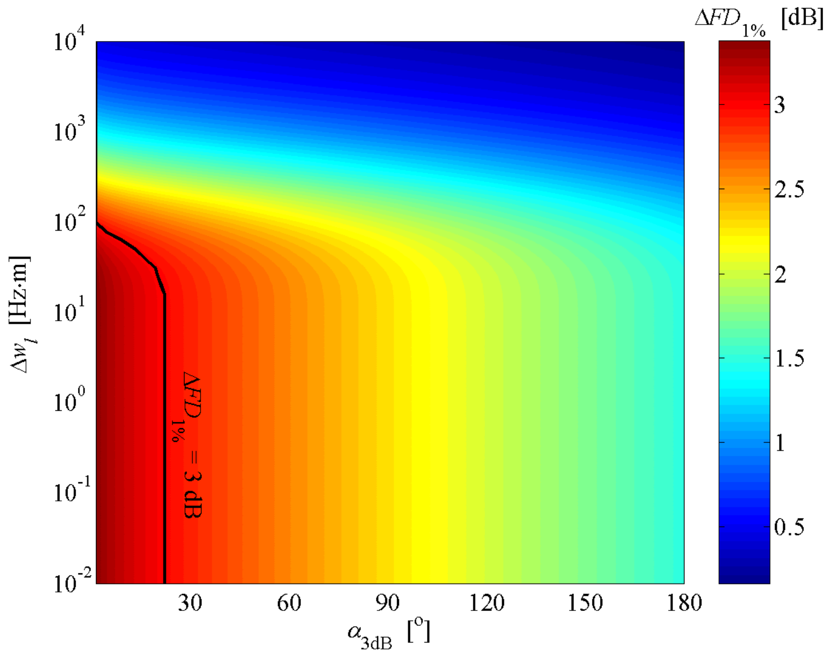

Figure VI.11 – Fading depth reduction as a function of Δw_l and α_{3dB}, K_{omni} = 12 dB.

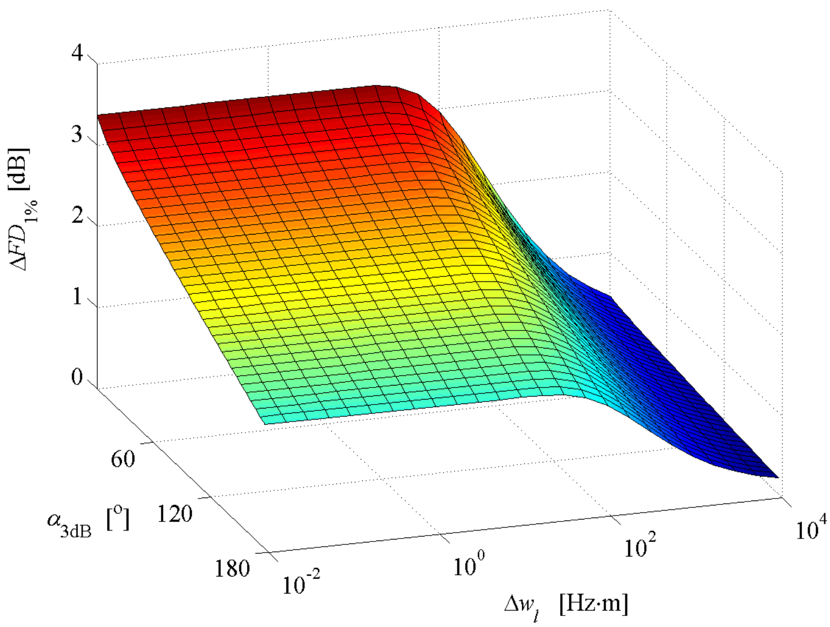

Figure VI.12 – Fading depth reduction as a function of Δw_l and α_{3dB}, K_{omni} = 12 dB.

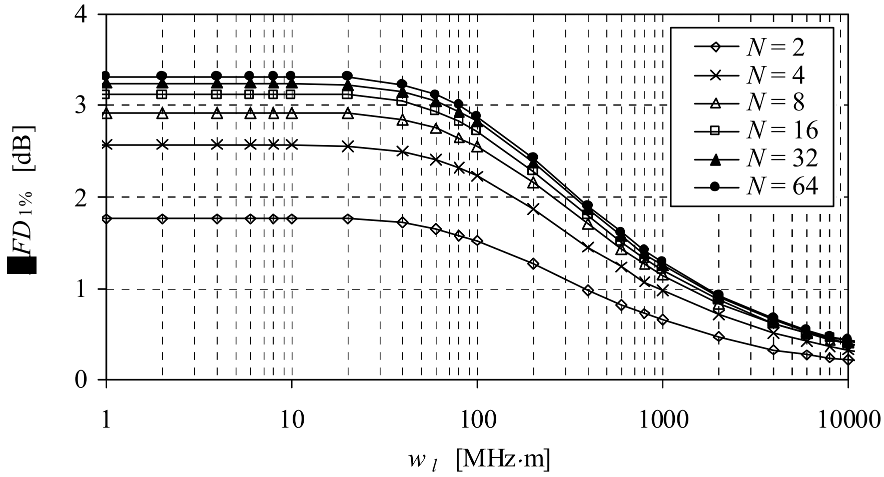

Figure VI.13 – Fading depth reduction for K_{omni} = 12 dB, ULA.

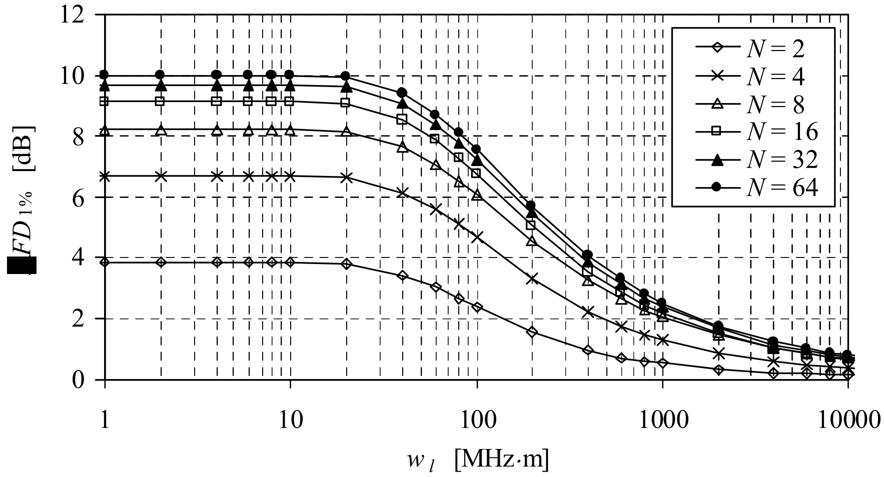

Figure VI.14 – Fading depth reduction for K_{omni} = 6 dB, UCA.

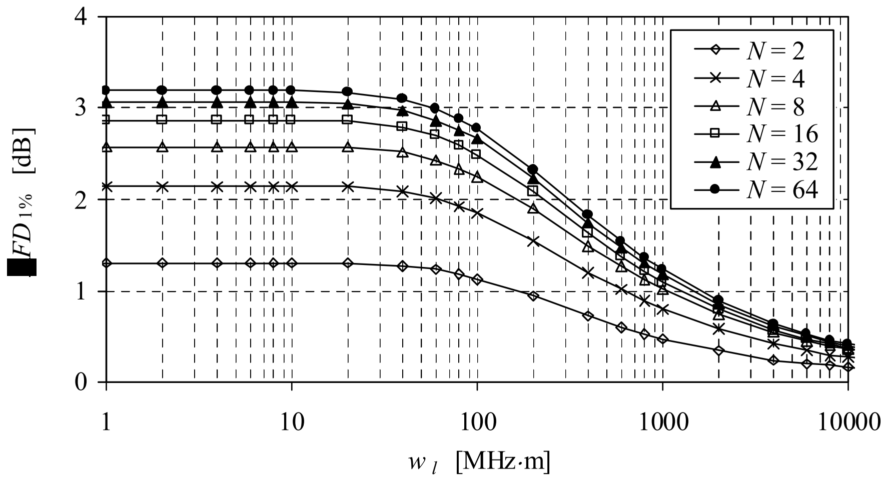

Figure VI.15 – Fading depth reduction for K_{omni} = 12 dB, UCA.

Appendix VII

Fading Depth Variation

In this Appendix, results on the fading depth variation for GSM, UMTS, and HIPERLAN/2 in pico-, micro- and macro-cellular LoS and NLoS environments, for different environment parameters, and for different statistical distributions for AoAs, are presented.

VII.1. Micro-cellular Environments

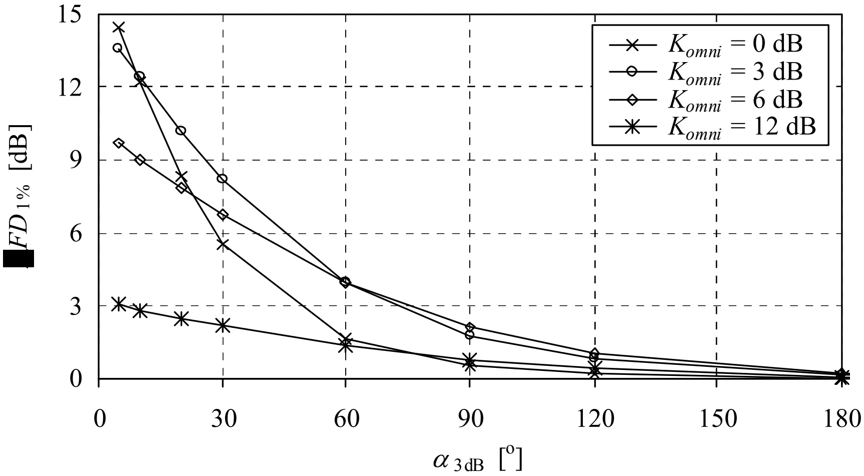

Figure VII.1 – Fading depth variation, micro-cellular, $\sigma_s = 40^o$, GSM.

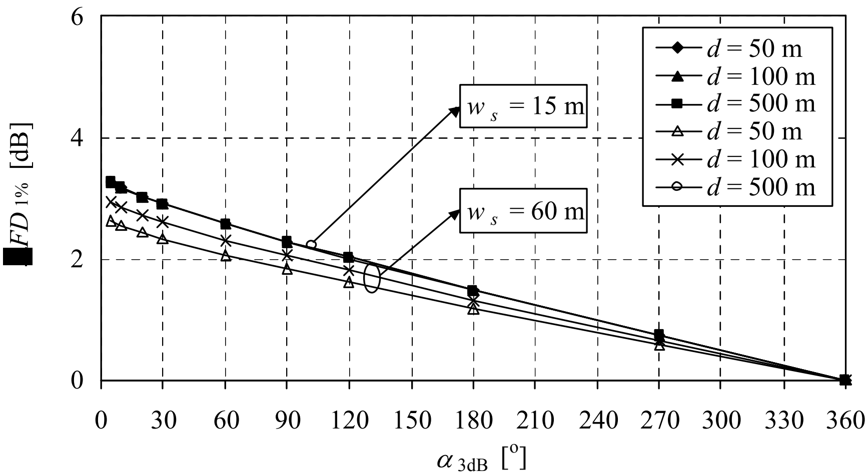

Figure VII.2 – Fading depth variation, micro-cellular, K_{omni} = 12 dB, UMTS.

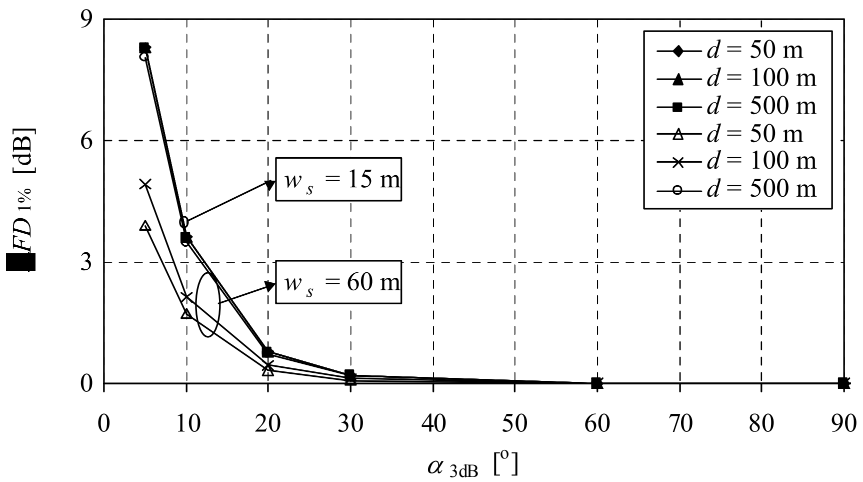

Figure VII.3 – Fading depth variation, micro-cellular, K_{omni} = 0 dB, $\sigma_s = 10^o$, UMTS.

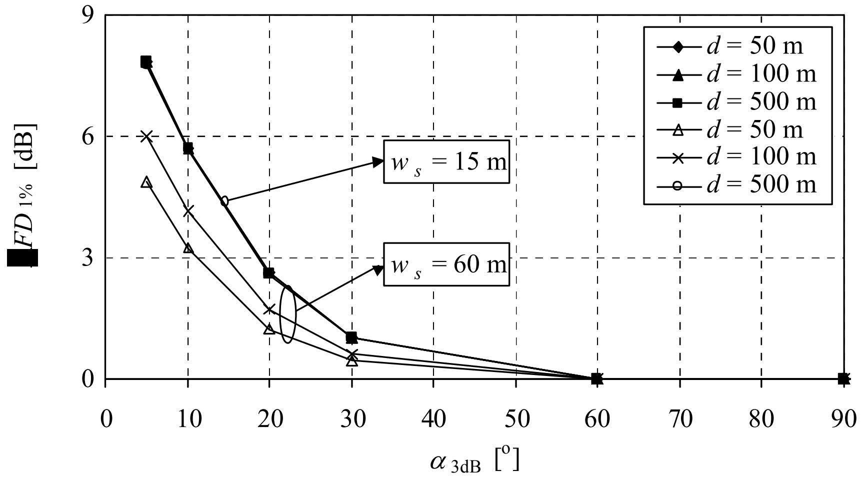

Figure VII.4 – Fading depth variation, micro-cellular, K_{omni} = 6 dB, σ_s = 10°, UMTS.

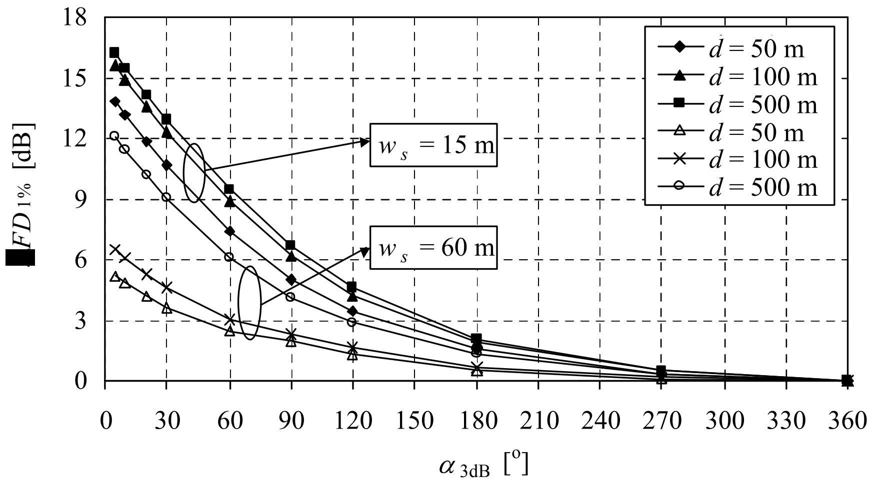

Figure VII.5 – Fading depth variation, micro-cellular, K_{omni} = 0 dB, HIPERLAN/2.

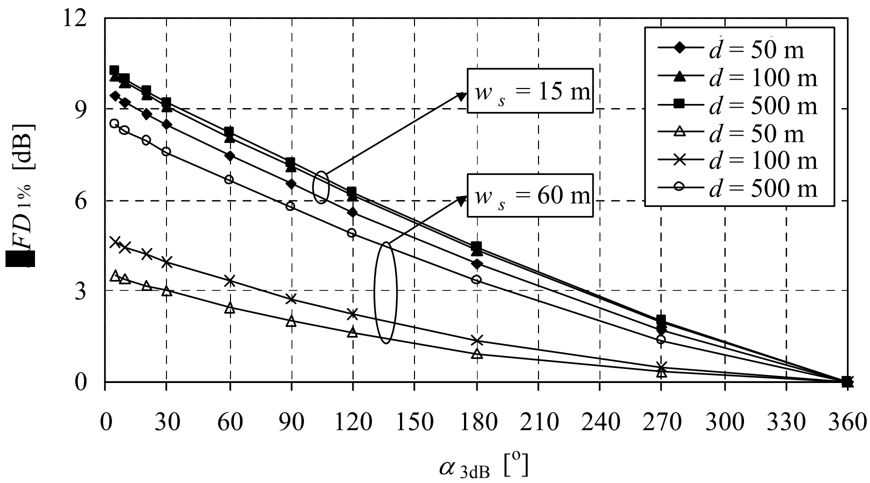

Figure VII.6 – Fading depth variation, micro-cellular, K_{omni} = 6 dB, HIPERLAN/2.

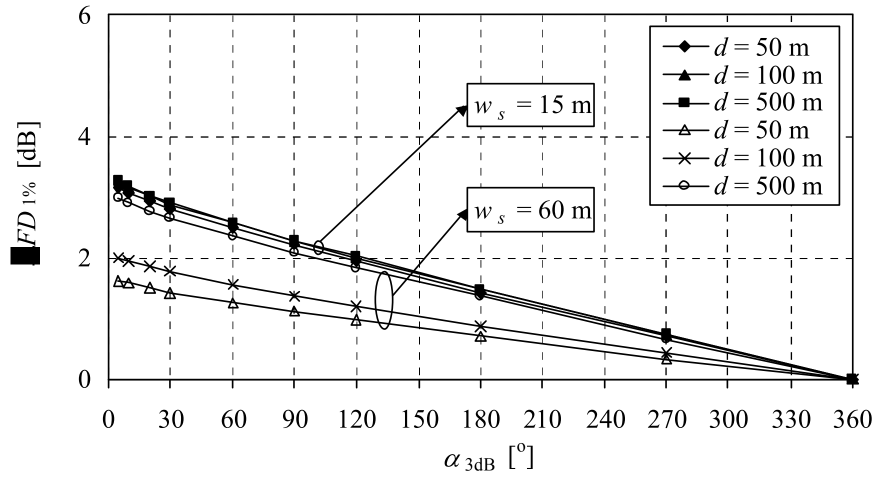

Figure VII.7 – Fading depth variation, micro-cellular, K_{omni} = 12 dB, HIPERLAN/2.

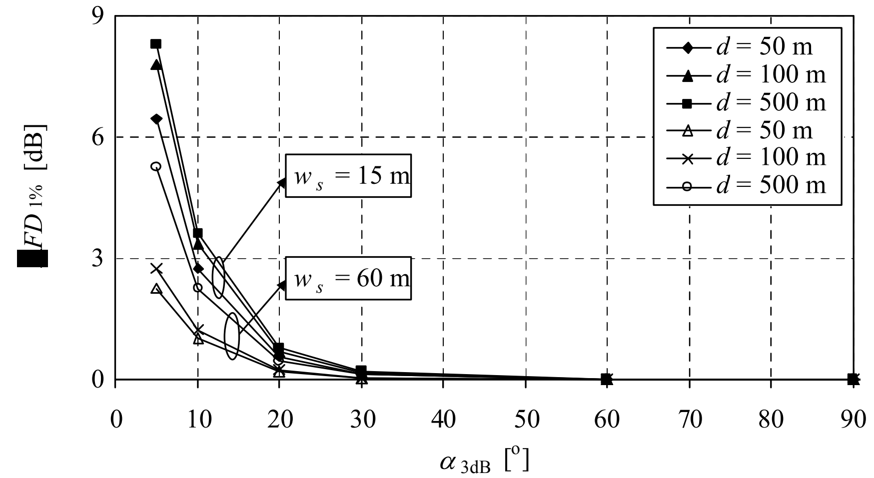

Figure VII.8 – Fading depth variation, micro-cellular, K_{omni} = 0 dB, σ_s = 10°, HIPERLAN/2.

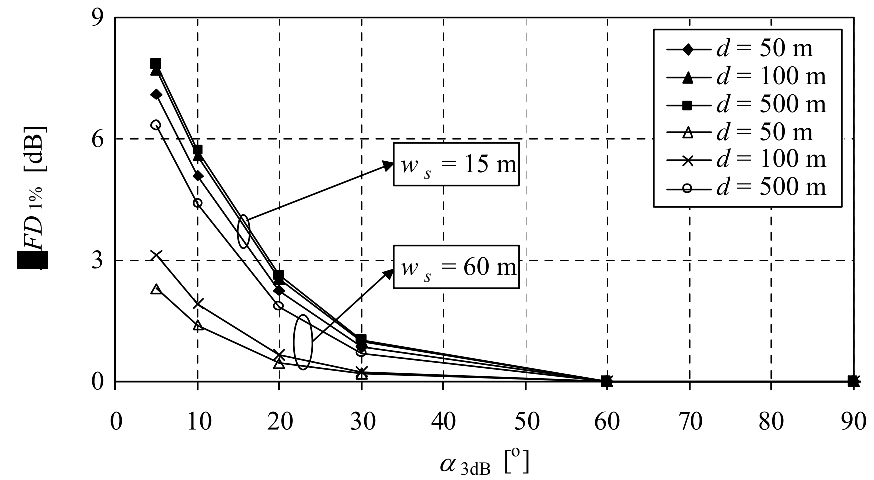

Figure VII.9 – Fading depth variation, micro-cellular, K_{omni} = 6 dB, σ_s = 10°, HIPERLAN/2.

VII.2. Macro-cellular Environments

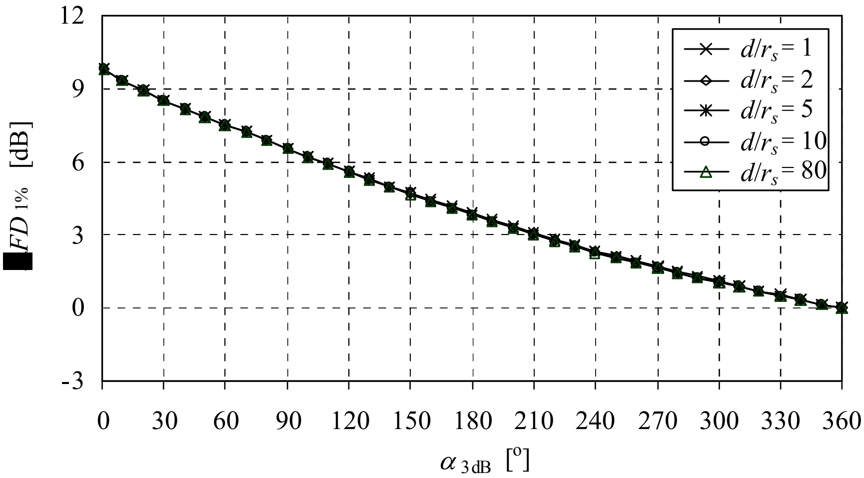

Figure VII.10 – Fading depth variation, macro-cellular, r_s = 100 m, K_{omni} = 6 dB, GSM.

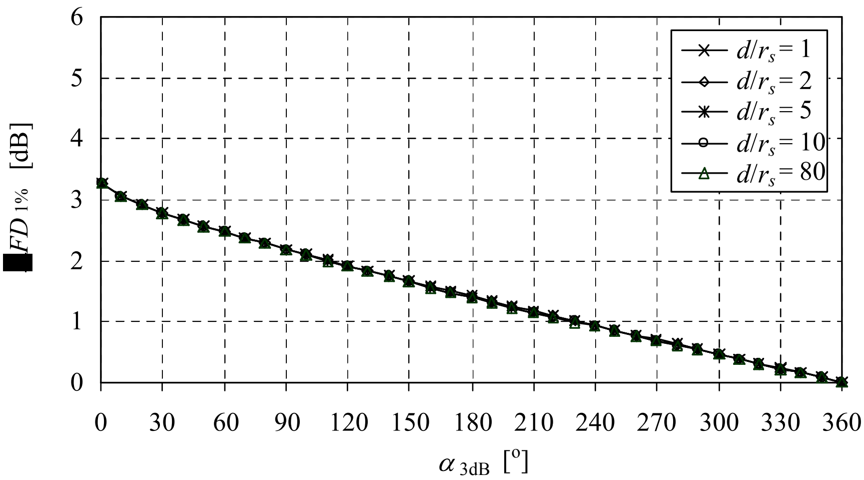

Figure VII.11 – Fading depth variation, macro-cellular, r_s = 100 m, K_{omni} = 12 dB, GSM.

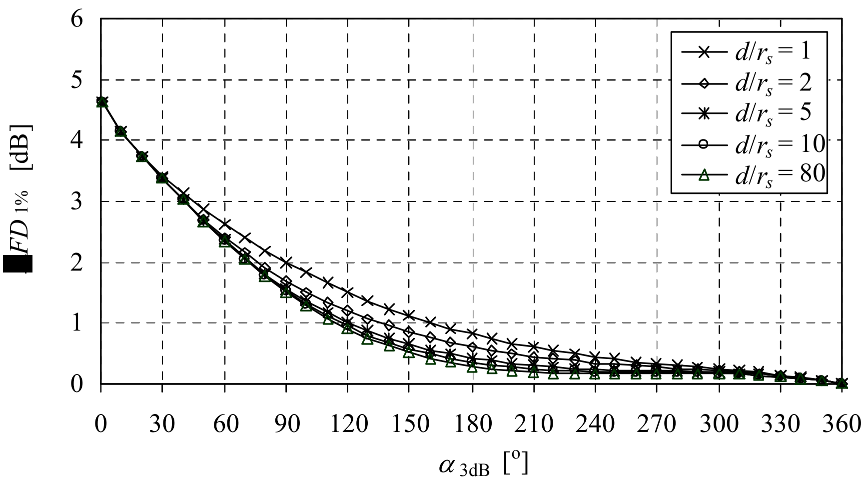

Figure VII.12 – Fading depth variation, macro-cellular, r_s = 800 m, K_{omni} = 6 dB, GSM.

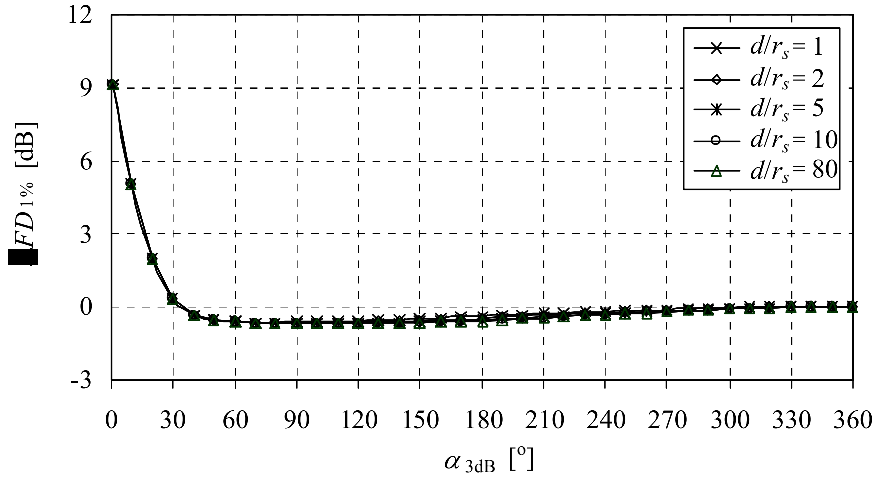

Figure VII.13 – Fading depth variation, macro-cellular, r_s = 100 m, K_{omni} = 6 dB, σ_s = 10º, GSM.

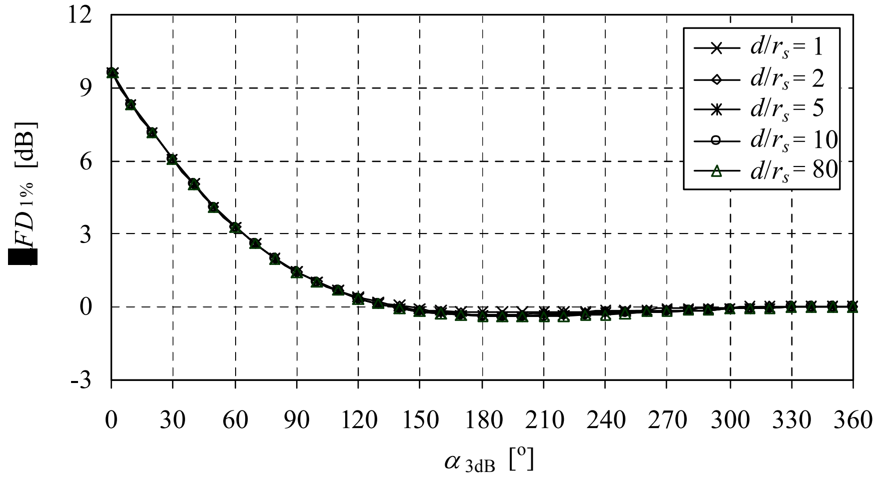

Figure VII.14 – Fading depth variation, macro-cellular, r_s = 100 m, K_{omni} = 6 dB, σ_s = 40º, GSM.

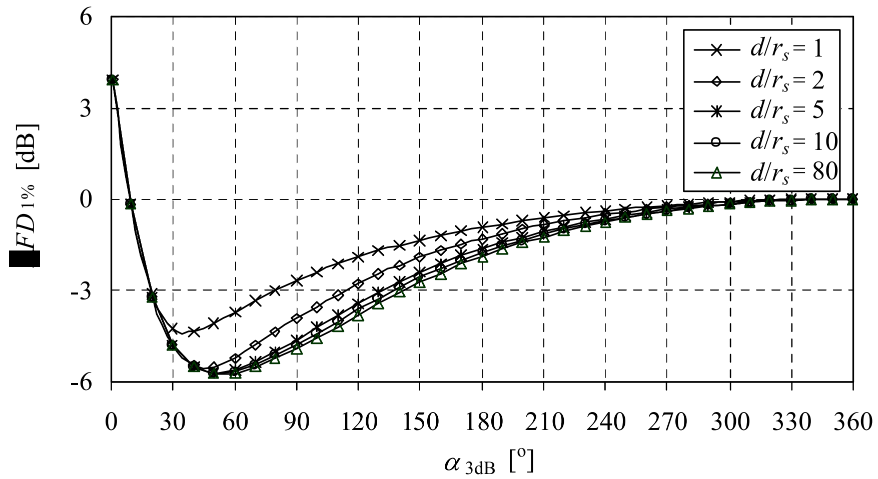

Figure VII.15 – Fading depth variation, macro-cellular, r_s = 800 m, K_{omni} = 6 dB, σ_s = 10º, GSM.

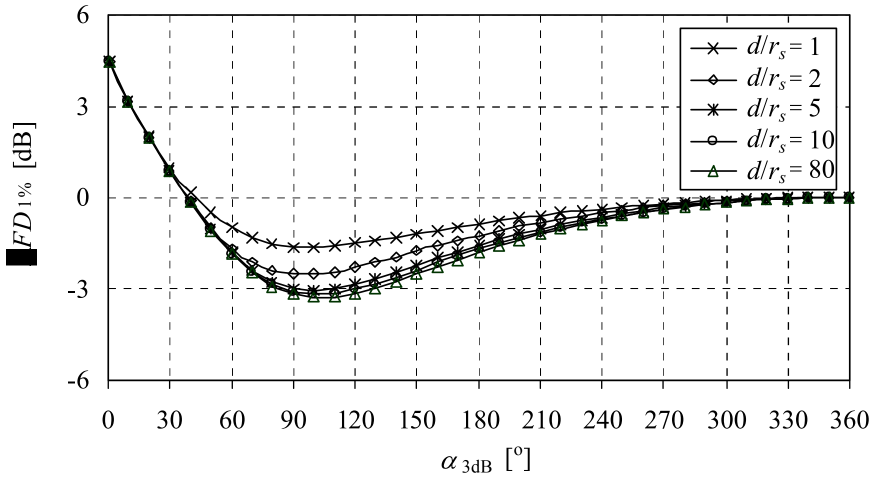

Figure VII.16 – Fading depth variation, macro-cellular, r_s = 800 m, K_{omni} = 6 dB, σ_s = 40º, GSM.

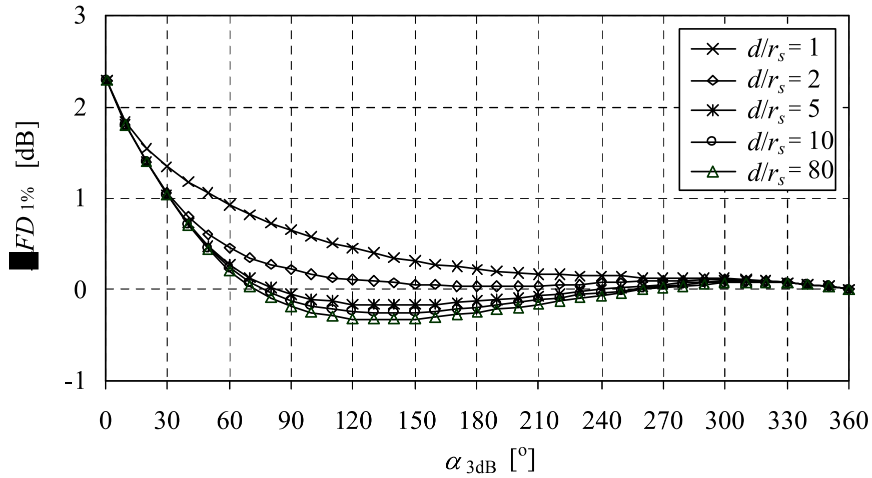

Figure VII.17 – Fading depth variation, macro-cellular, r_s = 100 m, K_{omni} = 6 dB, UMTS.

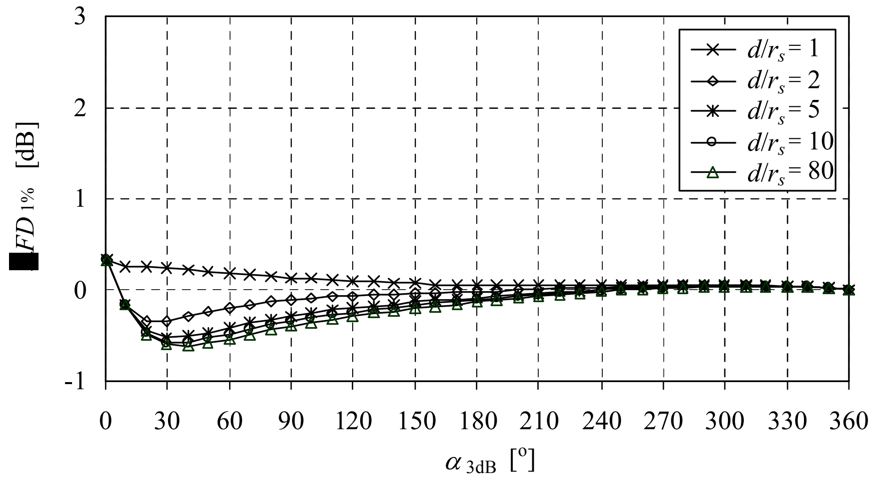

Figure VII.18 – Fading depth variation, macro-cellular, r_s = 800 m, K_{omni} = 6 dB, UMTS.

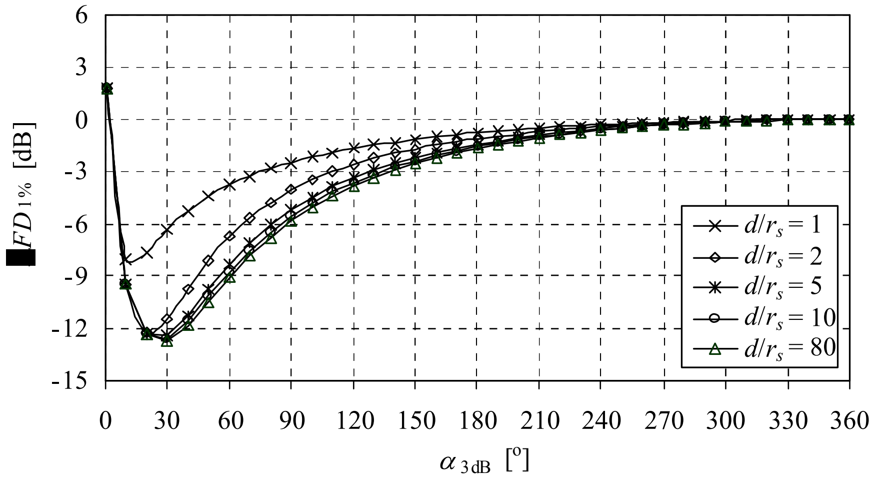

Figure VII.19 – Fading depth variation, macro-cellular, r_s = 100 m, K_{omni} = 0 dB, σ_s = 10º, UMTS.

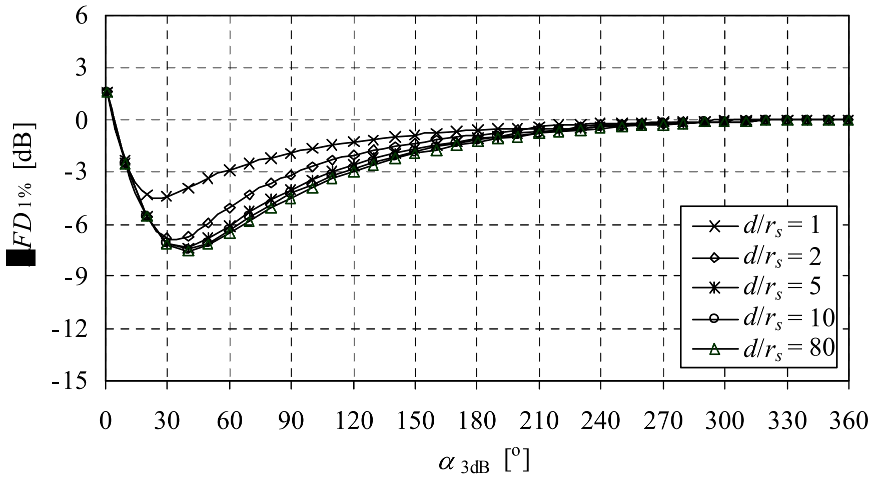

Figure VII.20 – Fading depth variation, macro-cellular, r_s = 100 m, K_{omni} = 6 dB, σ_s = 10º, UMTS.

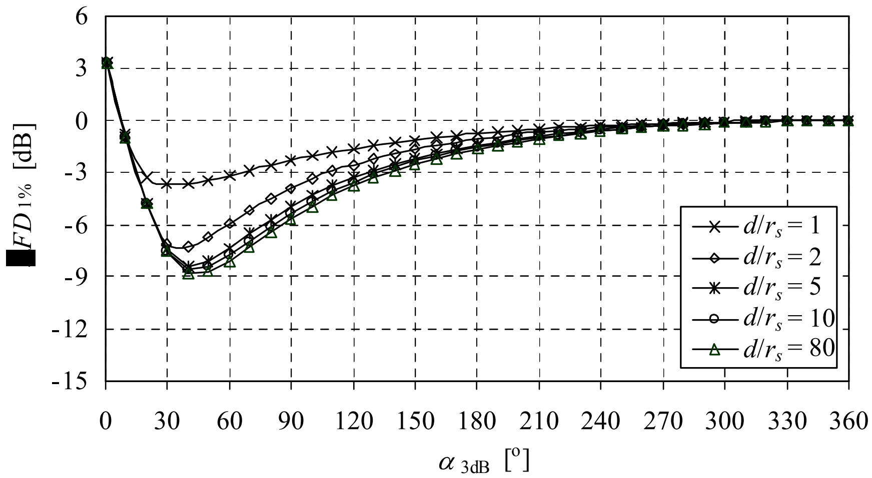

Figure VII.21 – Fading depth variation, macro-cellular, r_s = 100 m, K_{omni} = 0 dB, σ_s = 40º, UMTS.

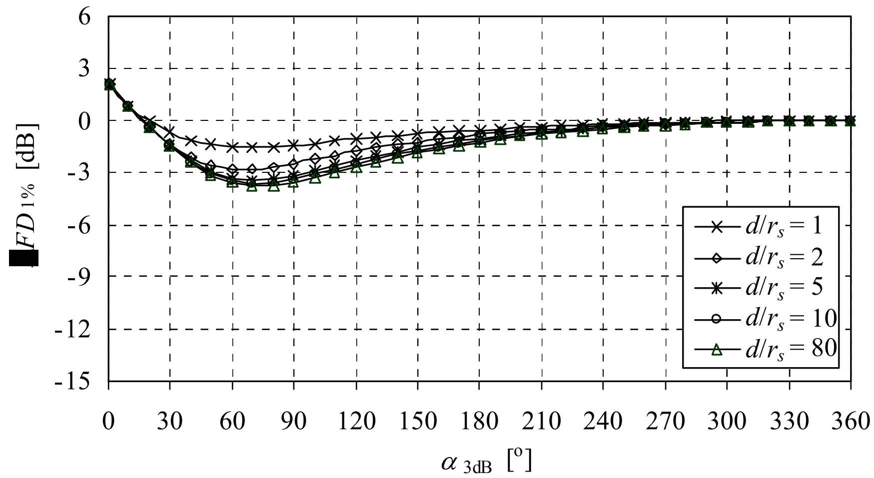

Figure VII.22 – Fading depth variation, macro-cellular, r_s = 100 m, K_{omni} = 6 dB, σ_s = 40^o, UMTS.

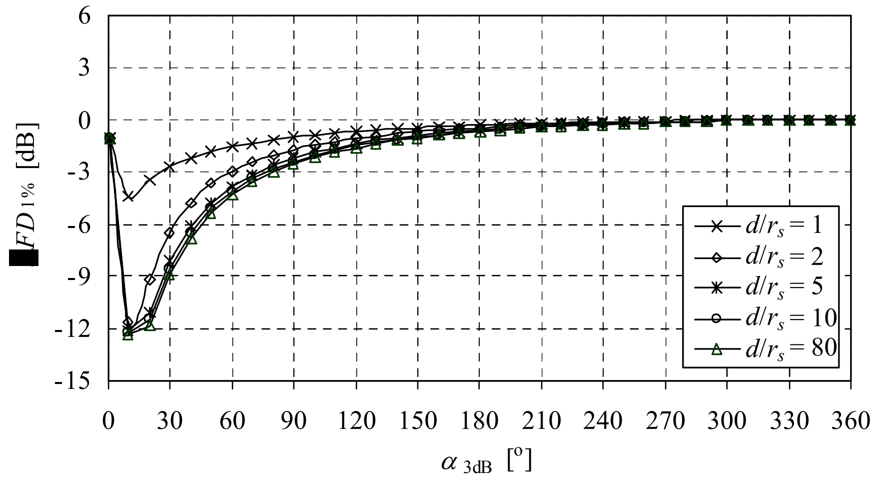

Figure VII.23 – Fading depth variation, macro-cellular, r_s = 800 m, K_{omni} = 0 dB, σ_s = 10^o, UMTS.

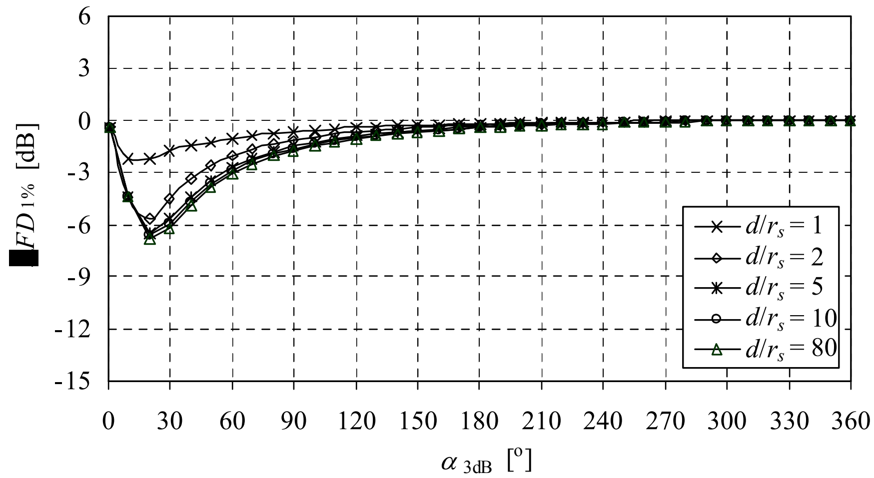

Figure VII.24 – Fading depth variation, macro-cellular, r_s = 800 m, K_{omni} = 6 dB, σ_s = 10^o, UMTS.

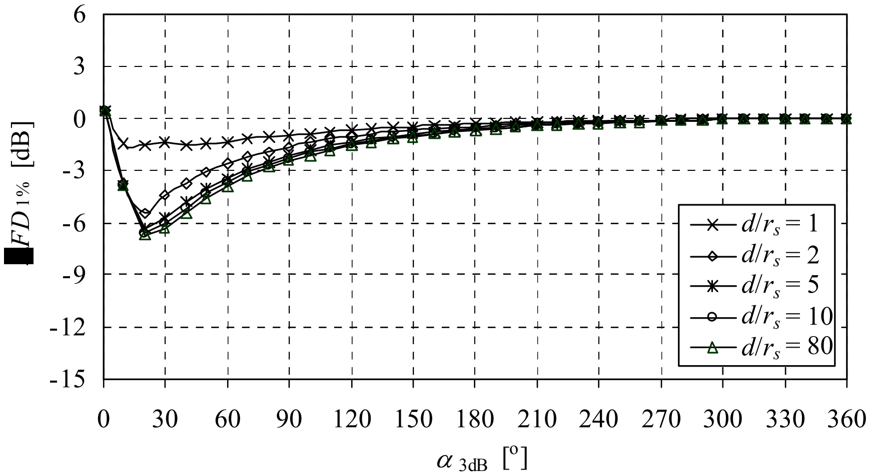

Figure VII.25 – Fading depth variation, macro-cellular, r_s = 800 m, K_{omni} = 0 dB, σ_s = 40º, UMTS.

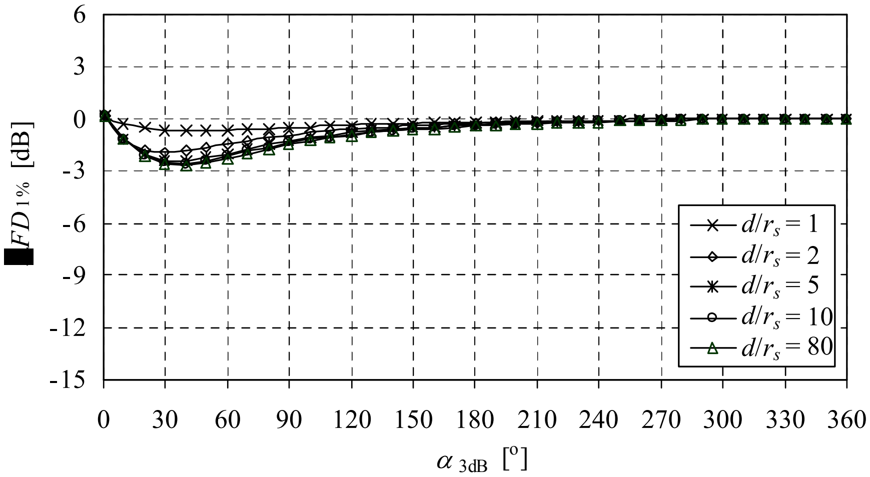

Figure VII.26 – Fading depth variation, macro-cellular, r_s = 800 m, K_{omni} = 6 dB, σ_s = 40º, UMTS.

VII.3. Pico-cellular Environments

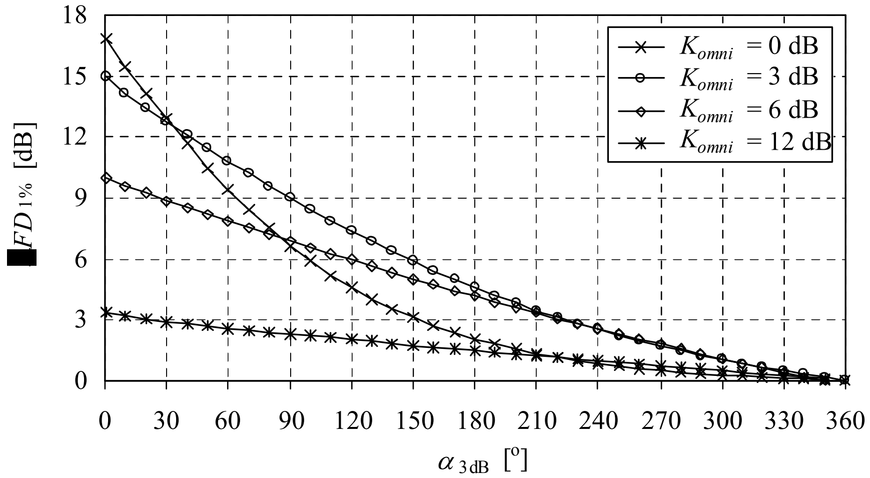

Figure VII.27 – Fading depth variation, pico-cellular, GSM.

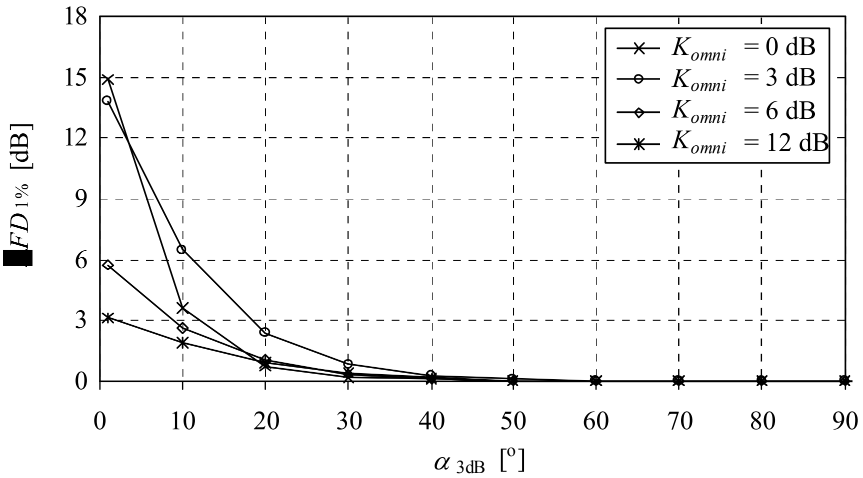

Figure VII.28 – Fading depth variation, pico-cellular, σ_s = 10º, GSM.

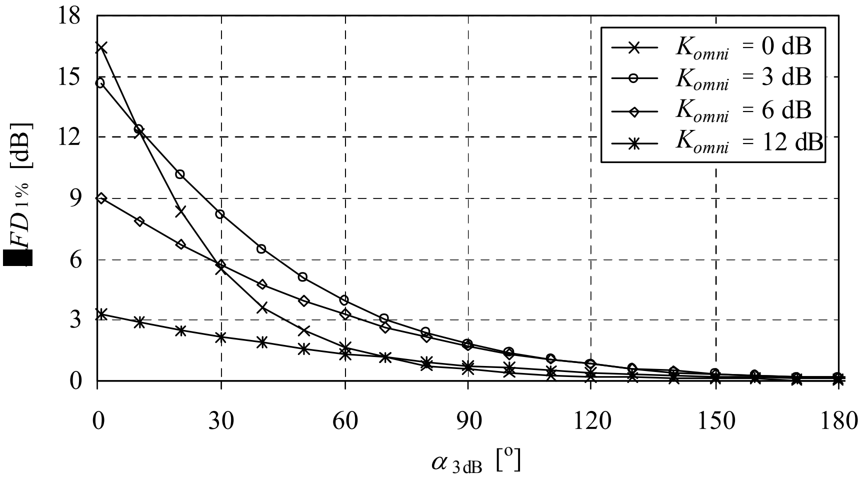

Figure VII.29 – Fading depth variation, pico-cellular, σ_s = 40º, GSM.

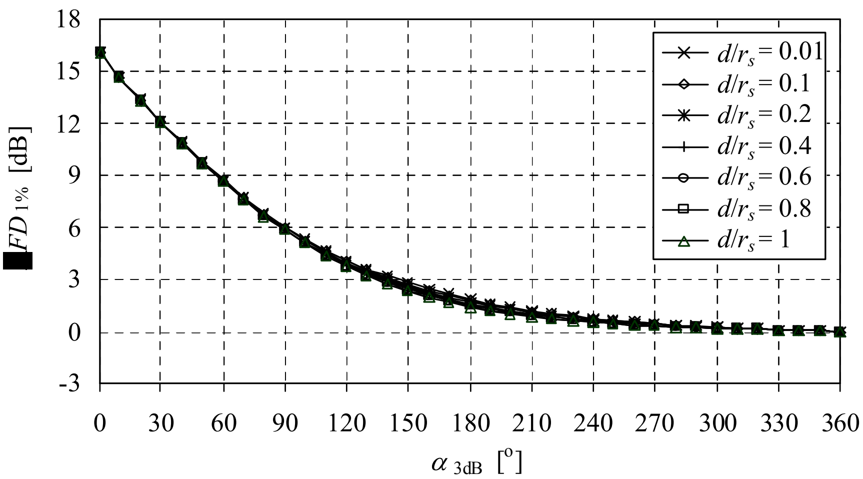

Figure VII.30 – Fading depth variation, pico-cellular, r_s = 2.5 m, K_{omni} = 0 dB, UMTS.

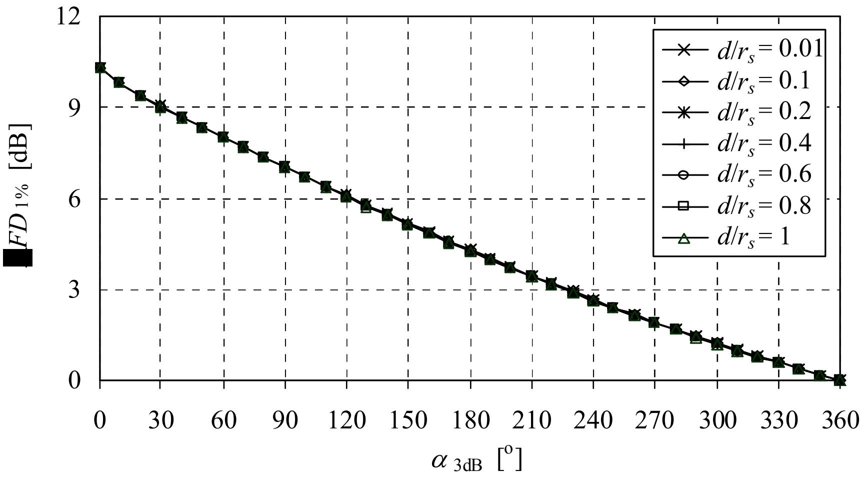

Figure VII.31 – Fading depth variation, pico-cellular, r_s = 2.5 m, K_{omni} = 6 dB, UMTS.

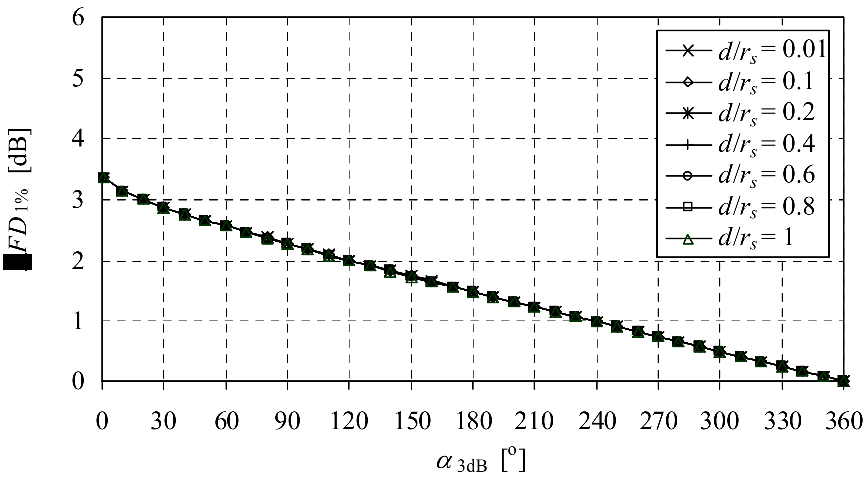

Figure VII.32 – Fading depth variation, pico-cellular, r_s = 2.5 m, K_{omni} =12 dB, UMTS.

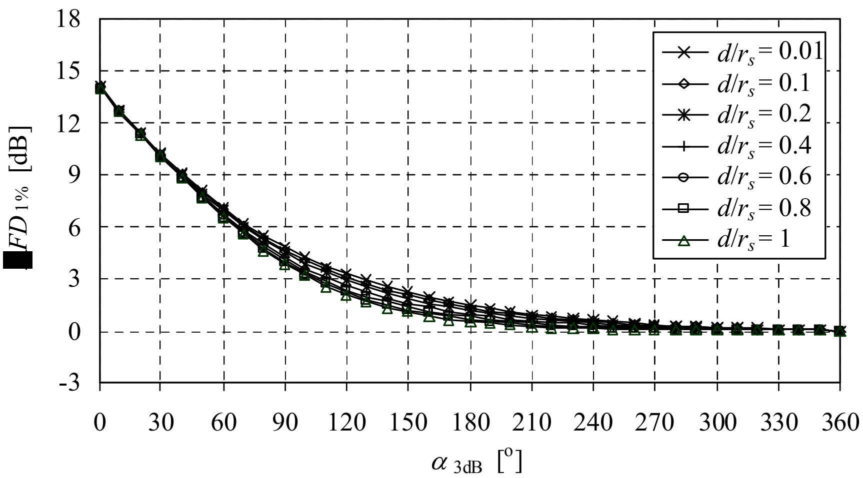

Figure VII.33 – Fading depth variation, pico-cellular, r_s = 5 m, K_{omni} = 0 dB, UMTS.

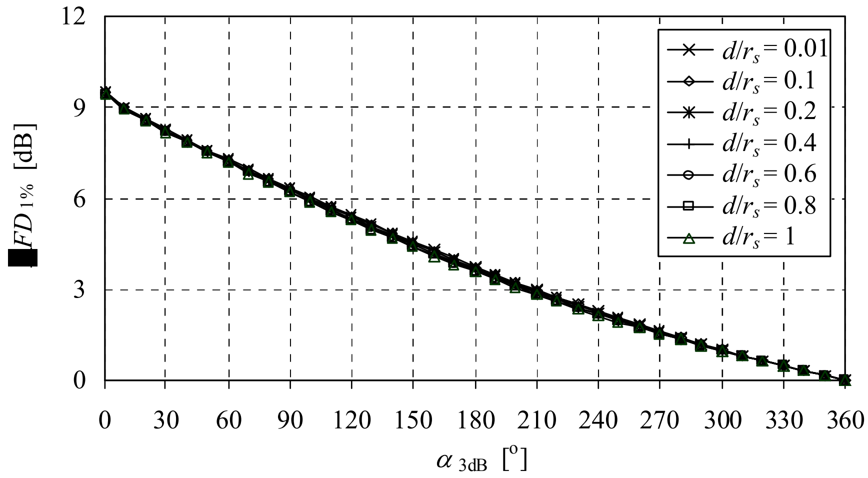

Figure VII.34 – Fading depth variation, pico-cellular, r_s =5 m, K_{omni} = 6 dB, UMTS.

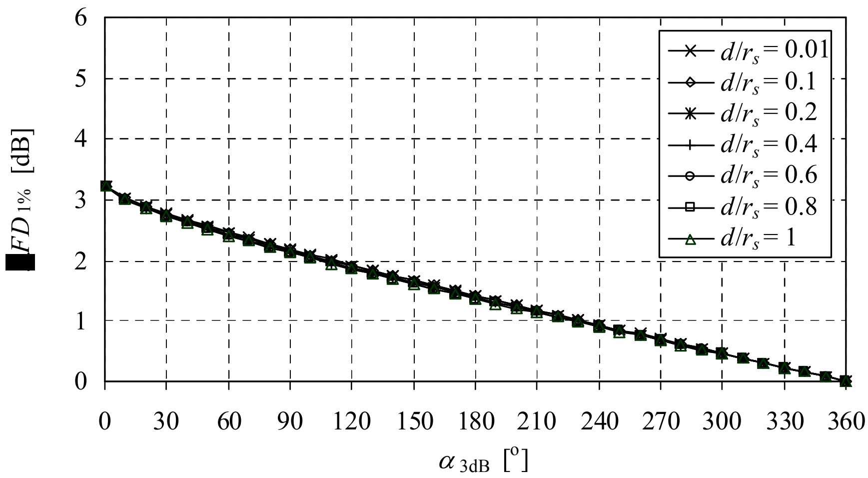

Figure VII.35 – Fading depth variation, pico-cellular, r_s = 5 m, K_{omni} = 12 dB, UMTS.

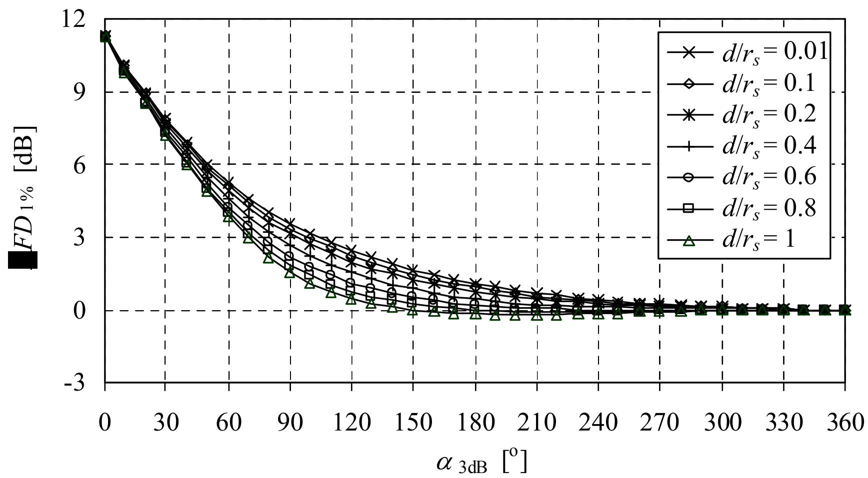

Figure VII.36 – Fading depth variation, pico-cellular, r_s = 2.5 m, K_{omni} = 0 dB, HIPERLAN/2.

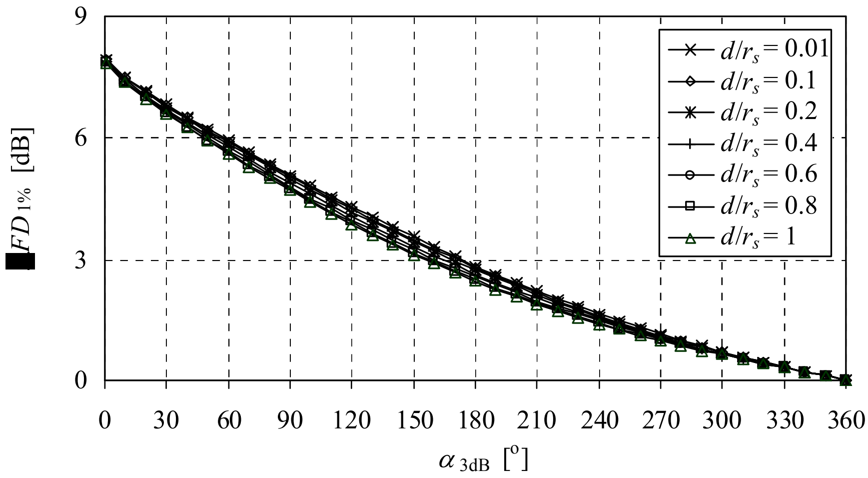

Figure VII.37 – Fading depth variation, pico-cellular, r_s = 2.5 m, K_{omni} = 6 dB, HIPERLAN/2.

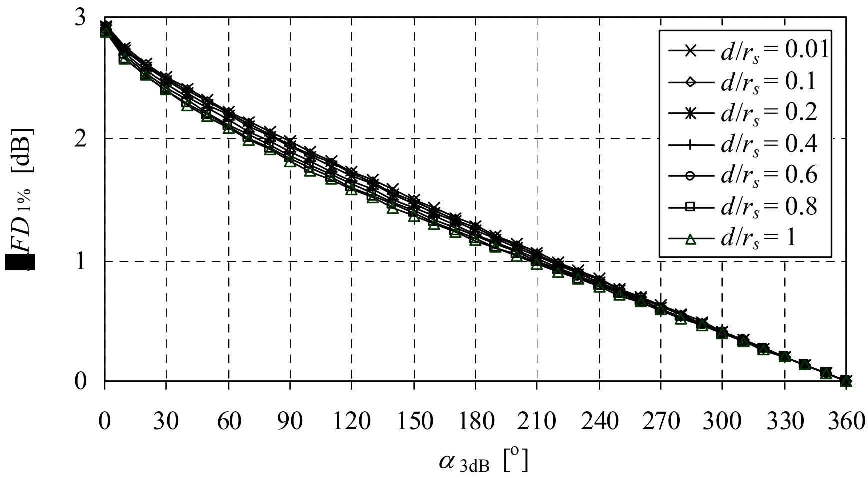

Figure VII.38 – Fading depth variation, pico-cellular, r_s = 2.5 m, K_{omni} = 12 dB, HIPERLAN/2.

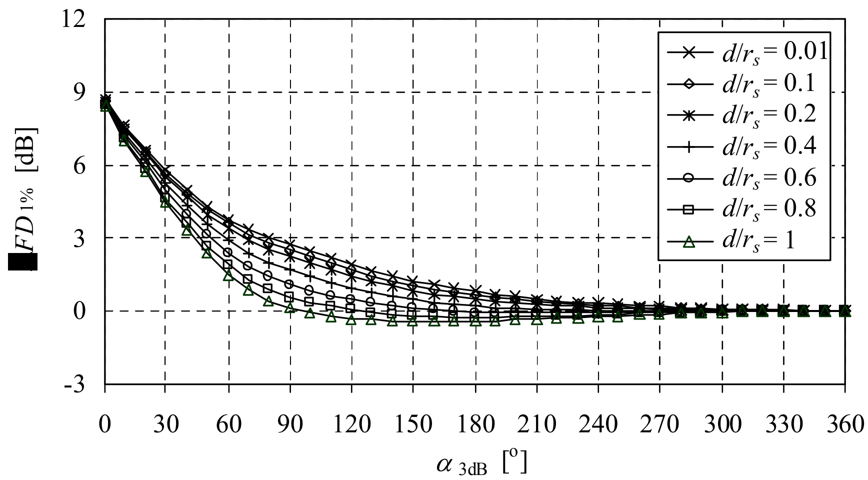

Figure VII.39 – Fading depth variation, pico-cellular, r_s = 5 m, K_{omni} = 0 dB, HIPERLAN/2.

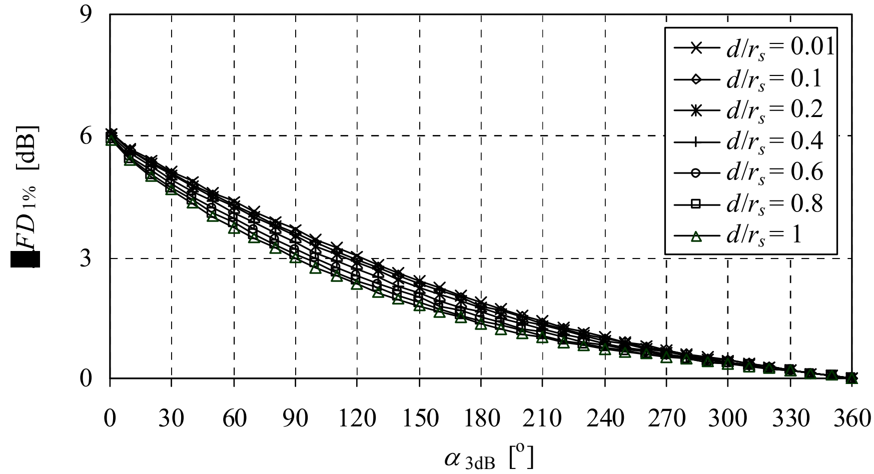

Figure VII.40 – Fading depth variation, pico-cellular, r_s = 5 m, K_{omni} = 6 dB, HIPERLAN/2.

VII.4. NLoS Environments

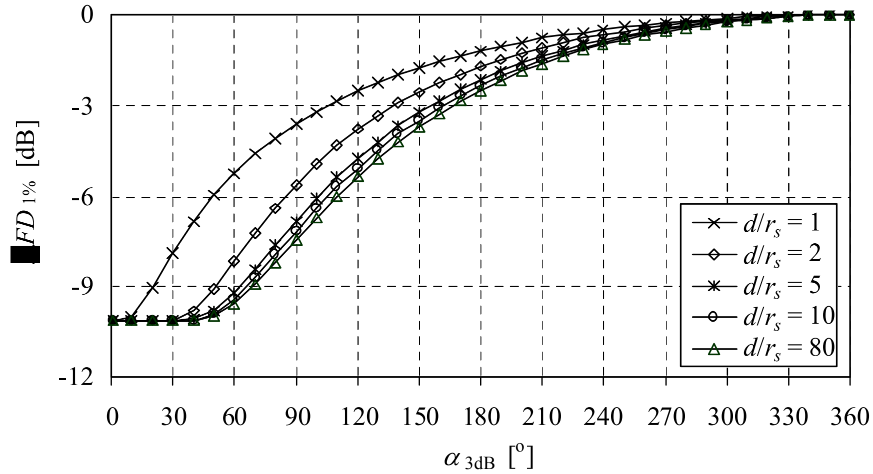

Figure VII.41 – Fading depth variation, macro-cellular, r_s = 800 m, GSM, NLoS.

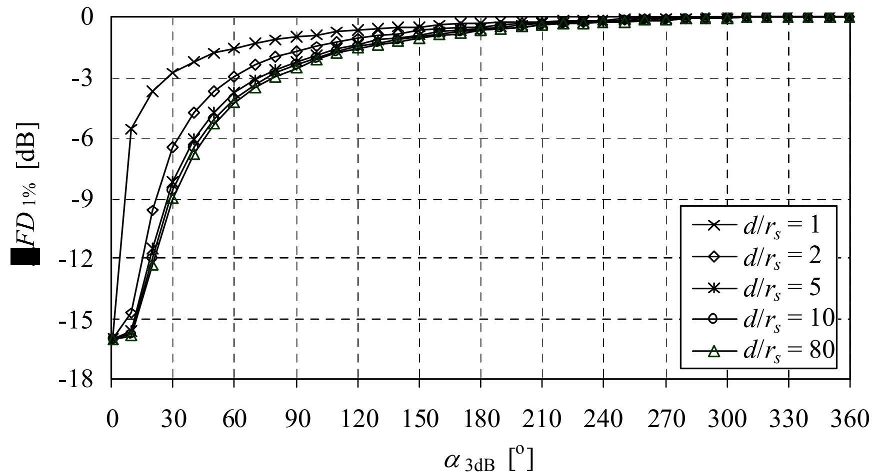

Figure VII.42 – Fading depth variation, macro-cellular, r_s = 800 m, UMTS, NLoS.

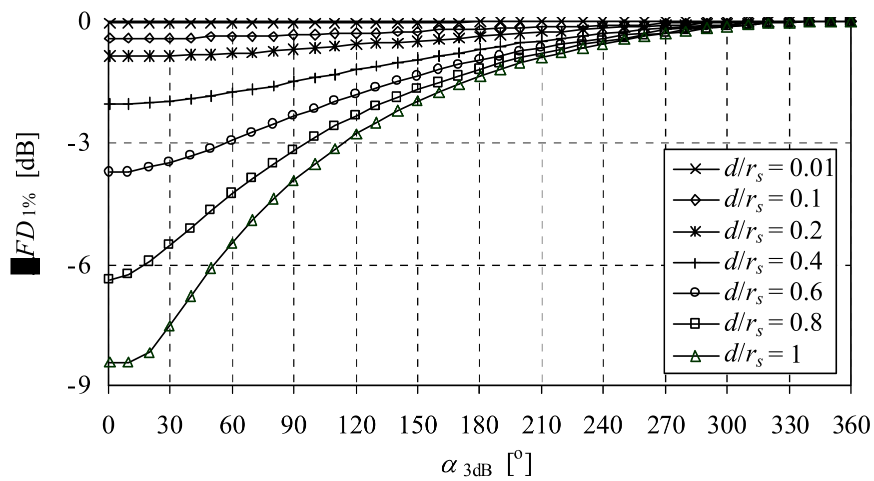

Figure VII.43 – Fading depth variation, pico-cellular, r_s = 5 m, HIPERLAN/2, NLoS.